AEROTHERM FINAL REPORT NO. 67-16, PART I

EXPERIMENTAL AND ANALYTICAL EVALUATION OF THE APOLLO THERMAL PROTECTION SYSTEM UNDER SIMULATED REENTRY CONDITIONS

by

John W. Schaefer
Donald T. Flood
John J. Reese, Jr.
Kimble J. Clark

July 15, 1967

PART I
PROGRAM DESCRIPTION AND PRESENTATION OF RESULTS

Prepared for

National Aeronautics and Space Administration

NASA Manned Spacecraft Center
Houston, Texas
Structures and Mechanics Division
Donald J. Tillian/ES

Contract NAS9-5430

Aerotherm Project 6007

AVAILABLE TO U.S. GOVERNMENT AGENCIES & U.S. GOVERNMENT CONTRACTORS ONLY

LIBRARY COPY
NOV 21 1967
MANNED SPACECRAFT CENTER
HOUSTON, TEXAS

TABLE OF CONTENTS

		Page No.
LIST OF FIGURES		iii
LIST OF TABLES		v
LIST OF SYMBOLS		vi
1.	INTRODUCTION	1-1
2.	PROGRAM DESCRIPTION	2-1
3.	TEST FACILITIES	3-1
3.1	Aerotherm Arc-Plasma Facility	3-1
3.2	NASA-Ames Entry Heating Simulator	3-10
REFERENCES		3-12
4.	TEST MODELS	4-1
4.1	Immersed Flow Models	4-1
4.2	Duct Flow Models	4-7
REFERENCES		4-12
5.	INSTRUMENTATION AND DATA REDUCTION	5-1
5.1	Pressure	5-1
5.2	Heating Rate	5-1
5.3	Enthalpy	5-5
5.4	Stream Composition and Contamination	5-8
5.5	Model Dimensional and Weight Change	5-9
5.6	Temperature	5-9
5.7	Photography	5-11
REFERENCES		5-12
6.	PRESENTATION OF TEST RESULTS	6-1
6.1	Calibration Tests	6-1
6.1.1	Calibration of Operating Conditions	6-1
6.1.2	Spherical Nose Heating Rate Distribution	6-60
6.1.3	Arc Column Radiation	6-60
6.1.4	Test Stream Composition	6-62
6.1.5	Test Stream Contamination	6-65
6.2	Model Test Results	6-68
6.3	Chemical and Physical Properties Tests	6-292
6.3.1	Photomicrograph Study	6-292
6.3.2	X-Ray Diffraction Analysis	6-309

TABLE OF CONTENTS (continued)

		Page No.
6.3.3	Microchemical Analysis	6-309
6.3.4	X-Ray Density Measurement	6-311
6.3.5	Infrared Spectra Analysis	6-315
REFERENCES		6-316
7.	ANALYTICAL PREDICTIONS	7-1
7.1	Introduction	7-1
7.2	Description of the Ablation Computer Programs Used in the Analytical Study	7-1
7.2.1	The Aerotherm Charring Material Ablation Program (CMA)	7-1
7.2.2	The Aerotherm Chemical Equilibrium Program (ACE)	7-3
7.3	Computer Program Input Information	7-4
7.3.1	Input Information for the ACE Program	7-4
7.3.1.1	Elemental Composition of the Char, Pyrolysis Gas, and Boundary-Layer Edge Gas	7-4
7.3.1.2	Thermodynamic Data for the Eligible Molecular Species	7-6
7.3.1.3	Miscellaneous Input Information	7-7
7.3.2	Input Information for the CMA Program	7-8
7.3.2.1	Arrhenius Material Decomposition Equation	7-8
7.3.2.2	Nodal Network	7-8
7.3.2.3	Back Wall Boundary Conditions	7-9
7.3.2.4	Material Properties	7-9
7.3.2.5	Pyrolysis Gas Enthalpy	7-13
7.3.2.6	Heats of Formation	7-13
7.3.2.7	Functions of Time Boundary Conditions	7-15
7.3.2.8	Ratio of Mass Transfer to Heat Transfer Coefficient	7-17
7.3.2.9	Radiation View Factor	7-17
7.3.2.10	Surface Thermochemistry	7-17
7.4	Results of the Analytical Predictions	7-20
7.4.1	Experimental Predictions	7-21
7.4.2	Parametric Predictions	7-21
REFERENCES		7-80
APPENDIX A - LIST OF INSTRUMENTATION		

LIST OF FIGURES

		Page No.
3-1	Aerotherm 1 Megawatt Arc Heater Mounted to Vacuum Test Chamber	3-3
3-2	Aerotherm 1 Megawatt Arc Heater in Atmospheric Discharge Configuration	3-3
3-3	Partial View of Aerotherm Arc-Plasma Facility Showing the Test Chamber, Steam Ejectors, and Condensors.	3-4
3-4	Stagnation Condition Envelopes for Several Flight Regimes	3-6
3-5	Sonic Duct Test Configuration	3-7
3-6	Heating Rate as a Function of Enthalpy for Sonic Duct Testing	3-8
3-7	Wall Shear Stress as a Function of Enthalpy for Sonic Duct Testing	3-9
3-8	NASA Ames Entry Heating Simulator	3-11
4-1	Shroud and Core Technique	4-2
4-2	Model Configurations	4-4
4-3	Typical 2 Inch Blunt Hemisphere Model Construction	4-6
4-4	Typical X-Ray Photograph of 2 Inch Blunt Hemisphere	4-8
4-5	Schematic View of Channel Flow Apparatus, Series "A"	4-9
4-6	Schematic View of Modified Channel Flow Apparatus, Series "B"	4-11
5-1	Radiation Flux and Total Flux Probes	5-3
5-2	Calculated Convective Heating Variation with Stagnation Pressure and Enthalpy	5-7
6-1	Enthalpy, Pressure and Heating Rate Spectrum of Operation	6-2
6-2	Calibration Data, Phase I	6-6
6-3	Calibration Data, Phase II	6-12
6-4	Calibration Data, Phase III	6-14
6-5	Calibration Data, Phase IV A	6-24
6-6	Calibration Data, Phase IV B	6-29
6-7	Calibration Data, Phase V	6-39
6-8	Calibration Data, Phase VI A	6-44
6-9	Calibration Data, Phase VI B	6-47
6-10	Calibration Data, Phase VII	6-56
6-11	Blunt Hemisphere Transient Calorimeter	6-61
6-12	Surface and Internal Temperature Histories, Phase I	6-79
6-13	Surface and Internal Temperature Histories, Phase II	6-101
6-14	Surface and Internal Temperature Histories, Phase III	6-124
6-15	Surface and Internal Temperature Histories, Phase IV A	6-152
6-16	Surface and Internal Temperature Histories, Phase IV B	6-167
6-17	Surface and Internal Temperature Histories, Phase V	6-189
6-18	Surface and Internal Temperature Histories, Phase VI A	6-204
6-19	Surface and Internal Temperature Histories, Phase VI B	6-218
6-20	Surface and Internal Temperature Histories, Phase VII	6-227

LIST OF FIGURES (continued)

		Page No.
6-21	Pre Test Model Photographs	6-235
6-22	Phase I Post Test Model Photographs	6-239
6-23	Phase II Post Test Model Photographs	6-245
6-24	Phase III Post Test Model Photographs	6-250
6-25	Phase IV A Post Test Model Photographs	6-259
6-26	Phase IV B Post Test Model Photographs	6-265
6-27	Phase V Post Test Model Photographs	6-273
6-28	Phase VI A Post Test Model Photographs	6-278
6-29	Phase VI B Post Test Model Photographs	6-282
6-30	Phase VII Post Test Model Photographs	6-285
6-31	Comparison of Surface Temperatures Indicated by Infrared and Total Radiation Pyrometer	6-288
6-32	Representative Micrographs	6-294
6-33	X-Ray Densitometer Trace	6-313
7-1	Char and Virgin Material Thermal Conductivity and f-Functions	7-12
7-2	Pyrolysis Gas Total Enthalpy vs Temperature	7-14
7-3	Typical Surface Thermochemical Response Results	7-18
7-4	Analytical Predictions of Material Performance for Models Exposed to Simulated Reentry Conditions (Option 1)	7-23
7-5	Analytical Predictions of Material Performance for Models Exposed to Simulated Reentry Conditions (Option 2)	7-51

LIST OF TABLES

		Page No.
4-1	Model Raw Material Information	4-3
5-1	Calorimeter Summary	5-4
5-2	Effective Spherical Nose Radii	5-4
6-1	Summary of Ablation Test Program	6-4
6-2	Radiation Probe Data	6-60
6-3	Results of Mass Spectrographic Analysis of Test Samples	6-63
6-4	Measured Nitrogen and Oxygen Concentration in Test Stream	6-64
6-5	Electrode Weight Loss	6-66
6-6	Nylon Sample Analysis	6-67
6-7	Ablation Model Test Results Phase I Shear	6-69
6-8	Ablation Model Test Results Phase II Combined Convective and Radiative Heating	6-70
6-9	Ablation Model Test Results Phase III High Stagnation Pressure	6-71
6-10	Ablation Model Test Results Phase IVA Low Stagnation Pressure and Exposure Time	6-73
6-11	Ablation Model Test Results Phase IVB Low Stagnation Pressure and Chemical Environment	6-74
6-12	Ablation Model Test Results Phase V Model Size and Exposure Time	6-75
6-13	Ablation Model Test Results Phase VIA Model Shape Constant Enthalpy and Constant Stagnation Pressure	6-76
6-14	Ablation Model Test Results Phase VIB Model Shape Constant Stagnation Pressure and Constant Stagnation Heating Rate	6-77
6-15	Ablation Model Test Results Phase VII Enthalpy and Stagnation Pressure at Constant Heating Rate	6-78
6-16	Summary of Chemical and Physical Properties Tests	6-293
6-17	X-Ray Diffraction Analysis Results	6-310
6-18	Microchemical Analysis Results	6-312
7-1	Predictions of Model Performance	7-22
7-2	Results of Parametric Study	7-79

LIST OF SYMBOLS

A	area (ft^2), or asymptotic calorimeter identification
a	channel (duct) height (inch), or a constant
B	pre-exponential factor (1/sec)
B'	dimensionless recession rate parameter
BH	blunt hemisphere model shape identification
C_p	specific heat (Btu/lb$^{\circ}$R)
D	model body diameter (inch), or diameter (inch), or duct
D_c	model core diameter (inch)
d_e	nozzle exit diameter (inch)
E_a/R	activation energy factor ($^{\circ}$R)
FF	flat face model shape identification
H	hemisphere model shape identification
h	enthalpy (Btu/lb)
K	mass fraction
K_c	char thermal conductivity (Btu/ft-sec-$^{\circ}$R)
K_p	virgin material thermal conductivity (Btu/ft-sec-$^{\circ}$R)
$\tilde{K}$	elemental mass fraction
Le	Lewis number
M	mass loss (gm)
m	mass (gm)
$\dot{m}$	mass flow rate of gas (lb/sec)
$\dot{m}_c$	mass loss rate of char (lb/sec)
$\dot{m}_g$	mass loss rate of pyrolysis gases (lb/sec)
$\mathcal{M}$	molecular weight (lb/lb-mol)
N	number of mols
Pr	Prandtl number
p_e	nozzle exit pressure (atm), or local static pressure (atm)
p_o	plenum (chamber) pressure (atm)
p_s	model stagnation pressure (atm)
p_v	vapor pressure (atm)
Q_{in}	arc input power (Btu/sec)

LIST OF SYMBOLS (continued)

Q_{loss}	total energy transfer rate to cooling water (Btu/sec)
q	heat flux (Btu/ft^{2}sec)
q_c	convective heat flux (Btu/ft^{2}sec)
$q_c\sqrt{R}$	stagnation point heating rate (Btu/ft$^{3/2}$sec)
R	effective spherical nose radius (ft), or radius (ft), or gas constant (ft-lb$_f$/lb$_m$)
$\overline{R}$	universal gas constant (ft-lb$_f$/lb-mol$^\circ$R)
RAD	radiation probe identification
r	nozzle radius (inch)
r_e	nozzle radius at exit (inch)
SUBS	subsonic anode arc configuration identification
SUPS	supersonic anode arc configuration identification
s	surface recession (inch)
$\dot{s}$	average surface recession rate (mils)
T	absolute temperature ($^\circ$R), or transient calorimeter identification
T_{ref}	reference temperature ($^\circ$R)
Z	compressibility
α	angle from stagnation point for a spherical nose
ΔT	temperature difference ($^\circ$R)
$\Delta\theta$	time increment (sec)
ϵ	emissivity
θ	exposure time or time (sec)
λ	blowing reduction parameter
μ	viscosity (lb/sec-ft)
ρ	density (lb/ft^3)
ρ_c	residual or fully-charred material density (lb/ft^3)
ρ_p	virgin material density (lb/ft^3)
$\rho_e u_e C_H$	heat transfer coefficient (lb/ft^{2}sec)
$\rho_e u_e C_M$	mass transfer coefficient (lb/ft^{2}sec)
τ_w	wall shear stress (lb/ft^2)
ψ	density factor exponent

LIST OF SYMBOLS (concluded)

Subscripts

cal	(based on) calorimeter
cpi	char-pyrolysis zone interface
cw	cold wall
eb	energy balance
hf	heat flux
hw	hot wall
mb	mass balance
n	nose
O	oxygen
o	non-ablating
ppi	pyrolysis zone - virgin material interface
N	nitrogen
r	radiative
t	total
w	wall
*	condensed phase, or evaluated at sonic throat conditions
0	centerline
1,2	species 1, species 2

SECTION 1
INTRODUCTION

The design and qualification of the Apollo thermal protection system requires an accurate knowledge of the system ablative material response to atmospheric entry conditions. For entry from the Apollo lunar mission, these conditions encompass a broad spectrum of enthalpy, pressure, heat flux, both convective and radiative, and shear. The response of the thermal protection material to this reentry environment must be known so that the system design has adequate protection capabilities but minimum weight. In order to define and evaluate this material response, ground tests that closely simulate the conditions of manned lunar return are required. Arc plasma generator testing provides an ideal means for simulating these conditions. An extensive test program on the Apollo thermal protection system material, using an arc plasma generator to simulate the broad spectrum of conditions experienced by the Apollo vehicle, was therefore performed. The results of this test program are presented in this report.

Because of scaling problems and the time variation of the above mentioned environmental parameters, it is not possible to exactly duplicate simultaneously all trajectory conditions in a ground test facility. The test results must therefore be related to empirical or theoretical prediction techniques which can then in turn be used to predict the thermal protection system response to flight trajectories. An analysis of the test results in the light of this requirement is also included herein.

This report is divided into two basic parts, Part I which presents all results obtained under the program and Part II which discusses and analyzes these results. Part I, contained herein, is divided into seven sections. Section 2 presents an outline of the overall program to provide the reader a brief but complete look at the total program. Section 3 presents the descriptions of the test facilities in which the reentry simulation tests were performed. Section 4 presents a detailed description of all test models of the thermal protection system material used in the program. Section 5 presents all instrumentation and the data reduction techniques. Section 6 presents all test results obtained under the program including the test model response to the broad spectrum of conditions to which they were exposed, the test conditions calibration results, and the results of chemical and physical properties tests on some of the tested models. Finally, Section 7 presents the results of analytical predictions of material performance made for a broad spectrum of conditions including several corresponding to model tests.

Part II is a separate document and provides the discussion and analysis of the test results. Section 8 is an introduction to Part II and briefly summarizes the overall program. Section 9 provides the interpretation and analysis of all results obtained under the program including the reentry simulation test results, the analytical prediction results, and the chemical and physical properties test results. Section 10 presents a summary of all results in the form of a descriptive characterization of the material response based on all program results. Finally, Section 11 presents recommendations for future work.

The authors express their appreciation to the many NASA and Aerotherm personnel who have contributed to the program. The contributions of Mr. Donald J. Tillian, the NASA-MSC Technical Monitor, and Mr. Donald M. Curry, also of NASA-MSC, are gratefully acknowledged. Particular thanks go to Mr. Roy M. Wakefield of the Gasdynamics Branch of NASA-Ames who conducted the combined convective and radiative heating test program in the NASA-Ames Entry Heating Simulator. The Aerotherm staff members who contributed to the program include Mr. Roald A. Rindal and Dr. Robert M. Kendall of the technical staff, Mr. Thomas Wong who performed all design work and assisted in the testing, and Mr. Francis J. McKinley who served as chief technician; their efforts are gratefully acknowledged.

SECTION 2
PROGRAM DESCRIPTION

The complete program performed under this contract, NAS9-5430, is outlined briefly below. The program was divided into three basic efforts for study of the Apollo thermal protection material as follows, the first of which being the main program effort:

Test and evaluation under simulated reentry conditions.
Analytical predictions of performance under test and reentry conditions.
Chemical and physical properties tests on models exposed to simulated reentry conditions.

The Avcoat 5026-39 HCG material was considered almost exclusively in the program; a few tests were also performed on other similar materials.

The reentry simulation test program was divided into seven phases. These phases are outlined below and the nominal range of test conditions noted.

Phase I Shear

Study of the effect of shear on material performance

Enthalpy	3000 to 10,000 Btu/lb
Local pressure	1 to 3 atm
Shear stress	3 to 20 psf
Convective heat flux	175 to 525 Btu/ft^{2}sec
Chemical environment	Air and Nitrogen

Phase II Combined Convective and Radiative Heating

Study of the effect of combined convective and radiative heating and radiative - only heating on material performance

Enthalpy	3000 to 6250 Btu/lb
Stagnation pressure	0.10 atm
Convective heat flux	0 to 175 Btu/ft^{2}sec
Radiative heat flux	0 to 600 Btu/ft^{2}sec
Chemical environment	Air

Phase III High Stagnation Pressure

Study of the effect of high heat flux and high pressure on material performance

Enthalpy	3500 to 5000 Btu/lb
Stagnation pressure	1 to 3 atm
Convective heat flux	800 to 1800 Btu/ft^{2}sec
Chemical environment	Air and Nitrogen

Phase IV A Low Stagnation Pressure and Exposure Time

Study of material performance at low stagnation pressure and study of the effect of exposure time on material performance

Enthalpy	3500 to 25,000 Btu/lb
Stagnation pressure	0.008 atm
Convective heat flux	30 to 250 Btu/ft^{2}sec
Chemical environment	Air

Phase IV B Low Stagnation Pressure and Chemical Environment

Study of the effect of chemical environment on material performance at low pressure

Enthalpy	5000 to 17,500 Btu/lb
Stagnation Pressure	0.028 atm
Convective heat flux	90 to 300 Btu/ft^{2}sec
Chemical environment	Air, Nitrogen, Helium, various Oxygen concentrations in Nitrogen

Phase V Model Size and Exposure Time

Study of material performance at low stagnation pressure, study of the effect of model size on test results, and study of the effect of exposure time on material performance

Enthalpy	5000 to 17,500 Btu/lb
Stagnation pressure	0.008 to 0.028 atm
Convective heat flux	60 to 450 Btu/ft^{2}sec
Chemical environment	Air

Phase VI A Model Shape, Constant Enthalpy and Constant Stagnation Pressure

B Model Shape, Constant Stagnation Pressure and Constant Stagnation Heating Rate

Study of material performance at low stagnation pressure, study of the effect of model shape on test results

Enthalpy	3500 to 25,000 Btu/lb
Stagnation pressure	0.028 atm
Convective heat flux	60 to 450 Btu/ft^{2}sec
Chemical environment	Air

Phase VII Enthalpy and Stagnation Pressure at Constant Heating Rate

Study of material performance at constant heating rate with enthalpy and pressure variable

Enthalpy	3500 to 25,000 Btu/lb
Stagnation pressure	0.028 to 0.4 atm
Convective heat flux	450 Btu/ft^{2}sec
Chemical environment	Air

A total of 158 models were tested over the above spectrum of conditions. The program also included a complete calibration of these test conditions.

The analytical predictions of material performance were made using the Aerotherm ablation computer programs and input information based on data provided by NASA-MSC. Predictions were made at conditions corresponding to several of the model tests and for a parametric array of environmental conditions.

The chemical and physical properties tests were performed on several models tested under simulated reentry conditions. These properties tests included microchemical quantitative analysis and X-ray diffraction studies of the surface materials and in-depth char, density distribution measurements as determined by X-ray transmission, infrared spectra measurements of the in-depth char and surface materials, and surface and in-depth photomicrographs.

The details of the program are presented in the following sections.

SECTION 3
TEST FACILITIES

The major part of the reentry simulation test program, Phases I and III through VII, was conducted in the Aerotherm Arc-Plasma Facility under stagnation point and duct flow convective heating conditions. One of the seven program phases, Phase II, was conducted in the NASA-Ames Entry Heating Simulator (Gasdynamics Branch, Test Series 56) under combined convective and radiative heating conditions. A description of the essential elements of each of the two facilities is presented below.

3.1 AEROTHERM ARC-PLASMA FACILITY

The Aerotherm Arc-Plasma Facility is a complete laboratory for study of the effects of high temperature and chemically reactive flows on thermal protection materials for planetary entry and rocket nozzle environments. The facility contains arc heaters ranging in input power from 100 to 1,000 kilowatts, a five-stage steam ejector vacuum pumping system, associated gas, cooling water and support equipment, and instrumentation for recording and monitoring operating conditions and test material response.

Two types of arc heaters are used in the facility. The arc heater used almost exclusively in this program is a gas stabilized, constricted arc device nominally rated at 1 megawatt. Various configurations of the same basic arc unit are used to cover the spectrum from very high enthalpy, low-to-moderate pressure testing to moderate and low enthalpy, high pressure testing. The basic design employs a tungsten cathode fitted at the bottom of a tubular well and a segmented constrictor tube and copper anode in line with the cathode. Both the cathode and anode configurations can be easily changed to obtain optimum performance at different test conditions and for different test gases. The gas is introduced tangentially at the insulated interface of the two electrodes causing the arc to run from the tungsten surface to the anode sleeve. The other unit used in the program is a 1-megawatt magnetically stabilized device which employs concentric water-cooled copper electrodes surrounded by a solenoid coil. The outer electrode serves as the cathode and pressure vessel, while the inner electrode, supported from an insulated rear flange, is the anode. The arc travels in the annulus formed by the two electrodes and is rotated by the magnetic field of the solenoid coil.

The two arc heaters have different operating characteristics and complementary capabilities. The constricted arc unit is the most versatile and covers the entire enthalpy range from very high to low. It is used in all testing for which the chamber pressures are below 125 psia. The magnetic arc unit is used for all testing requiring high chamber pressure and is limited

to moderate and low enthalpies. Both units have the capability of operating with a wide variety of chemically reactive and inert gases.

The solenoid arc-plasma generator has an operating power range from 0.45 to 1.2 megawatts. The chamber pressure range, when exhausting to atmosphere, can presently be varied from 1 to 30 atmospheres with nozzle throat sizes of 1.0- to 0.25-inch diameters, respectively. At these pressures, enthalpy levels up to 6,000 Btu/lb are achievable with air or nitrogen as the test gas.

The constrictor arc heater has an operating power range from 100 kilowatts to 1 megawatt. (Other constrictor units within this power range and for lower power levels are also available.) Experience to date indicates a maximum enthalpy with simulated air of about 72,000 Btu/lb at model stagnation pressures up to 0.2 atm and a maximum enthalpy of about 5,000 Btu/lb at a model stagnation pressure of 3.0 atmospheres. The unit is capable of over 8 atmospheres chamber pressure. For operation below 15,000 Btu/lb a plenum chamber is used upstream of the nozzle expansion whereas a supersonic anode and no plenum chamber is used for the ultra-high enthalpy regime (15,000 to 72,000 Btu/lb). The arc heater is shown mounted to the vacuum test chamber in Figure 3-1 and in Figure 3-2 is positioned for atmospheric discharge testing.

The Aerotherm vacuum-pumping system consists of a test chamber, five-stage steam ejector complex, two 110-boiler-horsepower steam generators, a cooling tower, and associated control equipment. A partial view of the system is shown in Figure 3-3.

The test chamber is a cylindrical steel vessel, 4 feet in diameter by 15 feet long, comprised of three sections. The first is the test chamber proper, which houses the supersonic nozzle and model support system and contains various ports for test observation and access. This is followed by an after-cooler which houses a heat exchanger to cool the arc-heated gases prior to entering the ejector system. The final section provides a transition from the test chamber diameter to the inlet of the steam-ejector system. Provision for radiant energy-flux simulation equipment is incorporated in the test chamber design.

The steam-ejector equipment consists of five ejector stages, two interstage condensers (each with condensate pumps), and an exhaust silencer. The motive steam for the ejector system is supplied by the two 110-boiler-horsepower steam generators. The two units together can provide a total steam load of 6,000 lb/hr at 240 psi. A recirculating cooling water system is provided to supply cooling water continuously to the two interstage condensers of the ejector system. The thermal energy in the cooling water is dissipated in the cooling tower.

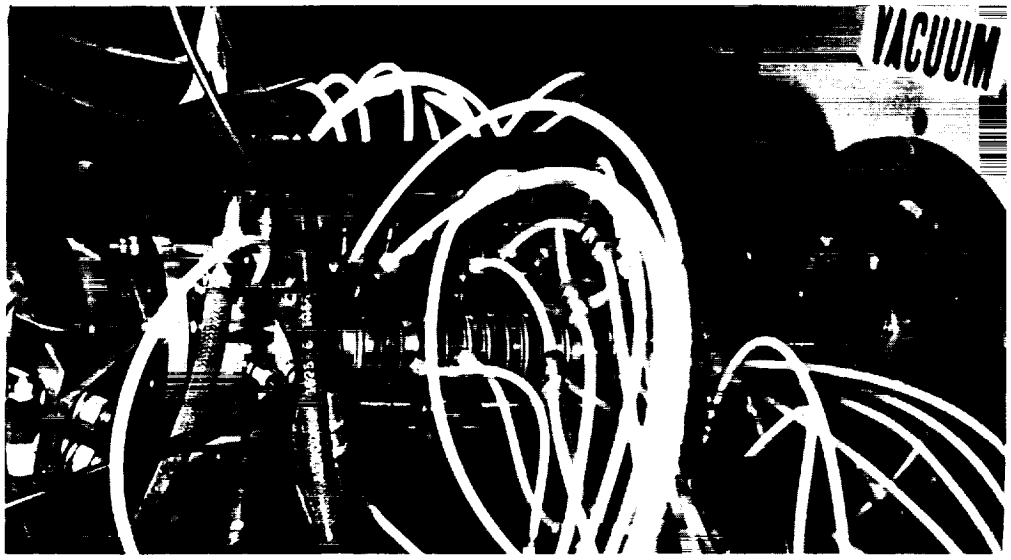

Figure 3-1. Aerotherm 1 Megawatt Arc Heater Mounted to Vacuum Test Chamber.

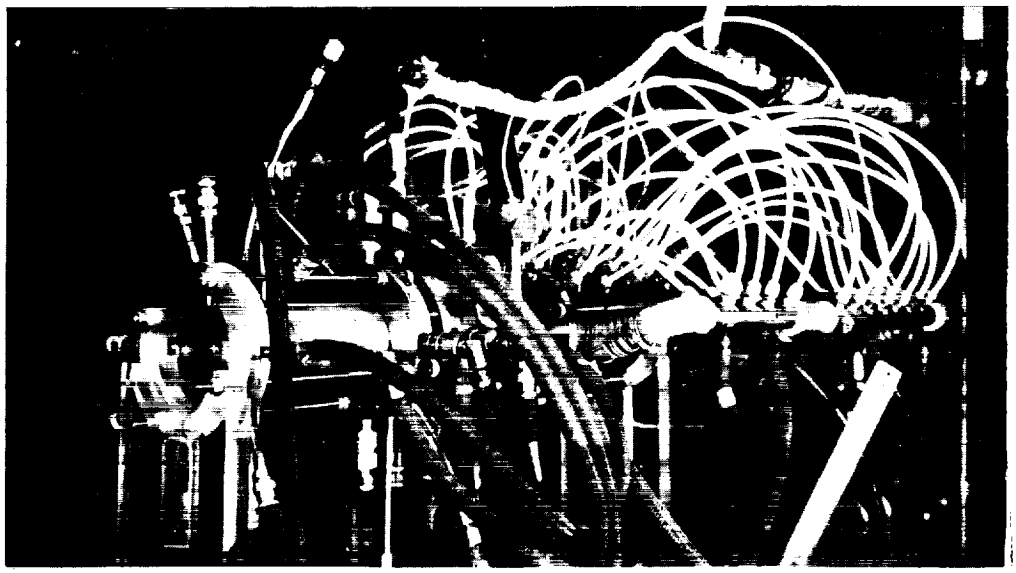

Figure 3-2. Aerotherm 1 Megawatt Arc Heater in Atmospheric Discharge Configuration.

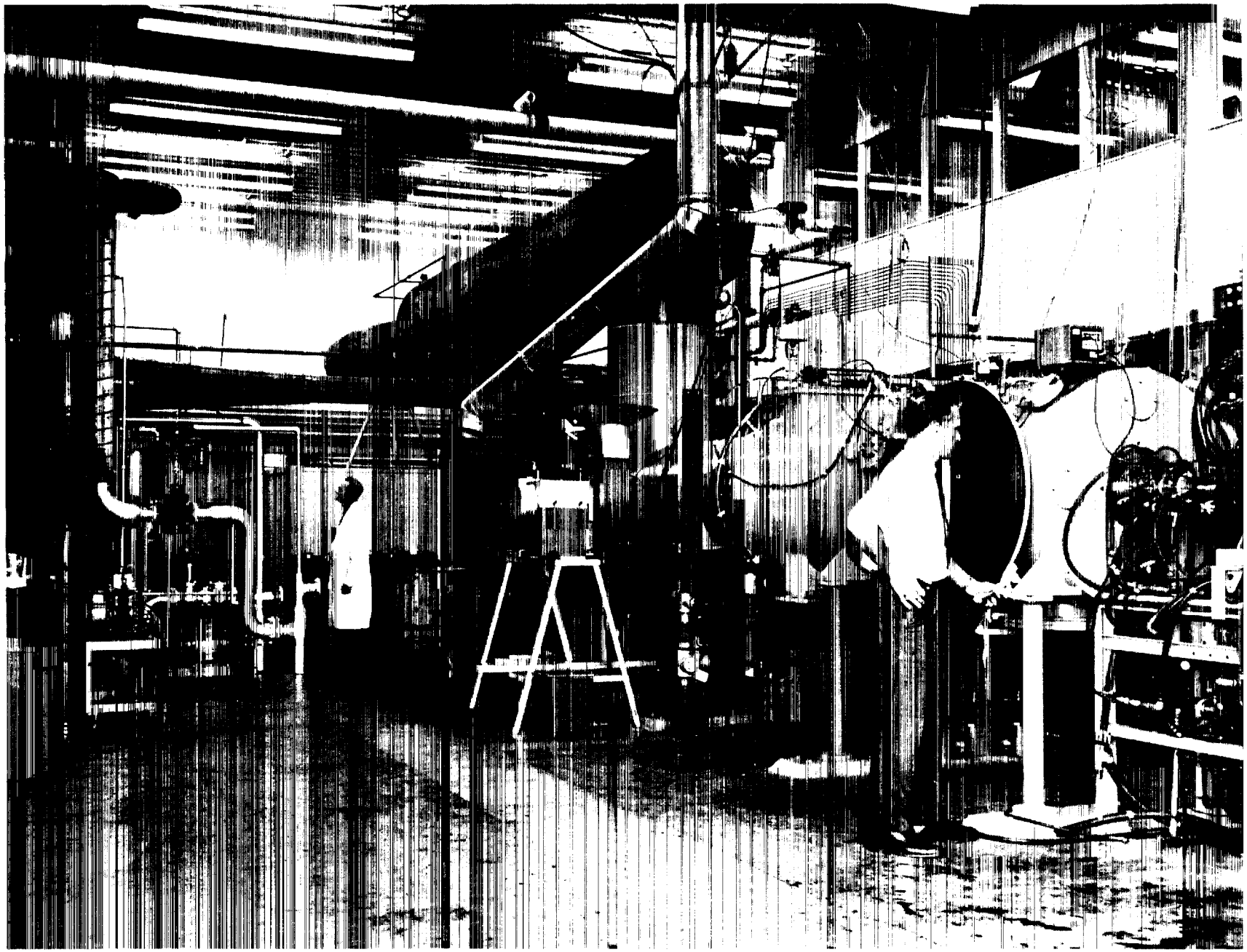

Figure 3-3. Partial View of Aerotherm Arc-Plasma Facility Showing the Test Chamber, Steam Ejectors, and Condensors.

The electric power for the arc heaters is provided by two diesel-electric generators and/or a battery power supply. The two arc heaters can be operated from either system independently or with both systems in parallel or series. In general, the constrictor arcs are run directly from the diesel generator units, with unrestricted run time, whereas the magnetic arc is operated from the battery power supply with run time limited to about one and a half minutes at the 1-megawatt power level. The diesel-generators are rated at 750 KW and 450 KW and can be operated separately or in parallel. Their power output and open circuit voltage are continuously variable, with a maximum combined continuous current of 3,000 amperes. A ballast resistor provides increments of resistance in series with the arc to control the input power level and electrical circuit stability.

The arc-plasma generators are instrumented to permit monitoring and continuous recording of the important operating variables required to define the test conditions, such as gas enthalpy, chamber pressure, and gas mass-flow rate. The facility instrumentation provides continuous high-speed recording and visual readout of the output from all sensors necessary to monitor the arc operating conditions and model or test section response. An analog-to-frequency converter with digital printout and a 36-channel oscillograph are used to record all transient data and to provide a time base for testing events. In addition, a visual readout is provided at a control console for the monitoring of operating conditions.

The capabilities for simulating stagnation reentry heating in the Aerotherm Arc-Plasma Facility are summarized in Figure 3-4, which shows the Aerotherm testing capabilities superimposed on various entry corridors. The operating envelope represents the limits of the present arc heaters and pumping system and are based on data acquired in the facility with nozzle exit diameters ranging from 0.6 inches through 8.0 inches.

Operation with a sonic duct configuration is also possible. Figure 3-5 shows the duct configuration wherein materials specimens form one or two walls of a long rectangular duct 1.0-inch wide and ranging in height between 0.15 and 1.0 inches. The sonic duct test capabilities are presented in Figures 3-6 and 3-7 which show heating rate and wall shear stress as a function of stagnation enthalpy.

The arc plasma facility has also been used for rocket propellant exhaust simulation, including exact composition duplication and/or simulation of liquid, solid, and hybrid propellants. In this case, the material test section is a sonic or supersonic nozzle that serves as the exit nozzle of the arc unit.

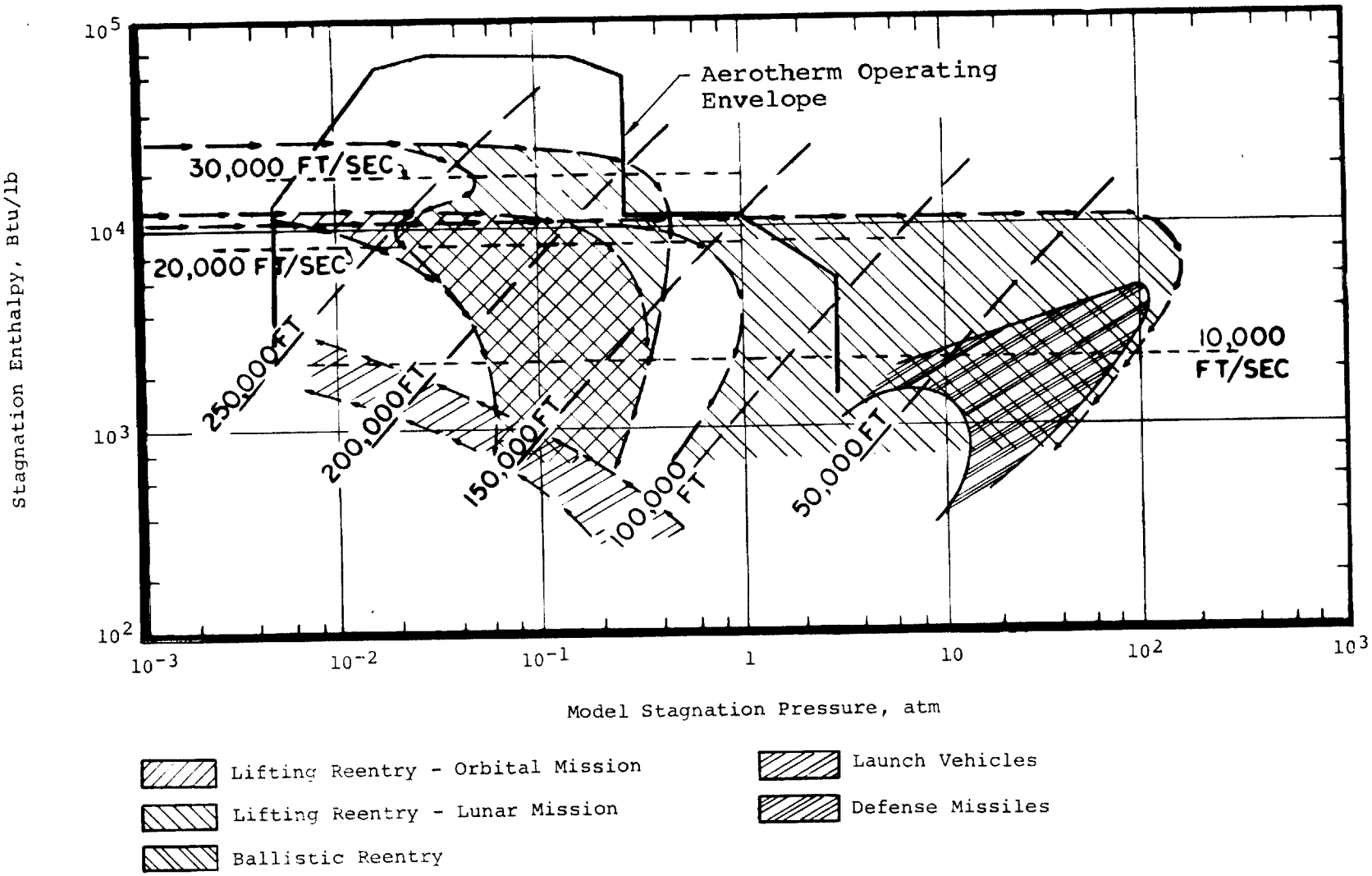

Figure 3-4. Stagnation Condition Envelopes for Several Flight Regimes.

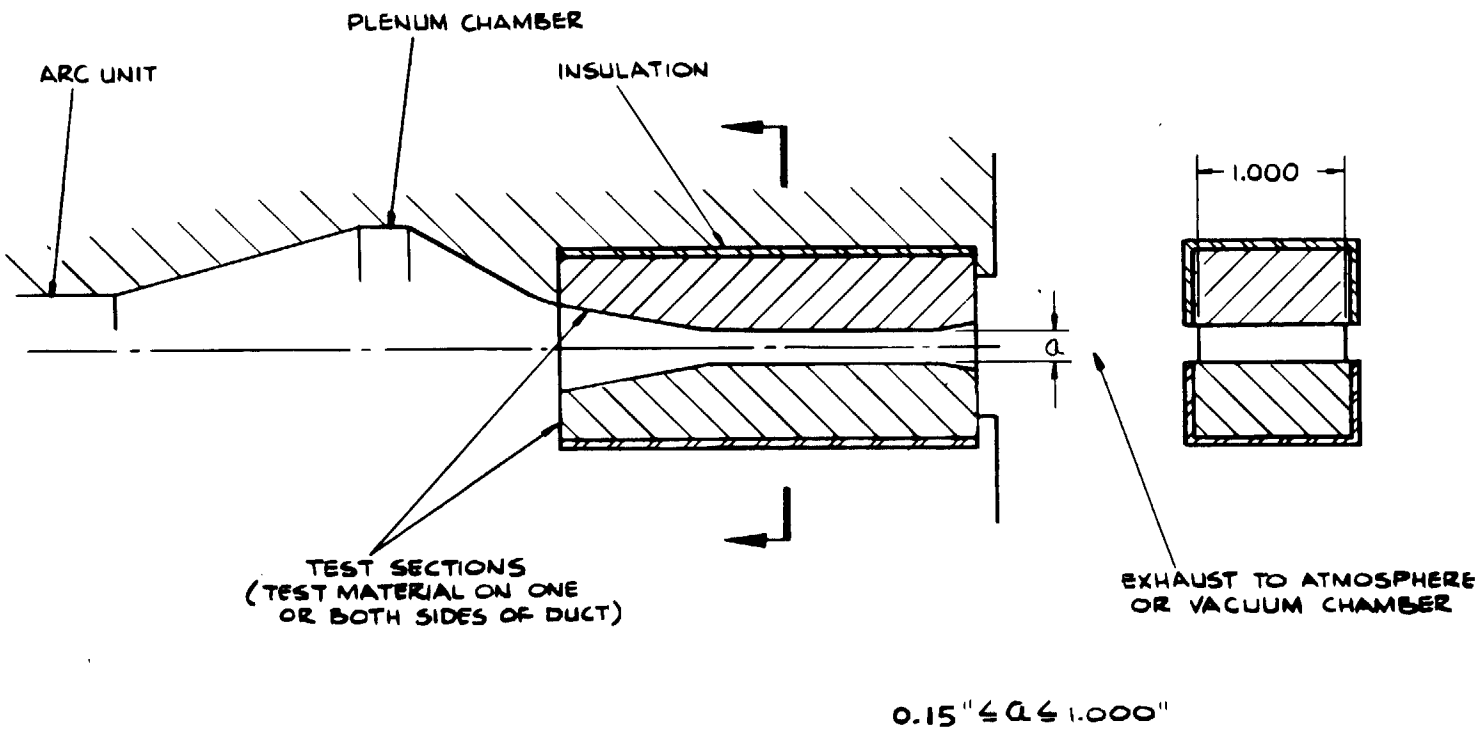

Figure 3-5. Sonic Duct Test Configuration.

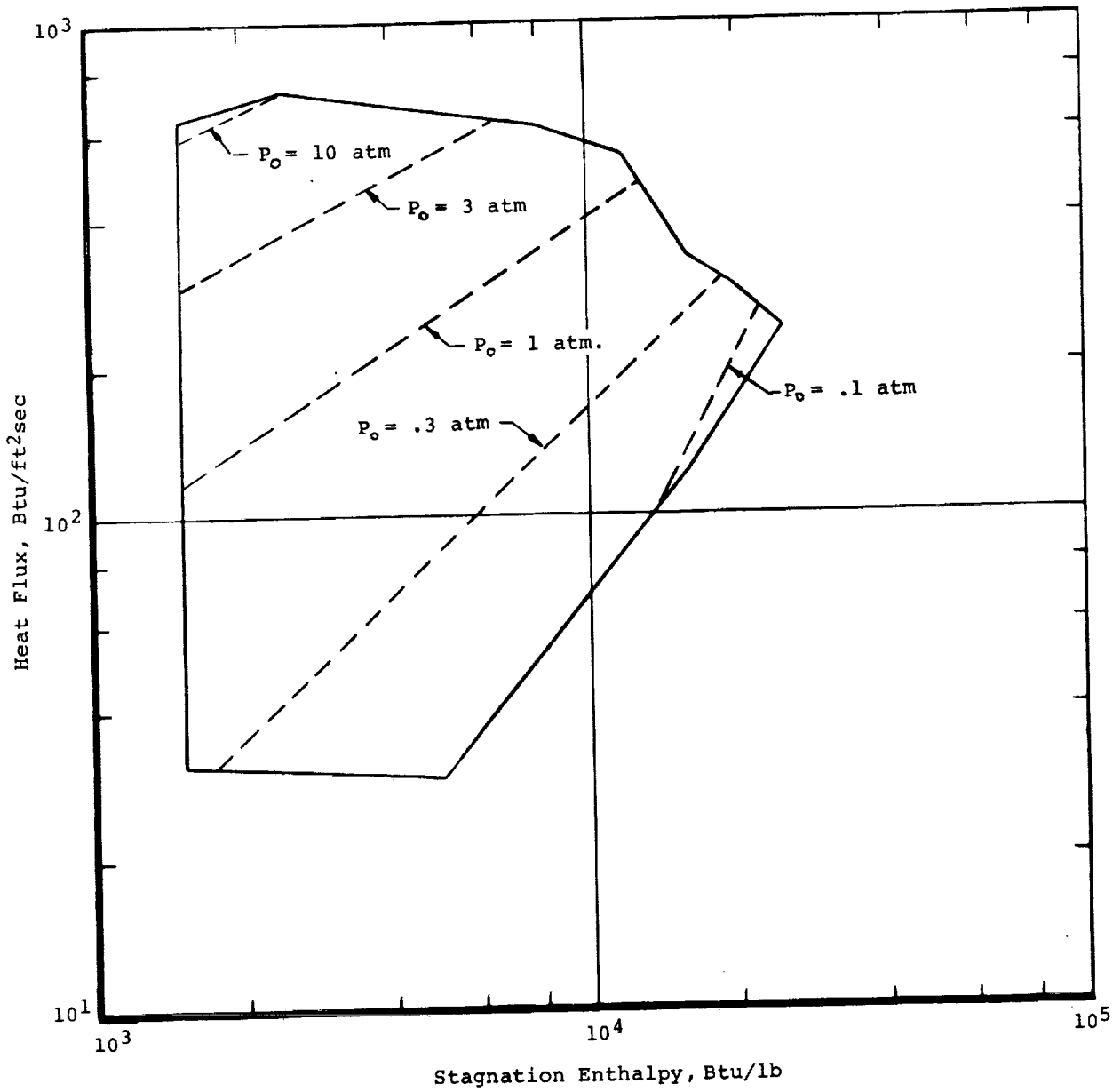

Figure 3-6. Heating Rate as a Function of Enthalpy for Sonic Duct Testing.

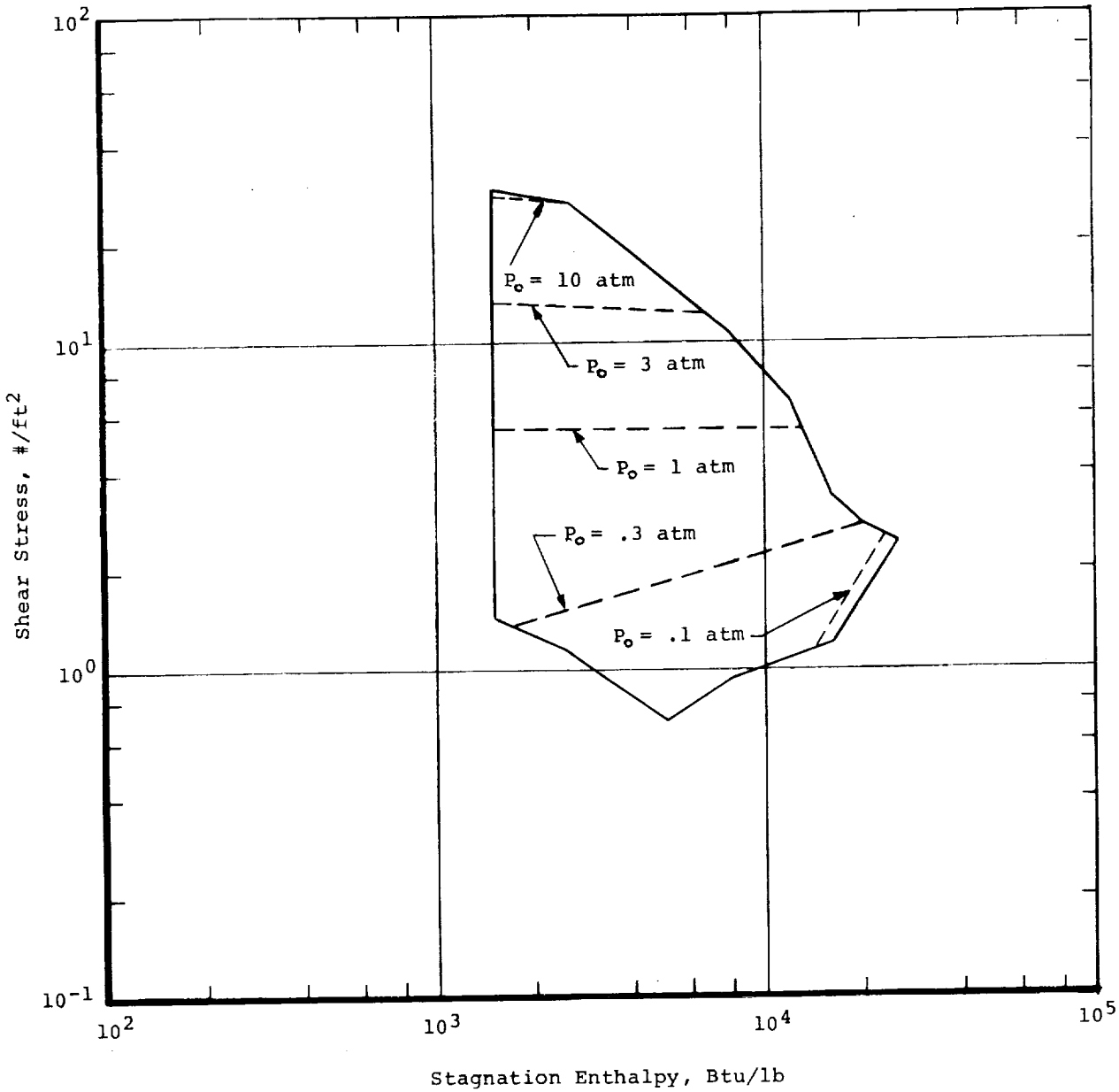

Figure 3-7. Wall Shear Stress as a Function of Enthalpy for Sonic Duct Testing.

3.2 NASA-AMES ENTRY HEATING SIMULATOR

The combined convective and radiative heating tests, Phase II, were conducted in the NASA-Ames Entry Heating Simulator, a facility capable of simulating both the convective and radiative heat fluxes encountered during a portion of the Apollo reentry trajectory.

The facility is comprised of two major components, one an air arc heater for producing hyperthermal, supersonic gas flows and the other a carbon arc lamp and optical system for producing an intense beam of thermal radiation. The arc heater is a copper electrode, magentically stabilized device capable of input power up to 1 megawatt. A supersonic nozzle having a throat diameter of 0.75 inch an an exit diameter of 2.67 inches is used in conjunction with the arc heater. The nozzle is contoured and operates at a Mach number between 3.4 to 4.2 depending upon operating conditions. The arc heater/nozzle combination is attached to a test chamber which in turn exhausts to a vacuum sphere.

The radiation source is housed in a separate vessel mounted in line with the arc heater and at the rear of the test chamber. The radiation source, a modified Strong Electric Company commercial grade carbon arc lamp, is separated from the chamber by a quartz window, a douser, several filters and an aperture plate. The system is shown schematically in Figure 3-8 which was taken from Reference 3-1. A more detailed discussion of the facility is given in References 3-1 and 3-2.

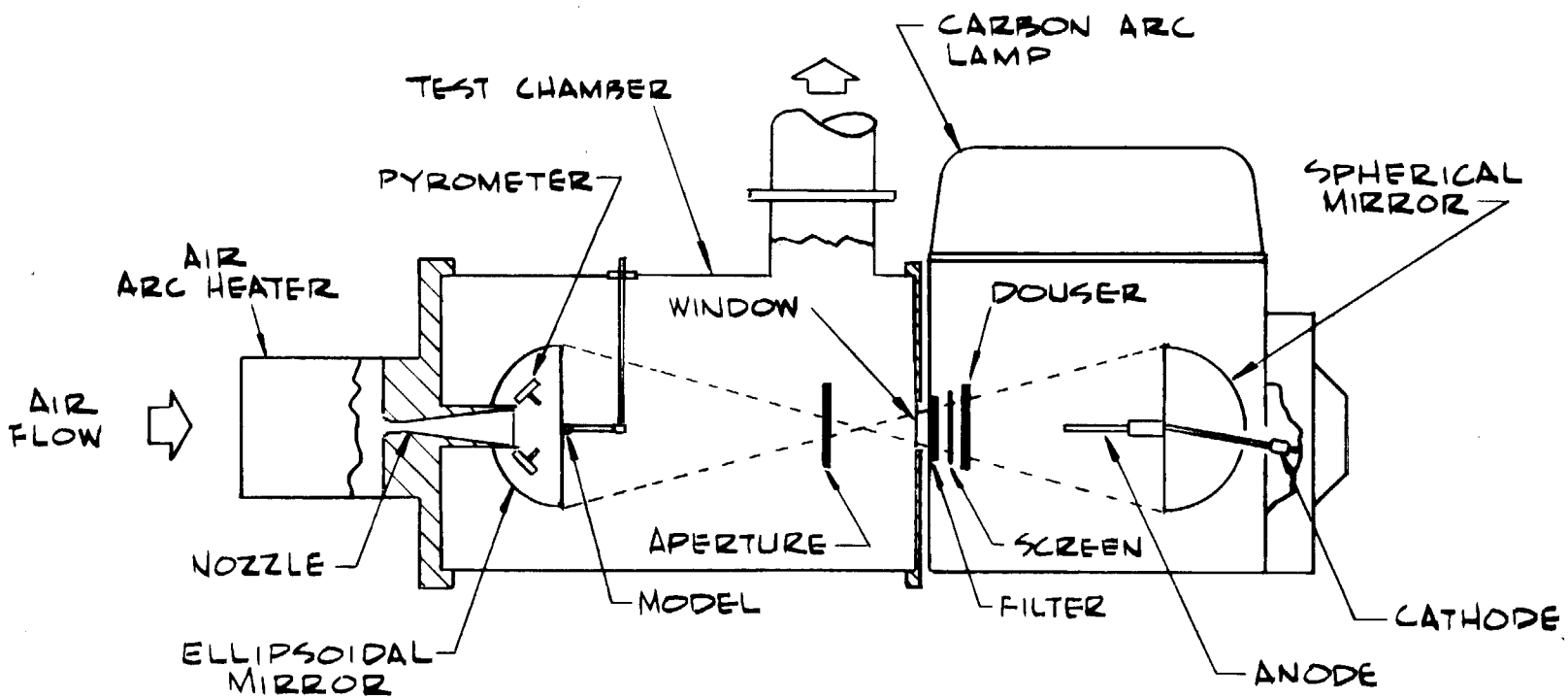

FIGURE 3-8 NASA AMES ENTRY HEATING SIMULATOR

REFERENCES

3-1 Lundell, John H., Winovich, Warren and Wakefield, Roy M.: Simulation of Convective and Radiative Entry Heating. Paper presented at Second National Symposium on Hypervelocity Techniques, Denver, Colorado, March 19 and 20, 1962.

3-2 Gowen, Forrest and Hopkins, Vaughn: A Wind Tunnel Using Arc Heated Air for Mach Numbers from 10 to 20. Paper presented at the Second National Symposium on Hypervelocity Techniques, Denver, Colorado, March 19 and 20, 1962.

SECTION 4
TEST MODELS

The ablation test models used in the program were fabricated from representative samples of the Apollo heat shield material and variations thereof as supplied by NASA-MSC. Two basic types of models were tested, one, an axisymmetric body of revolution for immersed flow exposure and the other a flat plate shape used as one wall of a rectangular duct for wall shear stress evaluation tests. Each of the models was constructed by the "shroud and core" technique as shown in Figure 4-1. This technique permitted measurements of material response on a sample ideally subjected to uniform one-dimensional heat flux. Each model core was instrumented with 3 to 5 fine wire thermocouples located at varying depths from the heated surface.

The ablation models were numbered for identification purposes, each having a serial number assigned at the time of fabrication and identified by this number throughout the remainder of the program. The models were fabricated from stock or "tiles" provided by NASA-MSC which also had a manufacturers serial number. A summary of the MSC model raw material information is shown in Table 4-1. The details of the design and construction of the immersed and duct flow models are discussed below.

4.1 IMMERSED FLOW MODELS

The models tested in immersed, supersonic flow were axisymmetric bodies of revolution constructed by the "shroud and core" technique discussed above. Three basic shapes were considered, a right circular cylinder (flat face) in end flow, designated as FF, a hemispherical nose cylinder, designated as H, and a blunted hemisphere cylinder, designated as BH, which had a hemisphere radius equal to the cylinder diameter. Each of these model shapes was instrumented with thermocouples for in-depth temperature measurement. All stagnation flow model configurations used in the program are presented in Figure 4-2. The body diameters, D, ranged from 1.0 to 4.0 inches. Using the abbreviations noted above, the model shape and size was coded by a shape/body diameter designation. As an example BH/2.0 indicates a blunt hemisphere shape having a body diameter D = 2.0 inches. This coding system is used throughout the remainder of the report.

The selection of the model shapes was based on two consideration, 1) investigation of the response of various configurations which had been previously tested under the Apollo program and 2) selection of the most desirable configuration for this test program. In view of these objectives three primary factors were established to identify the desirability of different model shapes: 1) the heating should be uniform over the test specimen core

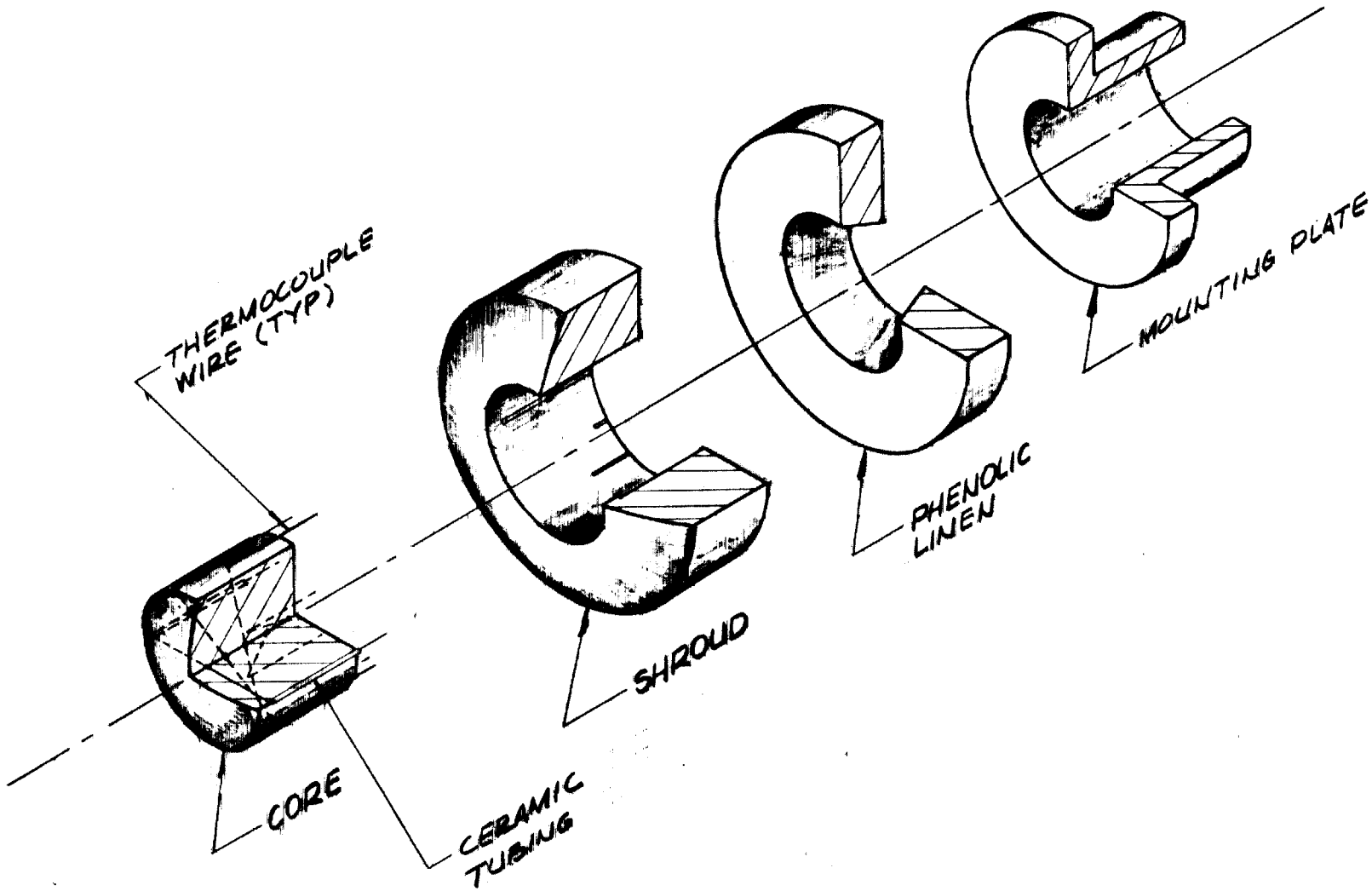

FIGURE 4-1 SHROUD AND CORE TECHNIQUE.

TABLE 4-1

MODEL RAW MATERIAL INFORMATION

Model No.	Material Type	Tile Serial No.
1-6/D	5026-39 HCG	S/N-13000-25
7-9/D	P2019	—
10-12/D	5026-22	—
13-15/D	C5 13093	—
16-22/FF/2.0	5026-39 HCG	S/N-13000-25
23-30/BH/2.0		
31-36/H/2.0		
37-63/FF/1.25		
37-63 shrouds	5026-39M	—
64-73/D	5026-39 HCG	S/N-13000-25
74 109/BH/2.0		K5-13002-5
110-113/BH/1.0		
110-113 shrouds	5026-39M	—
114-121/BH/4.0	5026-39 HCG	E6-80660-1
122-128/BH/4.0		E6-80133
129-158/BH/1.0		E6-80161
129-158 shrouds	5026-39M	F6-80578-4
159-160/H/2.0	5026-39 HCG	E6-80161
161-166/BH/2.0		

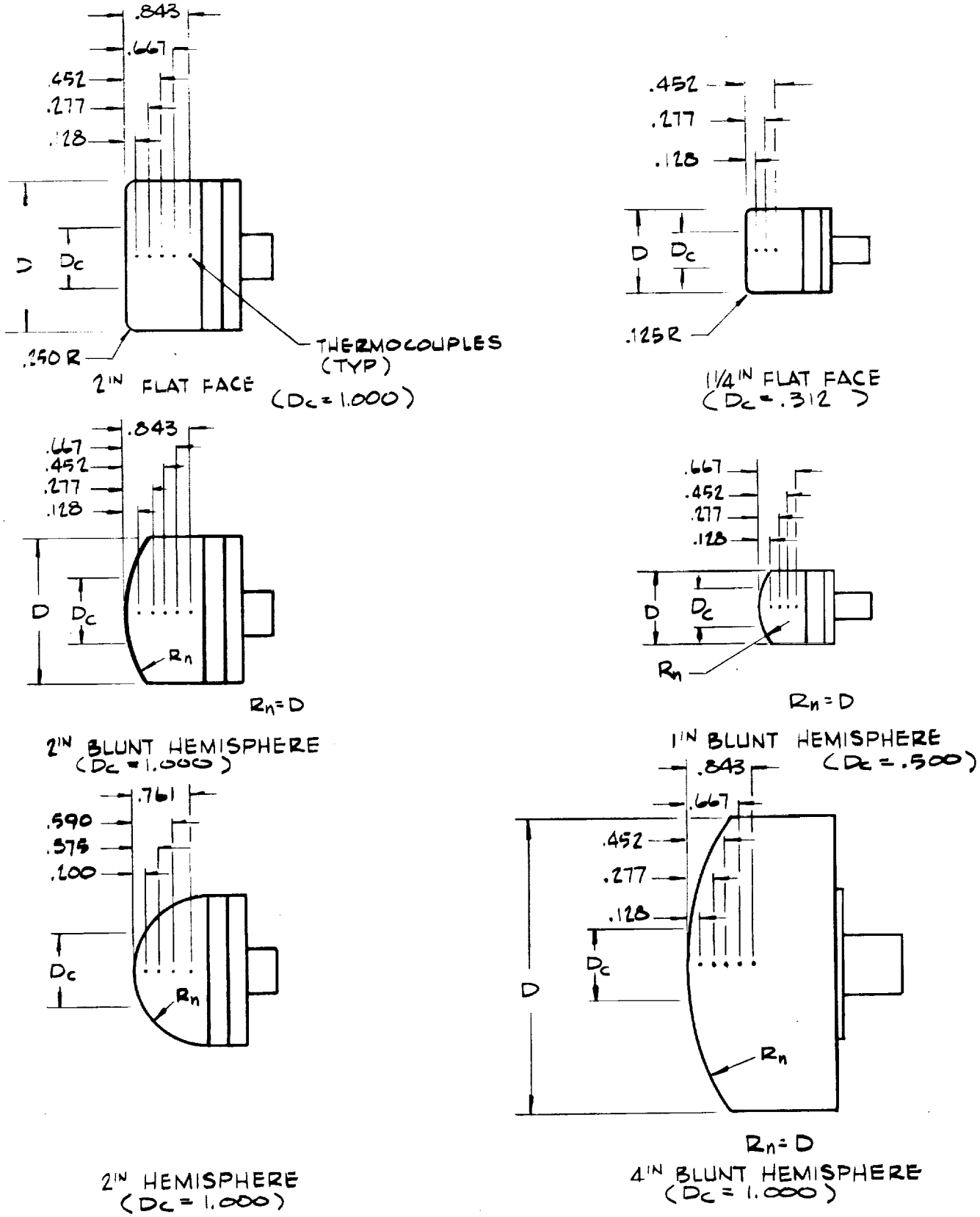

FIGURE 4-2 MODEL CONFIGURATIONS

in order that one-dimensional data reduction techniques be valid, 2) a body shape (core and shroud) should be selected for which an accurate evaluation of the stagnation point velocity gradient may be made in order to correlate measured heat flux data with existing theories, and 3) the core and shroud combination should ablate in such a manner that the body shape retains a similar contour throughout the test duration in order that the stagnation point velocity gradient does not change appreciably during model exposure.

In addition to the three body shapes presented above, the so-called iso-q shape was also considered. The analysis from which the iso-q shape was defined (Reference 4-1) was based on the pressure distribution for the hypersonic Newtonian approximation ($p_e/p_s = \cos^2\alpha$). However, this approximation, based on the results of Reference 4-2, does not adequately represent the pressure distribution (and stagnation point velocity gradient) for the iso-q shape. Because of this, the iso-q shape was not chosen for test under this program.

Because it is desirable to utilize a model shape for which the inviscid flow field (pressure distribution) has been characterized, it was recommended that a spherically blunted cylinder or the blunt hemisphere, BH, such as those described in Reference 4-2, be utilized as the primary shape for the program. The flat face (FF) and hemispherical (H) model shapes (Figure 4-2) were used in addition to the blunt hemisphere shape (BH) to investigate the effect of shape on material response and interpretation of results (part of Phase VI). The different model sizes (Figure 4-2) were used for a similar investigation of model size, relative to test stream diameter (part of Phases IV - VI), and to provide model sizes compatible with the nozzle exit diameters for all program phases.

The details of the model construction for a typical 2 inch blunt hemisphere are shown in Figure 4-3. The core and shroud were machined from the raw stock supplied by NASA-MSC. Each core was drilled with 3 to 5 holes which were 0.018 inch in diameter and perpendicular to the centerline to accommodate the thermocouples. A 0.005-inch diameter Chromel-Alumel lap welded thermocouple with a nominal 0.020-inch diamter junction was pulled through each port in such a fashion as to extrude the port locally, forcing intimate contact between the thermocouple junction and the virgin material as shown in the sketch. The thermocouple wires were brought out of the

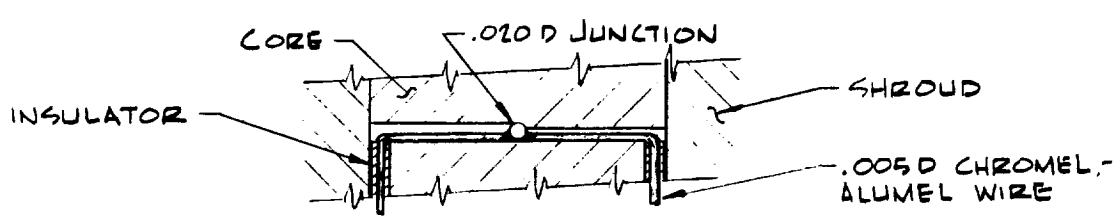

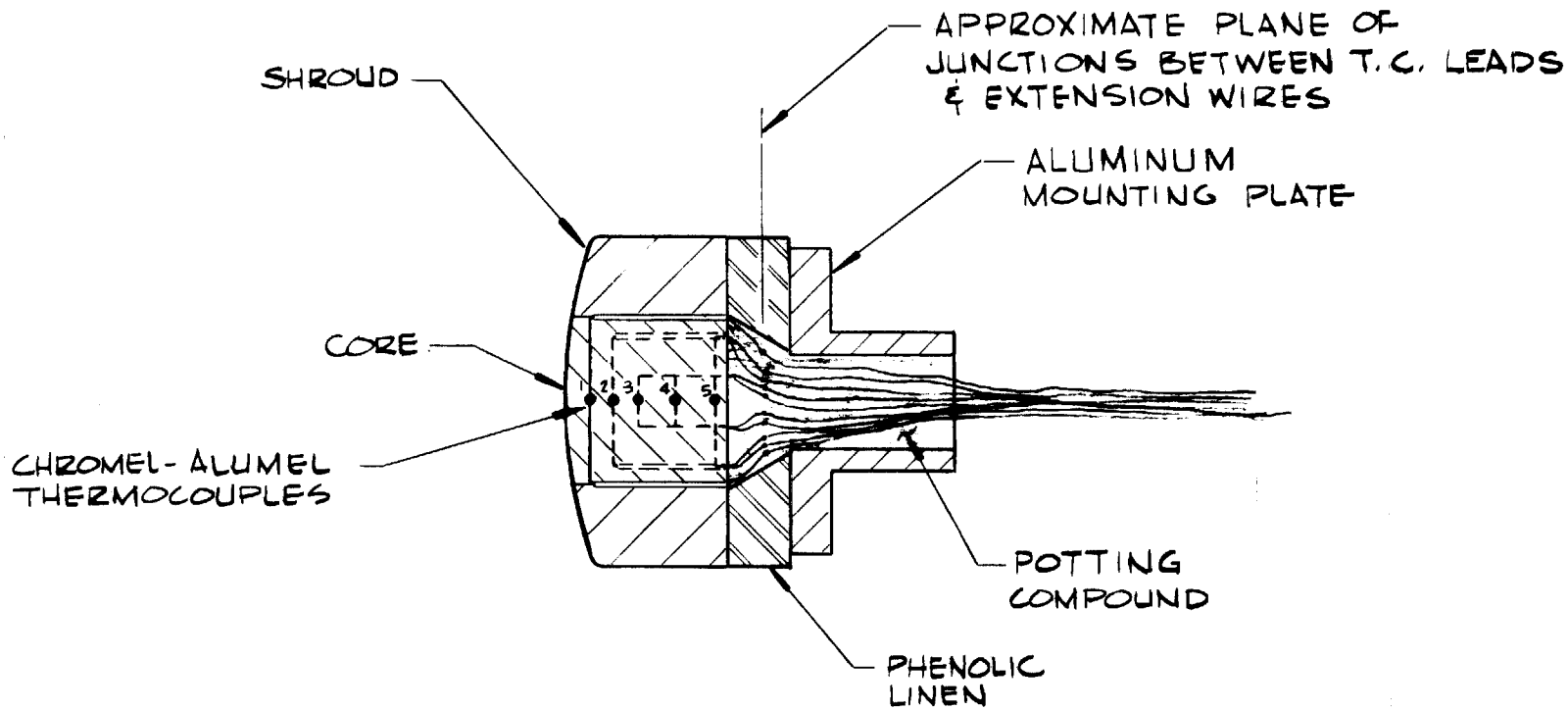

FIGURE 4-3 TYPICAL 2IN BLUNT HEMISPHERE MODEL CONSTRUCTION.

model down the sides of the core and insulated with 0.032-inch diameter ceramic tubing to prevent shorting or "bridging" across the char zone.

The core was assembled into the shroud and this assembly was bonded (General Electric RTV-106) to a phenolic linen base 0.25-inch thick to seal the core-shroud interface. This base was in turn bonded to an aluminum mounting plate for attachment to the horizontal sting in the model support system. Thermocouple extension wires were brought out of the rear of the mounting stud and the hole in the stud was completely potted (General Electric RTV-106). The exact position of the thermocouple junctions were located by X-ray inspection. A typical X-ray photograph is shown in Figure 4-4. The estimated resolution of the location technique is 0.010 inch.

In certain cases the molded version of the Apollo material, 5026-39M, was used as the shroud material whereas the standard honeycomb version, 5026-39 HCG, was used exclusively as the test specimen core. The molded shroud technique was employed for all of the 1.25- and 1.0-inch diameter models to prevent side gas leakage at elevated pressure ($p_s > 0.1$ atm) and to provide greater structural integrity of the smaller size models. In both cases the core was the standard 5026-39 HCG material and was machined from one honeycomb cell of the raw stock (1.25-inch models) or such that one honeycomb cell occupied the central portion of the core (1-inch models).

4.2 DUCT FLOW MODELS

The models for the duct flow or shear testing, Phase II, consisted of flat plates 3.75 inch long, 1.0 inch wide and nominally 5/8 inch thick. The models were also constructed by the core and shroud technique described above with an instrumented core located in the geometric center of the test specimen.

The shear tests were divided into two series, A and B. For Series A, a straight nonconverging duct 0.22 inch high, 1.0 inch wide and 2.75 inch long was used as shown in Figure 4-5. A water cooled transition inlet region converged the flow into the rectangular duct which included a cooled straightening inlet and the ablation model forming one wall, opposed by another cooled wall which housed a Gardon-type calorimeter directly opposing the geometric center of the test specimen and model core. For this series, the models were flat slabs of the ablation material backed with a phenolic plate which was in turn bonded to an aluminum model holder. The core was instrumented with 4 Chromel-Alumel 0.005-inch diameter thermocouples which were installed and X-ray located in a manner similar to that described in Section 4.1. The test specimens were constructed from stock supplied by NASA-MSC which included Avcoat 5026-39 HCG, 5026-22, and P2019 materials.

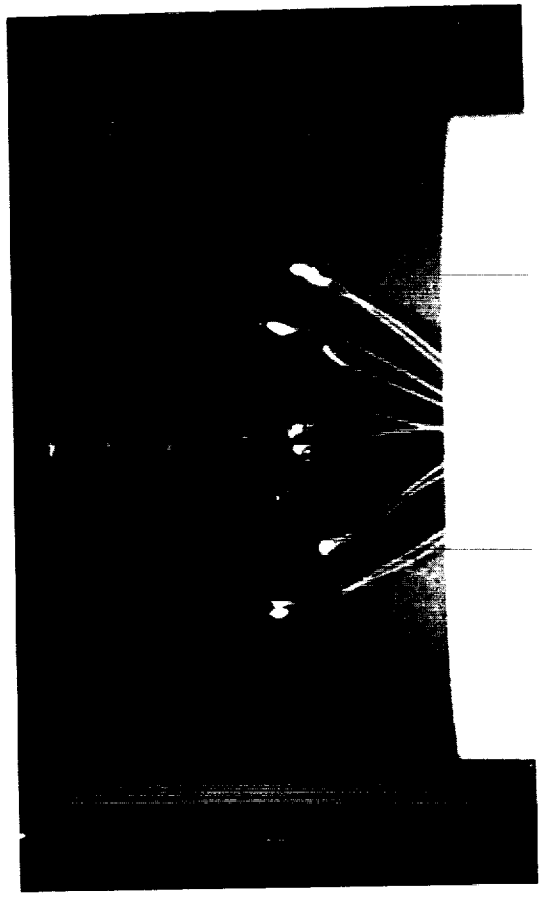

Figure 4-4. Typical X-Ray Photograph of 2 Inch Blunt Hemisphere.

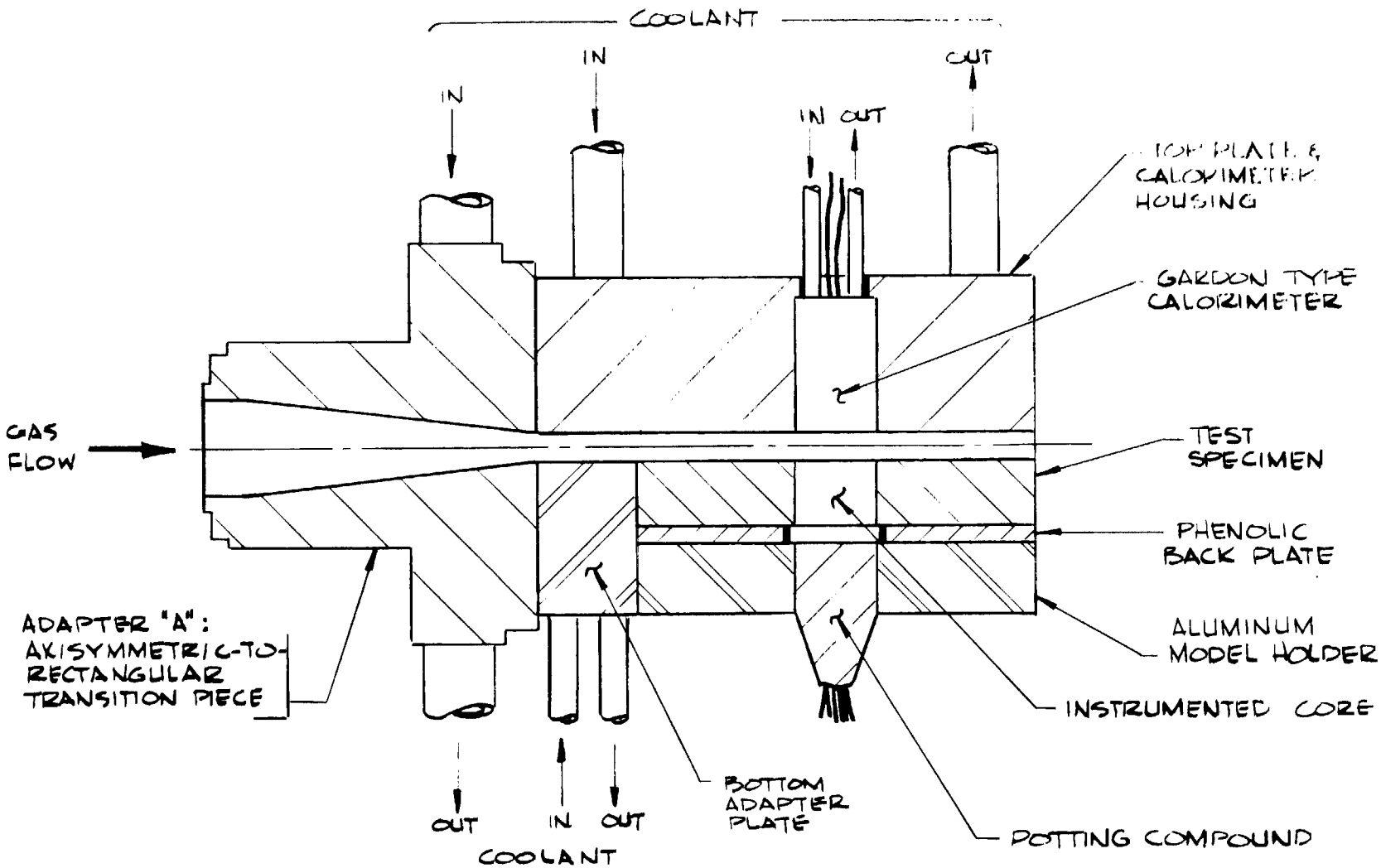

FIGURE 4-5 SCHEMATIC VIEW OF CHANNEL FLOW APPARATUS, SERIES "A"

ORIGINAL PAGE IS OF POOR QUALITY

The second series of duct flow tests, Series B, were much the same as Series A, however the duct configuration was modified to incorporate a larger transition inlet (0.45 inch high) with the remainder of the convergence to the original duct height (0.22 inch) created by the ablation model. The modified duct configuration is shown in Figure 4-6. The purpose of the change was to avoid local supersonic flow in the duct once the model had receded below the bottom adaptor plate surface upstream of the model (Figure 4-5). Otherwise the model construction and duct wall components were similar to those used in the Series A tests. All models for Series B tests were constructed from the honeycomb Avcoat 5026-39 HCG material.

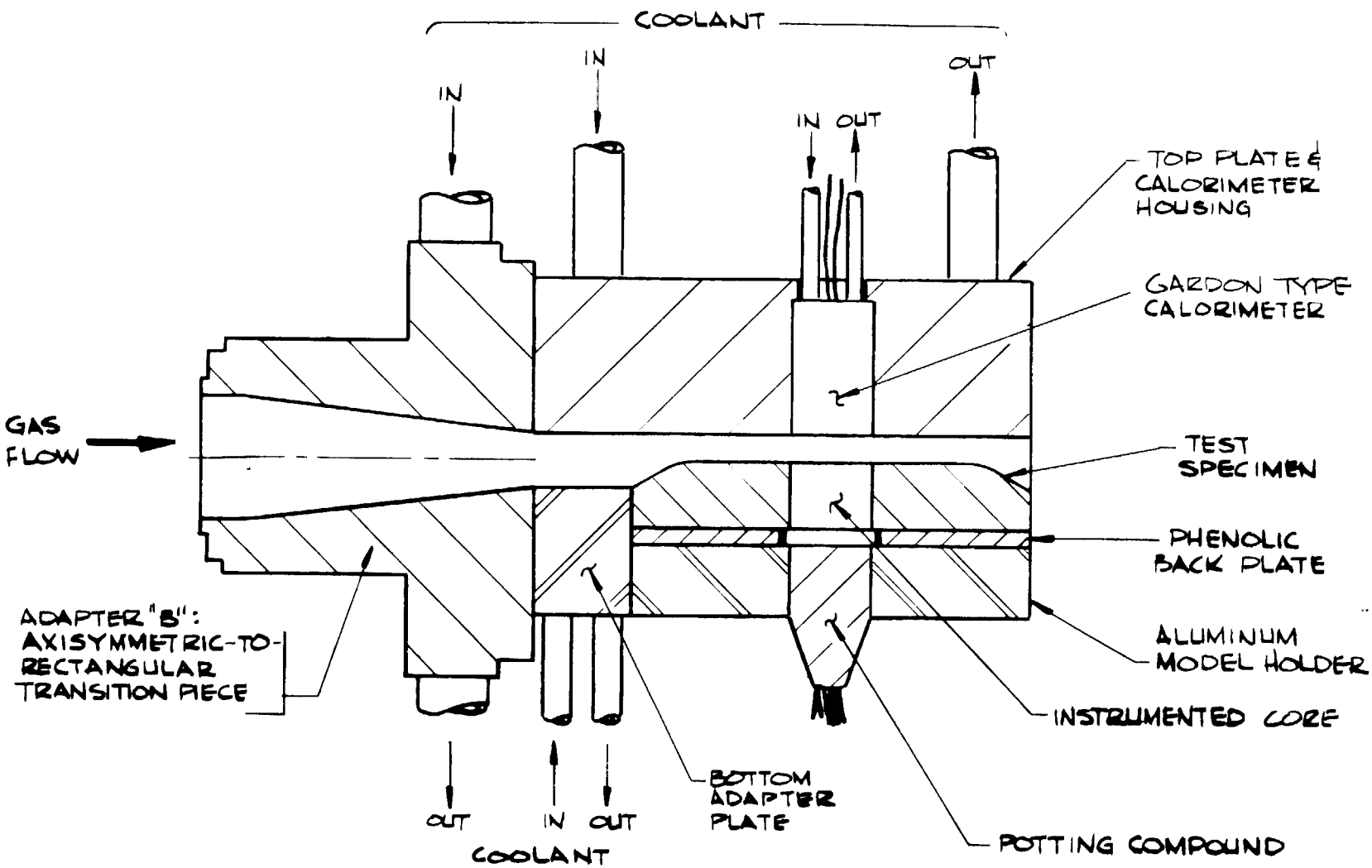

FIGURE 4-6 SCHEMATIC VIEW OF MODIFIED CHANNEL FLOW APPARATUS, SERIES "B"

REFERENCES

4-1 Hankey, W. L. Jr. and Hooks, L. E.: Constant Convective Heating Rate Surfaces for Lifting Reentry Vehicles. AIAA Jour. Vol. 1, No. 7, July 1963.

4-2 Boison, J. C. and Curtis, H. A.: An Experimental Investigation of Blunt Body Stagnation Point Velocity Gradient. ARS Jour. Vol. 29, No. 2, February 1959.

SECTION 5
INSTRUMENTATION AND DATA REDUCTION

The determination of the test environment and measurement of the model response was accomplished by conventional instrumentation procedures. The measured independent variables were pressure, heating rate, enthalpy, and stream composition and contamination. The measured dependent variables included model exposure time, surface and internal temperature histories, surface recession, char thickness, pyrolysis zone thickness, mass loss, and photographic recording of the model surface during the heating cycle. A general list of the instrumentation employed is presented in Appendix A. In this section a description of the specific instrumentation, measurement techniques, and the methods employed to interpret the raw data is presented.

5.1 PRESSURE

Measurements were made of total and static pressures at various locations throughout the system. Specifically for each immersed flow test, measurements were generally made of 1) stagnation point pressure through the use of a 0.375-inch diameter water cooled impact pressure probe, 2) arc heater chamber pressure at a tap in the plenum chamber or, when the arc was used in the supersonic anode mode, at the upstream end of the constrictor column, 3) nozzle exit static pressure at a tap located just upstream of the nozzle exit plane and 4) test cabin-to-nozzle exit differential pressure, which was measured so adjustment could be made to balance the free jet and cabin pressures. The most critical measurement, the stagnation point pressure, was measured with various absolute pressure transducers having a recorded output. Chamber pressure was similarly measured and recorded whereas the nozzle exit static pressure and cabin-to-nozzle differential pressure were measured with bourdon tube gauges. The calibration of the subatmospheric tranducers was compared with a precision McLeod gauge and manometer whereas the superatmospheric gauges were referenced to calibrated standard gauges.

5.2 HEATING RATE

The convective and radiative heating rates were measured with calorimeters which duplicated the basic model shapes and/or sizes. Each immersed flow calorimeter had a sensor at the stagnation point except for one case in which two sensors were also located off the stagnation point. Two calorimeter types were employed, a transient or "slug" type sensor and a steady state Gardon gauge or Asymptotic[1] type sensor. The former were fabricated

[1] Trade name of calorimeter manufactured by Hy-Cal Engineering.

by Aerotherm whereas the Asymptotic sensors were mounted in bodies fabricated by Aerotherm. The calorimeters were identified by a coding procedure similar to that discussed in Section 4 wherein abbreviations were used to identify the shape and body diameter. For the calorimeters, an additional code designating the sensor type was also used to identify either a transient (T) or an Asymptotic (A) (e.g., BH/2.0/T). The surface of the transient calorimeters was polished copper whereas the Asymptotic sensors had a factory applied black coating. A standard copper transient calorimeter with a blackening agent was used in the NASA-Ames Entry Heating Simulator to measure the radient heating rate whereas the same sensor in a polished surface condition was used for the convective measurements.

In addition to the conventional calorimeters, a special calorimeter was employed to measure the arc column radiative heat flux at the model location when using the supersonic anode configuration. The instrument consisted of a transient copper calorimeter mounted at the base of a cylindrical well of polished aluminum. The well was designed to simulate a black body cavity in which all reflected rays would remain in the cavity. A calculation indicated that at least 95 percent of the incident radiation would reach the calorimeter slug. A helium gas purge was introduced into the cavity to prevent convective heating of the sensor. The purge flow was very low and was adjusted to maintain positive cold gas pressure in the cavity without disrupting the shock shape. A standard transient calorimeter of similar nose shape was used to measure the total (convective plus radiative) heating rate for comparative purposes. The transient radiation cavity calorimeter has an outside diameter of 0.75 inch and is shown in Figure 5-1. The designation RAD is used to identify this sensor in all subsequent figures and tables.

A summary of the calorimeters utilized in the test program is shown in Table 5-1. The construction techniques employed in fabricating the transient calorimeters included sapphire ball or pin support of the slug, an 0.005-inch diameter, Chromel-Alumel thermocouple peened into a small hole in the rear face of the slug and copper body shapes similar to the model configuration.

For the transient calorimeters, the heat flux was determined in the conventional manner from the heat capacity equation for the slug:

$$q = \left(\frac{mC_p}{A}\right)_{slug} \frac{\Delta T}{\Delta \theta} \tag{5-1}$$

The slug mass, m, was measured and the wetted surface area, A, calculated thus defining the calorimeter constant (mC_p/A). The heat flux was then calculated from the recorded temperature-time trace which defined $\Delta T/\Delta\theta$.

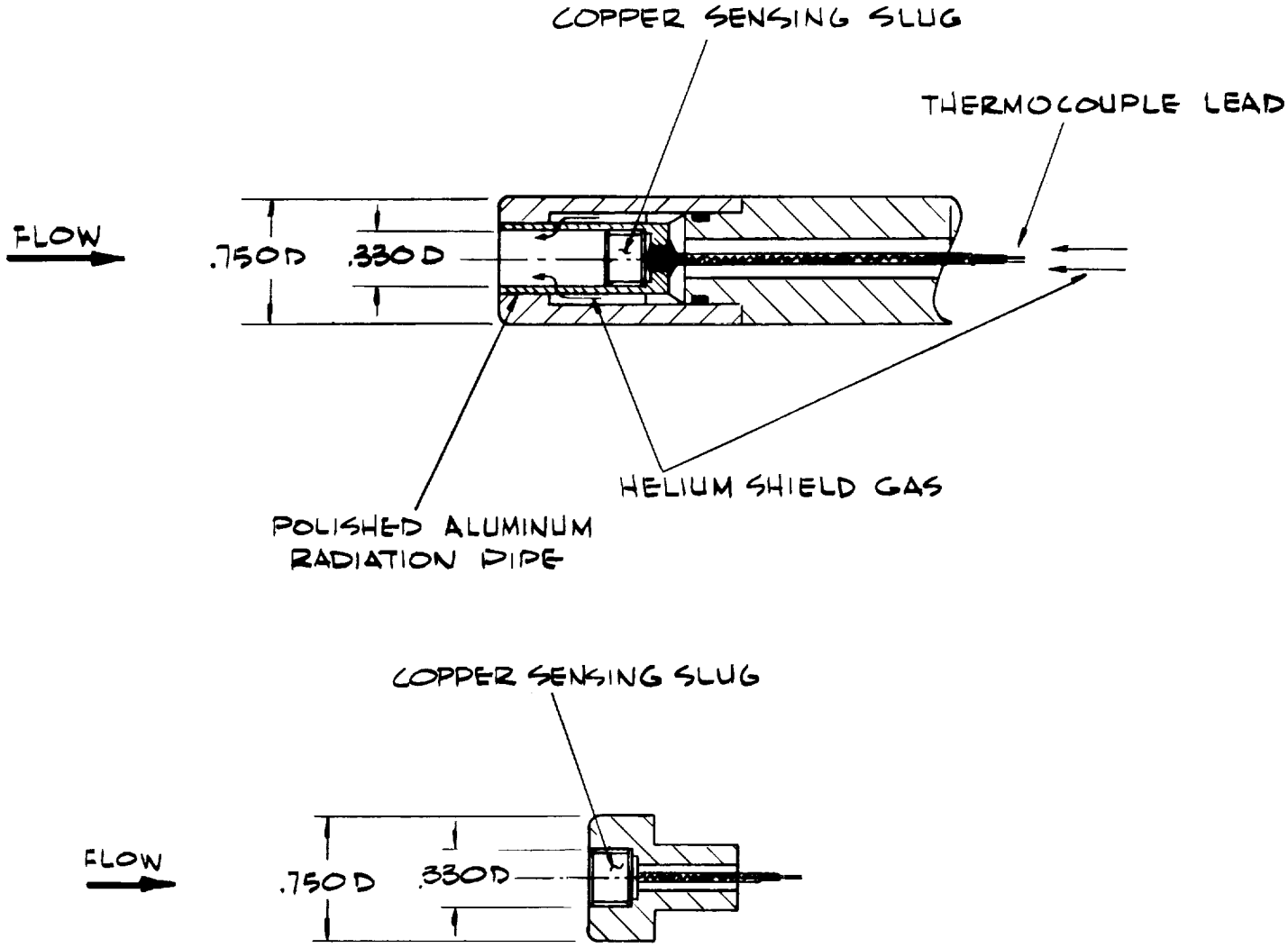

FIGURE 5-1 RADIATION FLUX AND TOTAL FLUX PROBES.

TABLE 5-1

CALORIMETER SUMMARY

Shape	Body Diameter D (in)	Sensor Diameter (in)	Type	Position of Sensor
BH	2.0	(1)	T	(1)
BH	1.0	0.490	T	Stagnation Point
H	2.0	0.225	T	|
FF	1.25	0.625	T	|
FF	|	0.311	T	|
FF	1.0	0.100	A	|
FF	1.50	|	A	|
FF	0.75	0.310	T	|
iso-q	2.0	0.085	A	|
RAD	0.75	0.315	T	|

(1) Three sensors: 0.248, 0.156, 0.156 at stagnation point, 15° and 90° off centerline, respectively.

TABLE 5-2

EFFECTIVE SPHERICAL NOSE RADII

Calorimeter Shape/Body Size/Type	Effective Spherical Nose Radius R (ft)	Nozzle Exit Diameter d_e (in)
BH/2.0/T	0.155	2.5-8.0
H/2.0/T	0.083	|
FF/1.25/T	0.179	|
FF/0.75/T	0.118	|
RAD/0.75/T	|	|
FF/1.0/A	0.158	|
FF/1.5/A	0.238	|
ISO-q/2.0/A	0.164	|
BH/1.0/T	0.076	1.5
FF/1.25/T	0.141	|
FF/0.75/T	0.095	|
BH/1.0/T	0.073	0.6-0.8
FF/0.75/T	0.091	|

For the Asymptotic calorimeters, the heat flux was defined by the recorded calorimeter output and the calorimeter calibration supplied by the manufacturer.

In the immersed flow tests, the calorimeter shapes ranged from flat face cylinders to full hemispheres. Due to the variation of the body shapes and sizes it was found convenient to present the various calorimeter measurements in terms of $q_c\sqrt{R}$. The effective spherical nose radius $\sqrt{R}$ was determined by the calculation of the velocity gradient for each shape at each Mach number using the results of Reference 4-2. A summary of the effective nose radius information for the calorimeters is presented in Table 5-2.

5.3 ENTHALPY

The measurement of enthalpy is the most difficult of all the variables critical to the precise definition of the environment. Conventional practice in the Aerotherm Arc Plasma Facility is to use the energy balance method of calculating the bulk mean enthalpy and to verify this value with calculations of enthalpy based on mass balance considerations (Reference 5-1) and on the measured heat flux and calculated heat transfer coefficient. Whenever possible, all three techniques were used. In the NASA-Ames Entry Heating Simulator tests (Phase II), the mass balance technique only was used. Each technique and its limitations are discussed below.

The energy balance technique is a determination of the net energy in the test stream with no consideration of its radial distribution. This method is practical for the arc configuration which includes a plenum chamber, for which the radial distribution of energy is reasonably uniform. This method is not practical, however, for the very high enthalpy regime of the supersonic anode configuration in which centerline enthalpies up to 3 times greater than the mean are obtained. The energy balance enthalpy is determined from measurements of input power, total energy loss to cooling water including the nozzle, and the gas mass flow rate. With these values the enthalpy is determined from

$$h_{eb} = \frac{Q_{in} - Q_{loss}}{\dot{m}} \qquad (5\text{-}2)$$

The enthalpy calculated by this method was used as the standard in all Aerotherm tests employing the subsonic anode/plenum chamber configuration (enthalpies less than about 14,000 Btu/lb).

The mass balance enthalpy is defined by the relation

$$\frac{\dot{m}}{p_o A_*} = f(h_{mb}) \tag{5-3}$$

where the unique function of enthalpy $f(h_{mb})$ is presented in Reference 5-1. This function is accurately defined for enthalpies below 10,000 Btu/lb and is based on an assumed nozzle discharge coefficient in the range of 0.98. At enthalpies above 10,000 Btu/lb, the technique is less accurate due to the significant real gas and non-uniform flow effects that occur. The enthalpy function was extended to high enthalpy, however, based on Reference 5-1 and on the high enthalpy results of Reference 5-2. The mass balance technique was used in this program as a check on the other calculated enthalpies. As noted from Equation (5-3), the technique requires the measruement of mass flow rate, chamber pressure, and throat area. A second mass balance method which relates the pressure rise from cold flow to hot flow may also be employed. This was not used by Aerotherm but was used as the standard in the NASA-Ames test series (Phase II) together with the other mass balance technique discussed above.

The heat flux potential method of determining enthalpy requires measurement of the heating rate and calculation of the heat transfer coefficient. The enthalpy is given by

$$h_{hf} = \frac{q_c}{\rho_e u_e C_H} + h_w \tag{5-4}$$

where q_c is the convective heat flux measured by a calorimeter, $\rho_e u_e C_H$ is the calorimeter heat transfer coefficient, and h_w is the enthalpy corresponding to the calorimeter surface temperature. The largest question mark in the calculation is the heat transfer coefficient and in this regard some detailed calculations were made to define the heat transfer coefficient for the broad spectrum of conditions under this program. Calculations were made using the Fay and Riddell equation (Reference 5-3) for enthalpies less than 10,000 Btu/lb and the Fay and Kemp relation (Reference 5-4) for higher enthalpies. The necessary boundary layer edge conditions were defined through expansion calculations which included consideration of real gas effects and frozen flow. The expansions were performed for nozzle exit area ratios of 7.5 and 36.7, corresponding to approximate exit Mach numbers of 3 and 4 respectively. The final results for these two area ratios, in terms of $q_c\sqrt{R}$ as a function of model stagnation pressure with enthalpy as a parameter, are presented in Figure 5-2. The effect of area ratio on the results is seen to

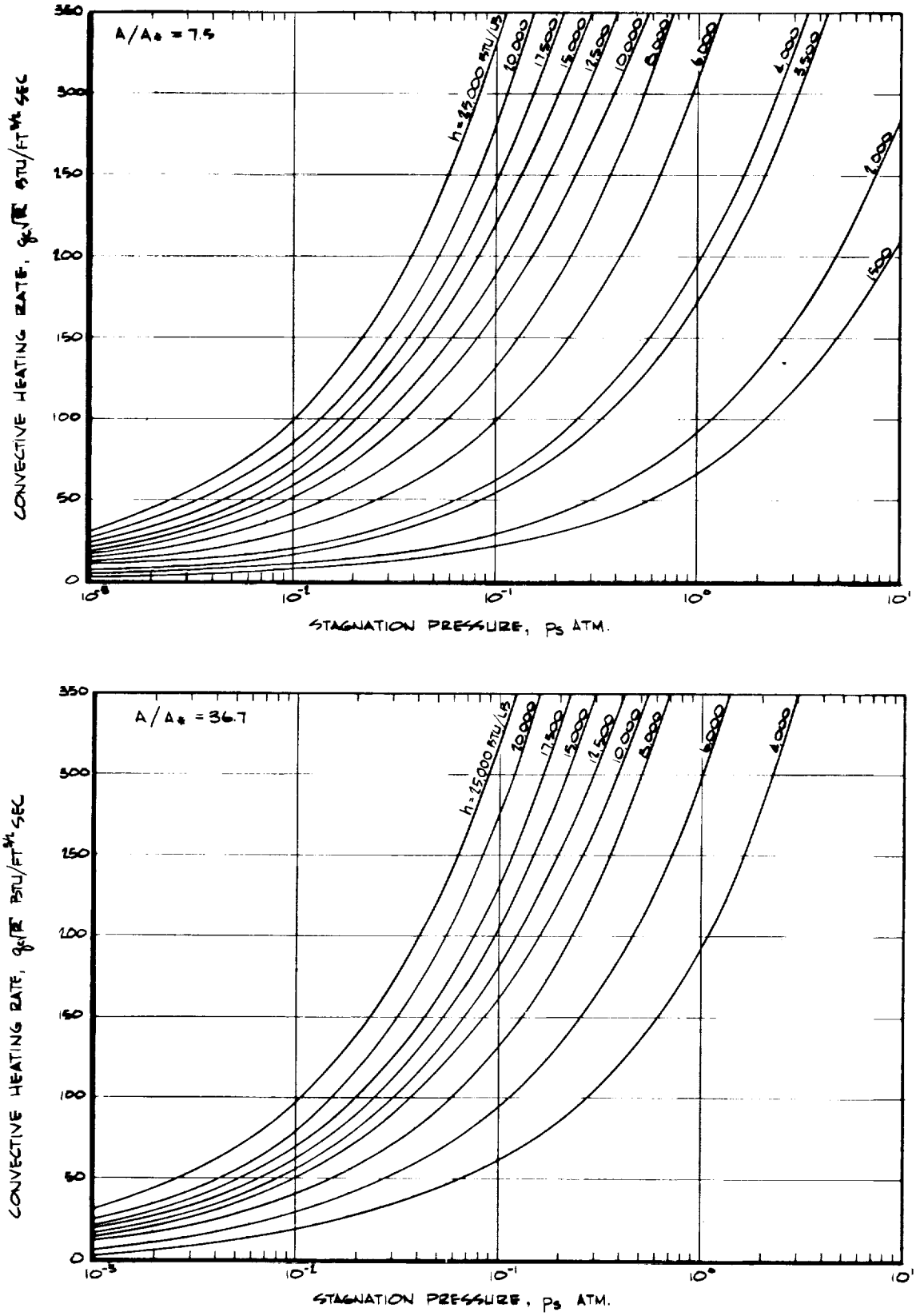

FIGURE 5-2 CALCULATED CONVECTIVE HEATING VARIATION WITH STAGNATION PRESSURE AND ENTHALPY.

be very small. These results were also compared with the simplified correlation equation suggested in Reference 5-5.

$$q_c\sqrt{R} = 0.042\sqrt{p_s}\,(h_{hf} - h_w) \tag{5-5}$$

For the range of enthalpies and stagnation pressures of this program, Equation (5-5) agreed very well with the more detailed results of Figure 5-2 except at high pressure ($p_s \geq 1$ atm) where the discrepancy was found to be significant. The enthalpy calculated by the heat flux potential method was used as the standard for all tests employing the supersonic anode configuration (enthalpies greater than about 15,000 Btu/lb). The simplified relation, Equation (5-5), is valid in this range and was used in this form

$$\rho_e u_e C_H = 0.042\sqrt{\frac{p_s}{R}} \tag{5-6}$$

in conjunction with Equation (5-4) to calculate the enthalpy. The effective nose radii used for the calorimeter shapes were presented previously in Table 5-2. This calculation was performed for all other Aerotherm test conditions as a check on the other enthalpy calculations and as a check on the measured heat fluxes.

The enthalpy distribution across the stream was to have been measured by enthalpy probe as part of the calibration of test conditions. This however was not done since a detailed study indicated that the then state-of-the-art in enthalpy probes for low density flows was not sufficiently advanced to yield reliable data. The enthalpy distribution was therefore calculated from the measured stagnation pressure and heating rate using Equations (5-4) and (5-6). Because of radial nonuniformities in the flow field and in other properties, this is a somewhat inexact approach. The results however are at least qualitative and indicative of the actual enthalpy profile.

5.4 STREAM COMPOSITION AND CONTAMINATION

The measurements made to characterize the test stream composition and contamination included the mass spectrographic analysis of gas samples taken at various radial locations, the assessment of electrode weight loss over a long period of operation and the surface chemical analysis of non-decomposing specimens immersed in the test stream.

The gas composition measurements were made with the impact pressure probe and evacuated sampling flasks. The sampling system was completely purged by

aspirating the collection line to the test chamber static pressure prior to acquiring a stream sample. With the probe positioned in the test stream, an evacuated flask was opened, allowed to fill and equilibrate and then sealed off. The contents of the sample flasks were analyzed for species concentration with a mass spectrometer.

The test stream contamination was qualitatively measured by electrode weight loss and surface chemical analysis of specially prepared models. The electrode weight loss method required measurements of component weight, total electrode exposure time, and cumulative gas mass flow rate, all of which were recorded over a period of many tests. The measurements were limited to the cathode and anode in that they were the only components which displayed any appreciable surface material loss. The model surface chemical analysis test consisted of immersing a nylon sample into the test stream for a brief period of time to attempt to collect any solid or liquid phase contaminants in the stream. The surface of the exposed samples was then semi-quantitatively examined for molecular composition by flame spectrographic techniques.

5.5 MODEL DIMENSIONAL AND WEIGHT CHANGE

Each model core was carefully weighed and measured before and after test to define model weight and dimensional changes. The weight measurements were made with a standard analytical balance having a sensitivity of approximately 50 micrograms. Both the pre- and post-test weights were taken with no thermocouple instrumentation in place. The dimensional measurements to define surface recession were made at the core centerline with either a sensitive dial gauge or a standard micrometer with a sensitivity of 0.0001 inch. The char and pyrolysis zone thickness were measured with a machinist's rule with a sensitivity of 0.010 inch; these measurements were made on the core centerline after sectioning with a diamond saw. In making these measurements, the pyrolysis zone-virgin material interface was defined by an abrupt change in the surface hardness, the pyrolysis zone being relatively "soft". The char-pyrolysis zone interface was defined by a reasonably distinct color change line. The model exposure time was measured by stopwatch and verified by the transient temperature response measurements recorded on the oscillograph.

5.6 TEMPERATURE

Measurements of surface and in-depth temperature were made for each model. The surface temperature measurement was made with an Infrared Industries "Thermodot" TD9-CH pyrometer which is a monochromatic device sensing at 800 millimicrons with a 15 millimicron band width. The output of the pyrometer was recorded on an oscillograph and the data were corrected for a surface

emissivity of 0.75.[2] For the supersonic, immersed flow tests the pyrometer was located outside of the test chamber and viewed the model stagnation point through a quartz window at an angle of incidence between 20 and 50 degrees. For the duct testing the pyrometer was located downstream of the exit plane viewing upstream to the model core at a very shallow angle of incidence.

The same type of pyrometer was used at NASA-Ames for the Phase II Combined Convective and Radiative tests. To eliminate the reflected radiation of the radiant source, a beam chopper was used and data were taken during the period of interruption. Tests were made at high chop rate to verify that the pyrometer time response was sufficient to yield accurate surface temperature measurements during the interrupted period. In the tests, the TD9 pyrometer was used in the standard operating mode and also in a fast response mode. The fast response mode essentially by-passed the complicated output circuit and indicated the TD9 radiometer output directly. The actual circuit was defined and the necessary modifications were made by NASA-Ames. The results of these tests confirmed that accurate data were obtained.

The infrared pyrometer viewing spot size for all cases was approximately 0.08-inch diameter with the pryometer focused in the model core at the stagnation point. The pryometer was periodically calibrated against a black body source at Infrared Industries (the manufacturer) and against a tungsten filament at Aerotherm yielding an overall accuracy of 2 percent of full scale for the three temperature ranges (1,500°C, 2,340°C and 4,600°C full scale).

A total radiation pyrometer was also employed for surface temperature measurement. The instrument used was a Minneapolis Honeywell "Radiomatic" pyrometer which has a thermopile sensor. The device required an 0.5-inch diameter target and hence was used only when the viewing port alignment permitted a very high angle of incidence with the model surface. The pryometer output was recorded and corrected for an emissivity of 0.75 as described above. The instrument was calibrated by the manufacturer and no facilities existed at Aerotherm to check the instrument because of the large target size required. Based on the manufacturer's information and the installation at Aerotherm, it was assumed that the recorded values of temperature were accurate to 3 percent.

The in-depth temperatures were measured with 0.005-inch diameter Chromel-Alumel thermocouples as described in Section 4. Each thermocouple had an ambient temperature reference junction and the outputs were recorded on an oscillograph. Each thermocouple recording circuit was calibrated prior to testing by imposing an EMF on the circuit which was measured with a self-balancing potentiometer and calculating the circuit sensitivity in millivolts. The recorded EMF output was then converted to temperature in the general Arc Facility Data Reduction Computer Program by means of a polynominal curve

[2] The value of emissivity used was based on information supplied by NASA-MSC.

fit equation based on the NBS data presented in Reference 5-6. This computer program also includes a machine plot output of temperature as a function of time.

5.7 PHOTOGRAPHY

Photographic coverage of each ablation model test included black and white still photographs of the models before and after test and color motion picture coverage of all immersed flow models. Motion picture coverage was not included for the duct flow tests since the heated surface could not be seen in any detail. A Photo-Sonics 1B 16 mm motor driven camera, Kodachrome II Type A film, and various neutral density filters were used for all motion pictures. The black and white still photographs were taken with a 35 mm camera and pan film.

REFERENCES

5-1 Winovich, Warren: On the Equilibrium Sonic-Flow Method for Evaluating Electric-Arc Air-Heater Performance. NASA TN D-2132, March 1964.

5-2 Shepard, Charles E., Watson, Velvin R., Stine, Howard A.: Evaluation of a Constricted-Arc Supersonic Jet. NASA TN D-2066, January 1964

5-3 Fay, J. A. and Riddell, F. R.: Theory of Stagnation Point Heat Transfer in Dissociated Air. Jour. of the Aeronautical Sciences, Vol. 25, No. 2, February 1958.

5-4 Fay, J. A. and Kemp, N. H.: Theory of Stagnation Point Heat Transfer in a Partially Ionized Diatomic Gas. IAS Paper No. 63-60, presented at IAS 31th Annual Meeting, January 21-23, 1963.

5-5 Hiester, N. K. and Clark, C. F.: Feasibility of Standard Evaluation Procedures for Ablating Materials, Stanford Research Institute, Menlo Park, Calif., NASA CR-379, February 1966.

5-6 Shenker, H., Lauritzen, Jr., J. I., Corruccini, R. J., and Lonberger, S. T.: Reference Tables for Thermocouples. National Bureau of Standards Circular 561, April 27, 1955.

SECTION 6
PRESENTATION OF TEST RESULTS

The results of the calibration and model tests are presented in this section. A total of 158 ablation models were tested at 75 different calibrated test conditions. The enthalpy, pressure and heating rate spectrum of operation is shown in Figure 6-1. Each test condition was characterized by the measurement of enthalpy, pressure, cold wall heating rate and radial distribution of these parameters where applicable. Furthermore, enthalpy, pressure and heating rate were measured prior to each ablation model test. The response of the model to the environment was characterized by measurements of surface and internal temperature, mass and dimensional change and in certain cases post-test surface and in-depth chemistry, in-depth density, and surface and cross-sectional photomicrographs.

The calibration and ablation model testing was carried out under seven separate program phases each with involved parametric variation of enthalpy, pressure, heating rate, shear stress, shape, and size. A recapitulation of the test program by phases is presented in Table 6-1 with the nominal operating conditions, model shape and size, and applicable test conditions listed for each phase. The test results are presented in detail with calibration data for each test condition in Section 6.1, followed by the results of the model tests presented in Section 6.2. The chemical and physical properties analysis is presented separately in Section 6.3.

6.1 CALIBRATION TESTS

Calibration tests were conducted for each test condition to which an ablation model was exposed. Each test condition was characterized by measurements of enthalpy, pressure, heating rate, chemical environment, arc heater operating conditions and information regarding the test configuration. Additional general calibration data included measurements of heating rate distribution, arc column radiation, and stream composition and contamination.

6.1.1 Calibration of Operating Conditions

The basic calibration data are presented in this section (Figures 6-2 through 6-10) in the form of a data sheet for each test condition. Each data sheet defines the test conditions and presents the information applicable to the particular test objective. The terms used in the figures are reasonably self-explanatory. The basic arc configurations are defined by SUBS denoting the subsonic anode/plenum chamber configuration and SUPS denoting the supersonic anode configuration (Section 3.1). Wherever air is the indicated environment, simulated air was used (a mass fraction of 0.768 for nitrogen and 0.232 for oxygen). For this test program the nitrogen was introduced in the cathode region while the oxygen was injected in the plenum (SUBS configuration)

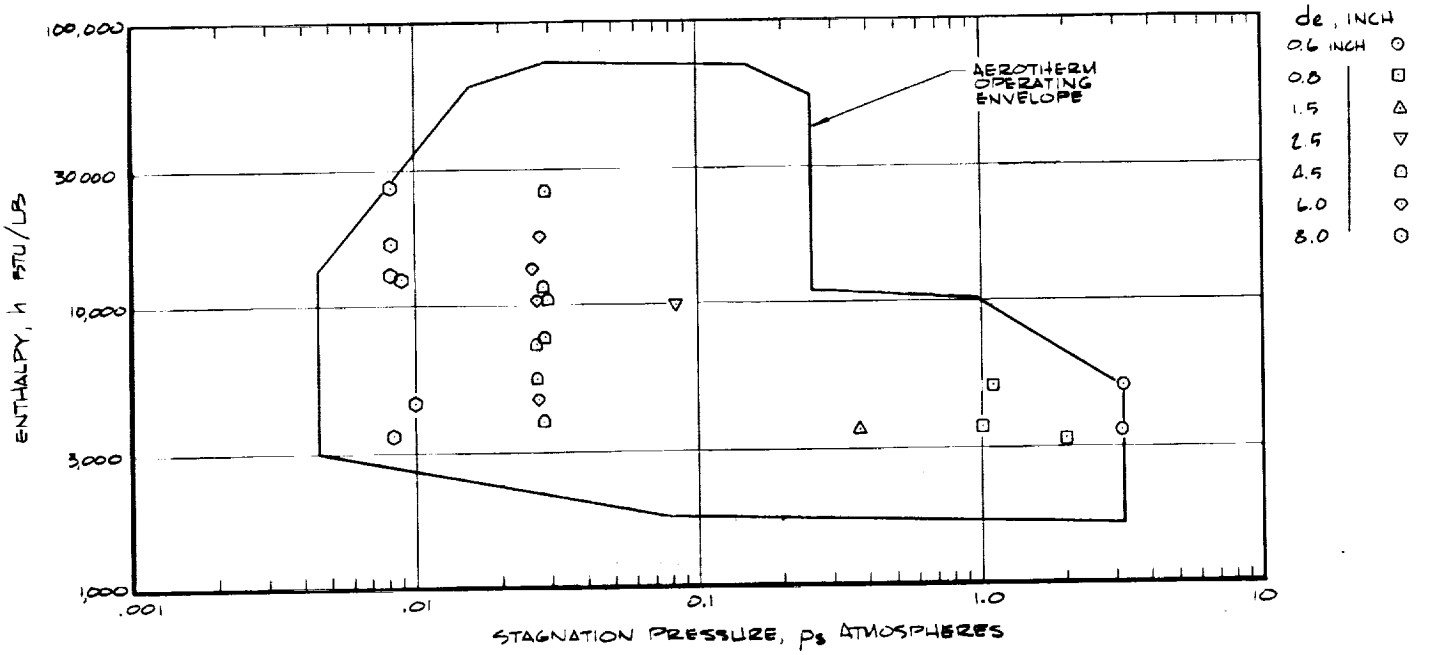

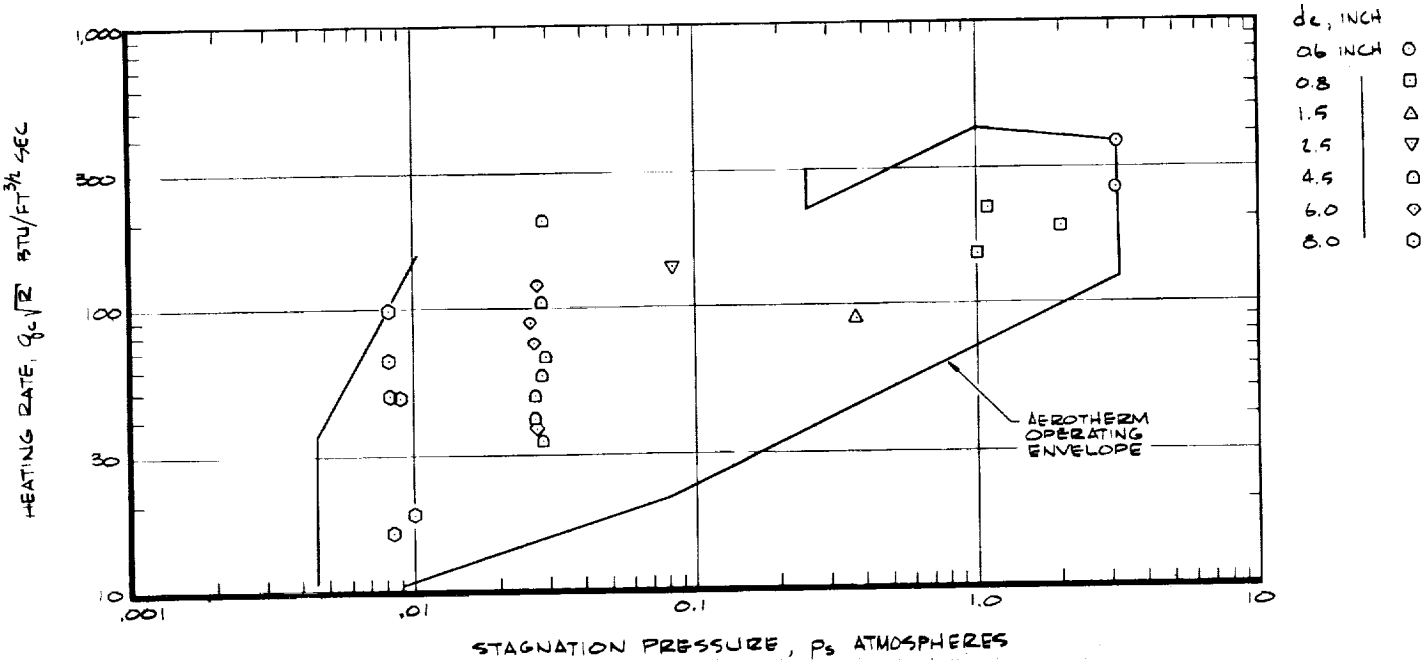

FIGURE 6-1 ENTHALPY, PRESSURE AND HEATING RATE SPECTRUM OF OPERATION.

IMMERSED FLOW SPECTRUM OTHER THAN AIR

Enthalpy h (Btu/lb)	Stagnation Pressure p_s (atm)	Heating rate $q_c\sqrt{R}$ (Btu/ft$^{3/2}$-sec)	Chemical Environment K
5,790	0.0275	44.9	$0.70N_2/0.30O_2$
5,670	0.0282	40.2	$0.85N_2/0.15O_2$
5,560	0.0275	35.8	$0.93N_2/0.07O_2$
5,830	|	70.5	Nitrogen
10,760	0.0288	|	$0.70N_2/0.30O_2$
11,090	0.0275	69.7	$0.85N_2/0.15O_2$
11,270	|	76.4	$0.93N_2/0.07O_2$
10,390	0.0268	127	Nitrogen
10,890	0.0280	69.0	Helium
15,800	0.0262	82.4	$0.70N_2/0.30O_2$
17,100	0.0271	116	$0.85N_2/0.15O_2$
17,400	|	152	$0.93N_2/0.07O_2$
17,600	0.0254	180	Nitrogen
18,260	0.0280	129	Helium
3,550	1.07	210	Nitrogen
4,860	1.13	352	|
3,370	2.02	309	|
3,410	3.19	354	|
4,980	3.15	449	|

DUCT FLOW SPECTRUM

Enthalpy h_{eb} (Btu/lb)	Chamber Pressure p_o (atm)	Heat Flux q (Btu/ft^2-sec)	Shear Stress τ_w (lb/ft^2)	Chemical Environment
3,560	2.04	228	7.95	Nitrogen
3,670	1.90	256	7.16	Air
4,140	1.25	208	2.71	|
8,560	1.20	347	3.25	|
4,040	1.26	194	3.38	Nitrogen
8,700	1.17	353	2.91	|
5,360	1.18	174	2.67	Air
3,730	1.97	305	10.5	|
|	4.99	540	19.1	|
5,120	1.15	173	2.67	Nitrogen
4,000	2.02	300	10.0	|
3,510	5.58	510	18.7	|

Figure 6-1. Concluded.

TABLE 6-1

SUMMARY OF ABLATION TEST PROGRAM

Phase	Enthalpy h (Btu/lb)	Chamber Pressure p_o (atm)	Heating Rate q (Btu/ft^{2}sec)	Shear Stress τ_w (psf)	Chemical Environment	Model Shape/Size	Test Condition
I Shear	5000	1.0	175	3	Air	D/.22	50
	3000	2.0	300	10			51
		3.0	525	20			52
	5000	1.0	175	3	Nitrogen		53
	3000	2.0	300	10			54
		3.0	525	20			55
	4000	2.0	250	7	Air		8
					Nitrogen		7
		1.0	190	3	Air		9
					Nitrogen		11
	9000		350		Air		10
					Nitrogen		12

	Enthalpy h_{mb} (Btu/lb)	Stagnation Pressure p_o (atm)	Heating Rate Convective q_c (Btu/ft^{2}sec)	Heating Rate Radiative q_r (Btu/ft^{2}sec)	Chemical Environment	Model Shape/Size	Test Condition
II Combined Convective and Radiative Heating	3000	0.10	94	0	Air	FF/1.25	56
				100			57
				175			58
				375			59
				475			60
	5000	0.08	140	0			61
				100			62
				175			63
				375			64
				475			65
	6250	0.10	195	0			66
				100			67
				175			68
				375			69
				475			70
	—	—	0	0			71
	—	—		100			72
	—	—		175			73
	—	—		375			74
	—	—		475			75

	Enthalpy h (Btu/lb)	Stagnation Pressure p_s (atm)	Heating Rate q_c (Btu/ft^{2}sec)	Chemical Environment	Model Shape/Size	Test Condition
III High Stagnation Pressure	5000	1.0	760	Air	BH/1.0	43
				Nitrogen		42
	3500		533	Air		40
				Nitrogen		41
		2.0	754	Air		44
				Nitrogen		45
	5000	3.0	1325	Air		49
				Nitrogen		48
	3500		925	Air		46
				Nitrogen		47

TABLE 6-1
CONCLUDED

Phase	Enthalpy h (Btu/lb)	Stagnation Pressure p_s (atm)	Heating Rate q_c (Btu/ft^{2}sec)	Chemical Environment	Model Shape/Size	Test Condition
IV A Low Stagnation Pressure and Exposure Time	3500	0.008	33	Air	BH/2.0	26
	5000		47			24
	10000		93			25
	17500		163			37
	25000		233			36
IV B Low Stagnation Pressure and Chemical Environment	5000	0.028	89	Air	BH/2.0	1
			—	0.700 N_2/0.300 O_2		14
			—	0.850 N_2/0.150 O_2		15
			—	0.930 N_2/0.070 O_2		16
			—	Nitrogen		17
	10000		179	Air		2
			—	0.700 N_2/0.300 O_2		18
			—	0.850 N_2/0.150 O_2		19
			—	0.930 N_2/0.070 O_2		20
			—	Nitrogen		21
			—	Helium		22
	17500		313	Air		30
			—	0.700 N_2/0.300 O_2		32
			—	0.850 N_2/0.150 O_2		33
			—	0.930 N_2/0.070 O_2		34
			—	Nitrogen		35
			—	Helium		23
V Model Size and Exposure Time	5000	0.008	33	Air	BH/4.0	24
	14100		93			38
	5000	0.028	63			28
	10000		127			29
	17500		221			30
VI A Model Shape, Constant Enthalpy and Constant Stagnation Pressure	5000	0.028	89	Air	BH/2.0	1
			62		FF/2.0	
			122		H/2.0	
	10000		179		BH/2.0	2
			120		FF/2.0	
			244		H/2.0	
	17500		313		BH/2.0	30
			218		FF/2.0	
			426		H/2.0	
VI B Model Shape, Constant Stagnation Pressure and Constant Stagnation Heating Rate	5000	0.028	89	Air	BH/2.0	1
	7180				FF/2.0	4
	3680				H/2.0	6
	10000		179		BH/2.0	2
	14400				FF/2.0	31
	7400				H/2.0	3
	17500		313		BH/2.0	30
	24400				FF/2.0	27
	12500				H/2.0	5
VII Enthalpy and Stagnation Pressure at Constant Heating Rate	25000	0.028	444	Air	BH/2.0	27
	10000	0.088			BH/1.0	13
			427		H/2.0	
	3500	0.400	444		BH/1.0	39

Enthalpy:

h_{eb}	=	3563	Btu/lb
h_{mb}	=	*	Btu/lb
h_{hf}	=	*	Btu/lb

Shear Stress:

τ_w	=	7.95	lb/ft^2

Duct Wall Heating Rate:

Cal No. 1	=	Duct/A	
q_c	=	228	$Btu/ft^2 sec$
$q_c \sqrt{R}$	=	*	$Btu/ft^{3/2} sec$
Cal No. 2	=	*	
q_c	=	*	$Btu/ft^2 sec$
$q_c \sqrt{R}$	=	*	$Btu/ft^{3/2} sec$

Environment:

K_1	=	1.00	N_2
K_2	=	0	O_2

Arc Conditions:

p_o	=	2.04	atm
$\dot{m}$	=	0.0306	lb/sec
p_e	=	*	mm Hg
a	=	0.220	inch
A/A_*	=	1.0	
Config.	=	SUBS	

Conditions for Duct Flow Tests.

(a) **TEST CONDITION** 7

Figure 6-2. Calibration Data, Phase I.

Enthalpy:

h_{eb}	=	3674	Btu/lb
h_{mb}	=	*	Btu/lb
h_{hf}	=	*	Btu/lb

Shear Stress:

τ_w	=	7.16	lb/ft^2

Duct Wall Heating Rate:

Cal No. 1	=	Duct/A	
q_c	=	256	$Btu/ft^2 sec$
$q_c \sqrt{R}$	=	*	$Btu/ft^{3/2} sec$
Cal No. 2	=	*	
q_c	=	*	$Btu/ft^2 sec$
$q_c \sqrt{R}$	=	*	$Btu/ft^{3/2} sec$

Environment:

K_1	=	0.768	N_2 } Air
K_2	=	0.232	O_2 } Air

Arc Conditions:

p_o	=	1.90	atm
$\dot{m}$	=	0.0304	lb/sec
p_e	=	*	mm Hg
a	=	0.220	inch
A/A_*	=	1.0	
Config.	=	SUBS	

Conditions for Duct Flow Tests.

*not applicable

(b) **TEST CONDITION** 8

Figure 6-2. Continued.

Enthalpy:

h_{eb}	=	4141	Btu/lb
h_{mb}	=	*	Btu/lb
h_{hf}	=	*	Btu/lb

Shear Stress:

τ_w	=	2.71	lb/ft^2

Duct Wall Heating Rate:

Cal No. 1	=	Duct/A	
q_c	=	208	$Btu/ft^2 sec$
$q_c\sqrt{R}$	=	*	$Btu/ft^{3/2} sec$
Cal No. 2	=	*	
q_c	=	*	$Btu/ft^2 sec$
$q_c\sqrt{R}$	=	*	$Btu/ft^{3/2} sec$

Environment:

K_1	=	0.768	N_2 } Air
K_2	=	0.232	O_2 } Air

Arc Conditions:

P_o	=	1.25	atm
$\dot{m}$	=	0.0152	lb/sec
P_e	=	*	mm Hg
a	=	0.220	inch
A/A_*	=	1.0	
Config.	=	SUBS	

Conditions for Duct Flow Tests.

(c) **TEST CONDITION** 9
Figure 6-2. Continued.

Enthalpy:

h_{eb}	=	8558	Btu/lb
h_{mb}	=	*	Btu/lb
h_{hf}	=	*	Btu/lb

Shear Stress

τ_w	=	3.25	lb/ft^2

Duct Wall Heating Rate:

Cal No. 1	=	Duct/A	
q_c	=	347	$Btu/ft^2 sec$
$q_c\sqrt{R}$	=	*	$Btu/ft^{3/2} sec$
Cal No. 2	=	*	
q_c	=	*	$Btu/ft^2 sec$
$q_c\sqrt{R}$	=	*	$Btu/ft^{3/2} sec$

Environment:

K_1	=	0.768	N_2 } Air
K_2	=	0.232	O_2 } Air

Arc Conditions:

P_o	=	1.20	atm
$\dot{m}$	=	0.0101	lb/sec
P_e	=	*	mm Hg
a	=	0.220	inch
A/A_*	=	1.0	
Config.	=	SUBS	

Conditions for Duct Flow Tests.

*not applicable

(d) **TEST CONDITION** 10
Figure 6-2. Continued.

Enthalpy:

h_{eb}	=	4045	Btu/lb
h_{mb}	=	*	Btu/lb
h_{hf}	=	*	Btu/lb

Shear Stress:

τ_w	=	3.38	lb/ft^2

Duct Wall Heating Rate:

Cal No. 1	=	Duct/A	
q_c	=	194	$Btu/ft^2 sec$
$q_c\sqrt{R}$	=	*	$Btu/ft^{3/2} sec$
Cal No. 2	=	*	
q_c	=	*	$Btu/ft^2 sec$
$q_c\sqrt{R}$	=	*	$Btu/ft^{3/2} sec$

Environment:

K_1	=	1.00	N_2
K_2	=	0	O_2

Arc Conditions:

p_o	=	1.26	atm
$\dot{m}$	=	0.0152	lb/sec
p_e	=	*	mm Hg
a	=	0.220	inch
A/A_*	=	1.0	
Config.	=	SUBS	

Conditions for Duct Flow Tests.

(e) TEST CONDITION 11
Figure 6-2. Continued.

Enthalpy:

h_{eb}	=	8703	Btu/lb
h_{mb}	=	*	Btu/lb
h_{hf}	=	*	Btu/lb

Shear Stress:

τ_w	=	2.91	lb/ft^2

Duct Wall Heating Rate:

Cal No. 1	=	Duct/A	
q_c	=	353	$Btu/ft^2 sec$
$q_c\sqrt{R}$	=	*	$Btu/ft^{3/2} sec$
Cal No. 2	=	*	
q_c	=	*	$Btu/ft^2 sec$
$q_c\sqrt{R}$	=	*	$Btu/ft^{3/2} sec$

Environment:

K_1	=	1.00	N_2
K_2	=	0	O_2

Arc Conditions:

p_o	=	1.17	atm
$\dot{m}$	=	0.0101	lb/sec
p_e	=	*	mm Hg
a	=	0.220	inch
A/A_*	=	1.0	
Config.	=	SUBS	

Conditions for Duct Flow Tests.

*not applicable

(f) TEST CONDITION 12
Figure 6-2. Continued.

Enthalpy:

h_{eb}	=	5380	Btu/lb
h_{mb}	=	*	Btu/lb
h_{hf}	=	*	Btu/lb

Shear Stress:

τ_w	=	2.67	lb/ft^2

Duct Wall Heating Rate:

Cal No. 1	=	Duct/A	
q_c	=	174	$Btu/ft^2 sec$
$q_c\sqrt{R}$	=	*	$Btu/ft^{5/2} sec$
Cal No. 2	=	*	
q_c	=	*	$Btu/ft^2 sec$
$q_c\sqrt{R}$	=	*	$Btu/ft^{5/2} sec$

Environment:

K_1	=	0.768	N_2 } Air
K_2	=	0.232	O_2 } Air

Arc Conditions:

p_o	=	1.18	atm
$\dot{m}$	=	0.0130	lb/sec
p_e	=	*	mm Hg
a	=	0.220	inch
A/A_*	=	1.0	
Config.	=	SUBS	

Conditions For Duct Flow Tests.

(g) **TEST CONDITION** 50
Figure 6-2. Continued.

Enthalpy:

h_{eb}	=	3730	Btu/lb
h_{mb}	=	*	Btu/lb
h_{hf}	=	*	Btu/lb

Shear Stress:

τ_w	=	10.50	lb/ft^2

Duct Wall Heating Rate:

Cal No. 1	=	Duct/A	
q_c	=	305	$Btu/ft^2 sec$
$q_c\sqrt{R}$	=	*	$Btu/ft^{5/2} sec$
Cal No. 2	=	*	
q_c	=	*	$Btu/ft^2 sec$
$q_c\sqrt{R}$	=	*	$Btu/ft^{5/2} sec$

Environment:

K_1	=	0.768	N_2 } Air
K_2	=	0.232	O_2 } Air

Arc Conditions:

p_o	=	1.97	atm
$\dot{m}$	=	0.0300	lb/sec
p_e	=	*	mm Hg
a	=	0.220	inch
A/A_*	=	1.0	
Config.	=	SUBS	

Conditions for Duct Flow Tests.

*not applicable

(h) **TEST CONDITION** 51
Figure 6-2. Continued.

Enthalpy:

h_{eb}	=	3730	Btu/lb
h_{mb}	=	*	Btu/lb
h_{hf}	=	*	Btu/lb

Shear Stress:

τ_w	=	19.10	lb/ft^2

Duct Wall Heating Rate:

Cal No. 1	=	Duct/A	
q_c	=	540	Btu/ft^2sec
$q_c\sqrt{R}$	=	*	$Btu/ft^{3/2}sec$
Cal No. 2	=	*	
q_c	=	*	Btu/ft^2sec
$q_c\sqrt{R}$	=	*	$Btu/ft^{3/2}sec$

Environment:

K_1	=	0.768	N_2 } Air
K_2	=	0.232	O_2 } Air

Arc Conditions:

p_o	=	4.99	atm
$\dot{m}$	=	0.075	lb/sec
p_e	=	*	mm Hg
a	=	0.220	inch
A/A_*	=	1.0	
Config.	=	SUBS	

Conditions for Duct Flow Tests.

(i) **TEST CONDITION** 52
Figure 6-2. Continued.

Enthalpy:

h_{eb}	=	5116	Btu/lb
h_{mb}	=	*	Btu/lb
h_{hf}	=	*	Btu/lb

Shear Stress:

τ_w	=	2.67	lb/ft^2

Duct Wall Heating Rate:

Cal No. 1	=	Duct/A	
q_c	=	173	Btu/ft^2sec
$q_c\sqrt{R}$	=	*	$Btu/ft^{3/2}sec$
Cal No. 2	=	*	
q_c	=	*	Btu/ft^2sec
$q_c\sqrt{R}$	=	*	$Btu/ft^{3/2}sec$

Environment:

K_1	=	1.00	N_2
K_2	=	0	O_2

Arc Conditions:

p_o	=	1.15	atm
$\dot{m}$	=	0.0132	lb/sec
p_e	=	*	mm Hg
a	=	0.220	inch
A/A_*	=	1.0	
Config.	=	SUBS	

Conditions for Duct Flow Tests.

*not applicable

(j) **TEST CONDITION** 53
Figure 6-2. Continued.

Enthalpy:

h_{eb}	=	4000	Btu/lb
h_{mb}	=	*	Btu/lb
h_{hf}	=	*	Btu/lb

Shear Stress:

τ_w	=	10.00	lb/ft^2

Duct Wall Heating Rate:

Cal No. 1	=	Duct/A	
q_c	=	300	$Btu/ft^2 sec$
$q_c\sqrt{R}$	=	*	$Btu/ft^{3/2} sec$
Cal No. 2	=	*	
q_c	=	*	$Btu/ft^2 sec$
$q_c\sqrt{R}$	=	*	$Btu/ft^{3/2} sec$

Environment:

K_1	=	1.00	N_2
K_2	=	0	O_2

Arc Conditions:

p_o	=	2.02	atm
$\dot{m}$	=	0.0300	lb/sec
p_e	=	*	mm Hg
	=	0.220	inch
A/A_*	=	1.0	
Config.	=	SUBS	

Conditions for Duct Flow Tests.

(k) **TEST CONDITION** 54
Figure 6-2. Continued.

Enthalpy:

h_{eb}	=	3510	Btu/lb
h_{mb}	=	*	Btu/lb
h_{hf}	=	*	Btu/lb

Shear Stress:

τ_w	=	18.70	lb/ft^2

Duct Wall Heating Rate:

Cal No. 1	=	Duct/A	
q_c	=	510	$Btu/ft^2 sec$
$q_c\sqrt{R}$	=	*	$Btu/ft^{3/2} sec$
Cal No. 2	=	*	
q_c	=	*	$Btu/ft^2 sec$
$q_c\sqrt{R}$	=	*	$Btu/ft^{3/2} sec$

Environment:

K_1	=	1.00	N_2
K_2	=	0	O_2

Arc Conditions:

p_o	=	5.58	atm
$\dot{m}$	=	0.075	lb/sec
p_e	=	*	mm Hg
	=	0.220	inch
A/A_*	=	1.0	
Config.	=	SUBS	

Conditions for Duct Flow Tests.

*not applicable

(l) **TEST CONDITION** 55
Figure 6-2. Concluded.

Enthalpy:

h_{eb}	=	*	Btu/lb
h_{mb}	=	3020	Btu/lb
h_{hf}	=	*	Btu/lb

Stagnation Pressure:

p_s	=	0.112	atm (1)

Stagnation Heating Rate:

Cal No. 1	=	FF/1.25/T	
q_c	=	152	Btu/ft^{2}sec
$q_c\sqrt{R}$	=	64.3	Btu/ft$^{3/2}$sec
Cal No. 2	=	FF/1.25/T	
q_c	=	163	Btu/ft^{2}sec
$q_c\sqrt{R}$	=	69.0	Btu/ft$^{3/2}$sec

Environment:

Air

Arc Conditions:

p_o	=	0.156	atm
$\dot{m}$	=	0.0198	lb/sec
p_e	=	*	mm Hg
d_e	=	2.674	inch
A/A_*	=	12.8	
Config.	=	Ames EHS	

Conditions at Stream Centerline.

(a) **TEST CONDITIONS** 56-60 (2)

Figure 6-3. Calibration Data, Phase II.

(1) This pressure was measured during a repeat calibration.

Enthalpy:

h_{eb}	=	*	Btu/lb
h_{mb}	=	5020	Btu/lb
h_{hf}	=	*	Btu/lb

Stagnation Pressure:

p_s	=	0.071	atm

Stagnation Heating Rate:

Cal No. 1	=	FF/1.25/T	
q_c	=	102	Btu/ft^{2}sec
$q_c\sqrt{R}$	=	43.1	Btu/ft$^{3/2}$sec
Cal No. 2	=	*	
q_c	=	*	Btu/ft^{2}sec
$q_c\sqrt{R}$	=	*	Btu/ft$^{3/2}$sec

Environment:

Air

Arc Conditions:

p_o	=	0.156	atm
$\dot{m}$	=	0.0210	lb/sec
p_e	=	*	mm Hg
d_e	=	2.674	inch
A/A_*	=	12.8	
Config.	=	Ames EHS	

Conditions at Stream Centerline.

*not applicable

(b) **TEST CONDITIONS** 61-65 (2)

Figure 6-3. Continued.

(2) These test conditions include variation in radiative heat flux for the same arc condition.

Enthalpy:

h_{eb}	=	*	Btu/lb
h_{mb}	=	6290	Btu/lb
h_{hf}	=	*	Btu/lb

Stagnation Pressure:

p_s	=	0.099	atm

Stagnation Heating Rate:

Cal No. 1	=	FF/1.25/T	
q_c	=	214	Btu/ft^2sec
$q_c\sqrt{R}$	=	90.5	$Btu/ft^{3/2}sec$
Cal No. 2	=	*	
q_c	=	*	Btu/ft^2sec
$q_c\sqrt{R}$	=	*	$Btu/ft^{3/2}sec$

Environment:

Air

Arc Conditions:

p_o	=	0.170	atm
$\dot{m}$	=	0.0229	lb/sec
p_e	=	*	mm Hg
d_e	=	2.674	inch
A/A_*	=	12.8	
Config.	=	Ames EHS	

Conditions at Stream Centerline.

*not applicable

(c) **TEST CONDITIONS** 66-70(1)

Figure 6-3. Concluded.

(1) These test conditions include variation in radiative heat flux for the same arc condition.

Enthalpy:

h_{eb}	=	3568	Btu/lb
h_{mb}	=	3400	Btu/lb
h_{hf}	=	*	Btu/lb

Stagnation Pressure:

p_s	=	1.00	atm

Stagnation Heating Rate:

Cal No. 1	=	BH/1.0/T	
q_c	=	777	Btu/ft^{2}sec
$q_c\sqrt{R}$	=	211	Btu/ft$^{3/2}$sec
Cal No. 2	=	FF/1.25/T	
q_c	=	794	Btu/ft^{2}sec
$q_c\sqrt{R}$	=	295	Btu/ft$^{3/2}$sec

Environment:

K_1	=	0.768	N_2 } Air
K_2	=	0.232	O_2 } Air

Arc Conditions:

p_o	=	1.71	atm
$\dot{m}$	=	0.0334	lb/sec
p_e	=	*	mm Hg
d_e	=	0.80	inch
A/A_*	=	2.00	
Config.	=	SUBS	

Conditions at Stream Centerline.

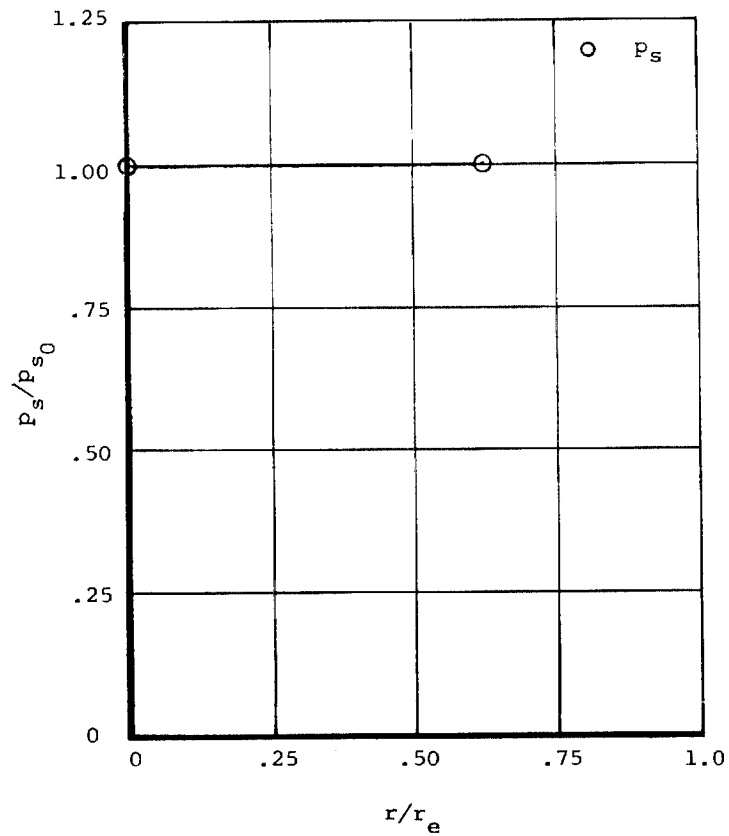

Distribution of Stagnation Pressure.

*not applicable

(a) **TEST CONDITION** 40

Figure 6-4. Calibration Data, Phase III.

Enthalpy:

h_{eb}	=	3547	Btu/lb
h_{mb}	=	*	Btu/lb
h_{hf}	=	*	Btu/lb

Stagnation Pressure:

p_s	=	1.07	atm

Stagnation Heating Rate:

Cal No. 1	=	BH/1.0/T	
q_c	=	774	Btu/ft^{2}sec
$q_c\sqrt{R}$	=	210	Btu/ft$^{3/2}$sec
Cal No. 2	=	FF/1.25/T	
q_c	=	764	Btu/ft^{2}sec
$q_c\sqrt{R}$	=	284	Btu/ft$^{3/2}$sec

Environment:

K_1	=	1.00	N_2
K_2	=	0	O_2

Arc Conditions:

p_o	=	1.78	atm
$\dot{m}$	=	0.0333	lb/sec
p_e	=	*	mm Hg
d_e	=	0.80	inch
A/A_*	=	2.00	
Config.	=	SUBS	

Conditions at Stream Centerline.

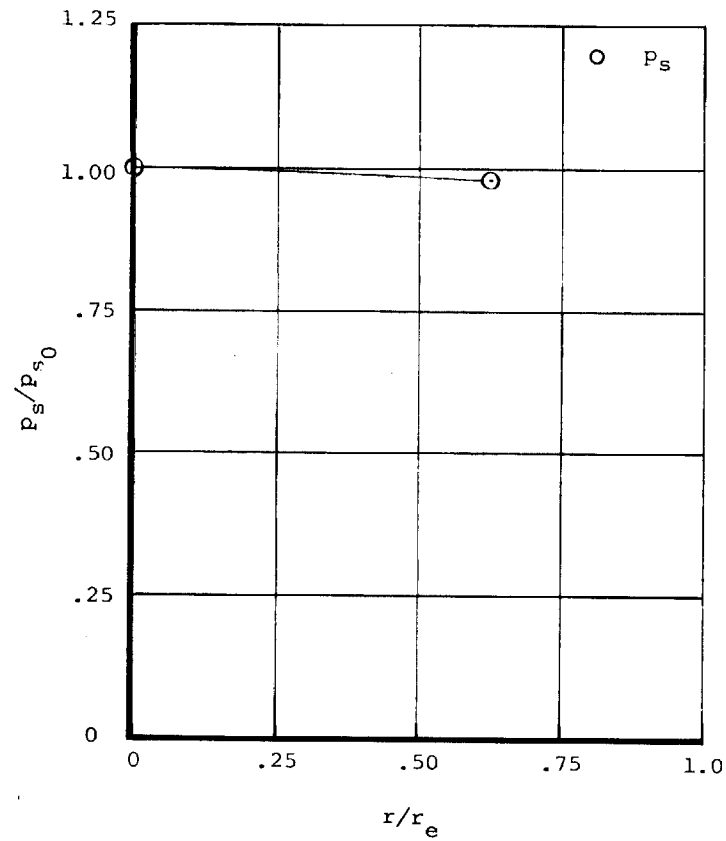

Distribution of Stagnation Pressure.

*not applicable

(b) **TEST CONDITION** 41
Figure 6-4. Continued.

Enthalpy:

h_{eb}	=	4860	Btu/lb
h_{mb}	=	*	Btu/lb
h_{hf}	=	*	Btu/lb

Stagnation Pressure:

p_s	=	1.13	atm

Stagnation Heating Rate:

Cal No. 1	=	BH/1.0/T	
q_c	=	1300	Btu/ft^{2}sec
$q_c\sqrt{R}$	=	352	Btu/ft$^{5/2}$sec
Cal No. 2	=	FF/1.25/T	
q_c	=	1319	Btu/ft^{2}sec
$q_c\sqrt{R}$	=	490	Btu/ft$^{5/2}$sec

Environment:

K_1	=	1.00	N_2
K_2	=	0	O_2

Arc Conditions:

p_o	=	1.82	atm
$\dot{m}$	=	0.0314	lb/sec
p_e	=	*	mm Hg
d_e	=	0.80	inch
A/A_*	=	2.00	
Config.	=	SUBS	

Conditions at Stream Centerline.

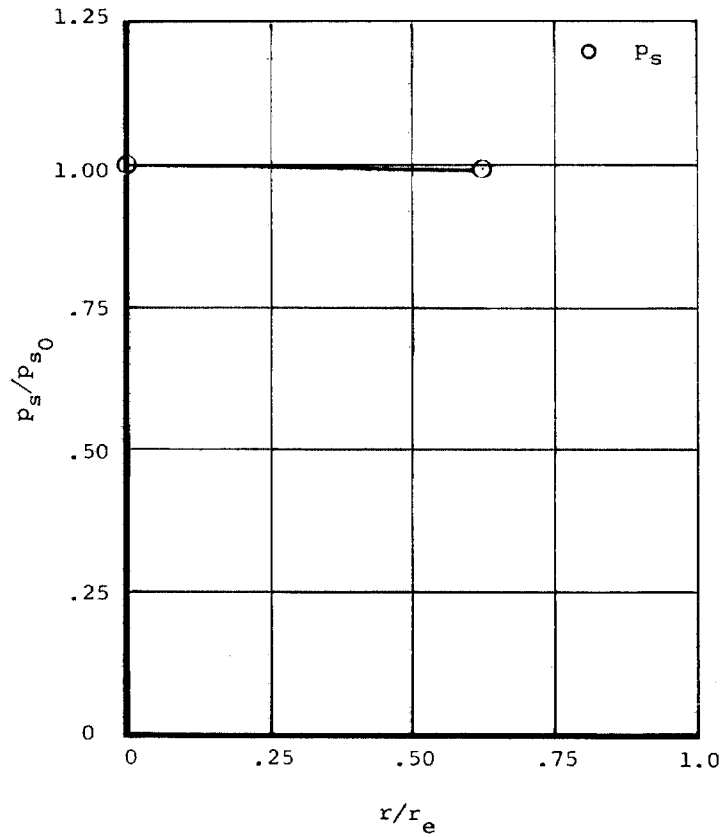

Distribution of Stagnation Pressure.

*not applicable

(c) **TEST CONDITION** 42

Figure 6-4. Continued.

Enthalpy:

h_{eb}	=	4992	Btu/lb
h_{mb}	=	4500	Btu/lb
h_{hf}	=	*	Btu/lb

Stagnation Pressure:

p_s	=	1.10	atm

Stagnation Heating Rate:

Cal No. 1	=	BH/1.0/T	
q_c	=	1268	Btu/ft^{2}sec
$q_c\sqrt{R}$	=	344	Btu/ft$^{5/2}$sec
Cal No. 2	=	FF/1.25/T	
q_c	=	1374	Btu/ft^{2}sec
$q_c\sqrt{R}$	=	511	Btu/ft$^{5/2}$sec

Environment:

K_1	=	0.768	N_2 } Air
K_2	=	0.232	O_2 } Air

Arc Conditions:

p_o	=	1.80	atm
$\dot{m}$	=	0.0313	lb/sec
p_e	=	*	mm Hg
d_e	=	0.80	inch
A/A_*	=	2.00	
Config.	=	SUBS	

Conditions at Stream Centerline.

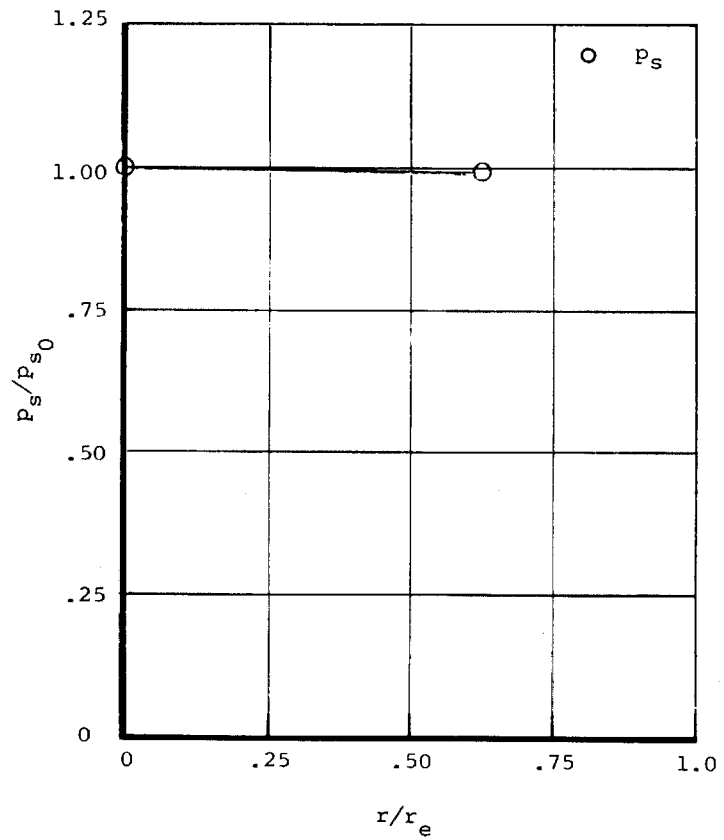

Distribution of Stagnation Pressure.

*not applicable

(d) **TEST CONDITION** 43

Figure 6-4. Continued.

Enthalpy:

h_{eb}	=	3200	Btu/lb
h_{mb}	=	3300	Btu/lb
h_{hf}	=	*	Btu/lb

Stagnation Pressure:

p_s	=	2.00	atm

Stagnation Heating Rate:

Cal No. 1	=	BH/1.0/T	
q_c	=	1226	Btu/ft^{2}sec
$q_c\sqrt{R}$	=	332	Btu/ft$^{5/2}$sec
Cal No. 2	=	FF/1.25/T	
q_c	=	1274	Btu/ft^{2}sec
$q_c\sqrt{R}$	=	475	Btu/ft$^{5/2}$sec

Environment:

K_1	=	0.768	N_2 } Air
K_2	=	0.232	O_2 } Air

Arc Conditions:

p_o	=	3.38	atm
$\dot{m}$	=	0.0666	lb/sec
p_e	=	*	mm Hg
d_e	=	0.80	inch
A/A_*	=	2.00	
Config.	=	SUBS	

Conditions at Stream Centerline.

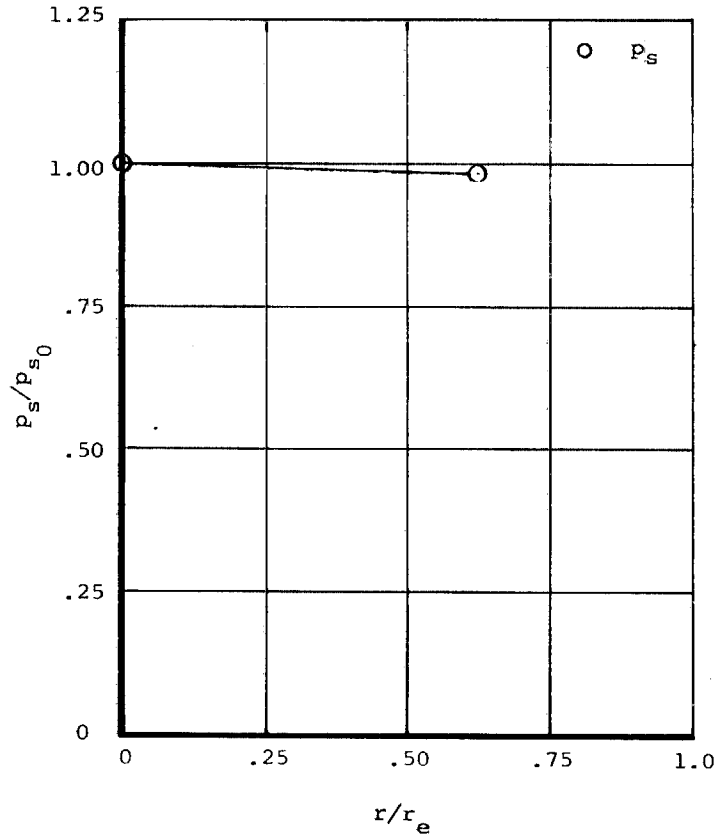

Distribution of Stagnation Pressure.

*not applicable

(e) **TEST CONDITION** 44

Figure 6-4. Continued.

Enthalpy:

h_{eb}	=	3370	Btu/lb
h_{mb}	=	3300	Btu/lb
h_{hf}	=	*	Btu/lb

Stagnation Pressure:

p_s	=	2.02	atm

Stagnation Heating Rate:

Cal No. 1	=	BH/1.0/T	
q_c	=	1138	Btu/ft^2 sec
$q_c\sqrt{R}$	=	309	Btu/ft$^{5/2}$sec
Cal No. 2	=	FF/1.25/T	
q_c	=	1196	Btu/ft^{2}sec
$q_c\sqrt{R}$	=	445	Btu/ft$^{5/2}$sec

Environment:

K_1	=	1.00	N_2
K_2	=	0	O_2

Arc Conditions:

p_o	=	3.42	atm
$\dot{m}$	=	0.0676	lb/sec
p_e	=	*	mm Hg
d_e	=	0.80	inch
A/A_*	=	2.00	
Config.	=	SUBS	

Conditions at Stream Centerline.

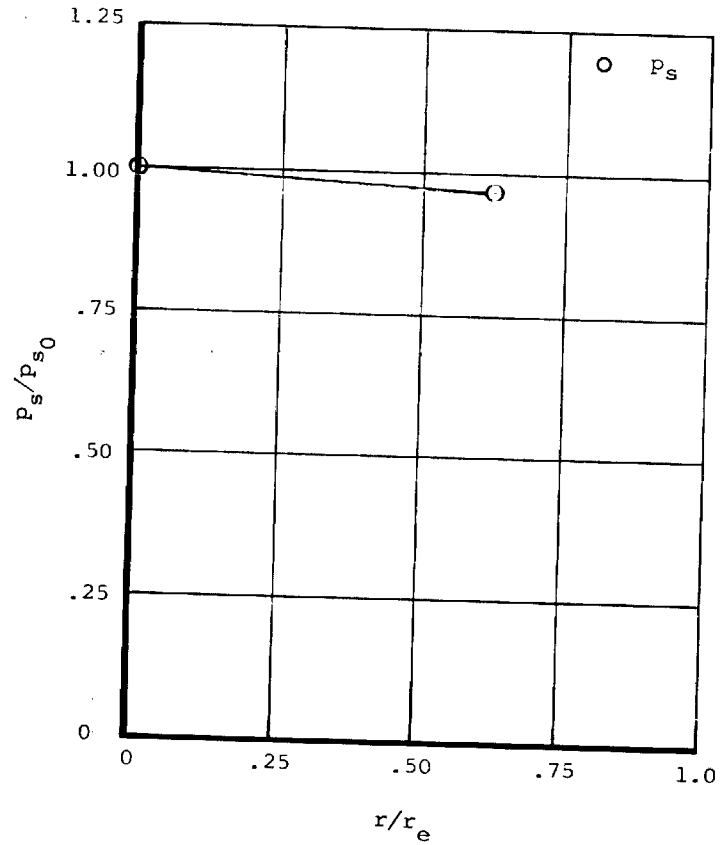

Distribution of Stagnation Pressure.

*not applicable

(f) **TEST CONDITION** 45
Figure 6-4. Continued.

Enthalpy:

h_{eb}	=	3456	Btu/lb
h_{mb}	=	4100	Btu/lb
h_{hf}	=	*	Btu/lb

Stagnation Pressure:

p_s	=	3.11	atm

Stagnation Heating Rate:

Cal No. 1	=	BH/1.0/T	
q_c	=	1329	Btu/ft^{2}sec
$q_c\sqrt{R}$	=	360	Btu/ft$^{3/2}$sec
Cal No. 2	=	FF/1.25/T	
q_c	=	1396	Btu/ft^{2}sec
$q_c\sqrt{R}$	=	524	Btu/ft$^{3/2}$sec

Environment:

K_1	=	0.768	N_2 } Air
K_2	=	0.232	O_2 } Air

Arc Conditions:

p_o	=	5.48	atm
$\dot{m}$	=	0.0556	lb/sec
p_e	=	*	mm Hg
d_e	=	0.60	inch
A/A_*	=	2.00	
Config.	=	SUBS	

Conditions at Stream Centerline.

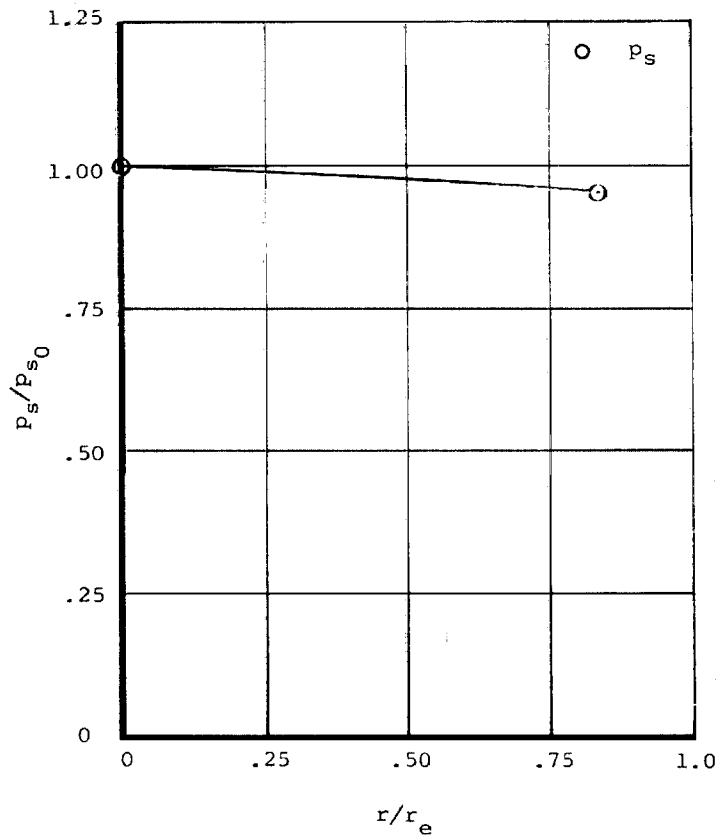

Distribution of Stagnation Pressure.

*not applicable

(g) **TEST CONDITION** 46

Figure 6-4. Continued.

Enthalpy:

h_{eb}	=	3410	Btu/lb
h_{mb}	=	*	Btu/lb
h_{hf}	=	*	Btu/lb

Stagnation Pressure:

p_s	=	3.19	atm

Stagnation Heating Rate:

Cal No. 1	=	BH/1.0/T	
q_c	=	1308	$Btu/ft^2 sec$
$q_c \sqrt{R}$	=	355	$Btu/ft^{3/2} sec$
Cal No. 2	=	FF/1.25/T	
q_c	=	1389	$Btu/ft^2 sec$
$q_c \sqrt{R}$	=	516	$Btu/ft^{3/2} sec$

Environment:

K_1	=	1.00	N_2
K_2	=	0	O_2

Arc Conditions:

p_o	=	5.74	atm
$\dot{m}$	=	0.0557	lb/sec
p_e	=	*	mm Hg
d_e	=	0.60	inch
A/A_*	=	2.00	
Config.	=	SUBS	

Conditions at Stream Centerline.

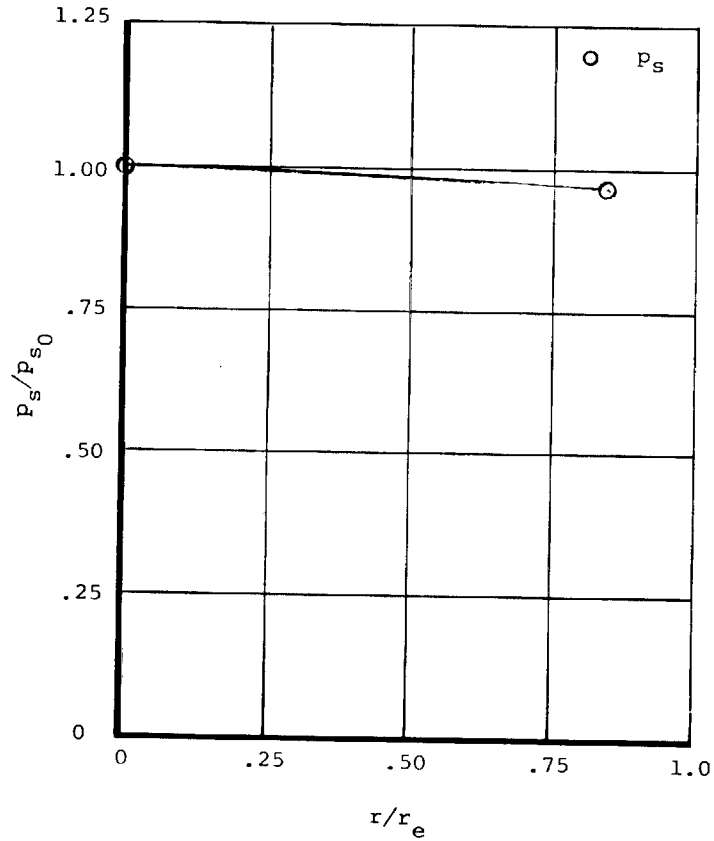

Distribution of Stagnation Pressure.

*not applicable

(h) **TEST CONDITION** 47
Figure 6-4. Continued.

Enthalpy:

h_{eb}	=	4984	Btu/lb
h_{mb}	=	*	Btu/lb
h_{hf}	=	*	Btu/lb

Stagnation Pressure:

p_s	=	3.15	atm

Stagnation Heating Rate:

Cal No. 1	=	BH/1.0/T	
q_c	=	1656	Btu/ft^{2}sec
$q_c\sqrt{R}$	=	449	Btu/ft$^{3/2}$sec
Cal No. 2	=	FF/1.25/T	
q_c	=	1866	Btu/ft^{2}sec
$q_c\sqrt{R}$	=	694	Btu/ft$^{3/2}$sec

Environment:

K_1	=	1.00	N_2
K_2	=	0	O_2

Arc Conditions:

p_o	=	5.60	atm
$\dot{m}$	=	0.0484	lb/sec
p_e	=	*	mm Hg
d_e	=	0.60	inch
A/A_*	=	2.00	
Config.	=	SUBS	

Conditions at Stream Centerline.

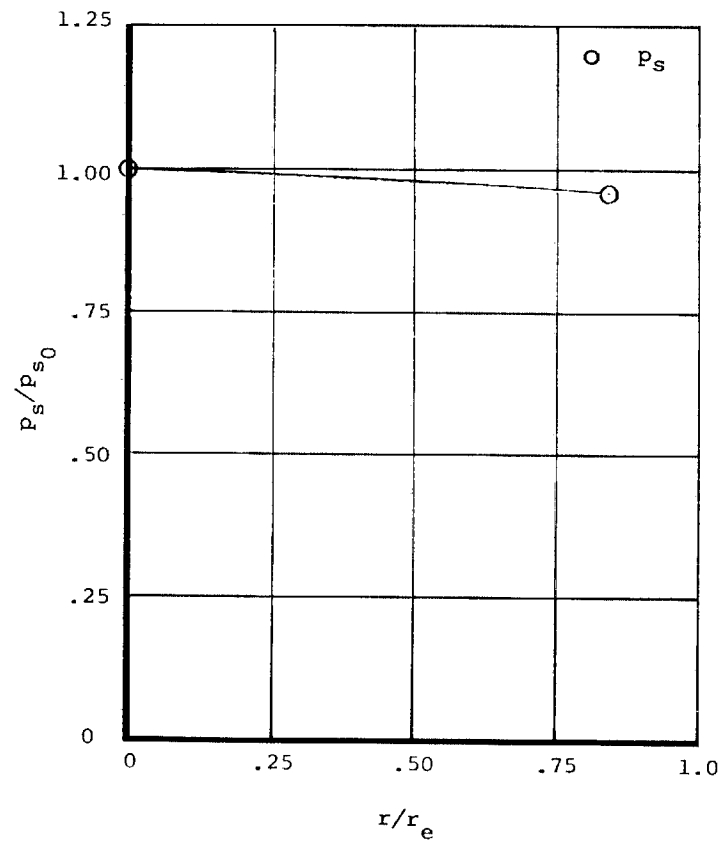

Distribution of Stagnation Pressure.

*not applicable

(i) **TEST CONDITION** 48

Figure 6-4 Continued.

Enthalpy:

h_{eb}	=	4982	Btu/lb
h_{mb}	=	5780	Btu/lb
h_{hf}	=	*	Btu/lb

Stagnation Pressure:

p_s	=	3.15	atm

Stagnation Heating Rate:

Cal No. 1	=	BH/1.0/T	
q_c	=	1739	$Btu/ft^2 sec$
$q_c \sqrt{R}$	=	471	$Btu/ft^{3/2} sec$
Cal No. 2	=	FF/1.25/T	
q_c	=	1933	$Btu/ft^2 sec$
$q_c \sqrt{R}$	=	720	$Btu/ft^{3/2} sec$

Environment:

K_1	=	0.768	N_2 } Air
K_2	=	0.232	O_2 } Air

Arc Conditions:

p_o	=	5.48	atm
$\dot{m}$	=	0.0483	lb/sec
p_e	=	*	mm Hg
d_e	=	0.60	inch
A/A_*	=	2.00	
Config.	=	SUBS	

Conditions at Stream Centerline.

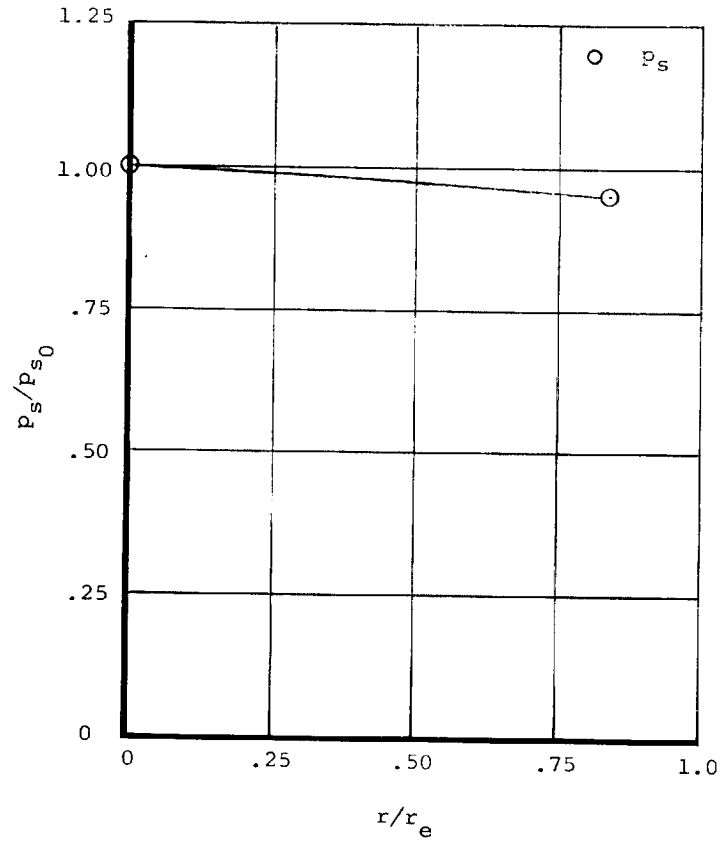

Distribution of Stagnation Pressure.

*not applicable

(j) **TEST CONDITION** 49
Figure 6-4. Concluded.

Enthalpy:

h_{eb}	=	4503	Btu/lb
h_{mb}	=	5400	Btu/lb
h_{hf}	=	4460	Btu/lb

Stagnation Pressure:

p_s	=	0.0098	atm

Stagnation Heating Rate:

Cal No. 1	=	BH/2.0/T	
q_c	=	46.9	Btu/ft^2sec
$q_c\sqrt{R}$	=	18.5	$Btu/ft^{3/2}sec$
Cal No. 2	=	FF/1.25/T	
q_c	=	53.1	Btu/ft^2sec
$q_c\sqrt{R}$	=	22.4	$Btu/ft^{3/2}sec$

Environment:

K_1	=	0.768	N_2 } Air
K_2	=	0.232	O_2 } Air

Arc Conditions:

p_o	=	0.258	atm
$\dot{m}$	=	0.013	lb/sec
p_e	=	0.2	mm Hg
d_e	=	8.00	inch
A/A_*	=	64.0	
Config.	=	SUBS	

Conditions at Stream Centerline.

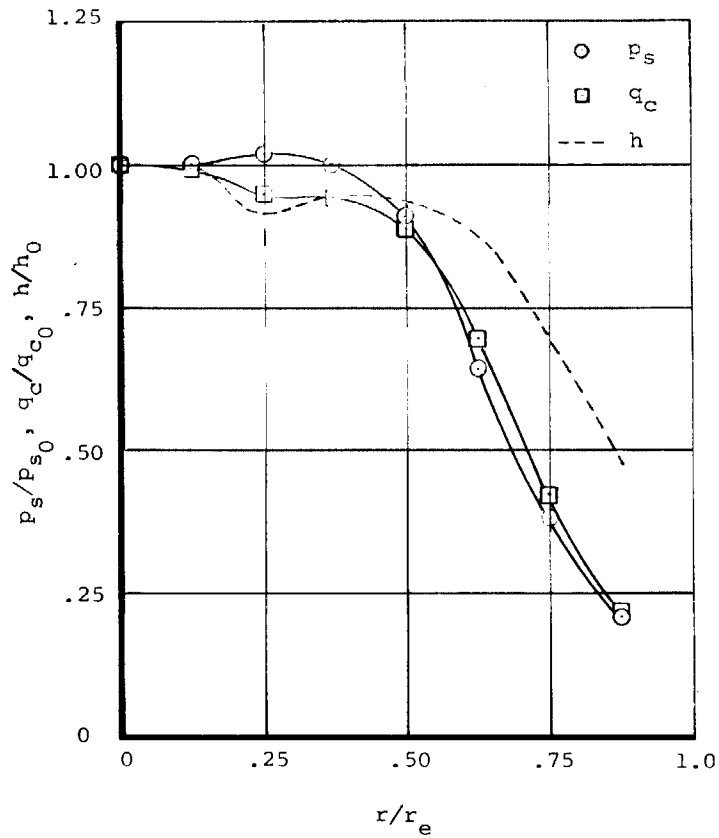

Distributions of Stagnation Pressure, Stagnation Heating Rate, and Stagnation Enthalpy.

(a) **TEST CONDITION** 24

Figure 6-5. Calibration Data, Phase IV A.

Enthalpy:

h_{eb}	=	12360	Btu/lb
h_{mb}	=	15700	Btu/lb
h_{hf}	=	12150	Btu/lb

Stagnation Pressure:

p_s	=	0.0089	atm

Stagnation Heating Rate:

Cal No. 1	=	BH/2.0/T	
q_c	=	122	Btu/ft^{2}sec
$q_c\sqrt{R}$	=	48.0	Btu/ft$^{5/2}$sec
Cal No. 2	=	FF/1.25/T	
q_c	=	115	Btu/ft^{2}sec
$q_c\sqrt{R}$	=	48.8	Btu/ft$^{5/2}$sec

Environment:

K_1	=	0.768	N_2 } Air
K_2	=	0.232	O_2 } Air

Arc Conditions:

p_o	=	0.197	atm
$\dot{m}$	=	0.0064	lb/sec
p_e	=	0.2	mm Hg
d_e	=	8.00	inch
A/A_*	=	64.0	
Config.	=	SUBS	

Conditions at Stream Centerline.

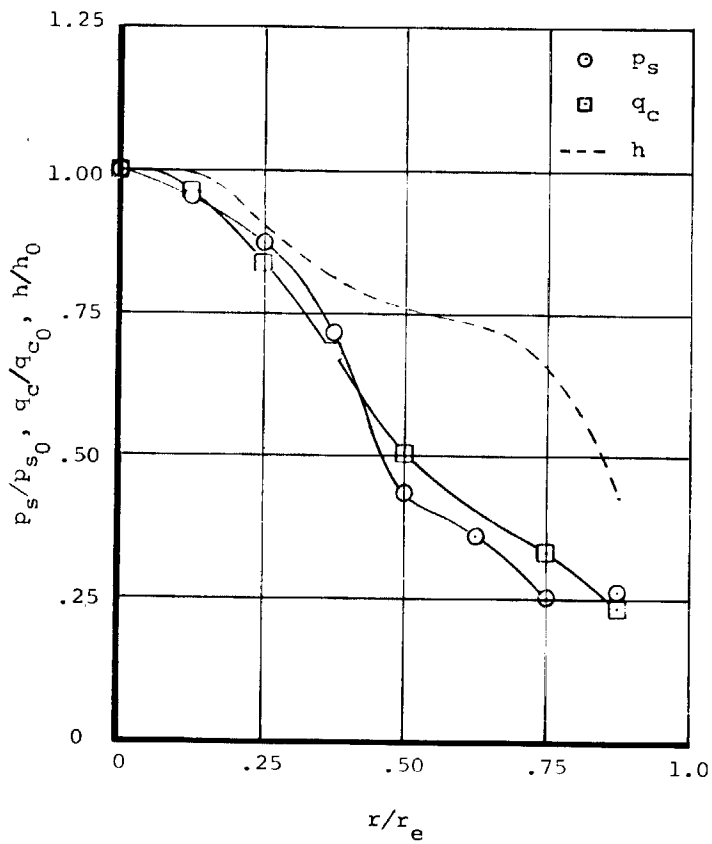

Distributions of Stagnation Pressure, Stagnation Heating Rate, and Stagnation Enthalpy.

(b) **TEST CONDITION** 25

Figure 6-5. Continued.

Enthalpy:

h_{eb}	=	3499	Btu/lb
h_{mb}	=	4050	Btu/lb
h_{hf}	=	4140	Btu/lb

Stagnation Pressure:

p_s	=	0.0083	atm

Stagnation Heating Rate:

Cal No. 1	=	BH/2.0/T	
q_c	=	40.2	Btu/ft^{2}sec
$q_c\sqrt{R}$	=	15.8	Btu/ft$^{3/2}$sec
Cal No. 2	=	FF/1.25/T	
q_c	=	38.2	Btu/ft^{2}sec
$q_c\sqrt{R}$	=	16.2	Btu/ft$^{3/2}$sec

Environment:

K_1	=	0.768	N_2 } Air
K_2	=	0.232	O_2 } Air

Arc Conditions:

p_o	=	0.289	atm
$\dot{m}$	=	0.0165	lb/sec
p_e	=	0.15	mm Hg
d_e	=	8.00	inch
A/A_*	=	64.0	
Config.	=	SUBS	

Conditions at Stream Centerline.

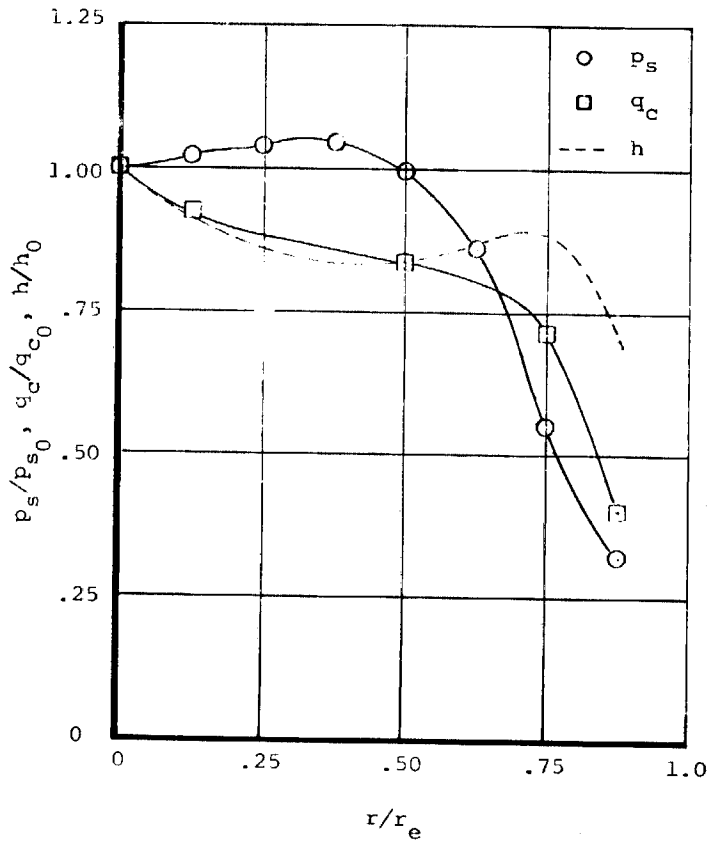

Distributions of Stagnation Pressure, Stagnation Heating Rate, and Stagnation Enthalpy.

(c) **TEST CONDITION** 26

Figure 6-5. Continued.

Enthalpy:

h_{eb}	=	9798	Btu/lb
h_{mb}	=	*	Btu/lb
h_{hf}	=	26100	Btu/lb

Stagnation Pressure:

p_s	=	0.0082	atm

Stagnation Heating Rate:

Cal No. 1	=	BH/2.0/T	
q_c	=	250	Btu/ft^{2}sec
$q_c\sqrt{R}$	=	98.6	Btu/ft$^{3/2}$sec
Cal No. 2	=	FF/1.25/T	
q_c	=	251	Btu/ft^{2}sec
$q_c\sqrt{R}$	=	106	Btu/ft$^{3/2}$sec

Environment:

K_1	=	0.768	N_2 } Air
K_2	=	0.232	O_2 } Air

Arc Conditions:

p_o	=	0.304	atm
$\dot{m}$	=	0.0070	lb/sec
p_e	=	*	mm Hg
d_e	=	8.00	inch
A/A_*	=	64.0	
Config.	=	SUPS	

Conditions at Stream Centerline.

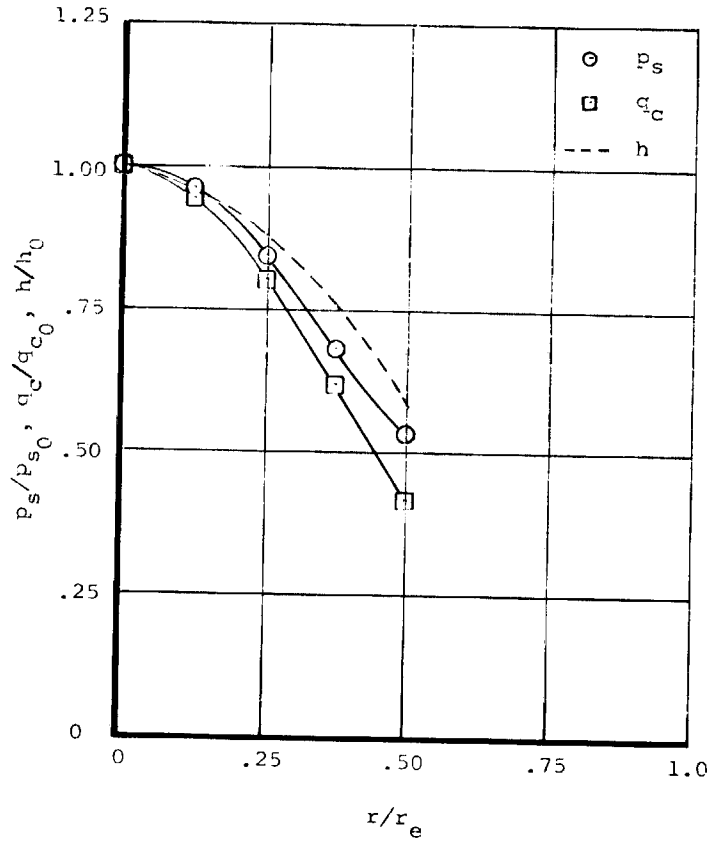

Distributions of Stagnation Pressure, Stagnation Heating Rate, and Stagnation Enthalpy.

*not applicable

(d) **TEST CONDITION** 36

Figure 6-5. Continued.

Enthalpy:

h_{eb}	=	7325	Btu/lb
h_{mb}	=	*	Btu/lb
h_{hf}	=	16600	Btu/lb

Stagnation Pressure:

p_s	=	0.0082	atm

Stagnation Heating Rate:

Cal No. 1	=	BH/2.0/T	
q_c	=	166	Btu/ft² sec
$q_c\sqrt{R}$	=	65.4	Btu/ft$^{3/2}$ sec
Cal No. 2	=	*	
q_c	=	*	Btu/ft² sec
$q_c\sqrt{R}$	=	*	Btu/ft$^{3/2}$ sec

Environment:

K_1	=	0.768	N_2 } Air
K_2	=	0.232	O_2 } Air

Arc Conditions:

p_o	=	0.205	atm
$\dot{m}$	=	0.0085	lb/sec
p_e	=	*	mm Hg
d_e	=	8.00	inch
A/A_*	=	64.0	
Config.	=	SUPS	

Conditions at Stream Centerline.

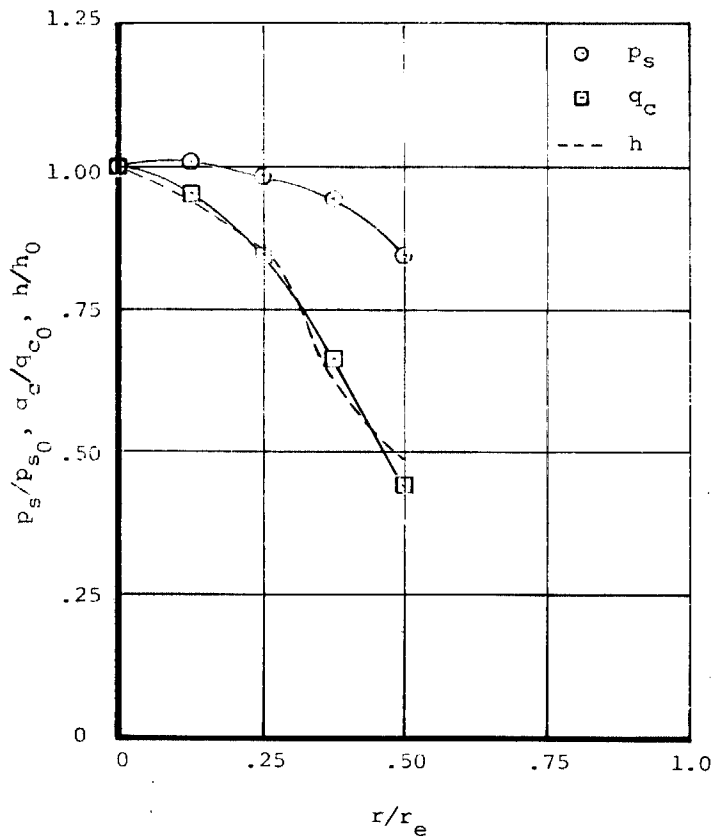

Distributions of Stagnation Pressure, Stagnation Heating Rate, and Stagnation Enthalpy.

*not applicable

(e) **TEST CONDITION** 37

Figure 6-5. Concluded.

Enthalpy:

h_{eb}	=	5545	Btu/lb
h_{mb}	=	4770	Btu/lb
h_{hf}	=	6000	Btu/lb

Stagnation Pressure:

p_s	=	0.0267	atm

Stagnation Heating Rate:

Cal No. 1	=	BH/2.0/T	
q_c	=	104	$Btu/ft^2 sec$
$q_c\sqrt{R}$	=	40.8	$Btu/ft^{3/2} sec$
Cal No. 2	=	FF/1.25/T	
q_c	=	107	$Btu/ft^2 sec$
$q_c\sqrt{R}$	=	45.4	$Btu/ft^{3/2} sec$

Environment:

K_1	=	0.768	N_2 } Air
K_2	=	0.232	O_2 } Air

Arc Conditions:

p_o	=	0.370	atm
$\dot{m}$	=	0.0196	lb/sec
p_e	=	1.00	mm Hg
d_e	=	4.50	inch
A/A_*	=	20.25	
Config.	=	SUBS	

Conditions at Stream Centerline.

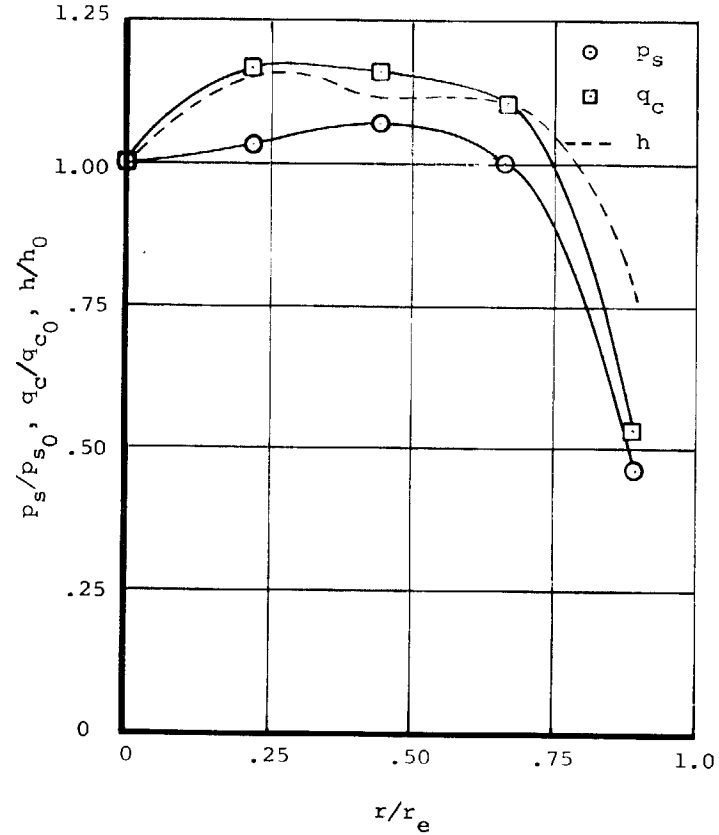

Distributions of Stagnation Pressure, Stagnation Heating Rate, and Stagnation Enthalpy.

(a) **TEST CONDITION** 1

Figure 6-6. Calibration Data, Phase IV B.

Enthalpy:

h_{eb}	=	10284	Btu/lb
h_{mb}	=	10500	Btu/lb
h_{hf}	=	9400	Btu/lb

Stagnation Pressure:

p_s	=	0.0291	atm

Stagnation Heating Rate:

Cal No. 1	=	BH/2.0/T	
q_c	=	169	Btu/ft^{2}sec
$q_c\sqrt{R}$	=	66.8	Btu/ft$^{3/2}$sec
Cal No. 2	=	FF/1.25/T	
q_c	=	204	Btu/ft^{2}sec
$q_c\sqrt{R}$	=	86.4	Btu/ft$^{3/2}$sec

Environment:

K_1	=	0.768	N_2 } Air
K_2	=	0.232	O_2 } Air

Arc Conditions:

p_o	=	0.325	atm
$\dot{m}$	=	0.0125	lb/sec
p_e	=	0.80	mm Hg
d_e	=	4.50	inch
A/A_*	=	20.25	
Config.	=	SUBS	

Conditions at Stream Centerline.

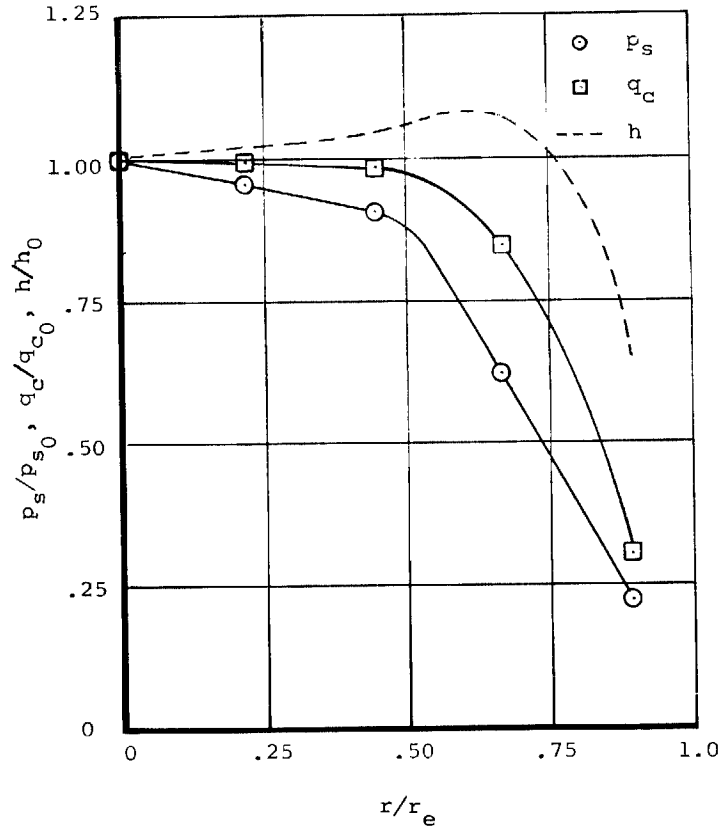

Distributions of Stagnation Pressure, Stagnation Heating Rate, and Stagnation Enthalpy.

(b) **TEST CONDITION** 2

Figure 6-6. Continued.

Enthalpy:

h_{eb}	=	5792	Btu/lb
h_{mb}	=	*	Btu/lb
h_{hf}	=	*	Btu/lb

Stagnation Pressure:

p_s	=	0.0275	atm

Stagnation Heating Rate:

Cal No. 1	=	BH/2.0/T	
q_c	=	114	Btu/ft^2sec
$q_c\sqrt{R}$	=	44.9	$Btu/ft^{3/2}sec$
Cal No. 2	=	FF/1.25/T	
q_c	=	110	Btu/ft^2sec
$q_c\sqrt{R}$	=	46.5	$Btu/ft^{3/2}sec$

Environment:

K_1	=	0.700	N_2
K_2	=	0.300	O_2

Arc Conditions:

p_o	=	0.417	atm
$\dot{m}$	=	0.0187	lb/sec
p_e	=	1.10	mm Hg
d_e	=	4.50	inch
A/A_*	=	20.25	
Config.	=	SUBS	

Conditions at Stream Centerline.

(c) **TEST CONDITION** 14
Figure 6-6. Continued.

Enthalpy:

h_{eb}	=	5668	Btu/lb
h_{mb}	=	*	Btu/lb
h_{hf}	=	*	Btu/lb

Stagnation Pressure:

p_s	=	0.0282	atm

Stagnation Heating Rate:

Cal No. 1	=	BH/2.0/T	
q_c	=	102	Btu/ft^2sec
$q_c\sqrt{R}$	=	40.2	$Btu/ft^{3/2}sec$
Cal No. 2	=	FF/1.25/T	
q_c	=	87.0	Btu/ft^2sec
$q_c\sqrt{R}$	=	36.8	$Btu/ft^{3/2}sec$

Environment:

K_1	=	0.850	N_2
K_2	=	0.150	O_2

Arc Conditions:

p_o	=	0.455	atm
$\dot{m}$	=	0.0208	lb/sec
p_e	=	1.0	mm Hg
d_e	=	4.50	inch
A/A_*	=	20.25	
Config.	=	SUBS	

Conditions at Stream Centerline.

*not applicable

(d) **TEST CONDITION** 15
Figure 6-6. Continued.

Enthalpy:

h_{eb}	=	5557	Btu/lb
h_{mb}	=	*	Btu/lb
h_{hf}	=	*	Btu/lb

Stagnation Pressure:

p_s	=	0.0275	atm

Stagnation Heating Rate:

Cal No. 1	=	BH/2.0/T	
q_c	=	91.0	Btu/ft^2sec
$q_c\sqrt{R}$	=	35.8	$Btu/ft^{3/2}sec$
Cal No. 2	=	H/2.0/T	
q_c	=	110	Btu/ft^2sec
$q_c\sqrt{R}$	=	31.7	$Btu/ft^{3/2}sec$

Environment:

K_1	=	0.930	N_2
K_2	=	0.070	O_2

Arc Conditions:

p_o	=	0.463	atm
$\dot{m}$	=	0.0205	lb/sec
p_e	=	1.10	mm Hg
d_e	=	4.50	inch
A/A_*	=	20.25	
Config.	=	SUBS	

Conditions at Stream Centerline.

(e) **TEST CONDITION** 16

Figure 6-6. Continued.

Enthalpy:

h_{eb}	=	5833	Btu/lb
h_{mb}	=	*	Btu/lb
h_{hf}	=	*	Btu/lb

Stagnation Pressure:

p_s	=	0.0275	atm

Stagnation Heating Rate:

Cal No. 1	=	BH/2.0/T	
q_c	=	179	Btu/ft^2sec
$q_c\sqrt{R}$	=	70.5	$Btu/ft^{3/2}sec$
Cal No. 2	=	H/2.0/T	
q_c	=	216	Btu/ft^2sec
$q_c\sqrt{R}$	=	62.2	$Btu/ft^{3/2}sec$

Environment:

K_1	=	1.00	N_2
K_2	=	0	O_2

Arc Conditions:

p_o	=	0.459	atm
$\dot{m}$	=	0.0230	lb/sec
p_e	=	0.90	mm Hg
d_e	=	4.50	inch
A/A_*	=	20.25	
Config.	=	SUBS	

Conditions at Stream Centerline.

*not applicable

(f) **TEST CONDITION** 17

Figure 6-6. Continued.

Enthalpy:

h_{eb}	=	10755	Btu/lb
h_{mb}	=	*	Btu/lb
h_{hf}	=	*	Btu/lb

Stagnation Pressure:

p_s	=	0.0288	atm

Stagnation Heating Rate:

Cal No. 1	=	BH/2.0/T	
q_c	=	179	Btu/ft^2sec
$q_c\sqrt{R}$	=	70.5	$Btu/ft^{3/2}sec$
Cal No. 2	=	H/2.0/T	
q_c	=	204	Btu/ft^2sec
$q_c\sqrt{R}$	=	58.7	$Btu/ft^{3/2}sec$

Environment:

K_1	=	0.700	N_2
K_2	=	0.300	O_2

Arc Conditions:

p_o	=	0.344	atm
$\dot{m}$	=	0.0122	lb/sec
p_e	=	1.00	mm Hg
d_e	=	4.50	inch
A/A_*	=	20.25	
Config.	=	SUBS	

Conditions at Stream Centerline.

(g) **TEST CONDITION** 18
Figure 6-6. Continued.

Enthalpy:

h_{eb}	=	11092	Btu/lb
h_{mb}	=	*	Btu/lb
h_{hf}	=	*	Btu/lb

Stagnation Pressure:

p_s	=	0.0275	atm

Stagnation Heating Rate:

Cal No. 1	=	BH/2.0/T	
q_c	=	177	Btu/ft^2sec
$q_c\sqrt{R}$	=	69.7	$Btu/ft^{3/2}sec$
Cal No. 2	=	H/2.0/T	
q_c	=	180	Btu/ft^2sec
$q_c\sqrt{R}$	=	51.8	$Btu/ft^{3/2}sec$

Environment:

K_1	=	0.850	N_2
K_2	=	0.150	O_2

Arc Conditions:

p_o	=	0.382	atm
$\dot{m}$	=	0.0131	lb/sec
p_e	=	1.00	mm Hg
d_e	=	4.50	inch
A/A_*	=	20.25	
Config.	=	SUBS	

Conditions at Stream Centerline.

*not applicable

(h) **TEST CONDITION** 19
Figure 6-6. Continued.

Enthalpy:

h_{eb}	=	11274	Btu/lb
h_{mb}	=	*	Btu/lb
h_{hf}	=	*	Btu/lb

Stagnation Pressure:

p_s	=	0.0275	atm

Stagnation Heating Rate:

Cal No. 1	=	BH/2.0/T	
q_c	=	194	Btu/ft^2sec
$q_c\sqrt{R}$	=	76.4	$Btu/ft^{3/2}sec$
Cal No. 2	=	H/2.0/T	
q_c	=	237	Btu/ft^2sec
$q_c\sqrt{R}$	=	68.2	$Btu/ft^{3/2}sec$

Environment:

K_1	=	0.930	N_2
K_2	=	0.070	O_2

Arc Conditions:

p_o	=	0.386	atm
$\dot{m}$	=	0.0137	lb/sec
p_e	=	0.95	mm Hg
d_e	=	4.50	inch
A/A_*	=	20.25	
Config.	=	SUBS	

Conditions at Stream Centerline.

(i) **TEST CONDITION** 20
Figure 6-6. Continued.

Enthalpy:

h_{eb}	=	10388	Btu/lb
h_{mb}	=	*	Btu/lb
h_{hf}	=	*	Btu/lb

Stagnation Pressure:

p_s	=	0.0268	atm

Stagnation Heating Rate:

Cal No. 1	=	FF/1.25/T	
q_c	=	300	Btu/ft^2sec
$q_c\sqrt{R}$	=	127	$Btu/ft^{3/2}sec$
Cal No. 2	=	*	
q_c	=	*	Btu/ft^2sec
$q_c\sqrt{R}$	=	*	$Btu/ft^{3/2}sec$

Environment:

K_1	=	1.00	N_2
K_2	=	0	O_2

Arc Conditions:

p_o	=	0.386	atm
$\dot{m}$	=	0.0141	lb/sec
p_e	=	0.95	mm Hg
d_e	=	4.50	inch
A/A_*	=	20.25	
Config.	=	SUBS	

Conditions at Stream Centerline.

*not applicable

(j) **TEST CONDITION** 21
Figure 6-6. Continued.

Enthalpy:

h_{eb}	=	10887	Btu/lb
h_{mb}	=	*	Btu/lb
h_{hf}	=	*	Btu/lb

Stagnation Pressure:

p_s	=	0.0280	atm

Stagnation Heating Rate:

Cal No. 1	=	BH/2.0/T	
q_c	=	175	Btu/ft^2sec
$q_c\sqrt{R}$	=	69.0	$Btu/ft^{3/2}sec$
Cal No. 2	=	H/2.0/T	
q_c	=	195	Btu/ft^2sec
$q_c\sqrt{R}$	=	56.2	$Btu/ft^{3/2}sec$

Environment:

K_1	=	1.00	He
K_2	=	*	

Arc Conditions:

p_o	=	0.374	atm
$\dot{m}$	=	0.0081	lb/sec
p_e	=	0.40	mm Hg
d_e	=	4.50	inch
A/A_*	=	20.25	
Config.	=	SUBS	

Conditions at Stream Centerline.

(k) **TEST CONDITION** 22
Figure 6-6. Continued.

Enthalpy:

h_{eb}	=	18263	Btu/lb
h_{mb}	=	*	Btu/lb
h_{hf}	=	*	Btu/lb

Stagnation Pressure:

p_s	=	0.0280	atm

Stagnation Heating Rate:

Cal No. 1	=	BH/2.0/T	
q_c	=	328	Btu/ft^2sec
$q_c\sqrt{R}$	=	129	$Btu/ft^{3/2}sec$
Cal No. 2	=	H/2.0/T	
q_c	=	372	Btu/ft^2sec
$q_c\sqrt{R}$	=	107	$Btu/ft^{3/2}sec$

Environment:

K_1	=	1.00	He
K_2	=	*	

Arc Conditions:

p_o	=	0.278	atm
$\dot{m}$	=	0.0056	lb/sec
p_e	=	0.40	mm Hg
d_e	=	4.50	inch
A/A_*	=	20.25	
Config.	=	SUBS	

Conditions at Stream Centerline.

*not applicable

(l) **TEST CONDITION** 23
Figure 6-6. Continued.

Enthalpy:

h_{eb}	=	8616	Btu/lb
h_{mb}	=	16300	Btu/lb
h_{hf}	=	17300	Btu/lb

Stagnation Pressure:

p_s	=	0.0275	atm

Stagnation Heating Rate:

Cal No. 1	=	FF/1.25/T	
q_c	=	283	$Btu/ft^2 sec$
$q_c \sqrt{R}$	=	120	$Btu/ft^{3/2} sec$
Cal No. 2	=	H/2.0/T	
q_c	=	346	$Btu/ft^2 sec$
$q_c \sqrt{R}$	=	99.8	$Btu/ft^{3/2} sec$

Environment:

K_1	=	0.768	N_2 } Air
K_2	=	0.232	O_2 } Air

Arc Conditions:

p_o	=	0.957	atm
$\dot{m}$	=	0.0304	lb/sec
p_e	=	1.20	mm Hg
d_e	=	6.00	inch
A/A_*	=	36.0	
Config.	=	SUPS	

Conditions at Stream Centerline.

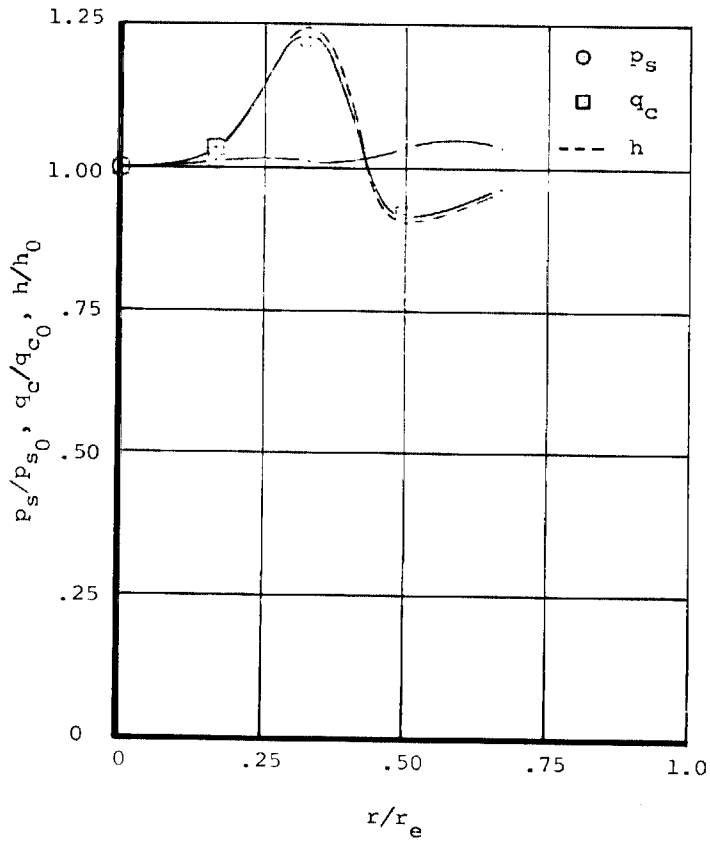

Distributions of Stagnation Pressure, Stagnation Heating Rate, and Stagnation Enthalpy.

*not applicable

(m) **TEST CONDITION** 30

Figure 6-6. Continued.

Enthalpy:

h_{eb}	=	7848	Btu/lb
h_{mb}	=	*	Btu/lb
h_{hf}	=	*	Btu/lb

Stagnation Pressure:

p_s	=	0.0262	atm

Stagnation Heating Rate:

Cal No. 1	=	BH/2.0/T	
q_c	=	209	Btu/ft^{2}sec
$q_c\sqrt{R}$	=	82.4	Btu/ft$^{5/2}$sec
Cal No. 2	=	FF/1.25/T	
q_c	=	199	Btu/ft^{2}sec
$q_c\sqrt{R}$	=	84.1	Btu/ft$^{5/2}$sec

Environment:

K_1	=	0.700	N_2
K_2	=	0.300	O_2

Arc Conditions:

p_o	=	0.933	atm
$\dot{m}$	=	0.0290	lb/sec
p_e	=	1.00	mm Hg
d_e	=	6.00	inch
A/A_*	=	36.0	
Config.	=	SUPS	

Conditions at Stream Centerline.

(n) **TEST CONDITION** 32
Figure 6-6. Continued.

Enthalpy:

h_{eb}	=	8529	Btu/lb
h_{mb}	=	*	Btu/lb
h_{hf}	=	*	Btu/lb

Stagnation Pressure:

p_s	=	0.0271	atm

Stagnation Heating Rate:

Cal No. 1	=	BH/2.0/T	
q_c	=	294	Btu/ft^{2}sec
$q_c\sqrt{R}$	=	116	Btu/ft$^{5/2}$sec
Cal No. 2	=	FF/1.25/T	
q_c	=	267	Btu/ft^{2}sec
$q_c\sqrt{R}$	=	113	Btu/ft$^{5/2}$sec

Environment:

K_1	=	0.850	N_2
K_2	=	0.150	O_2

Arc Conditions:

p_o	=	1.00	atm
$\dot{m}$	=	0.0273	lb/sec
p_e	=	1.20	mm Hg
d_e	=	6.00	inch
A/A_*	=	36.0	
Config.	=	SUPS	

Conditions at Stream Centerline.

*not applicable

(o) **TEST CONDITION** 33
Figure 6-6. Continued.

Enthalpy:

h_{eb}	=	8678	Btu/lb
h_{mb}	=	*	Btu/lb
h_{hf}	=	*	Btu/lb

Stagnation Pressure:

p_s	=	0.0271	atm

Stagnation Heating Rate:

Cal No. 1	=	BH/2.0/T	
q_c	=	387	Btu/ft^{2}sec
$q_c\sqrt{R}$	=	152	Btu/ft$^{5/2}$sec
Cal No. 2	=	FF/1.25/T	
q_c	=	316	Btu/ft^{2}sec
$q_c\sqrt{R}$	=	134	Btu/ft$^{5/2}$sec

Environment:

K_1	=	0.930	N_2
K_2	=	0.070	O_2

Arc Conditions:

p_o	=	1.04	atm
$\dot{m}$	=	0.0315	lb/sec
p_e	=	1.35	mm Hg
d_e	=	6.00	inch
A/A_*	=	36.0	
Config.	=	SUPS	

Conditions at Stream Centerline.

(p) **TEST CONDITION** 34

Figure 6-6. Continued.

Enthalpy:

h_{eb}	=	8772	Btu/lb
h_{mb}	=	*	Btu/lb
h_{hf}	=	*	Btu/lb

Stagnation Pressure:

p_s	=	0.0254	atm

Stagnation Heating Rate:

Cal No. 1	=	FF/1.25/T	
q_c	=	426	Btu/ft^{2}sec
$q_c\sqrt{R}$	=	180	Btu/ft$^{5/2}$sec
Cal No. 2	=	FF/1.25/T	
q_c	=	435	Btu/ft^{2}sec
$q_c\sqrt{R}$	=	184	Btu/ft$^{5/2}$sec

Environment:

K_1	=	1.00	N_2
K_2	=	0	O_2

Arc Conditions:

p_o	=	1.05	atm
$\dot{m}$	=	0.0354	lb/sec
p_e	=	1.35	mm Hg
d_e	=	6.00	inch
A/A_*	=	36.0	
Config.	=	SUPS	

Conditions at Stream Centerline.

*not appplicable

(q) **TEST CONDITION** 35

Figure 6-6. Concluded.

Enthalpy:

h_{eb}	=	4503	Btu/lb
h_{mb}	=	5400	Btu/lb
h_{hf}	=	4460	Btu/lb

Stagnation Pressure:

p_s	=	0.0098	atm

Stagnation Heating Rate:

Cal No. 1	=	BH/2.0/T	
q_c	=	46.9	Btu/ft^{2}sec
$q_c\sqrt{R}$	=	18.5	Btu/ft$^{5/2}$sec
Cal No. 2	=	FF/1.25/T	
q_c	=	53.1	Btu/ft^{2}sec
$q_c\sqrt{R}$	=	22.4	Btu/ft$^{5/2}$sec

Environment:

K_1	=	0.768	N_2 } Air
K_2	=	0.232	O_2 } Air

Arc Conditions:

p_o	=	0.258	atm
$\dot{m}$	=	0.013	lb/sec
p_e	=	0.2	mm Hg
d_e	=	8.00	inch
A/A_*	=	64.0	
Config.	=	SUBS	

Conditions at Stream Centerline.

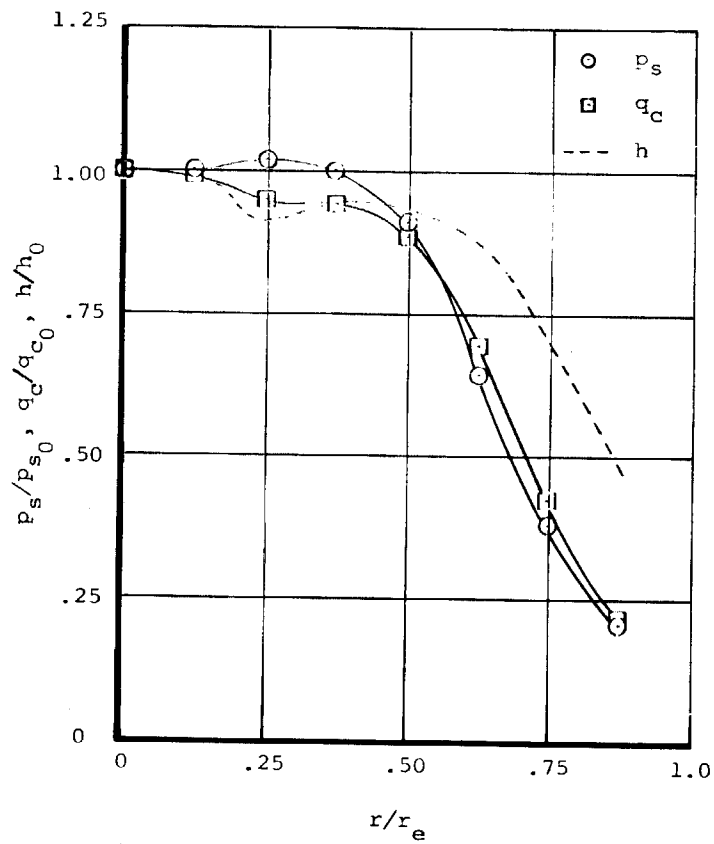

Distributions of Stagnation Pressure, Stagnation Heating Rate, and Stagnation Enthalpy.

(a) **TEST CONDITION** 24 (1)

Figure 6-7. Calibration Data, Phase V.

(1) Also used in Phase IV A.

Enthalpy:

h_{eb}	=	4660	Btu/lb
h_{mb}	=	4850	Btu/lb
h_{hf}	=	5390	Btu/lb

Stagnation Pressure:

p_s	=	0.0270	atm

Stagnation Heating Rate:

Cal No. 1	=	BH/2.0/T	
q_c	=	93.8	Btu/ft^2sec
$q_c\sqrt{R}$	=	37.0	$Btu/ft^{3/2}sec$
Cal No. 2	=	FF/1.25/T	
q_c	=	73.3	Btu/ft^2sec
$q_c\sqrt{R}$	=	31.0	$Btu/ft^{3/2}sec$

Environment:

K_1	=	0.768	N_2 } Air
K_2	=	0.232	O_2 } Air

Arc Conditions:

p_o	=	0.769	atm
$\dot{m}$	=	0.0405	lb/sec
p_e	=	1.00	mm Hg
d_e	=	6.00	inch
A/A_*	=	36.0	
Config.	=	SUBS	

Conditions at Stream Centerline.

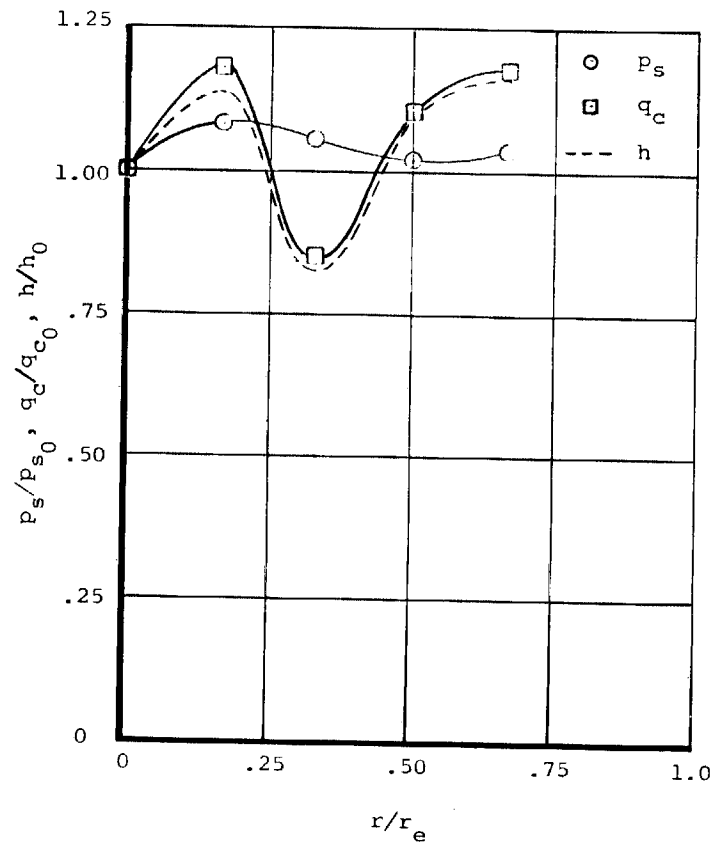

Distributions of Stagnation Pressure, Stagnation Heating Rate, and Stagnation Enthalpy.

(b) **TEST CONDITION** 28

Figure 6-7. Continued.

Enthalpy:

h_{eb}	=	10162	Btu/lb
h_{mb}	=	10000	Btu/lb
h_{hf}	=	11100	Btu/lb

Stagnation Pressure:

p_s	=	0.0266	atm

Stagnation Heating Rate:

Cal No. 1	=	BH/2.0/T	
q_c	=	192	Btu/ft^2sec
$q_c\sqrt{R}$	=	75.6	$Btu/ft^{3/2}sec$
Cal No. 2	=	FF/1.25/T	
q_c	=	172	Btu/ft^2sec
$q_c\sqrt{R}$	=	72.9	$Btu/ft^{3/2}sec$

Environment:

K_1	=	0.768	N_2 } Air
K_2	=	0.232	O_2 } Air

Arc Conditions:

p_o	=	0.566	atm
$\dot{m}$	=	0.0222	lb/sec
p_e	=	1.00	mm Hg
d_e	=	6.00	inch
A/A_*	=	36.0	
Config.	=	SUBS	

Conditions at Stream Centerline.

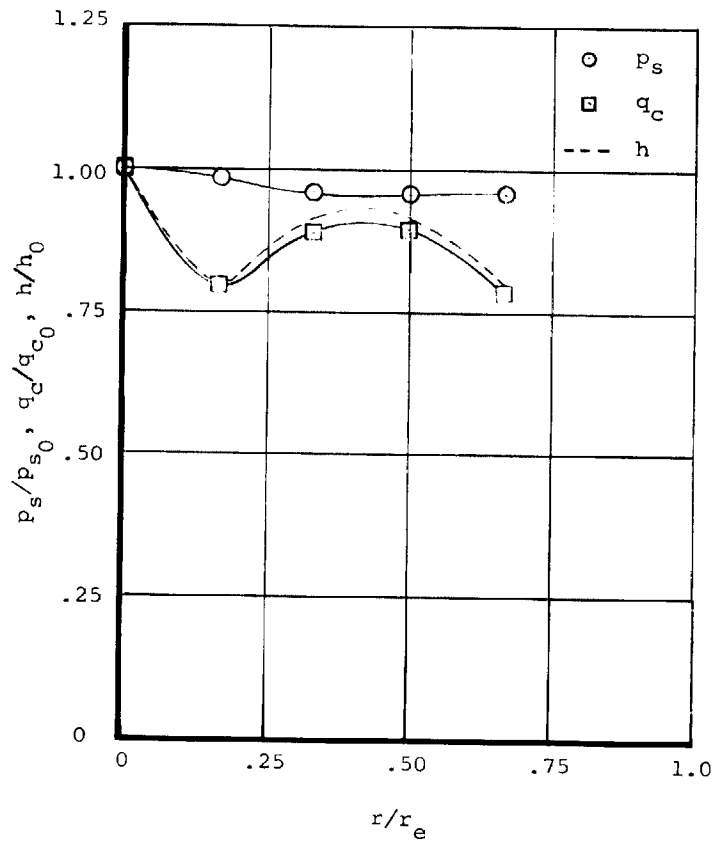

Distributions of Stagnation Pressure, Stagnation Heating Rate, and Stagnation Enthalpy.

(c) **TEST CONDITION** 29

Figure 6-7. Continued.

Enthalpy:

h_{eb}	=	8616	Btu/lb
h_{mb}	=	16300	Btu/lb
h_{hf}	=	17300	Btu/lb

Stagnation Pressure:

p_s	=	0.0275	atm

Stagnation Heating Rate:

Cal No. 1	=	FF/1.25/T	
q_c	=	283	$Btu/ft^2 sec$
$q_c \sqrt{R}$	=	120	$Btu/ft^{3/2} sec$
Cal No. 2	=	H/2.0/T	
q_c	=	346	$Btu/ft^2 sec$
$q_c \sqrt{R}$	=	99.8	$Btu/ft^{3/2} sec$

Environment:

K_1	=	0.768	N_2 } Air
K_2	=	0.232	O_2 } Air

Arc Conditions:

p_o	=	0.957	atm
$\dot{m}$	=	0.0304	lb/sec
p_e	=	1.20	mm Hg
d_e	=	6.00	inch
A/A_*	=	36.0	
Config.	=	SUPS	

Conditions at Stream Centerline.

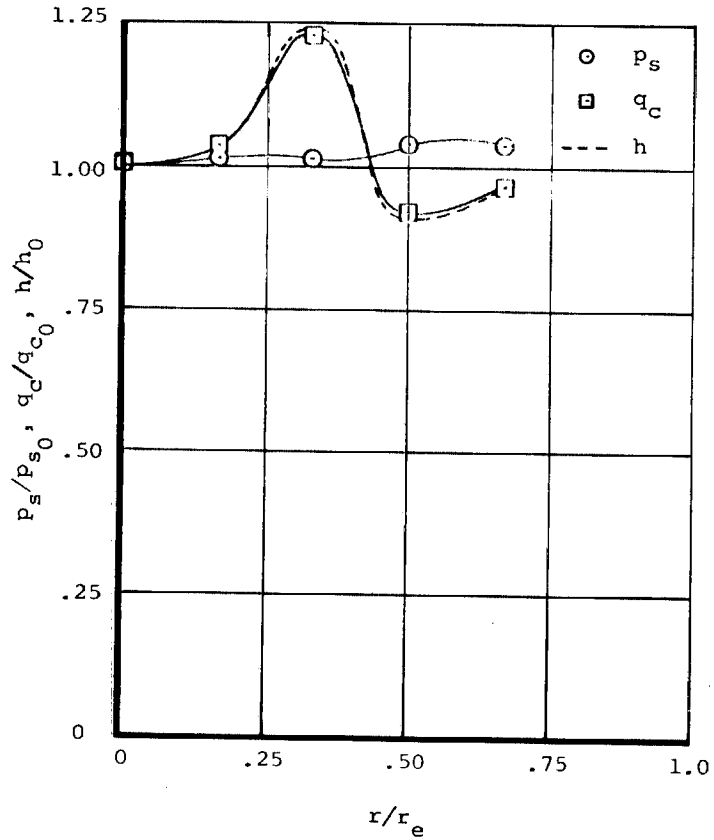

Distributions of Stagnation Pressure, Stagnation Heating Rate, and Stagnation Enthalpy.

(d) **TEST CONDITION** 30 (1)

Figure 6-7. Continued.

(1) Also used in Phases IV B, VI A, B.

Enthalpy:

h_{cb}	=	6226	Btu/lb
h_{mb}	=	14800	Btu/lb
h_{hf}	=	12940	Btu/lb

Stagnation Pressure:

p_s	=	0.0082	atm

Stagnation Heating Rate:

Cal No. 1	=	BH/2.0/T	
q_c	=	124	Btu/ft² sec
$q_c\sqrt{R}$	=	48.9	Btu/ft$^{3/2}$ sec
Cal No. 2	=	*	
q_c	=	*	Btu/ft² sec
$q_c\sqrt{R}$	=	*	Btu/ft$^{3/2}$ sec

Environment:

K_1	=	0.768	N_2 } Air
K_2	=	0.232	O_2 } Air

Arc Conditions:

P_o	=	0.281	atm
$\dot{m}$	=	0.0090	lb/sec
p_e	=	*	mm Hg
d_e	=	8.00	inch
A/A_*	=	64.0	
Config.	=	SUPS	

Conditions at Stream Centerline.

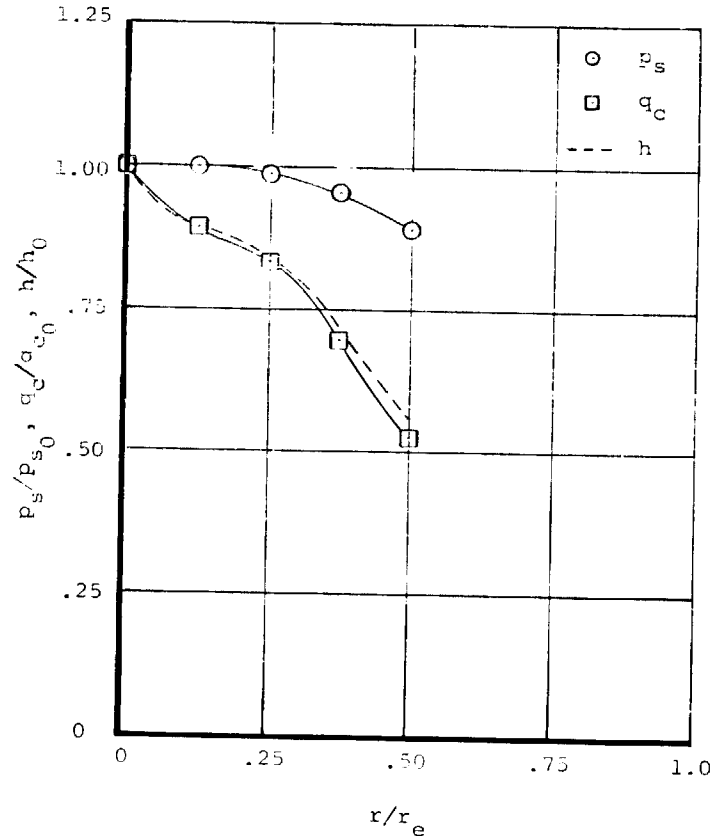

Distributions of Stagnation Pressure, Stagnation Heating Rate, and Stagnation Enthalpy.

*not applicable

(e) **TEST CONDITION** 38

Figure 6-7. Concluded.

Enthalpy:

h_{eb}	=	5545	Btu/lb
h_{mb}	=	4770	Btu/lb
h_{hf}	=	6000	Btu/lb

Stagnation Pressure:

p_s	=	0.0267	atm

Stagnation Heating Rate:

Cal No. 1	=	BH/2.0/T	
q_c	=	104	Btu/ft^{2}sec
$q_c\sqrt{R}$	=	40.8	Btu/ft$^{5/2}$sec
Cal No. 2	=	FF/1.25/T	
q_c	=	107	Btu/ft^{2}sec
$q_c\sqrt{R}$	=	45.4	Btu/ft$^{5/2}$sec

Environment:

K_1	=	0.768	N_2 } Air
K_2	=	0.232	O_2 } Air

Arc Conditions:

p_o	=	0.370	atm
$\dot{m}$	=	0.0196	lb/sec
p_e	=	1.00	mm Hg
d_e	=	4.50	inch
A/A_*	=	20.25	
Config.	=	SUBS	

Conditions at Stream Centerline.

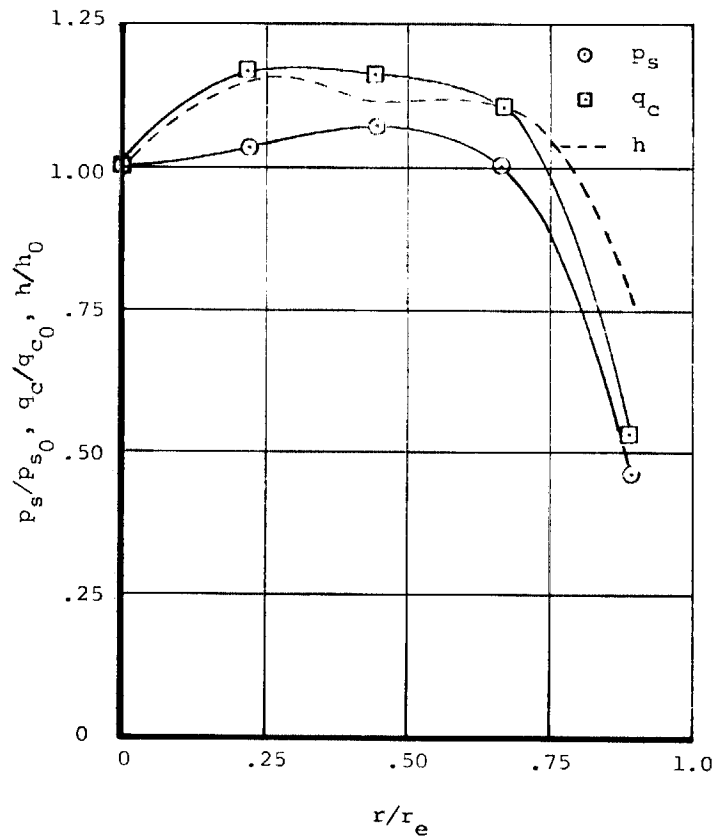

Distributions of Stagnation Pressure, Stagnation Heating Rate, and Stagnation Enthalpy.

(a) **TEST CONDITION** 1

Figure 6-8. Calibration Data, Phase VI A.

(1) Also used in Phases IV B, VI B.

Enthalpy:

h_{eb}	=	10284	Btu/lb
h_{mb}	=	10500	Btu/lb
h_{hf}	=	9400	Btu/lb

Stagnation Pressure:

p_s	=	0.0291	atm

Stagnation Heating Rate:

Cal No. 1	=	BH/2.0/T	
q_c	=	169	Btu/ft^{2}sec
$q_c\sqrt{R}$	=	66.8	Btu/ft$^{5/2}$sec
Cal No. 2	=	FF/1.25/T	
q_c	=	204	Btu/ft^{2}sec
$q_c\sqrt{R}$	=	86.4	Btu/ft$^{5/2}$sec

Environment:

K_1	=	0.768	N_2 } Air
K_2	=	0.232	O_2 } Air

Arc Conditions:

p_o	=	0.325	atm
$\dot{m}$	=	0.0125	lb/sec
p_e	=	0.80	mm Hg
d_e	=	4.50	inch
A/A_*	=	20.25	
Config.	=	SUBS	

Conditions at Stream Centerline.

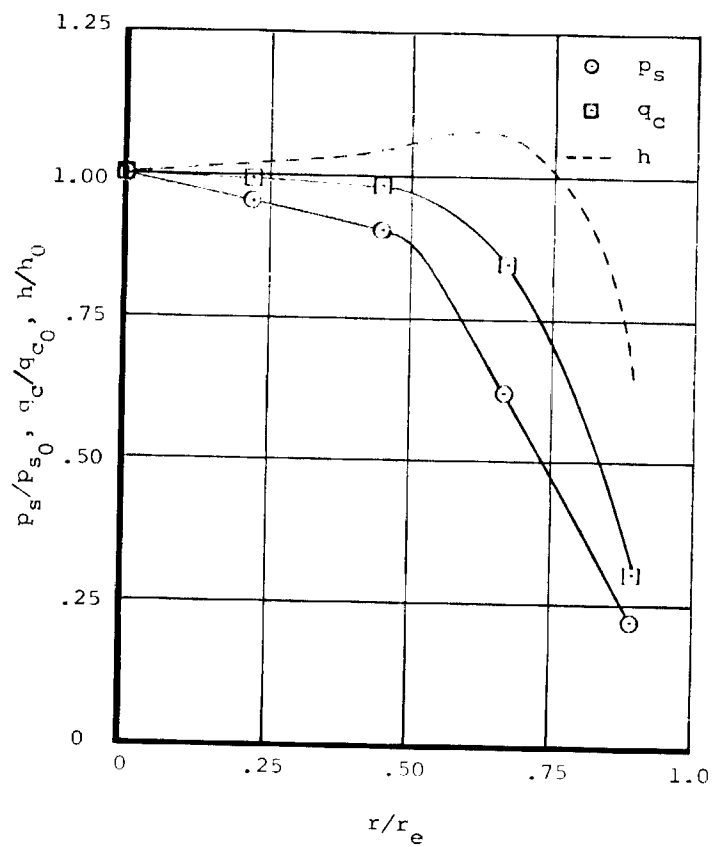

Distributions of Stagnation Pressure, Stagnation Heating Rate, and Stagnation Enthalpy.

(b) **TEST CONDITION** 2 (1)

Figure 6-8. Continued.

(1) Also used in Phases IV B, VI B.

Enthalpy:

h_{eb}	=	8616	Btu/lb
h_{mb}	=	16300	Btu/lb
h_{hf}	=	17300	Btu/lb

Stagnation Pressure:

p_s	=	0.0275	atm

Stagnation Heating Rate:

Cal No. 1	=	FF/1.25/T	
q_c	=	283	Btu/ft^{2}sec
$q_c\sqrt{R}$	=	120	Btu/ft$^{3/2}$sec
Cal No. 2	=	H/2.0/T	
q_c	=	346	Btu/ft^{2}sec
$q_c\sqrt{R}$	=	99.8	Btu/ft$^{3/2}$sec

Environment:

K_1	=	0.768	N_2 } Air
K_2	=	0.232	O_2 } Air

Arc Conditions:

p_o	=	0.957	atm
$\dot{m}$	=	0.0304	lb/sec
p_e	=	1.20	mm Hg
d_e	=	6.00	inch
A/A_*	=	36.0	
Config.	=	SUPS	

Conditions at Stream Centerline.

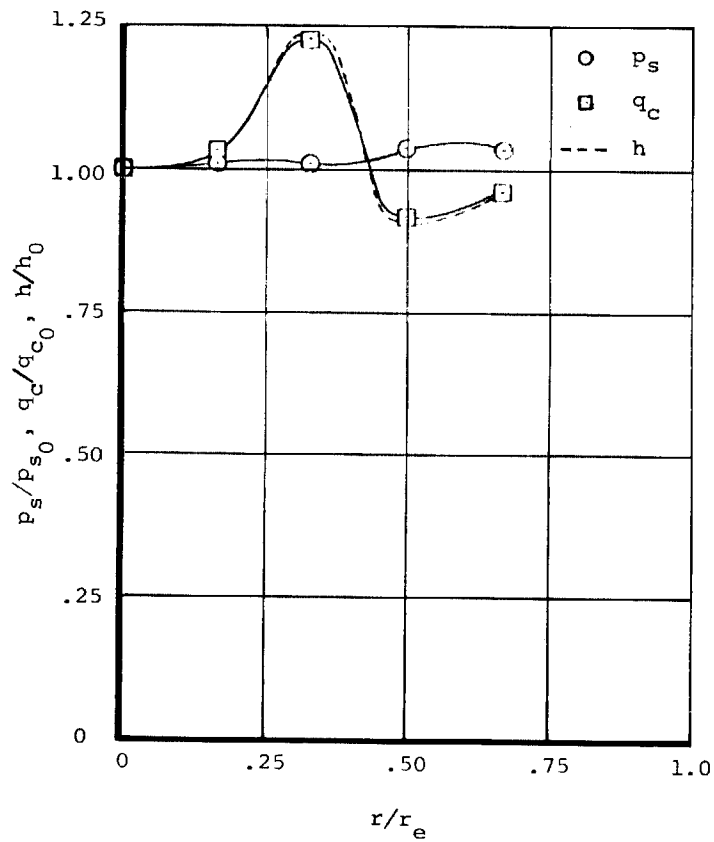

Distributions of Stagnation Pressure, Stagnation Heating Rate, and Stagnation Enthalpy.

(c) **TEST CONDITION** 30 (1)
Figure 6-8. Concluded.

(1) Also used in Phases IV B, V, VI B.

C-2.

Enthalpy:

h_{eb}	=	5545	Btu/lb
h_{mb}	=	4770	Btu/lb
h_{hf}	=	6000	Btu/lb

Stagnation Pressure:

p_s	=	0.0267	atm

Stagnation Heating Rate:

Cal No. 1	=	BH/2.0/T	
q_c	=	104	Btu/ft^{2}sec
$q_c\sqrt{R}$	=	40.8	Btu/ft$^{3/2}$sec
Cal No. 2	=	FF/1.25/T	
q_c	=	107	Btu/ft^{2}sec
$q_c\sqrt{R}$	=	45.4	Btu/ft$^{3/2}$sec

Environment:

K_1	=	0.768	N_2 } Air
K_2	=	0.232	O_2 } Air

Arc Conditions:

P_o	=	0.370	atm
$\dot{m}$	=	0.0196	lb/sec
P_e	=	1.00	mm Hg
d_e	=	4.50	inch
A/A_*	=	20.25	
Config.	=	SUBS	

Conditions at Stream Centerline.

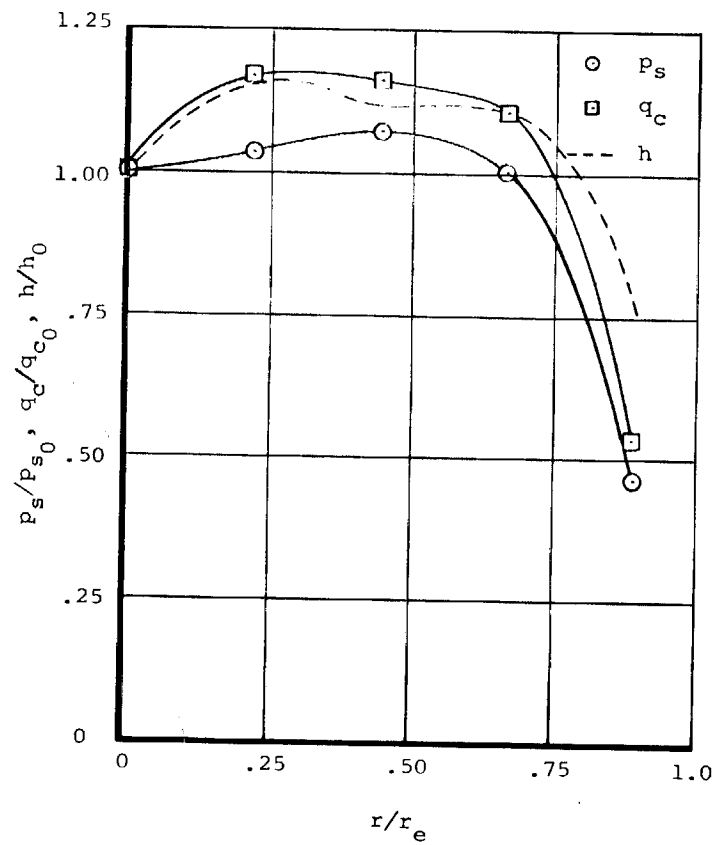

Distributions of Stagnation Pressure, Stagnation Heating Rate, and Stagnation Enthalpy.

(a) **TEST CONDITION** 1 (1)

Figure 6-9. Calibration Data, Phase VI B.

(1) Also used in Phases IV B, VI A.

Enthalpy:

h_{eb}	=	10284	Btu/lb
h_{mb}	=	10500	Btu/lb
h_{hf}	=	9400	Btu/lb

Stagnation Pressure:

p_s	=	0.0291	atm

Stagnation Heating Rate:

Cal No. 1	=	BH/2.0/T	
q_c	=	169	Btu/ft^2sec
$q_c\sqrt{R}$	=	66.8	$Btu/ft^{3/2}sec$
Cal No. 2	=	FF/1.25/T	
q_c	=	204	Btu/ft^2sec
$q_c\sqrt{R}$	=	86.4	$Btu/ft^{3/2}sec$

Environment:

K_1	=	0.768	N_2 } Air
K_2	=	0.232	O_2 } Air

Arc Conditions:

p_o	=	0.325	atm
$\dot{m}$	=	0.0125	lb/sec
p_e	=	0.80	mm Hg
d_e	=	4.50	inch
A/A_*	=	20.25	
Config.	=	SUBS	

Conditions at Stream Centerline.

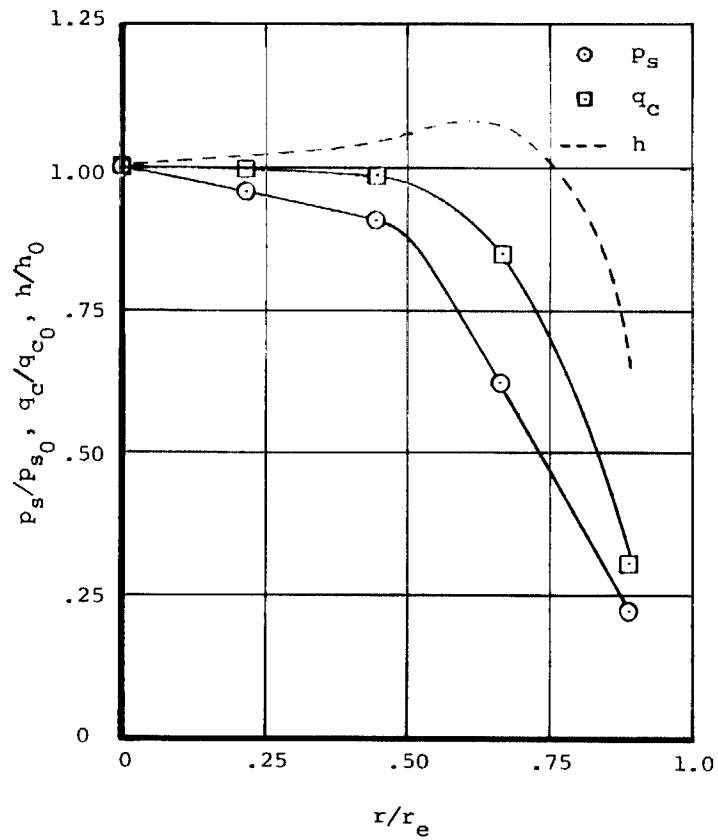

Distributions of Stagnation Pressure, Stagnation Heating Rate, and Stagnation Enthalpy.

(b) **TEST CONDITION** 2 (1)

Figure 6-9. Continued.

(1) Also used in Phases IV B, VI A.

Enthalpy:

h_{eb}	=	7654	Btu/lb
h_{mb}	=	7400	Btu/lb
h_{hf}	=	8220	Btu/lb

Stagnation Pressure:

p_s	=	0.0285	atm

Stagnation Heating Rate:

Cal No. 1	=	BH/2.0/T	
q_c	=	147	Btu/ft^{2}sec
$q_c\sqrt{R}$	=	57.8	Btu/ft$^{3/2}$sec
Cal No. 2	=	H/2.0/T	
q_c	=	162	Btu/ft^{2}sec
$q_c\sqrt{R}$	=	46.8	Btu/ft$^{3/2}$sec

Environment:

K_1	=	0.768	N_2 } Air
K_2	=	0.232	O_2 } Air

Arc Conditions:

p_o	=	0.348	atm
$\dot{m}$	=	0.0154	lb/sec
p_e	=	0.85	mm Hg
d_e	=	4.50	inch
A/A_*	=	20.25	
Config.	=	SUBS	

Conditions at Stream Centerline.

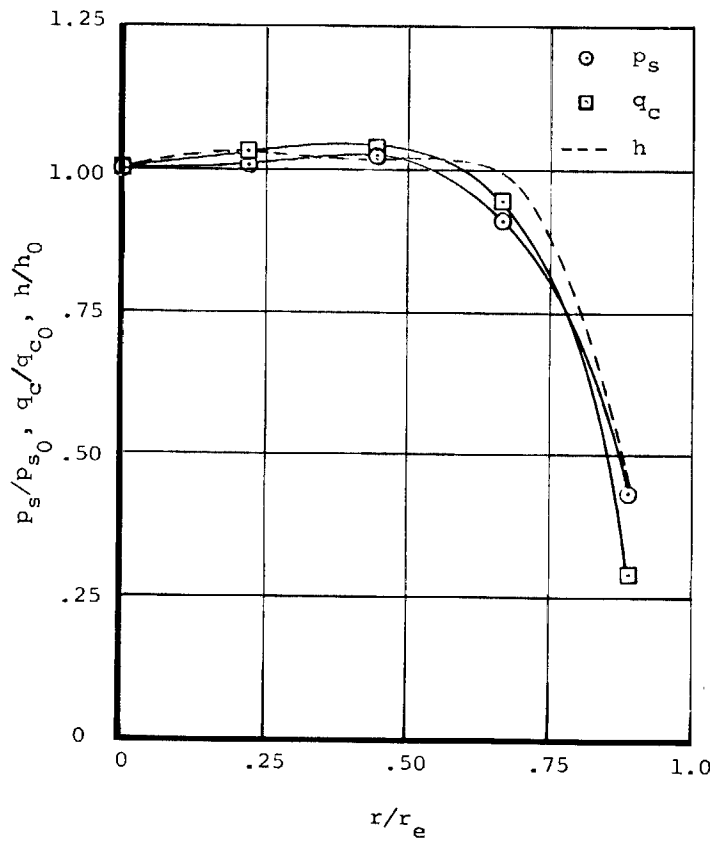

Distributions of Stagnation Pressure, Stagnation Heating Rate, and Stagnation Enthalpy.

(c) **TEST CONDITION** 3

Figure 6-9. Continued.

Enthalpy:

h_{eb}	=	7276	Btu/lb
h_{mb}	=	6950	Btu/lb
h_{hf}	=	7100	Btu/lb

Stagnation Pressure:

p_s	=	0.0265	atm

Stagnation Heating Rate:

Cal No. 1	=	BH/2.0/T	
q_c	=	123	$Btu/ft^2 sec$
$q_c\sqrt{R}$	=	48.3	$Btu/ft^{3/2} sec$
Cal No. 2	=	FF/1.25/T	
q_c	=	146	$Btu/ft^2 sec$
$q_c\sqrt{R}$	=	61.6	$Btu/ft^{3/2} sec$

Environment:

K_1	=	0.768	N_2 } Air
K_2	=	0.232	O_2 } Air

Arc Conditions:

p_o	=	0.362	atm
$\dot{m}$	=	0.0165	lb/sec
p_e	=	1.10	mm Hg
d_e	=	4.50	inch
A/A_*	=	20.25	
Config.	=	SUBS	

Conditions at Stream Centerline.

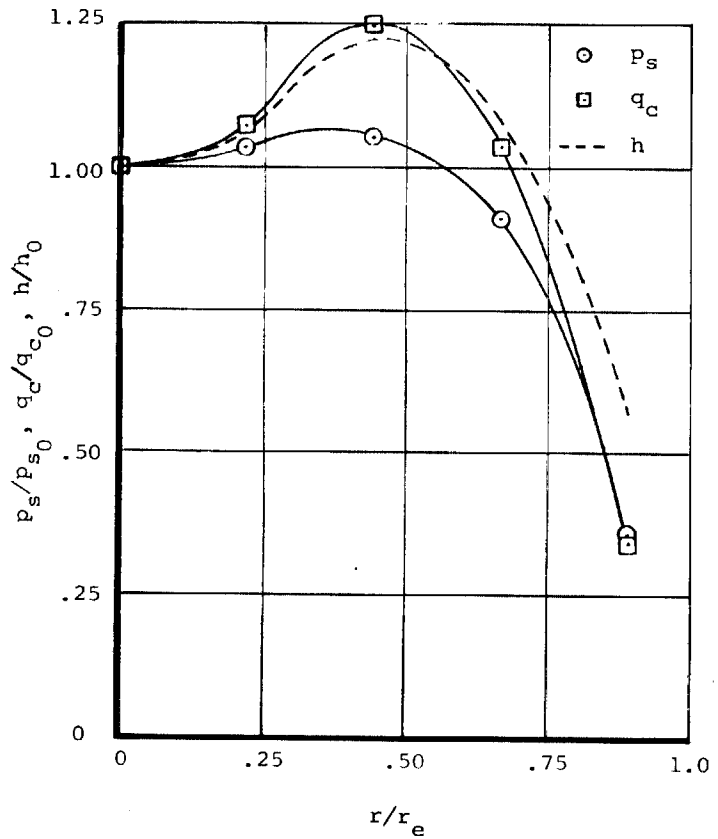

Distributions of Stagnation Pressure, Stagnation Heating Rate, and Stagnation Enthalpy.

(d) **TEST CONDITION** 4

Figure 6-9. Continued.

Enthalpy:

h_{eb}	=	11397	Btu/lb
h_{mb}	=	12600	Btu/lb
h_{hf}	=	14700	Btu/lb

Stagnation Pressure:

p_s	=	0.0282	atm

Stagnation Heating Rate:

Cal No. 1	=	BH/2.0/T	
q_c	=	262	Btu/ft^{2}sec
$q_c\sqrt{R}$	=	103	Btu/ft$^{3/2}$sec
Cal No. 2	=	H/2.0/T	
q_c	=	280	Btu/ft^{2}sec
$q_c\sqrt{R}$	=	80.7	Btu/ft$^{3/2}$sec

Environment:

K_1	=	0.768	N_2 } Air
K_2	=	0.232	O_2 } Air

Arc Conditions:

p_o	=	0.281	atm
$\dot{m}$	=	0.010	lb/sec
p_e	=	*	mm Hg
d_e	=	4.50	inch
A/A_*	=	20.25	
Config.	=	SUBS	

Conditions at Stream Centerline.

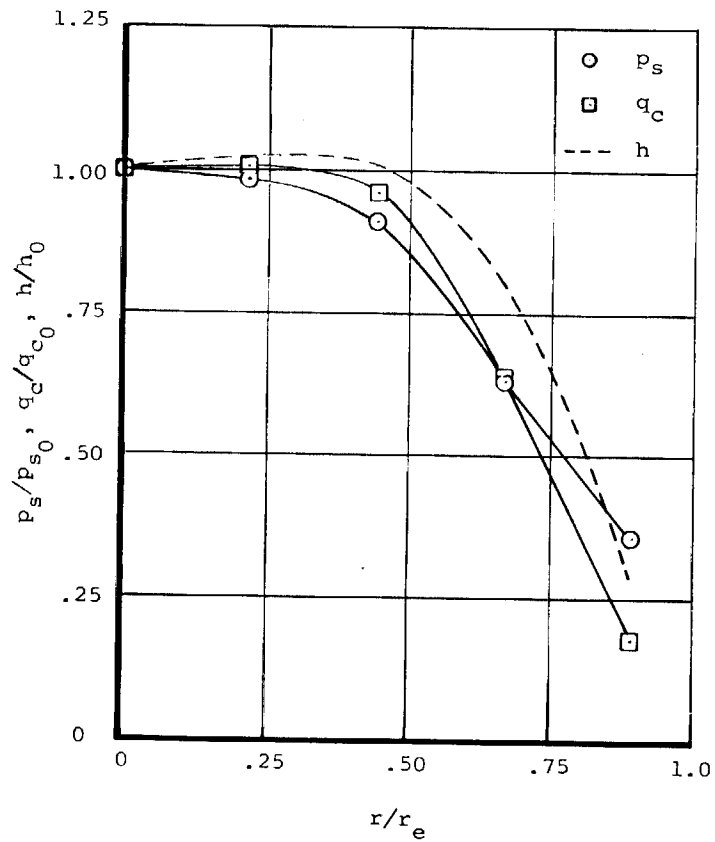

Distributions of Stagnation Pressure, Stagnation Heating Rate, and Stagnation Enthalpy.

(e) **TEST CONDITION** 5

Figure 6-9. Continued.

Enthalpy:

h_{eb}	=	3819	Btu/lb
h_{mb}	=	3600	Btu/lb
h_{hf}	=	4780	Btu/lb

Stagnation Pressure:

p_s	=	0.0281	atm

Stagnation Heating Rate:

Cal No. 1	=	BH/2.0/T	
q_c	=	85.0	Btu/ft^{2}sec
$q_c\sqrt{R}$	=	33.5	Btu/ft$^{3/2}$sec
Cal No. 2	=	H/2.0/T	
q_c	=	105	Btu/ft^{2}sec
$q_c\sqrt{R}$	=	30.2	Btu/ft$^{3/2}$sec

Environment:

K_1	=	0.762	N_2 } Air
K_2	=	0.232	O_2 } Air

Arc Conditions:

p_o	=	0.428	atm
$\dot{m}$	=	0.0252	lb/sec
p_e	=	1.20	mm Hg
d_e	=	4.50	inch
A/A_*	=	20.25	
Config.	=	SUBS	

Conditions at Stream Centerline.

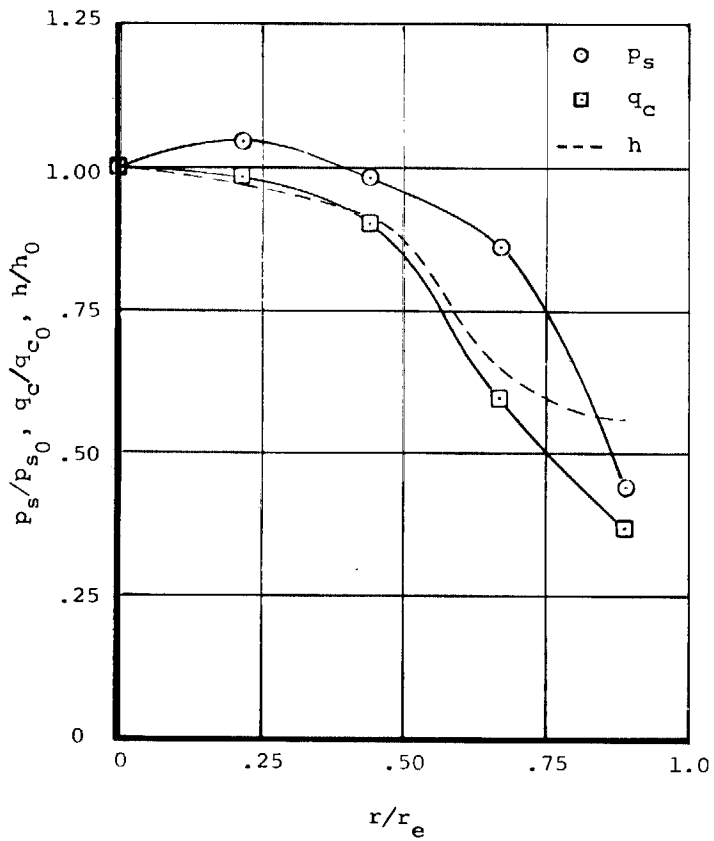

Distributions of Stagnation Pressure, Stagnation Heating Rate, and Stagnation Enthalpy.

(f) **TEST CONDITION** 6

Figure 6-9. Continued.

Enthalpy:

h_{eb}	=	6510	Btu/lb
h_{mb}	=	10000	Btu/lb
h_{hf}	=	25500	Btu/lb

Stagnation Pressure:

p_s	=	0.0285	atm

Stagnation Heating Rate:

Cal No. 1	=	BH/2.0/T	
q_c	=	512	Btu/ft^{2}sec
$q_c\sqrt{R}$	=	202	Btu/ft$^{5/2}$sec
Cal No. 2	=	FF/1.25/T	
q_c	=	426	Btu/ft^{2}sec
$q_c\sqrt{R}$	=	180	Btu/ft$^{5/2}$sec

Environment:

K_1	=	0.768	N_2 } Air
K_2	=	0.232	O_2 } Air

Arc Conditions:

p_o	=	0.524	atm
$\dot{m}$	=	0.0205	lb/sec
p_e	=	1.45	mm Hg
d_e	=	4.50	inch
A/A_*	=	20.25	
Config.	=	SUPS	

Conditions at Stream Centerline.

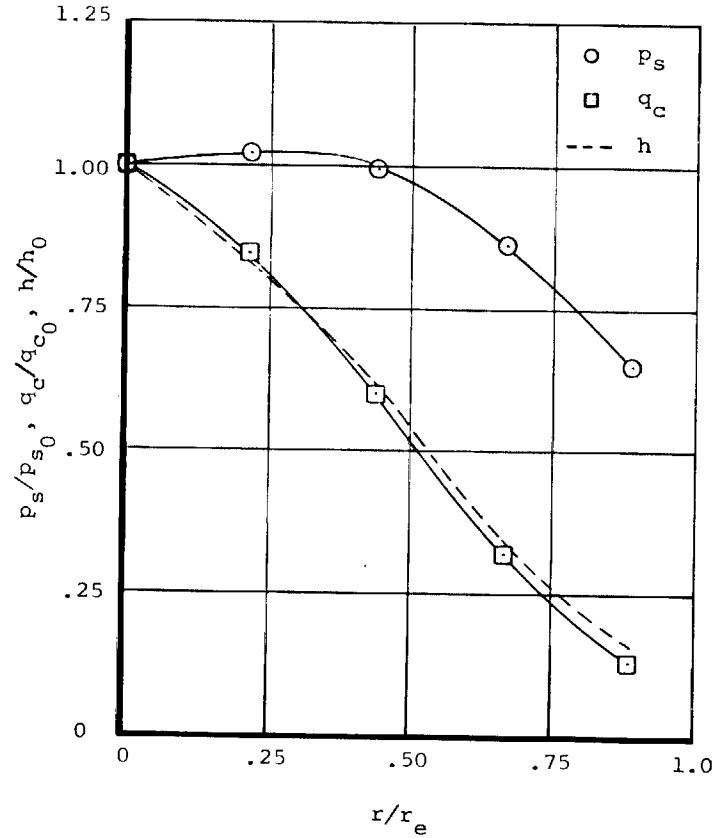

Distributions of Stagnation Pressure, Stagnation Heating Rate, and Stagnation Enthalpy.

(g) **TEST CONDITION** 27

Figure 6-9. Continued.

Enthalpy:

h_{eb}	=	8616	Btu/lb
h_{mb}	=	16300	Btu/lb
h_{hf}	=	17300	Btu/lb

Stagnation Pressure:

p_s	=	0.0275	atm

Stagnation Heating Rate:

Cal No. 1	=	FF/1.25/T	
q_c	=	283	Btu/ft^{2}sec
$q_c\sqrt{R}$	=	120	Btu/ft$^{3/2}$sec
Cal No. 2	=	H/2.0/T	
q_c	=	346	Btu/ft^{2}sec
$q_c\sqrt{R}$	=	99.8	Btu/ft$^{3/2}$sec

Environment:

K_1	=	0.768	N_2 } Air
K_2	=	0.232	O_2 } Air

Arc Conditions:

p_o	=	0.957	atm
$\dot{m}$	=	0.0304	lb/sec
p_e	=	1.20	mm Hg
d_e	=	6.00	inch
A/A_*	=	36.0	
Config.	=	SUPS	

Conditions at Stream Centerline.

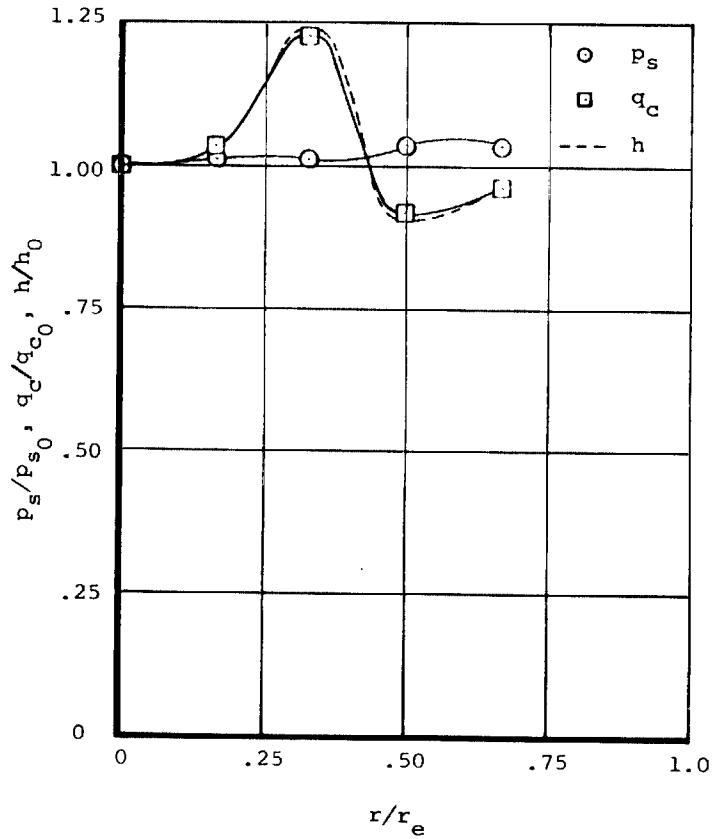

Distributions of Stagnation Pressure, Stagnation Heating Rate, and Stagnation Enthalpy.

(h) **TEST CONDITION** 30 (1)

Figure 6-9. Continued.

(1) Also used in Phases IV B, V, VI A.

Enthalpy:

h_{eb}	=	7188	Btu/lb
h_{mb}	=	15400	Btu/lb
h_{hf}	=	13300	Btu/lb

Stagnation Pressure:

p_s	=	0.0258	atm

Stagnation Heating Rate:

Cal No. 1	=	FF/1.25/T	
q_c	=	210	Btu/ft^{2}sec
$q_c\sqrt{R}$	=	88.9	Btu/ft$^{5/2}$sec
Cal No. 2	=	H/2.0/T	
q_c	=	260	Btu/ft^{2}sec
$q_c\sqrt{R}$	=	75.0	Btu/ft$^{5/2}$sec

Environment:

K_1	=	0.768	N_2 } Air
K_2	=	0.232	O_2 } Air

Arc Conditions:

p_o	=	0.925	atm
$\dot{m}$	=	0.0304	lb/sec
p_e	=	1.20	mm Hg
d_e	=	6.00	inch
A/A_*	=	36.0	
Config.	=	SUPS	

Conditions at Stream Centerline.

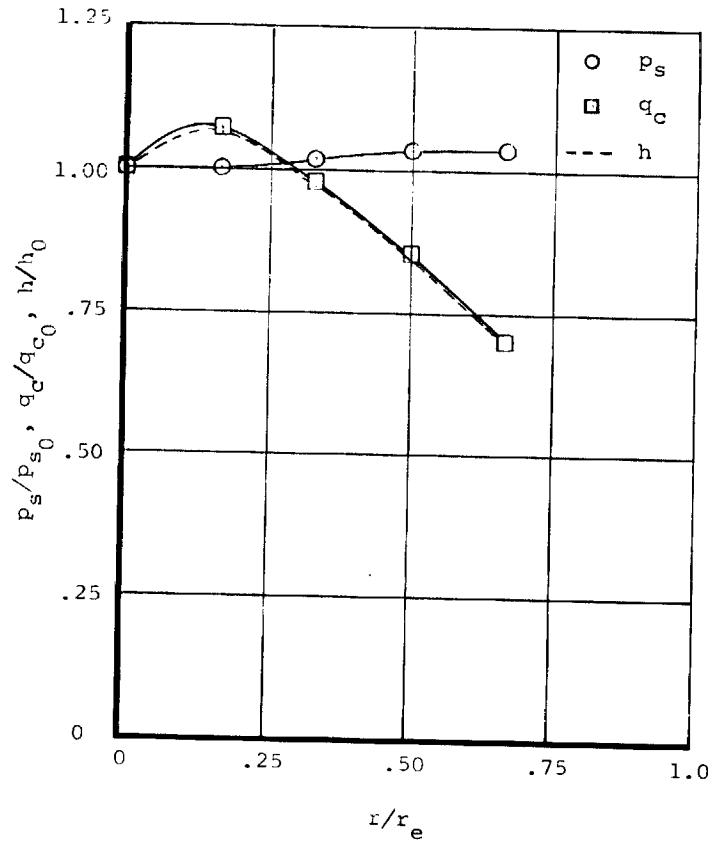

Distributions of Stagnation Pressure, Stagnation Heating Rate, and Stagnation Enthalpy.

(i) **TEST CONDITION** 31

Figure 6-9. Concluded.

Enthalpy:

h_{eb}	=	9954	Btu/lb
h_{mb}	=	9200	Btu/lb
h_{hf}	=	11500	Btu/lb

Stagnation Pressure:

p_s	=	0.0828	atm

Stagnation Heating Rate:

Cal No. 1	=	BH/2.0/T	
q_c	=	351	Btu/ft^{2}sec
$q_c\sqrt{R}$	=	138	Btu/ft$^{3/2}$sec
Cal No. 2	=	H/2.0/T	
q_c	=	390	Btu/ft^{2}sec
$q_c\sqrt{R}$	=	112	Btu/ft$^{3/2}$sec

Environment:

K_1	=	0.768	N_2 } Air
K_2	=	0.232	O_2 } Air

Arc Conditions:

p_o	=	0.606	atm
$\dot{m}$	=	0.0139	lb/sec
p_e	=	*	mm Hg
d_e	=	2.50	inch
A/A_*	=	11.11	
Config.	=	SUBS	

Conditions at Stream Centerline.

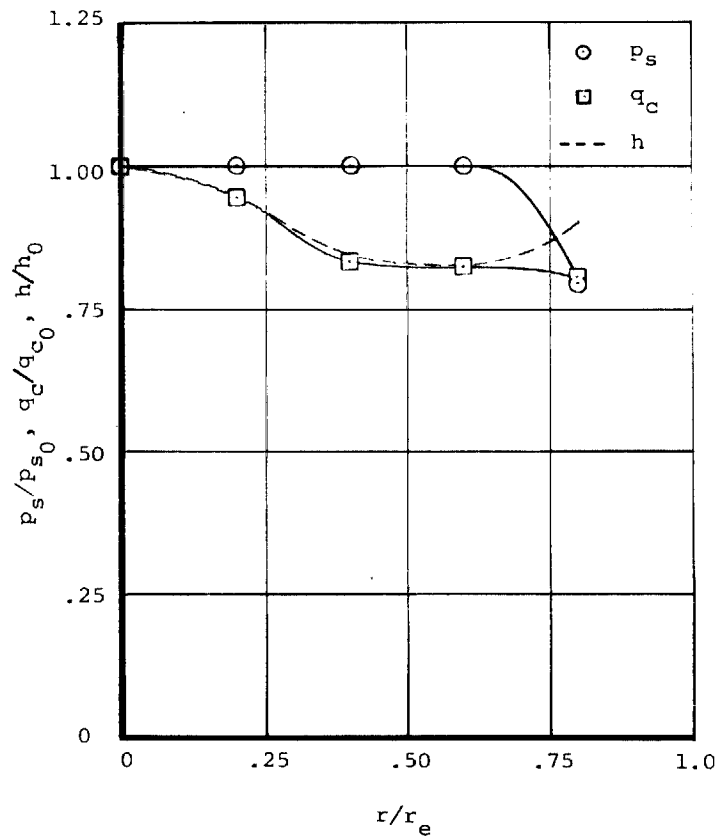

Distributions of Stagnation Pressure, Stagnation Heating Rate, and Stagnation Enthalpy.

*not applicable

(a) **TEST CONDITION** 13

Figure 6-10. Calibration Data, PhaseVII.

Enthalpy:

h_{eb}	=	6510	Btu/lb
h_{mb}	=	10000	Btu/lb
h_{hf}	=	25500	Btu/lb

Stagnation Pressure:

p_s	=	0.0285	atm

Stagnation Heating Rate:

Cal No. 1	=	BH/2.0/T	
q_c	=	512	Btu/ft^{2}sec
$q_c\sqrt{R}$	=	202	Btu/ft$^{3/2}$sec
Cal No. 2	=	FF/1.25/T	
q_c	=	426	Btu/ft^{2}sec
$q_c\sqrt{R}$	=	180	Btu/ft$^{3/2}$sec

Environment:

K_1	=	0.768	N_2 } Air
K_2	=	0.232	O_2 } Air

Arc Conditions:

p_o	=	0.524	atm
$\dot{m}$	=	0.0205	lb/sec
p_e	=	1.45	mm Hg
d_e	=	4.50	inch
A/A_*	=	20.25	
Config.	=	SUPS	

Conditions at Stream Centerline.

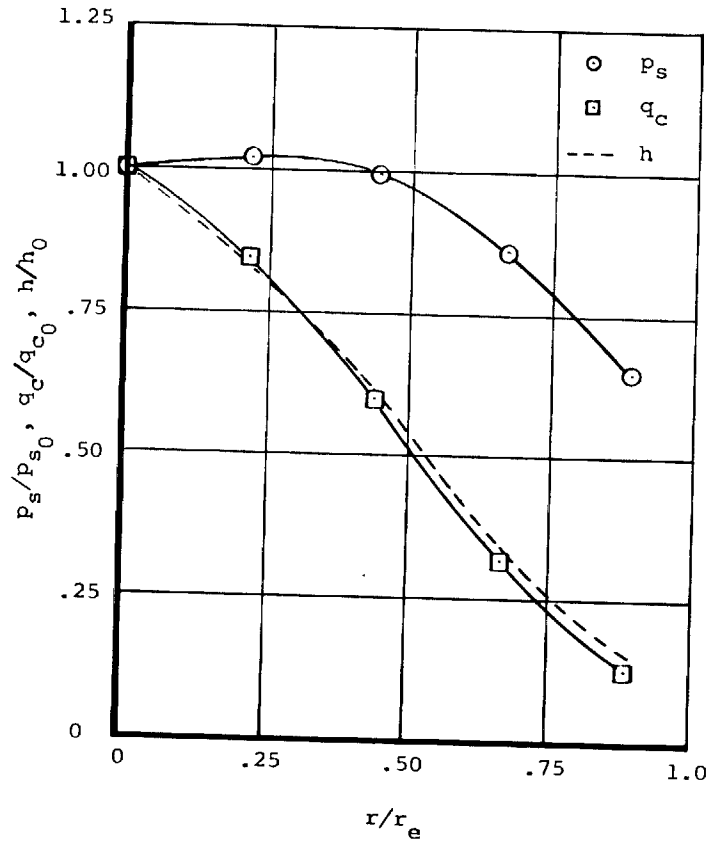

Distributions of Stagnation Pressure, Stagnation Heating Rate, and Stagnation Enthalpy.

(b) **TEST CONDITION** 27 (1)
Figure 6-10. Continued.

(1) Also used in Phase VI B.

Enthalpy:

h_{eb}	=	3532	Btu/lb
h_{mb}	=	*	Btu/lb
h_{hf}	=	*	Btu/lb

Stagnation Pressure:

p_s	=	0.370	atm

Stagnation Heating Rate:

Cal No. 1	=	BH/1.0/T	
q_c	=	599	Btu/ft^{2}sec
$q_c\sqrt{R}$	=	165	Btu/ft$^{3/2}$sec
Cal No. 2	=	FF/1.25/T	
q_c	=	436	Btu/ft^{2}sec
$q_c\sqrt{R}$	=	164	Btu/ft$^{3/2}$sec

Environment:

K_1	=	0.768	N_2 } Air
K_2	=	0.232	O_2 } Air

Arc Conditions:

p_o	=	1.44	atm
$\dot{m}$	=	0.0349	lb/sec
p_e	=	37	mm Hg
d_e	=	1.50	inch
A/A_*	=	4.00	
Config.	=	SUBS	

Conditions at Stream Centerline.

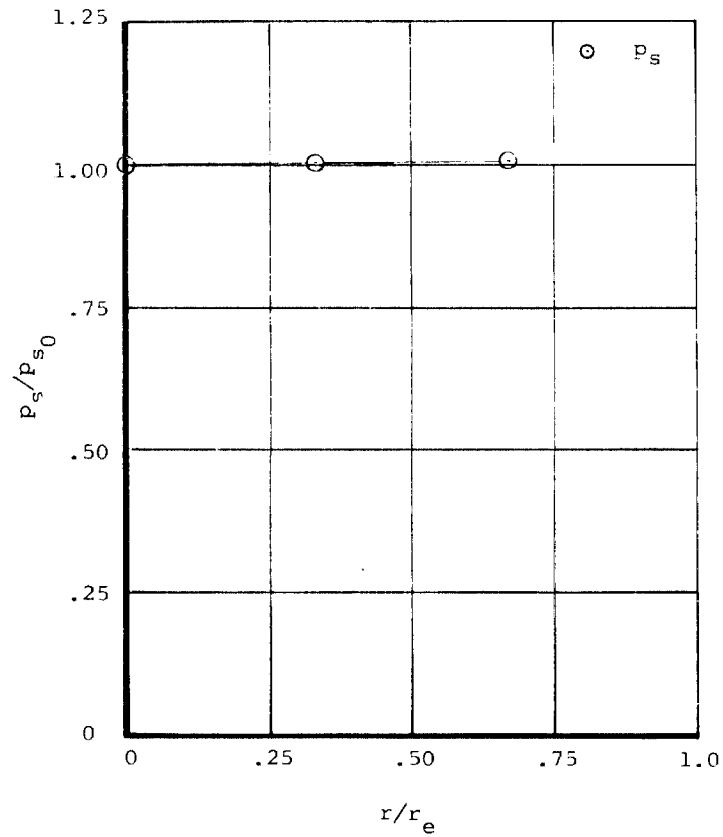

Distribution of Stagnation Pressure

*not applicable

(c) **TEST CONDITION** 39

Figure 6-10. Concluded.

or along the constrictor column (SUPS configuration). Certain explanation of the data presented is also appropriate and is presented in the succeeding paragraphs.

The calibration data for Phase I - Shear (Test Conditions 8-12 and 50-55) are presented in Figure 6-2. The wall shear stress was calculated by Reynolds analogy using the measured cold wall heating rate, a calculated edge velocity, and the measured total enthalpy. The duct flow calibration data were acquired with a cooled wall replacing the ablation model and hence these data represent the conditions prior to the onset of ablation. The Phase II - Combined Convective and Radiative Heating tests were conducted in the NASA Ames Entry Heating Simulator. The calibration data were acquired by measuring the mass balance enthalpy and convective heating conditions and then varying the radiative heating to obtain selected ratios of radiative to convective heating. The radiative heating was measured prior to and after each model test. Hence the calibration data (Test Conditions 56 through 70), presented in Figure 6-3, represent the 3 convective heating conditions each with 5 separate radiative heating conditions imposed. In addition, 5 purely radiative test conditions (71 through 75) were used but are not included in the calibration data since they involved only the radiative heat rate. The NASA-Ames facility did not have provision for radial survey of the various measurements; therefore, no streamwise profiles are presented.

The calibration data for Phase III - High Stagnation Pressure (test conditions 40 through 49) is presented in Figure 6-4. There are no radial profiles of heating rate due to the small test stream size which did not permit discrete measurements with the calorimeters employed; hence, there are no profiles of enthalpy. Also it should be noted that the calorimeter and model size were larger than the jet size which precluded an accurate evaluation of the stagnation point velocity gradient and in turn the $q_c\sqrt{R}$ heating rate.

The balance of the calibration data for Phase IV through VII are presented in Figures 6-5 through 6-10. The basic data including pressure, heating rate and enthalpy, radial profiles of the parameters and other pertinent test information are presented. The enthalpy profile shown was calculated as discussed in Section 5.3. The results of two calorimeter measurements are shown for comparative purposes, however the primary data were always taken from Calorimeter Number 1 which was considered to be the most accurate and reliable instrument for the particular configuration. It should be noted that certain test conditions were duplicated between phases and are so indicated on the calibration data figures. Exceptions to the standard format occur in Phase IV B (Figure 6-6) wherein no radial profiles were measured for the test conditions which did not involve air.

In addition to the basic calibration data taken for each test condition, other measurements were made at selected conditions to aid in defining the environment. These included measurements of heating rate distribution over a spherically blunted body, radiation from the arc column, radial variation of stream composition and measurements of test stream contamination.

6.1.2 Spherical Nose Heating Rate Distribution

The heating rate distribution was measured over the face of the 2.0 inch diameter blunt hemisphere (BH/2.0/T) configuration using 3 transient or slug sensors located at the stagnation point, 15 degrees away from the stagnation point and in the cylindrical region of the body (90°). A schematic of this calorimeter is shown in Figure 6-11. Measurements were made at 5 test conditions, each with the arc heater in the supersonic anode configuration which induces the largest radial gradients in conditions away from the stagnation point. The data acquired with this calorimeter are unfortunately of questionable value since the 15° and 90° sensors worked only intermittently. In the cases where the 15° calorimeter did work, its indicated heat flux was found to correlate with the radial heat flux distribution measured by traversing the test stream at the same test condition. The model heat flux distribution is therefore influenced directly by the stream heat flux distribution as might be expected. The 90° calorimeter results indicated that the side wall heating was low, about 10 to 15 percent of the stangation point value. No other conclusions from these results are possible.

6.1.3 Arc Column Radiation

A special calorimeter was constructed to assess the level of radiant heating emitted from the arc column while testing with the supersonic anode configuration. The radiation calorimeter, designated RAD/0.75/T, described in Section 5-2, was used to compare the total incident and radiant heating rates existing in the test stream at 3 operating conditions. The measurements are shown below in Table 6-2 which reveals the radiative component of the

TABLE 6-2

RADIATION PROBE DATA

Enthalpy h_{hf} (Btu/lb)	Stagnation Pressure p_s (atm)	Incident Heating Rate q_t (Btu/ft^2 sec)	Radiant Heating Rate q_{RAD} (Btu/ft^2 sec)
32,100	0.032	875	4.5
31,800	0.026	463	< 10
20,500	0.022	258	< 10

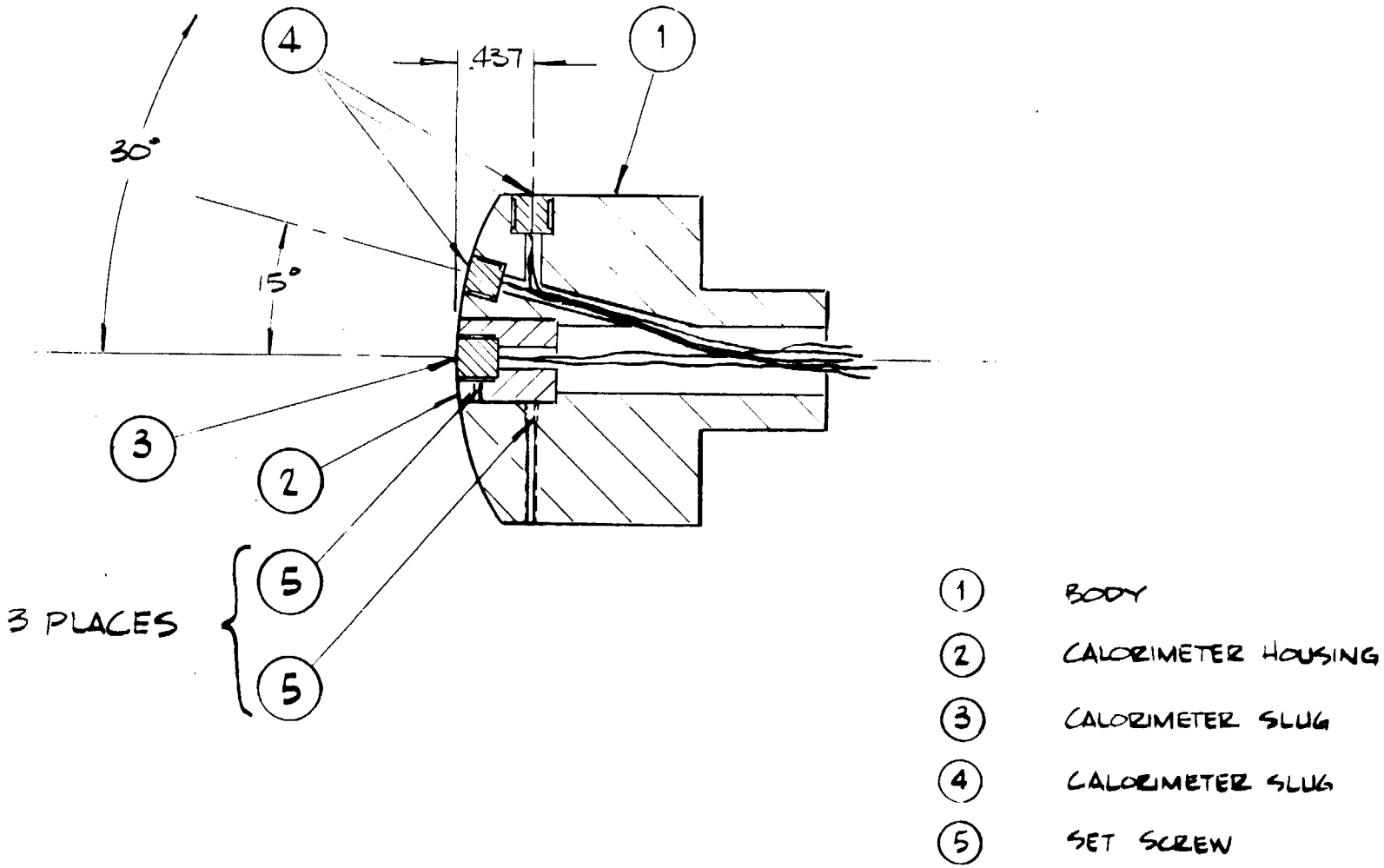

FIGURE 6-11 BLUNT HEMISPHERE TRANSIENT CALORIMETER.

heating on the calorimeter surface to be negligible for these high enthalpy conditions.

6.1.4 Test Stream Composition

Evaluation of the test stream composition was made at the centerline and 3 radial locations for 5 test conditions. The technique involved aspirating samples of the test stream into flasks and analyzing their contents by mass spectrometry. (See Section 5-4 for further discussion of the technique.) The sampling tests were conducted at varied arc heater operating conditions to insure a representative spread of data over the pressure and enthalpy spectrum. Unfortunately the results from one of the five tests were lost during the gas analysis due to equipment malfunction. Hence the results of gas sample analysis are presented for four test conditions representing enthalpies between 3,800 and 10,200 Btu/lb and stagnation pressures between 0.055 and 0.375 atmospheres.

The analysis revealed varying amounts of nitrogen, oxygen, argon, carbon dioxide and nitric oxide. The data as determined from the mass spectrograph are shown in Table 6-3. These results have been further reduced to measured mass fractions of total nitrogen and oxygen and compared in Table 6-4 to the ideal or injected concentrations of nitrogen and oxygen as determined from the flow meter readings recorded during the sampling tests. It should be noted that no contaminates existed in the nitrogen and oxygen gas supply systems. From Table 6-4 it can be seen that the measured oxygen concentration varied by as much as a factor of about three lower than the ideal (perfectly mixed test stream) value shown. Examination of the results reveals a deficiency of oxygen at all locations across the stream or a total deficiency on an integrated basis. Since the input metering systems were thoroughly calibrated it can only be assumed that the oxygen reacted with the arc heater walls or reacted with or was adsorbed by the sampling apparatus (lines, tubes, valves, and flasks) and was not detected in the analysis. The latter is strongly suspected since a flexible hose and valve seals of organic material were used in the sampling line. Although it was originally assumed that the sample would cool sufficiently in the water cooled portion of the sample probe to preclude these problems, it is entirely possible that a reaction of the sample with the flexible hose and valve seals could have occurred during the aspiration of the sample into the collection flask. The possibility of sample flask contaminates and analysis error, of course, also exists. Furthermore, in that the samples were taken at subatmospheric pressure, the total sample mass was small. Therefore the slightest unaccounted consumption by reaction or adsorption would alter the results significantly and small amounts of contaminates could cause large errors. The results of previous stream

TABLE 6-3

RESULTS OF MASS SPECTROGRAPHIC ANALYSIS
OF TEST STREAM SAMPLES

Test Condition	Radial Position r/r_e	Percent by Mass						Enthalpy h_{eb} (Btu/lb)	Stagnation Pressure p_s (atm)
		He (1)	N_2	O_2	A	CO_2	NO		
39	0	80.8	16.8	2.35	0.022	0.022	0.007	3817	0.375
	0.333	81.0	16.1	2.70	0.019	0.019	0.099		
	0.667	81.0	15.3	3.28	0.012	0.043	0.406		
	1.0	—	75.2	21.8	0.069	0.281	2.577		
28	0	0	79.9	19.0	0.601	0.271	0.221	4432	0.067
	0.286		83.8	15.4	0.095	0.268	0.348		
	0.572		79.3	19.8	0.124	0.176	0.515		
	0.856		93.5	5.88	0.068	0.250	0.340		
29	0		81.7	17.7	0.110	0.316	0.160	10207	0.055
	0.286		93.0	5.80	0.103	0.544	0.579		
	0.572		95.0	3.84	0.095	0.444	0.646		
	0.856		89.6	9.61	0.112	0.239	0.457		
13	0		76.9	18.1	0.337	4.44	0.194	9580	0.162
	0.333		81.2	18.2	0.111	0.212	0.269		
	0.667		78.9	17.5	0.078	0.412	3.02		
	1.0		82.1	17.4	0.080	0.163	0.230		

(1) For test condition 39 Helium was used as an inert diluent to raise bottle pressures to superatmospheric pressure.

TABLE 6-4

MEASURED NITROGEN AND OXYGEN CONCENTRATION IN TEST STREAM

Test Condition	Radial Position r/r_e	Sample Concentration Mass Percent N_2	Sample Concentration Mass Percent O_2	Ideal Concentration Mass Percent N_2	Ideal Concentration Mass Percent O_2
39	0	87.6	12.4	76.8	23.2
	0.333	85.4	14.6		
	0.667	81.4	18.5		
	1	76.6	23.4		
28	0	80.5	19.5		
	0.286	84.1	15.9		
	0.572	79.7	20.3		
	0.856	93.7	6.3		
29	0	81.8	18.2		
	0.286	93.4	6.61		
	0.572	95.4	4.61		
	0.856	89.9	10.1		
13	0	79.0	21.0		
	0.333	81.5	18.5		
	0.667	80.7	19.3		
	1	82.2	17.7		

sampling at superatmospheric pressures have revealed excellent results (Reference 6-1). In this case no organic materials were used and the sample pressures were high. In summary, the mass spectrographic results of Tables 6-3 and 6-4 are felt to be in error and are not representative of the overall nitrogen and oxygen concentrations or of their distribution across the stream.

6.1.5 Test Stream Contamination

A semi-quantitative calibration of stream contamination was conducted by two methods: 1) measurement of arc heater electrode weight loss and 2) the surface chemistry analysis of nylon samples exposed to the test stream for a short period of time. The electrode weight loss evaluation was made to determine if the amount of electrode material expended over a long period of time amounted to a significant percentage of the effluent gas. Measurements were made on 3 anodes and 3 cathodes each operated for cumulative times in excess of an hour and each subjected to many arc ignitions. In addition, a gas mass flow rate time history was maintained to estimate the total gas flow during the period of each electrode exposure. The results are presented in Table 6-5 in terms of apparent contamination level in parts per million. Although there were other arc heater components exposed to the gas it was found that their weight loss was negligible. The total contamination level in the stream therefore should not exceed 200 parts per million (0.02 percent) even at the highest pressure operation achieved under this contract. Note that this level also includes several arc starts, the condition for which most of the electrode losses are felt to occur. The test stream should have a much lower contamination level during a model test when conditions are stable. Note also that the above maximum contamination level will decrease with decreasing chamber pressure.

The nylon sample tests were run to qualitatively evaluate the existence of any solid or liquid phase contaminates in the test stream which might deposit on an ablation model. The nylon samples, 2-inch diameter flat face cylinders, were exposed to the jet for approximately 3 seconds. After testing, the samples were carefully encapsulated to preserve the surface composition. The sample surfaces were then analyzed by semi-quantitative spectrographic analysis in which a layer of the surface was removed, reduced to ash and quantitatively analyzed by flame spectroscopy. The basic constituents of nylon (carbon, hydrogen, oxygen and nitrogen) were reduced to oxides and nitrides leaving only the contaminates of the raw material and any matter from the test stream. The results of the analysis are shown in Table 6-6. Specimen G-5 was a control model which was taken from the same nylon stock but was not exposed to the test stream. As evident from the results, the nylon itself contained all of the observed elements in varying amounts and

TABLE 6-5

ELECTRODE WEIGHT LOSS

Electrode Type/Serial No.	Mass Loss (lb)	Exposure Time (sec)	Mass Loss Rate (lb/sec)	Estimated Average Gas Flow Rate (lb/sec)	Apparent Contamination Level (PPM)	Operating Conditions		
						Range of p_o (atm)	Range of h_{eb} (Btu/lb)	Number of Starts(1)
Anode/48	476×10^{-4}	132×10^{2}	36.1×10^{-7}	4.9×10^{-2}	73.8	1-6	3500-5000	67
Cathode/9	35.2×10^{-4}	27.2×10^{2}	12.9×10^{-7}	5.1×10^{-2}	25.4	2-6	|	28
Cathode/10	11.0×10^{-4}	59.2×10^{2}	1.86×10^{-7}	3.9×10^{-2}	4.78	.5-3	1600-9000	29
Anode/31	8.81×10^{-4}	21.2×10^{2}	4.16×10^{-7}	2.4×10^{-2}	17.4	.5-1.2	5000-10000	15
Anode/56		4.79×10^{2}	18.4×10^{-7}	2.6×10^{-2}	70.6	1.5-2.5	|	6

(1) Estimated number of starts for exposure time.

TABLE 6-6

NYLON SAMPLE ANALYSIS

	Sample Number			
	G1	G2	G4	G5 (1)
Test Condition	39	13	29	—
Exposure Time (sec)	3.5	3.8	4.0	—
Element and Qualitative Amount Present (PPM)				
Si	7.9	5.4	7.8	12
Mn	0.8	1	1	0.8
Mg	1.8	0.5	0.4	1.6
Fe	1.2	1.1	0.6	1
Al	2.6	1.4	2.3	3.4
Cu	1.4	0.9	0.4	0.5
Na	7.9	11	2.9	2.6
Ti	0.2	0.1	0.1	0.2
Ca	3.4	8.9	5.8	2
Cr	0.2	0.2	0.1	0.1
Ba	0.03	0.03	0.03	0.2
W	<4	<4	<4	<4
Ni	0.2	—	—	—
Ag	0.2	—	—	—
Rh	1	—	—	—

(1) Control sample, not exposed.

the expected contaminates, copper, zirconium, boron nitride and tungsten, were not present in significant amounts.

6.2 MODEL TEST RESULTS

A total of 158 ablation model tests were conducted at different test conditions under the seven phases of the program. Measurements of the operating conditions, model dimensional and weight change, surface and internal temperature histories and photographic documentation were made for each model test. The seven phases of the program, discussed in Section 6.1.1, included detailed examination of the effects of shear, combined convective and radiative heating, high and low stagnation pressure, model shape, model size, chemical environment, enthalpy, and convective heating rate.

The test results are presented in three major groups of data: first, a tabulation of the operating conditions and test model response; second, the surface and internal temperature histories; and last, the pre- and post-test photographs of each model. The operating conditions and model response information are presented by phase in Tables 6-7 through 6-15 respectively. The operating condition measurements and model response measurements presented in the tables were made as presented in Section 5. Data lost due to instrumentation failure are indicated by a dashed line in the tables. The surface and internal temperature histories are presented by phase in Figures 6-12 through 6-20. A fine grid transparent overlay for these plots is included in the cover flap for ease in the quantitative review of the plots. The temperature measurements were made as presented in Section 5. In all cases, the surface temperature is that indicated by the infrared pyrometer. The pre-test photographs of typical models, including all configurations used in the program, are presented in Figure 6-21. The post-test photographs of each model are presented by phase in Figures 6-22 through 6-30.

In 42 model tests, duplicate surface temperature measurements were made with a total radiation pyrometer. Representative results for four tests and their comparison with the infrared pyrometer results are presented in Figure 6-31 (in all cases $\varepsilon = 0.75$). Seventy-five percent of the comparisons agree to within about 5 percent while the remainder show the total radiation pryometer to give results generally 10 percent below the infrared pyrometer. This is felt to be due to the large spot size for the total radiation pyrometer and the associated problems of measuring temperature over a large surface area, sensitivity to incidence angle, and the loss of full view of the model as surface recession occurs. Because of these problems, the infrared pyrometer was used as the standard in all tests.

TABLE 6-7

ABLATION MODEL TEST RESULTS

PHASE I SHEAR

Model No.	Test Condition	Enthalpy h (Btu/lb)	Chamber Pressure p_o (atm)	Heating Rate q (Btu/ft^{2}sec)	Shear Stress τ_w (1) (psf)	Chemical Environment	Exposure Time θ (sec)	Surface Recession s (inch)	Char Thickness (inch)	Pyrolysis Zone Thickness (inch)	Mass Loss M (gm)	Avg. Recession Rate $\dot{s}$ (mils/sec)	Aerotherm Test No.
6/D/.22	50	5430	1.38	348	2.67	Air	29.6	0.308	0.078	—	0.807	10.4	377
9/D/.22			1.40	337			29.7	0.283	0.062	—	1.040	9.52	378
12/D/.22		5220	1.41	319			30.4	0.096	0.125	—	0.729	3.16	379
1/D/.22	51	5310	2.25	464	10.50		16.1	0.280	0.060	—	0.866	17.4	1481
8/D/.22		4750	2.32	509				0.233	0.046	—	0.949	14.5	1482
11/D/.22		5800	2.76	683			17.5	0.155		—	0.849	8.86	1495
2/D/.22	52	3780	5.08	414	19.10		10.7	0.428	0.020	—	1.204	40.0	1483
7/D/.22		4500	5.11	432			12.1	0.353	0.015	—	1.241	29.2	1484
10/D/.22		4310		536			5.9	0.154	0.005	—	0.609	26.1	1499
5/D/.22	53	5250	1.16	248	2.67	Nitrogen	30.2	0.011	0.218	—	0.382	0.36	382
3/D/.22	54	4740	2.48	609	10.00		16.4	0.231	0.030	—	0.659	14.1	1490
4/D/.22	55	3740	5.62	409	18.70		11.9	0.333	0.046	—	1.275	28.0	1491
67/D/.22	8	4290	1.38	413	7.16	Air	11.6	0.210/.295	0.035	0.015	0.695	18.1/25.4	712
68/D/.22		4050	1.42	370			11.4	0.175/.270	0.07	0.01	0.612	15.3/23.7	713
64/D/.22	7	4030	1.65	472	7.95	Nitrogen	27.4	0.050/.380			0.743	1.82/13.9	710
65/D/.22		3970	1.64	423			28.8	0.260/.465	0.14	0.02	0.934	9.0/16.1	711
73/D/.22	9	3730	1.14	383	2.71	Air	8.3	0.061	0.08	0.01	0.242	7.35	721
70/D/.22		4240	1.12	310			15.7	0.165/.210	0.055	0.015	0.630	10.5/13.4	722
69/D/.22	11	4340	1.20	262	3.38	Nitrogen	27.9	0.014	0.19	0.05	0.320	0.50	720
72/D/.22	10	10180	1.10	556	3.25	Air	12.5	0.086	0.08	0.02	0.833	6.88	723
71/D/.22		10130		508			15.7	0.110	0.10		0.426	7.00	724
66/D/.22	12	9700	1.13	545	2.91	Nitrogen	28.7	0.021	0.22	0.05	0.399	0.73	719

(1) Nominal initial shear stress.

TABLE 6-8

ABLATIVE MODEL TEST RESULTS

PHASE II COMBINED CONVECTIVE AND RADIATIVE HEATING

Model No.	Test Condition	Enthalpy h (Btu/lb)	Stagnation Pressure p_s (1) (atm)	Heating Rate Convective q_c (2) (Btu/ft²sec)	Heating Rate Radiative q_r (3) (Btu/ft²sec)	Chemical Environment	Exposure Time θ (sec)	Surface Recession s (inch)	Char Thickness (inch)	Pyrolysis Zone Thickness (inch)	Mass Loss M (gm)	Avg. Recession Rate $\dot{s}$ (mils/sec)	Test No.
46/FF/1.25	56	3090	0.112	157	0/0	Air	20.1	0.070	0.09	0.02	0.063	3.48	66
38/FF/1.25	57	3100		164	80/83			0.095	0.07		0.105	4.73	69
45/FF/1.25	58	3210		168	154/151		15.1	0.090		0.01	0.076	6.00	72
50/FF/1.25	59	3120			340/332		10.1	0.069		0.02	0.065	6.73	73
62/FF/1.25	60	3050		170	490/510		8.1	0.105	0.05	0.01	0.068	12.96	76
51/FF/1.25	56	3290		148	0/0		30.2	0.112	0.07	0.015	0.088	3.71	216
61/FF/1.25		3260			0/0		—	0.110	0.08	0.01	0.080	—	217
54/FF/1.25	58	3250			149/150		20.2	0.138	0.05	0.02	0.099	6.83	218
55/FF/1.25	59	3420			343/360		20.1	0.121	0.07		0.096	6.02	219
37/FF/1.25	61	5020	0.071	102	0/0		25.1	0.025	0.11	0.01	0.070	1.00	156
39/FF/1.25	62	5130			68/64		26.0	0.081	0.09	0.02	0.064	3.12	157
63/FF/1.25	63	5120		95	108/106		25.1	0.032	0.11		0.083	1.27	160
40/FF/1.25	64	5130			230/199		25.2	0.072	0.12	0.03	0.086	2.86	161
47/FF/1.25	65	5060			475/470		15.1	0.090	0.08	0.02	0.093	5.96	162
49/FF/1.25	66	6290	0.099	214	0/0		25.3	0.103	0.09		0.092	4.07	201
53/FF/1.25	67	6780			117/105			0.140			0.105	5.53	203
60/FF/1.25	68	6410			240/190		20.2	0.082	0.10		0.094	4.06	204
52/FF/1.25	69	6390			355/343		15.1	0.065	0.105	0.03	0.078	4.30	207
44/FF/1.25	70	6170			406/375		15.2	0.082	0.10	0.015	0.094	5.39	208
48/FF/1.25	71	—	0	0	101/91	Vacuum	20.8	0.012	0.09	0.02	0.045	0.58	220
42/FF/1.25	72	—			220/216		20.0	0.032	0.08		0.065	1.60	221
56/FF/1.25	73	—			309/281			0.022	0.12	0.01	0.047	1.10	222
57/FF/1.25	74	—			486/488		15.0	0.059	0.11	0.02	0.059	3.93	223
58/FF/1.25	75	—			592/546		15.1	0.104		0.01	0.130	6.89	224

(1) Stagnation pressure as measured during calibration run previous to model test.

(2) Convective heat flux as measured during calibration run previous to model test.

(3) Prerun/postrun radiative heating rates.

TABLE 6-9

ABLATION MODEL TEST RESULTS

PHASE III HIGH STAGNATION PRESSURE

Model No.	Test Condition	Enthalpy h (Btu/lb)	Stagnation Pressure p_s (atm)	Heating Rate $q_c\sqrt{R}$ (Btu/ft$^{3/2}$sec)	Chemical Environment	Exposure Time Θ (sec)	Surface Recession s (inch)	Char Thickness (inch)	Pyrolysis Zone Thickness (inch)	Mass Loss M (gm)	Avg. Recession Rate $\dot{s}$ (mils/sec)	Aerotherm Test No.
154/BH/1.0	43	5031	1.06	318	Air	15.2	0.585	0.04	0.008	0.670	38.5	869A
158/BH/1.0						10.2	0.509		0.01	0.833	50.0	869B
113/BH/1.0		5047	1.05	326		5.1	0.240	0.02/.05	0.005	0.383	47.0	870A
151/BH/1.0	42	4975	1.11	302	Nitrogen	20.2	0.435/0.465	0.06/.10	0.01/.035	0.797	21.5/23.0	867A
152/BH/1.0						10.1	0.275/0.435	0.02/.06	0.01	0.617	27.2/43.0	867B
156/BH/1.0	40	3456	1.02	218	Air	20.6	0.635/0.735	0.03/.04	0.005	1.088	30.8/35.6	868A
157/BH/1.0						10.5	0.355/0.525	0.033	0.007	0.643	33.8/50.0	868B
134/BH/1.0		3310	1.01	226		5.1	0.311	0.02	0.005	0.442	61.0	870B
149/BH/1.0	41	3556		239	Nitrogen	30.1	0.598/0.875	0/.06	0.005/.01	1.266	19.0/29.0	866A
150/BH/1.0						15.0	0.292	0.065	0.02	0.522	19.4	866B
139/BH/1.0	44	3251	1.93	313	Air	7.3	—	—	—	—	—	875A
153/BH/1.0						5.4	0.485/0.875	0/.025	0.005	0.952	90.0/162	875B
144/BH/1.0		3115	1.94	305		1.9	0.203	0.015		0.300	107	876A
145/BH/1.0							0.305/0.515	0.01/.02	0.008	0.582	160/271	876B
146/BH/1.0	45	3460	2.05	288	Nitrogen	10.2	0.759	0.025	0.00[illegible]	1.223	74.4	874A
147/BH/1.0						5.4	0.220	0.040		0.424	40.7	874B
136/BH/1.0	49	5015	3.16	493	Air	3.2	0.365	0/.015		0.490	114	882A
135/BH/1.0		5224	3.08	489			0.375/0.545	0		0.785	117/186	885A
155/BH/1.0		5367	3.10	480		1.84	0.227	0.007		0.317	123	886
137/BH/1.0		5015	3.16	493		2.8	0.365/0.455	0/.01		0.648	130/162	882B
148/BH/1.0		5224	3.08	489		1.8	0.205/0.335	0.005/.03	0.003/.015	0.428	114/186	885B
140/BH/1.0		5151	3.10	480		2.9	0.418	0.01	0.005	0.717	144	884B
132/BH/1.0	48	4602	3.16	484	Nitrogen	3.98	0.405/0.632	0/.03		0.792	101/158	881A
133/BH/1.0							0.275/0.365	0.02/.04		0.439	68.8/91.3	881B
142/BH/1.0	46	3518	3.01	332	Air	4.28	0.405/0.525	0.01		0.778	94.2/122	883A
143/BH/1.0						2.54	0.255/0.445	0.007		0.517	101/175	883B
141/BH/1.0		3519	3.08	327		3.40	0.345/0.475	0.01		0.639	101/140	884A

TABLE 6-9 CONCLUDED

ABLATION MODEL TEST RESULTS

PHASE III HIGH STAGNATION PRESSURE

Model No.	Test Condition	Enthalpy h (Btu/lb)	Stagnation Pressure p_s (atm)	Heating Rate $q_c\sqrt{R}$ (Btu/ft$^{1/2}$ sec)	Chemical Environment	Exposure Time Θ (sec)	Surface Recession s (inch)	Char Thickness (inch)	Pyrolysis Zone Thickness (inch)	Mass Loss M (gm)	Avg. Recession Rate $\dot{s}$ (mils/sec)	Aerotherm Test No.
130/BH/1.0	47	3471	3.23	351	Nitrogen	3.67	0.384	0.01	0.008	0.594	104	880A
131/BH/1.0		3532	3.28	346		2.90	0.235/0.495	0.025	0.005	0.640	81.0/171	880B

TABLE 6-10

ABLATION MODEL TEST RESULTS

PHASE IV A LOW STAGNATION PRESSURE AND EXPOSURE TIME

Model No.	Test Condition	Enthalpy h (Btu/lb)	Stagnation Pressure p_s (atm)	Heating Rate $q_c\sqrt{R}$ (Btu/ft$^{3/2}$sec)	Chemical Environment	Exposure Time Θ (sec)	Surface Recession s (inch)	Char Thickness (inch)	Pyrolysis Zone Thickness (inch)	Mass Loss M (gm)	Avg. Recession Rate $\dot{s}$ (mils/sec)	Aerotherm Test No.
93/BH/2.0	26	3442	0.0082	12.8	Air	210.2	0.100	0.22	0.10	1.689	0.48	772B
95/BH/2.0		3539		13.3		120.3	0.076	0.16	0.05	1.187	0.63	773B
94/BH/2.0						60.6	0.049	0.10	0.045	0.713	0.81	773A
89/BH/2.0	24	4944	0.0090	18.7		210.5	0.114	0.26	0.07	1.882	0.54	769A
88/BH/2.0		5044	0.0110	17.9		121.1	0.077	0.16	0.09	1.349	0.64	768A
87/BH/2.0		4910	0.0112	18.5		61.0	0.055	0.10	0.04	0.823	0.90	767A
92/BH/2.0	25	10193	0.0079	48.6		120.3	0.300	0.18	0.06	2.361	2.49	772A
91/BH/2.0		10969	0.0079	45.8		60.5	0.152	0.085	0.08	1.274	2.51	770B
90/BH/2.0						30.3	0.077	0.07	.03	0.723	2.54	770A
106/BH/2.0	37	16880(1)	0.0082	63.6		90.4	0.217	0.14	0.05	1.832	2.40	856A
108/BH/2.0		16301(1)	0.0080	60.8		60.4	0.147	0.10	0.07	1.515	2.44	855B
99/BH/2.0						30.3	0.078		0.04	0.800	2.57	855A
163/BH/2.0	36	25800(1)	0.0085	99.0		31.5	—	—	—	—	—	857B
166/BH/2.0		29400(1)		113		70.0	0.184	0.26	0.06	2.129	2.63	859B
162/BH/2.0		25800(1)		99.0		60.5	0.153	0.14	0.06	2.697	2.53	857A
109/BH/2.0		25600(1)		98.1		30.3	0.076	0.11	0.04	0.930	2.50	856B

(1) h_{hf}

TABLE 6-11

ABLATION MODEL TEST RESULTS

PHASE IV B LOW STAGNATION PRESSURE AND CHEMICAL ENVIRONMENT

Model No.	Test Condition	Enthalpy h (Btu/lb)	Stagnation Pressure P_s (atm)	Heating Rate $q_c\sqrt{R}$ (Btu/ft$^{1/2}$ sec)	Chemical Environment K	Exposure Time Θ (sec)	Surface Recession s (inch)	Char Thickness (inch)	Pyrolysis Zone Thickness (inch)	Mass Loss M (gm)	Avg. Recession Rate $\dot{s}$ (mils/sec)	Aerotherm Test No.
74/BH/2.0	1	6322	0.0261	51.4	Air	60.7	0.160	0.10	0.04	1.531	2.64	746A
79/BH/2.0	14	5730	0.0276	39.0	.700 N_2/.300 O_2	61.0	0.196	0.09	|	1.669	3.21	748B
78/BH/2.0	15	5640	0.0283	34.9	.850 N_2/.150 O_2	60.6	0.144	0.15	|	1.299	2.38	748A
77/BH/2.0	16	5511	0.0296	29.9	.930 N_2/.070 O_2	61.4	0.114	0.16	|	1.232	1.86	747B
23/BH/2.0	17	5801	0.0278	59.5	Nitrogen	60.8	0.050	0.21	0.06	2.273	0.82	751A
76/BH/2.0	|	5961	0.0297	74.0	|	60.5	0.082	|	0.05	1.230	1.36	747A
84/BH/2.0	22	10918	0.0298	|	Helium	60.3	0.023	0.19	0.12	1.024	0.38	758A
85/BH/2.0	|	|	|	|	|	60.9	0.022	0.25	0.055	1.071	0.36	758B
75/BH/2.0	2	11578	0.0283	79.1	Air	60.6	0.301	0.10	0.03	2.152	4.97	746B
81/BH/2.0	18	10100	0.0269	74.8	.700 N_2/.300 O_2	60.4	0.316	0.09	0.04	2.203	5.23	749B
83/BH/2.0	19	10850	0.0290	68.5	.850 N_2/.150 O_2	61.0	0.242	0.14	|	1.982	3.97	750B
82/BH/2.0	20	10445	|	84.3	.930 N_2/.070 O_2	60.3	0.215	0.16	|	1.912	3.57	750A
80/BH/2.0	21	9960	0.0276	107	Nitrogen	60.6	0.172	0.12	0.11	1.767	2.84	749A
24/BH/2.0	|	11013	0.0264	110	|	60.4	0.109	0.22	0.05	1.748	1.80	751B
101/BH/2.0	30	17400(1)	0.0287	123	Air	45.2	0.215	0.08	0.04	1.746	4.76	834A
104/BH/2.0	32	15620(1)	0.0266	85.9	.700 N_2/.300 O_2	44.9	0.229	|	|	1.768	5.10	841A
98/BH/2.0	33	17290(2)	0.0283	114	.850 N_2/.150 O_2	45.0	0.181	0.125	0.035	1.641	4.02	842A
107/BH/2.0	34	18040(1)	0.0275	117	.930 N_2/.070 O_2	|	0.135	0.16	0.04	1.527	3.00	843A
105/BH/2.0	35	16930(2)	0.0254	143	Nitrogen	45.3	0.120	0.19	0.055	1.563	2.65	841B
103/BH/2.0	|	16830(2)	0.0258	152	|	45.1	0.121	|	0.05	1.488	2.68	842B
161/BH/2.0	|	17000(1)	0.0254	165	|	44.9	0.107	0.20	0.02	1.347	2.38	843B
86/BH/2.0	23	18019	0.0278	118	Helium	45.0	0.029	0.27	0.05	1.242	0.64	759

(1) h_{hf}

(2) Based on the assumption that $\frac{h_{hf}}{h_{eb}} = \left(\frac{h_{hf}}{h_{eb}}\right)_{air}$

TABLE 6-12

ABLATION MODEL TEST RESULTS

PHASE V MODEL SIZE AND EXPOSURE TIME

Model No.	Test Condition	Enthalpy h (Btu/lb)	Stagnation Pressure p_s (atm)	Heating Rate $q_c\sqrt{R}$ (Btu/ft$^{1/2}$ sec)	Chemical Environment	Exposure Time θ (sec)	Surface Recession s (inch)	Char Thickness (inch)	Pyrolysis Zone Thickness (inch)	Mass Loss M (gm)	Avg. Recession Rate $\dot{s}$ (mils/sec)	Aerotherm Test No.
114/BH/4.0	24	4910	0.0112	18.5	Air	211.4	0.085	0.22	0.15	1.624	0.40	767B
115/BH/4.0		5044	0.0110	18.0		120.5	0.061	0.17	0.05	1.185	0.51	768B
116/BH/4.0		4944	0.0090	18.8		60.4	0.035	0.10	0.08	0.735	0.58	769B
128/BH/4.0	38	13500(1)	0.0081	50.9		90.2	0.137	0.13	0.06	1.641	1.52	859A
127/BH/4.0		14480(1)		54.2		59.9	0.082	0.17	0.04	1.189	1.37	858B
126/BH/4.0						30.6	0.043	0.10	0.02	0.696	1.40	858A
120/BH/4.0	28	4510	0.0275	27.5		90.3	—	—	—	1.213	—	821B
118/BH/4.0		4612	0.0279	29.3		54.2	—	—	—	0.930	—	820B
117/BH/4.0						30.3	0.026	0.08	0.04	0.582	0.86	820A
122/BH/4.0	29	10434	0.0275	74.8		60.6	0.168	0.14	0.04	1.724	2.77	822B
121/BH/4.0		11119	0.0283	66.1		28.0	—	—	—	1.393	—	822A
119/BH/4.0		10976	0.0279	65.0		30.8	0.096	0.10	0.04	0.990	3.12	821A
123/BH/4.0	30	15186(1)	0.0283	107		45.2		0.16	0.045	1.372	2.12	835B
125/BH/4.0		15891(1)	0.0279	111		29.8	0.056	0.12	0.04	1.058	1.88	836B
124/BH/4.0		19040(1)		133		20.0	0.045	0.08	0.04	0.717	2.25	836A

(1) h_{hf}

TABLE 6-13

ABLATION MODEL TEST RESULTS

PHASE VI A MODEL SHAPE CONSTANT ENTHALPY AND CONSTANT STAGNATION PRESSURE

Model No.	Test Condition	Enthalpy h (Btu/lb)	Stagnation Pressure p_s (atm)	Heating Rate $q_c\sqrt{R}$ (Btu/ft$^{1/2}$-sec)	Chemical Environment	Exposure Time θ (sec)	Surface Recession s (inch)	Char Thickness (inch)	Pyrolysis Zone Thickness (inch)	Mass Loss M (gm)	Avg. Recession Rate $\dot{s}$ (mils/sec)	Aerotherm Test No.
30/BH/2.0	1	5937	0.0275	45.8	Air	90.0	0.218	0.17	0.07	2.153	2.42	675A
25/BH/2.0		5447	0.0270	47.9		45.6	0.112	0.12	0.03	1.154	2.46	676A
19/FF/2.0		5582		33.4		90.0	0.139	0.17		1.701	1.54	674B
33/H/2.0		5640	0.0275	45.8		93.5	0.356	0.11	0.04	2.860	3.81	675B
28/BH/2.0	2	10357	0.0281	74.8		90.0	0.384	0.12		3.132	4.27	673B
29/BH/2.0		9554	0.0283	62.6		45.2	0.171	0.11		1.717	3.78	676B
17/FF/2.0		10357	0.0281	74.8		90.0	0.293	0.12	0.035	2.627	3.26	673A
35/H/2.0		10463		69.4			0.499	0.11	0.02	3.998	5.54	674A
100/BH/2.0	30	15800(1)	0.0285	111		27.3	0.132	0.09		0.995	4.84	831B
165/BH/2.0		17300(1)	0.0283	120		45.4	0.177	0.13	0.04	1.929	3.90	835A
164/BH/2.0		15800(1)	0.0285	111		30.5	0.106	0.11	0.03	1.330	3.48	831A
21/FF/2.0		14287(1)	0.0287	101		45.7	0.147	0.12	0.05	1.553	3.22	832B
20/FF/2.0		14844(1)		105		30.4	0.083	0.10	0.04	1.073	2.73	832A
159/H/2.0		17204(1)	0.0279	120		30.0	0.154	0.085	0.02	1.557	5.13	833B

(1) h_{hf}

TABLE 6-14

ABLATION MODEL TEST RESULTS

PHASE VI B MODEL SHAPE CONSTANT STAGNATION PRESSURE AND CONSTANT STAGNATION HEATING RATE

Model No.	Test Condition	Enthalpy h (Btu/lb)	Stagnation Pressure p_s (atm)	Heating Rate $q_c\sqrt{R}$ (Btu/ft$^{3/2}$/sec)	Chemical Environment	Exposure Time θ (sec)	Surface Recession s (inch)	Char Thickness (inch)	Pyrolysis Zone Thickness (inch)	Mass Loss M (gm)	Avg. Recession Rate $\dot{s}$ (mils/sec)	Aerotherm Test No.
26/BH/2.0	1	5549	0.0269	34.1	Air	90.0	0.255	0.16	0.02	2.286	2.84	682B
22/FF/2.0	4	7236	0.0265	45.3			0.205	0.14	0.04	2.029	2.28	683B
34/H/2.0	6	3692	0.0289	33.0			0.241	0.125	0.05	2.352	2.68	691
27/BH/2.0	2	10269	0.0282	71.3			0.391	0.16	0.06	3.219	4.34	683A
16/FF/2.0	31	14200(1)	0.0271	89.6		90.1	0.300	0.11	0.04	2.851	3.33	833A
36/H/2.0	3	7145	0.0272	49.6		90.0	0.402	0.09	0.03	3.330	4.47	682A
102/BH/2.0	30	16517(1)	0.0271	113		44.7	0.218	0.11	0.06	1.687	4.88	834B
18/FF/2.0	27	19201(1)	0.0293	137		42.5	0.165	0.13	0.04	0.891	3.88	804
32/H/2.0	5	10692	0.0286	111		45.0	0.261	0.11	0.03	2.258	5.80	684

(1) h_{hf}

TABLE 6-15

ABLATION MODEL TEST RESULTS

PHASE VII ENTHALPY AND STAGNATION PRESSURE AT CONSTANT HEATING RATE

Model No.	Test Condition	Enthalpy h (Btu/lb)	Stagnation Pressure p_s (atm)	Heating Rate $q_c\sqrt{R}$ (Btu/ft$^{1/2}$ sec)	Chemical Environment (inch)	Exposure Time θ (sec)	Surface Recession s (inch)	Char Thickness (inch)	Pyrolysis Zone Thickness (inch)	Mass Loss M (gm)	Avg. Recession Rate $\dot{s}$ (mils/sec)	Aerotherm Test No.
96/BH/2.0	27	18860(1)	0.0285	133	Air	30.8	0.148	0.11	0.03	0.924	4.81	803A
97/BH/2.0	|	|	|	|	|	31.0	0.155	0.13	0.10	1.350	5.00	803B
111/BH/1.0	13	10588	0.0817	156	|	39.6	0.388	0.08	0.02	0.724	9.80	732
112/BH/1.0	|	10548	0.0831	152	|	40.7	0.382	0.08	0.02	0.711	9.39	733
110/BH/1.0	|	10167	0.0827	154	|	24.6	0.232	0.06	0.01	0.448	9.43	731
31/H/2.0	|	10443	0.0842	145	|	40.5	0.338	0.045	0.03	2.538	8.35	734
129/BH/1.0	39	3515	0.373	140	|	20.1	0.325	0.04	0.01	0.586	16.20	889A
138/BH/1.0	|	|	|	|	|	15.4	0.247	0.055	0.015	0.422	16.00	889B

(1) h_{hf}

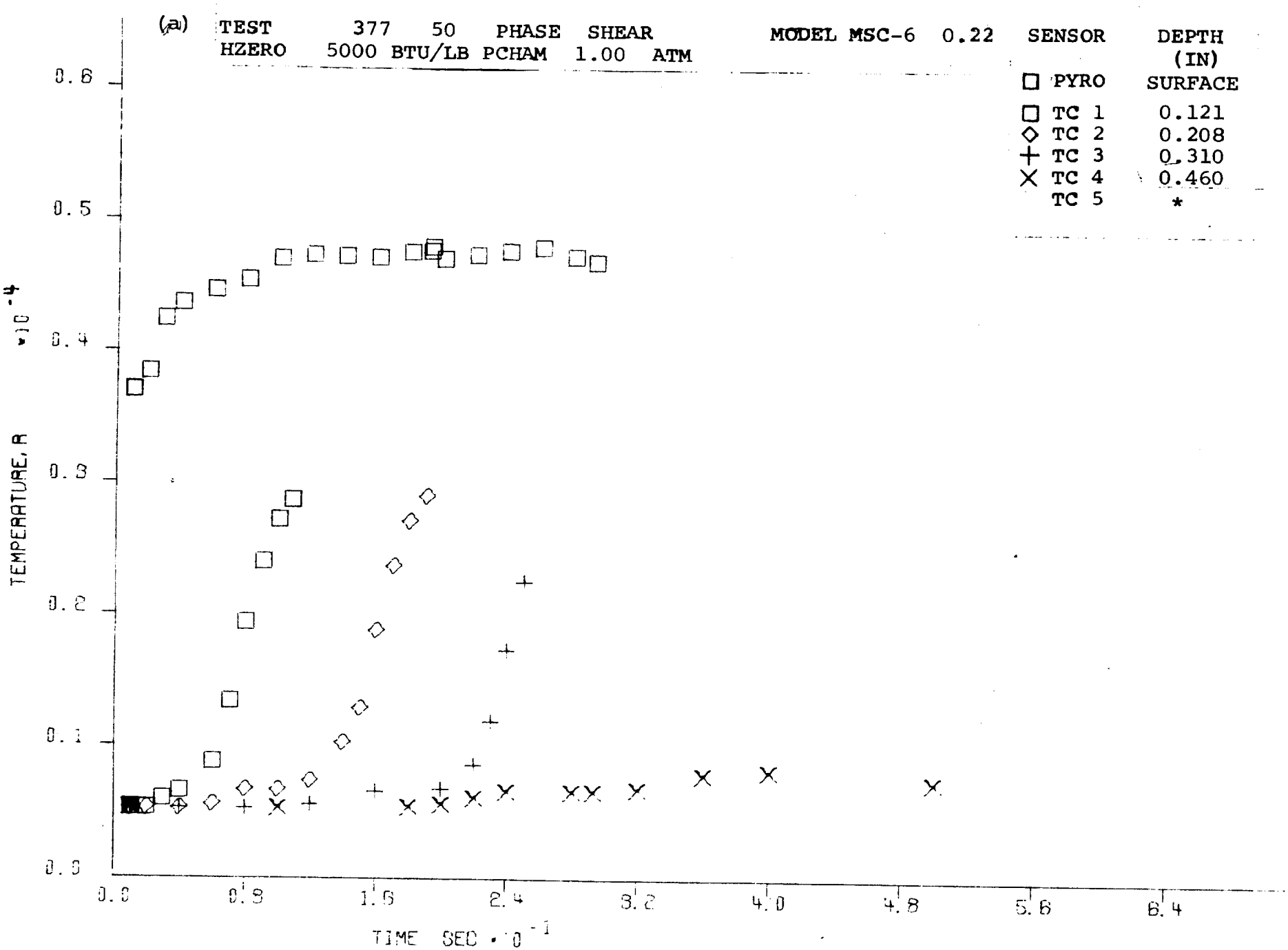

Figure 6-12. Surface and Internal Temperature Histories, Phase I.

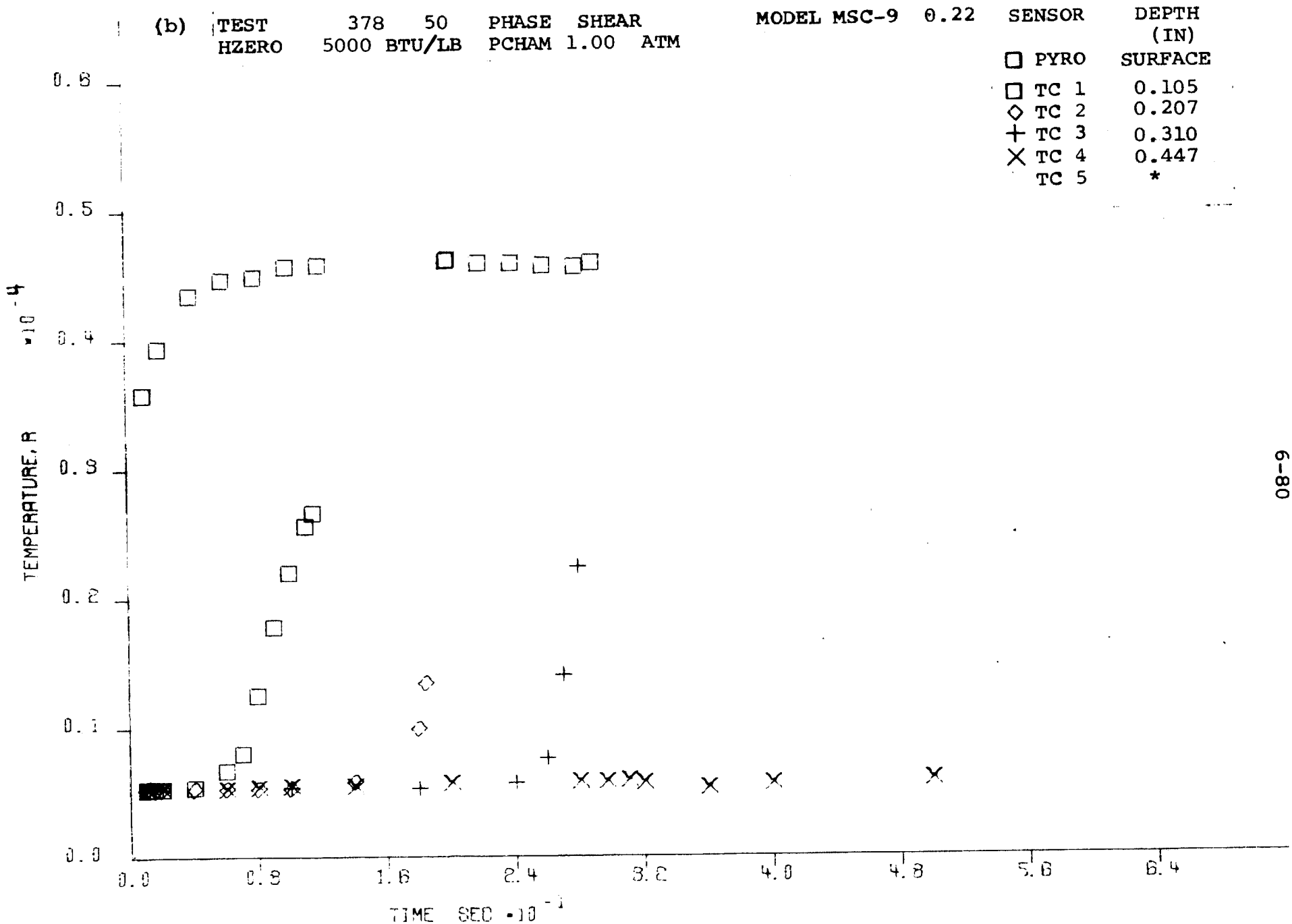

Figure 6-12. Continued.

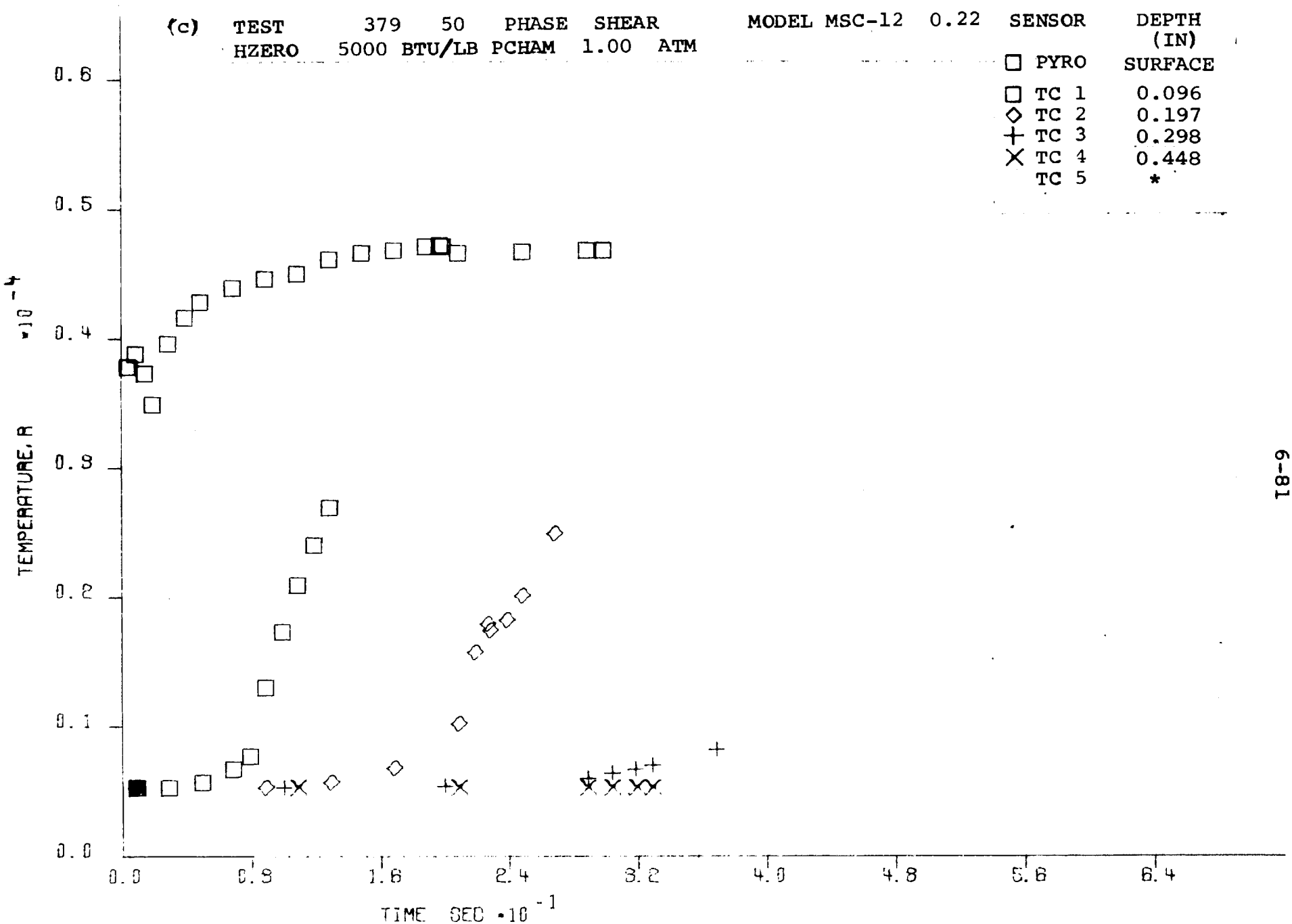

Figure 12. Continued.

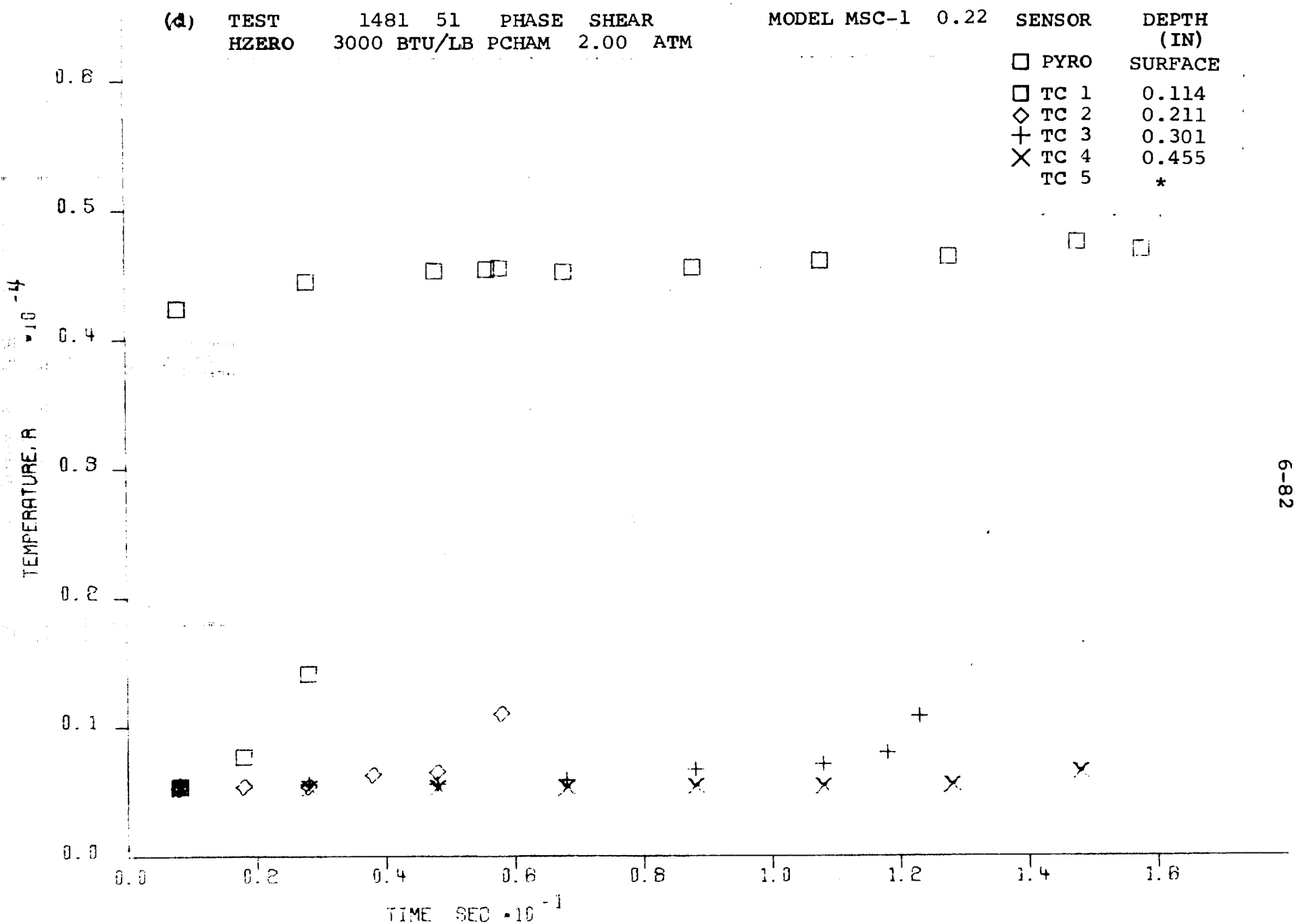

Figure 6-12. Continued.

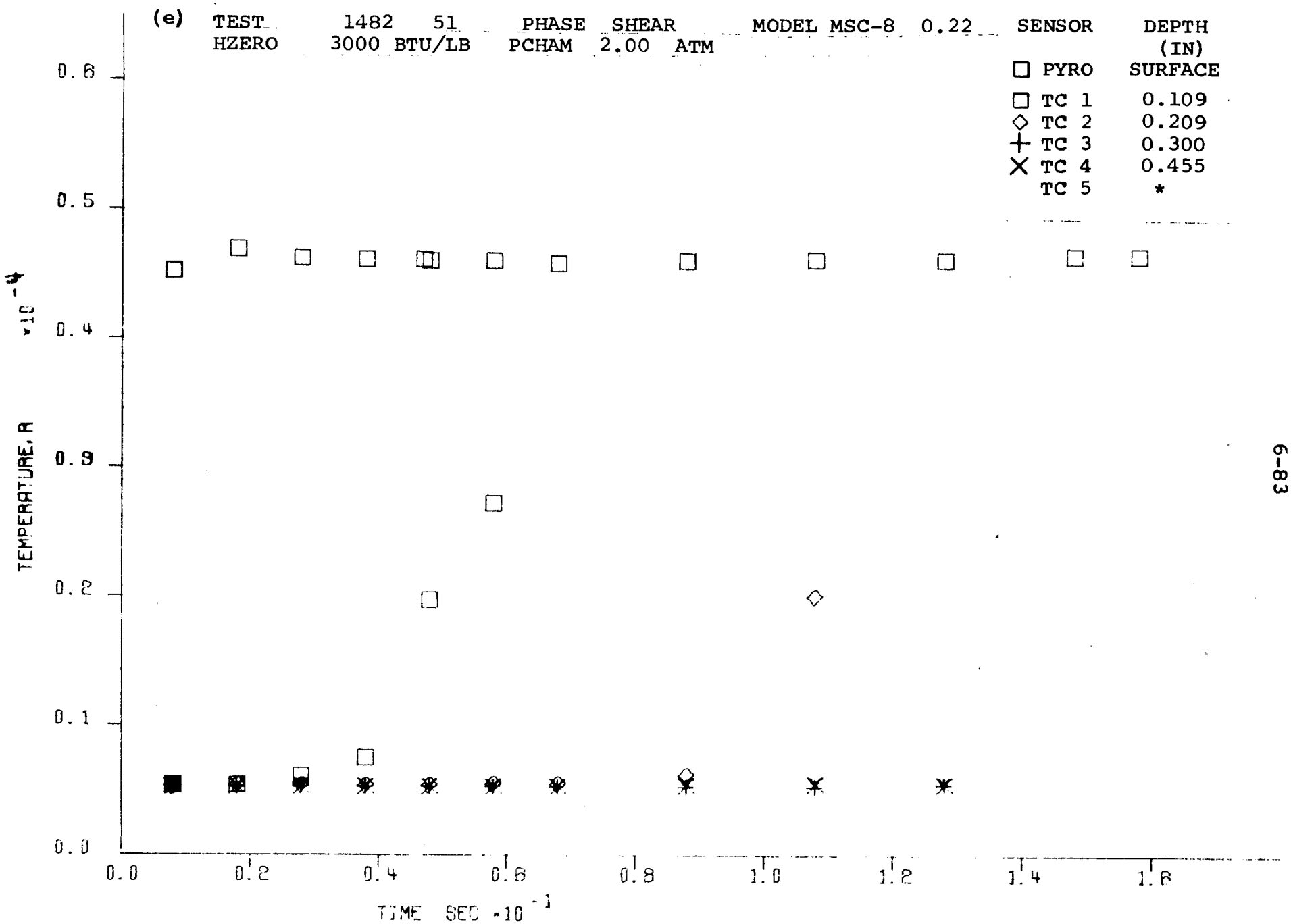

Figure 6-12. Continued.

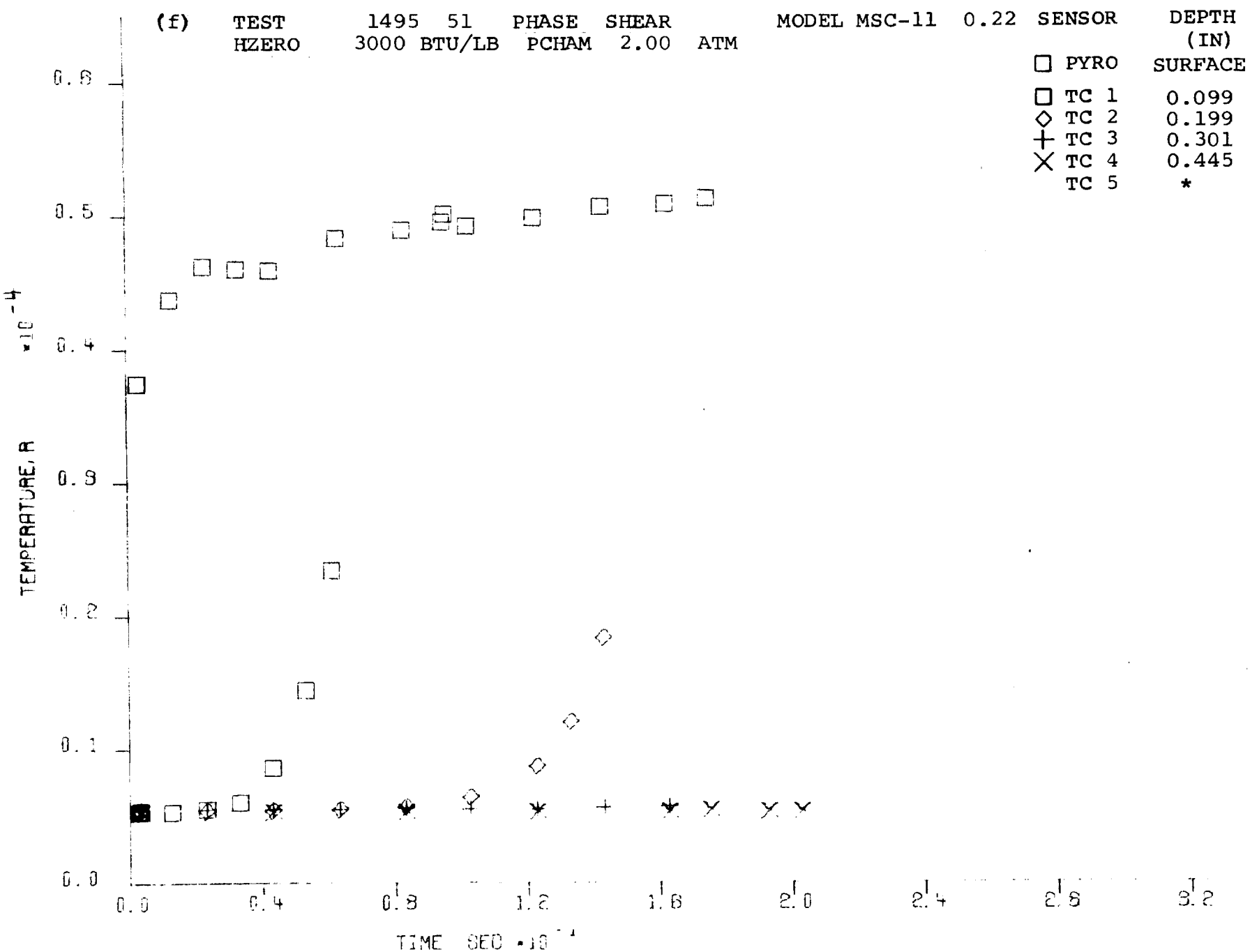

Figure 6-12. Continued.

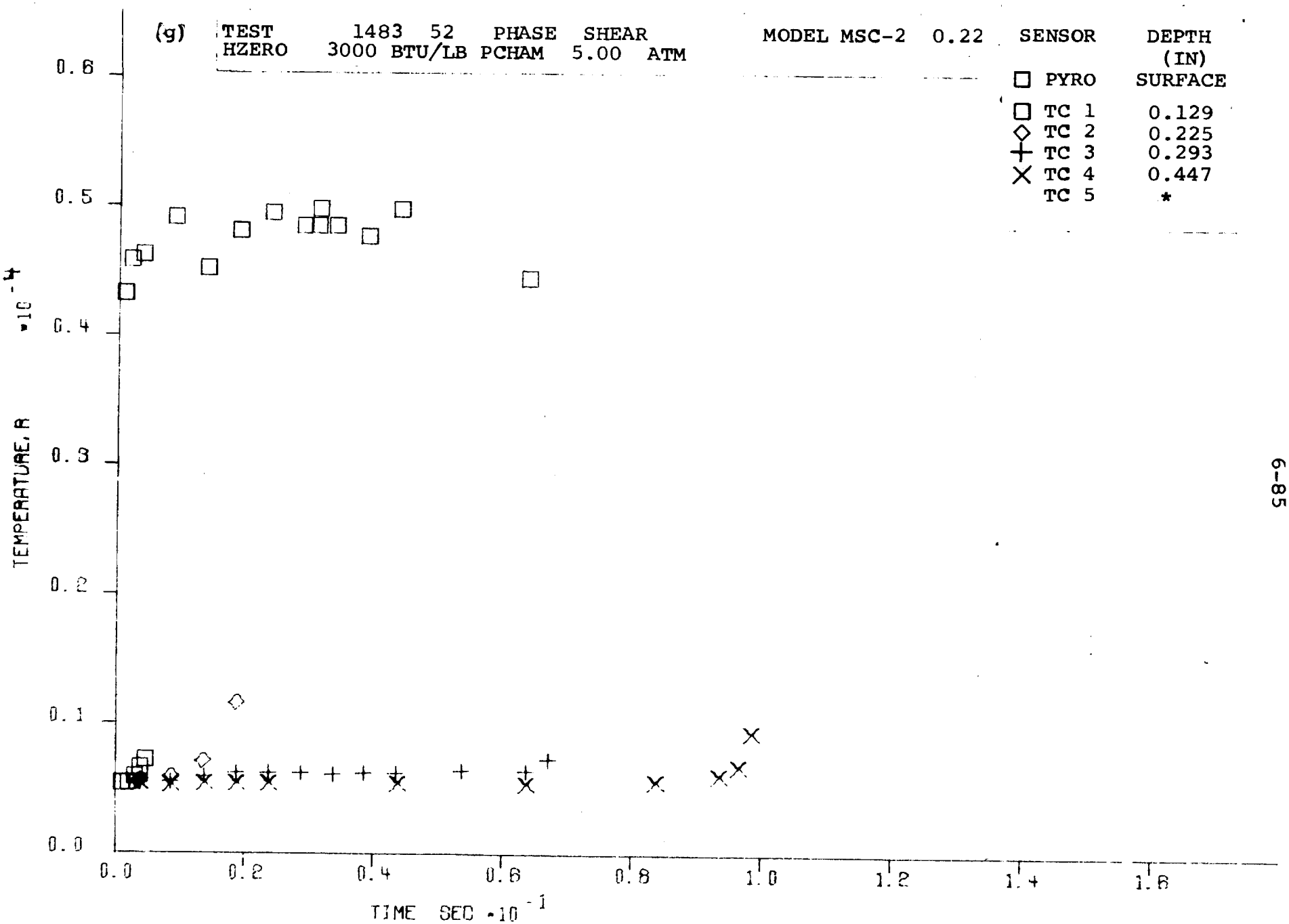

Figure 6-12. Continued.

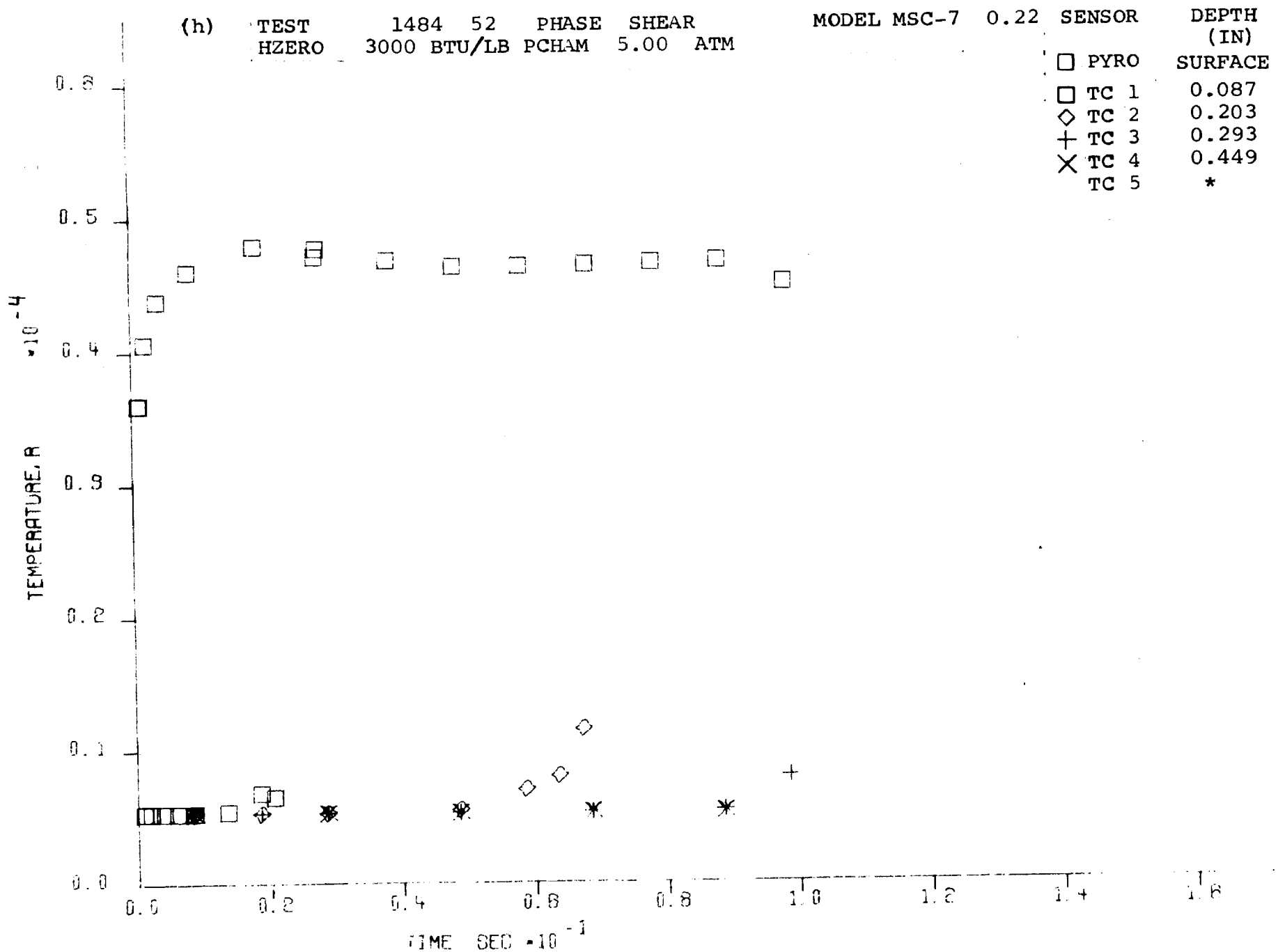

Figure 6-12. Continued.

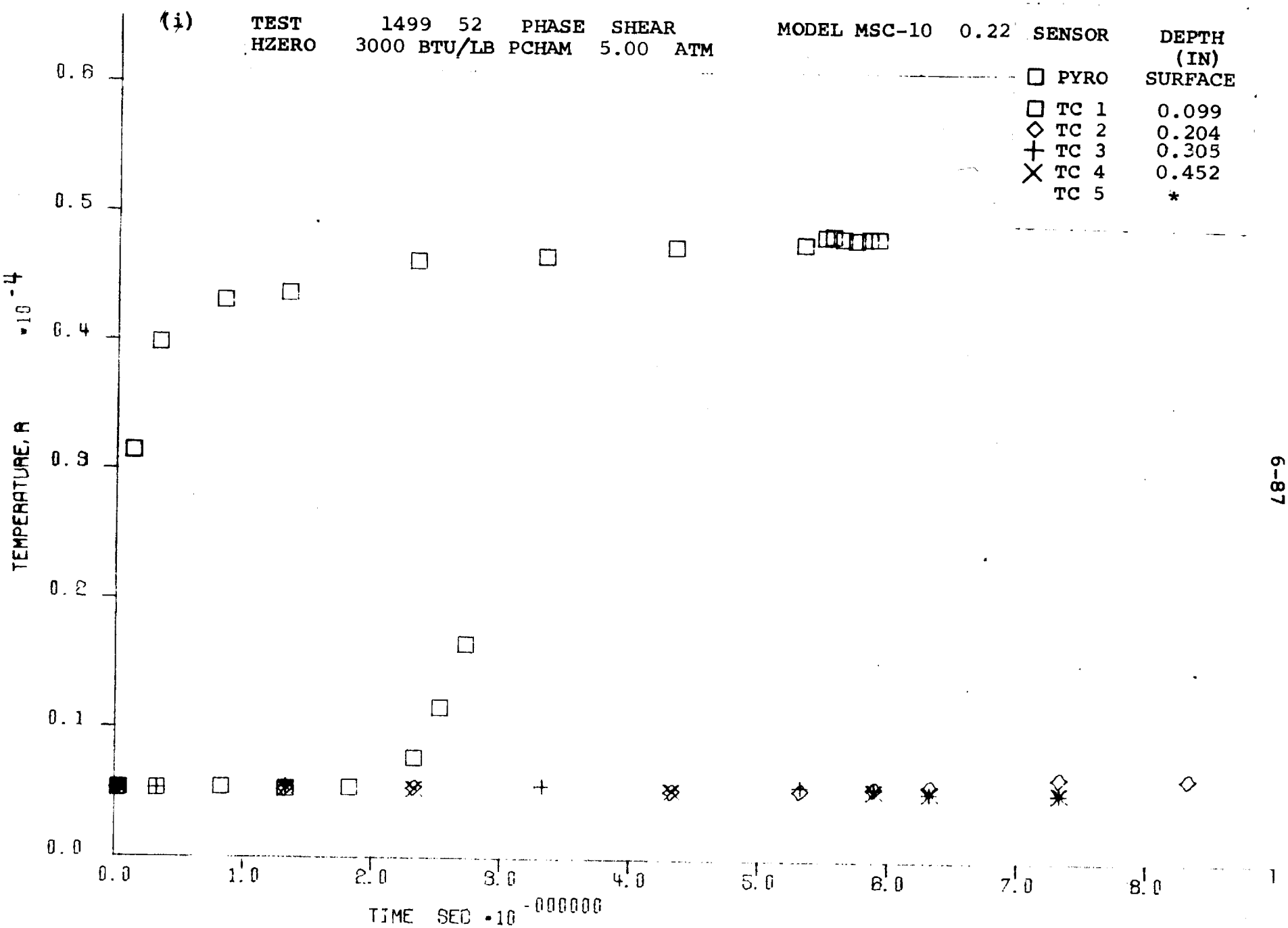

Figure 6-12. Continued.

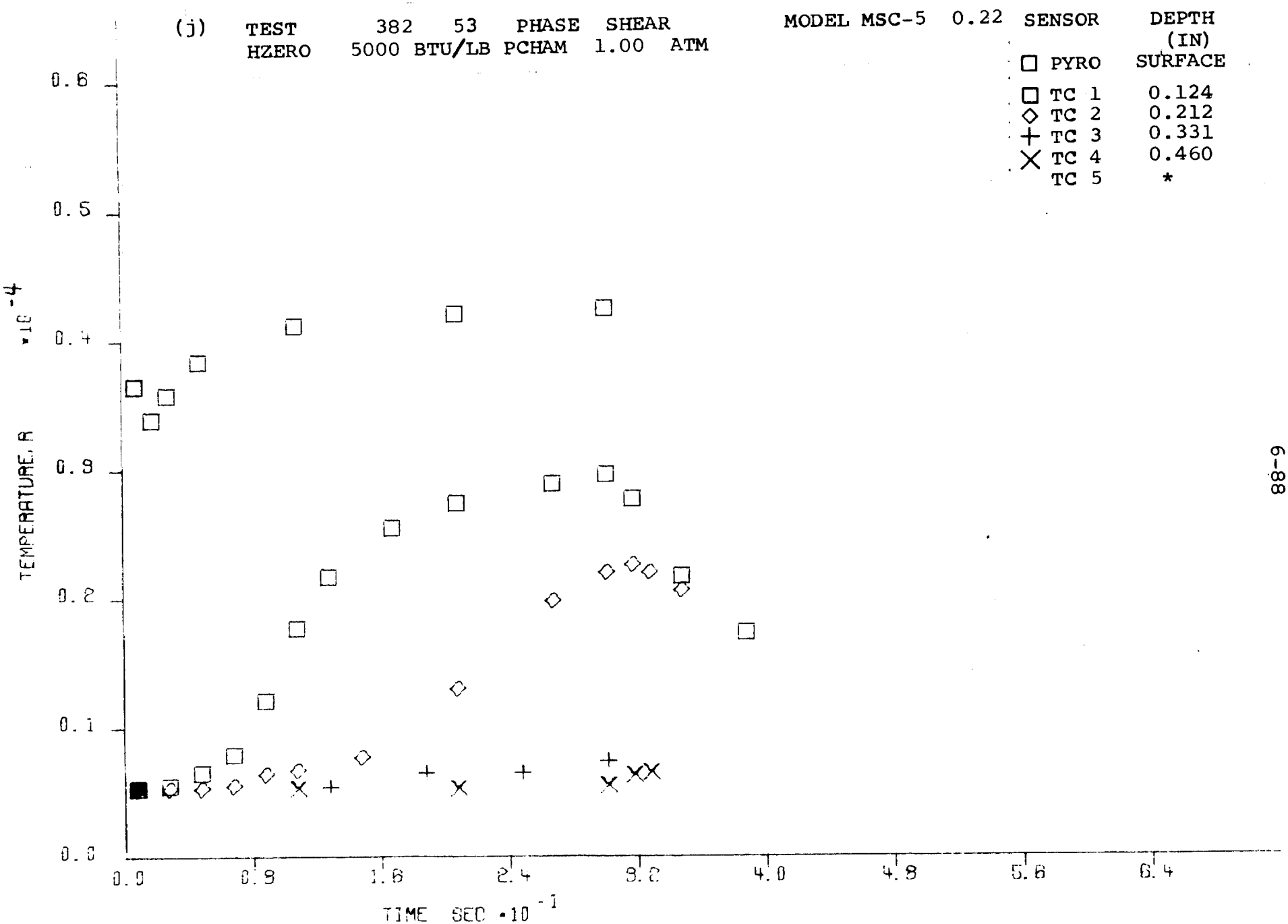

Figure 6-12. Continued.

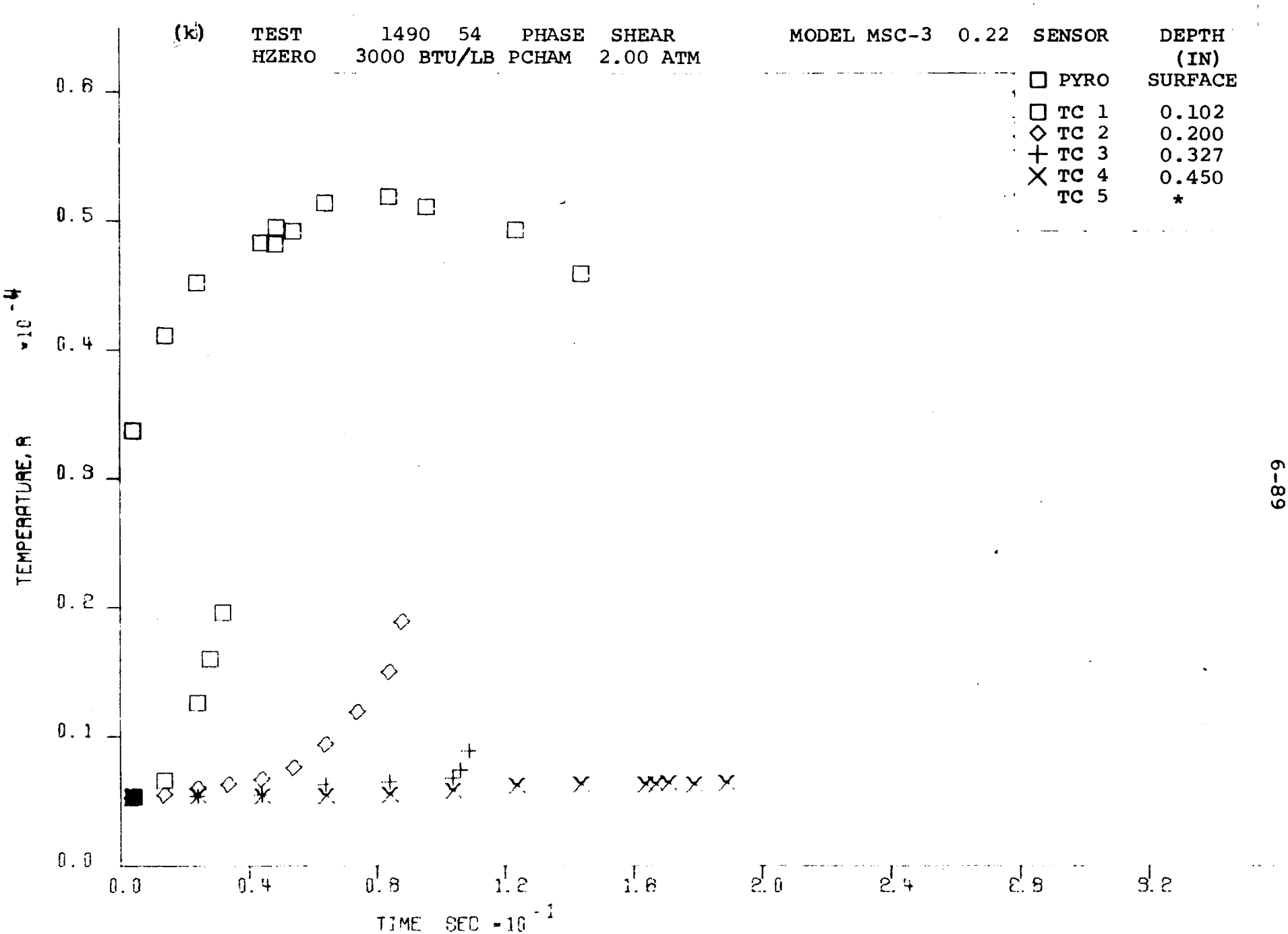

Figure 6-12. Continued.

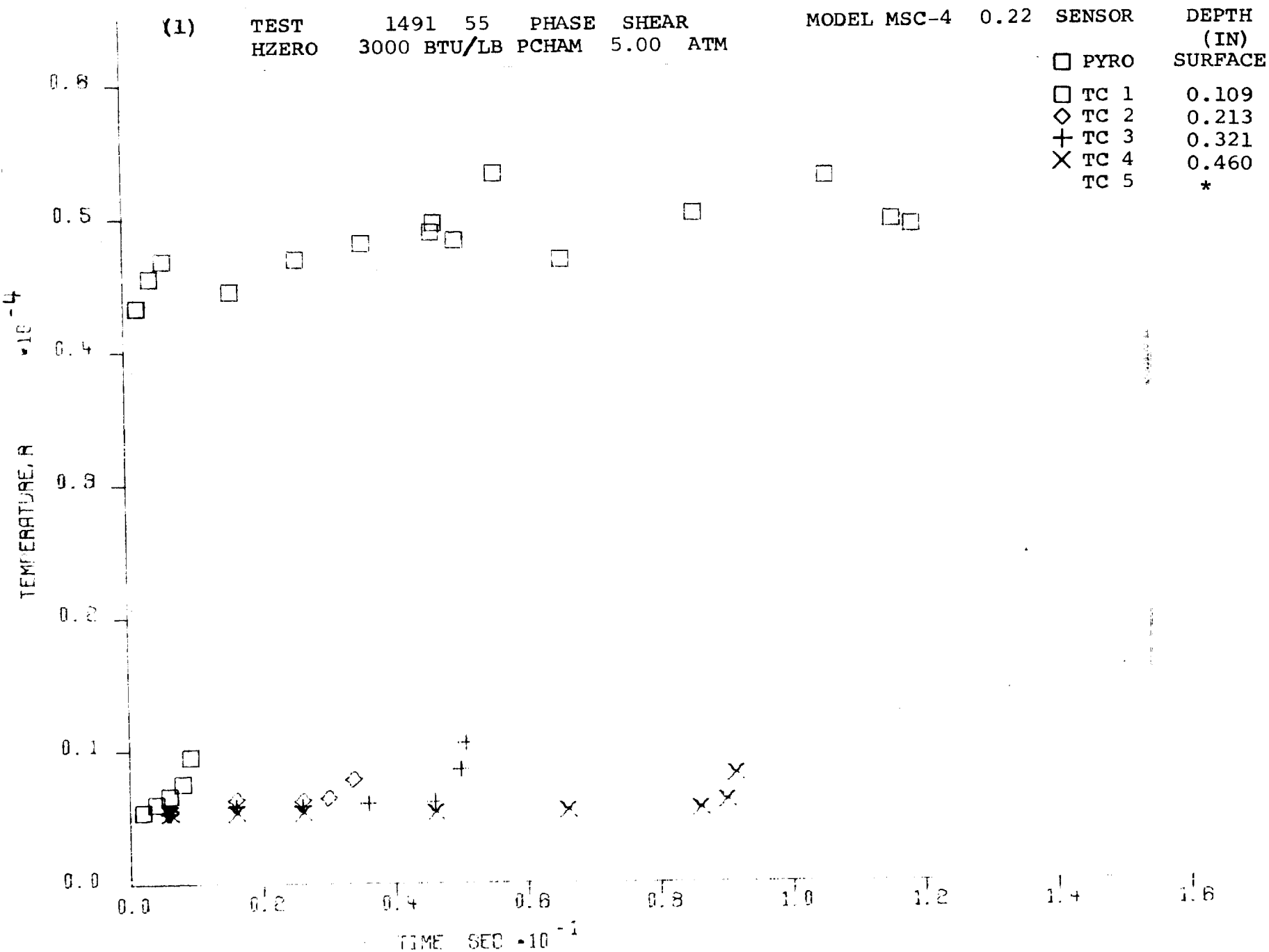

Figure 6-12. Continued.

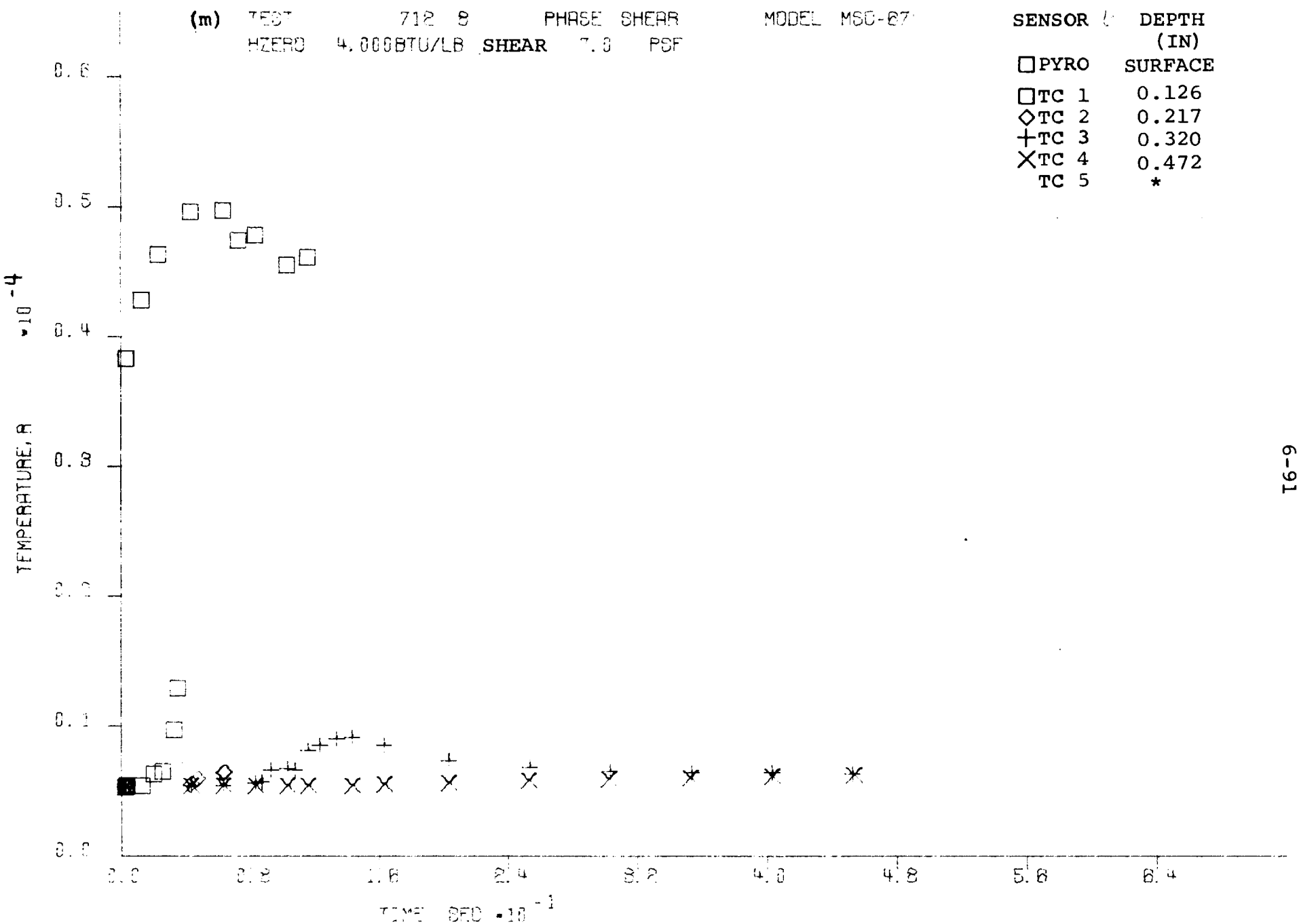

Figure 6-12. Continued.

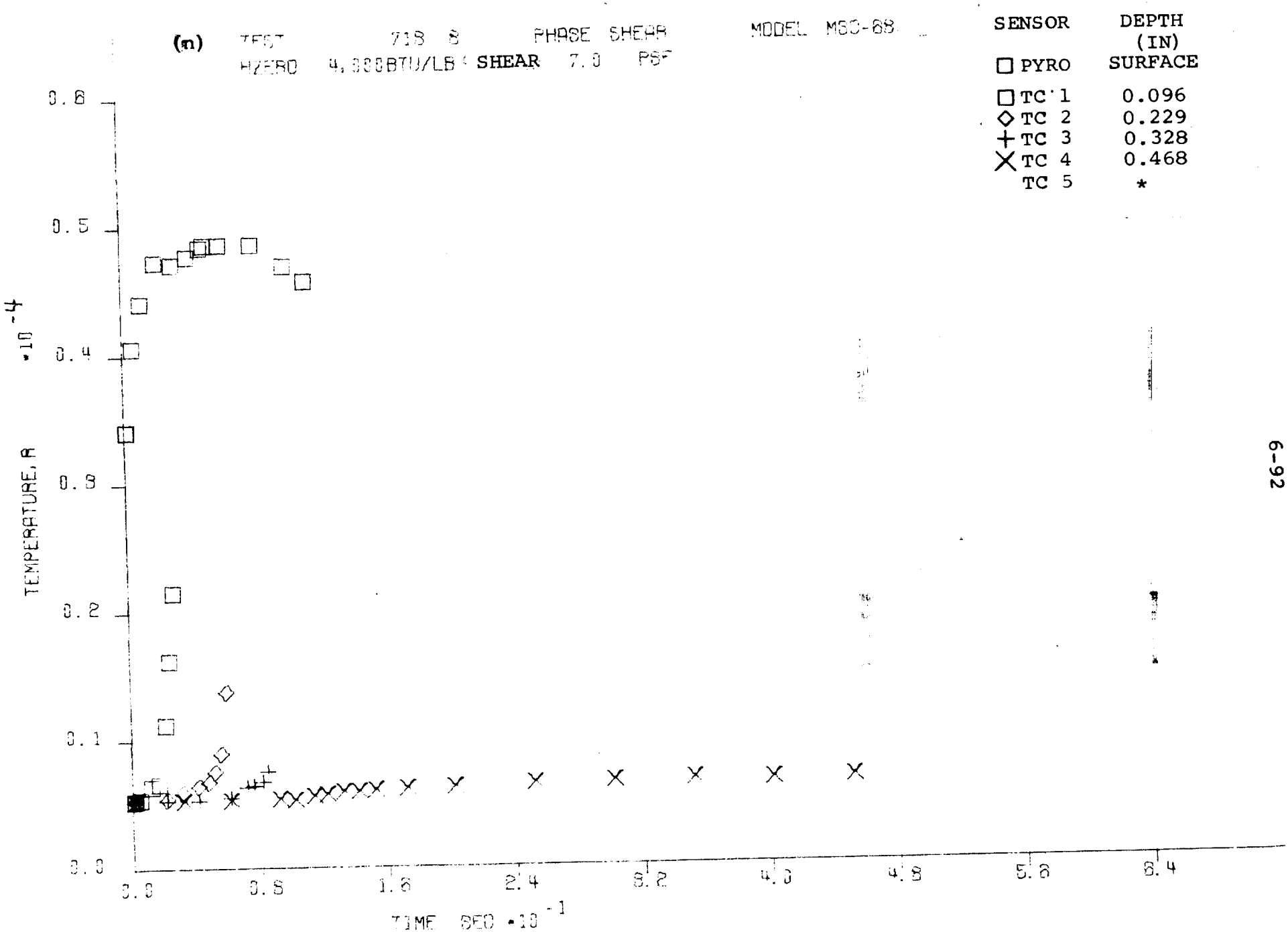

Figure 6-12. Continued.

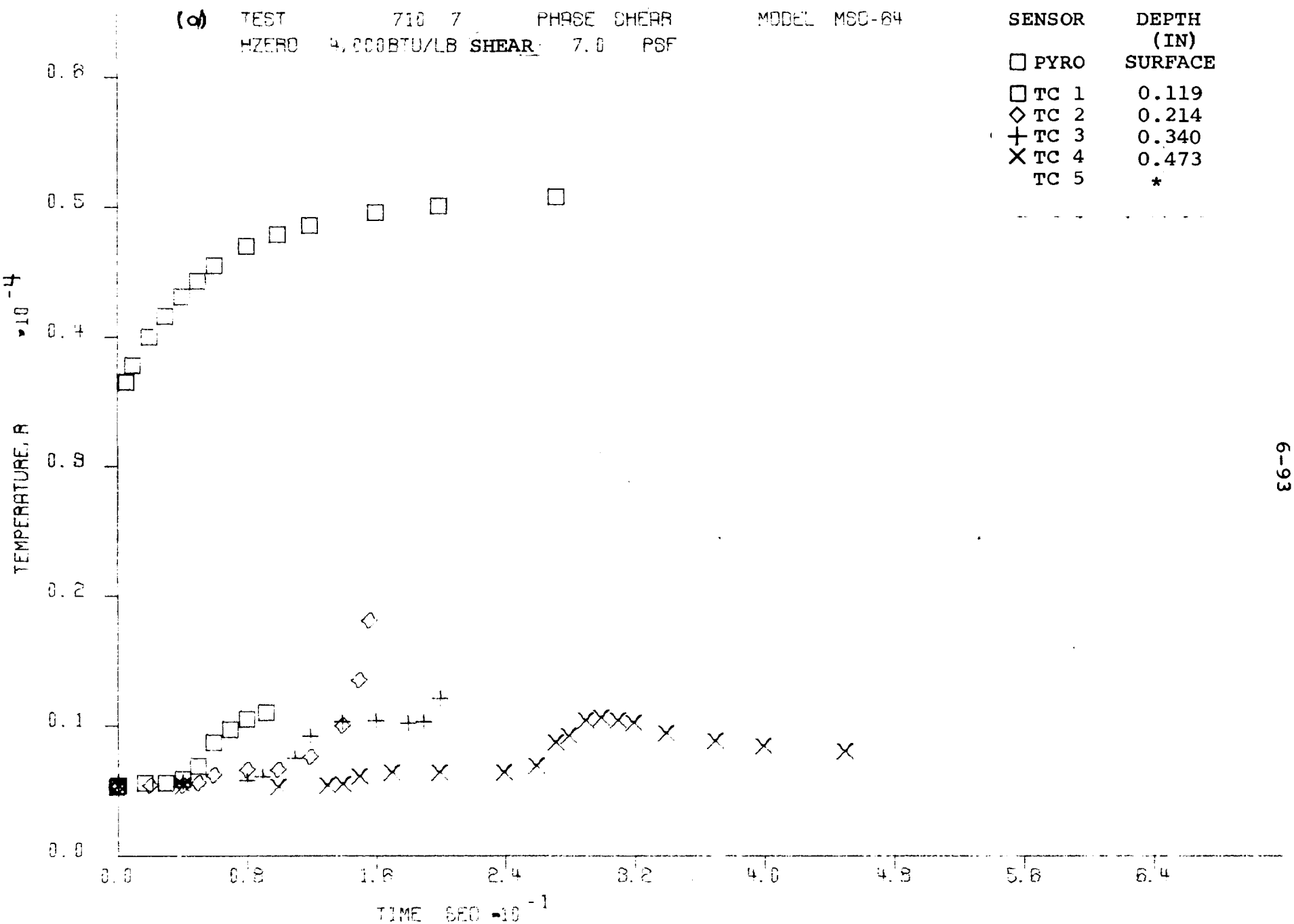

Figure 6-12. Continued.

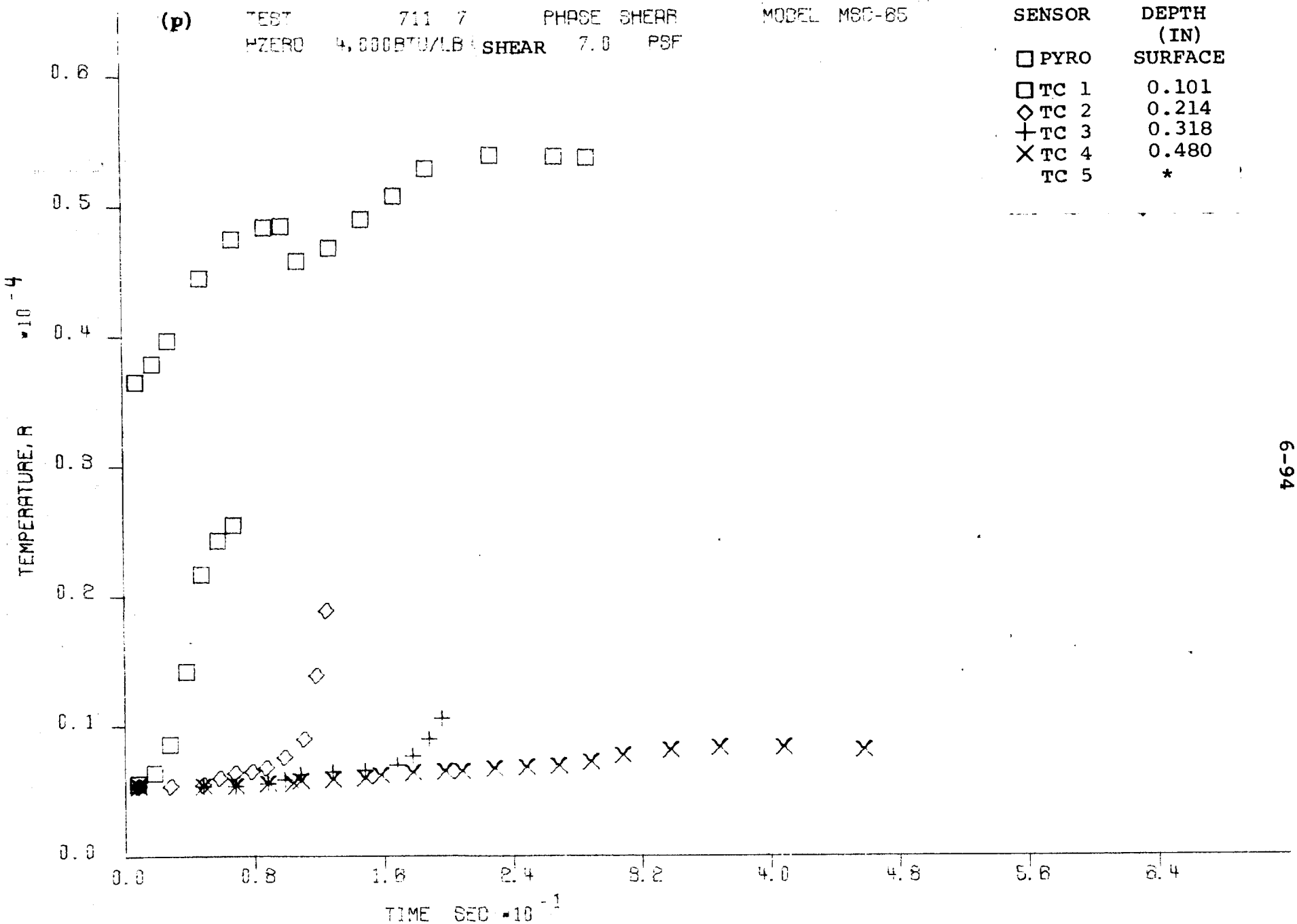

Figure 6-12. Continued.

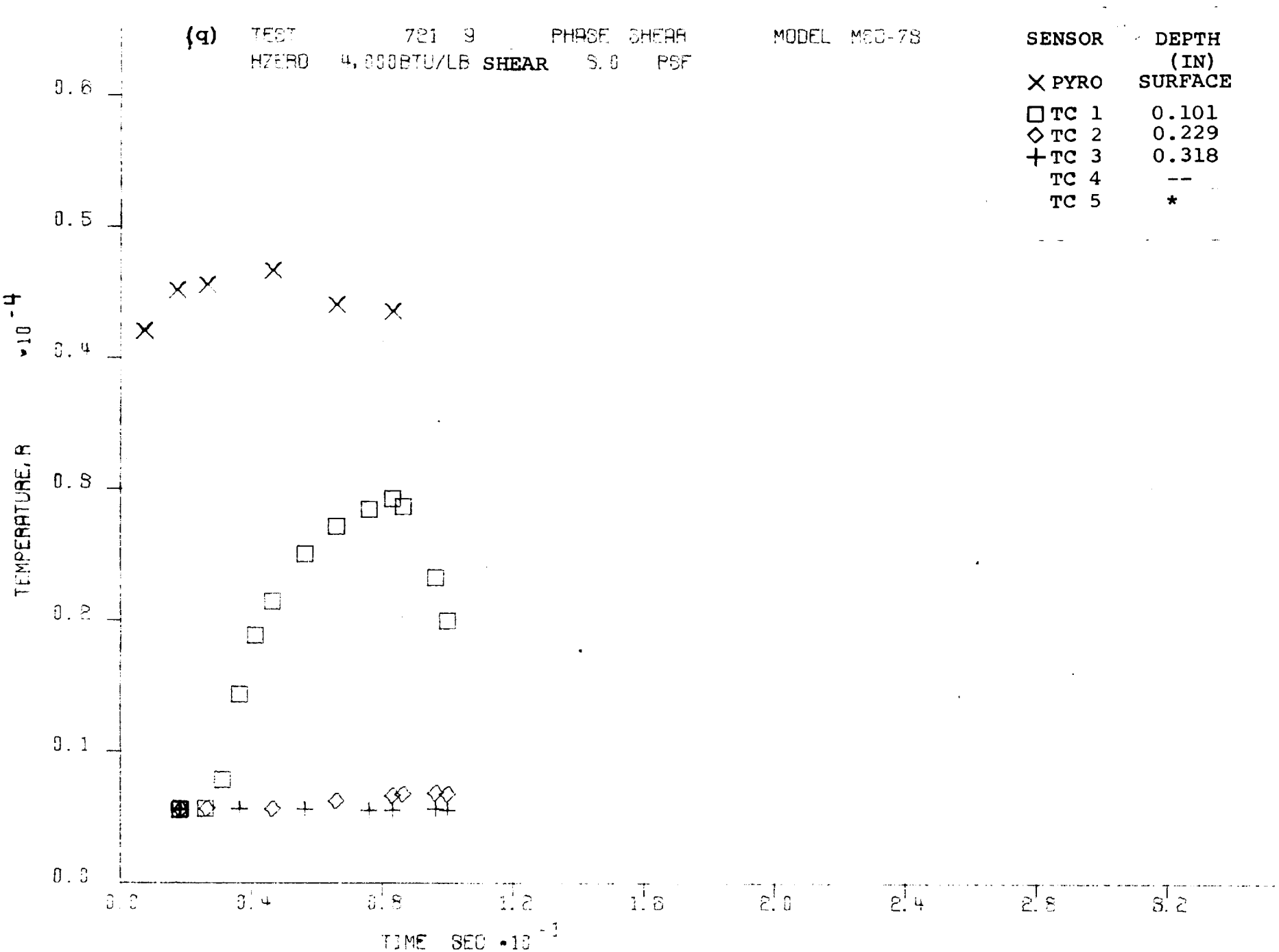

Figure 6-12. Continued.

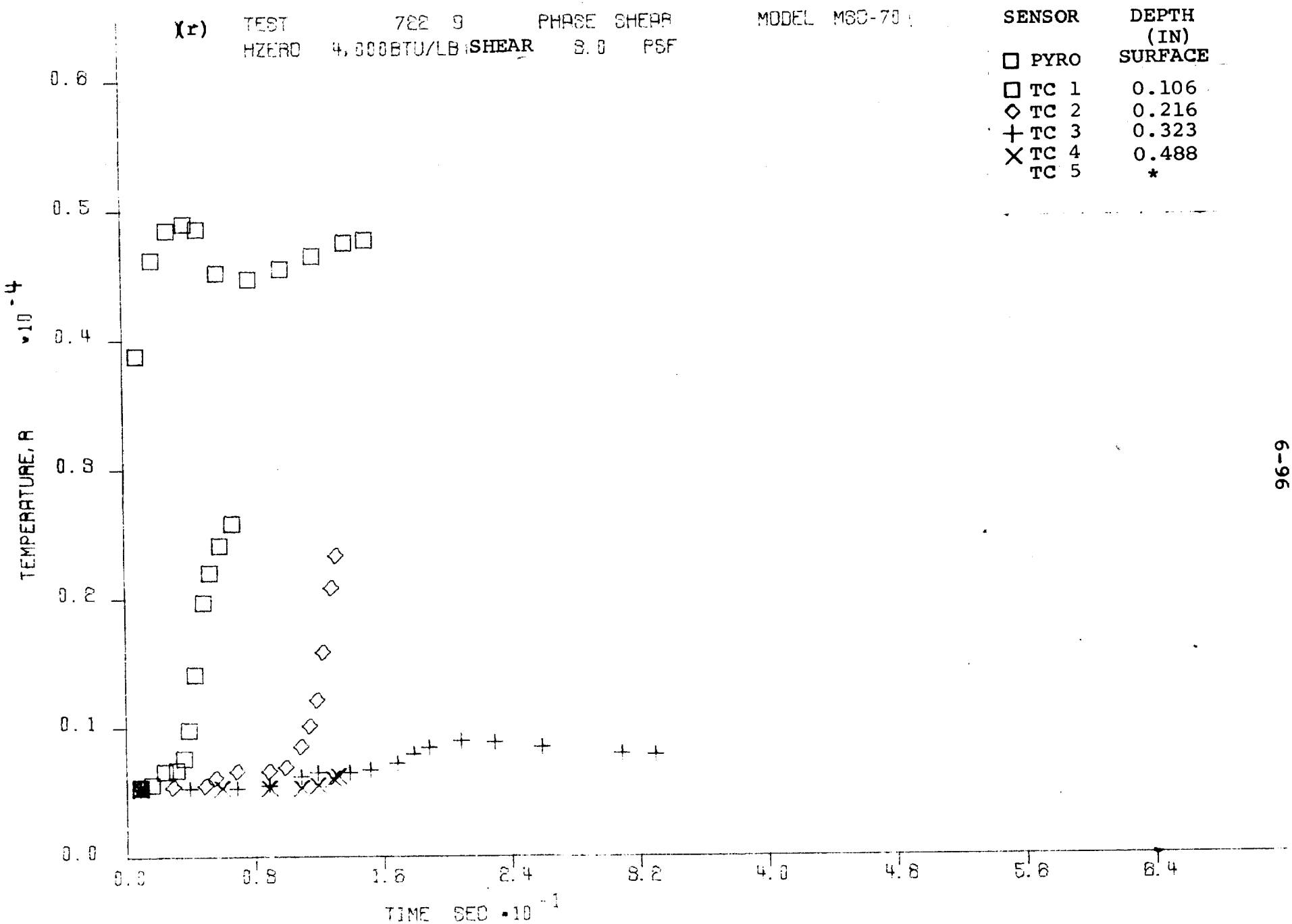

Figure 6-12. Continued.

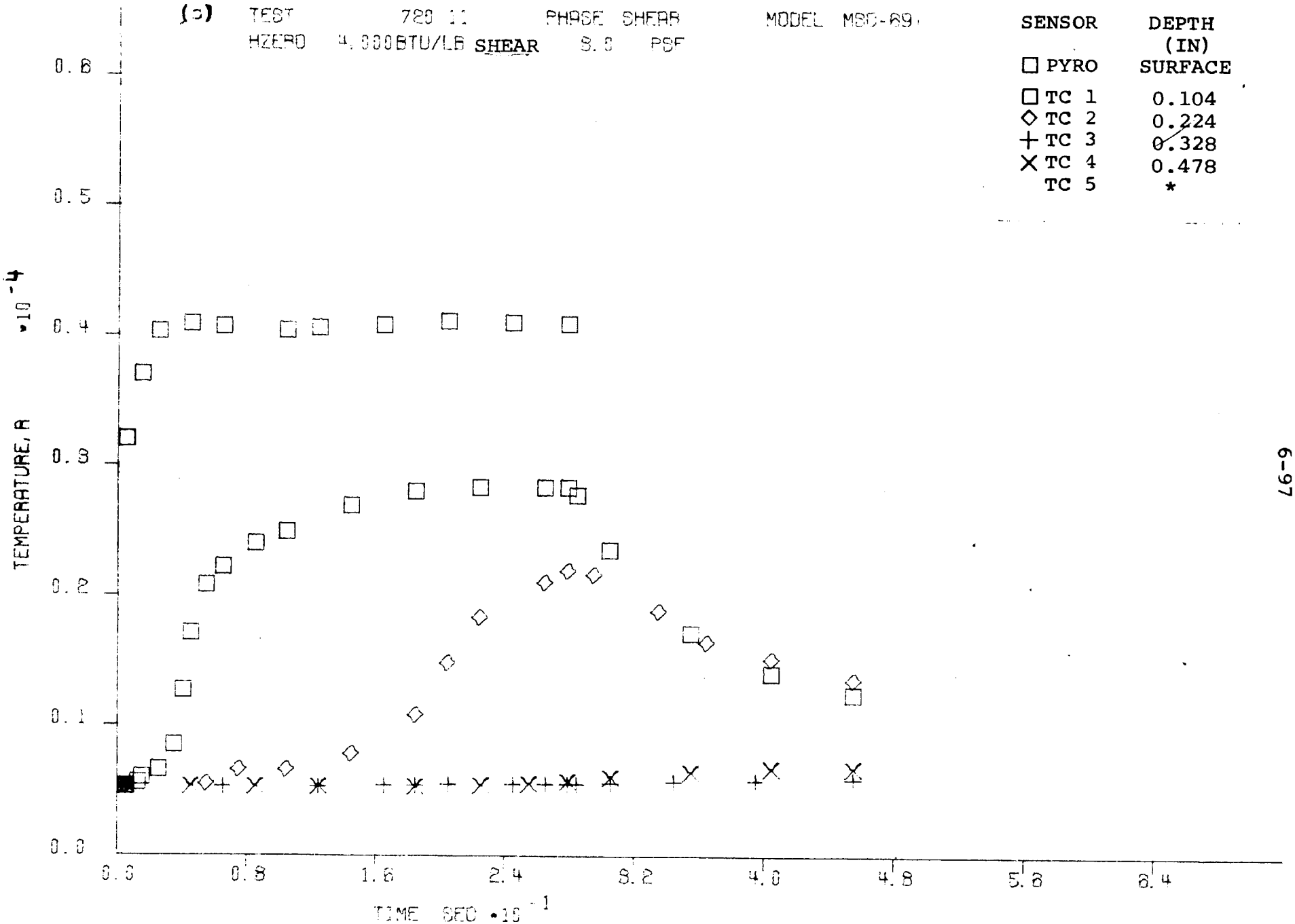

Figure 6-12. Continued.

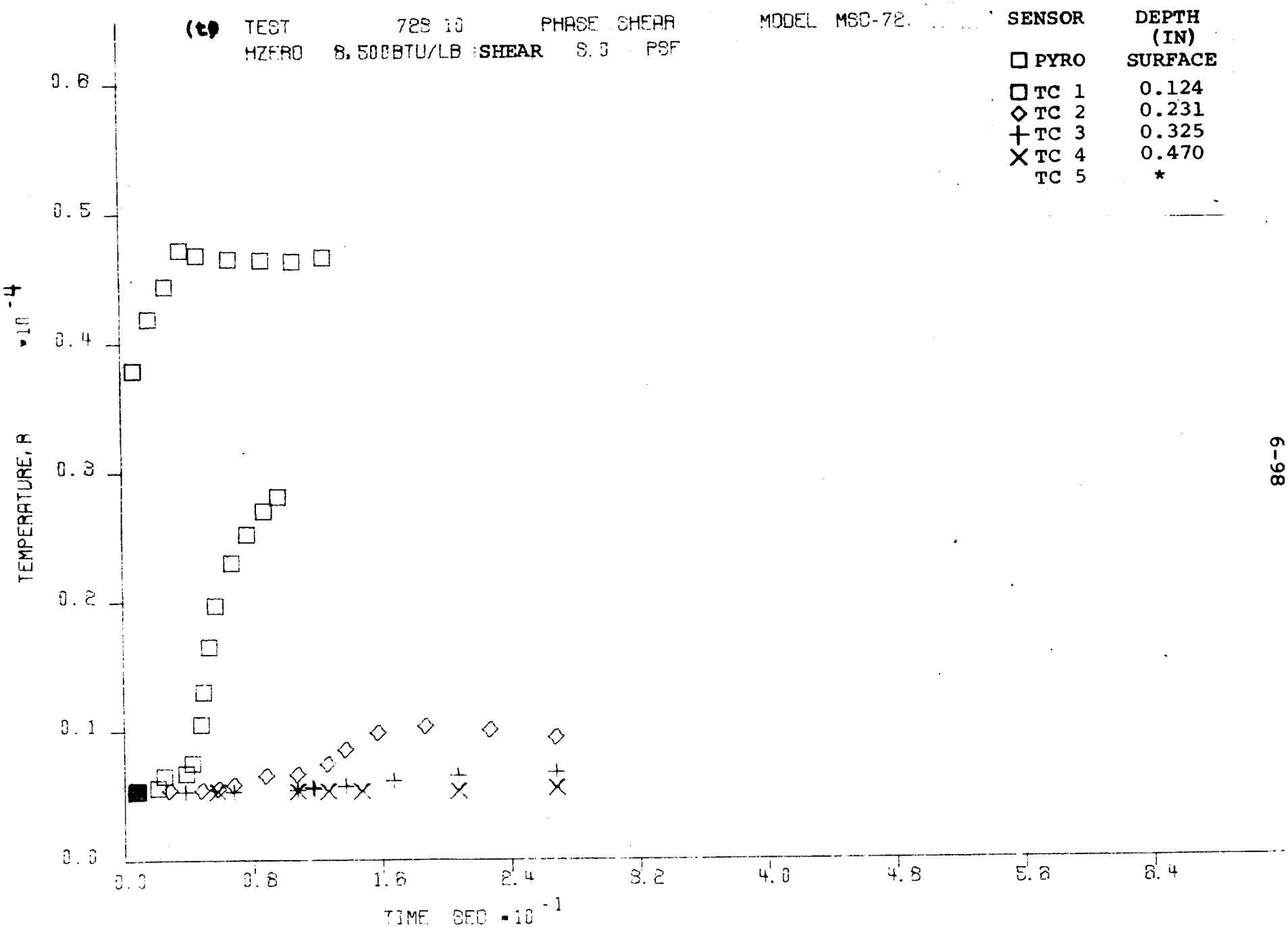

Figure 6-12. Continued.

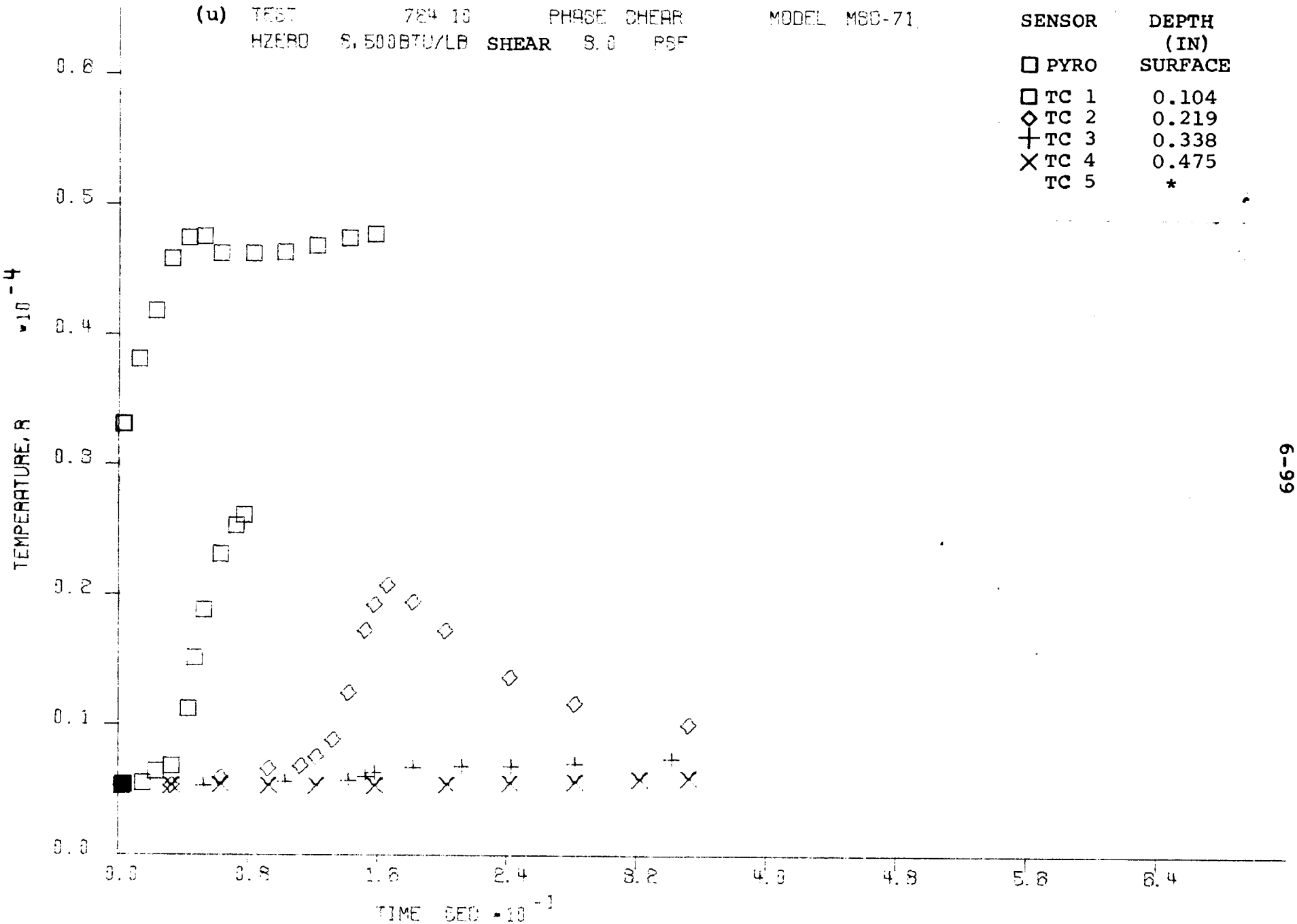

Figure 6-12. Continued.

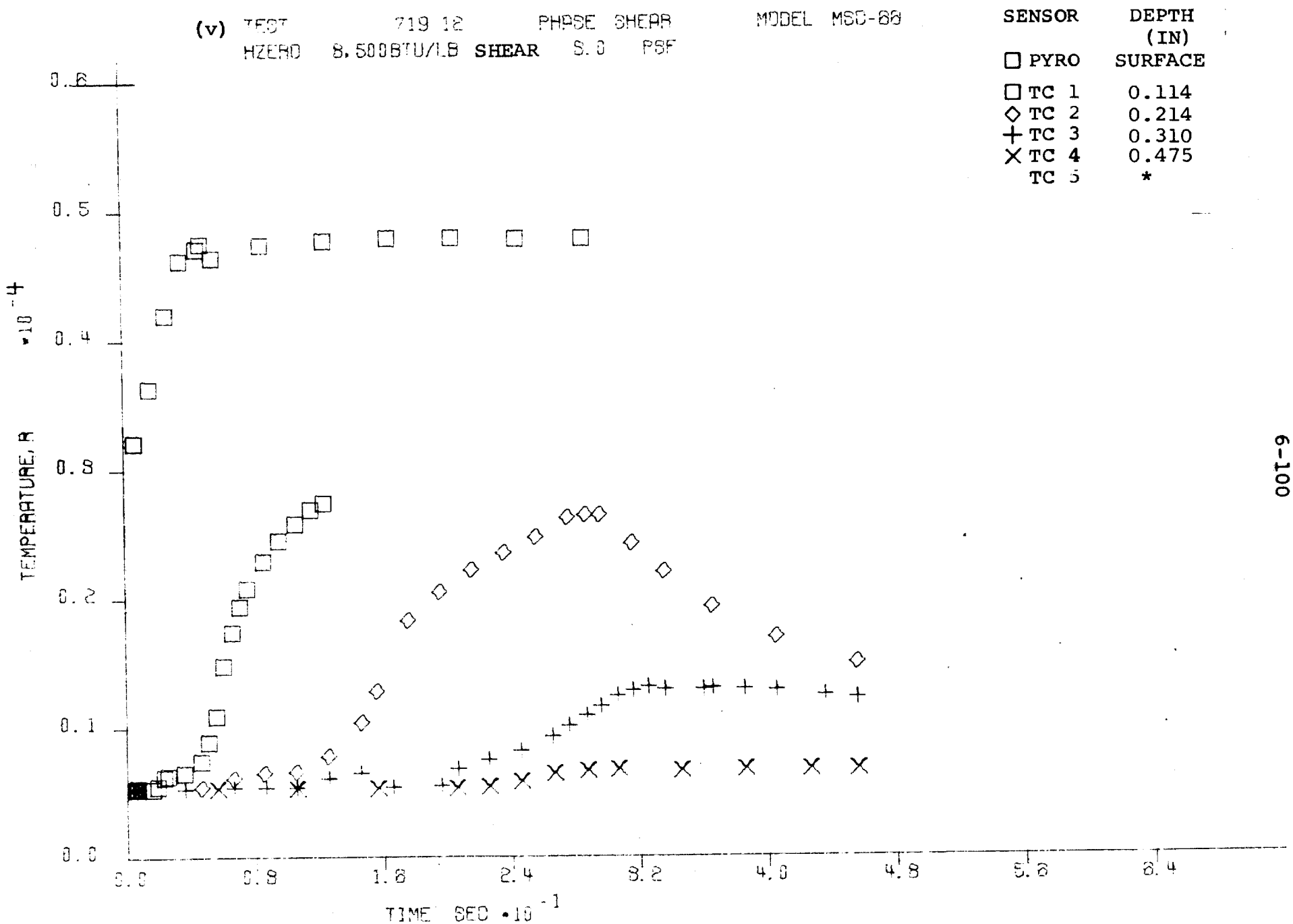

Figure 12. Concluded.

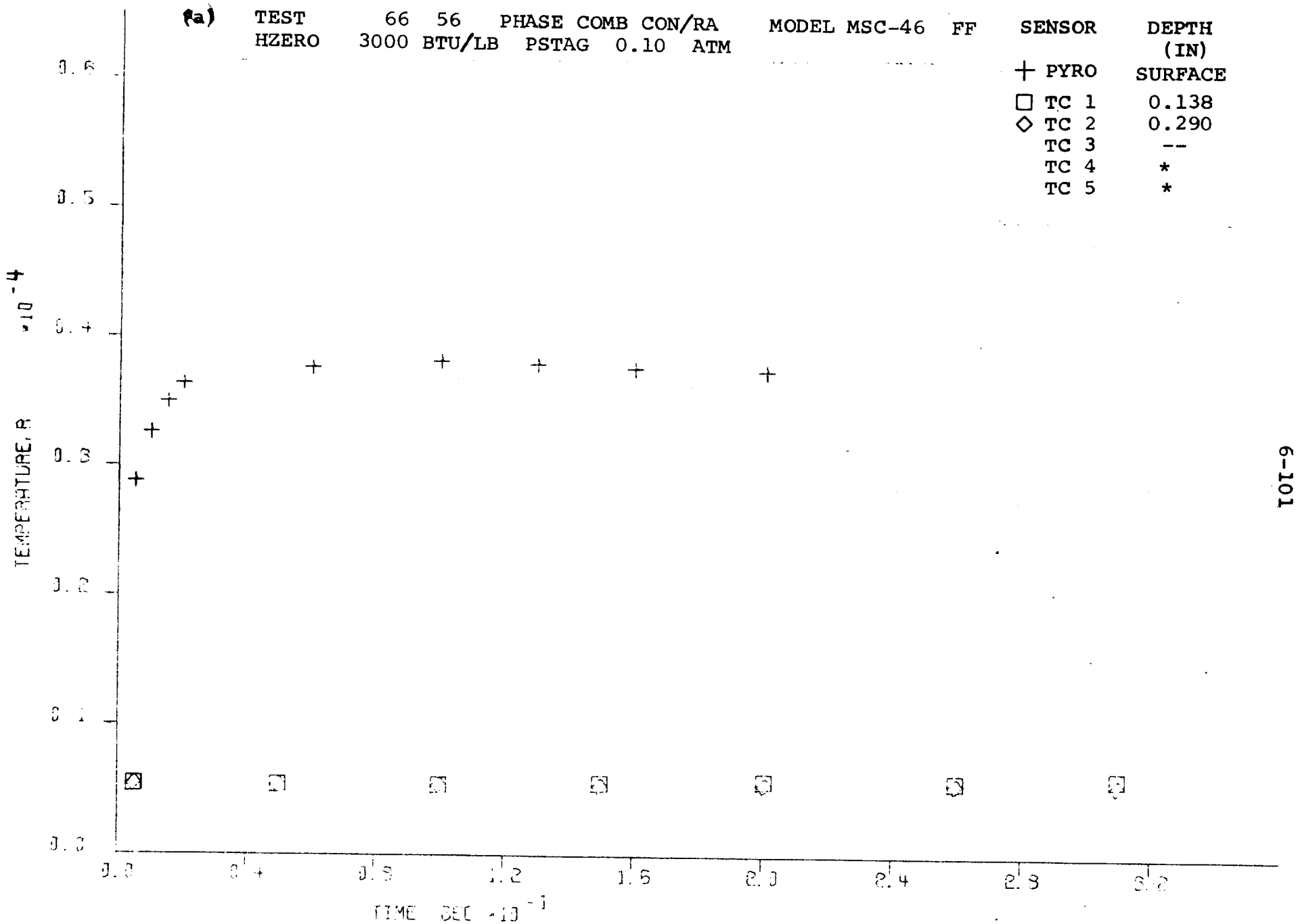

Figure 6-13. Surface and Internal Temperature Histories, Phase II.

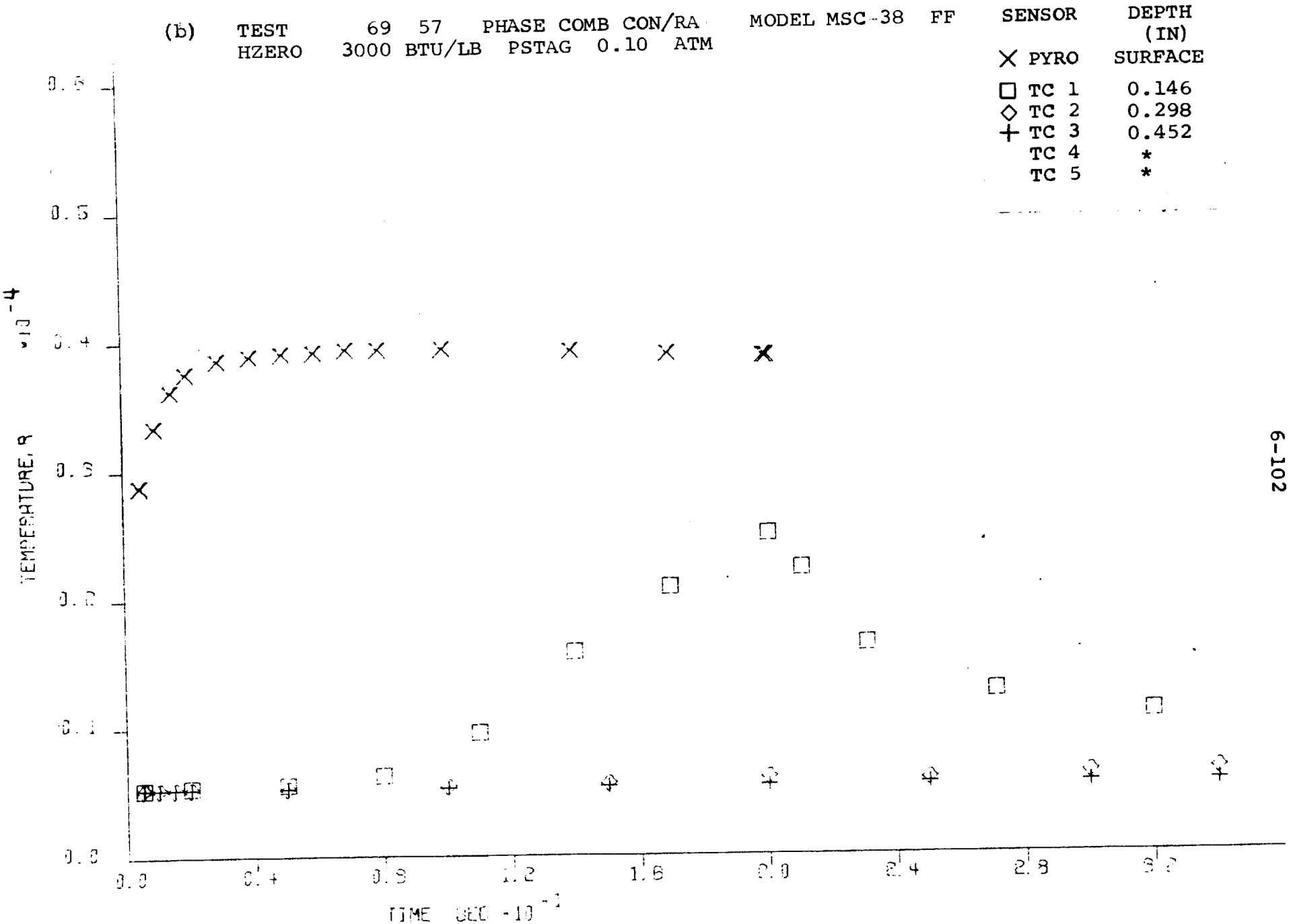

Figure 6-13. Continued.

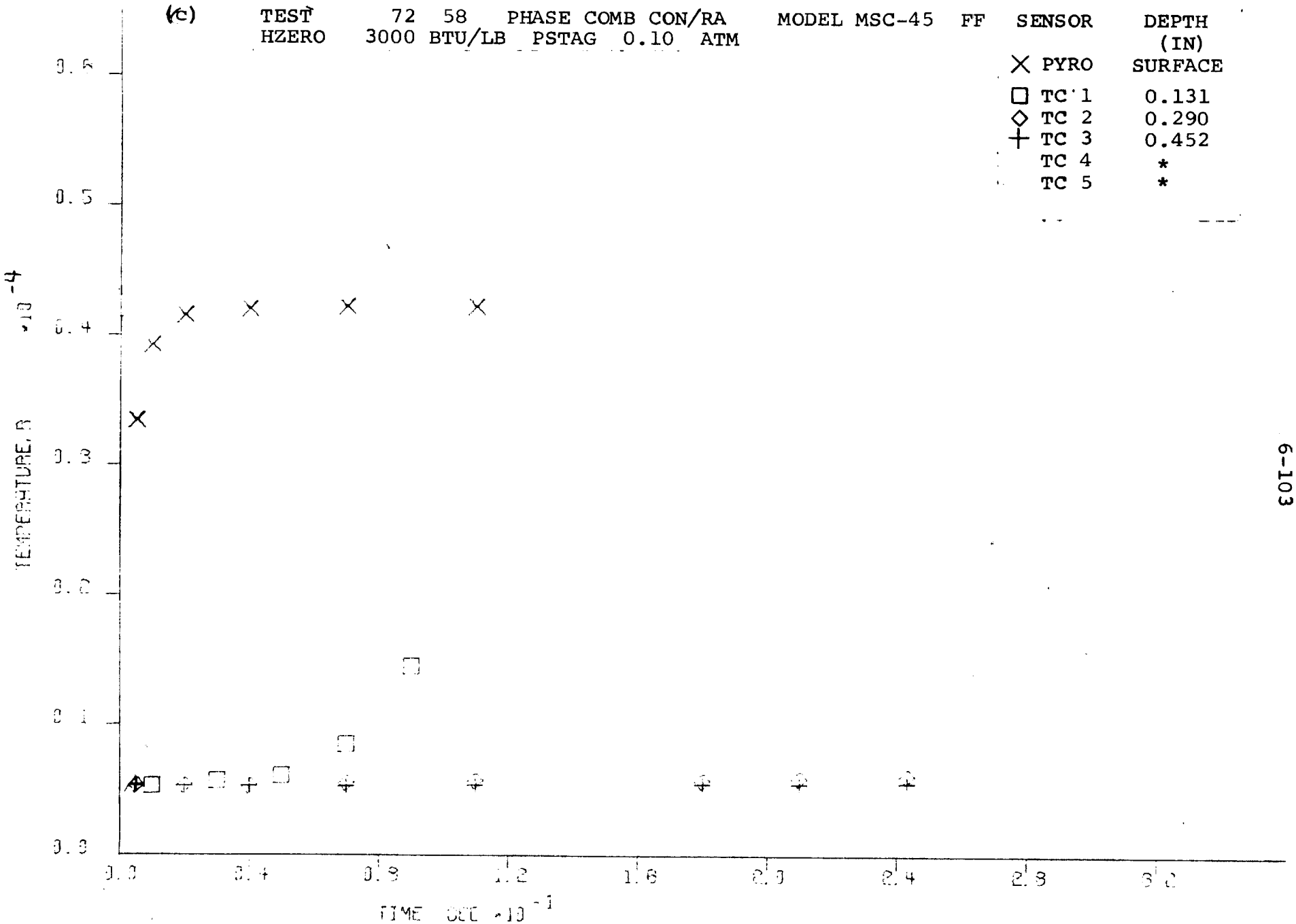

Figure 6-13. Continued.

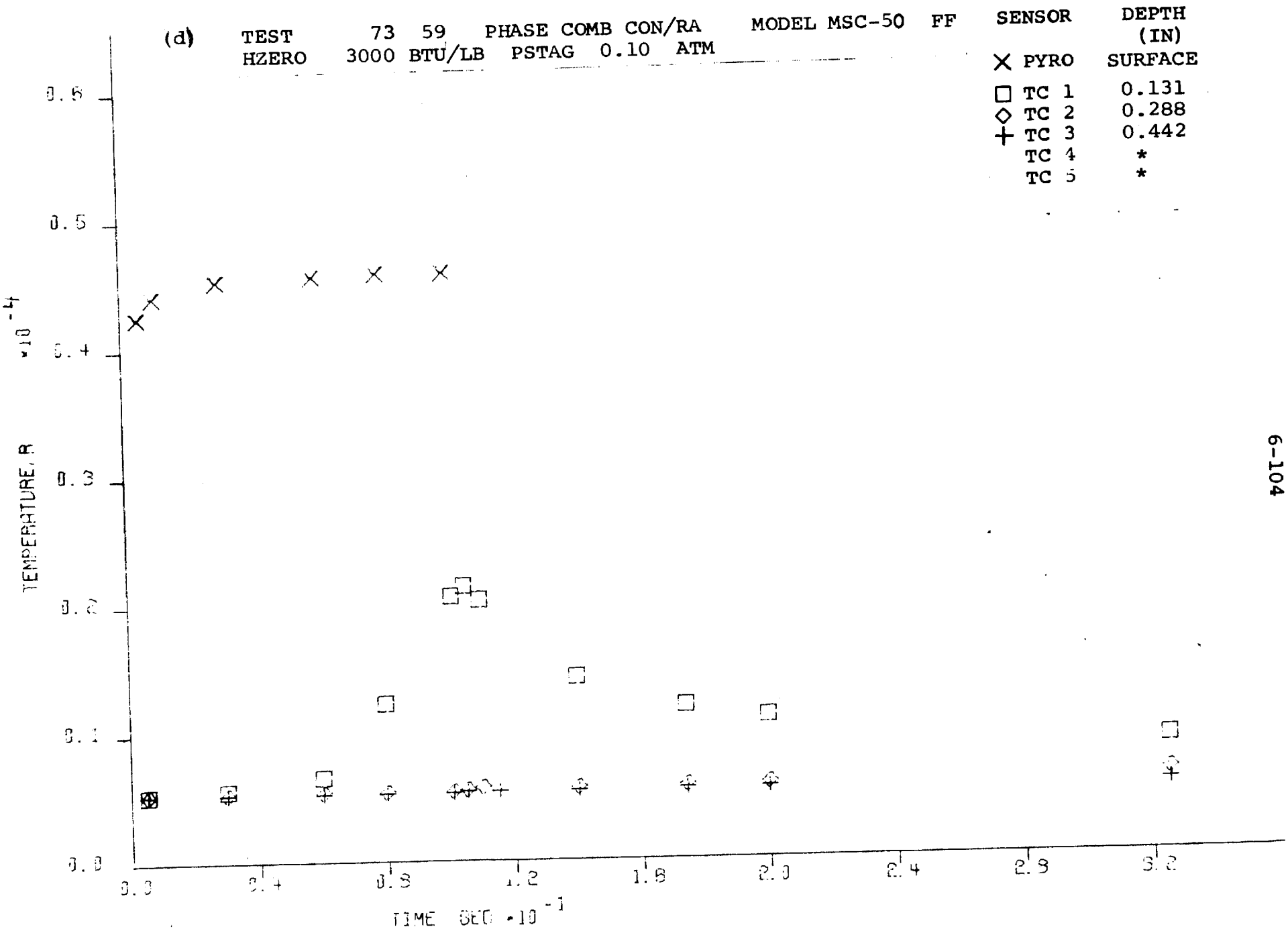

Figure 6-13. Continued.

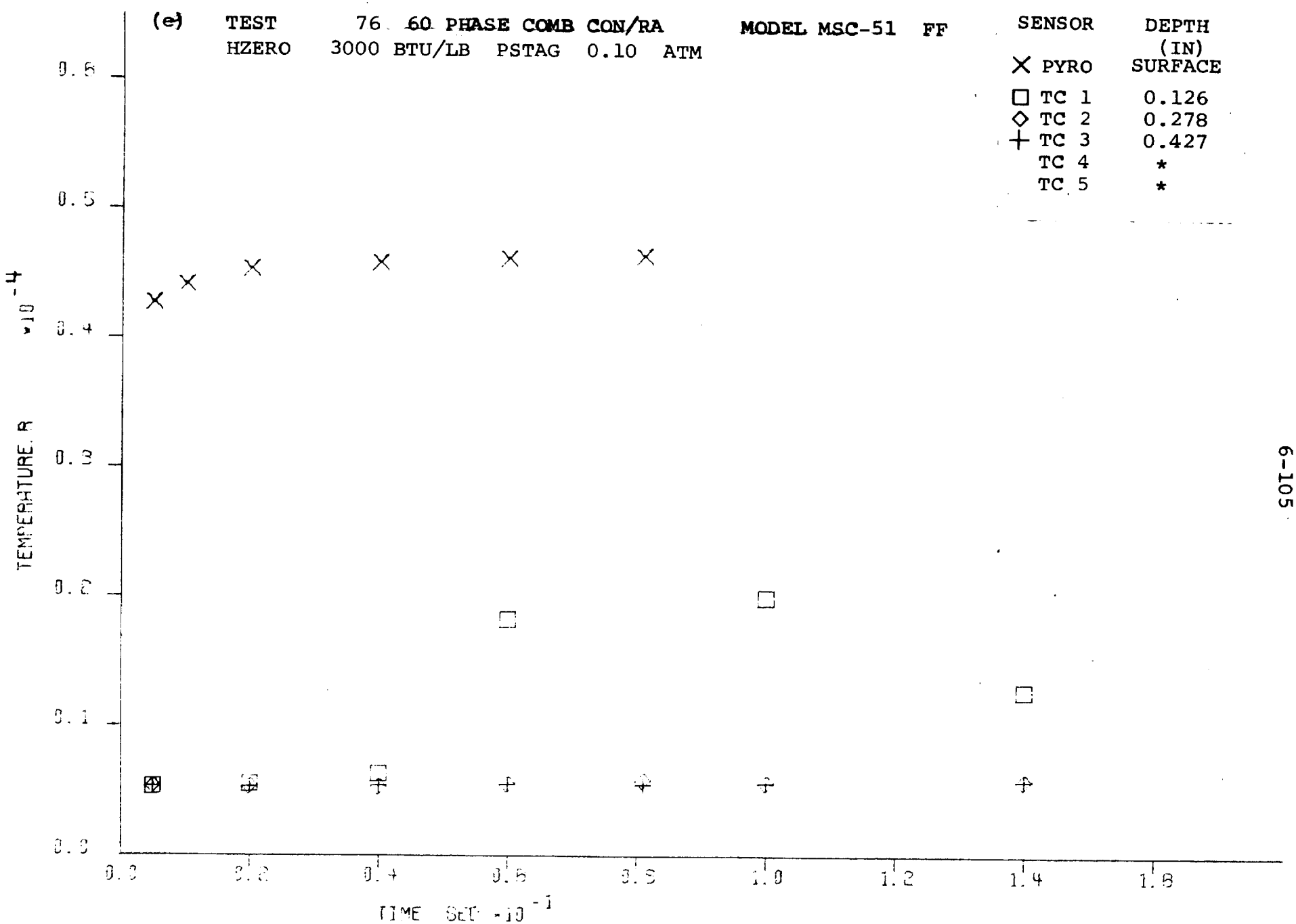

Figure 6-13. Continued.

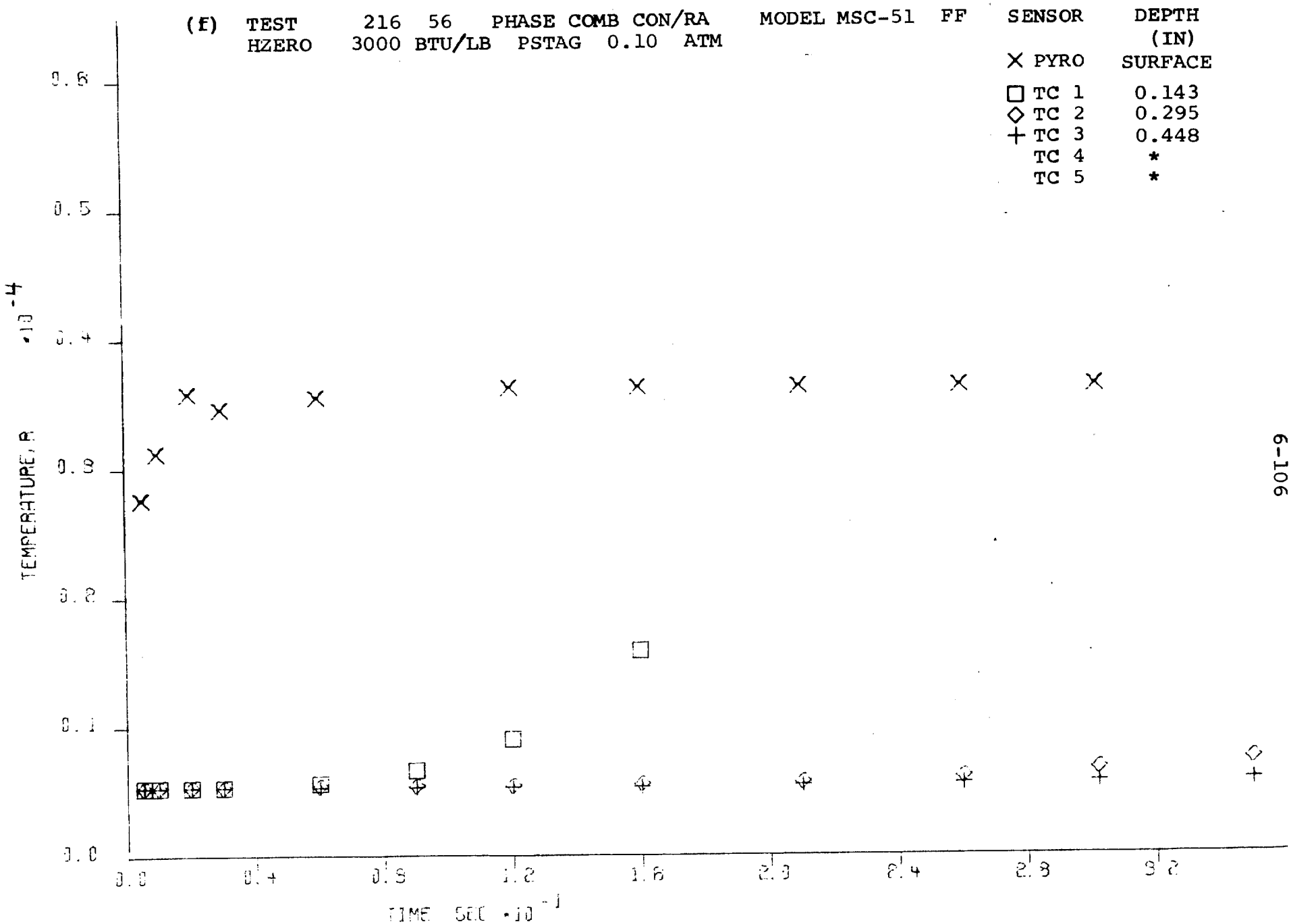

Figure 6-13. Continued.

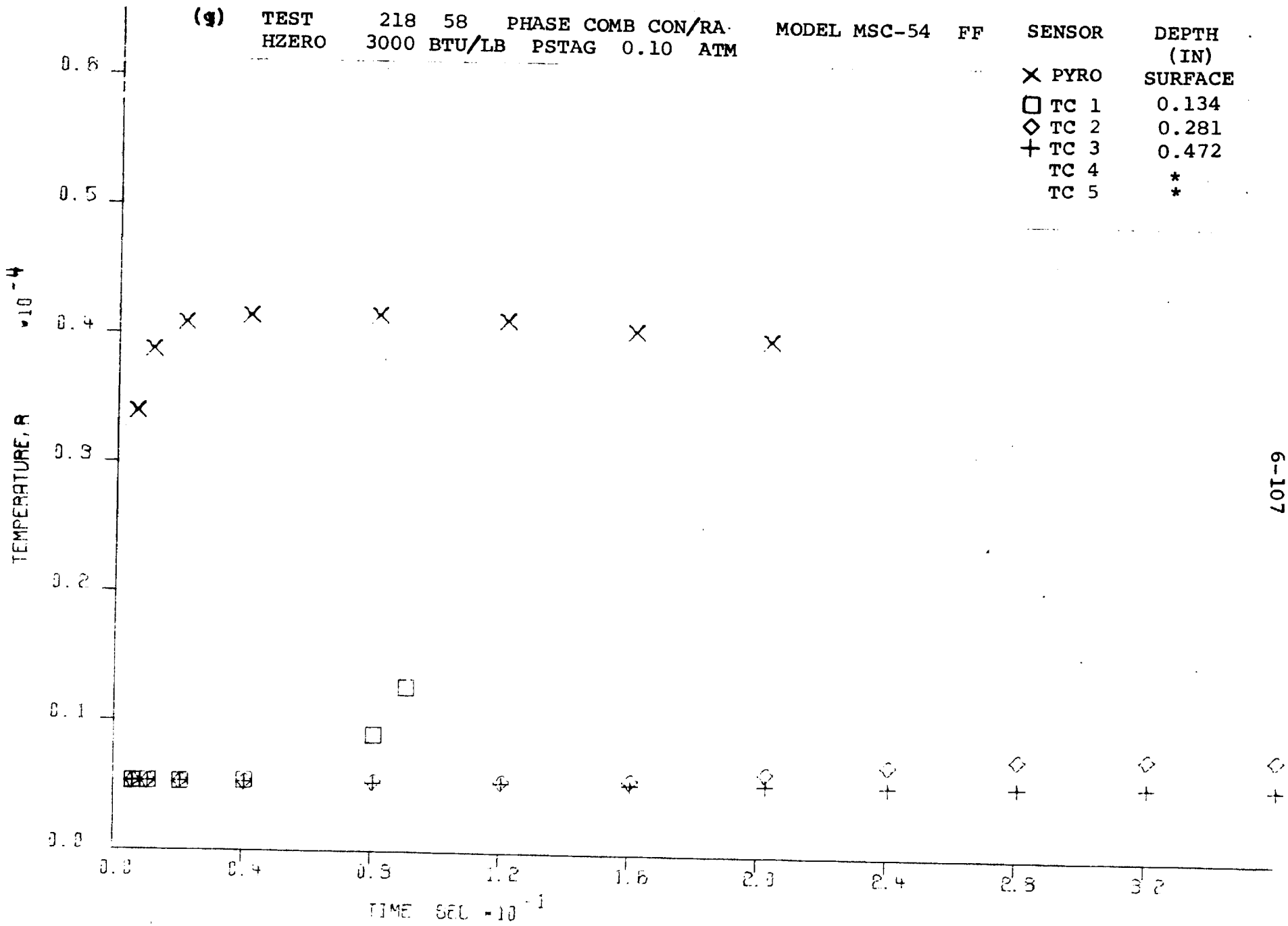

Figure 6-13. Continued.

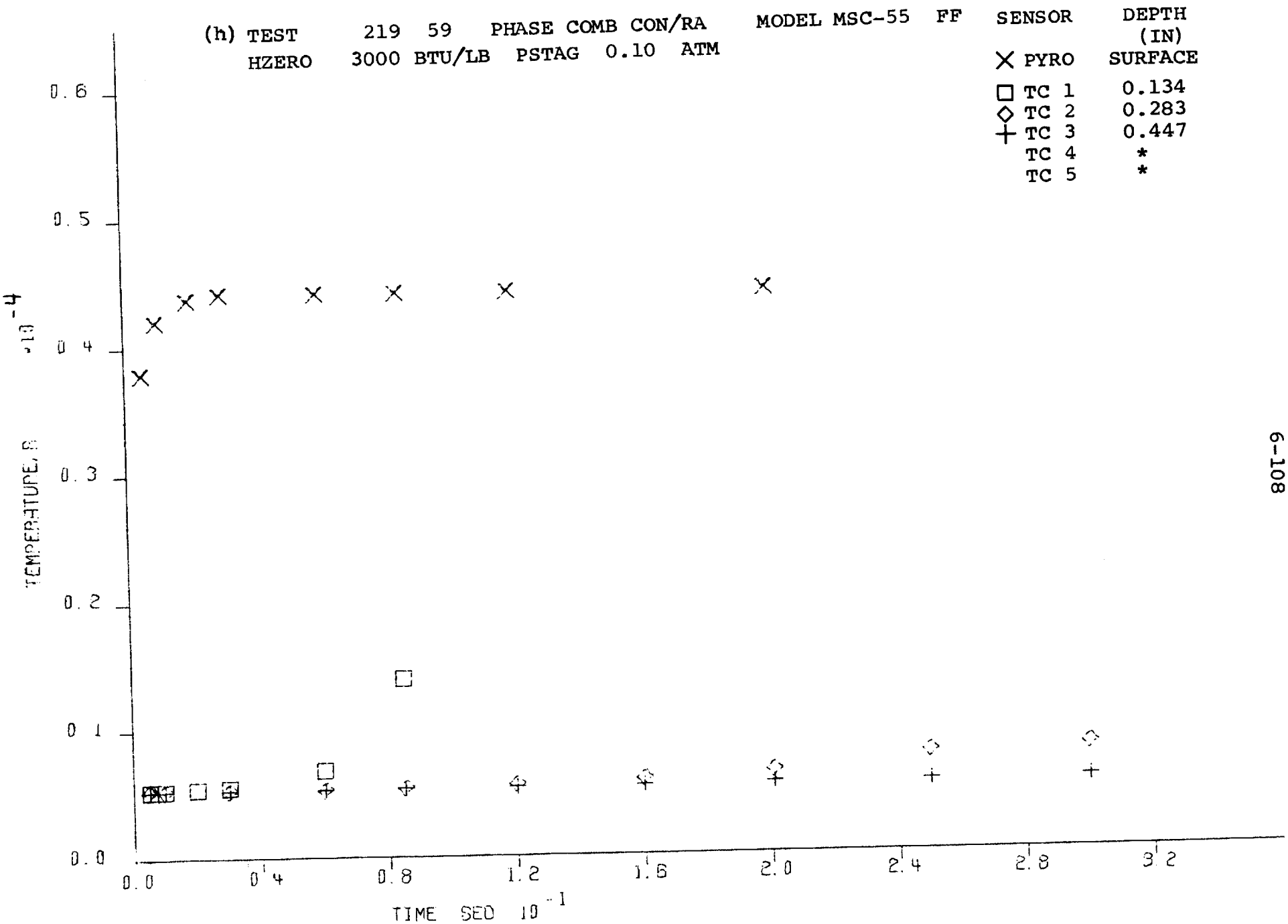

Figure 6-13. Continued.

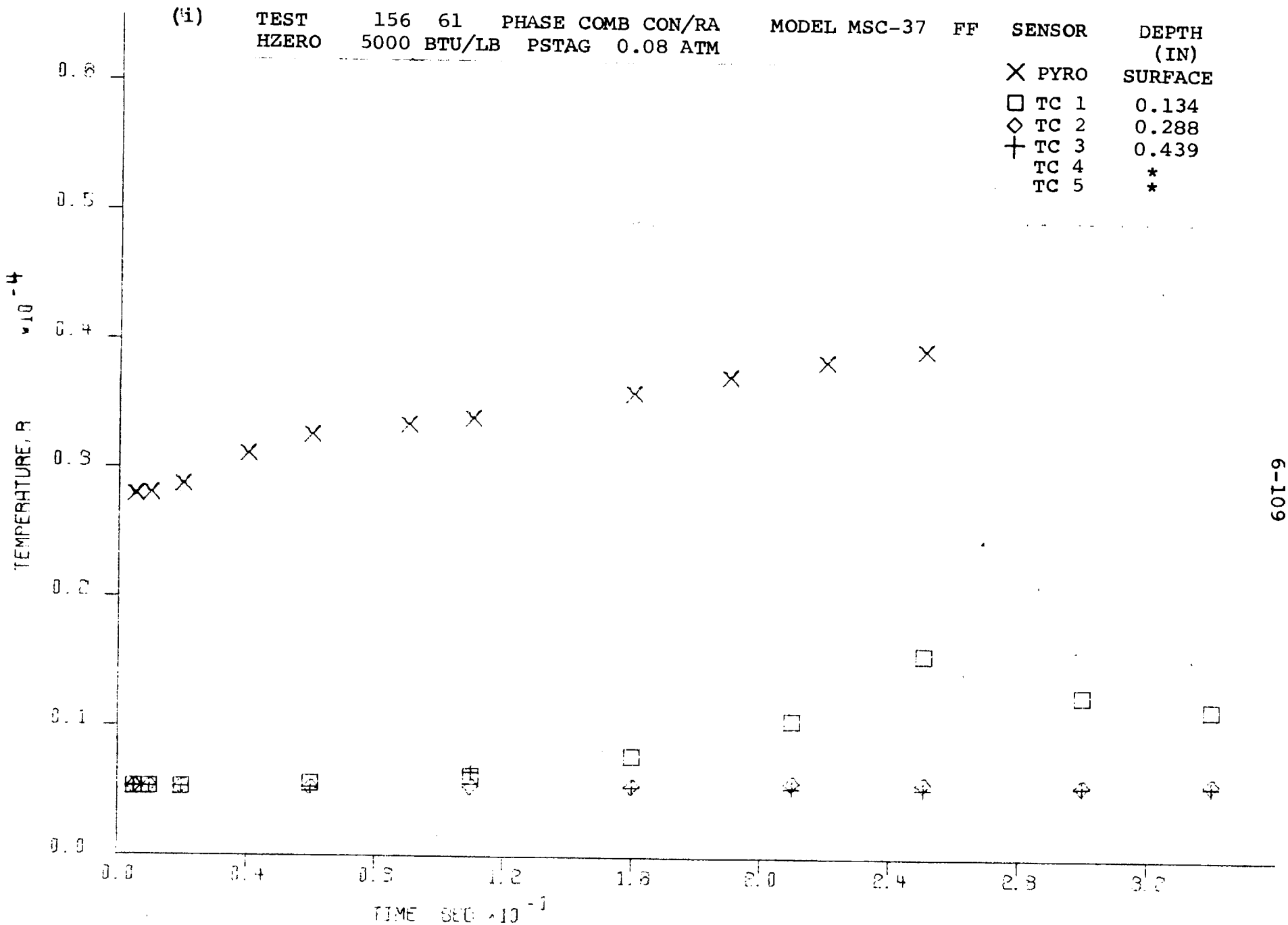

Figure 6-13. Continued.

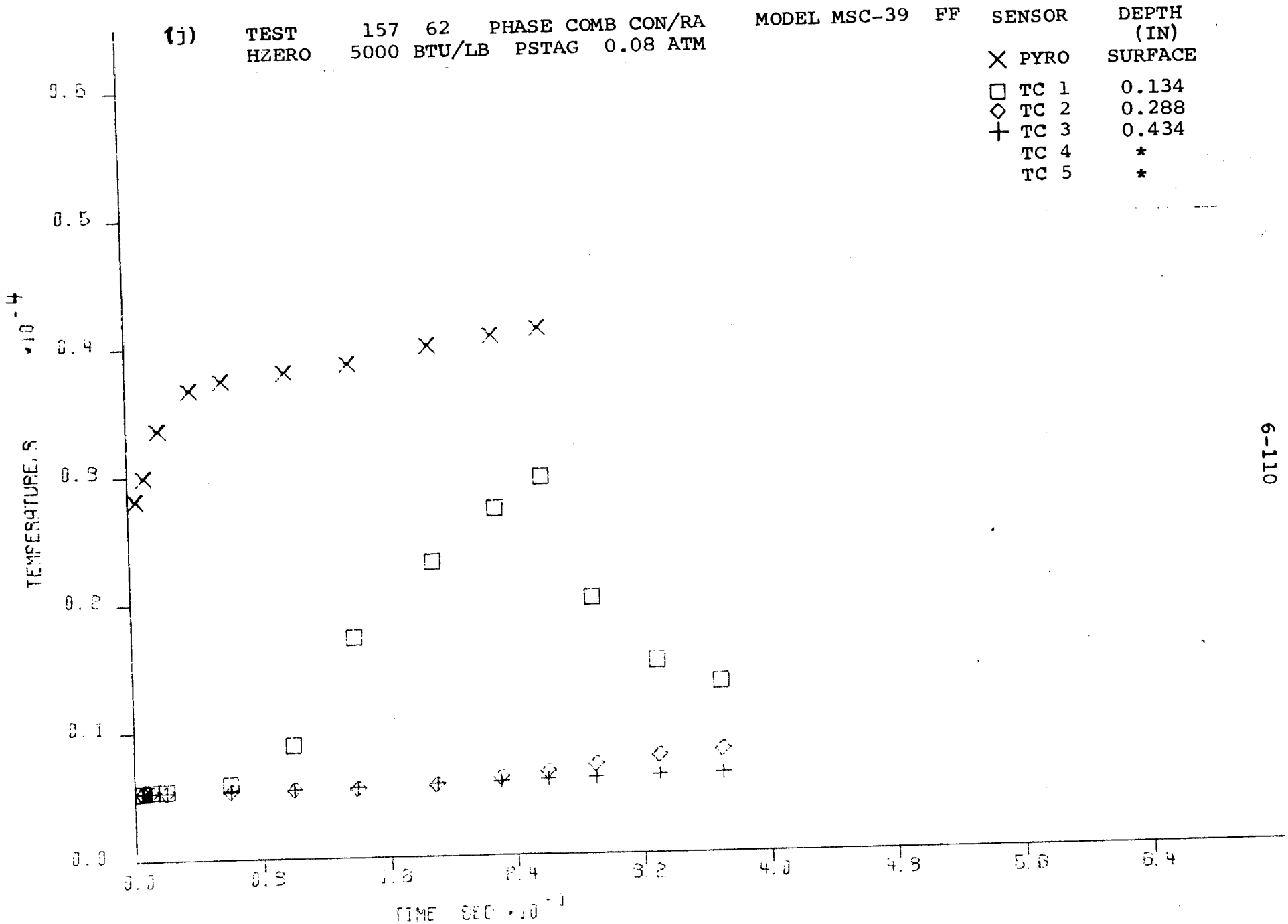

Figure 6-13. Continued.

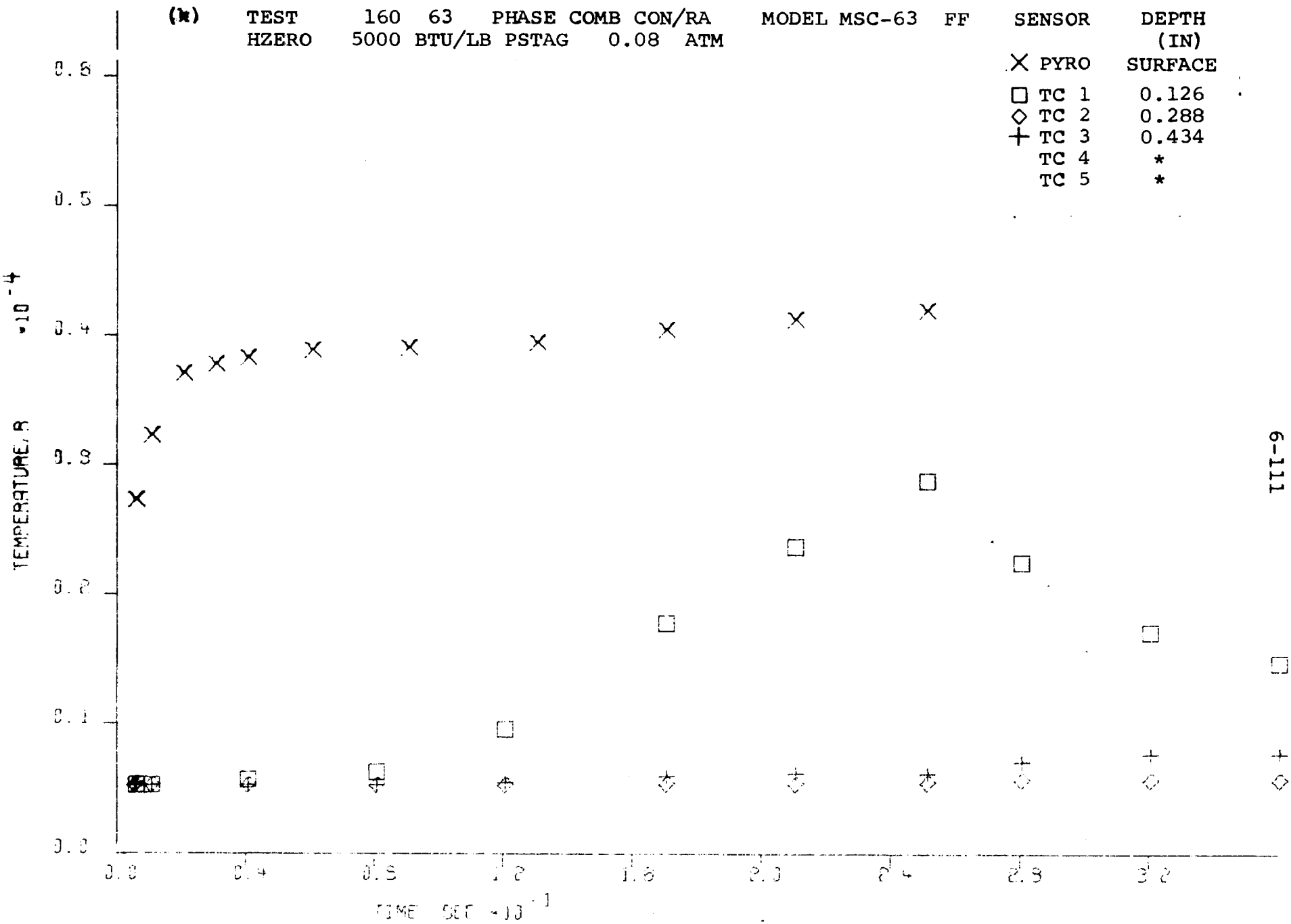

Figure 6-13. Continued.

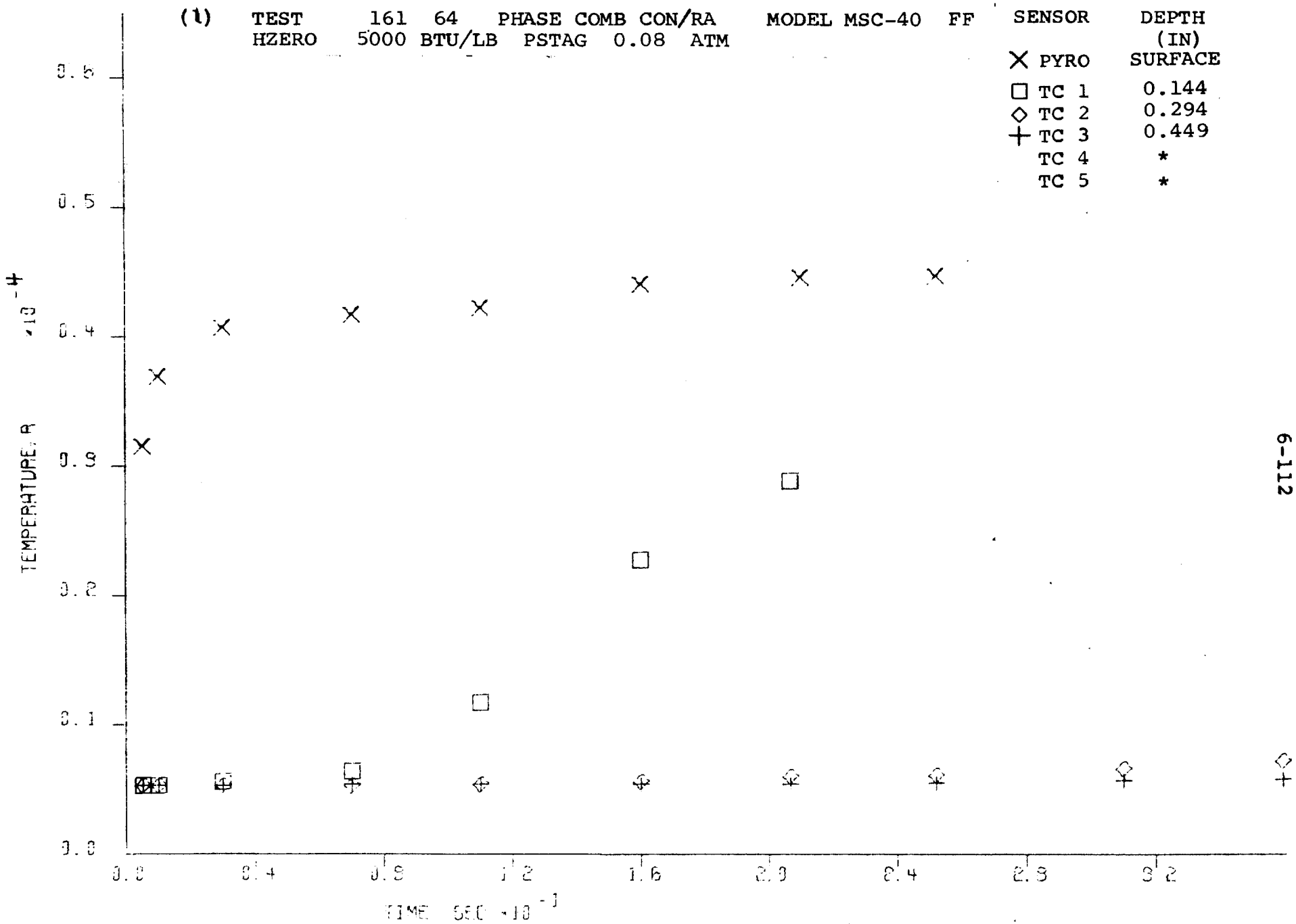

Figure 6-13. Continued.

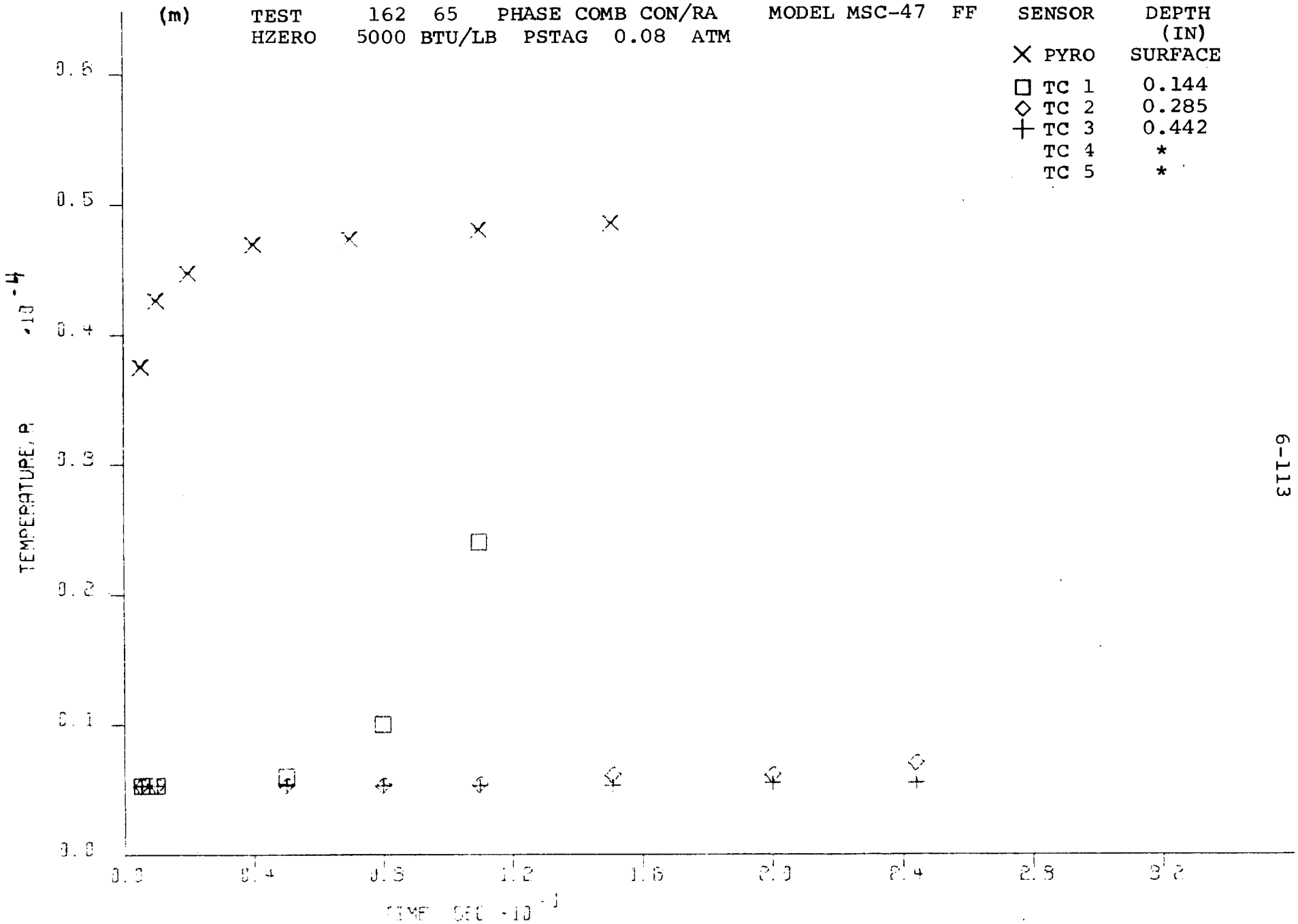

Figure 6-13. Continued.

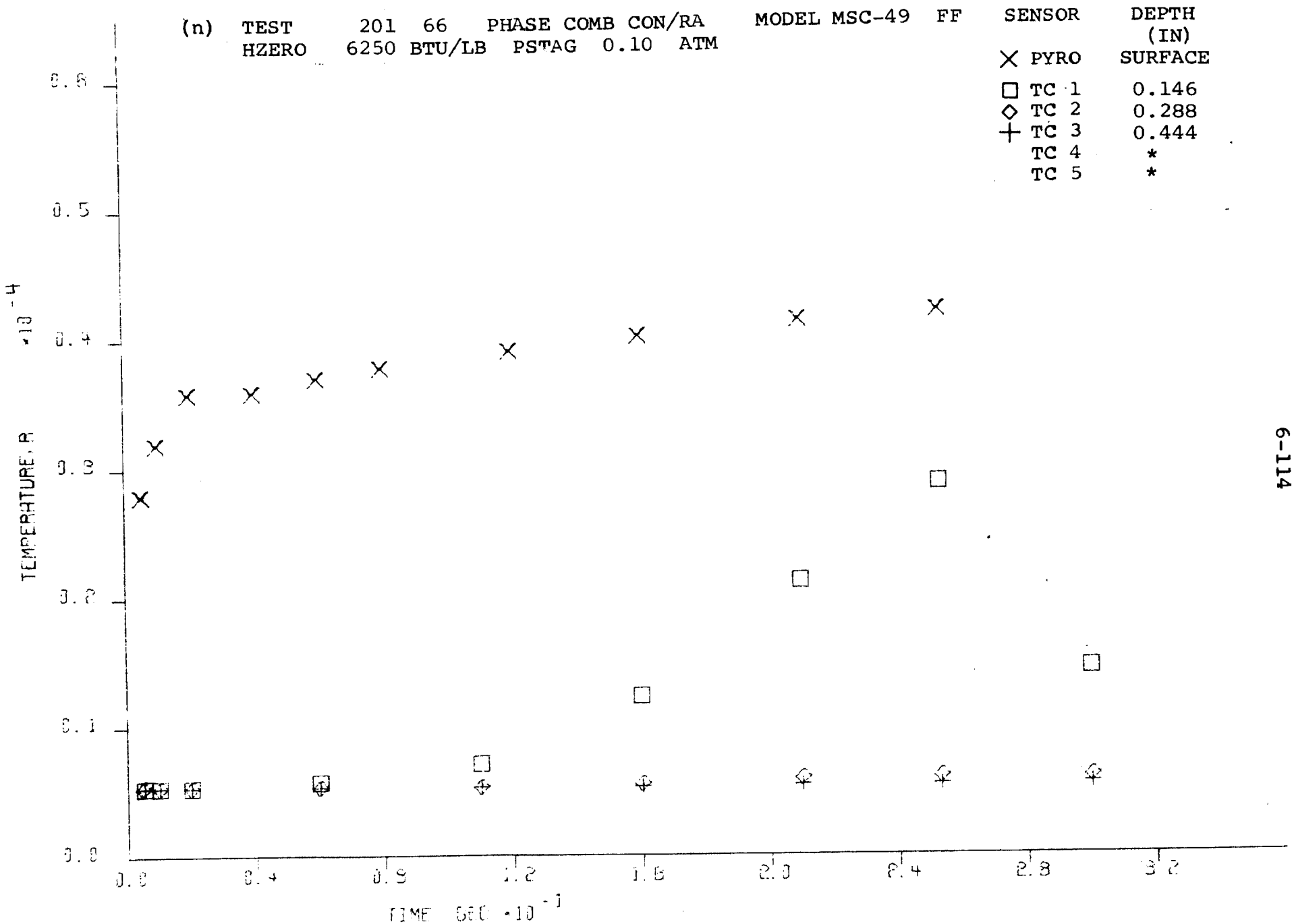

Figure 6-13. Continued.

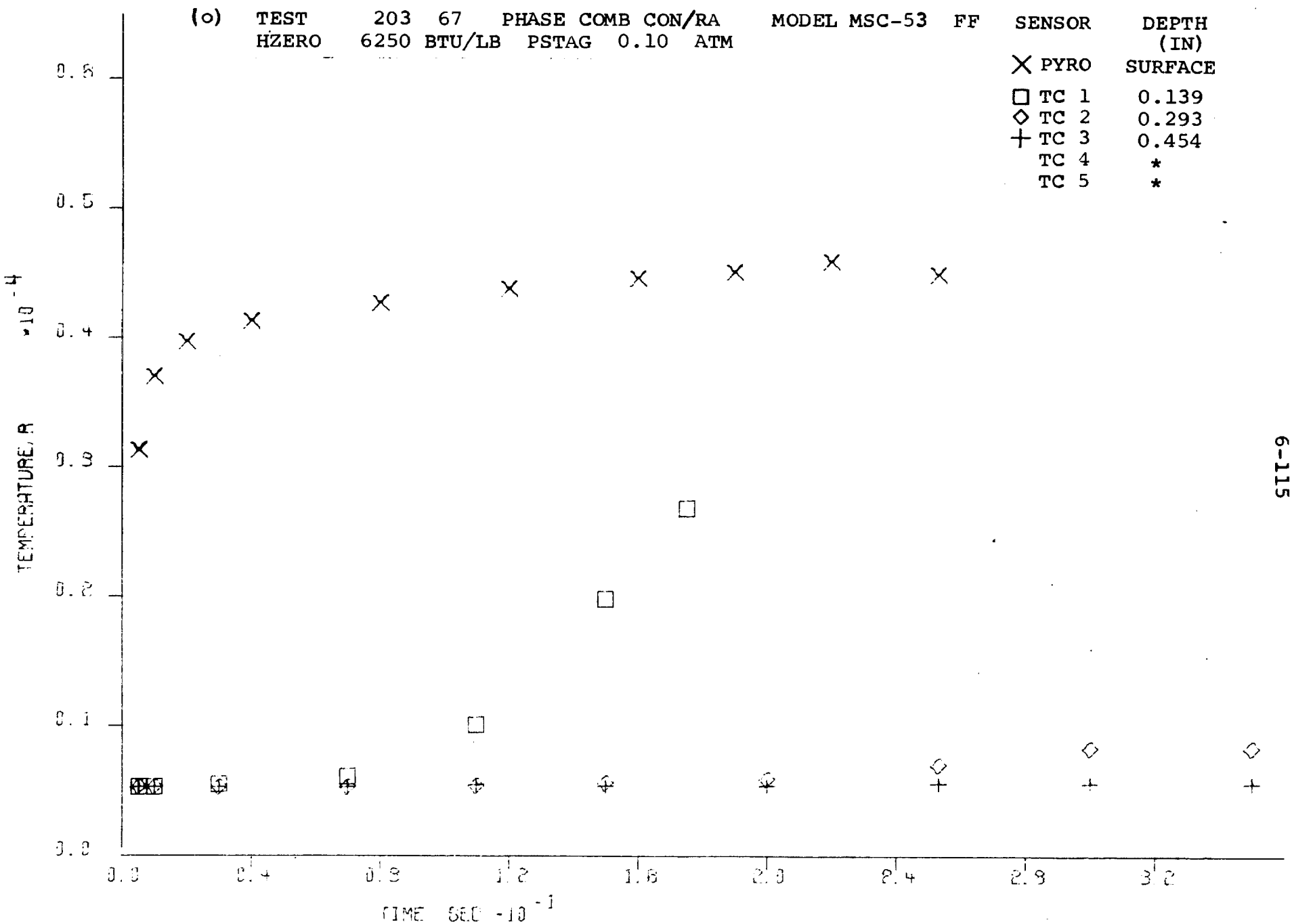

Figure 6-13. Continued.

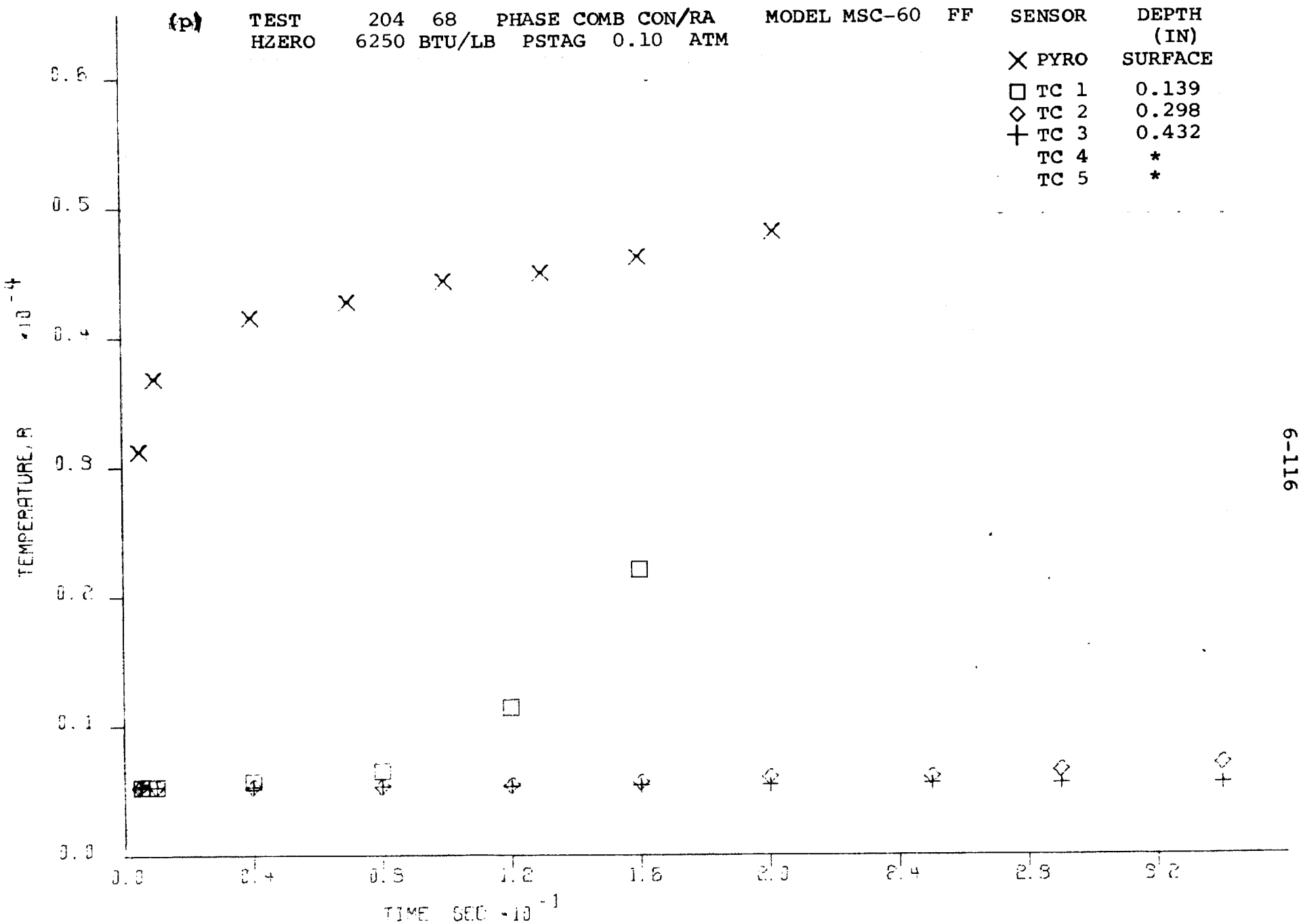

Figure 6-13. Continued.

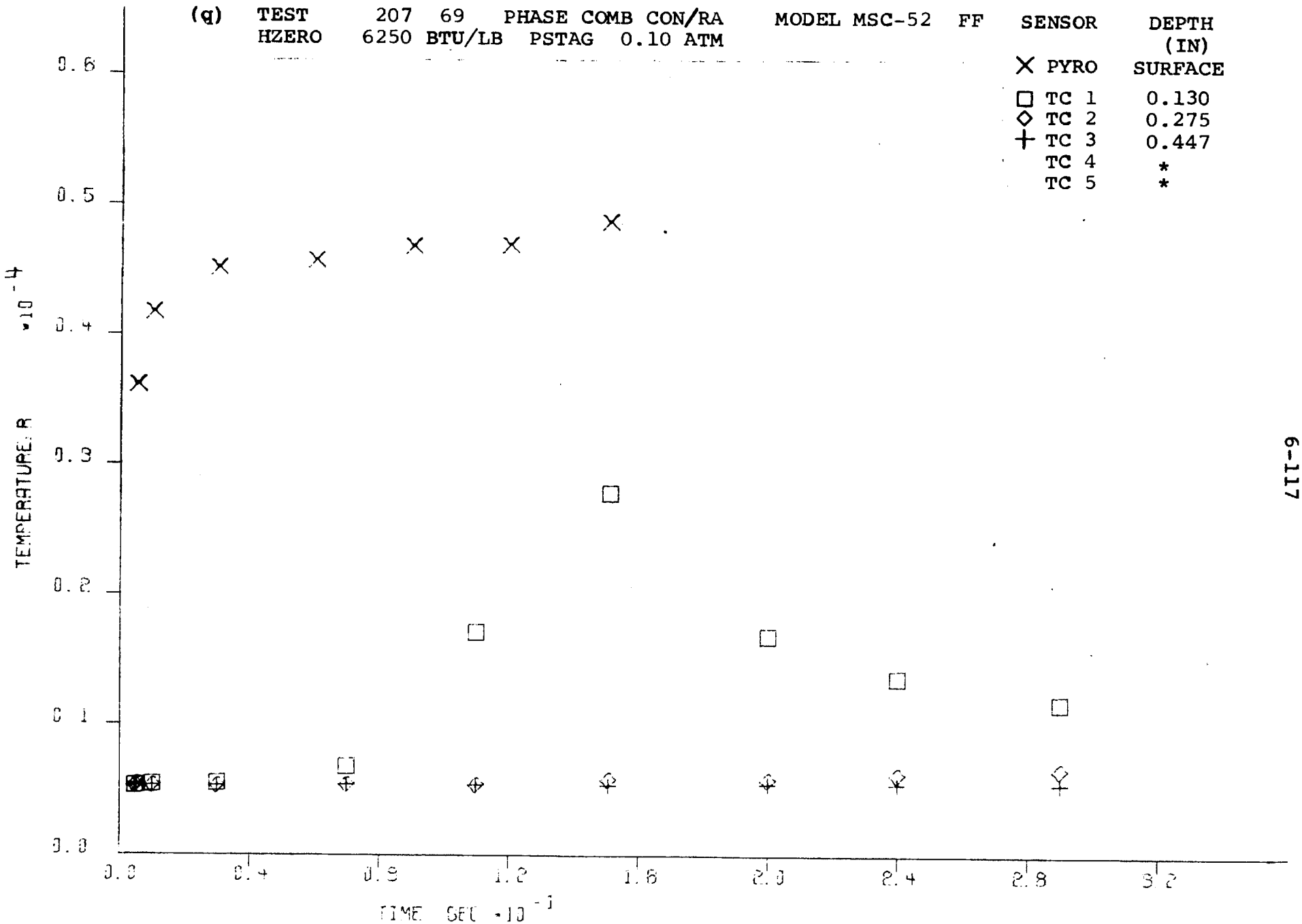

Figure 6-13. Continued.

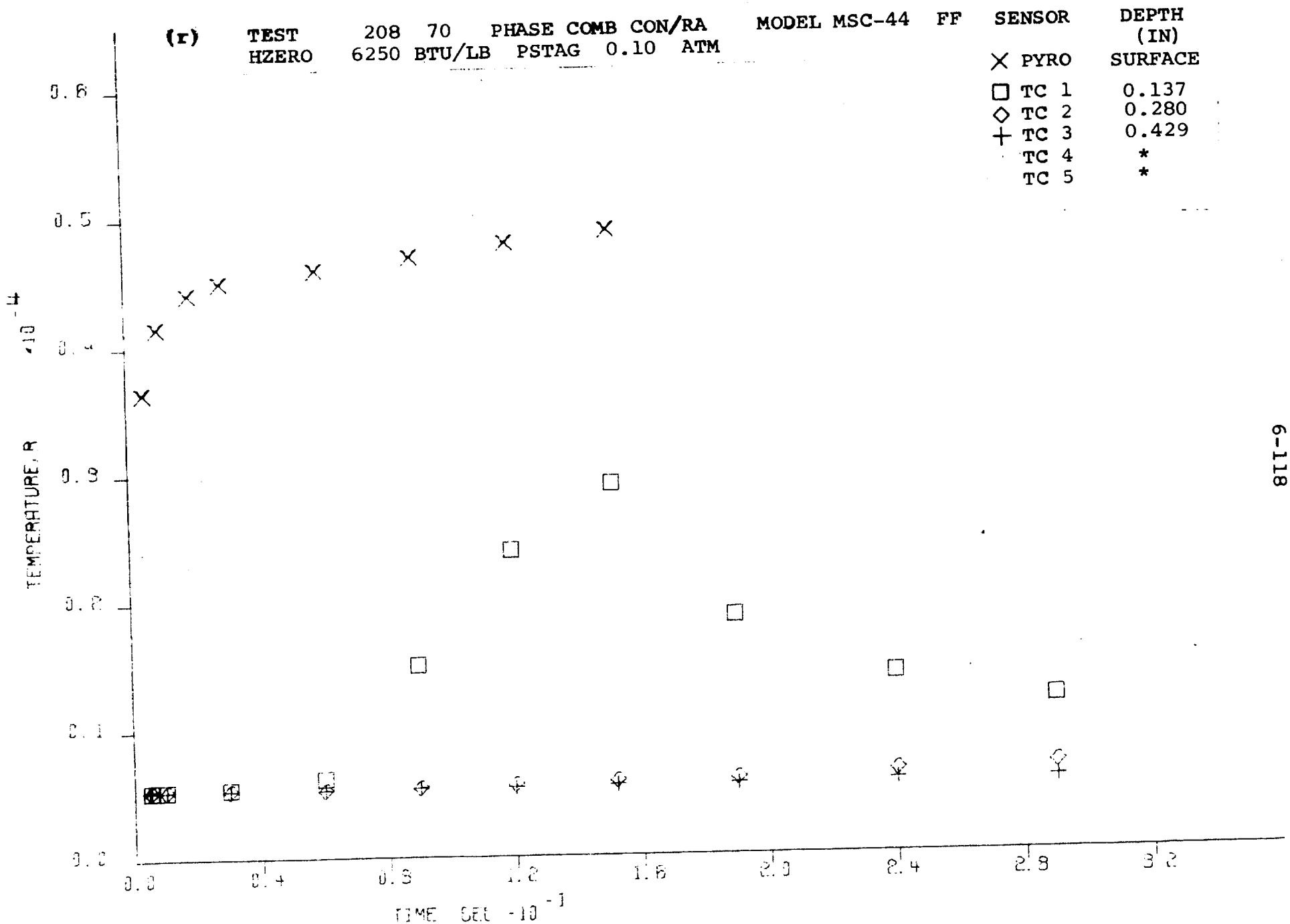

Figure 6-13. Continued.

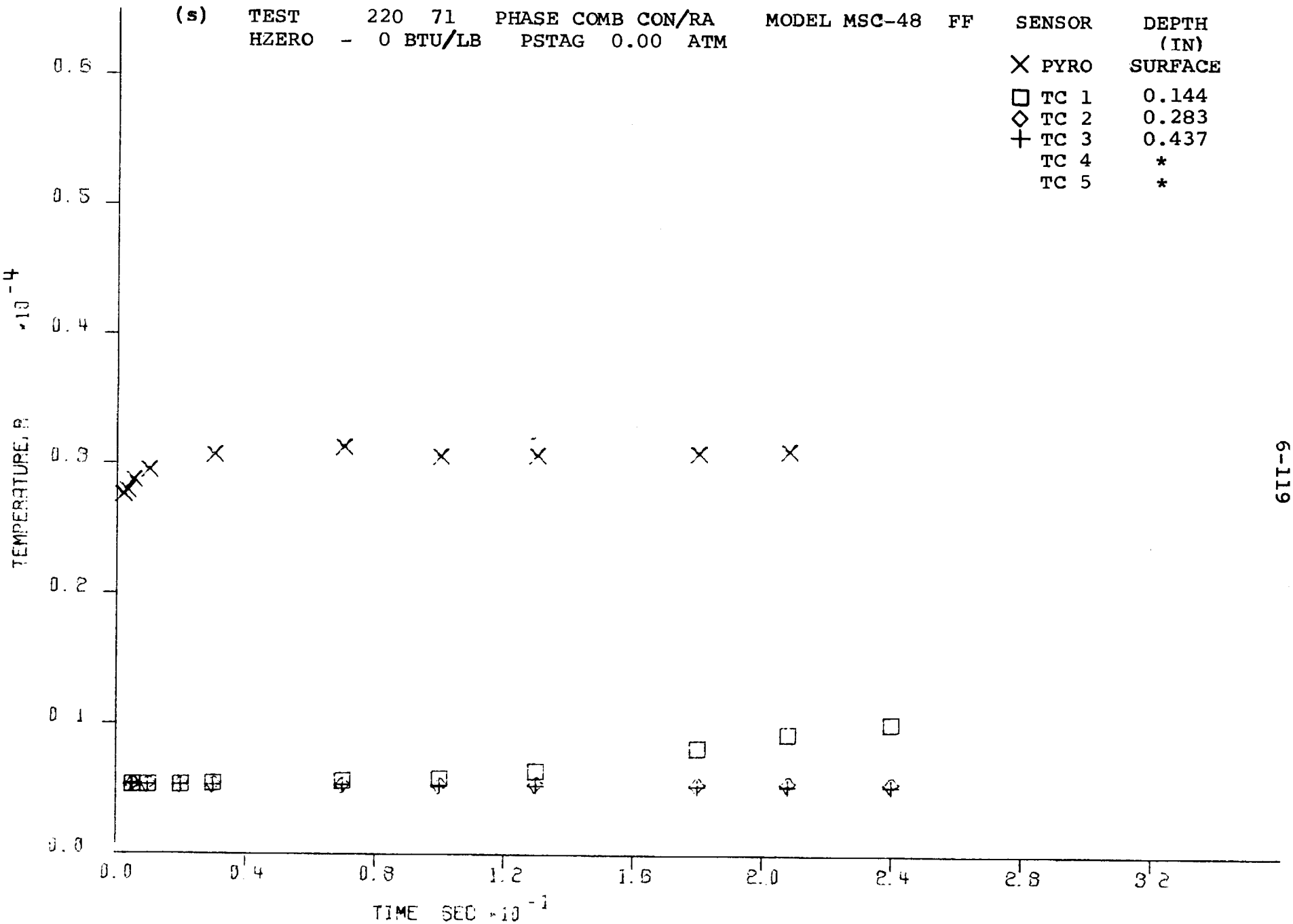

Figure 6-13. Continued.

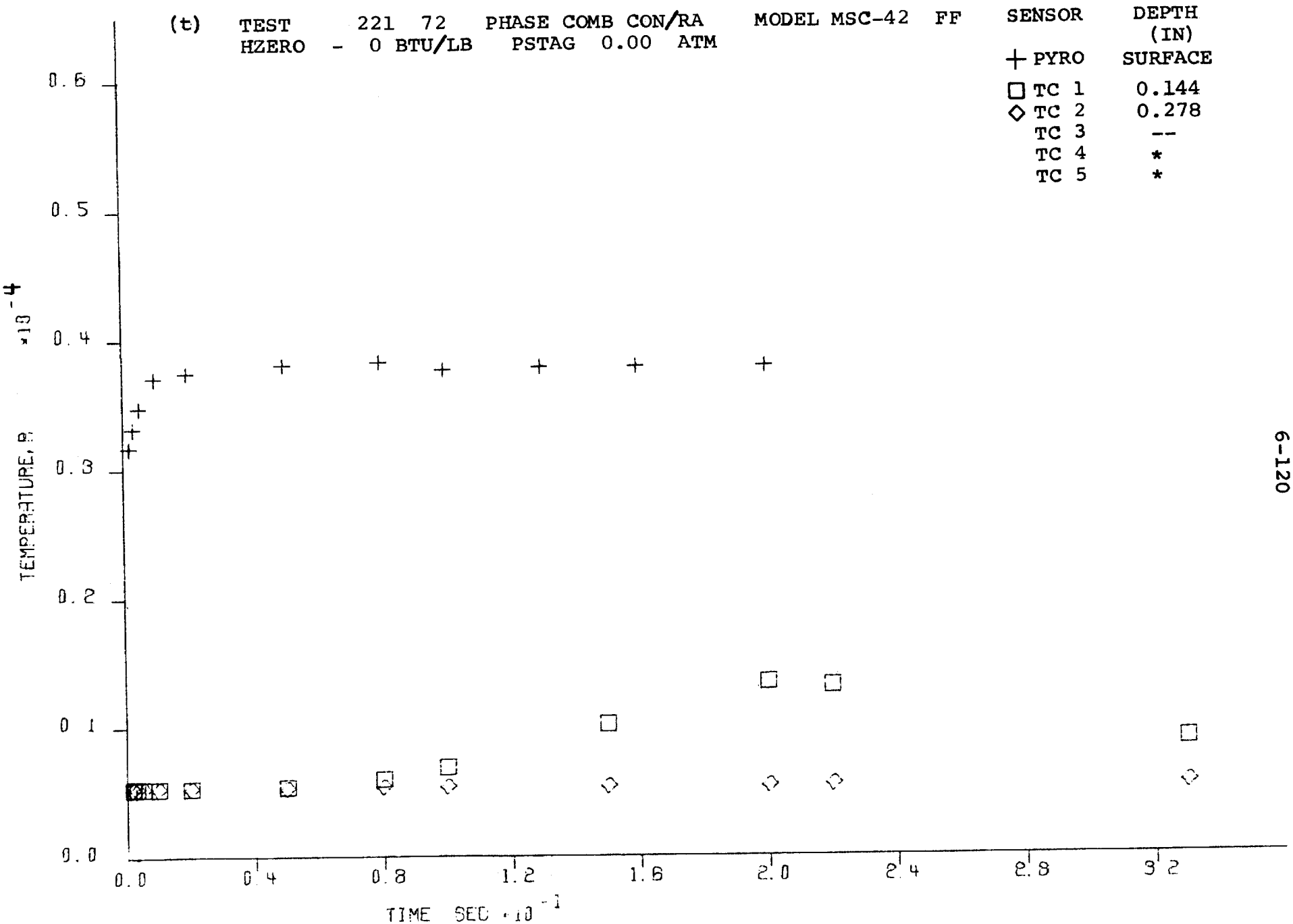

Figure 6-13. Continued.

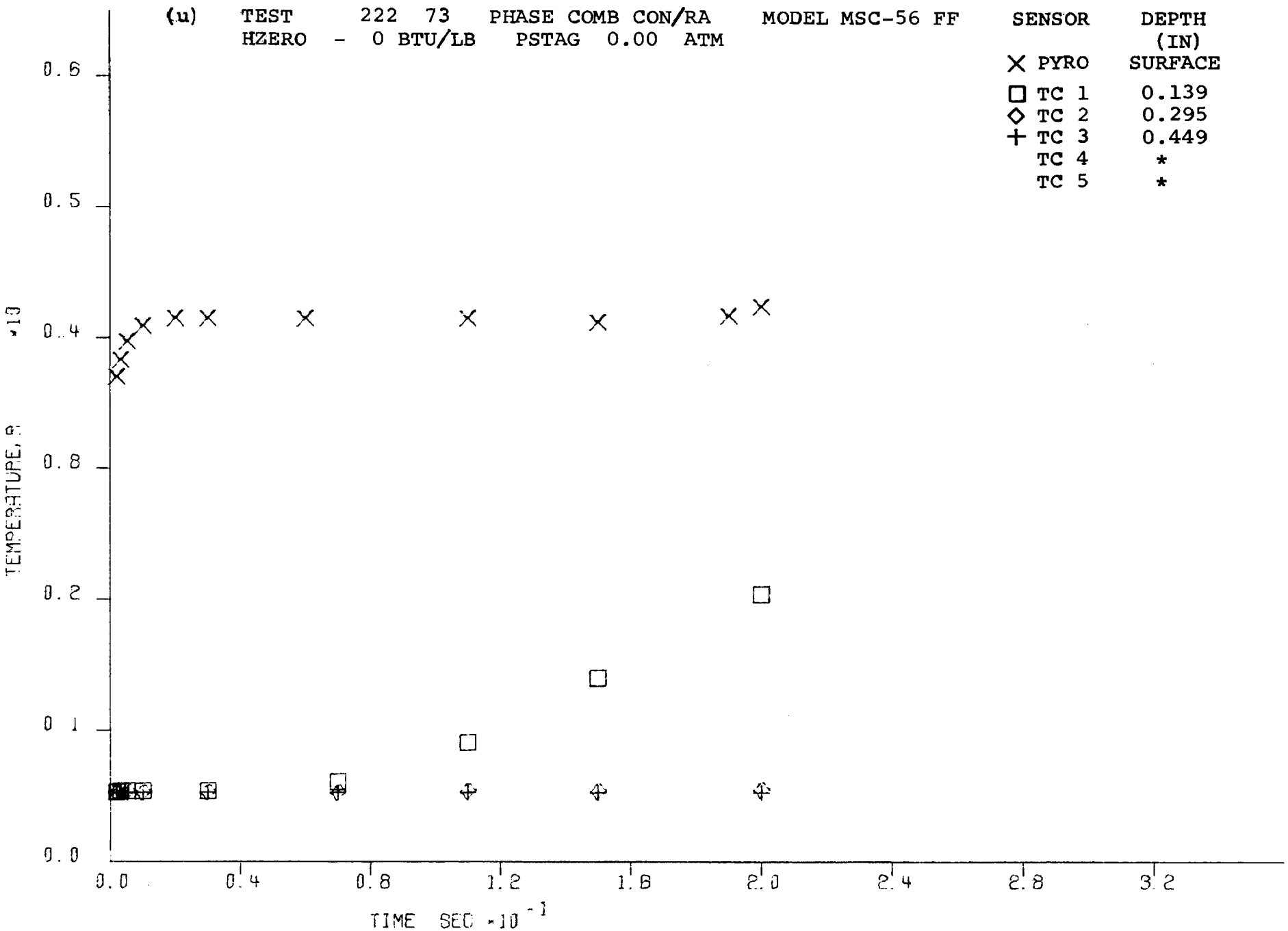

Figure 6-13. Continued.

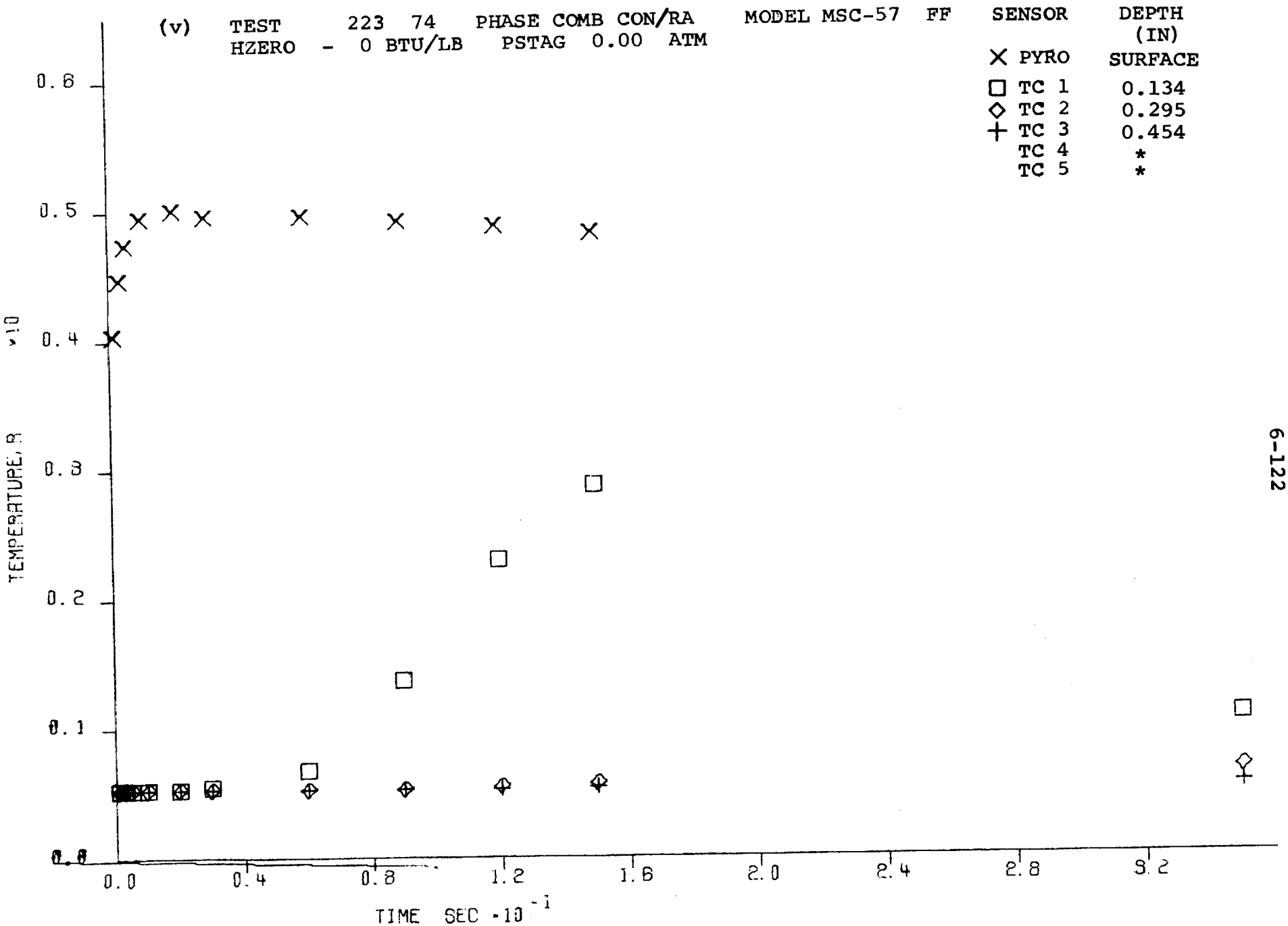

Figure 6-13. Continued.

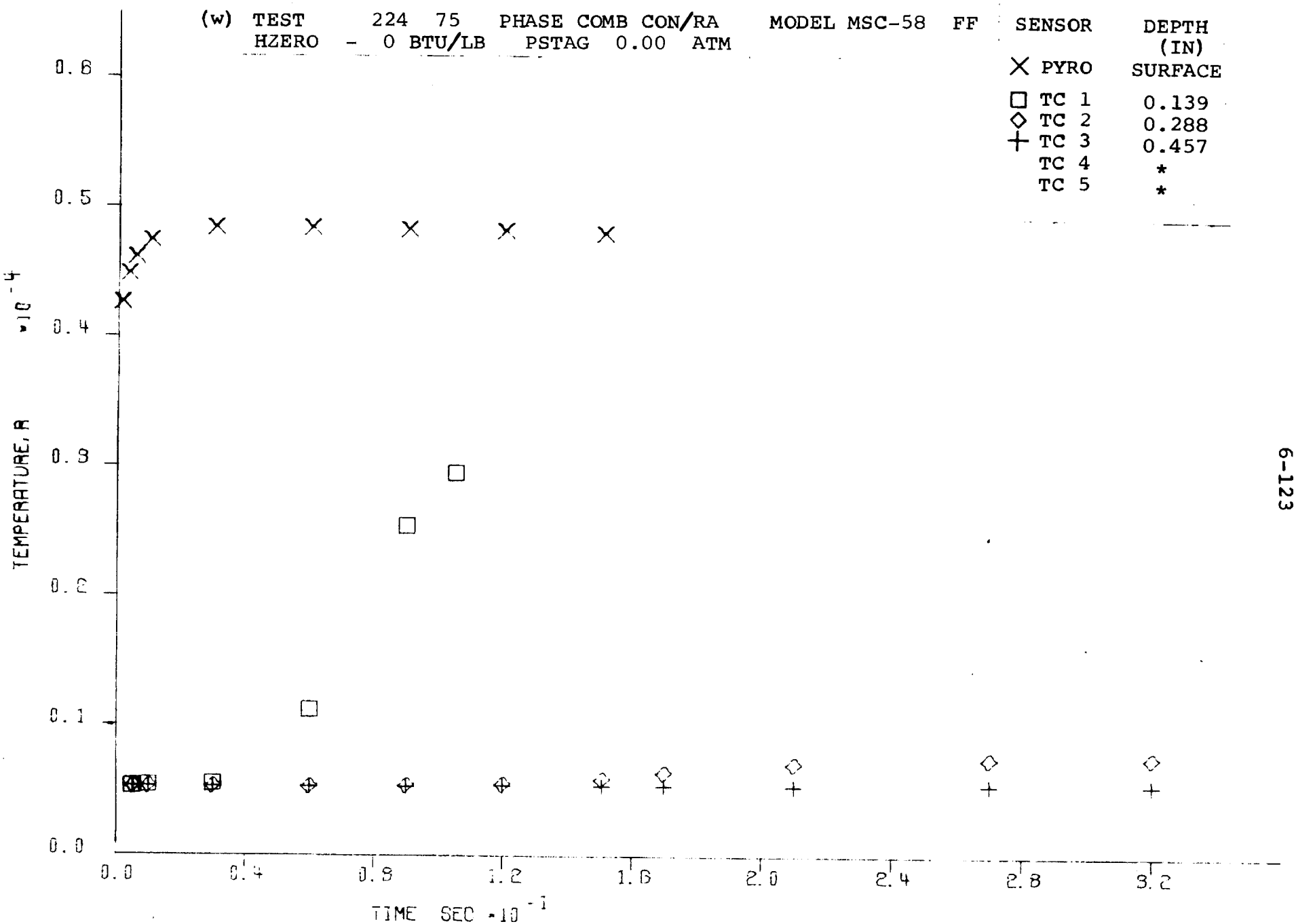

Figure 6-13. Concluded.

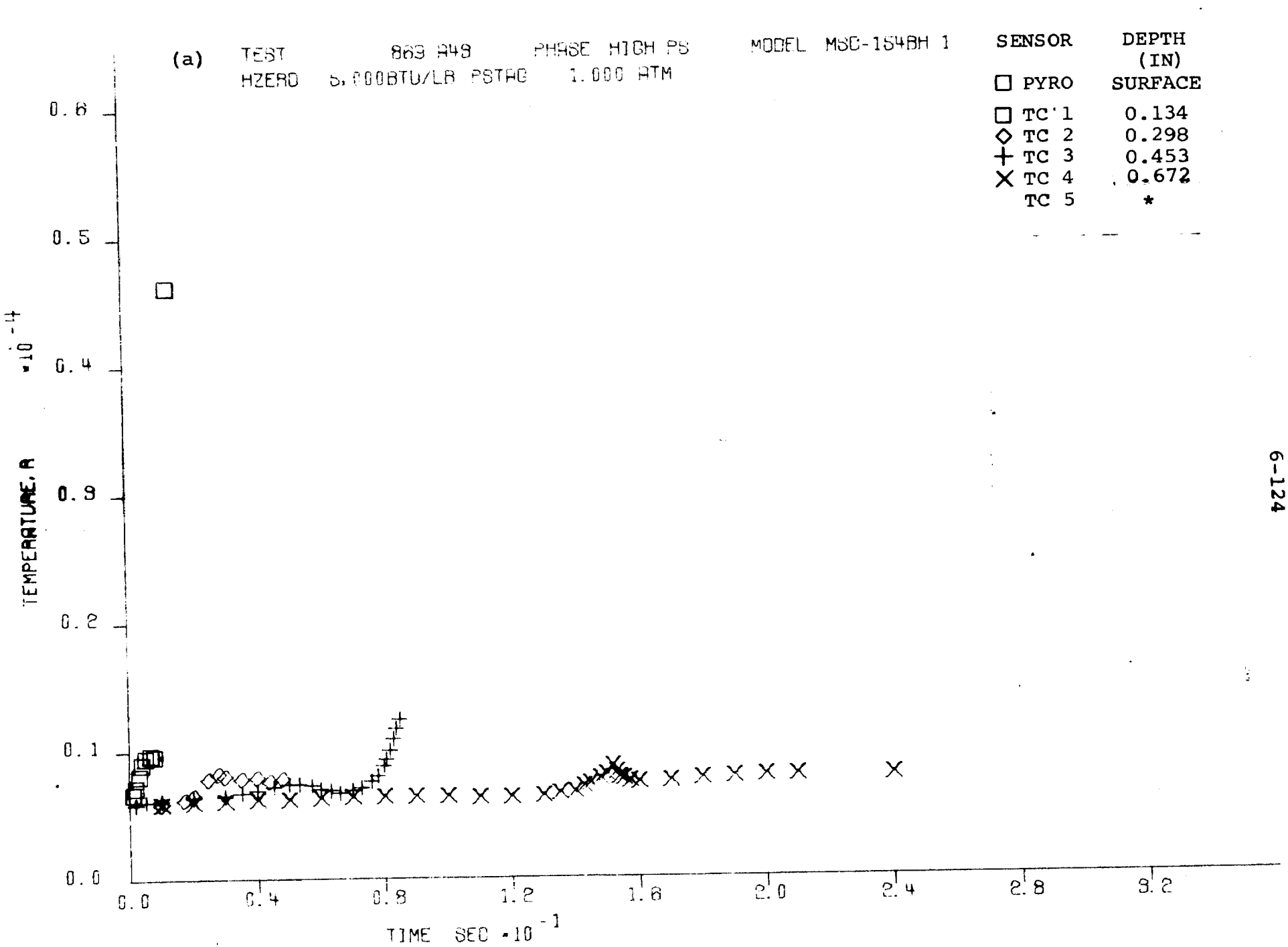

Figure 6-14. Surface and Internal Temperature Histories, Phase III.

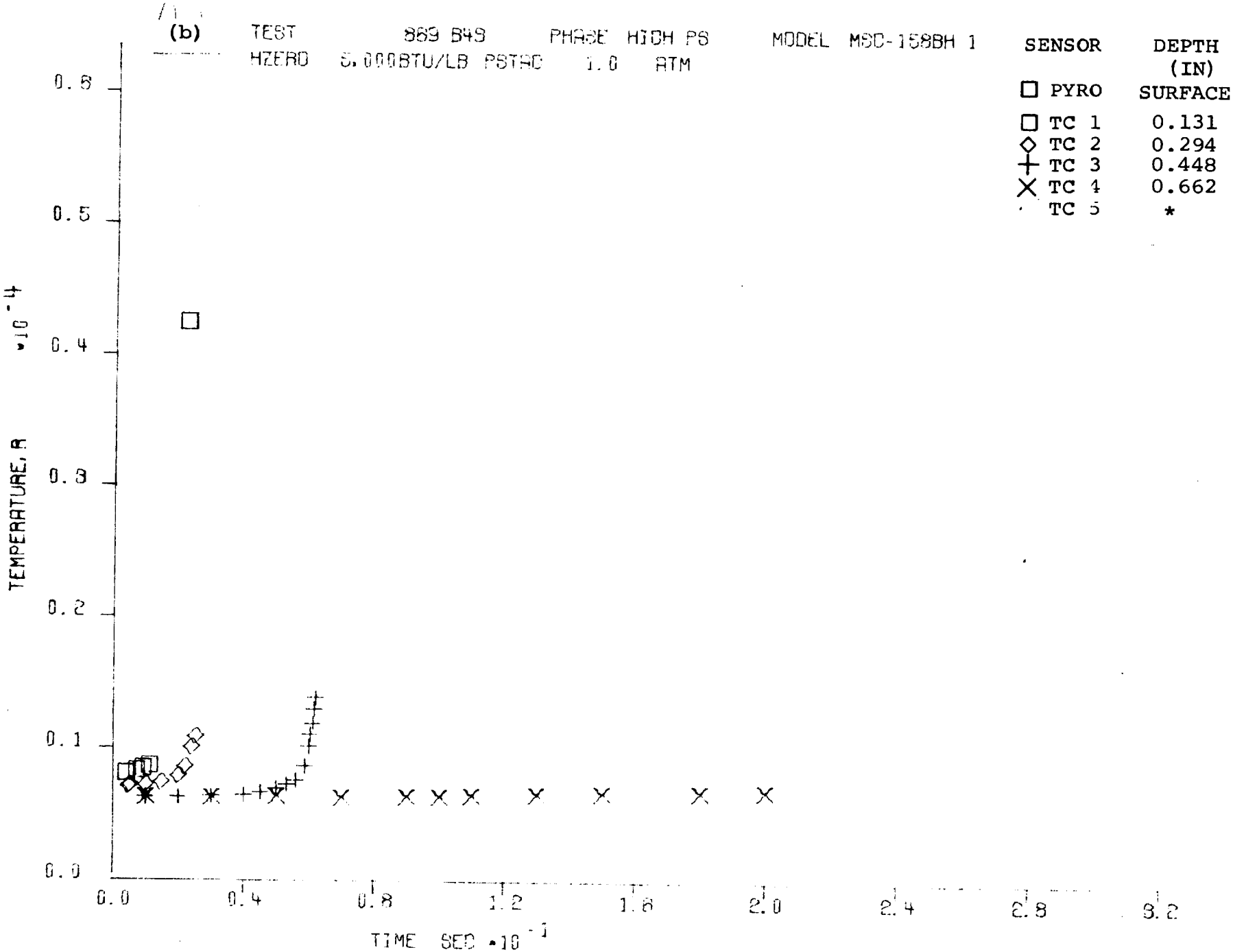

Figure 6-14. Continued.

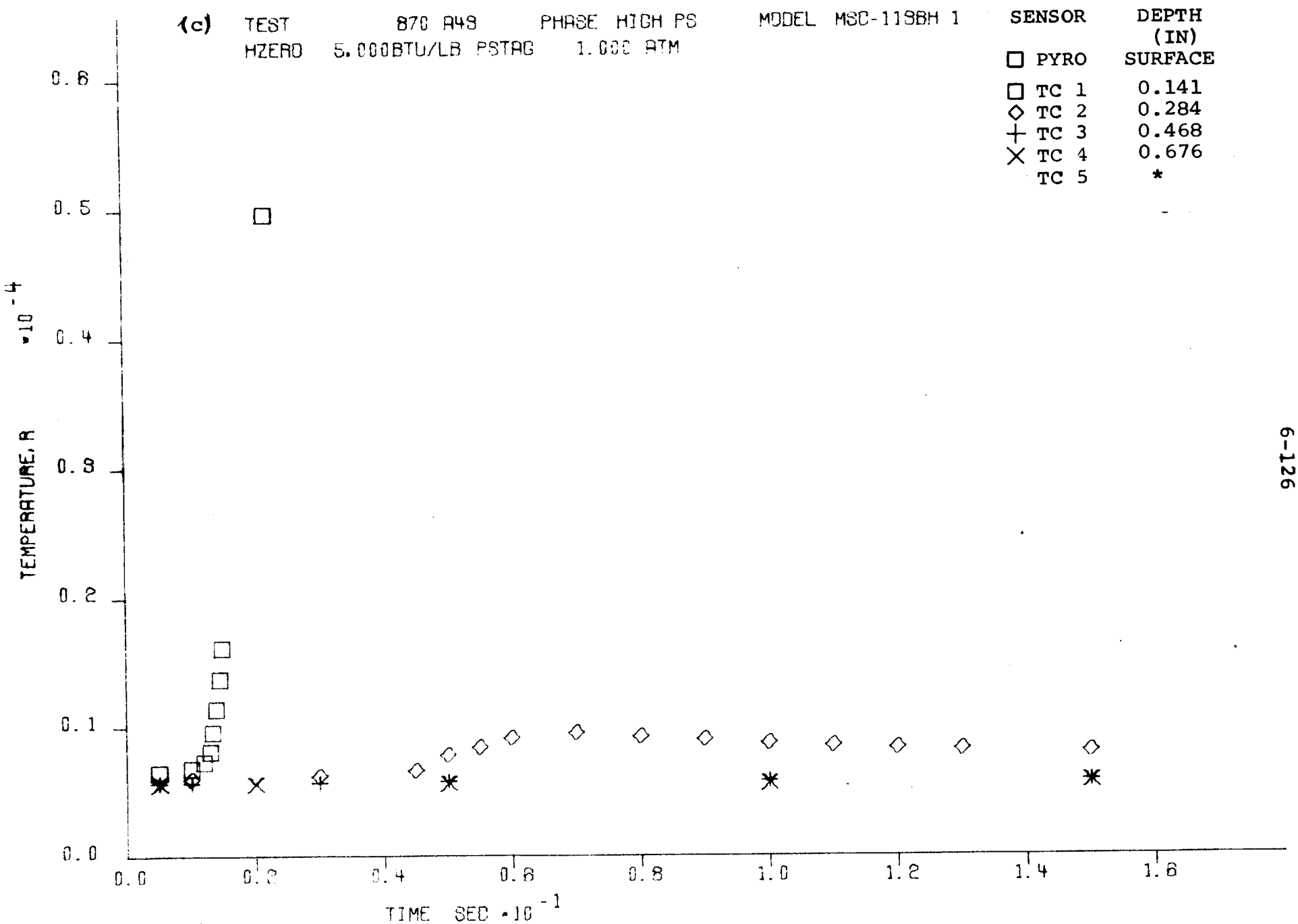

Figure 6-14. Continued.

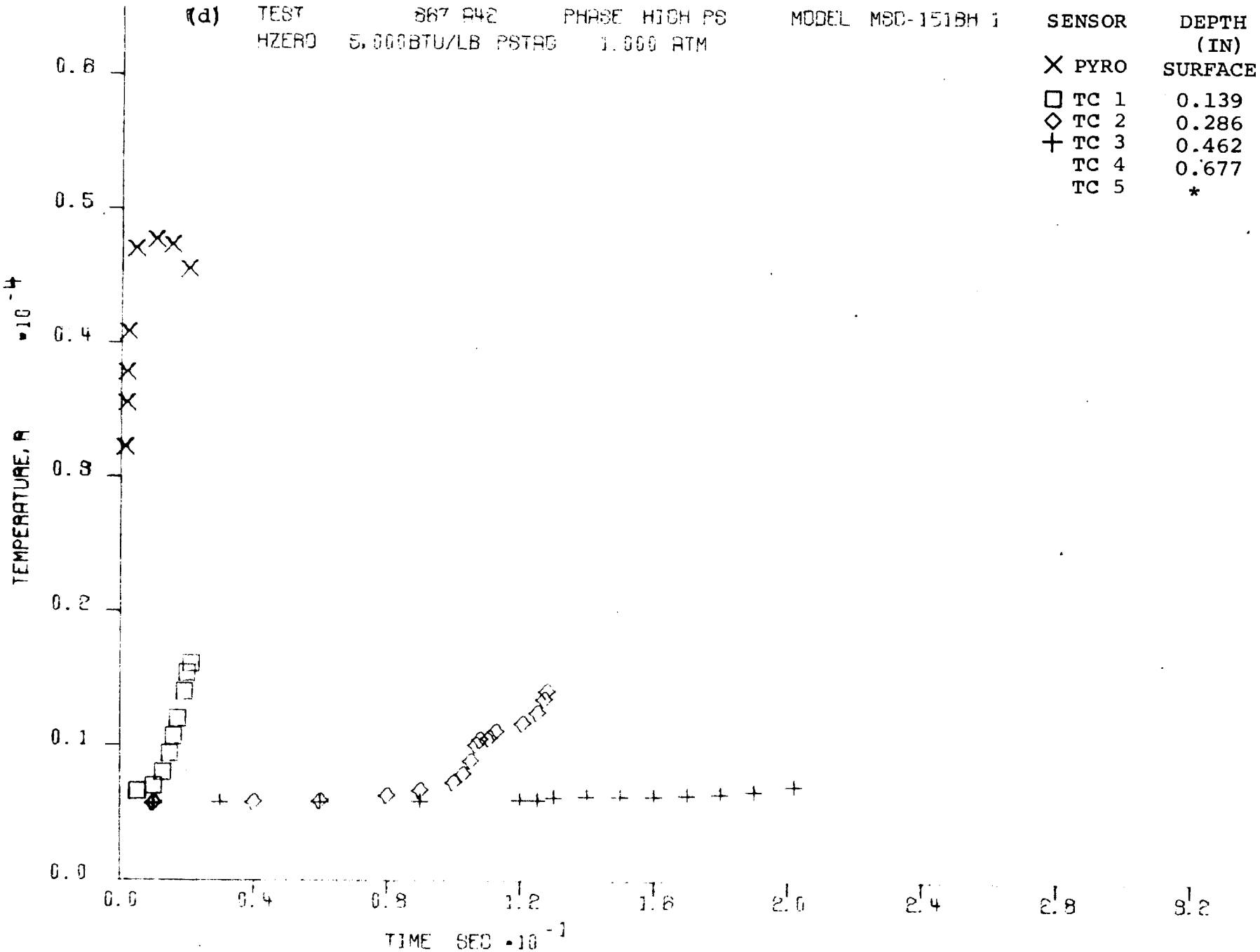

Figure 6-14. Continued.

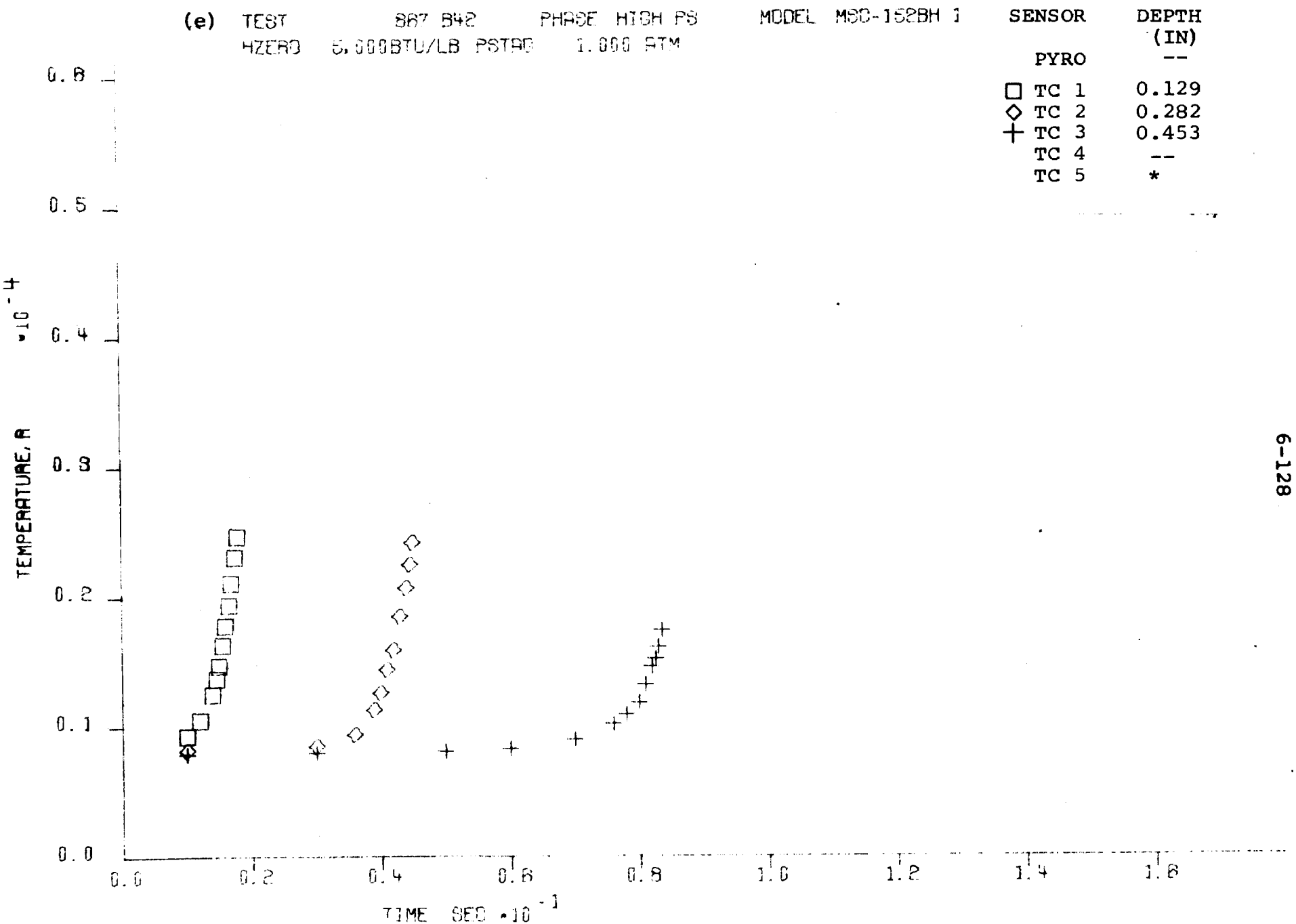

Figure 6-14. Continued.

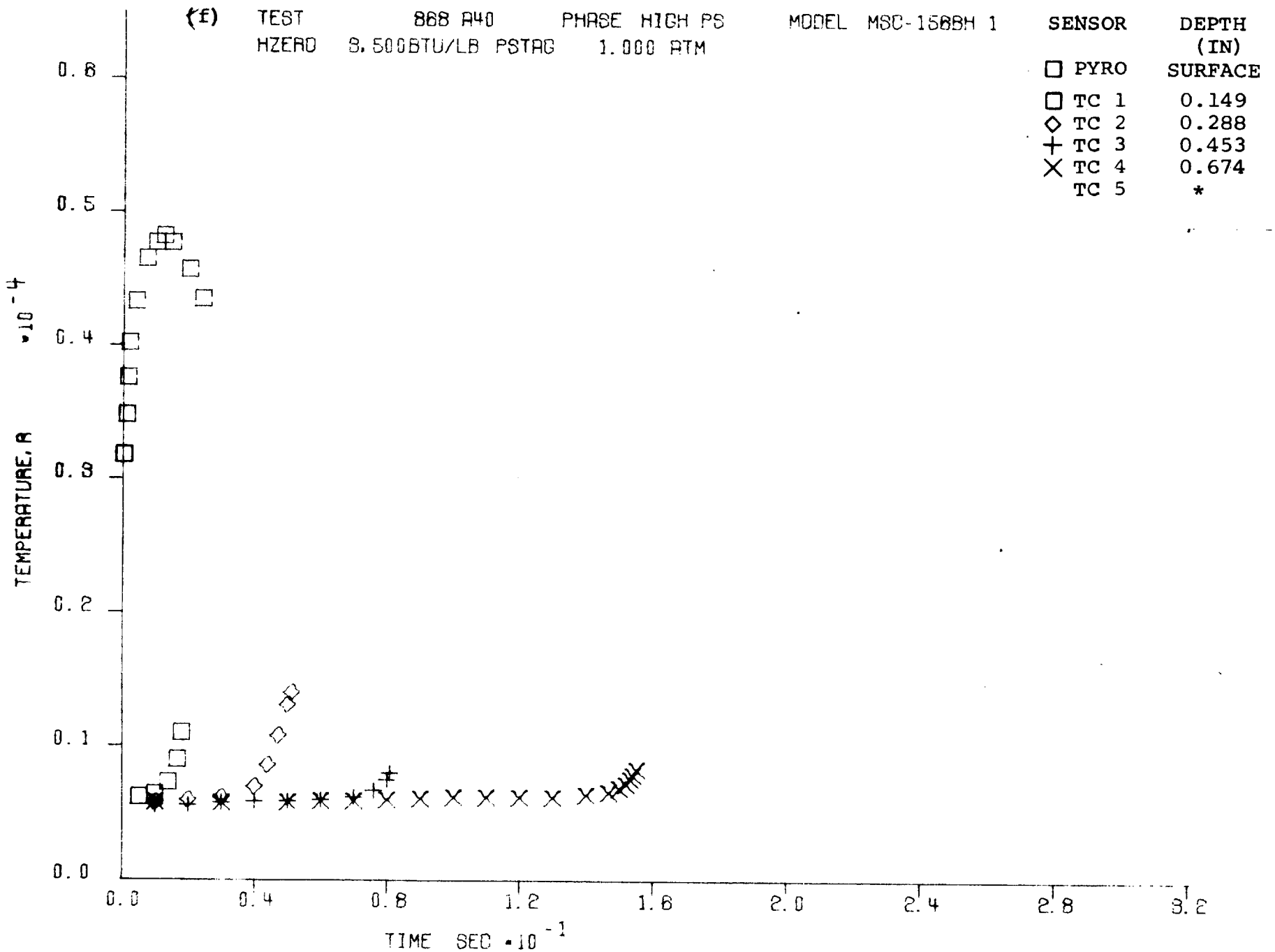

Figure 6-14. Continued.

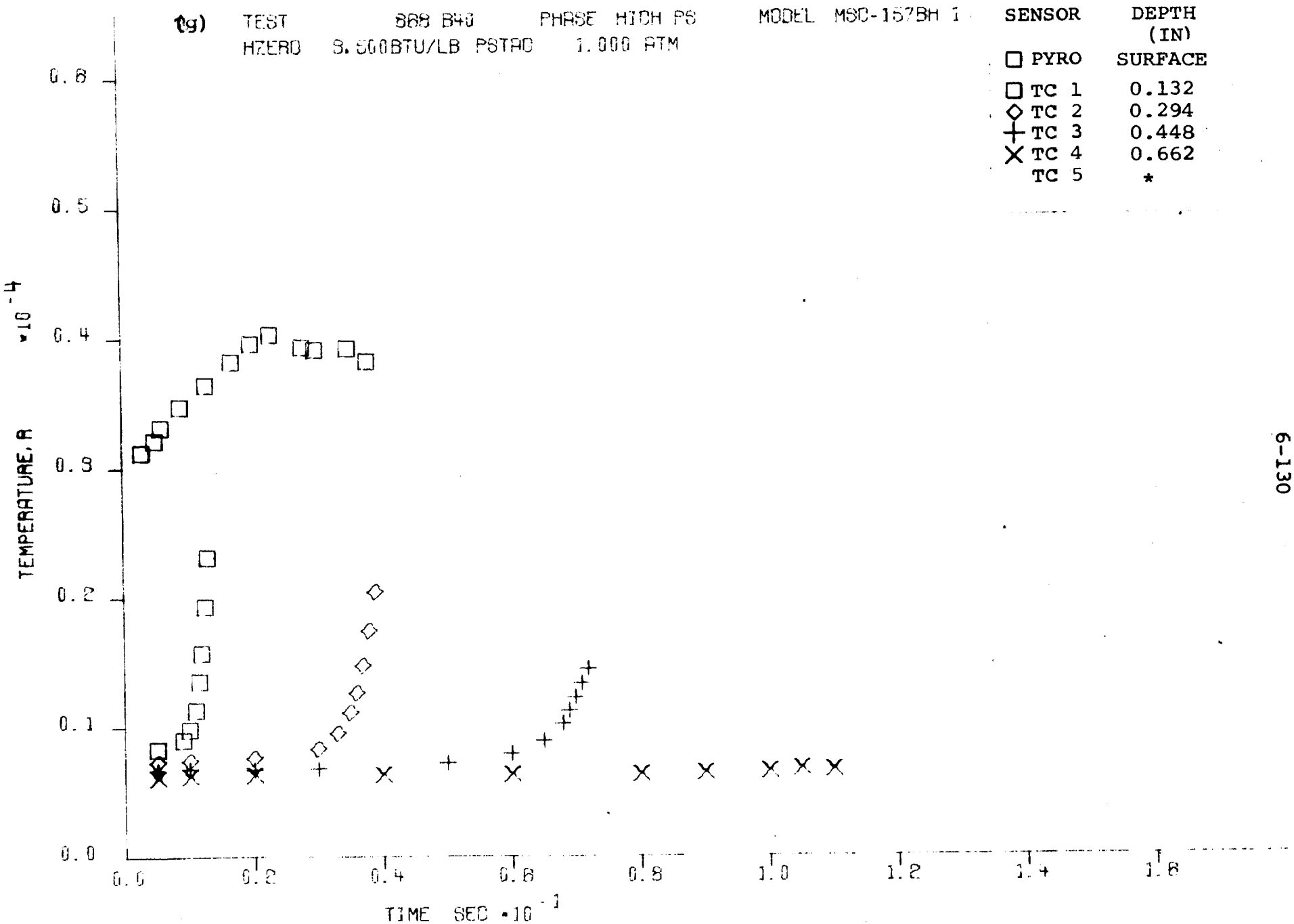

Figure 6-14. Continued.

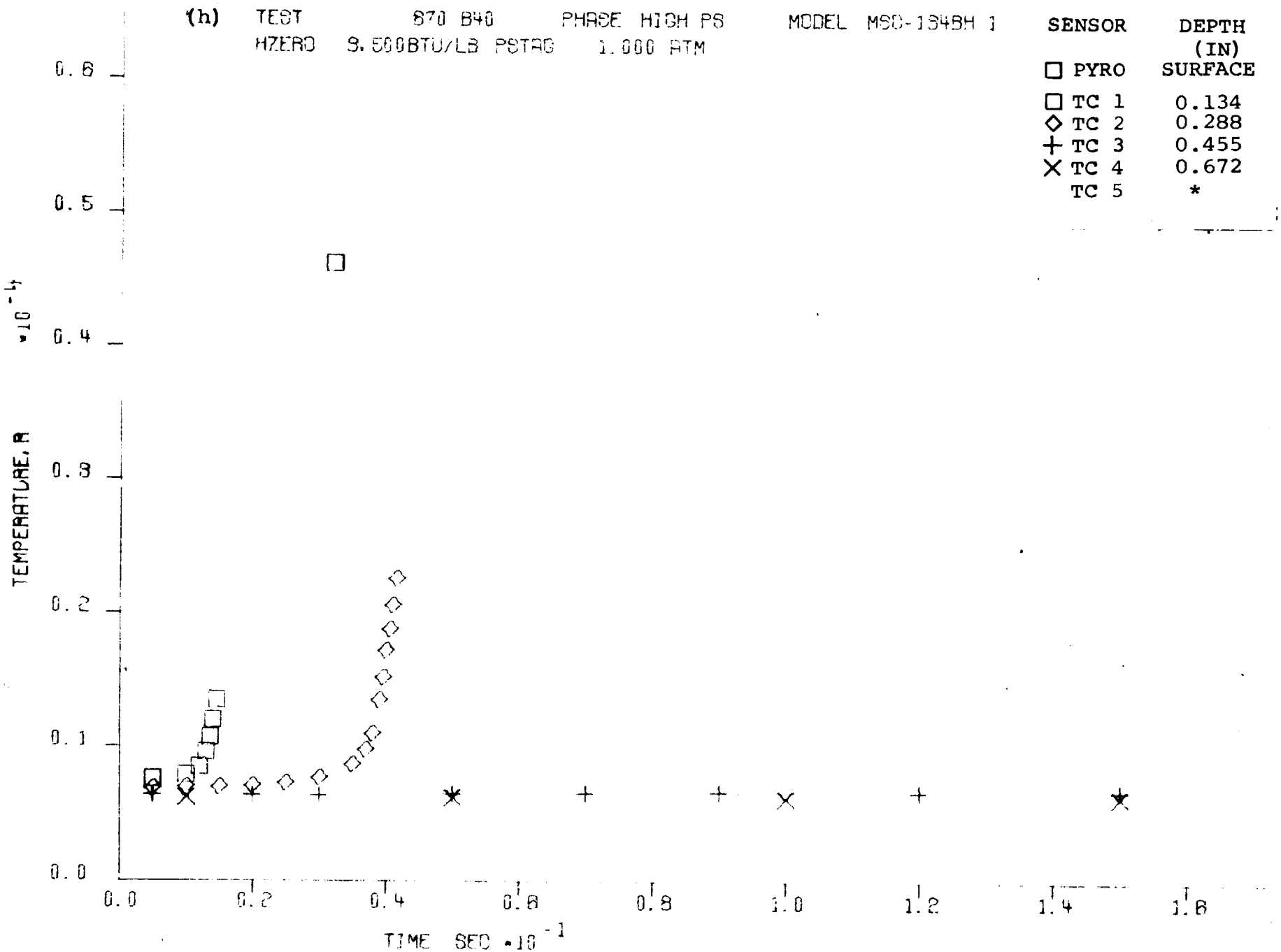

Figure 6-14. Continued.

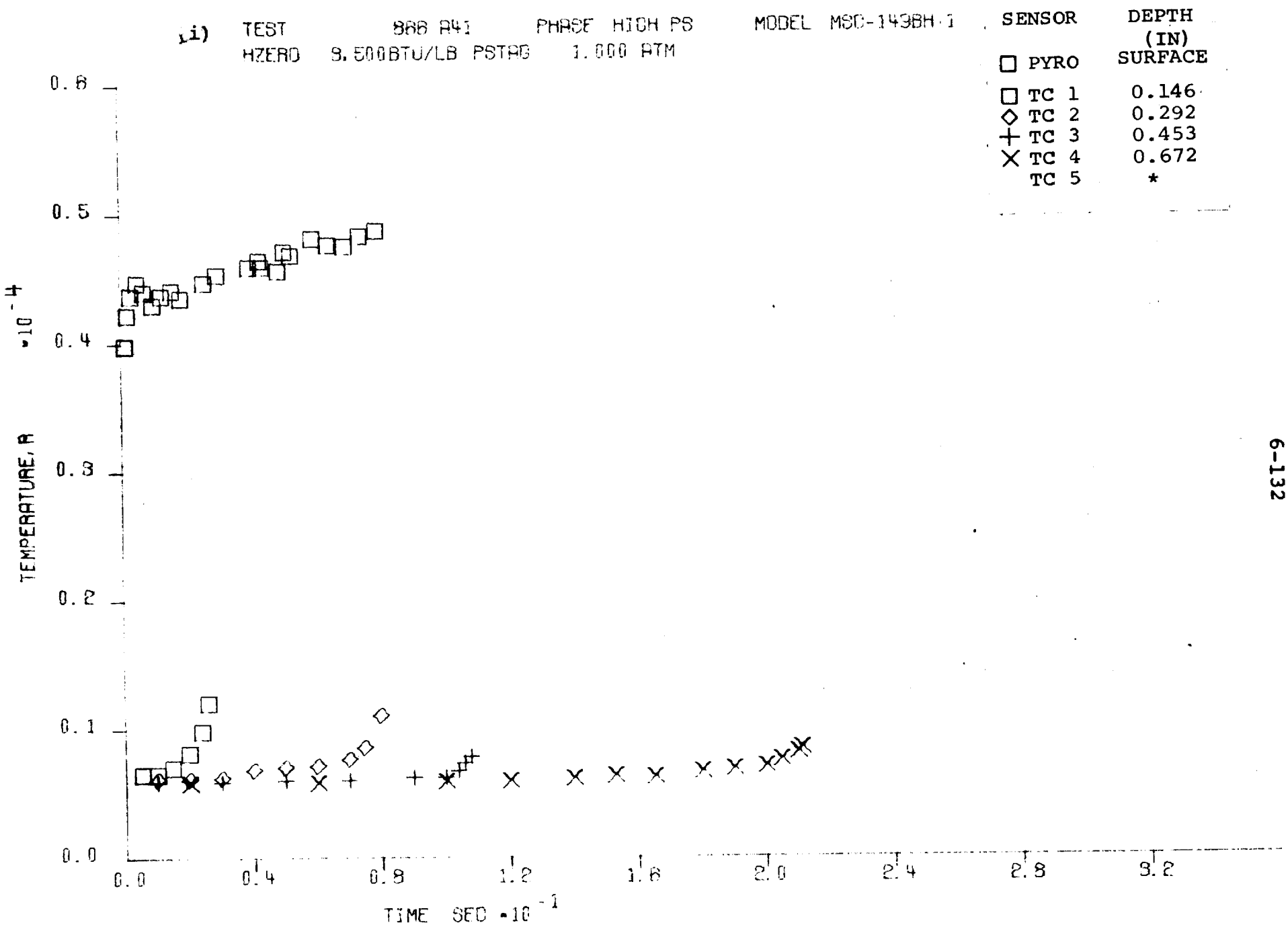

Figure 6-14. Continued.

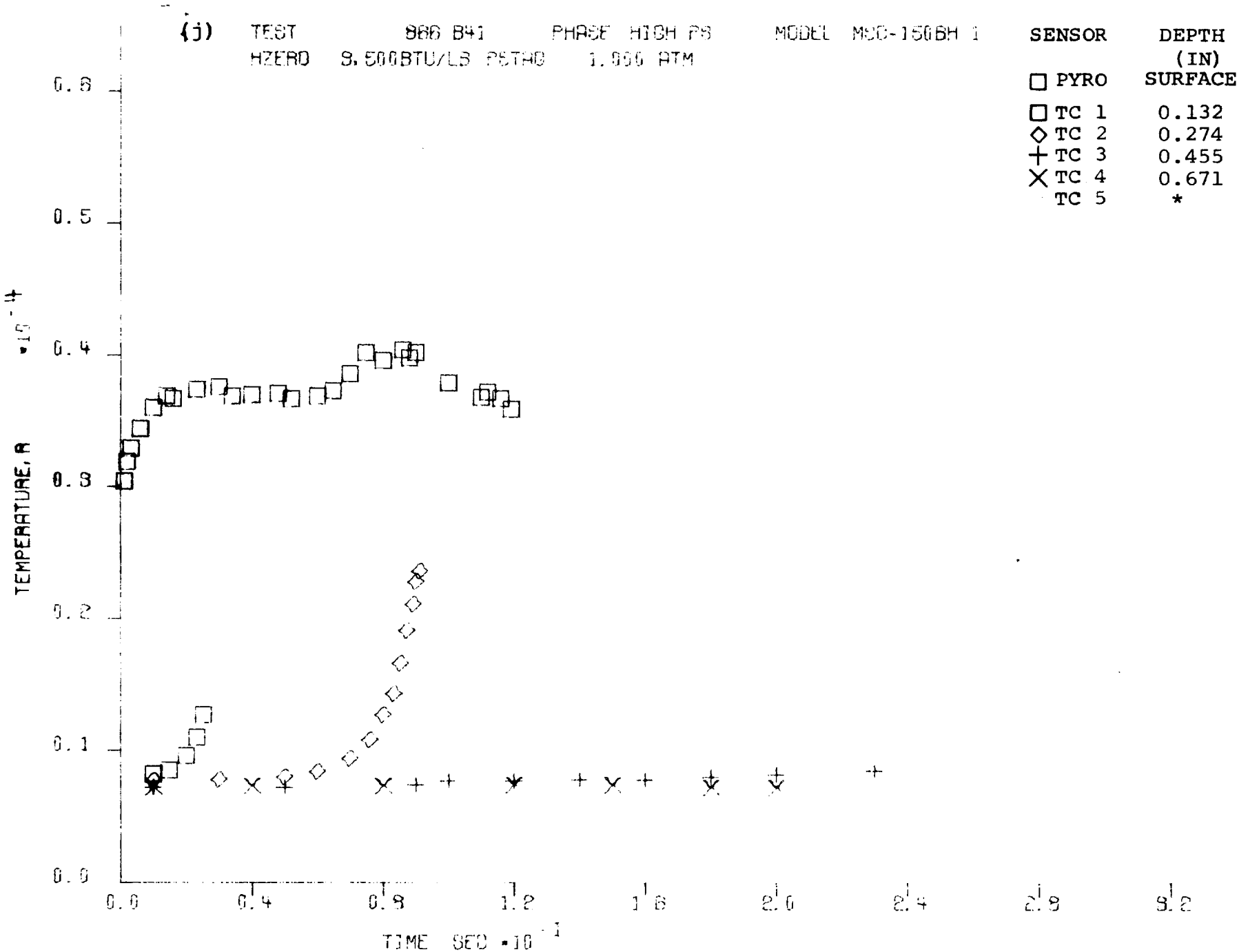

Figure 6-14. Continued.

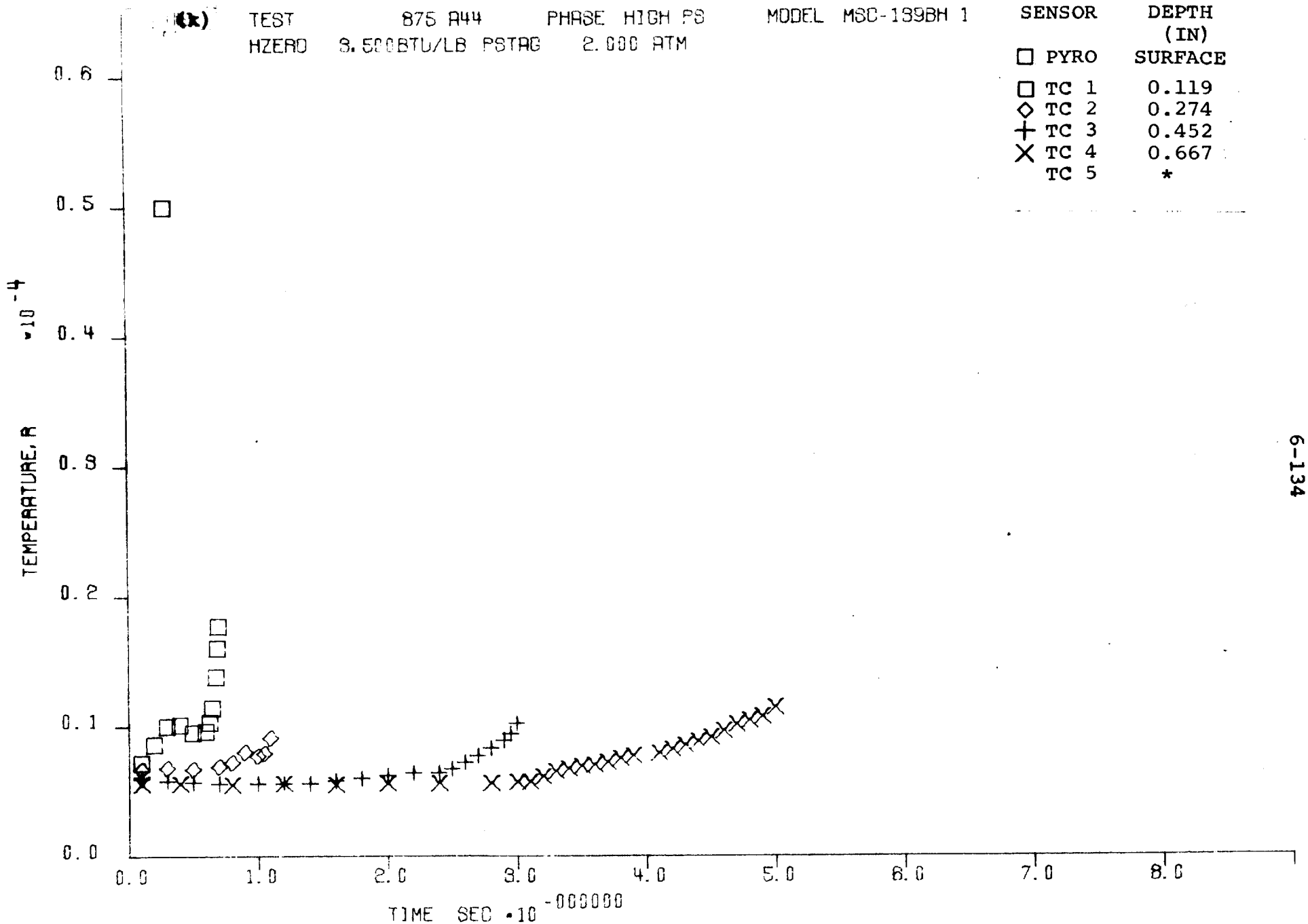

Figure 6-14. Continued.

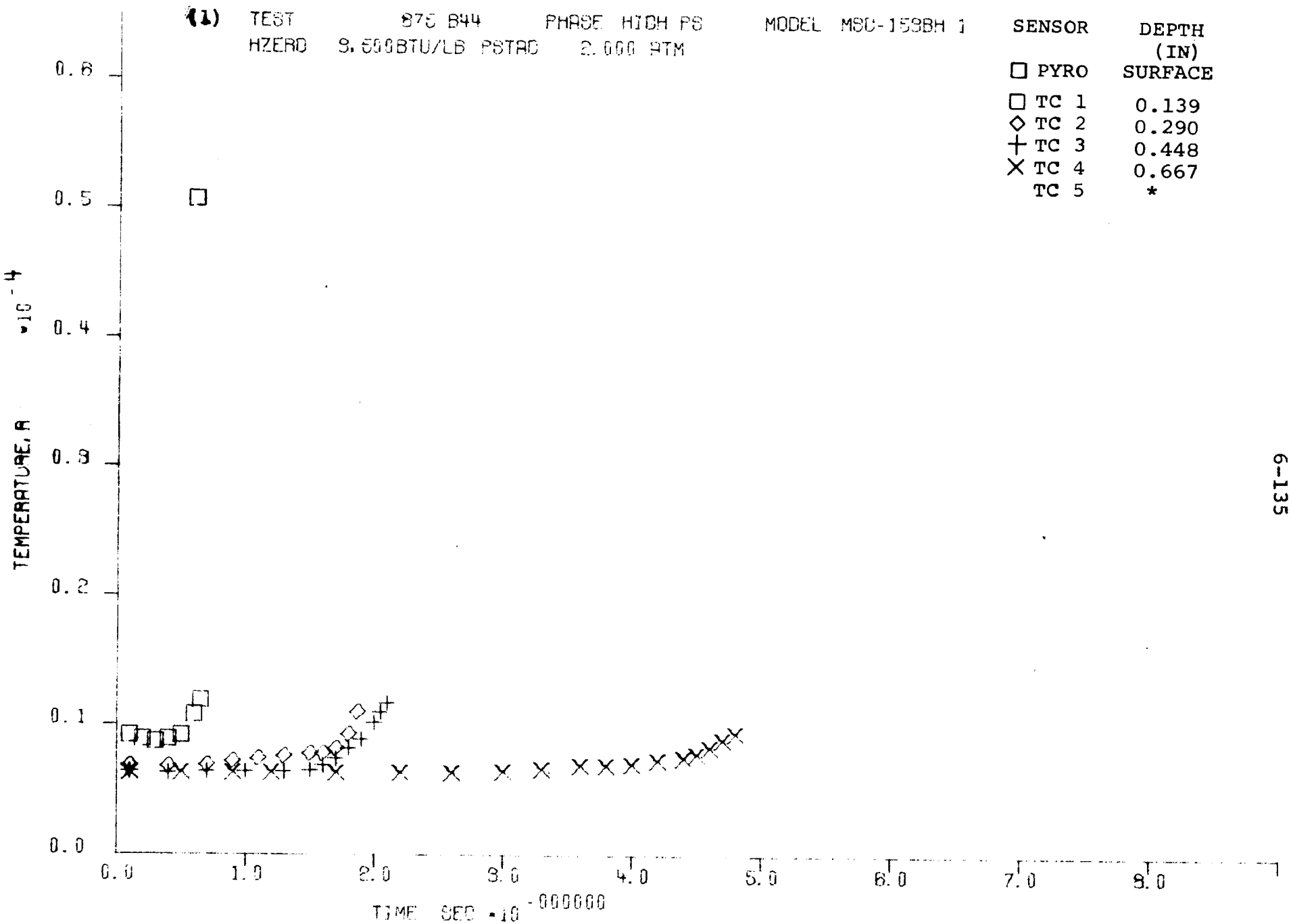

Figure 6-14. Continued.

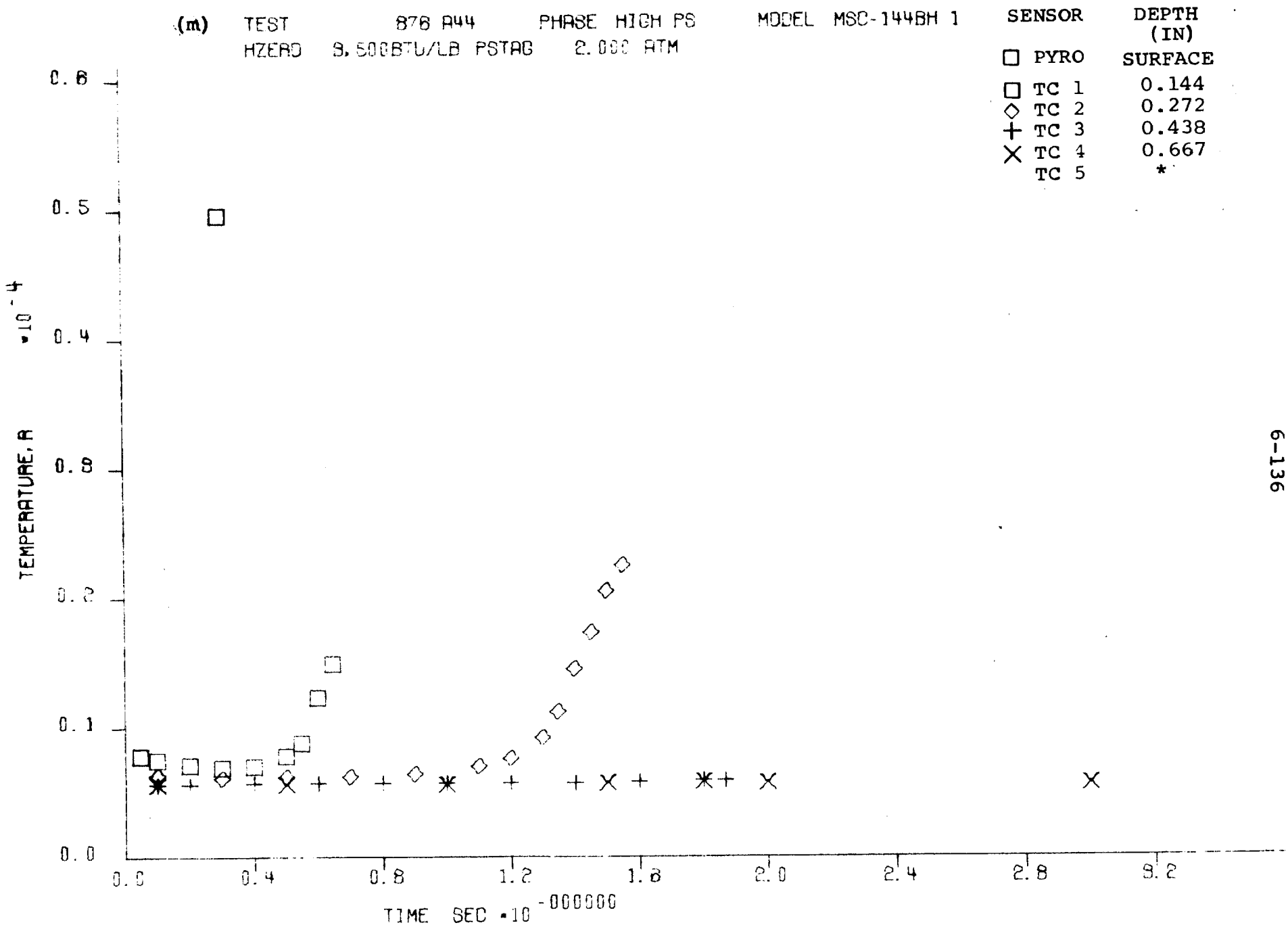

Figure 6-14. Continued.

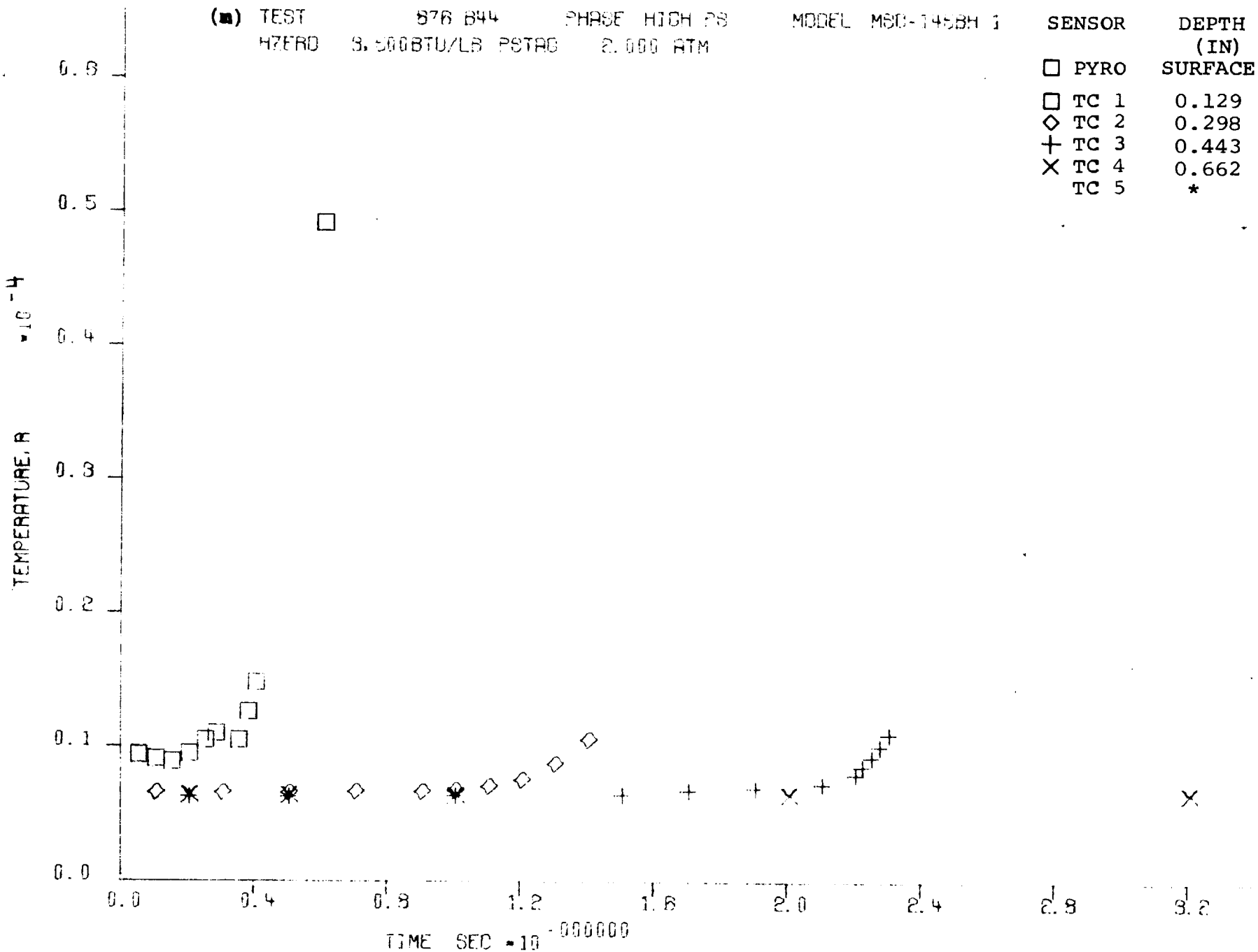

Figure 6-14. Continued.

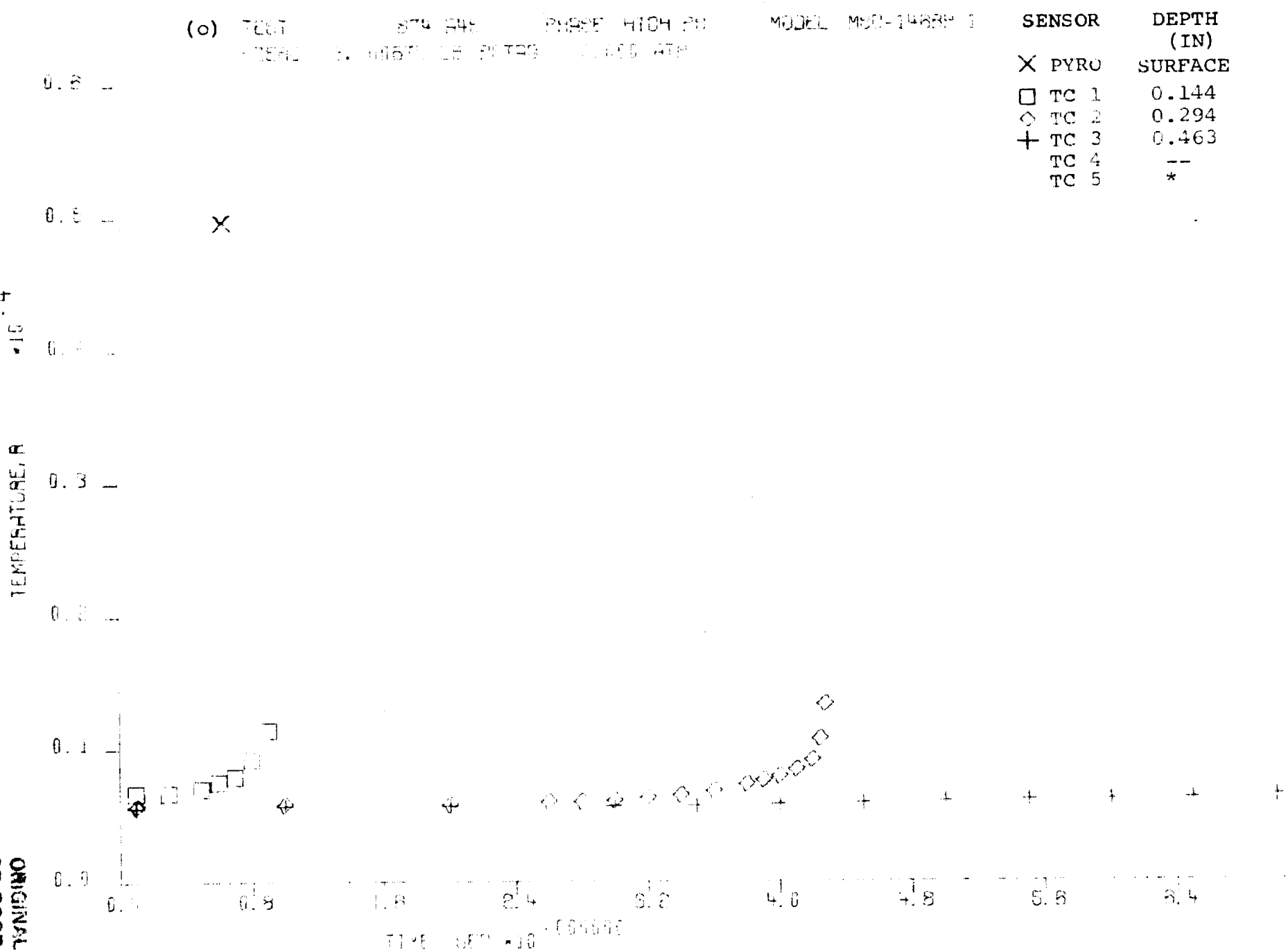

Figure 6-14. Continued.

ORIGINAL PAGE IS
OF POOR QUALITY

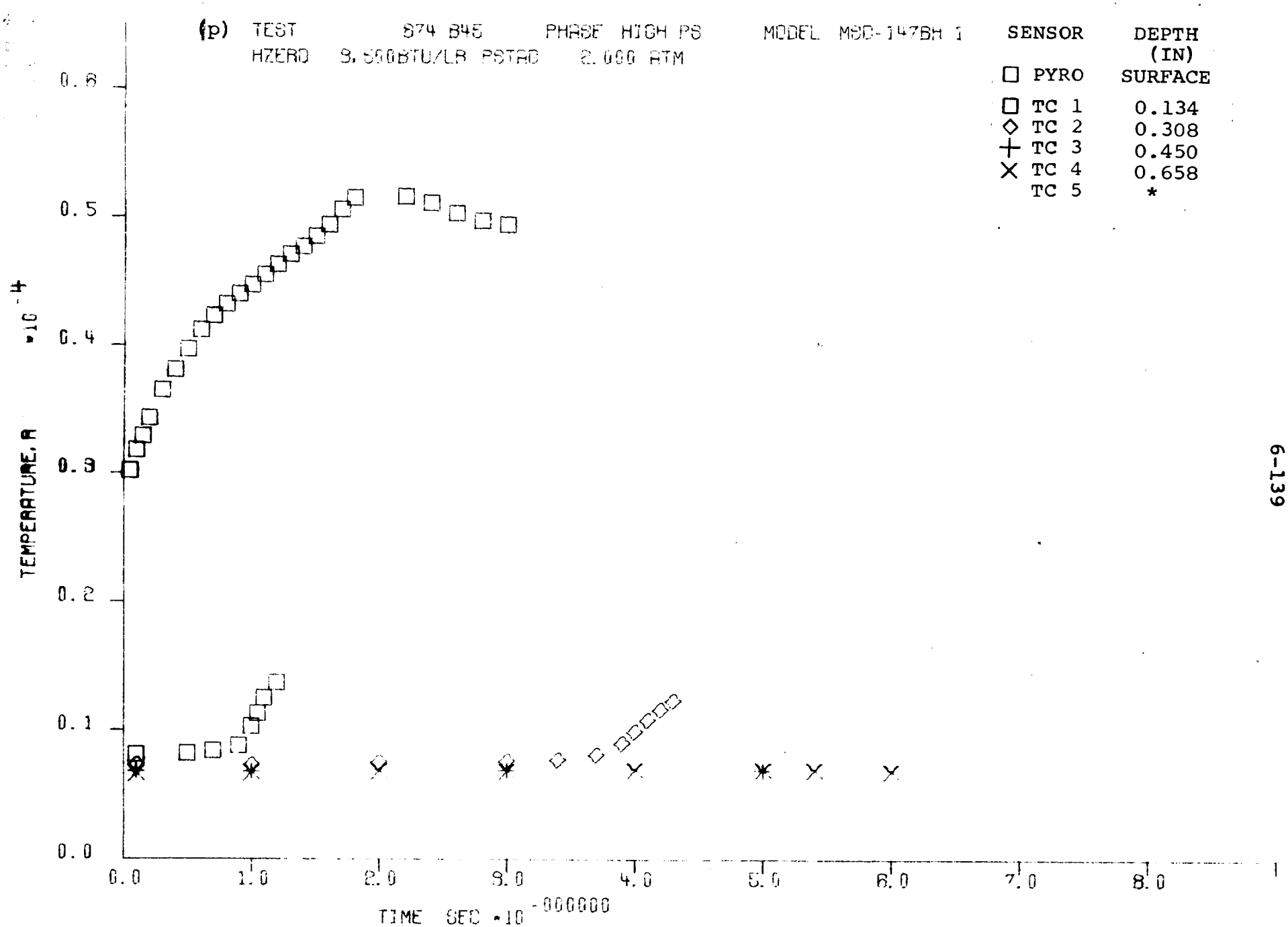

Figure 6-14. Continued.

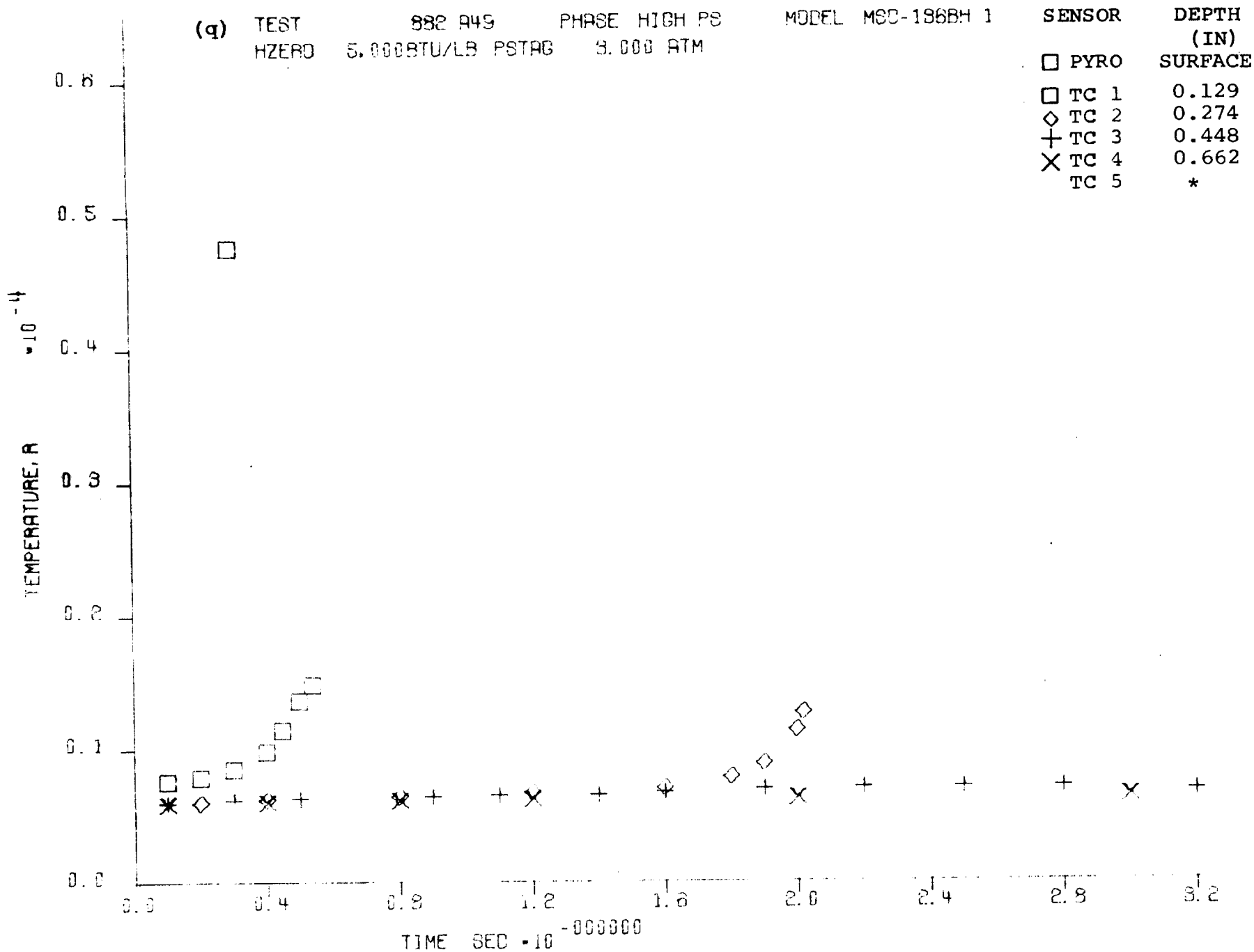

Figure 6-14. Continued.

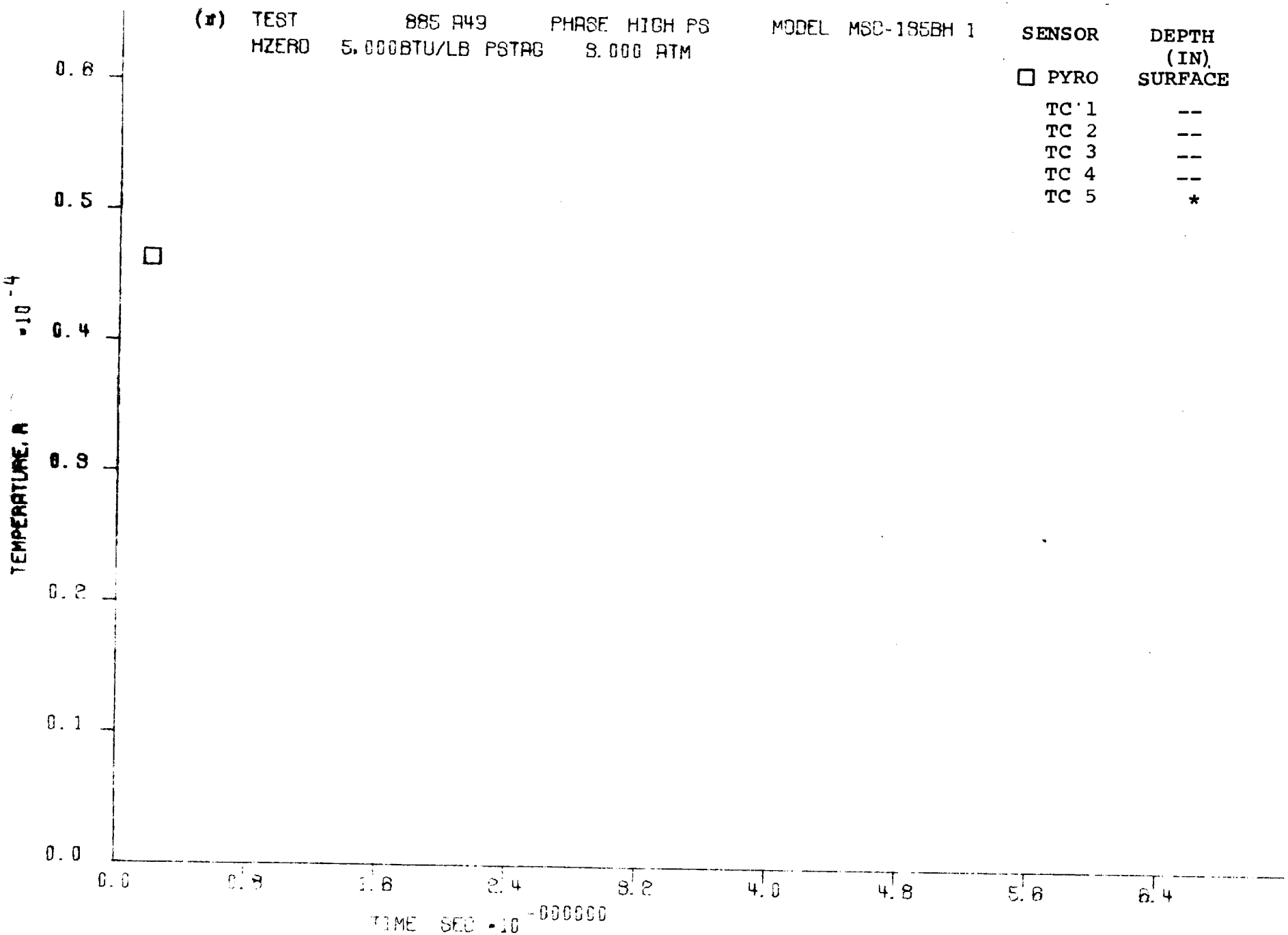

Figure 6-14. Continued.

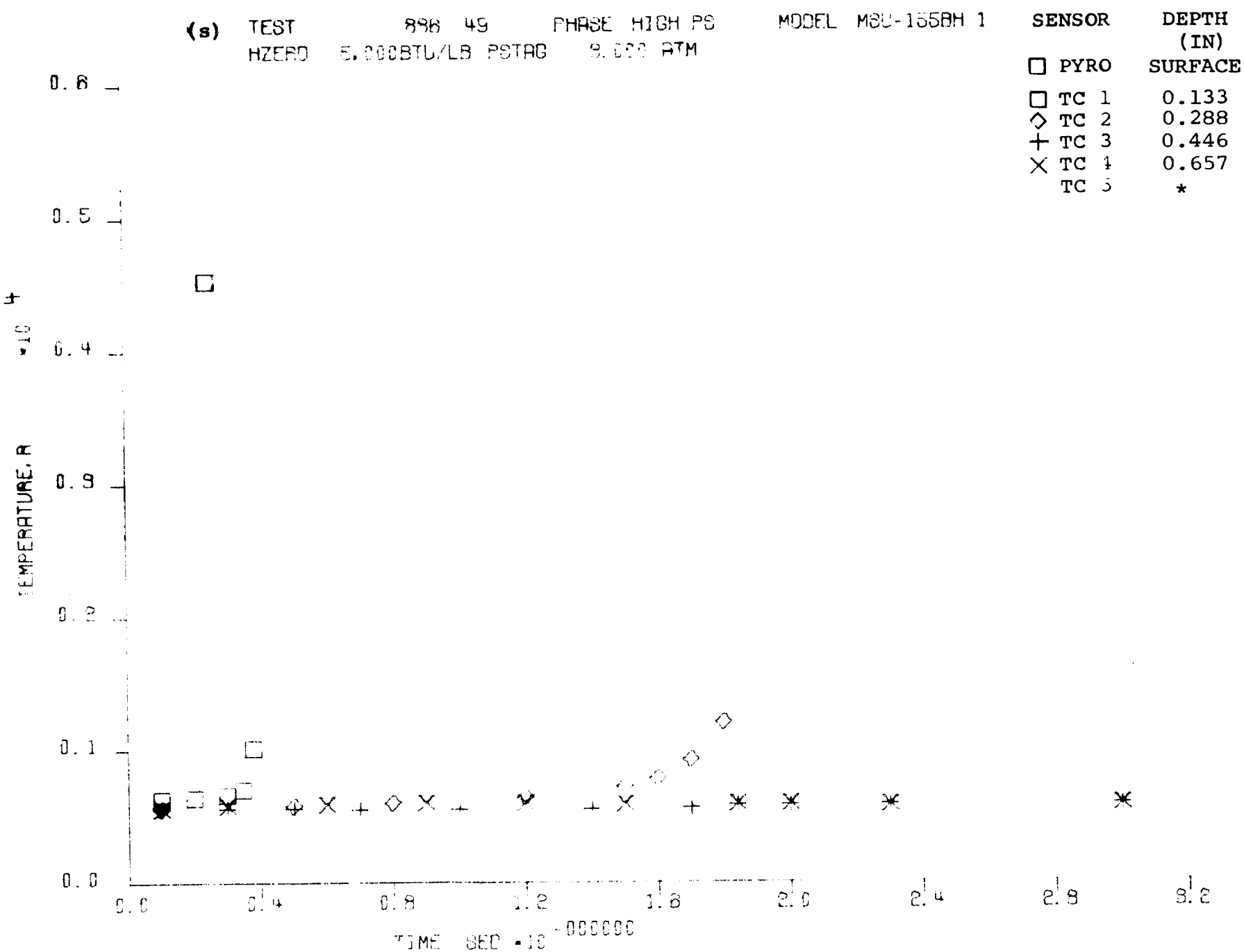

Figure 6-14. Continued.

ORIGINAL PAGE IS
OF POOR QUALITY

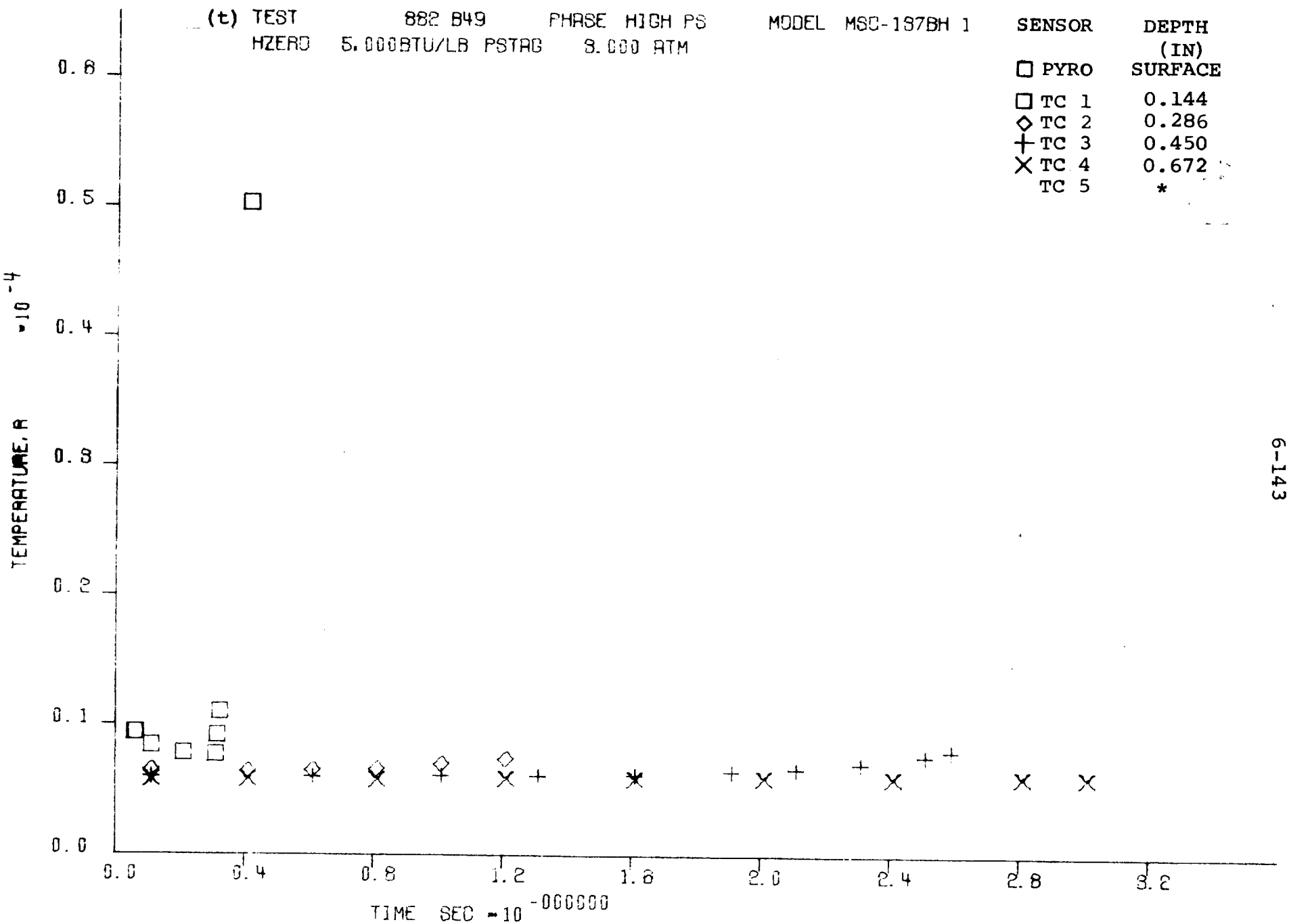

Figure 6-14. Continued.

C-3.

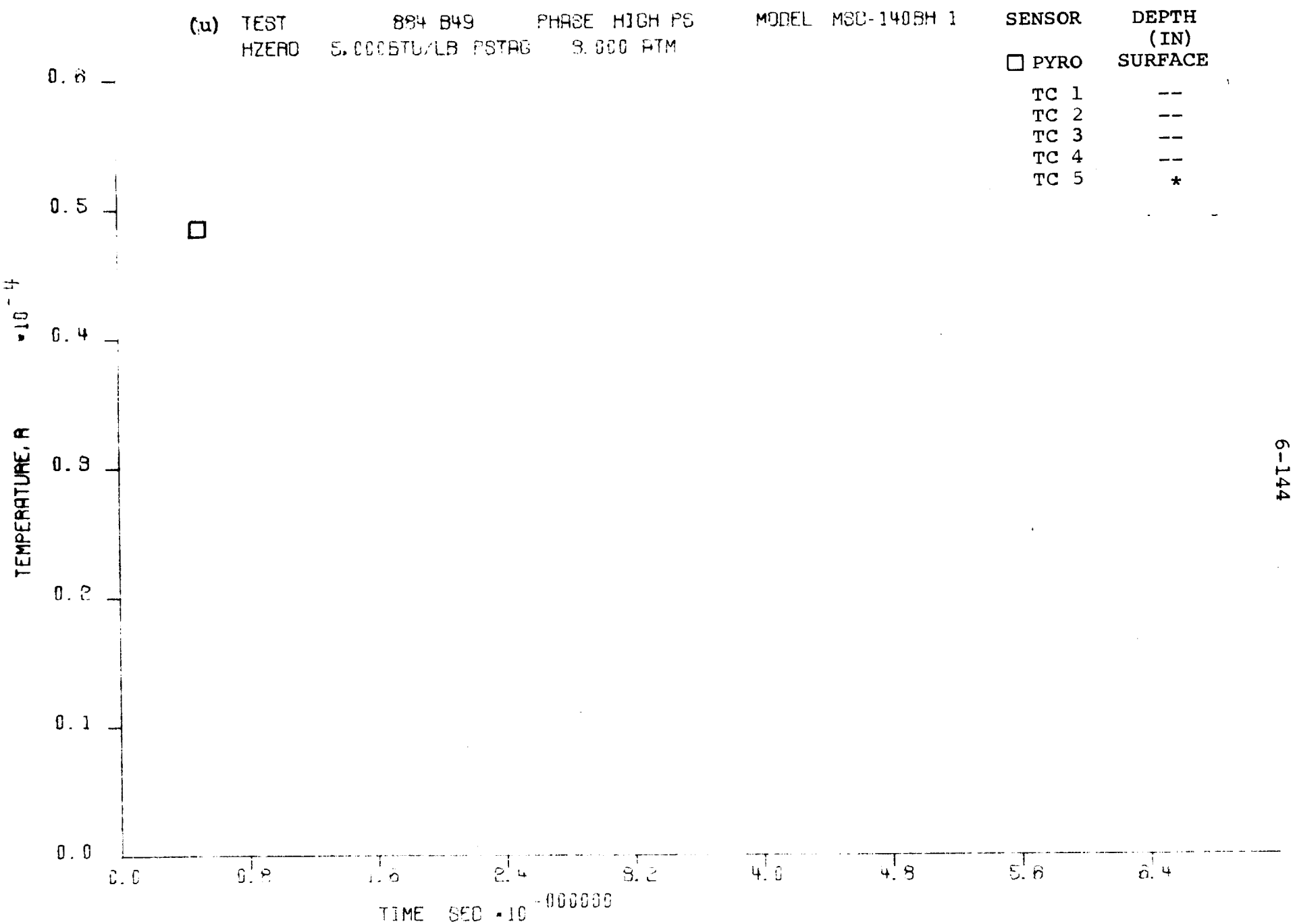

Figure 6-14. Continued.

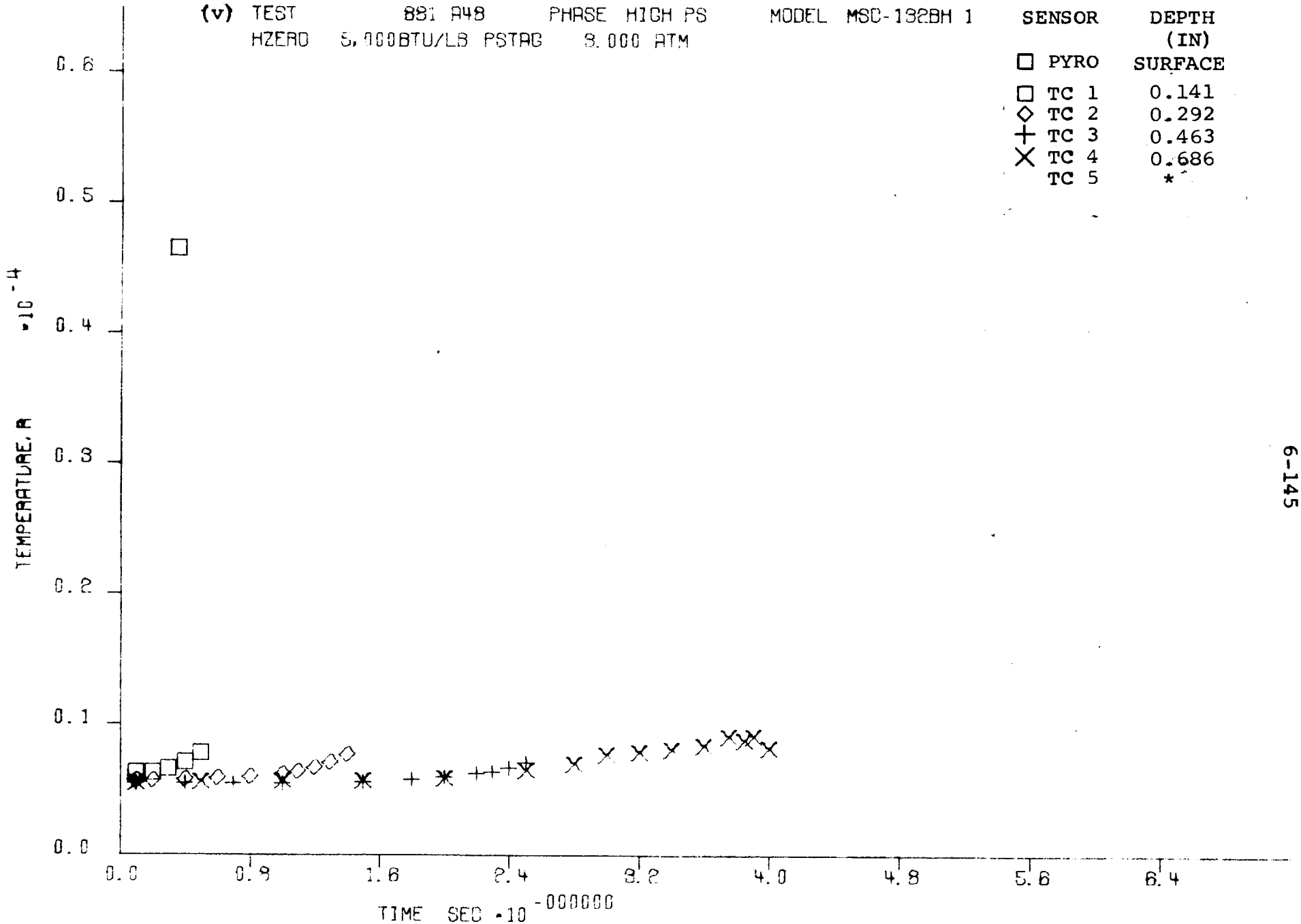

Figure 6-14. Continued.

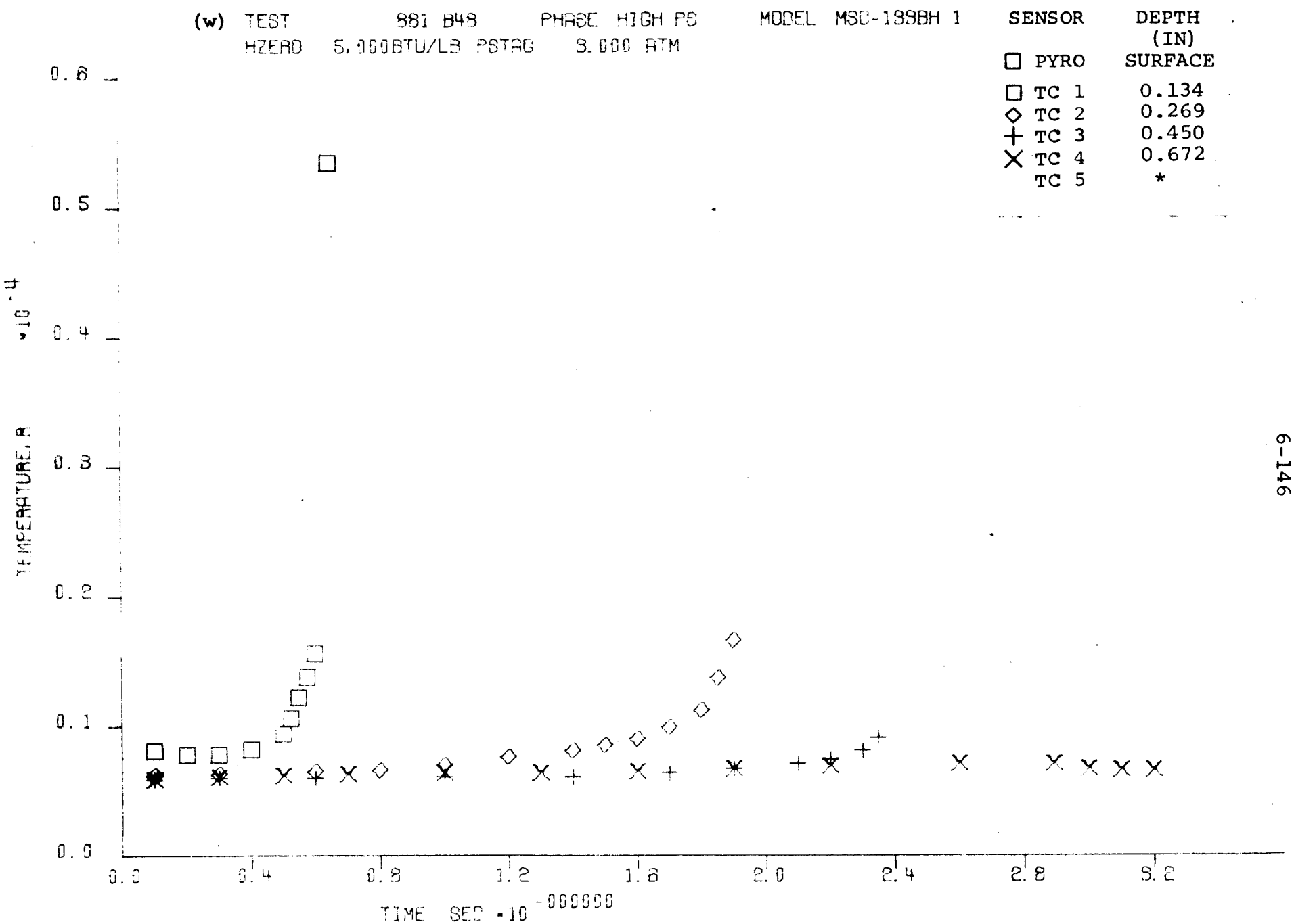

Figure 6-14. Continued.

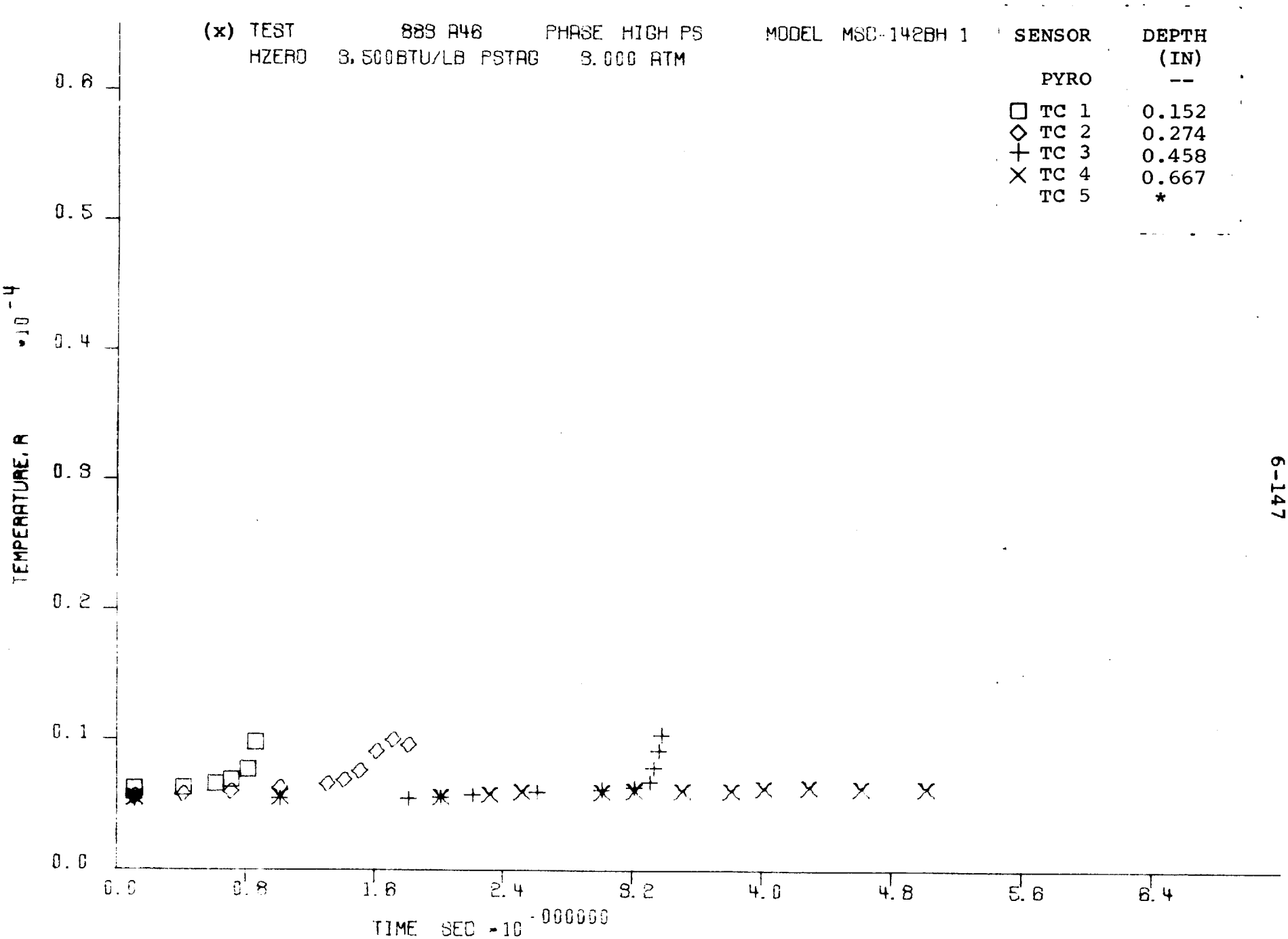

Figure 6-14. Continued.

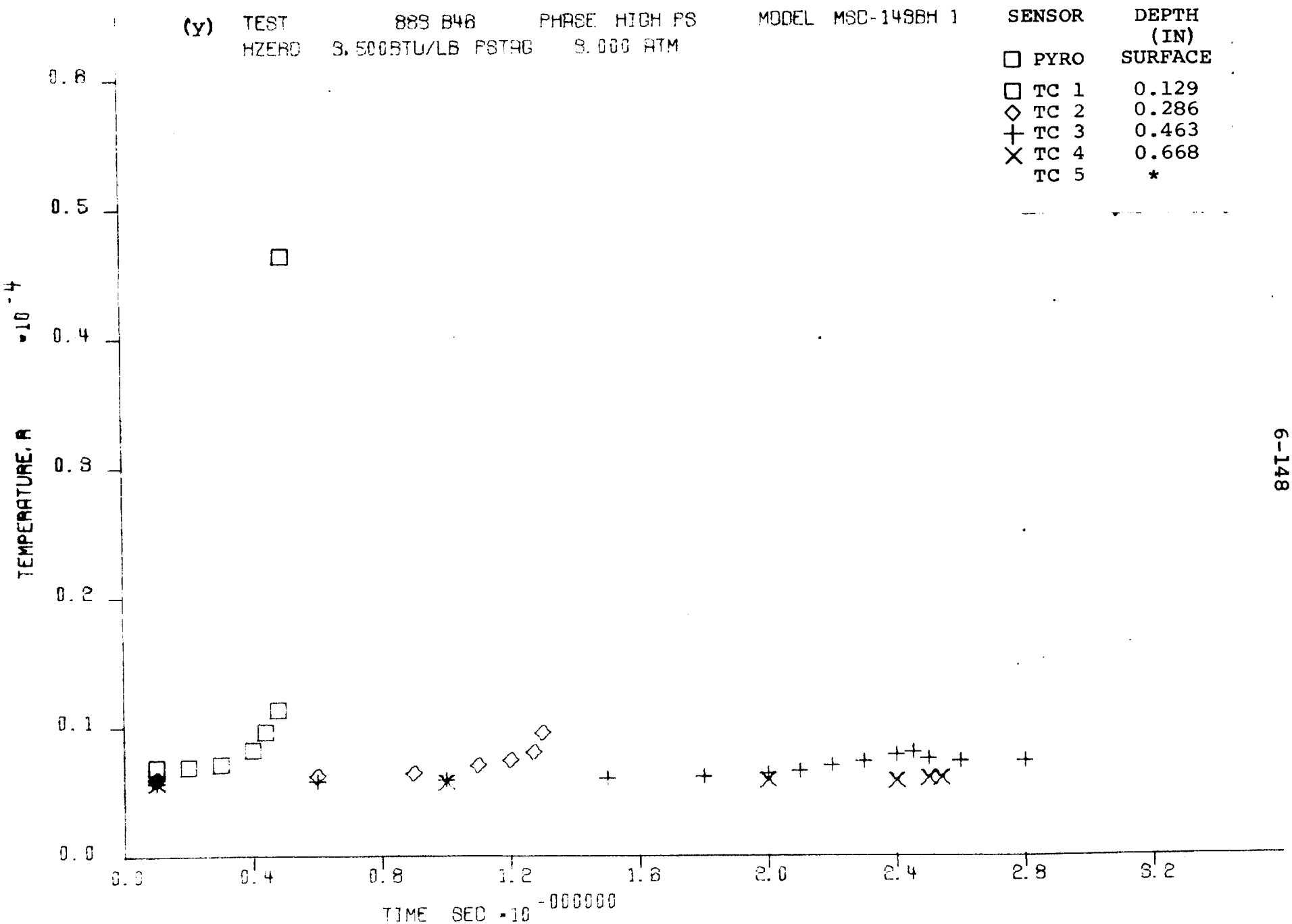

Figure 6-14. Continued.

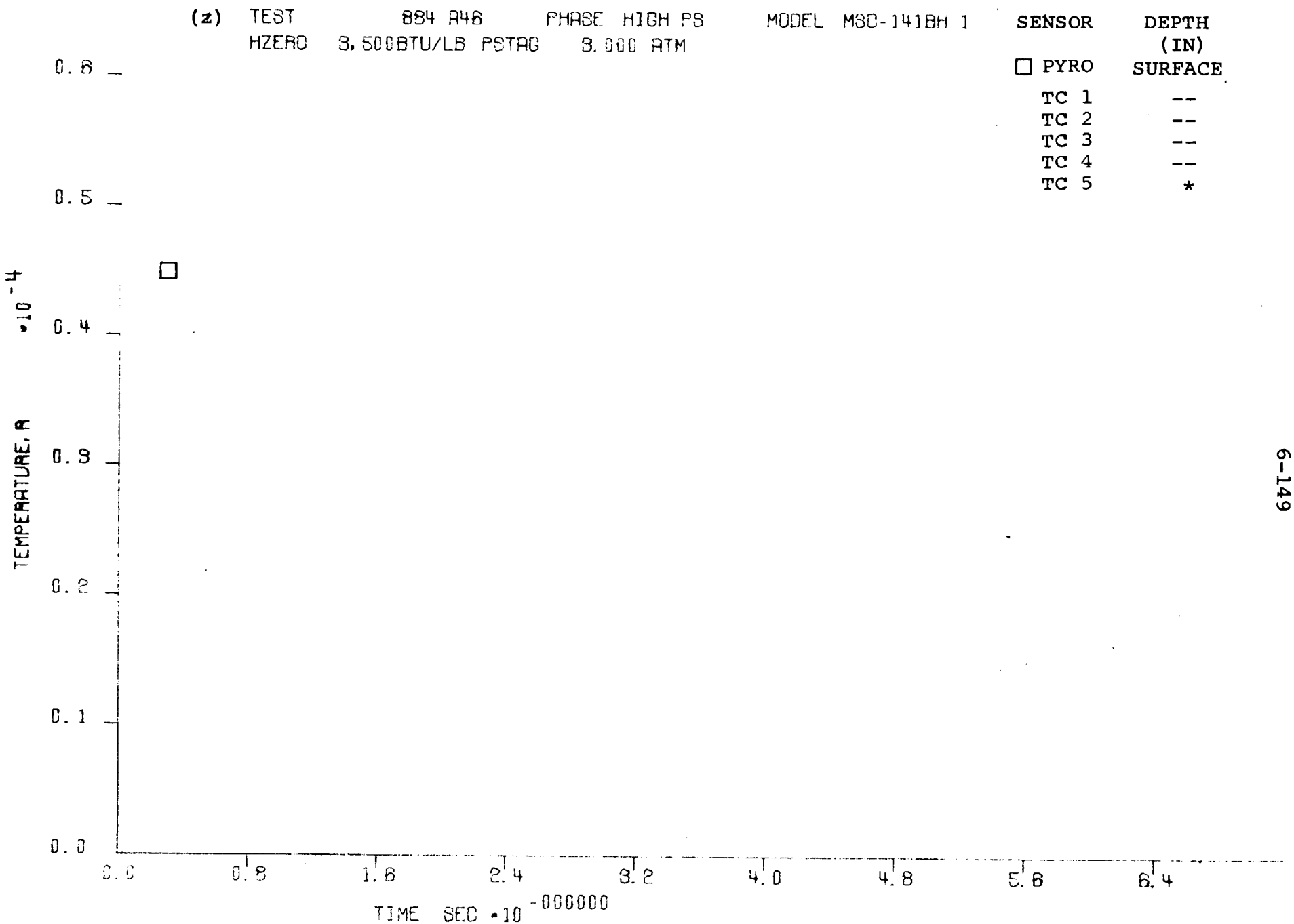

Figure 6-14. Continued.

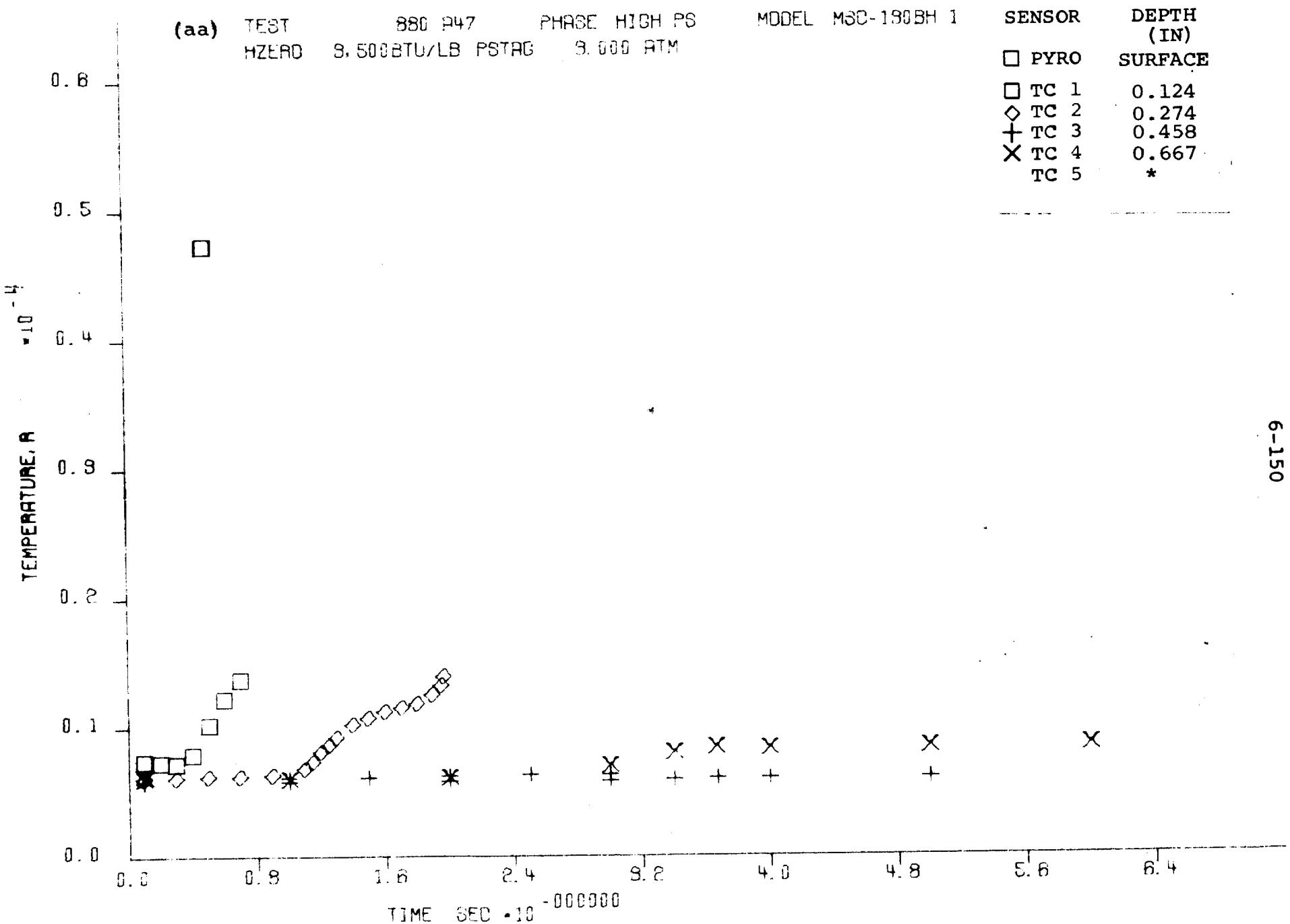

Figure 6-14. Continued.

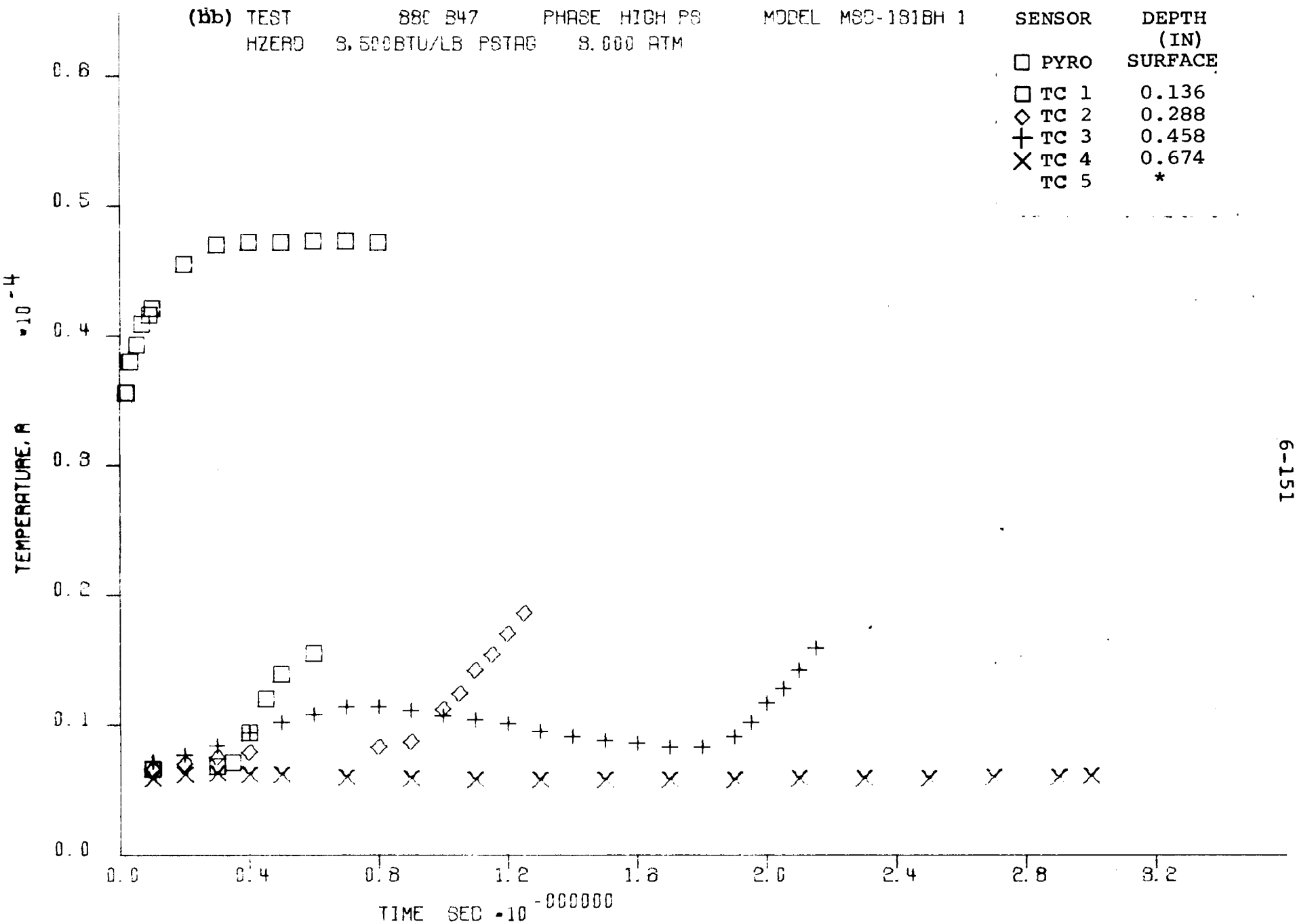

Figure 6-J4 Concluded.

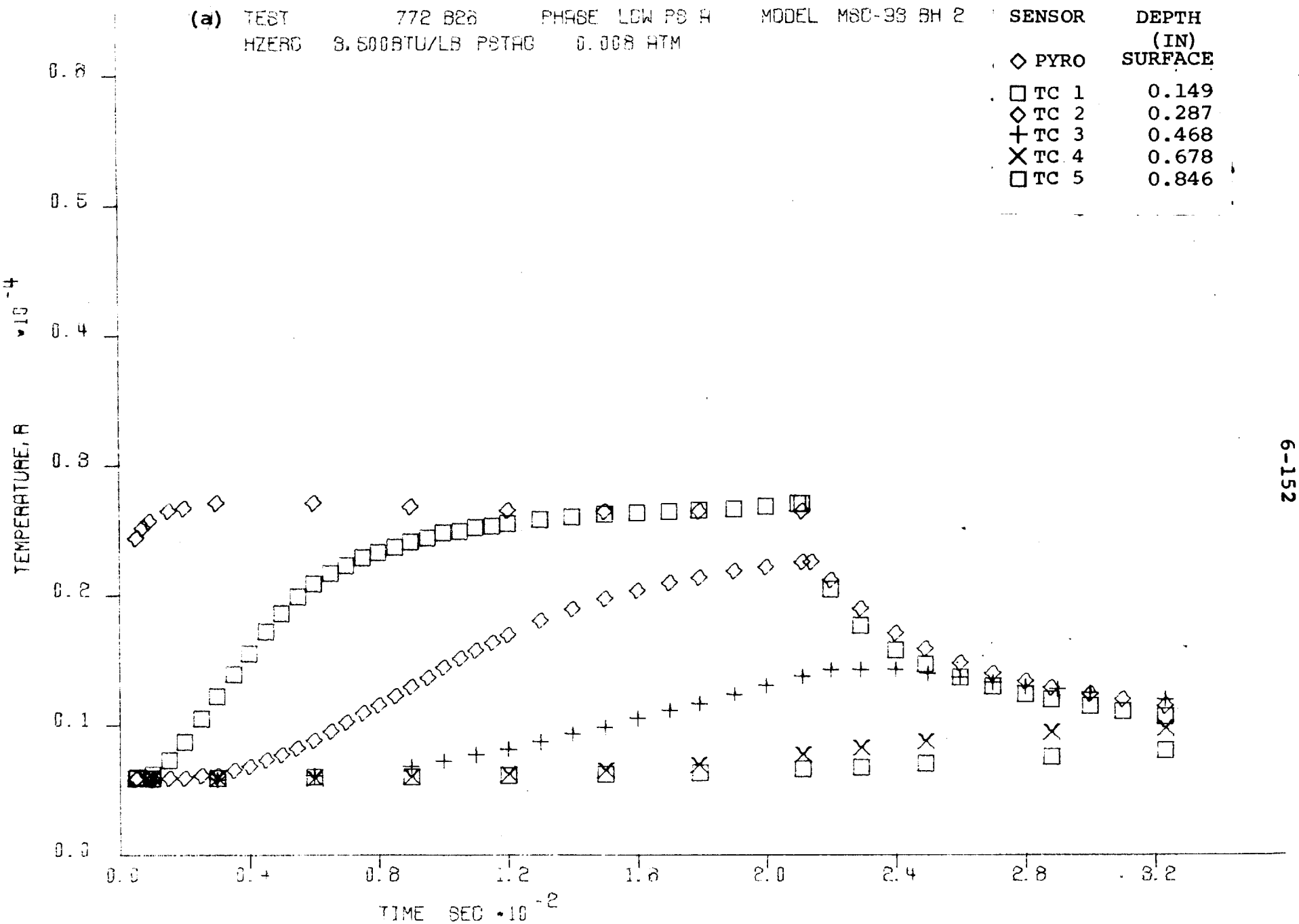

Figure 6-15. Surface and Internal Temperature Histories, Phase IV A.

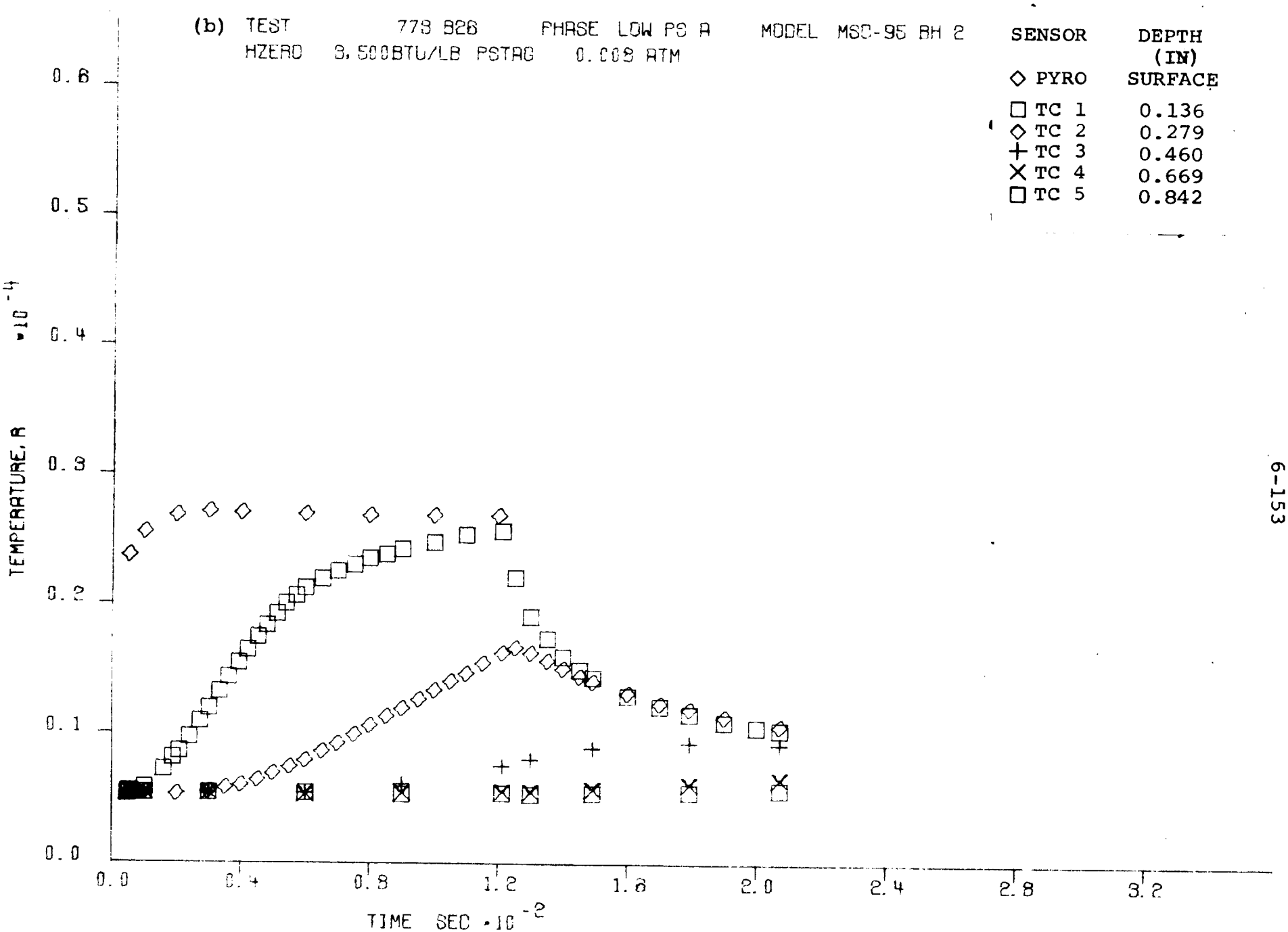

Figure 6-15. Continued.

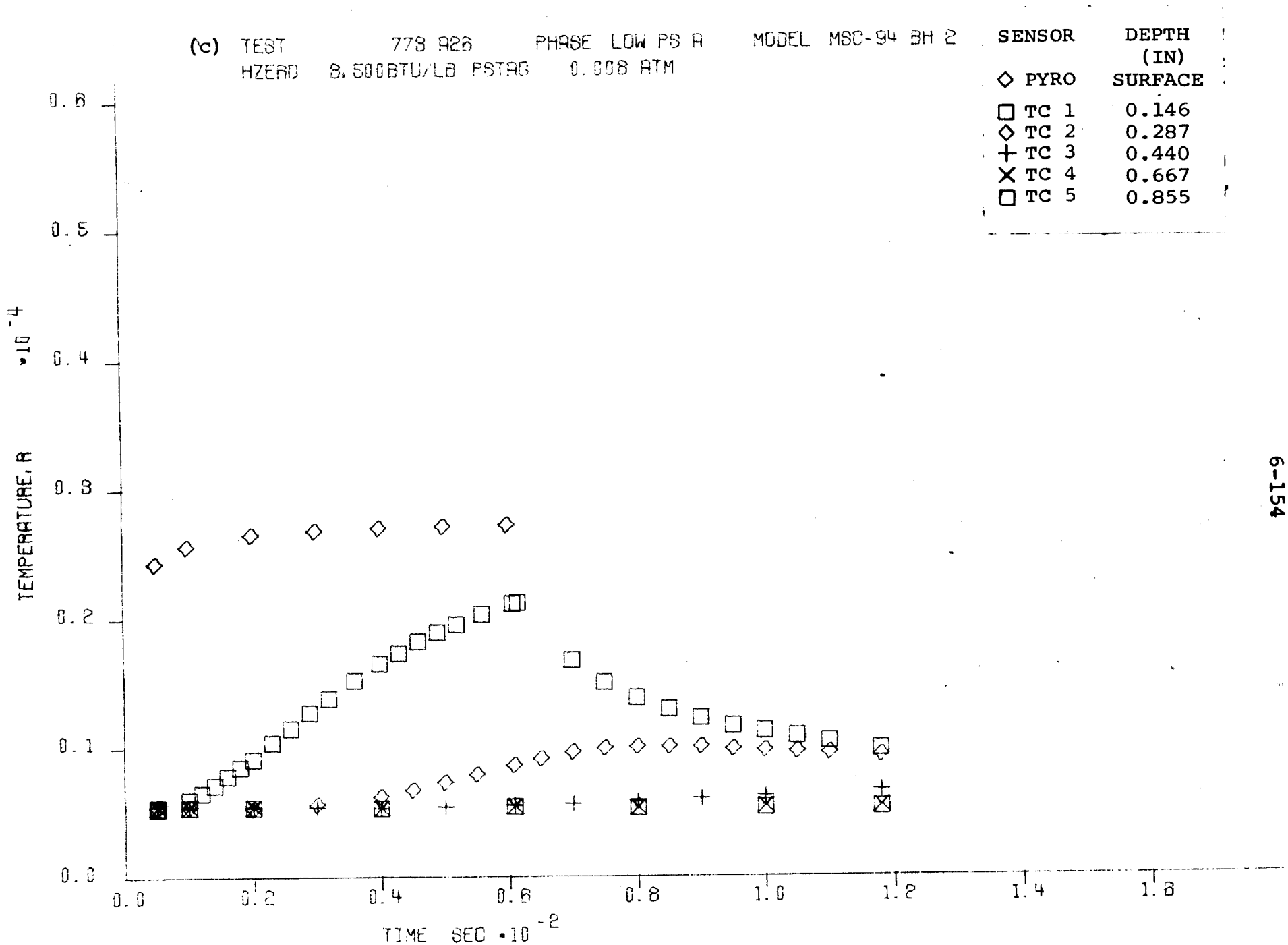

Figure 6-15. Continued.

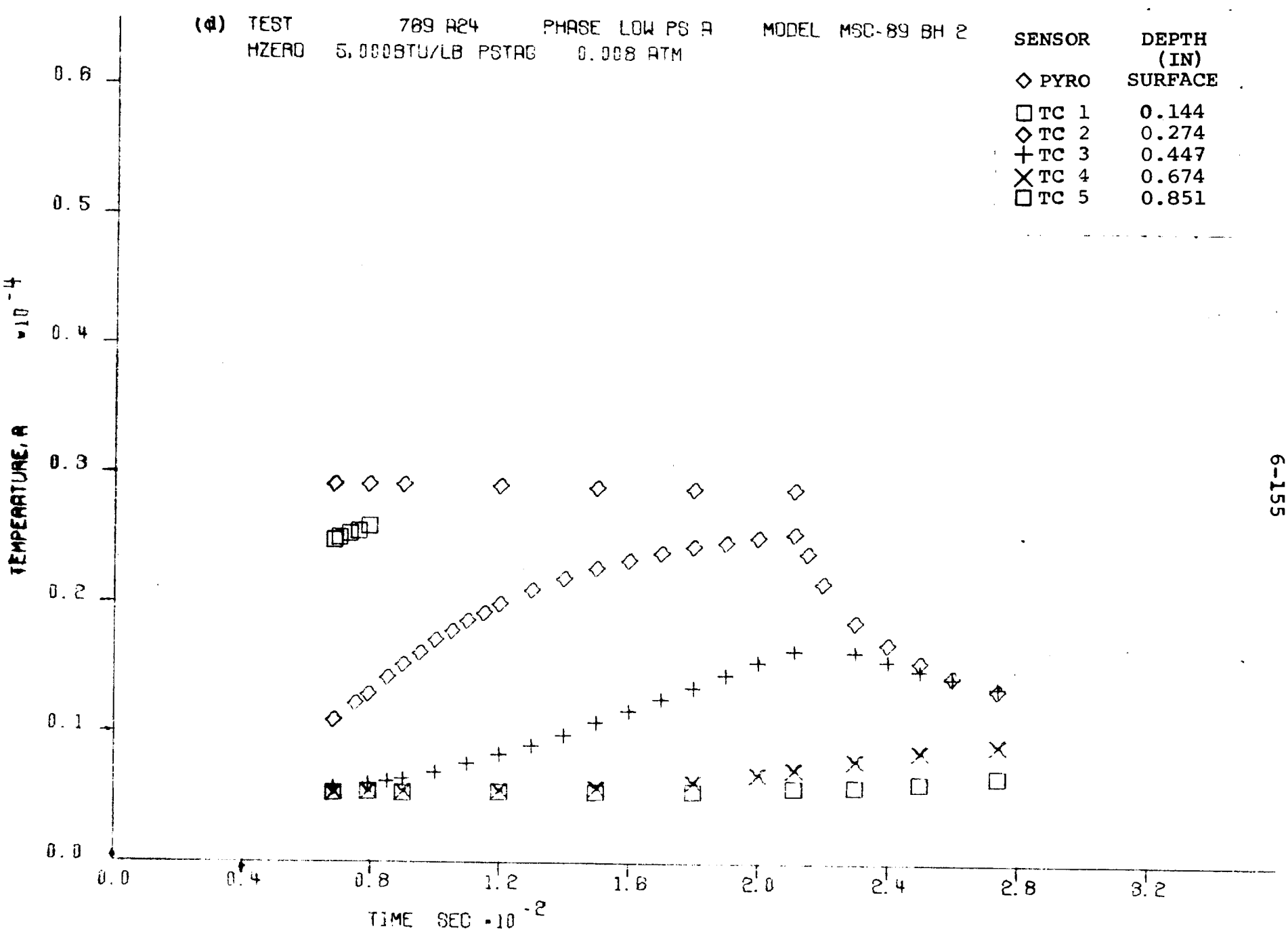

Figure 6-15. Continued.

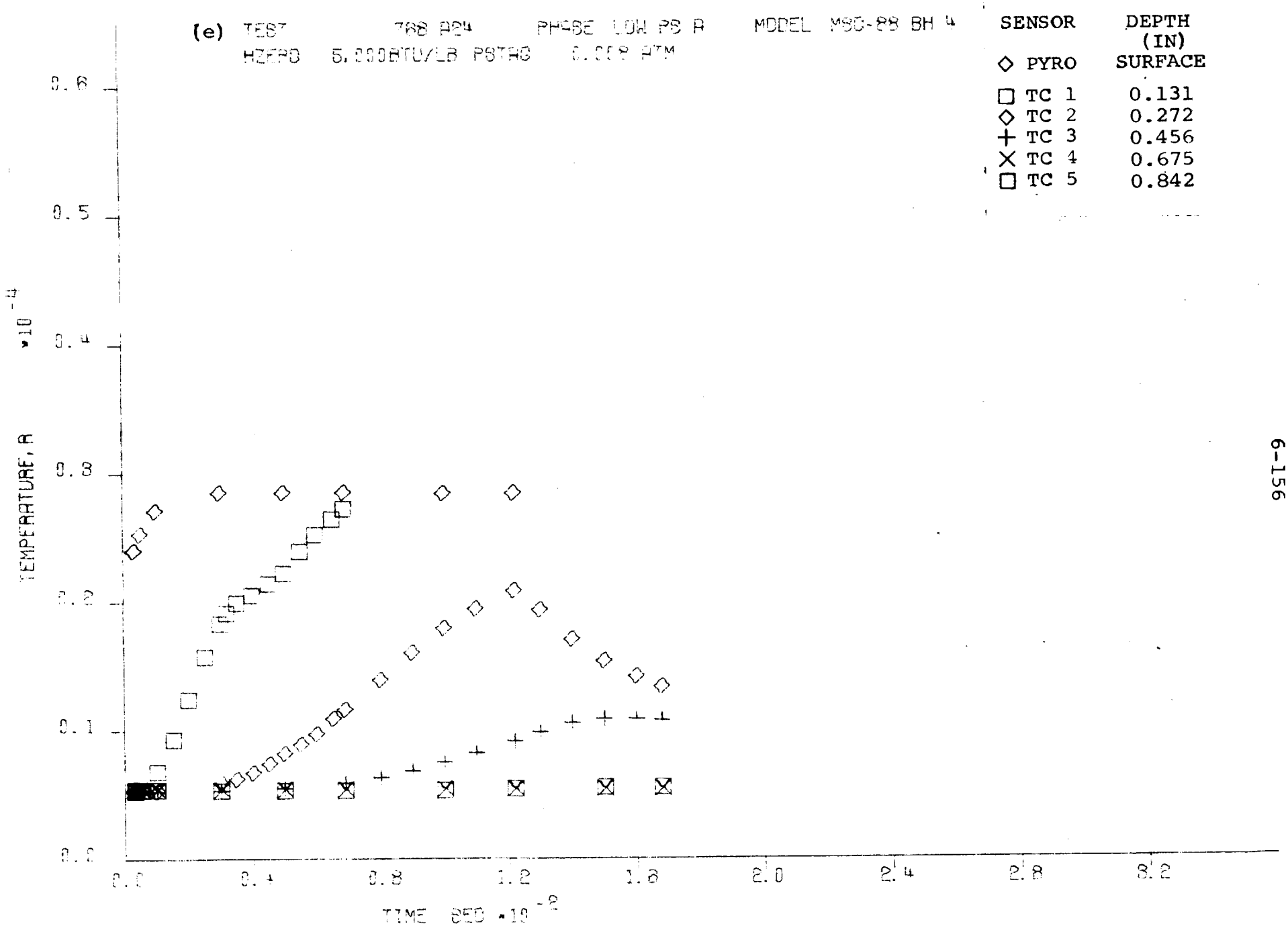

Figure 6-15. Continued.

ORIGINAL PAGE IS OF POOR QUALITY

ORIGINAL PAGE IS
OF POOR QUALITY

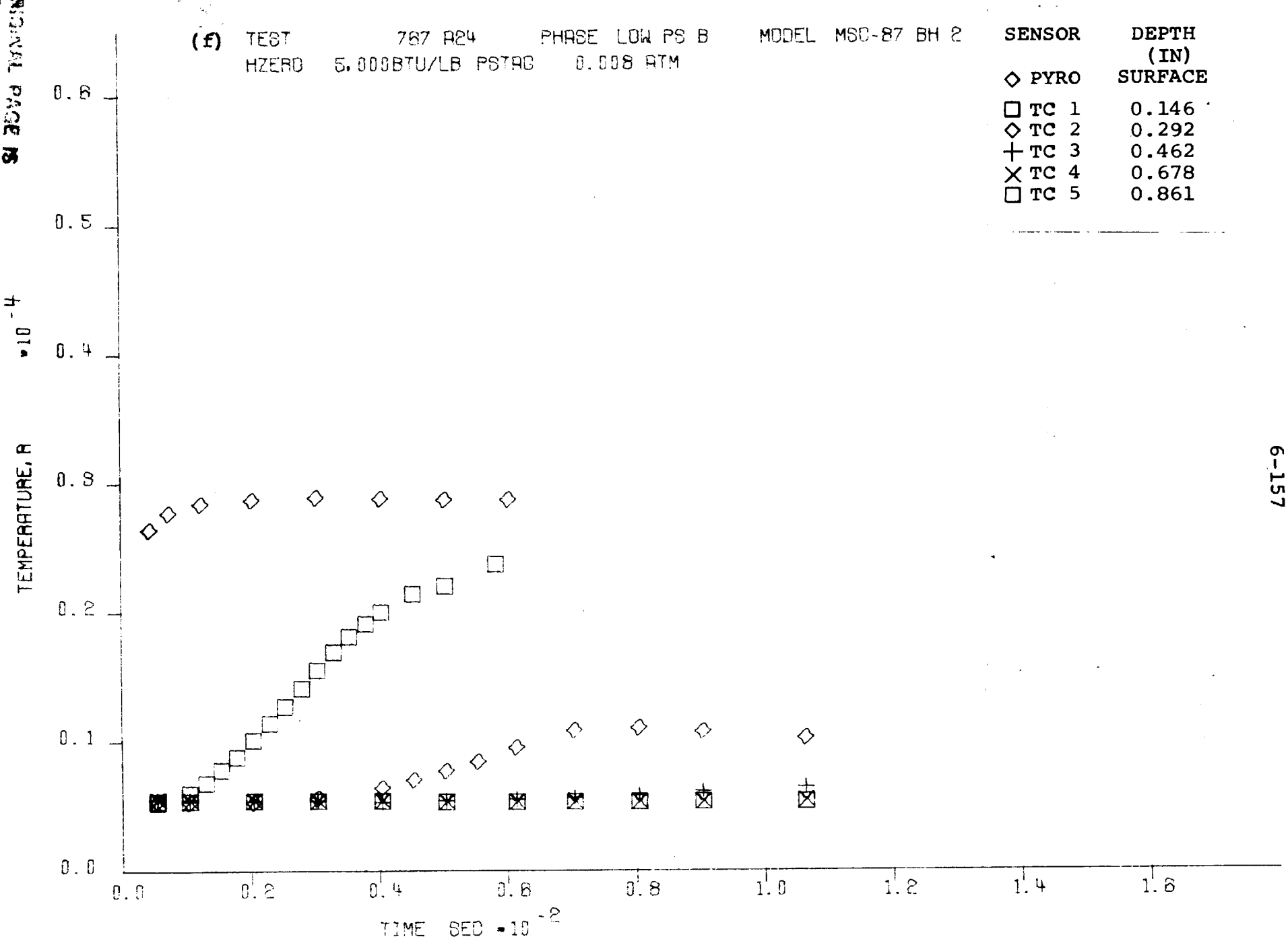

Figure 6-15. Continued.

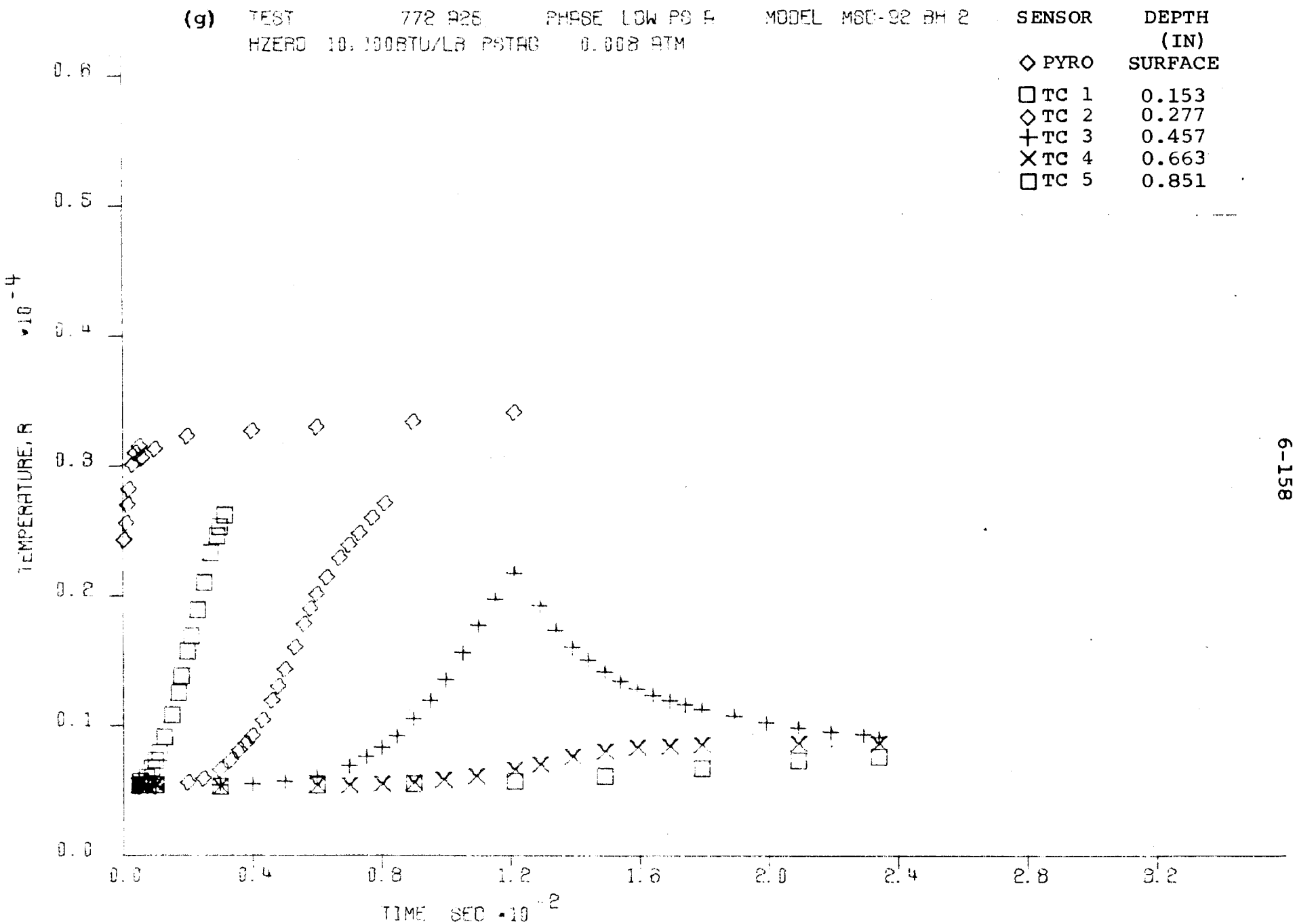

Figure 6-15. Continued.

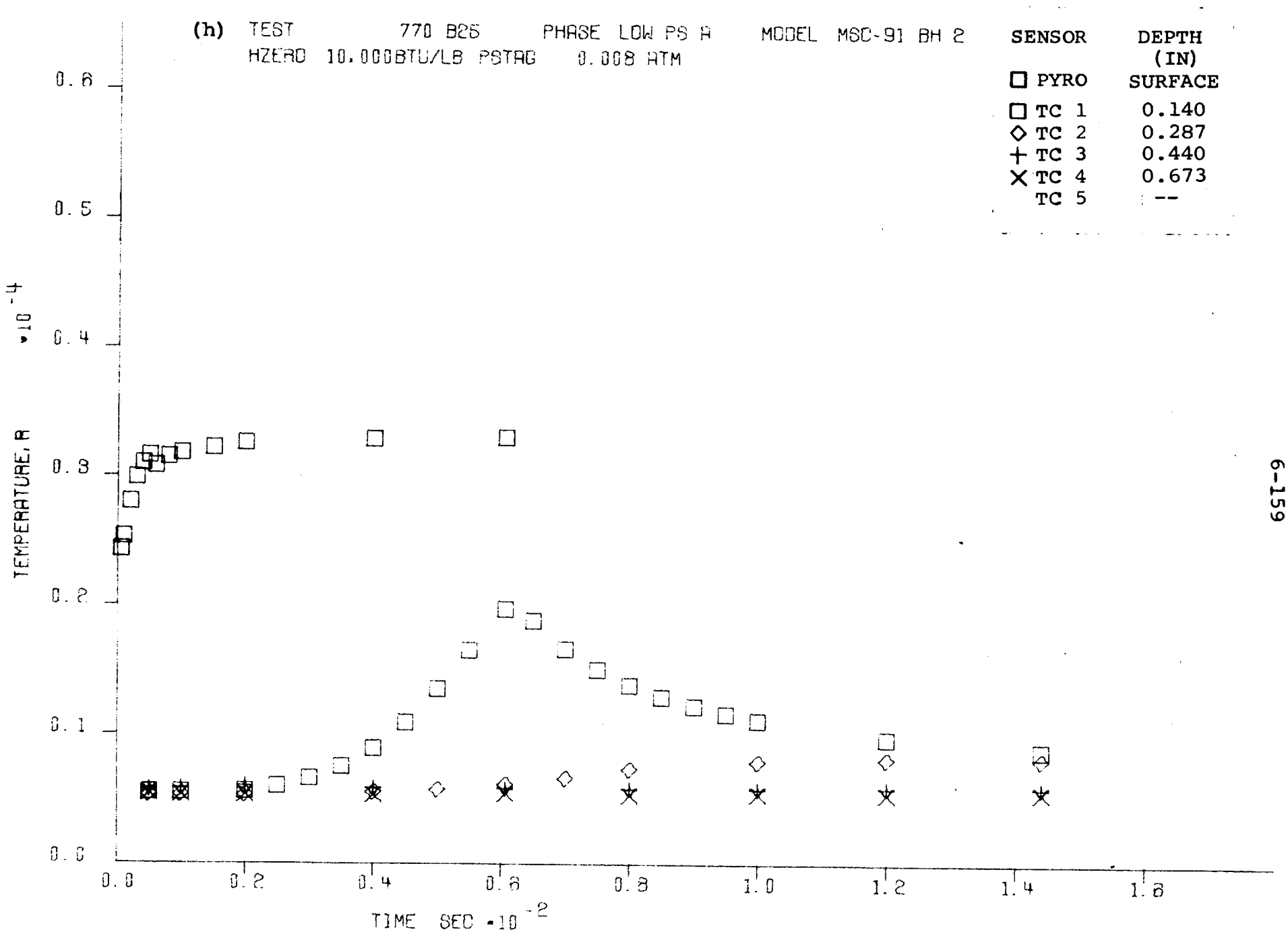

Figure 6-15. Continued.

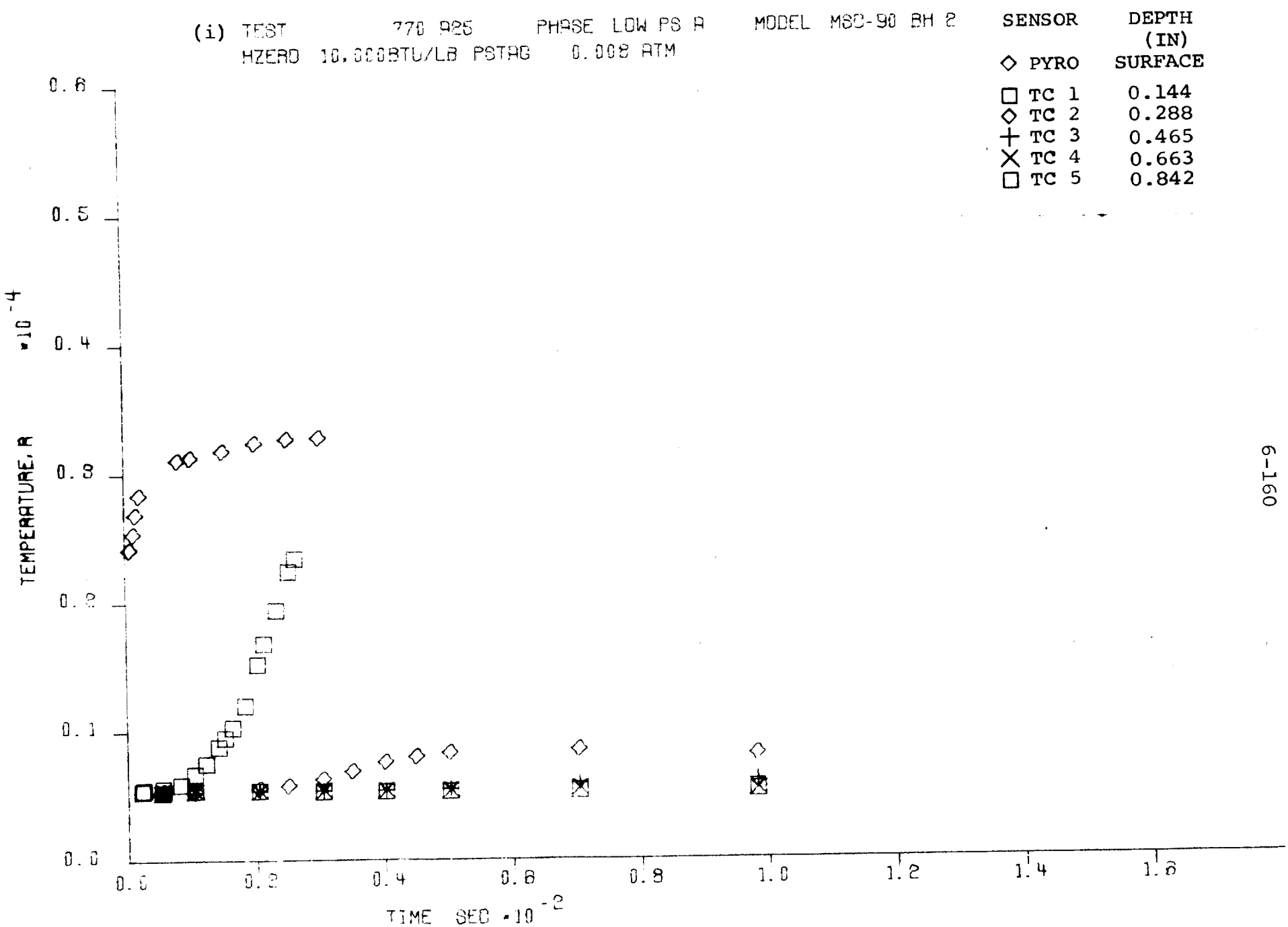

Figure 6-15. Continued.

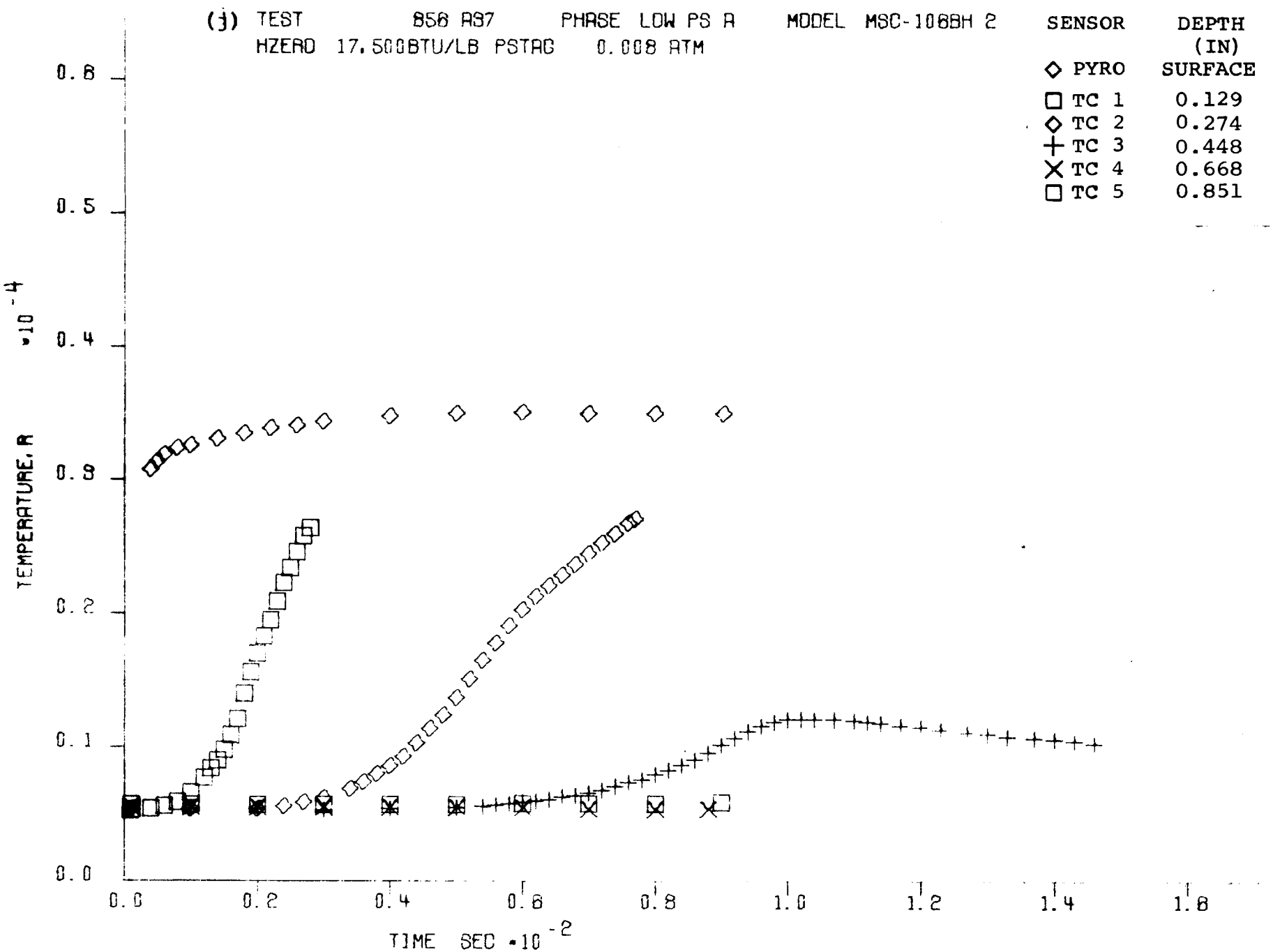

Figure 6-15. Continued.

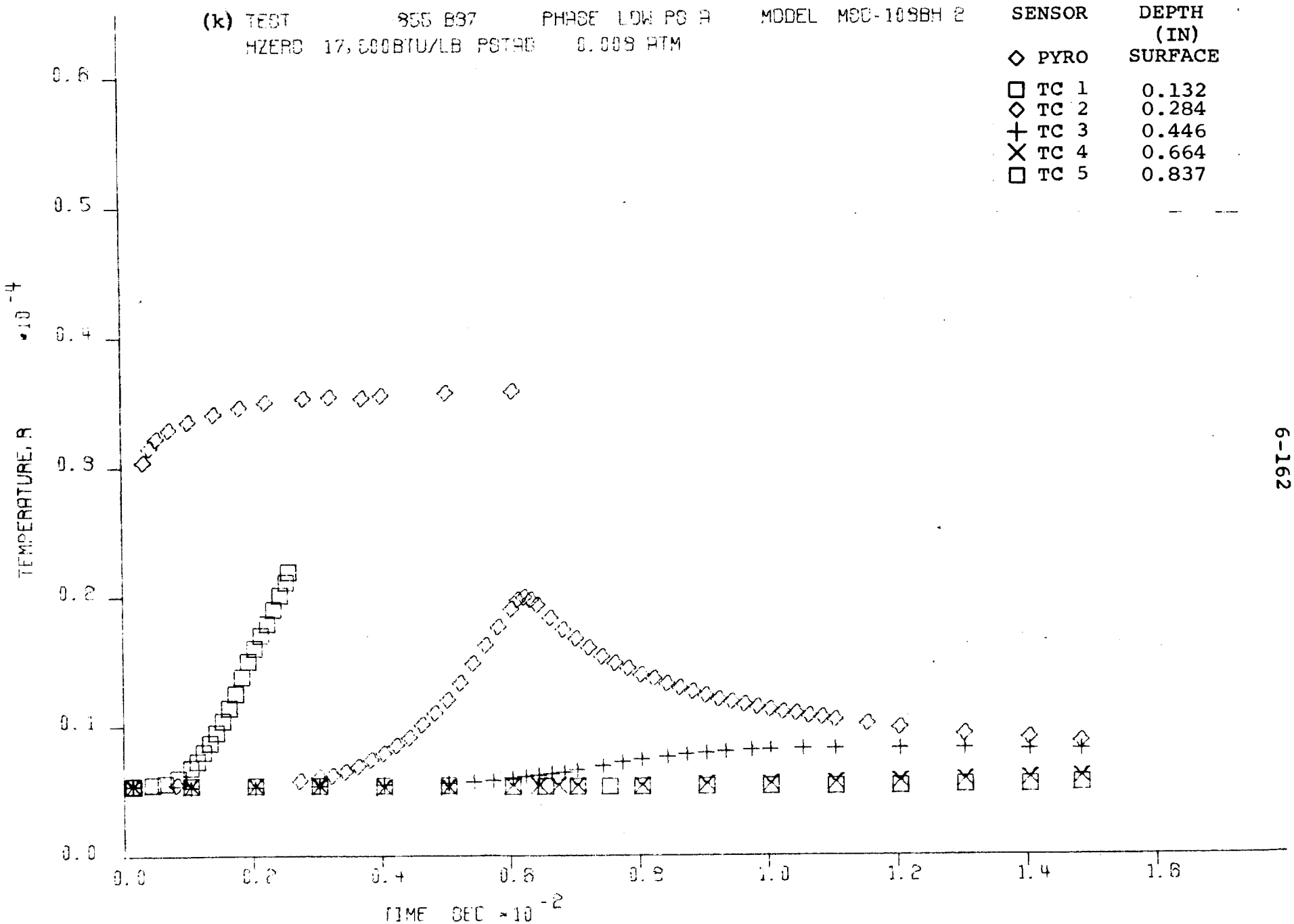

Figure 6-15. Continued.

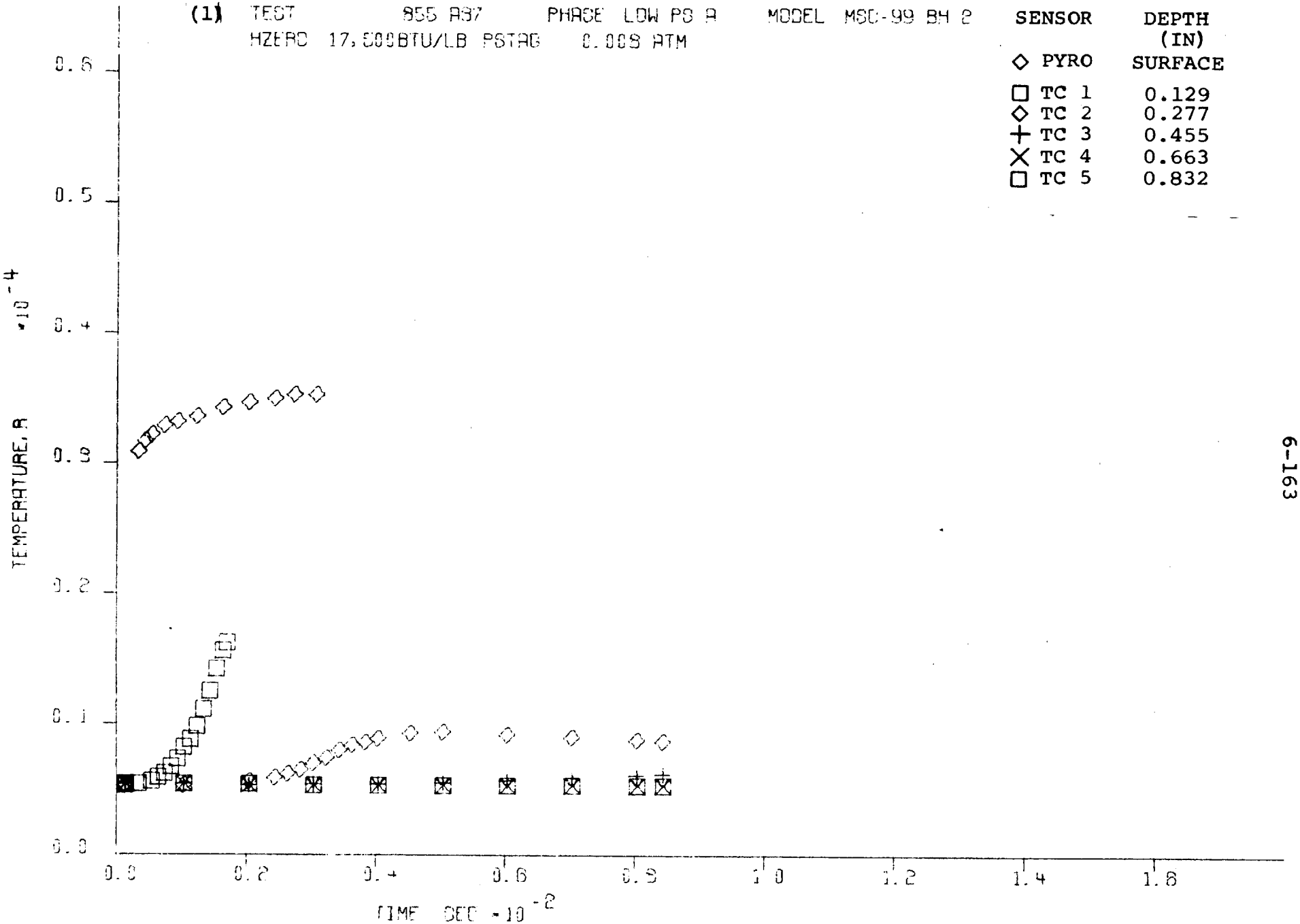

Figure 6-15. Continued.

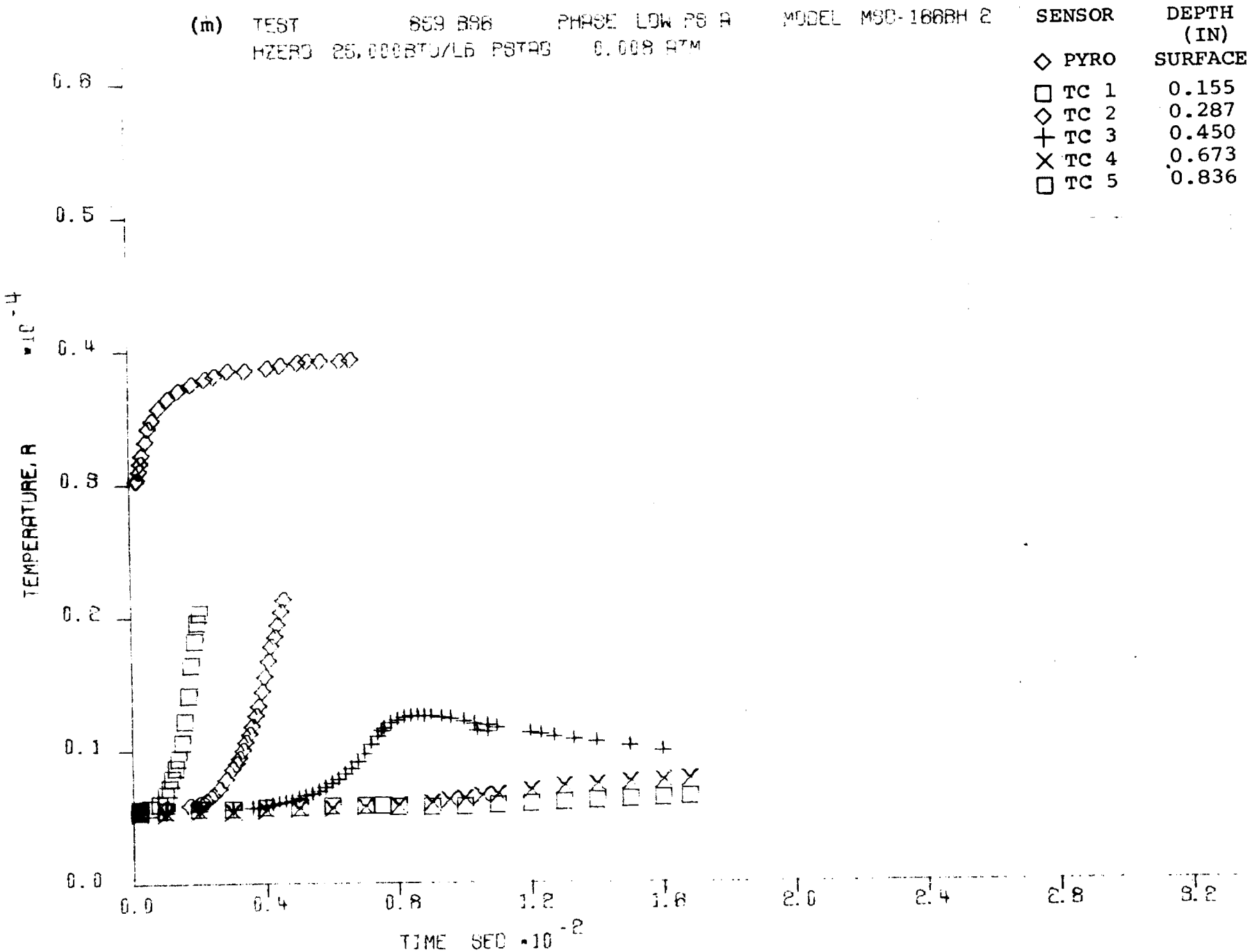

Figure 6-15. Continued.

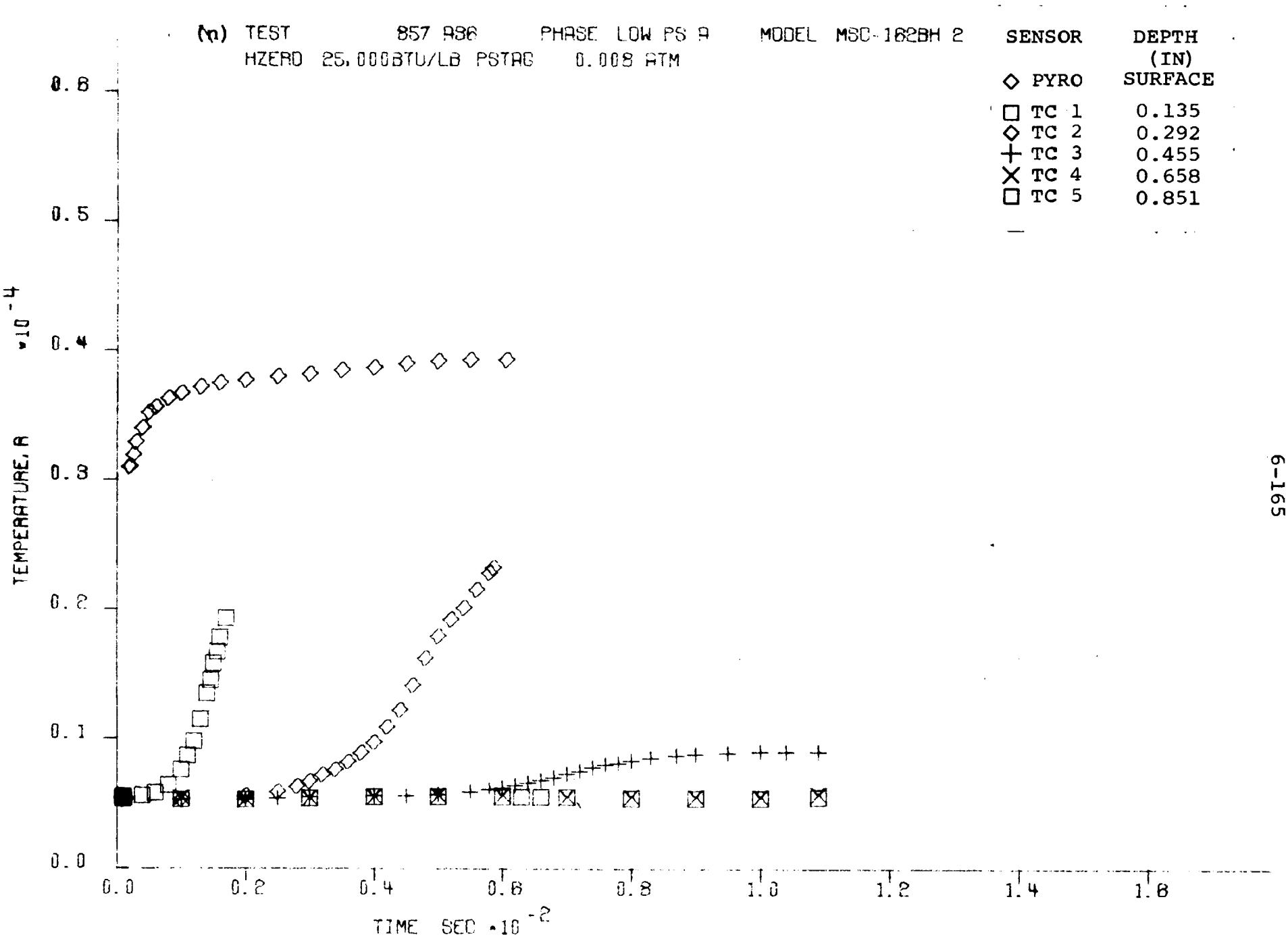

Figure 6-15. Continued.

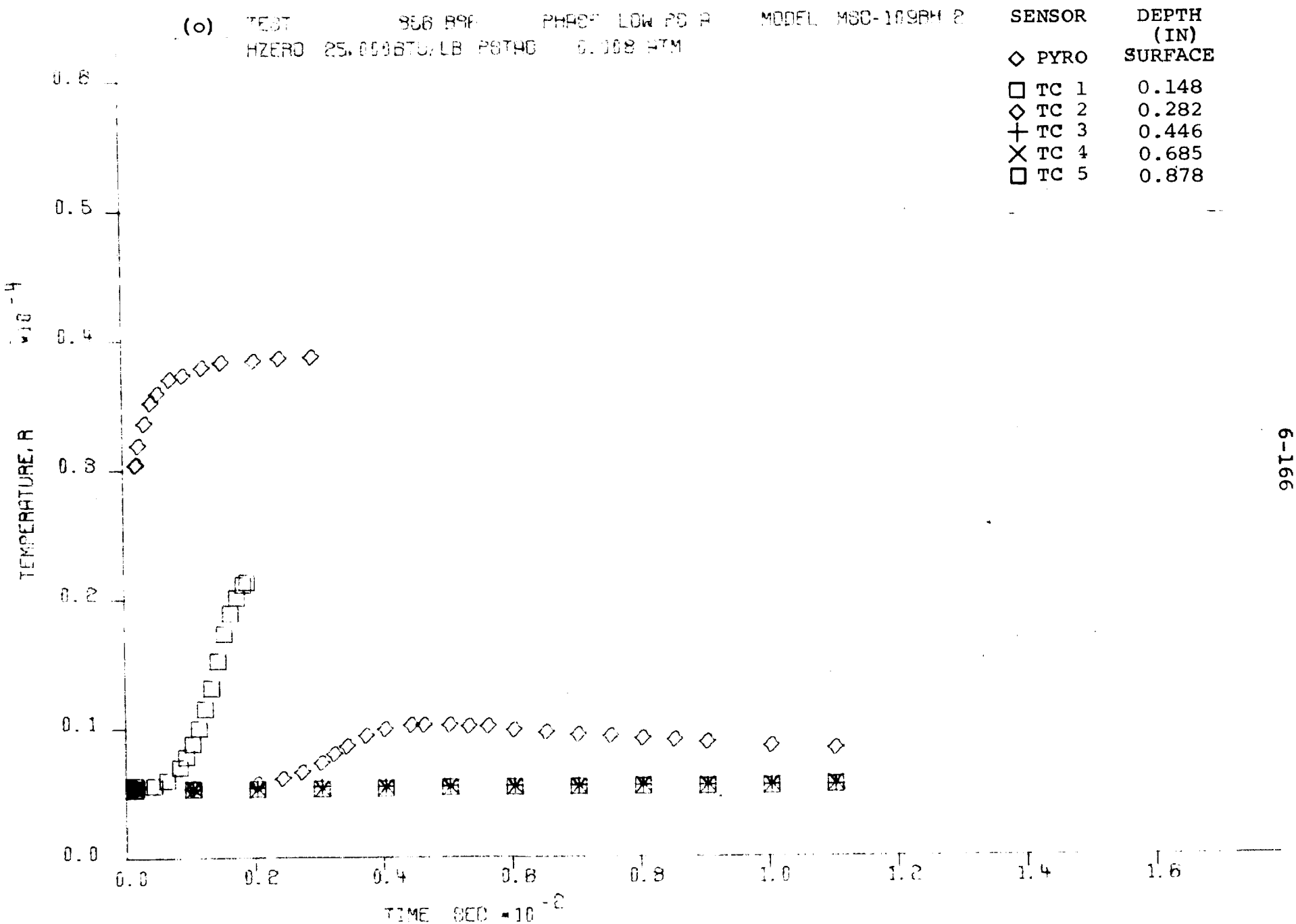

Figure 6-15. Concluded.

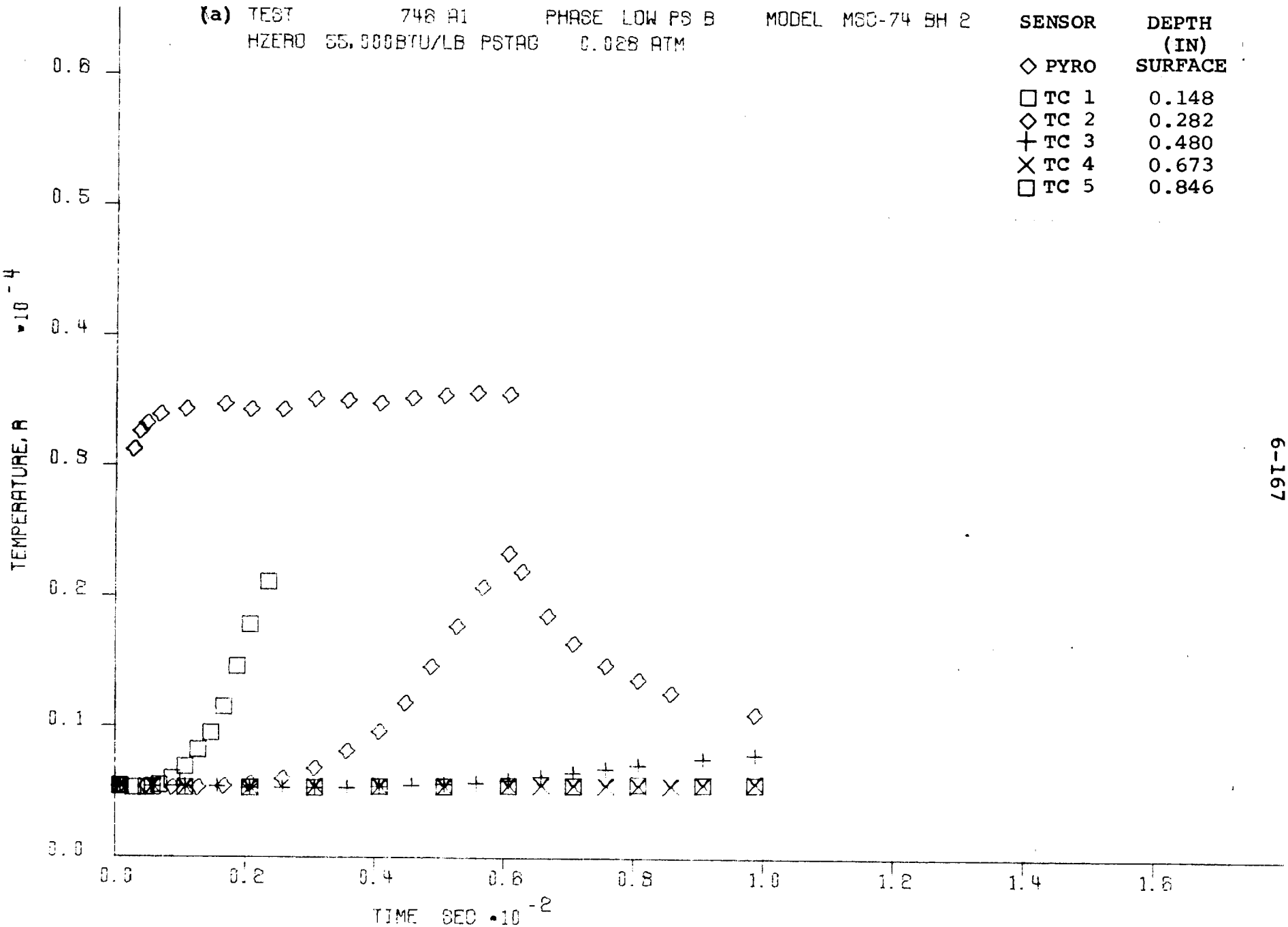

Figure 6-16. Surface and Internal Temperature Histories, Phase IV B.

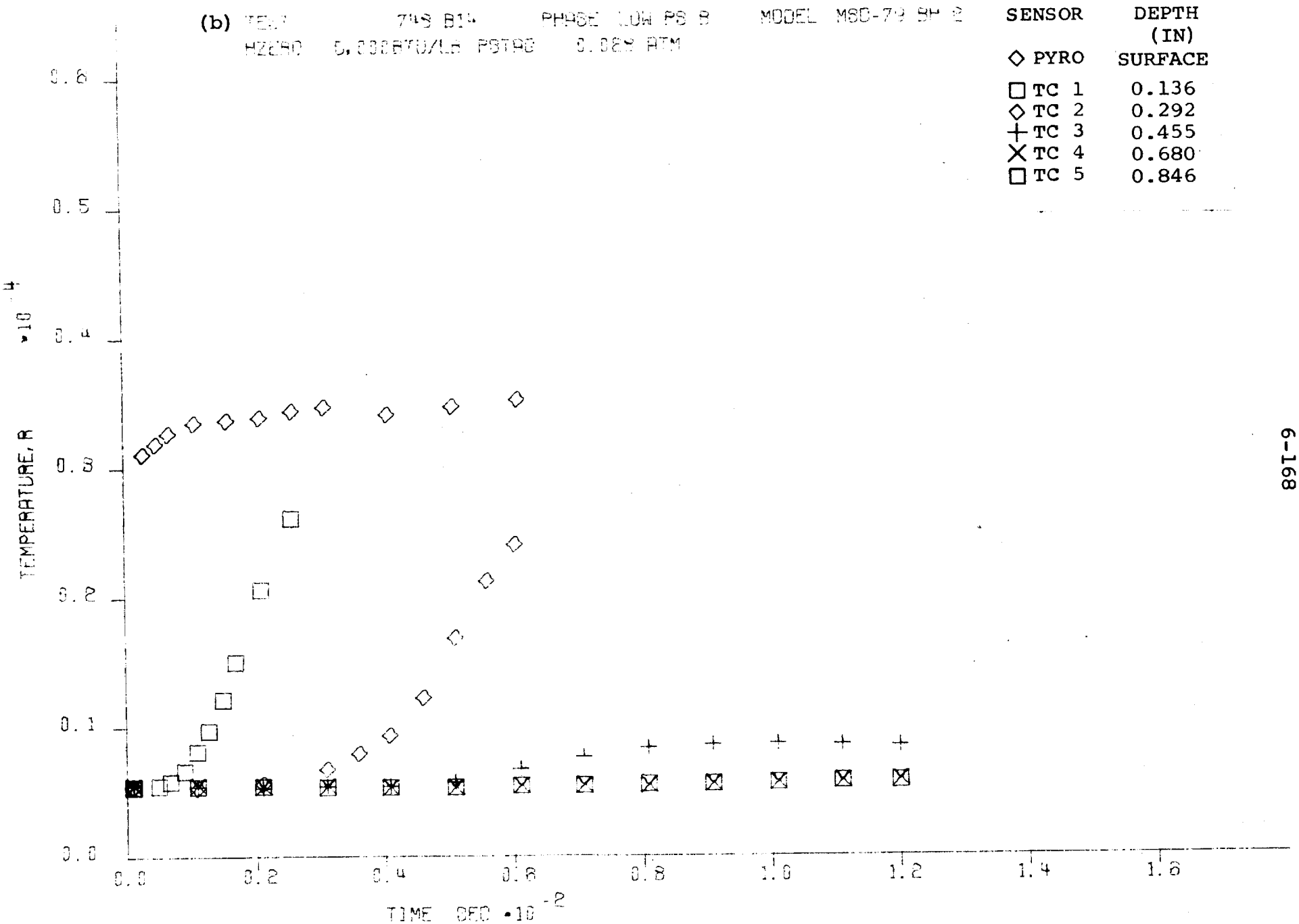

Figure 6-16. Continued.

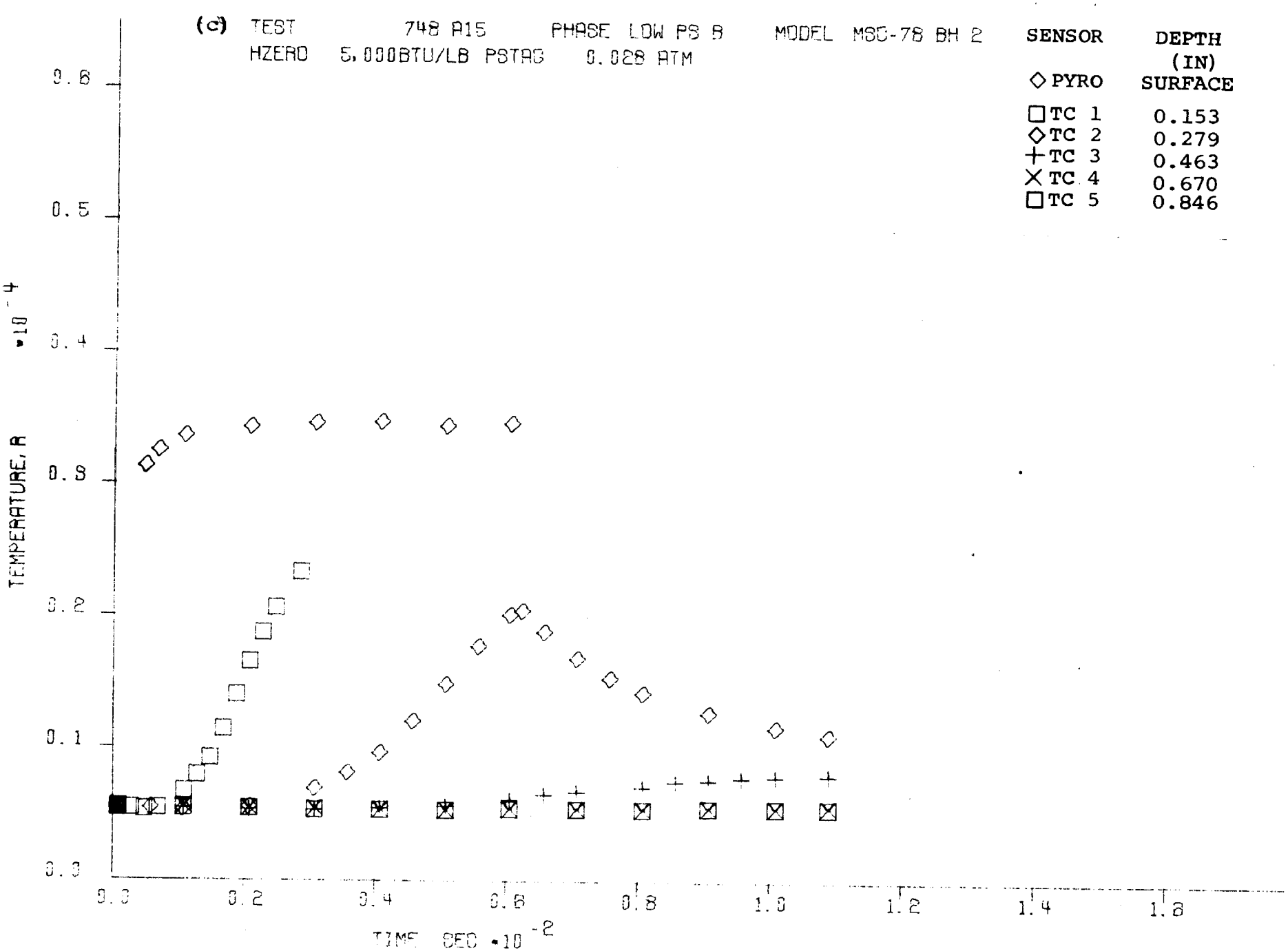

Figure 6-16. Continued.

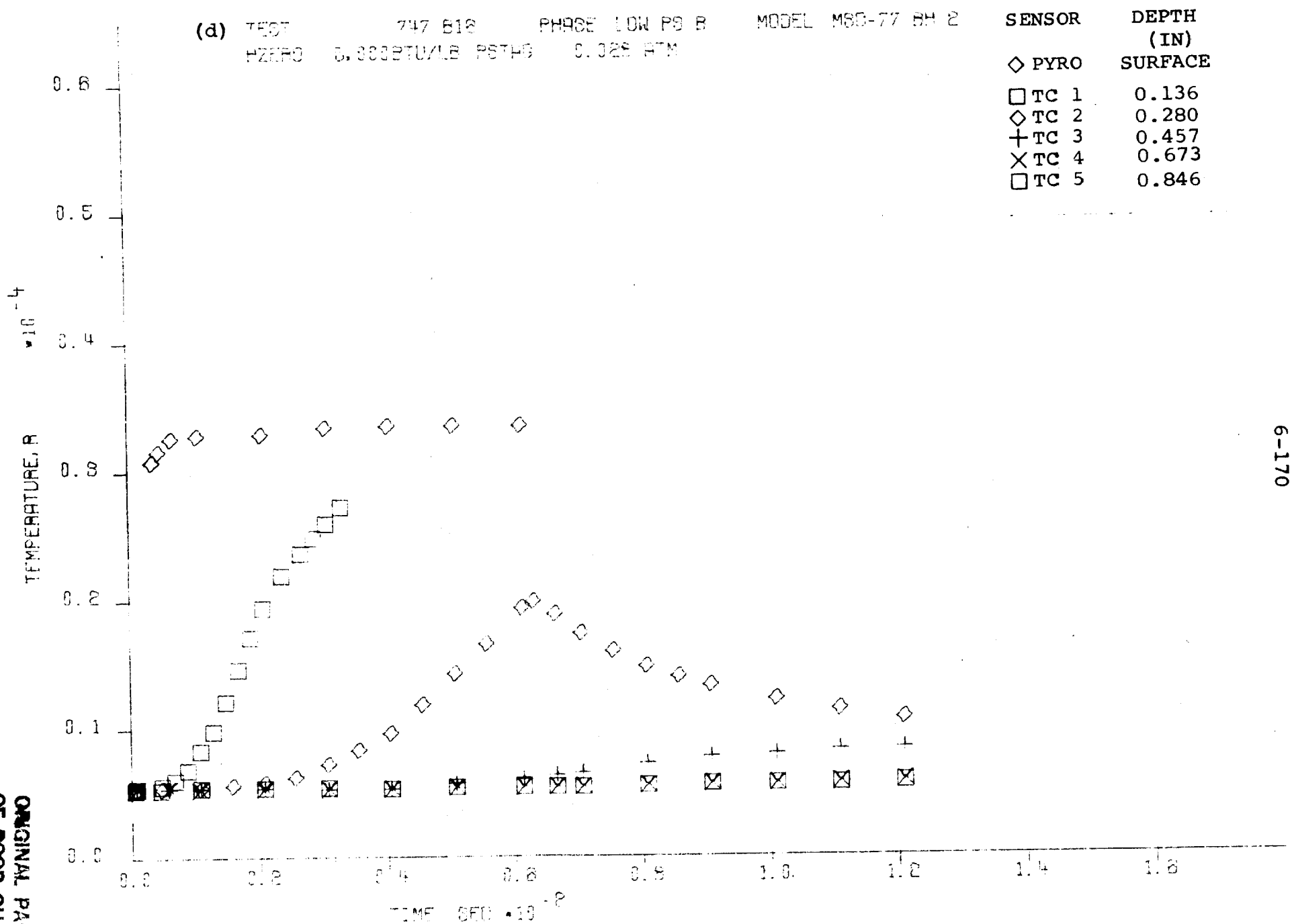

Figure 6-16. Continued.

ORIGINAL PAGE IS OF POOR QUALITY

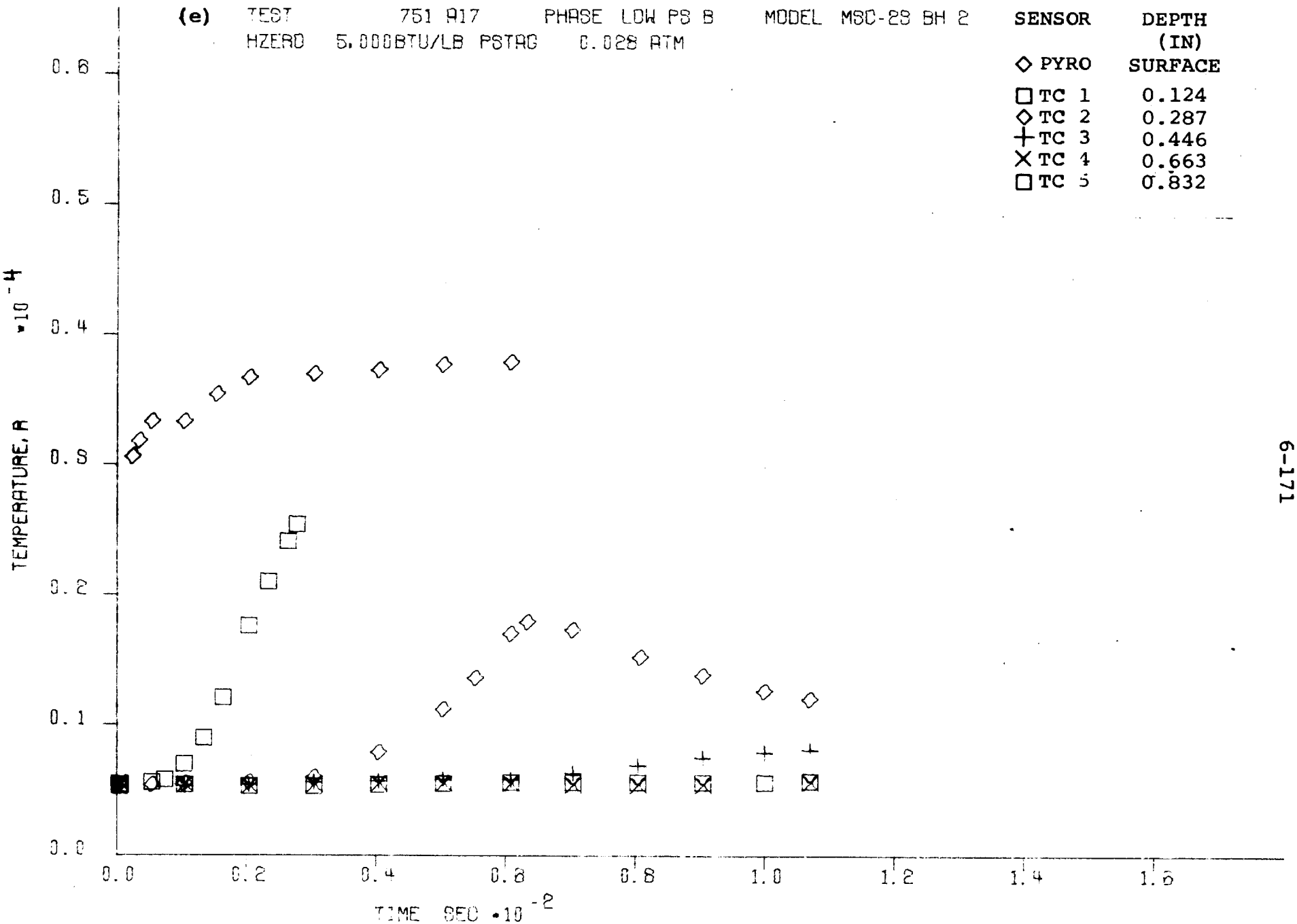

Figure 6-16. Continued.

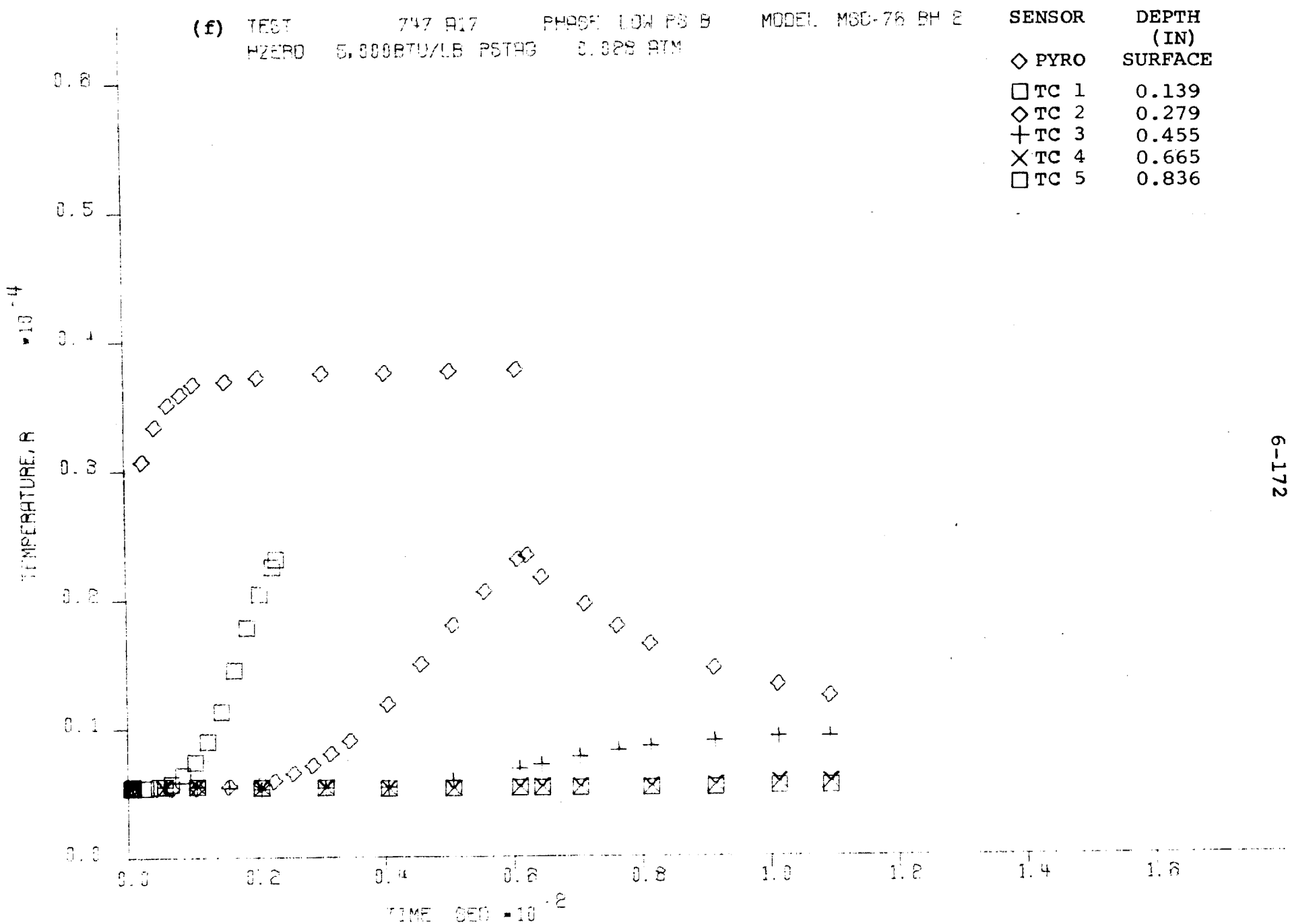

Figure 6-16. Continued.

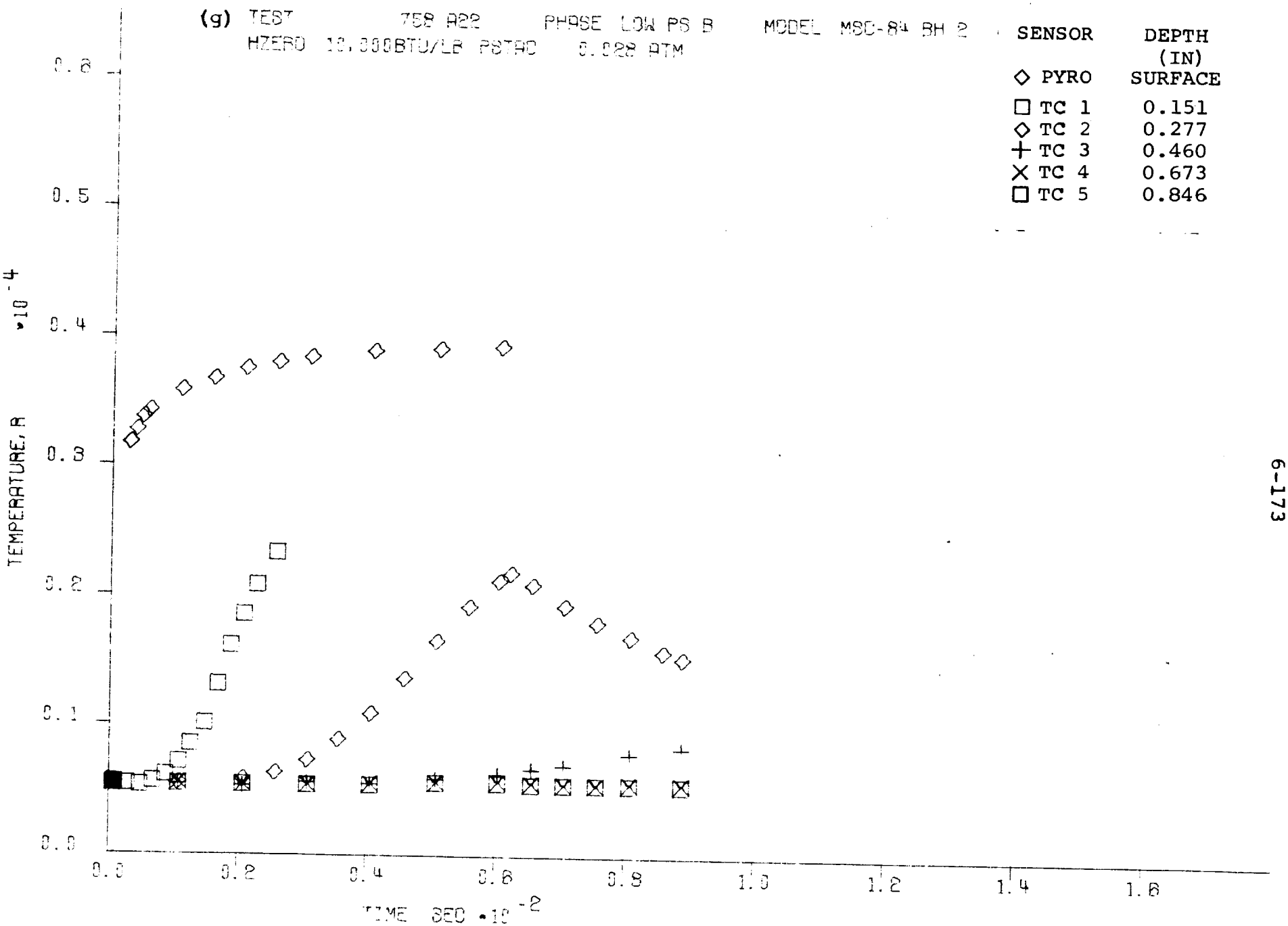

Figure 6-16. Continued.

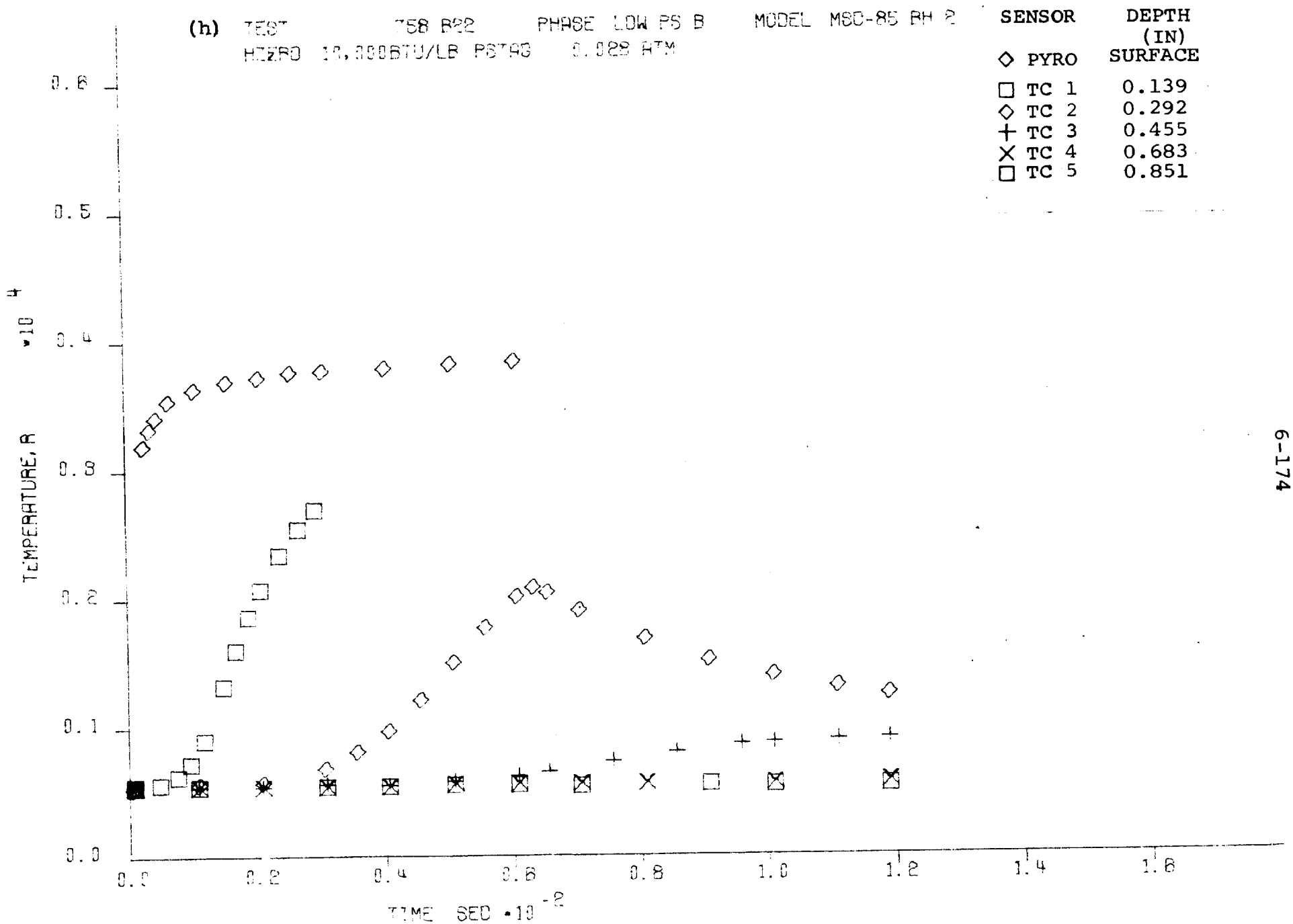

Figure 6-16. Continued.

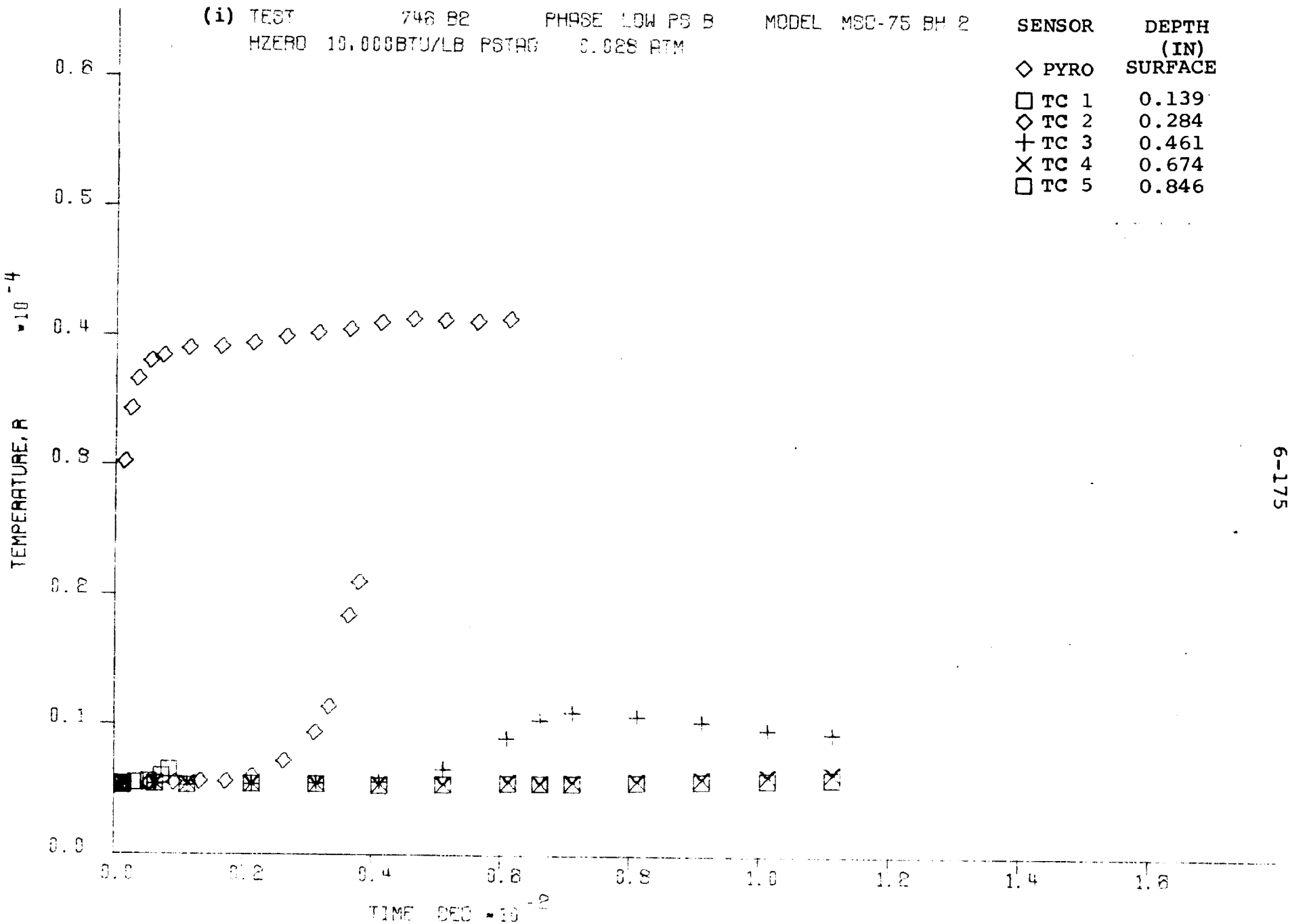

Figure 6-16. Continued.

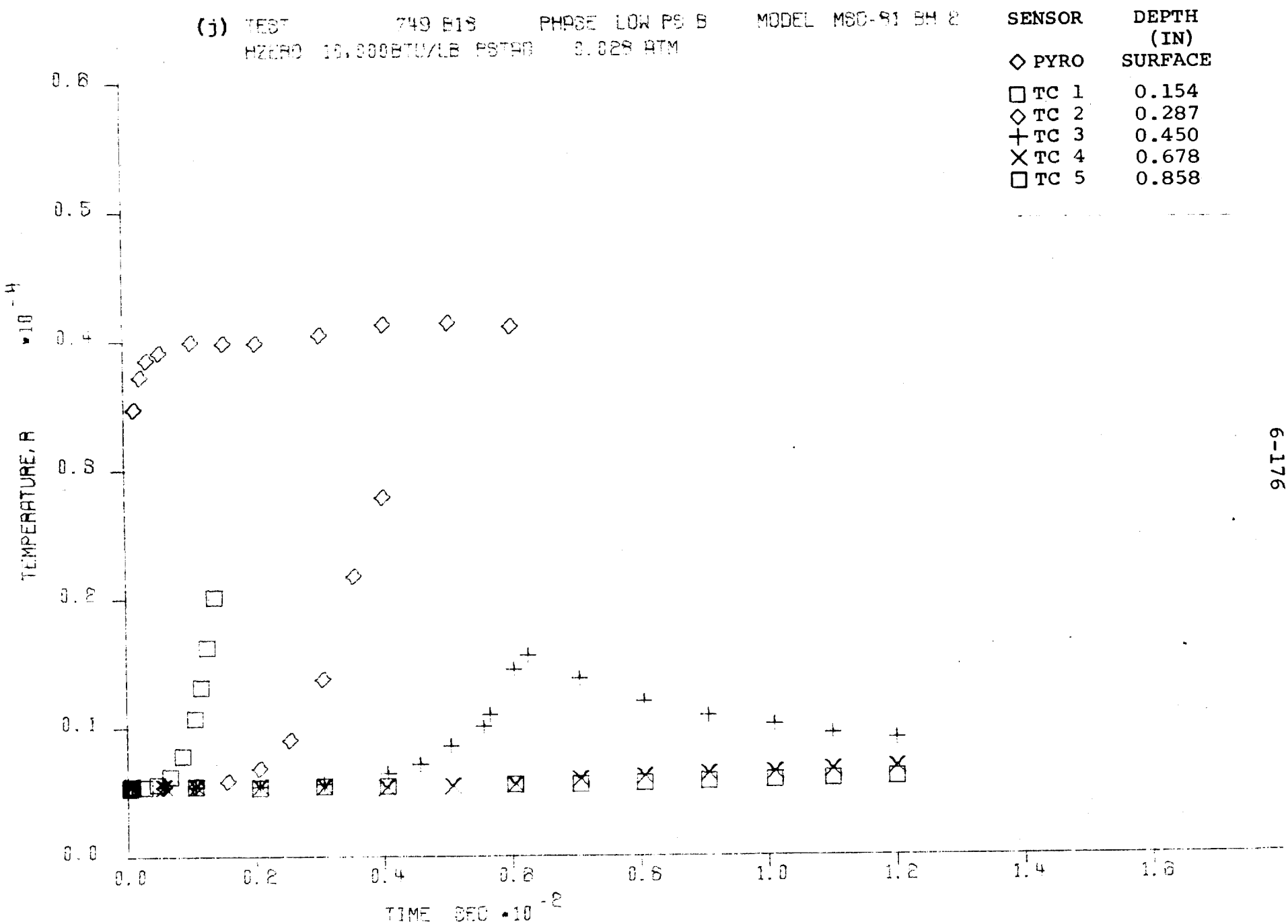

Figure 6-16. Continued.

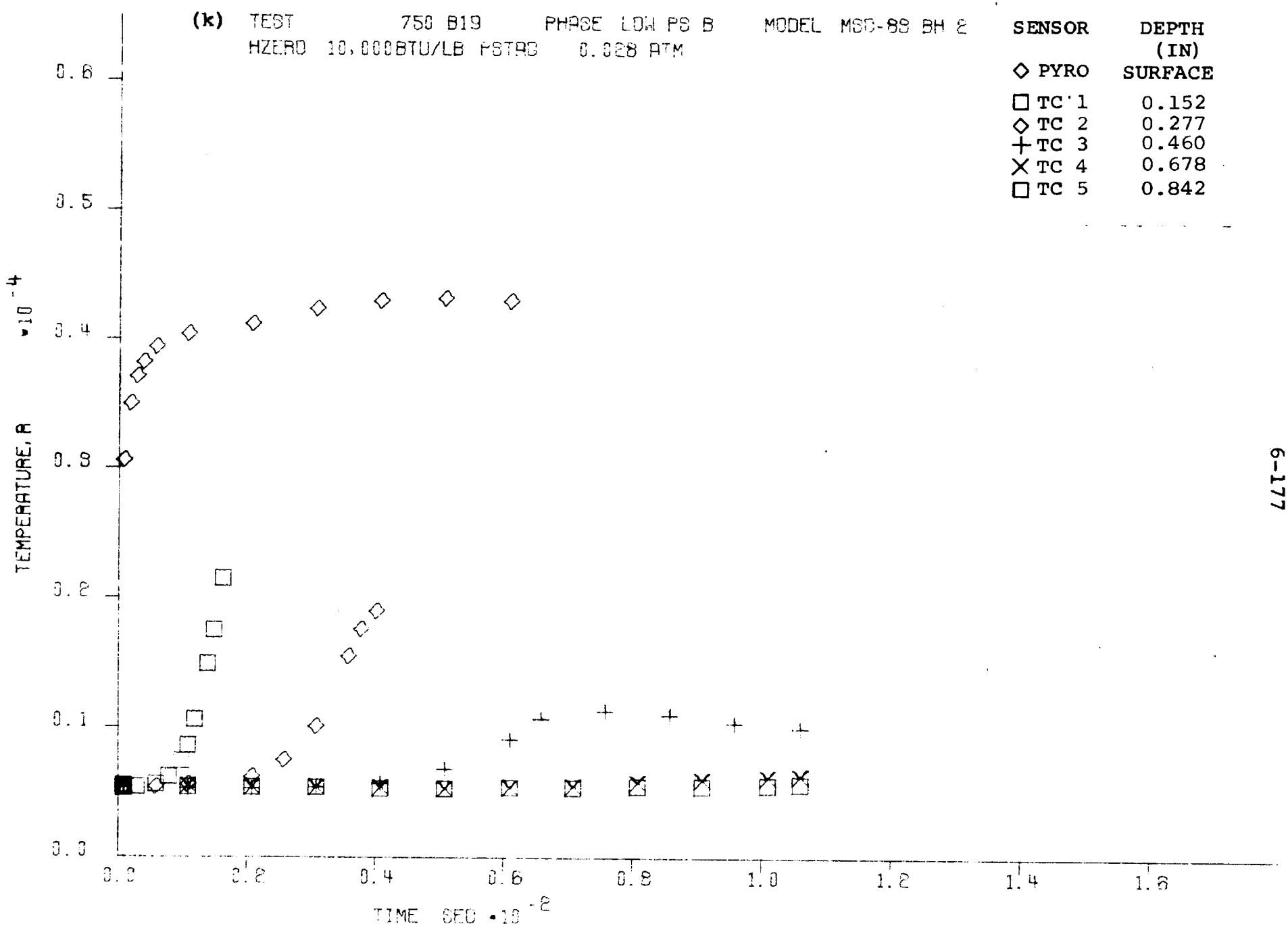

Figure 6-16. Continued.

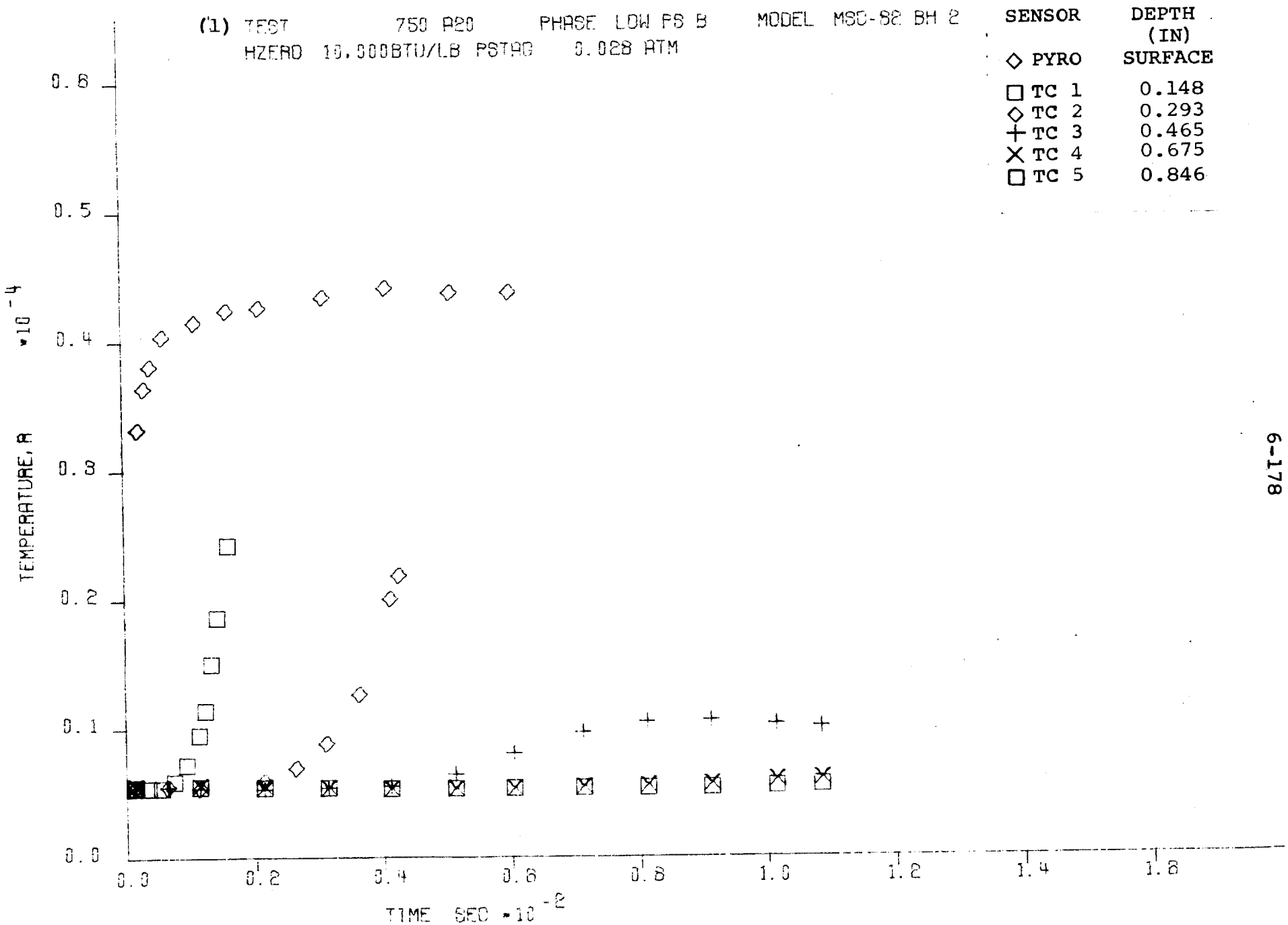

Figure 6-16. Continued.

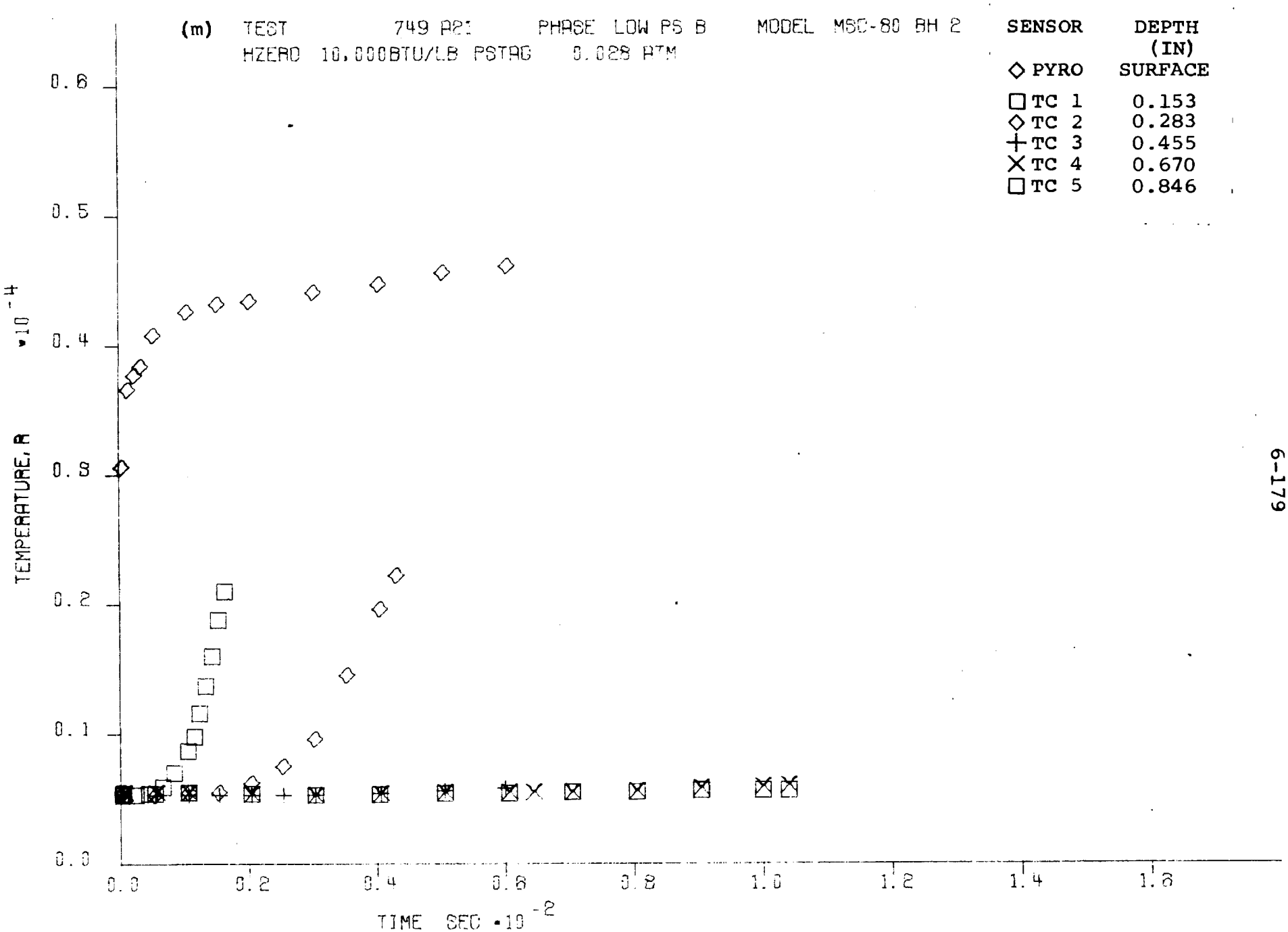

Figure 6-16. Continued.

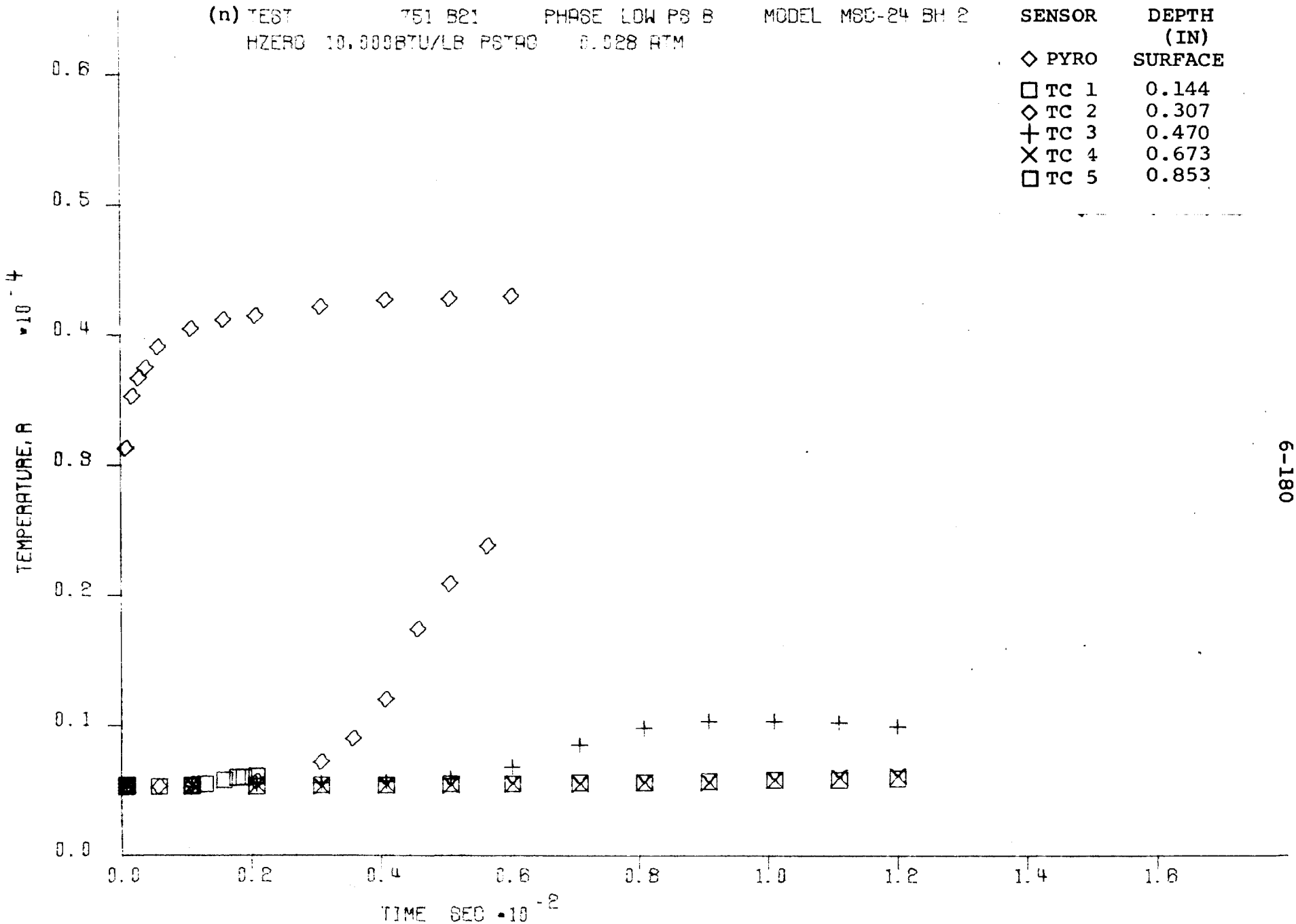

Figure 6-16. Continued.

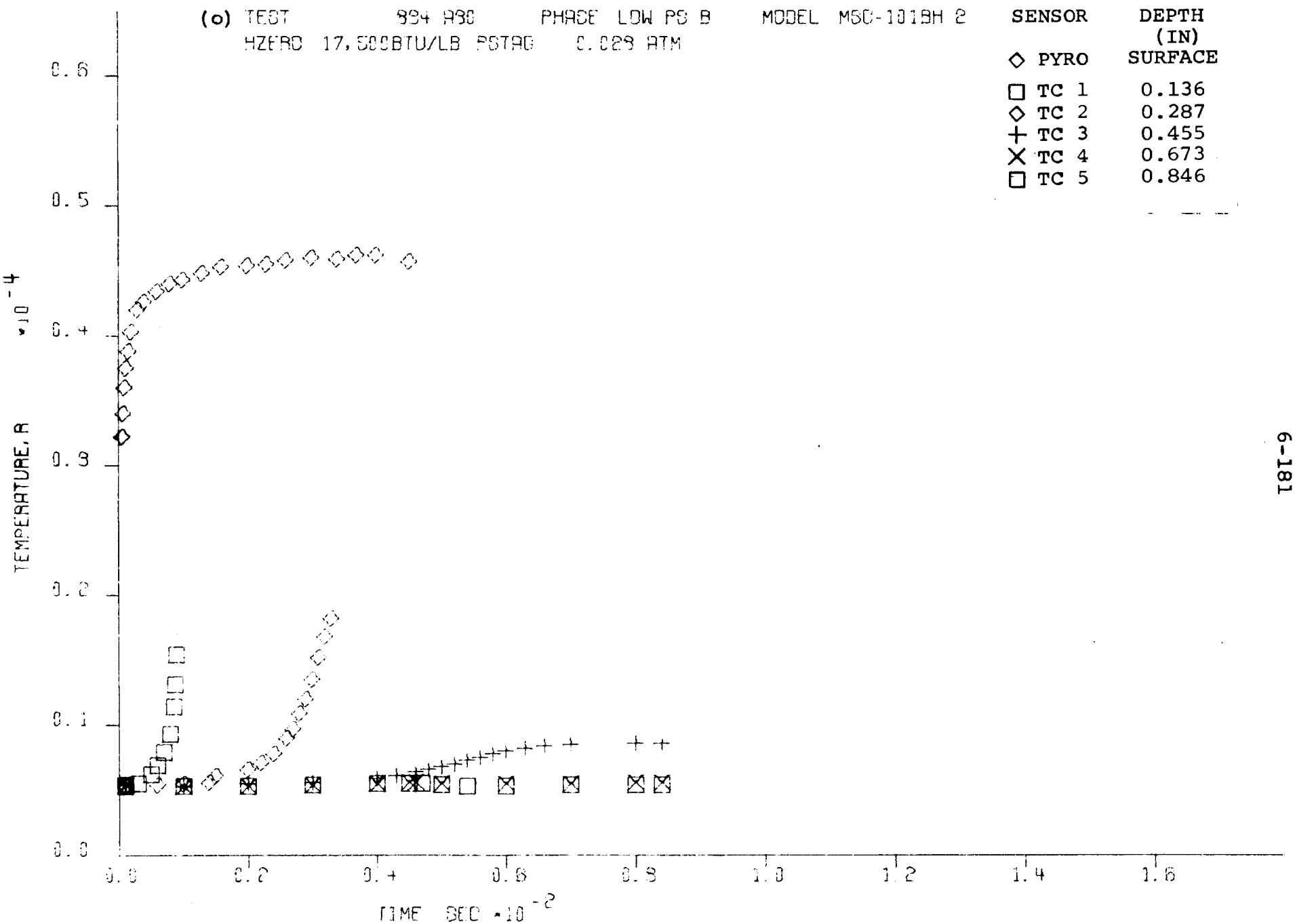

Figure 6-16. Continued.

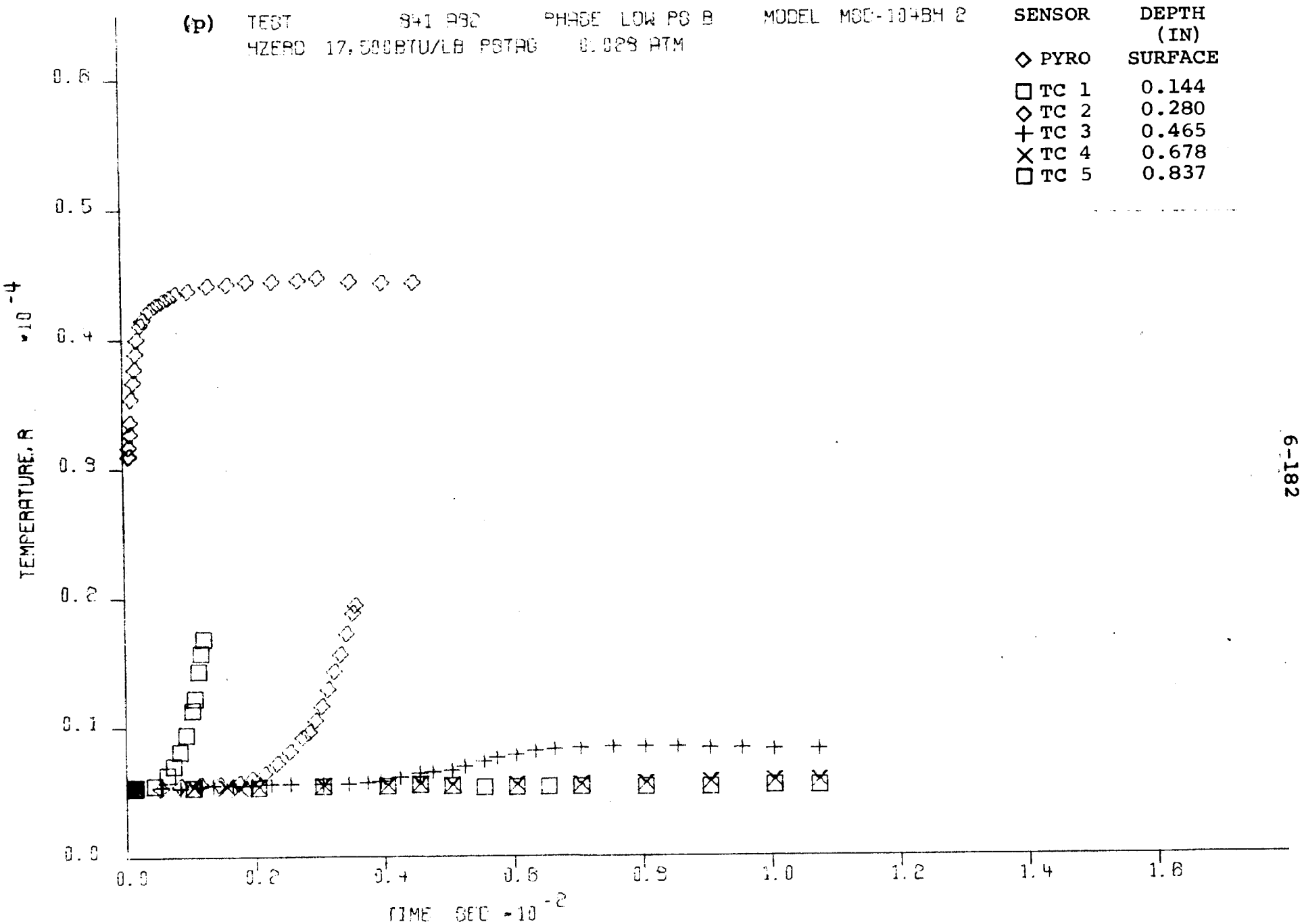

Figure 6-16. Continued.

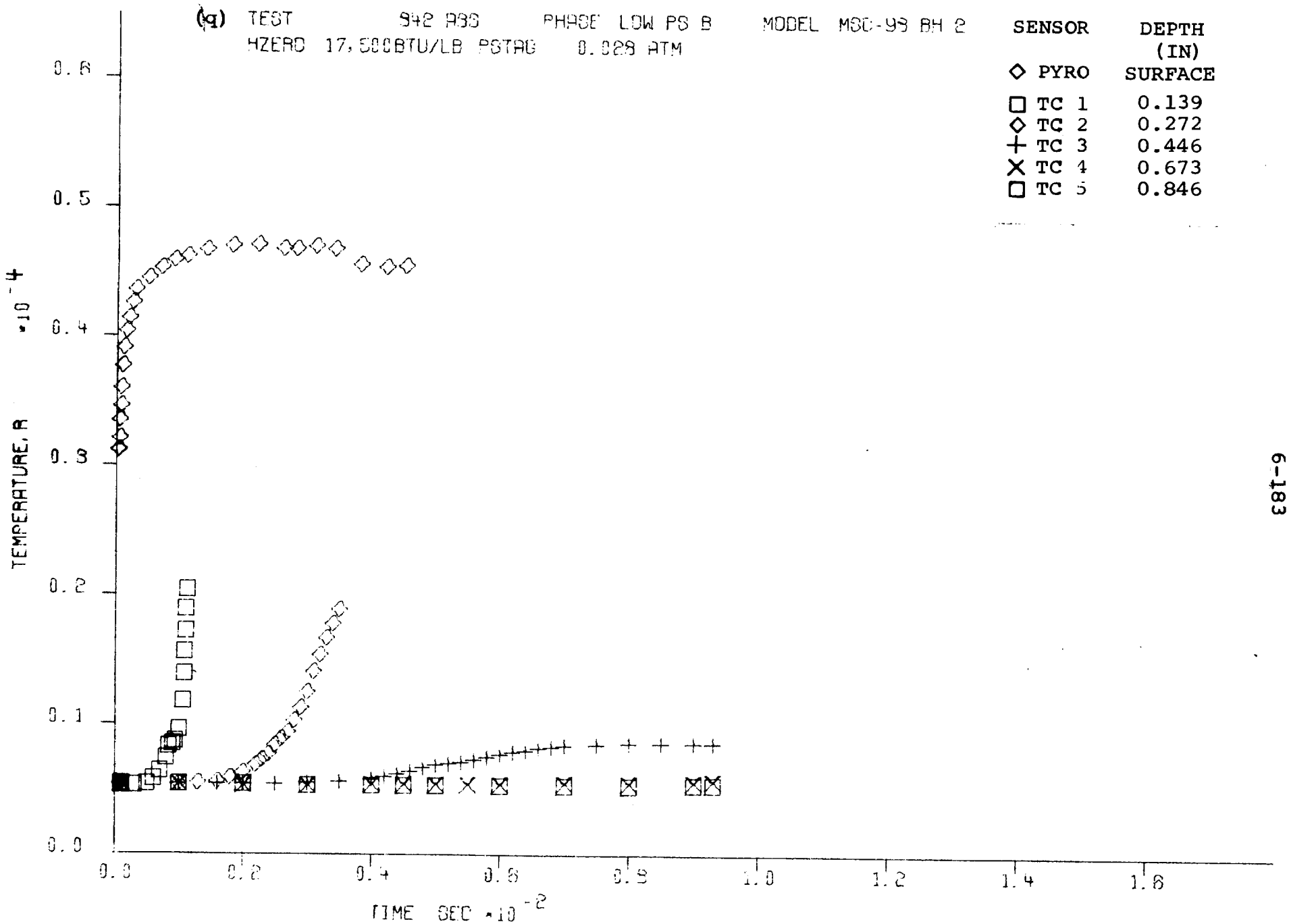

Figure 6-16. Continued.

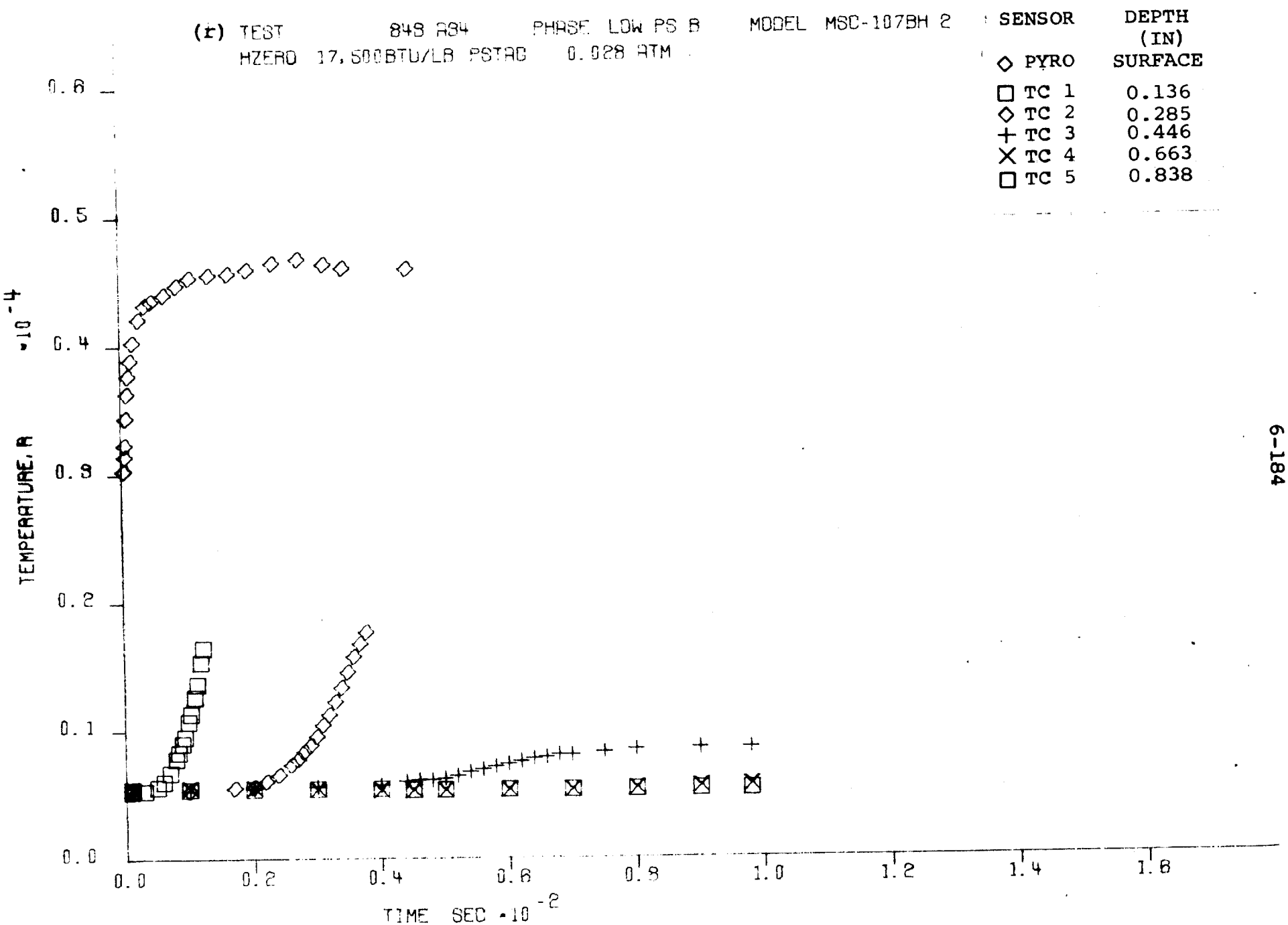

Figure 6-16. Continued.

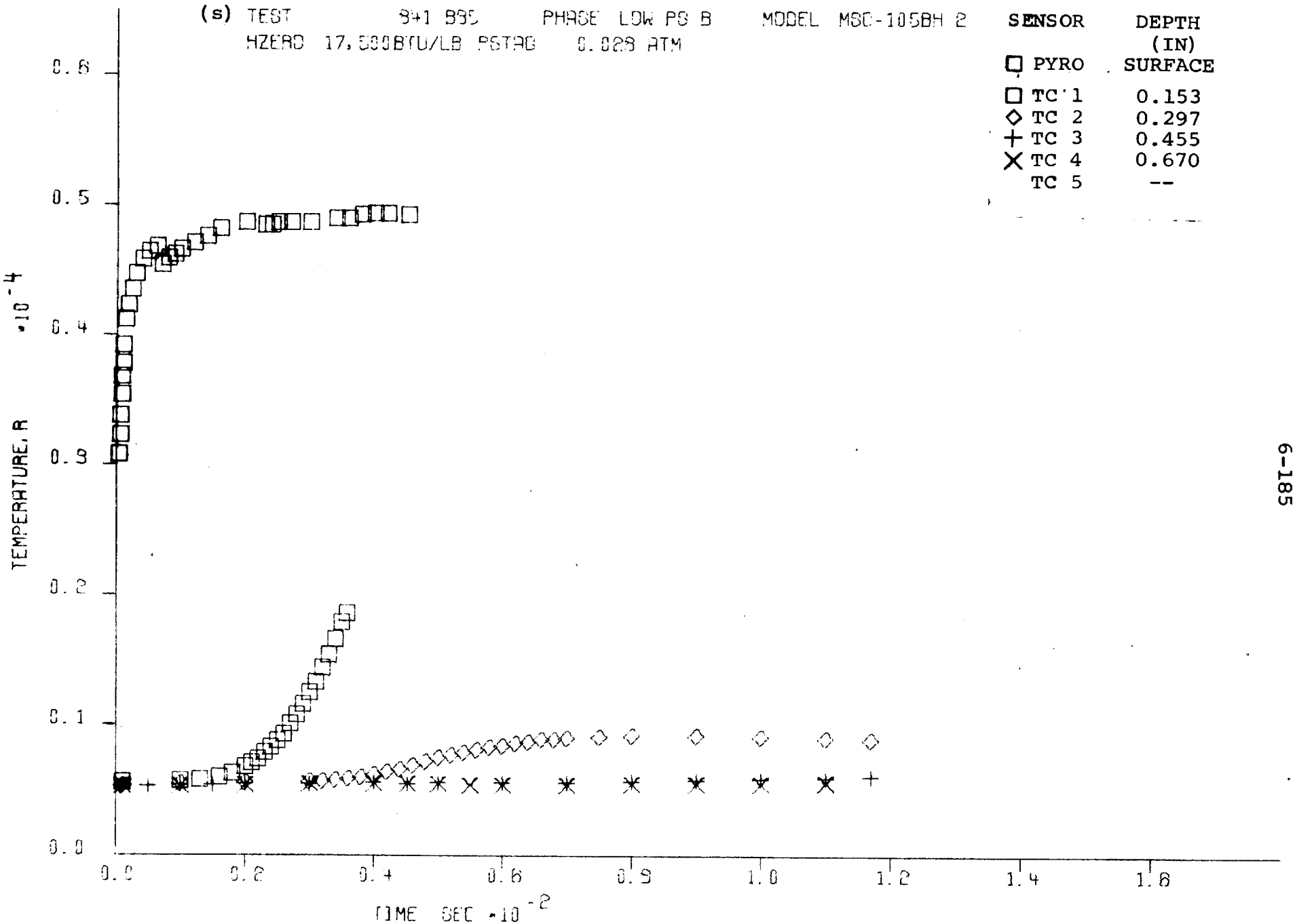

Figure 6-16. Continued.

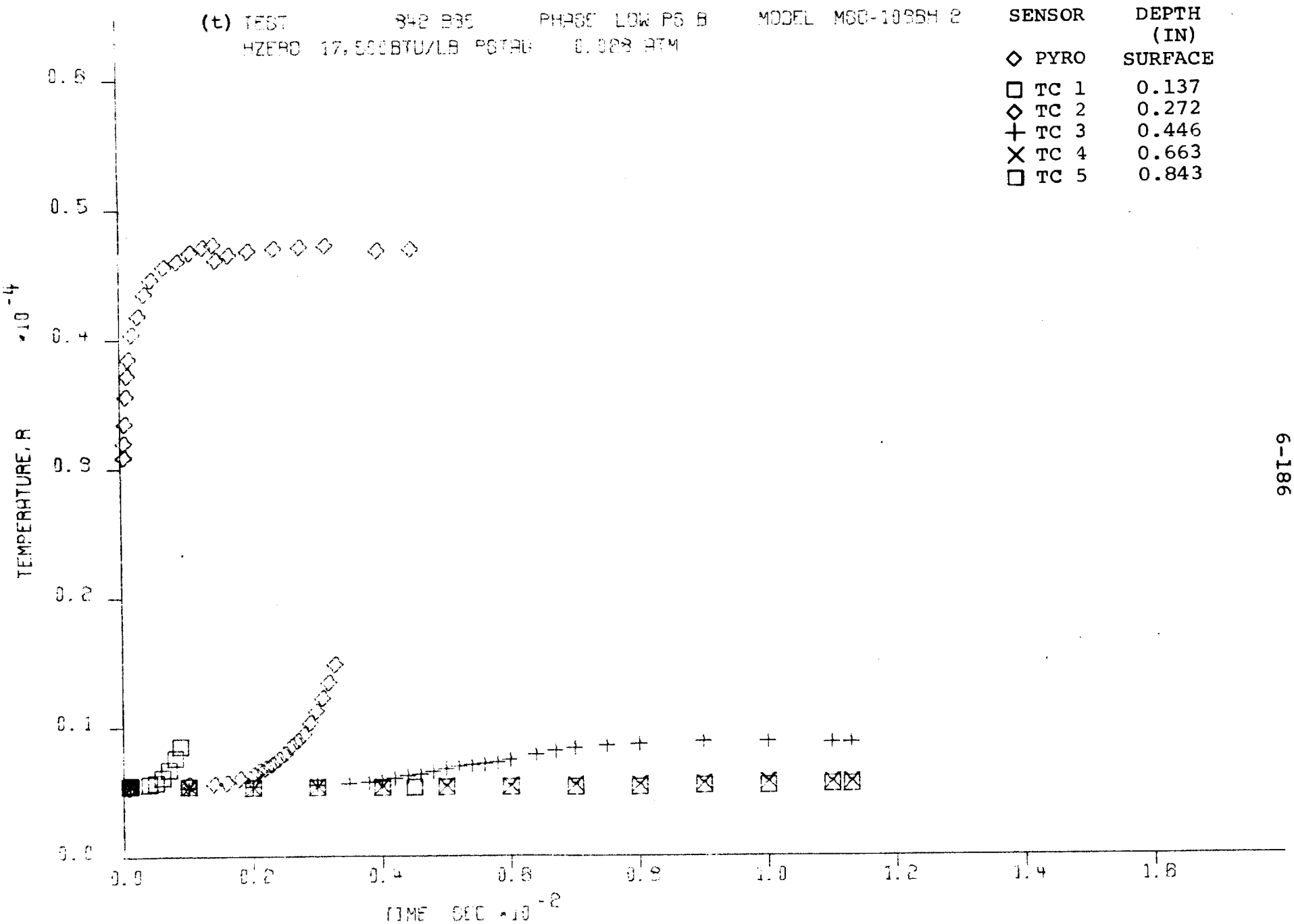

Figure 6-16. Continued.

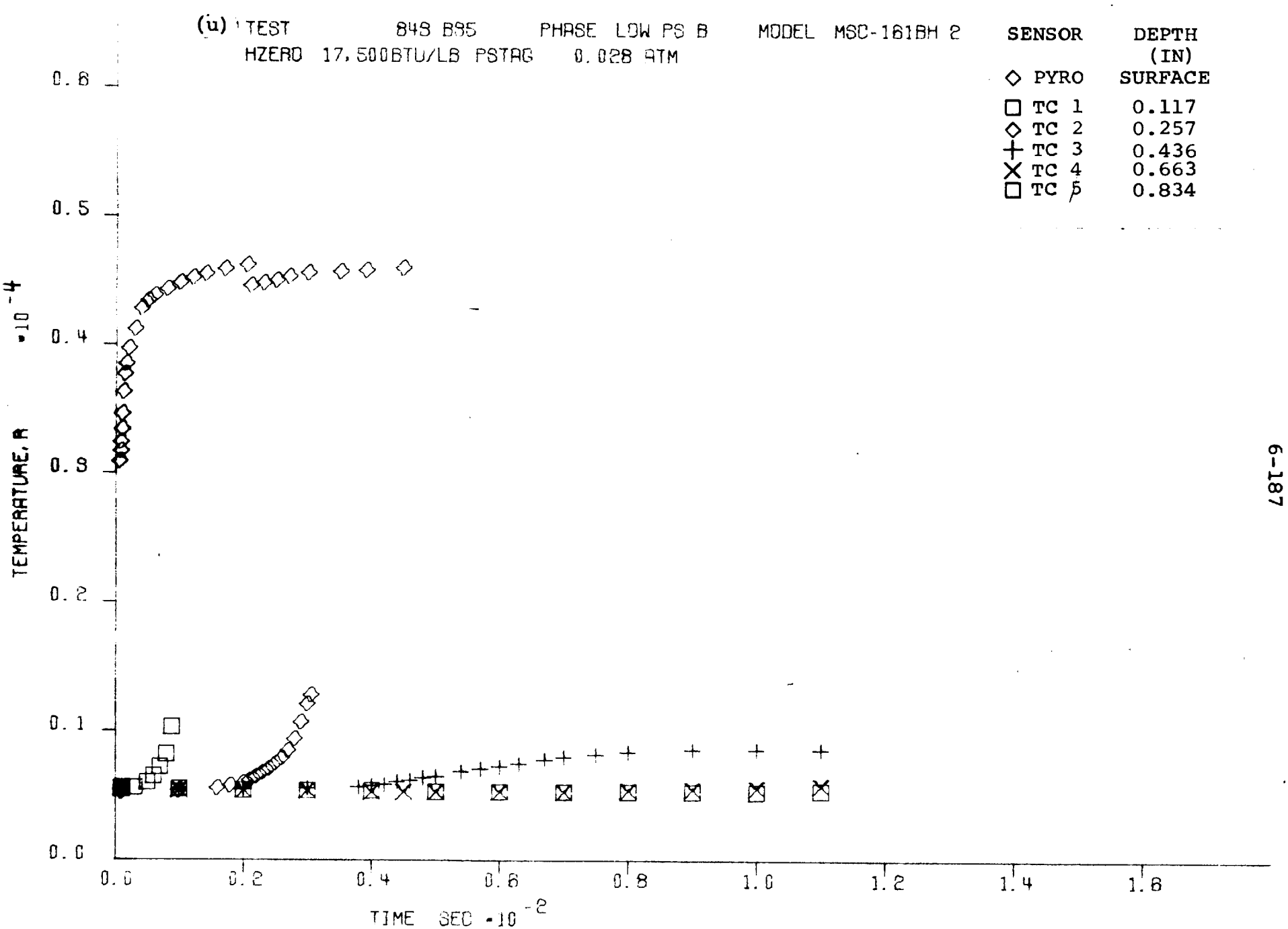

Figure 6-16. Continued.

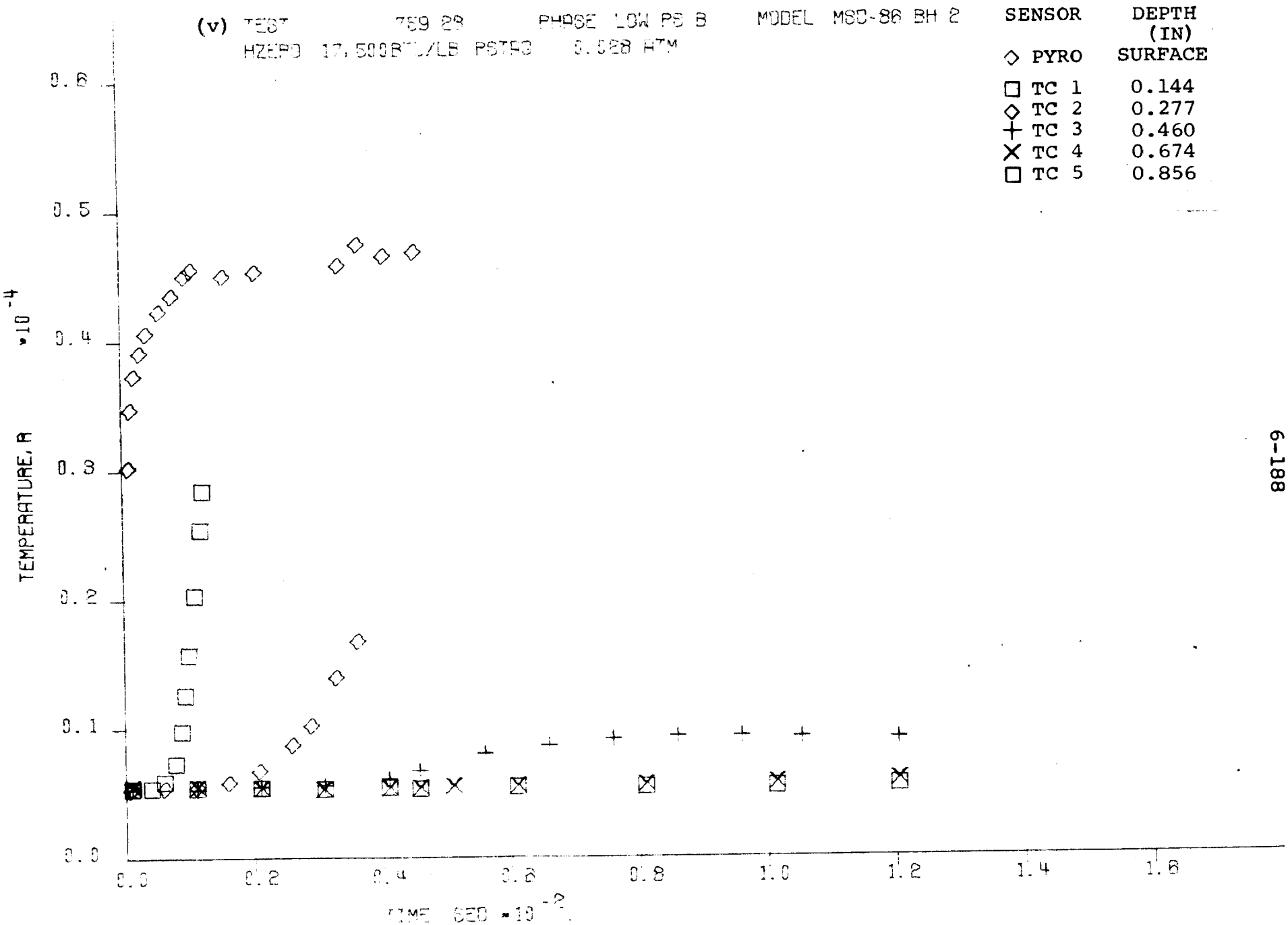

Figure 6-16. Concluded.

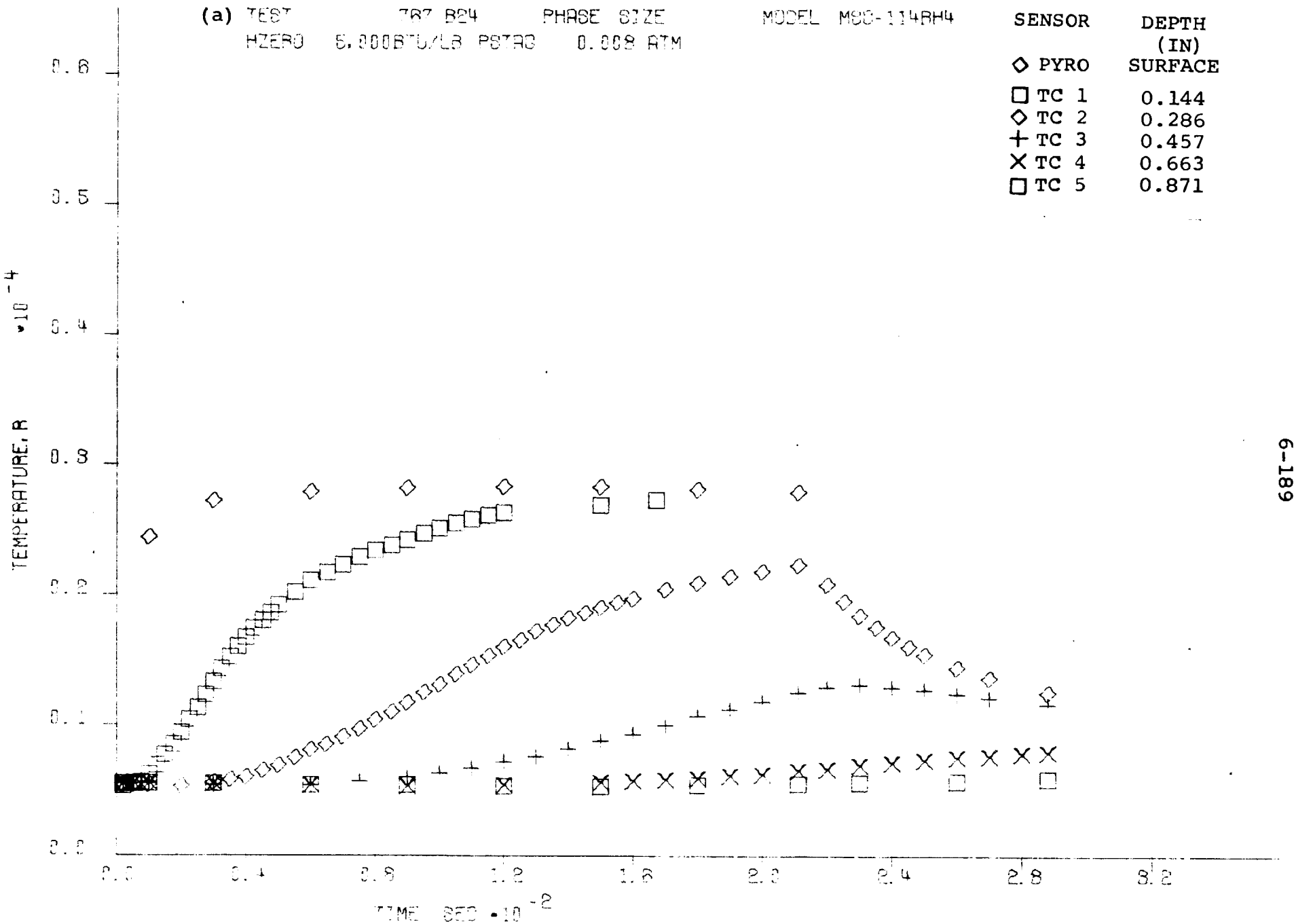

Figure 6-17. Surface and Internal Temperature Histories, Phase V.

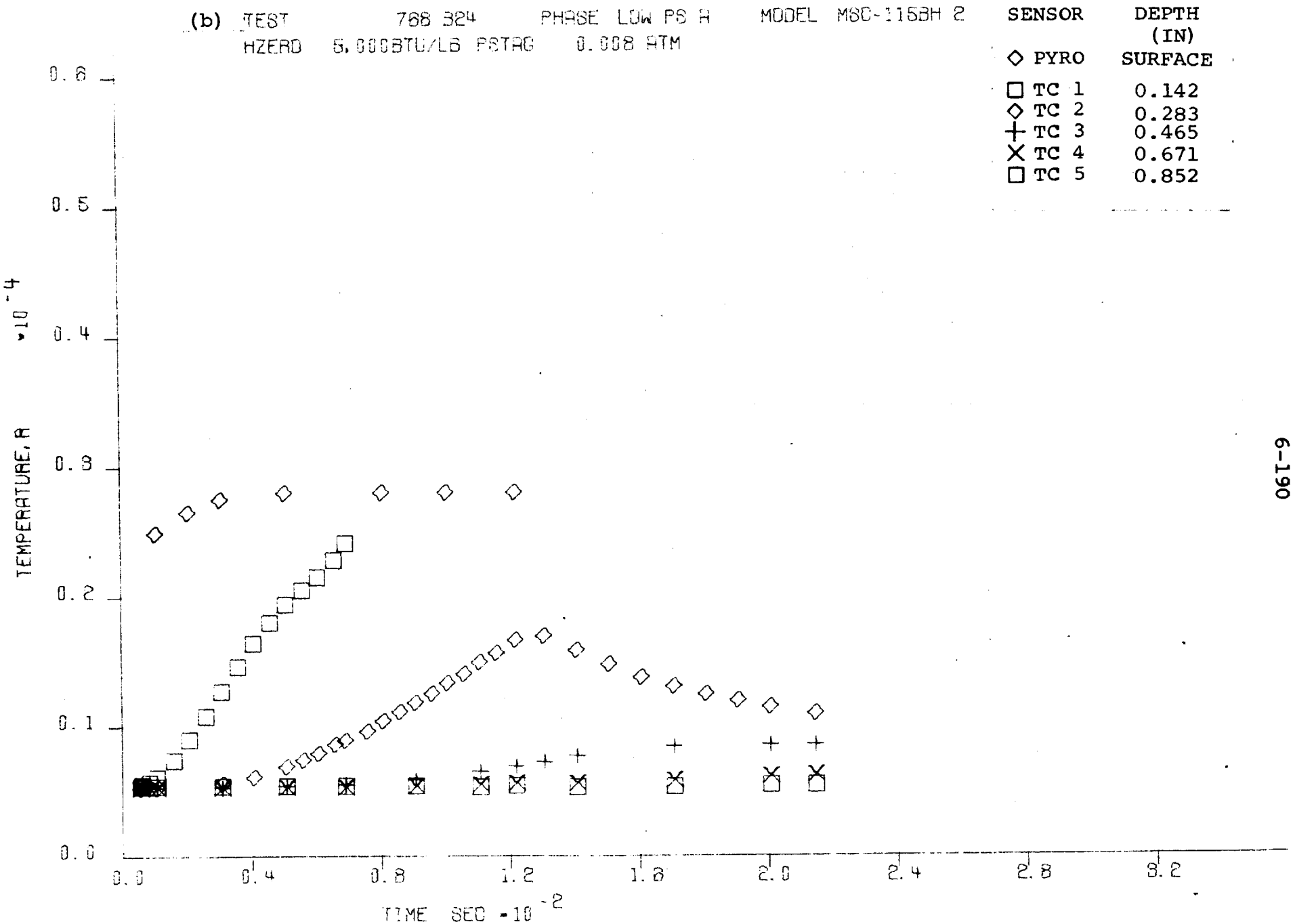

Figure 6-17. Continued.

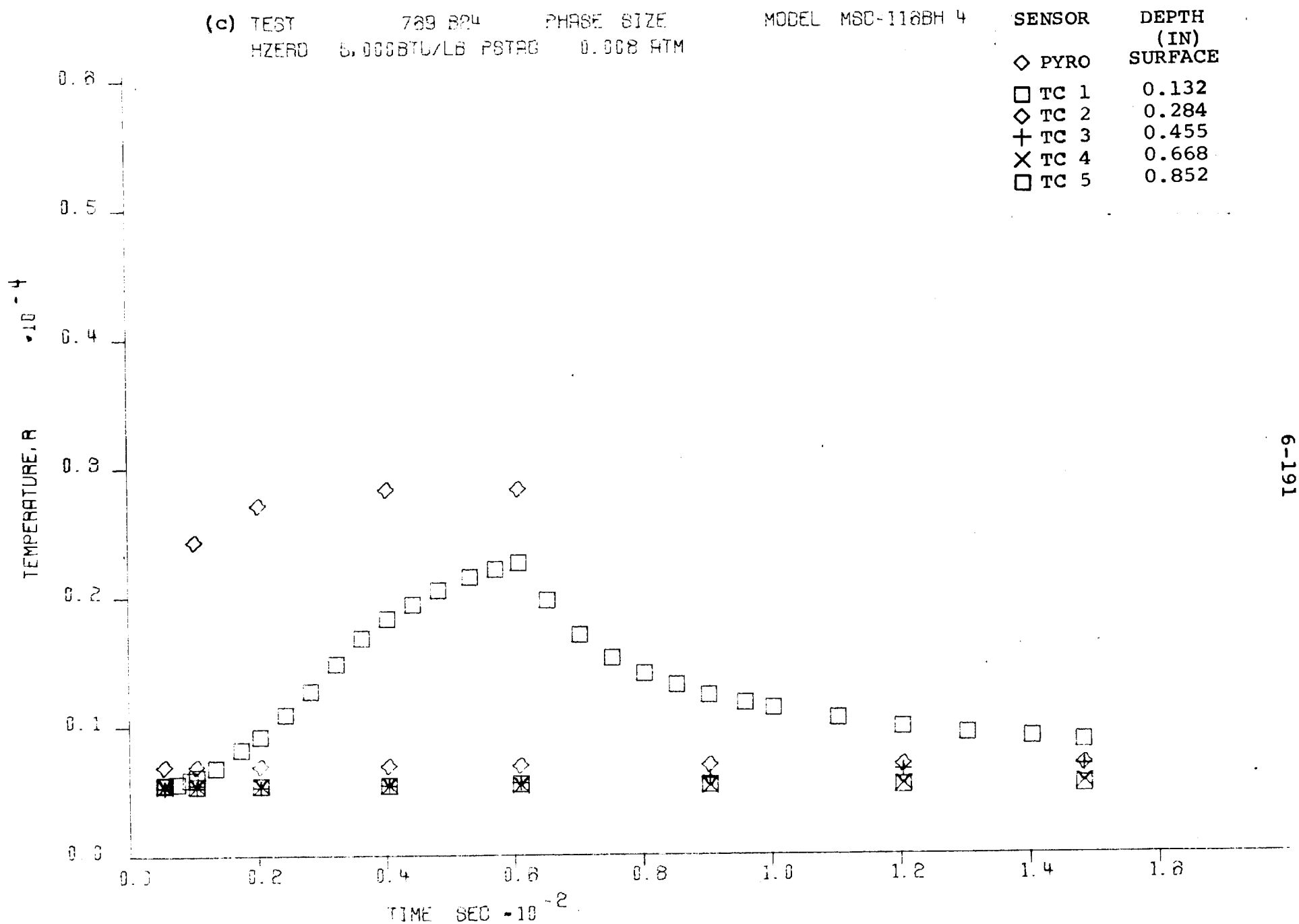

Figure 6-17. Continued.

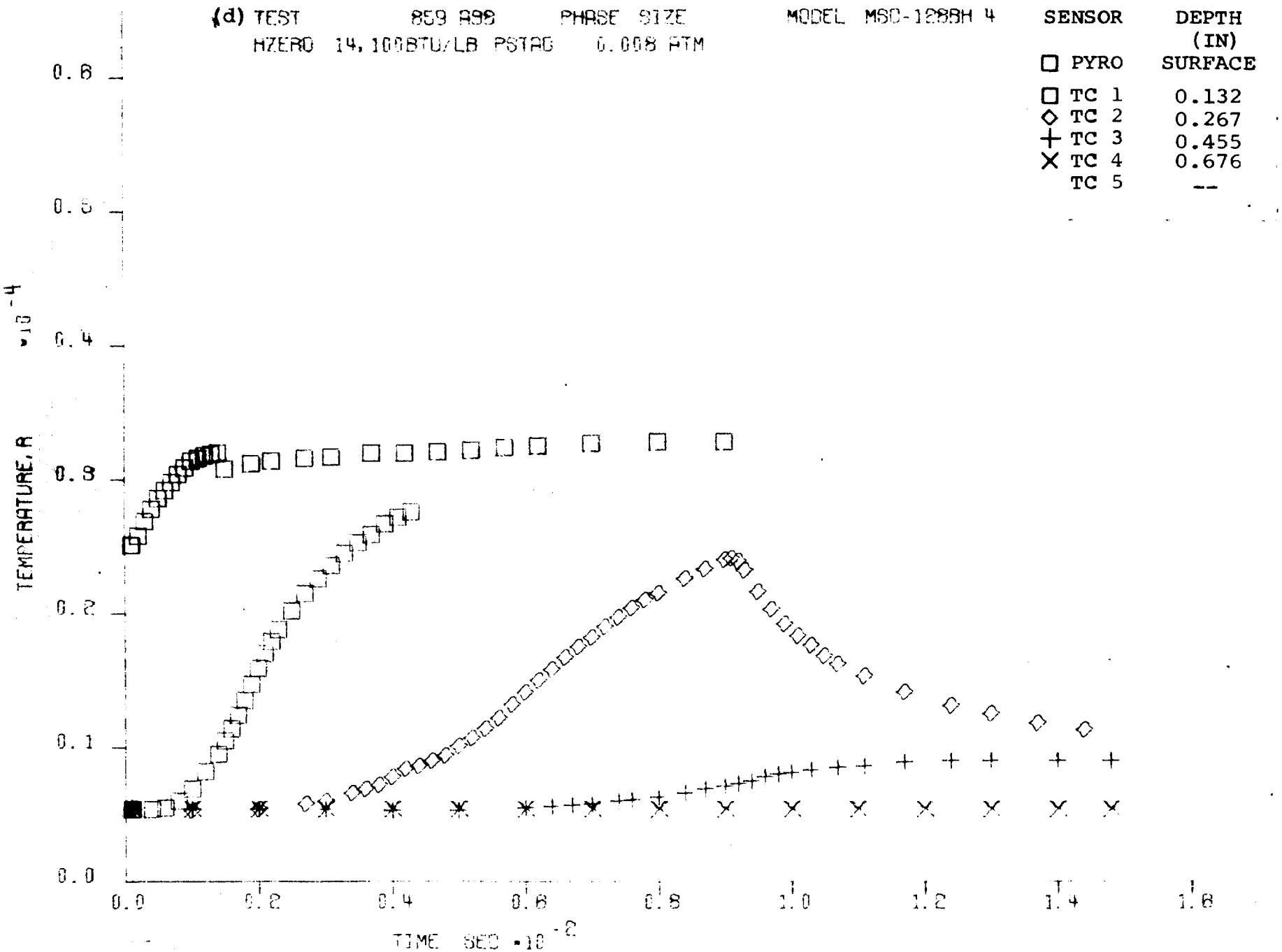

Figure 6-17. Continued.

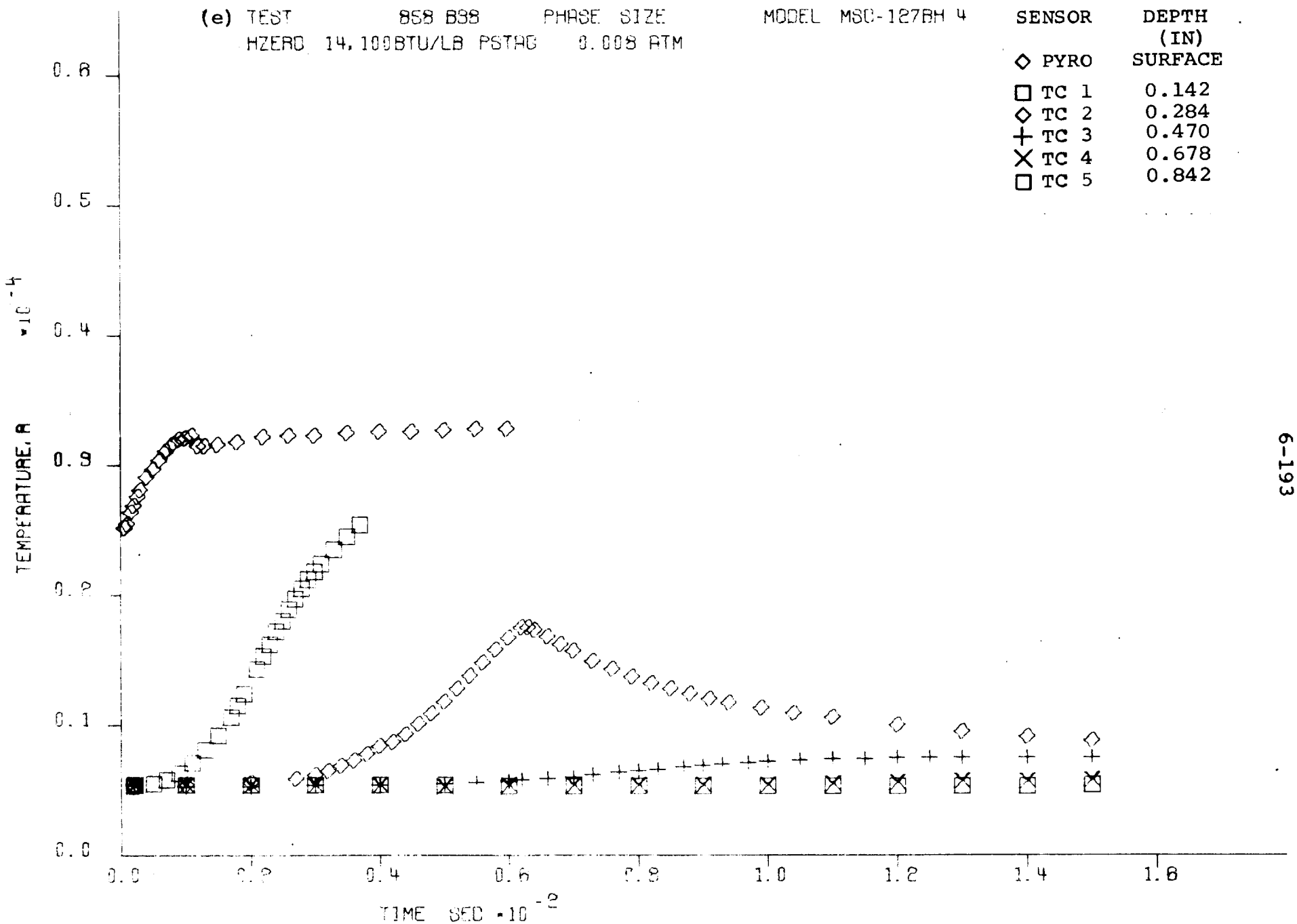

Figure 6-17. Continued.

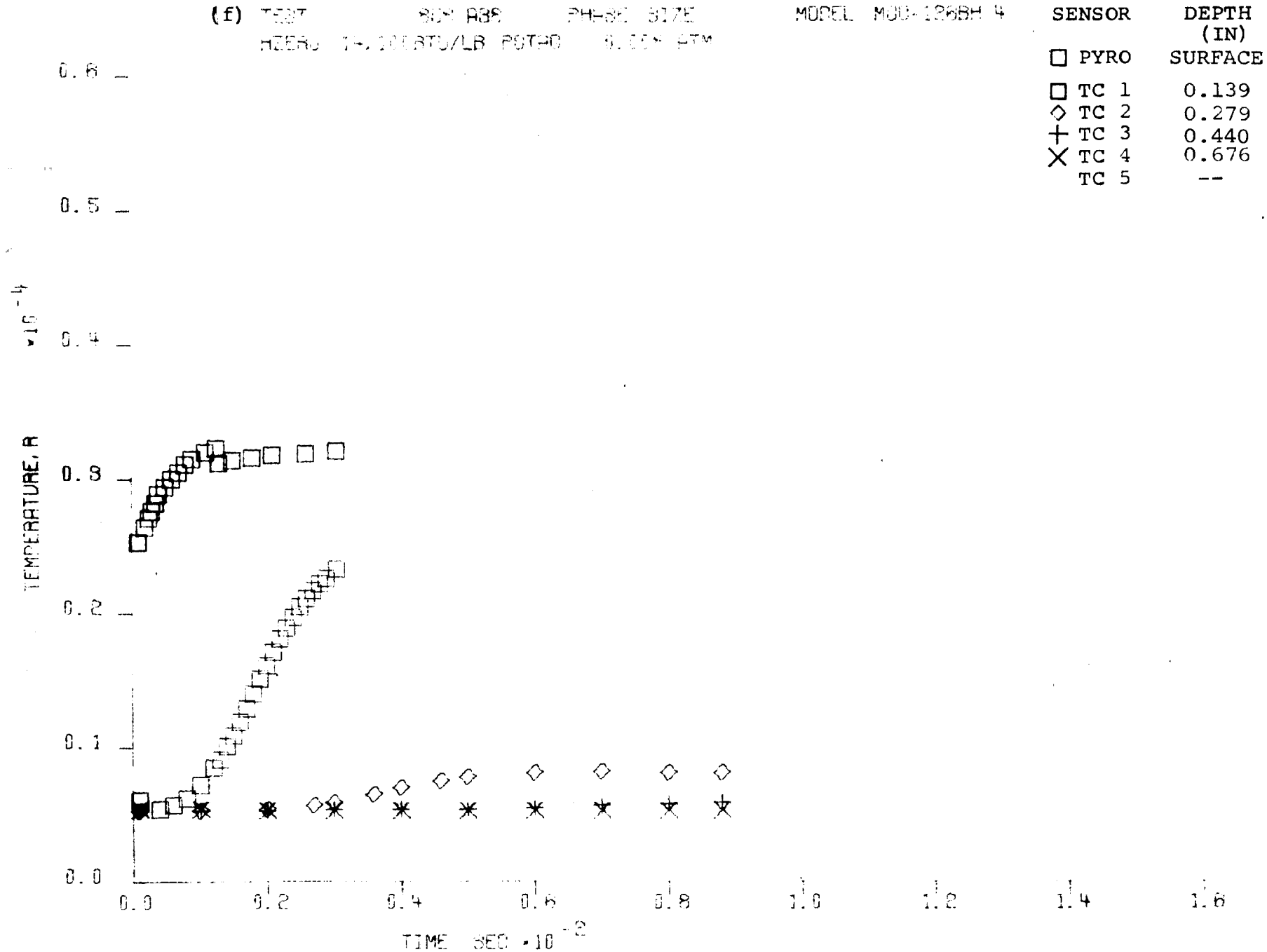

Figure 6-17. Continued.

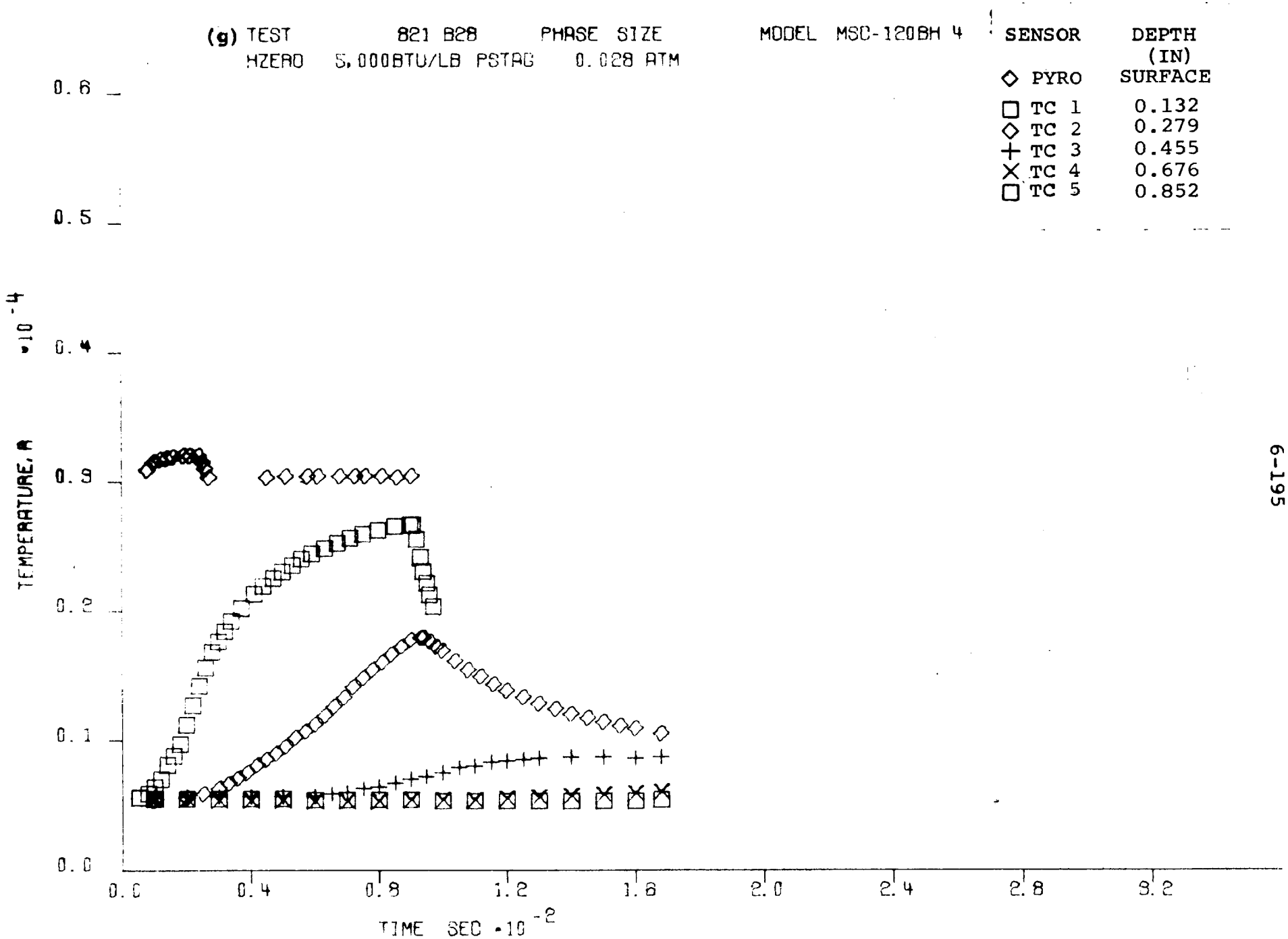

Figure 6-17. Continued.

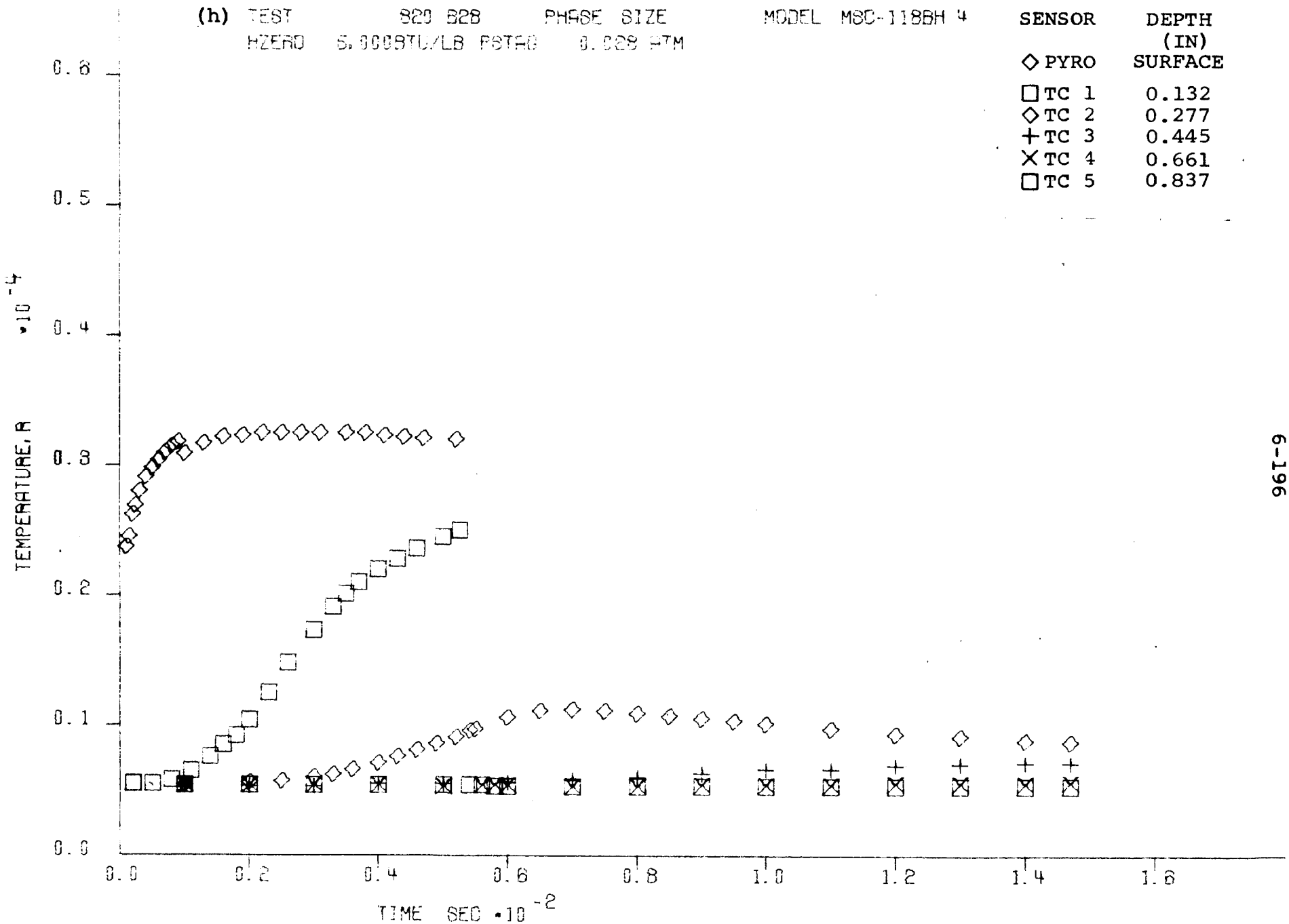

Figure 6-17. Continued.

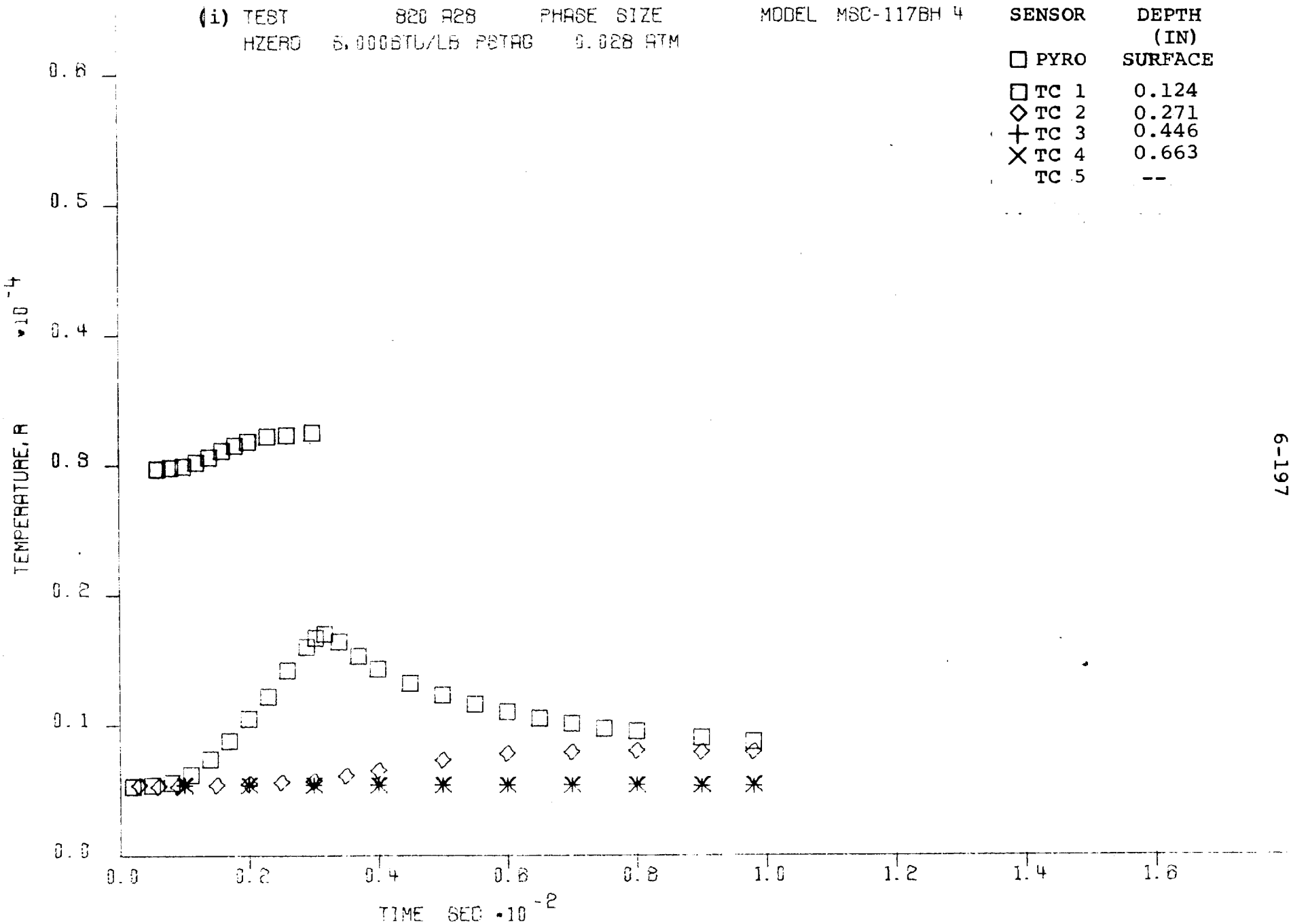

Figure 6-17. Continued.

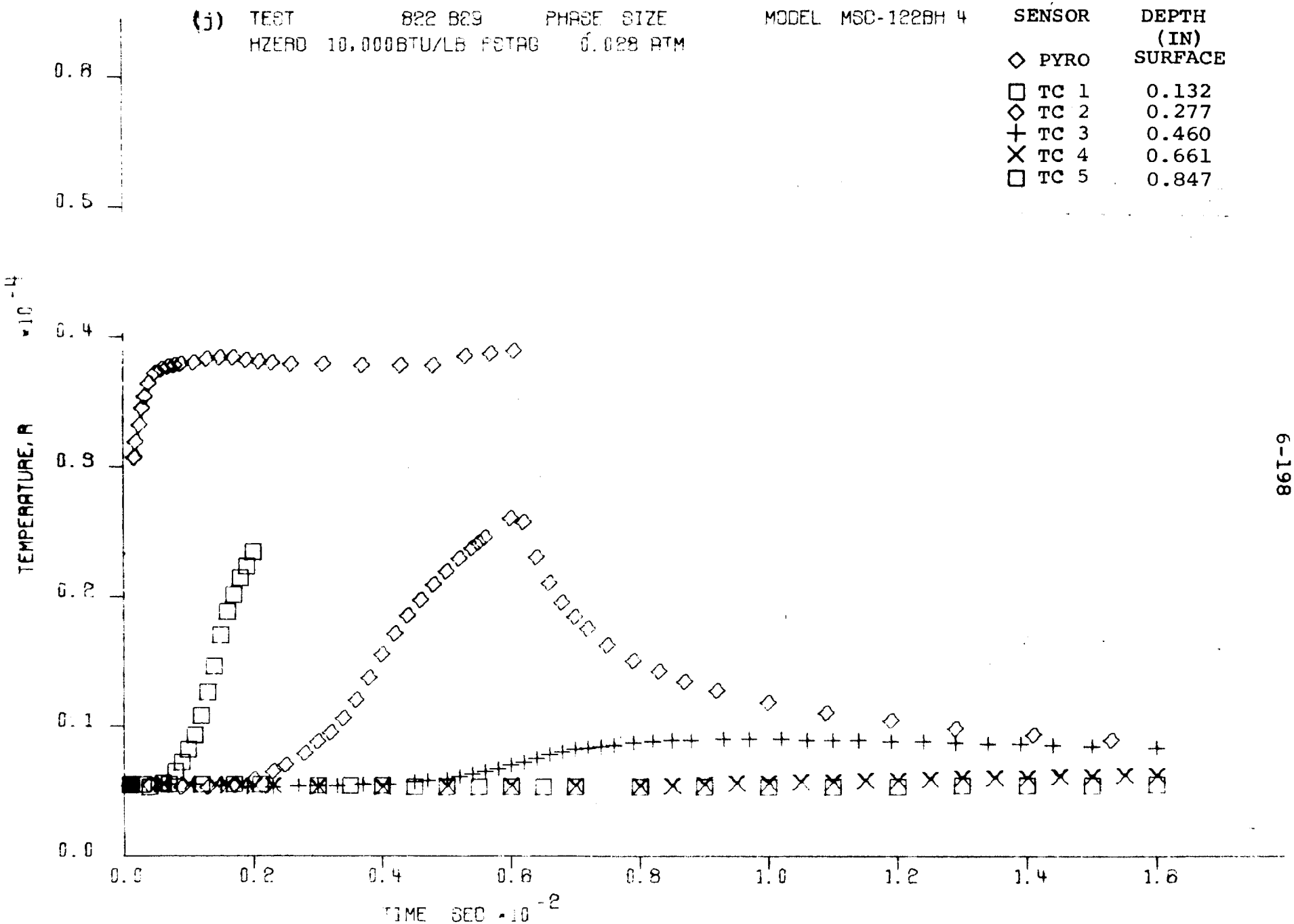

Figure 6-17. Continued.

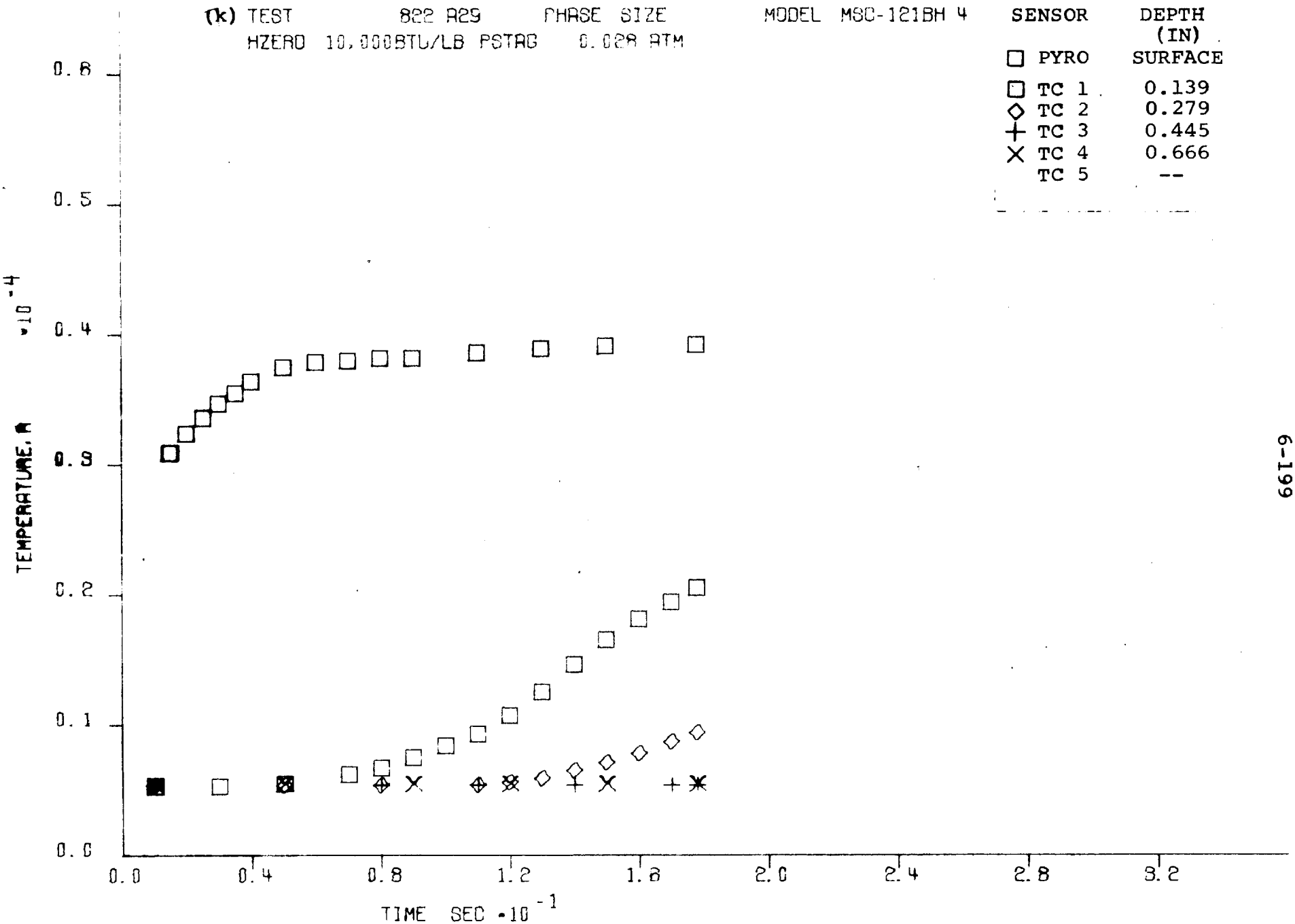

Figure 6-17. Continued.

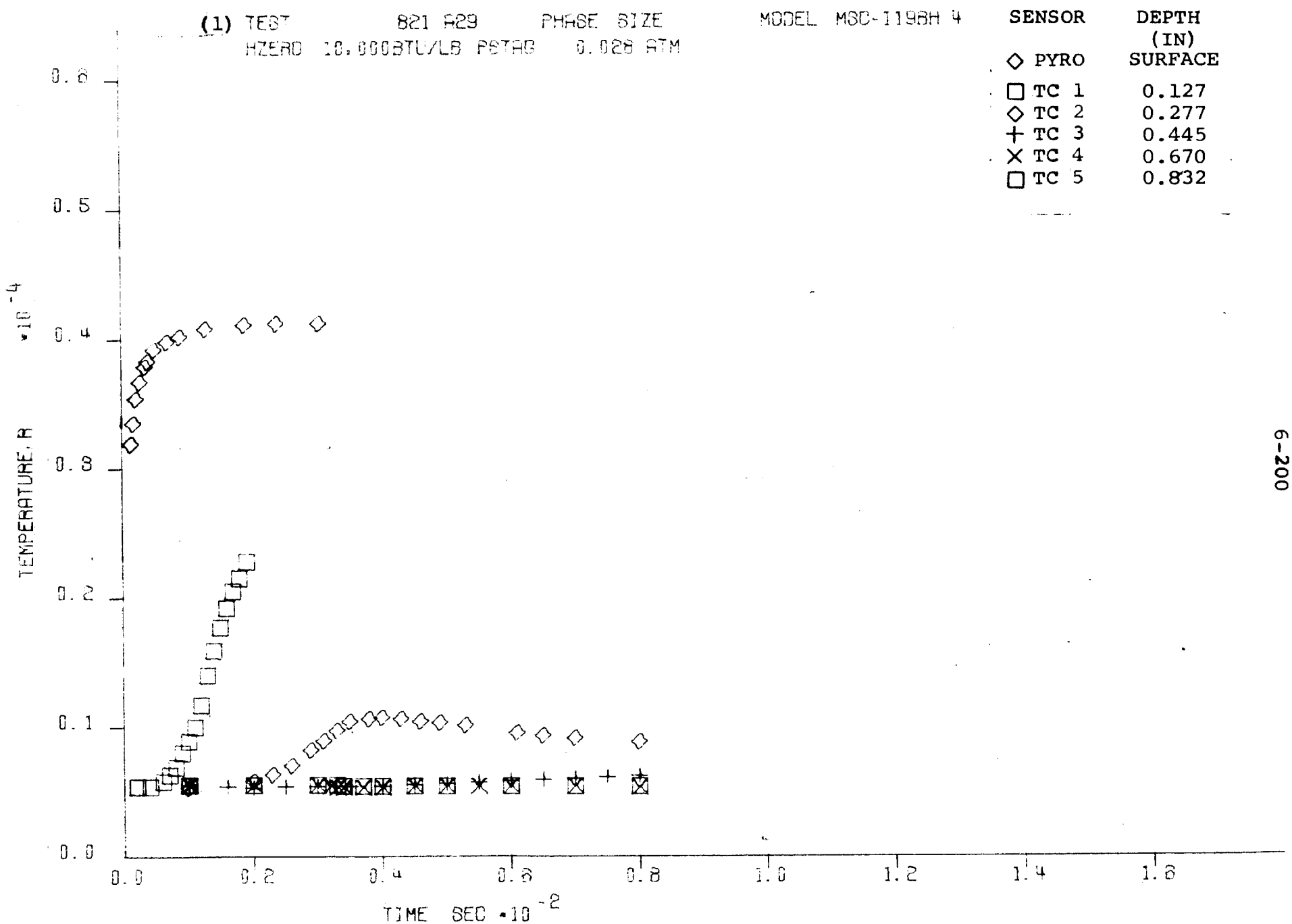

Figure 6-17. Continued.

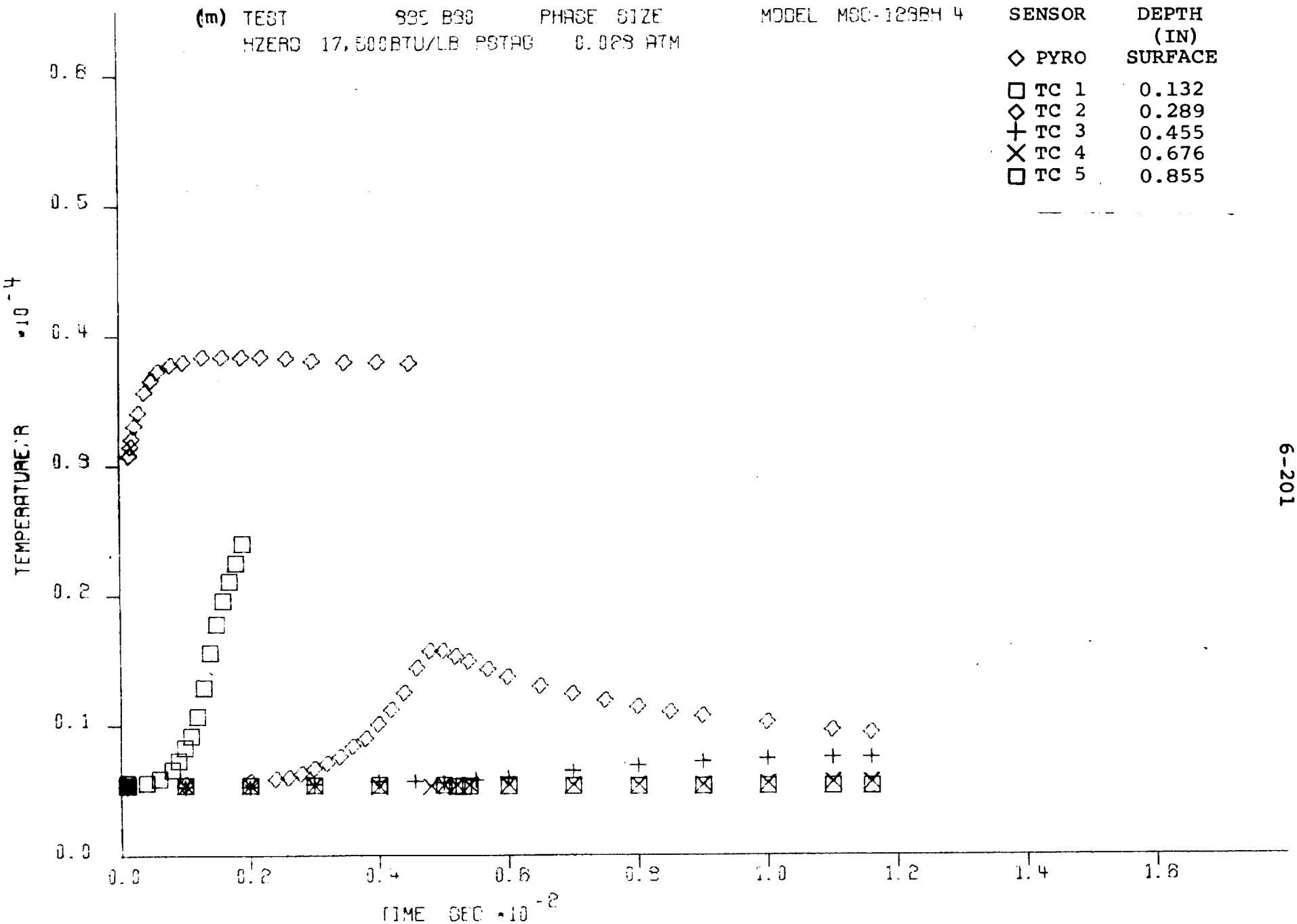

Figure 6-17. Continued.

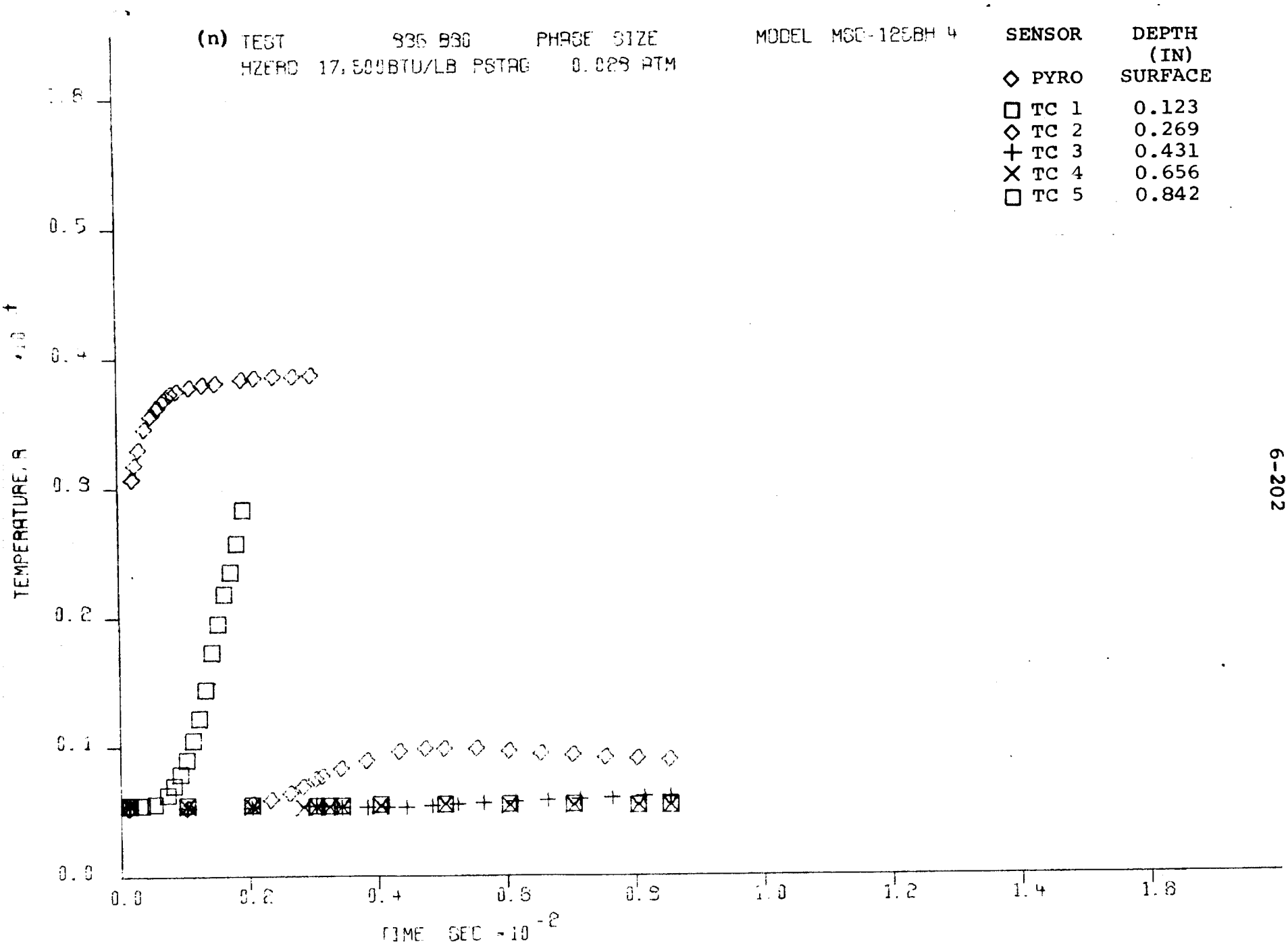

Figure 6-17. Continued

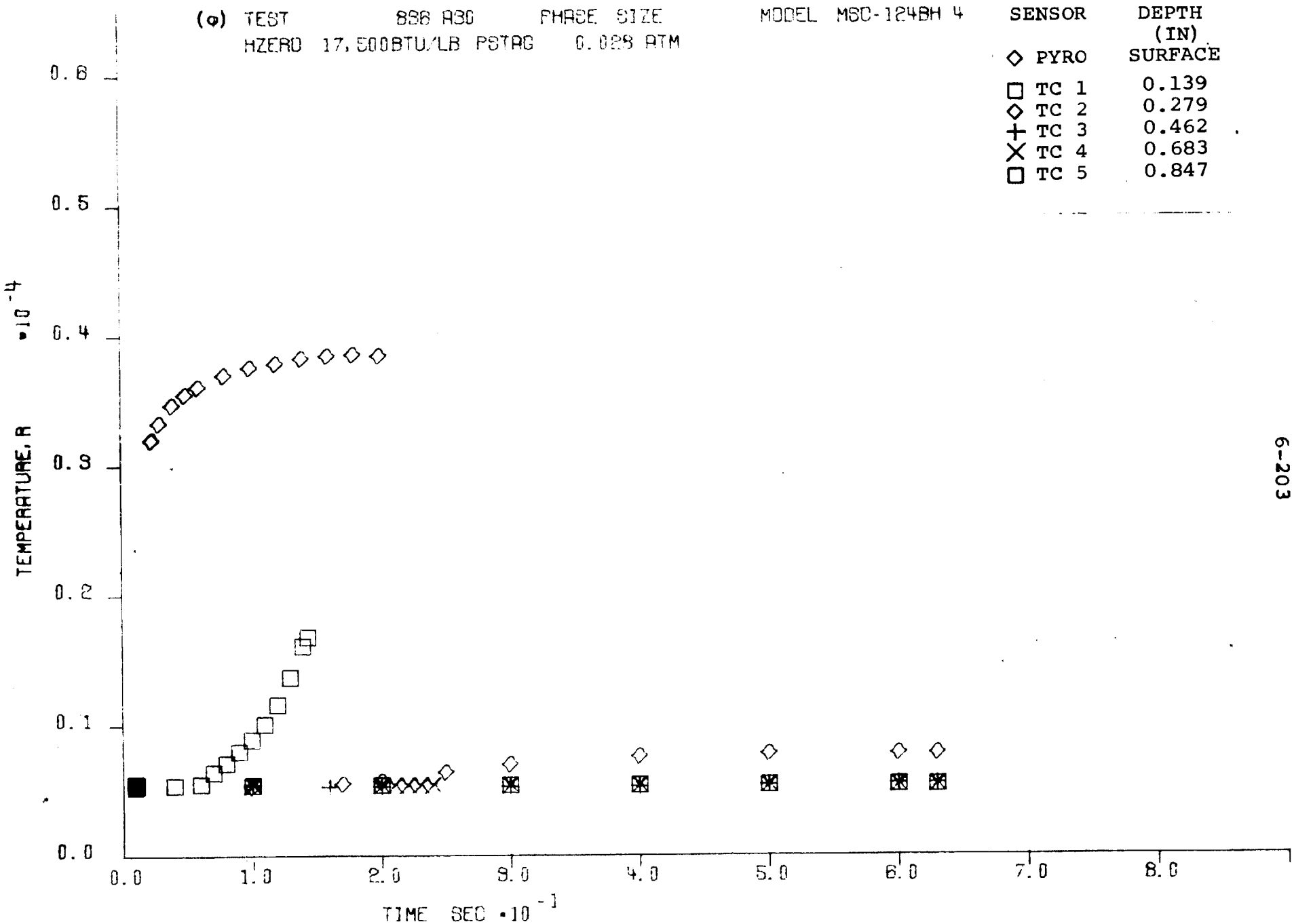

Figure 6-17. Concluded.

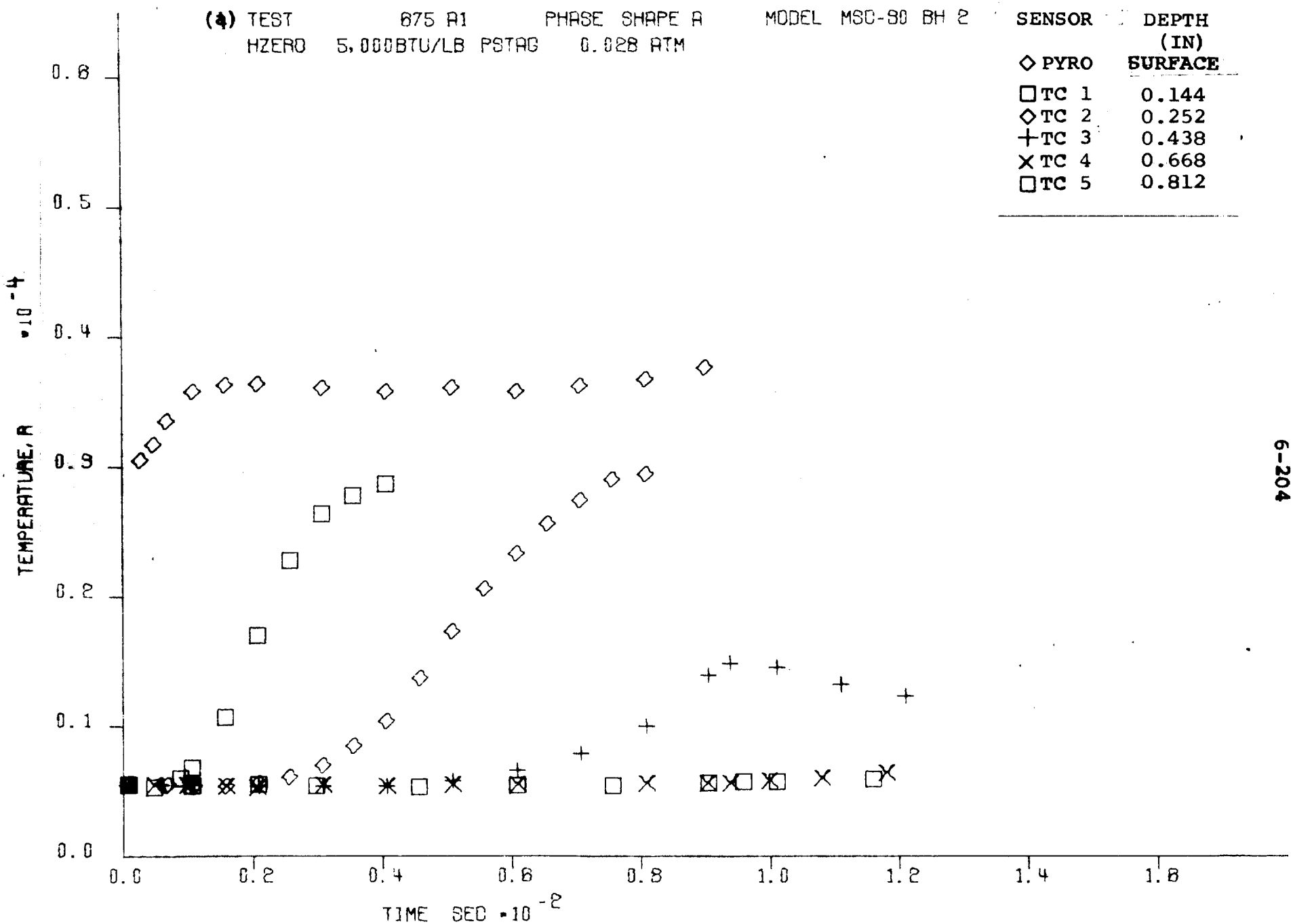

Figure 6-18. Surface and Internal Temperature Histories, Phase VI A.

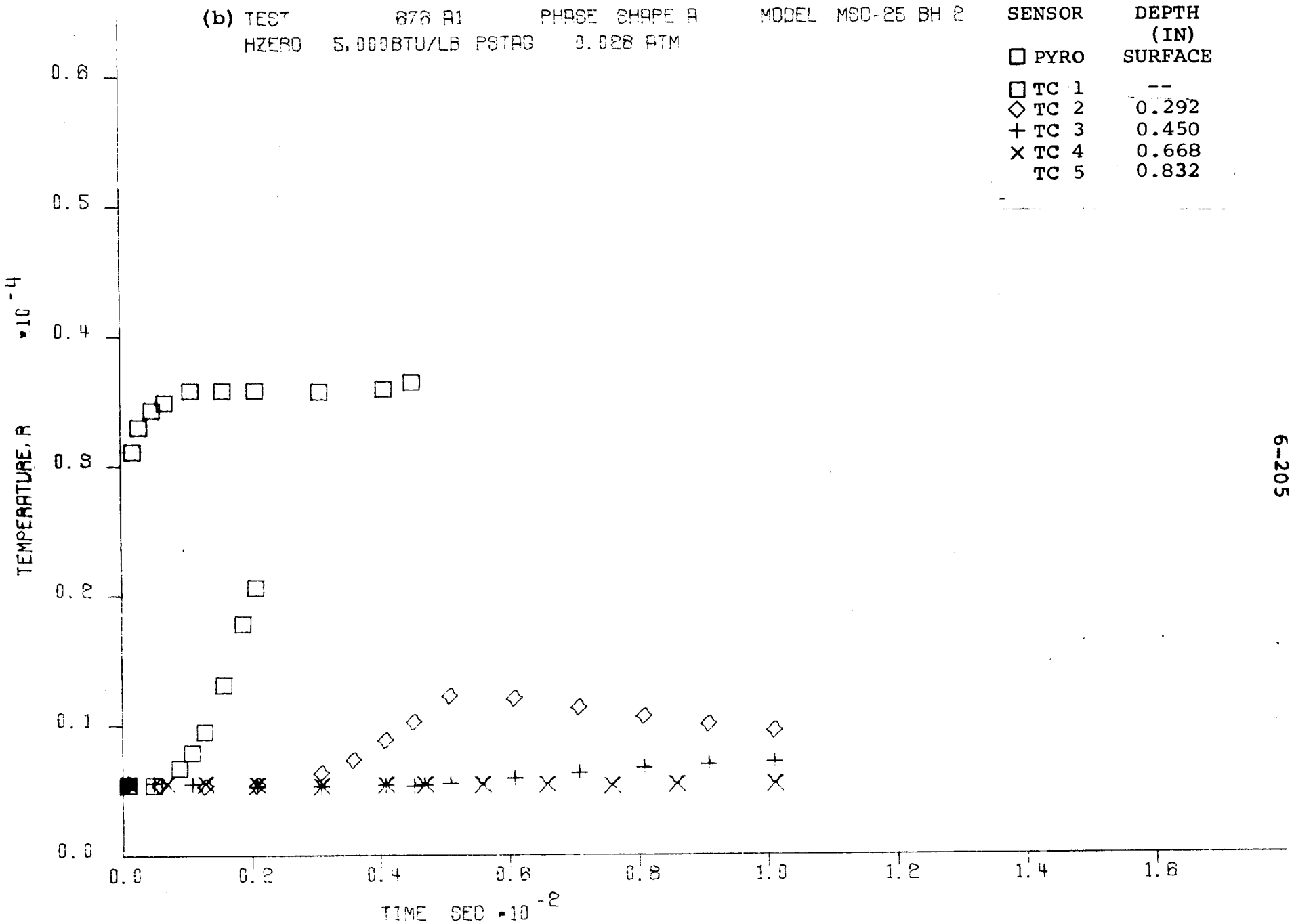

Figure 6-18. Continued.

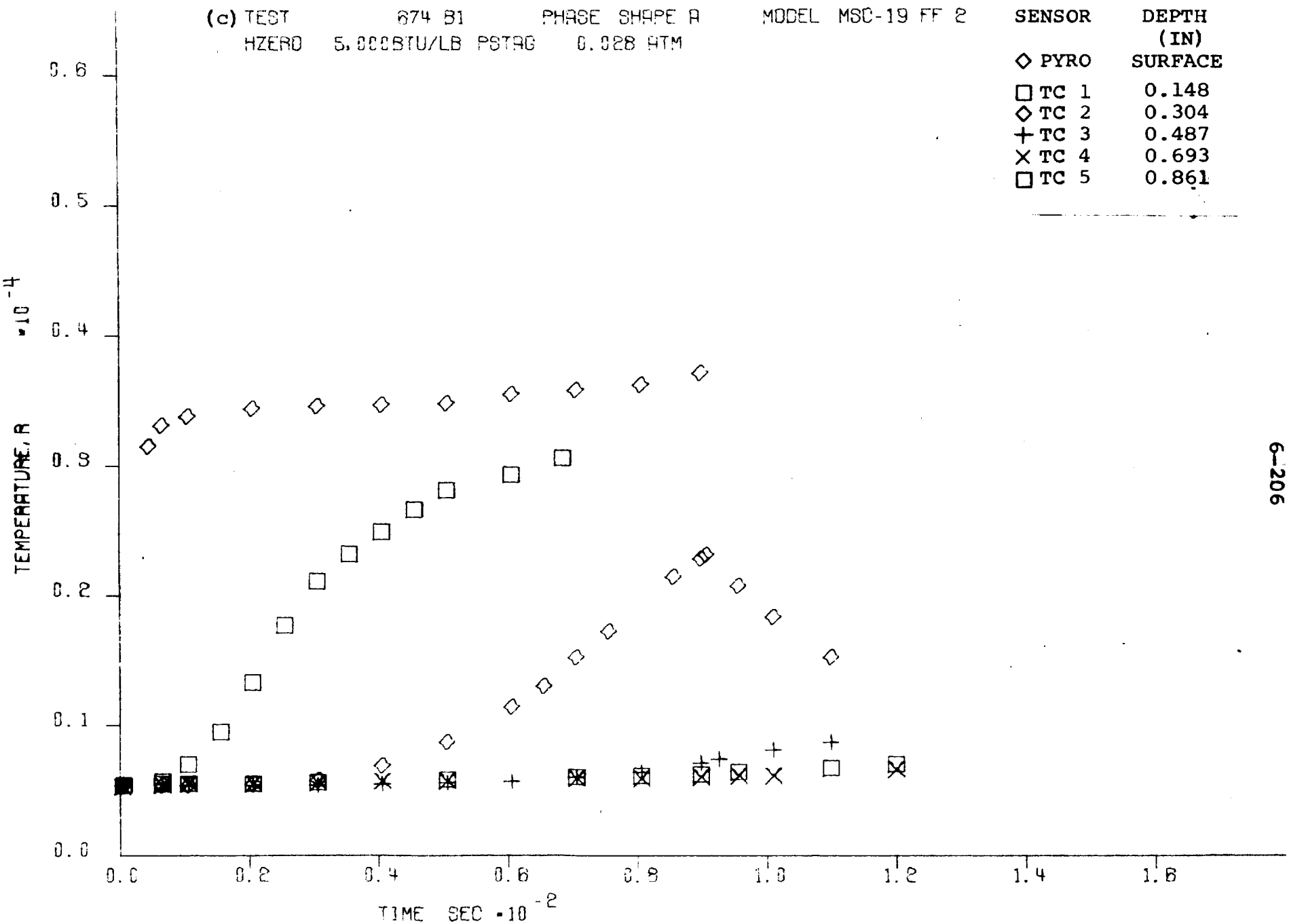

Figure 6-18. Continued.

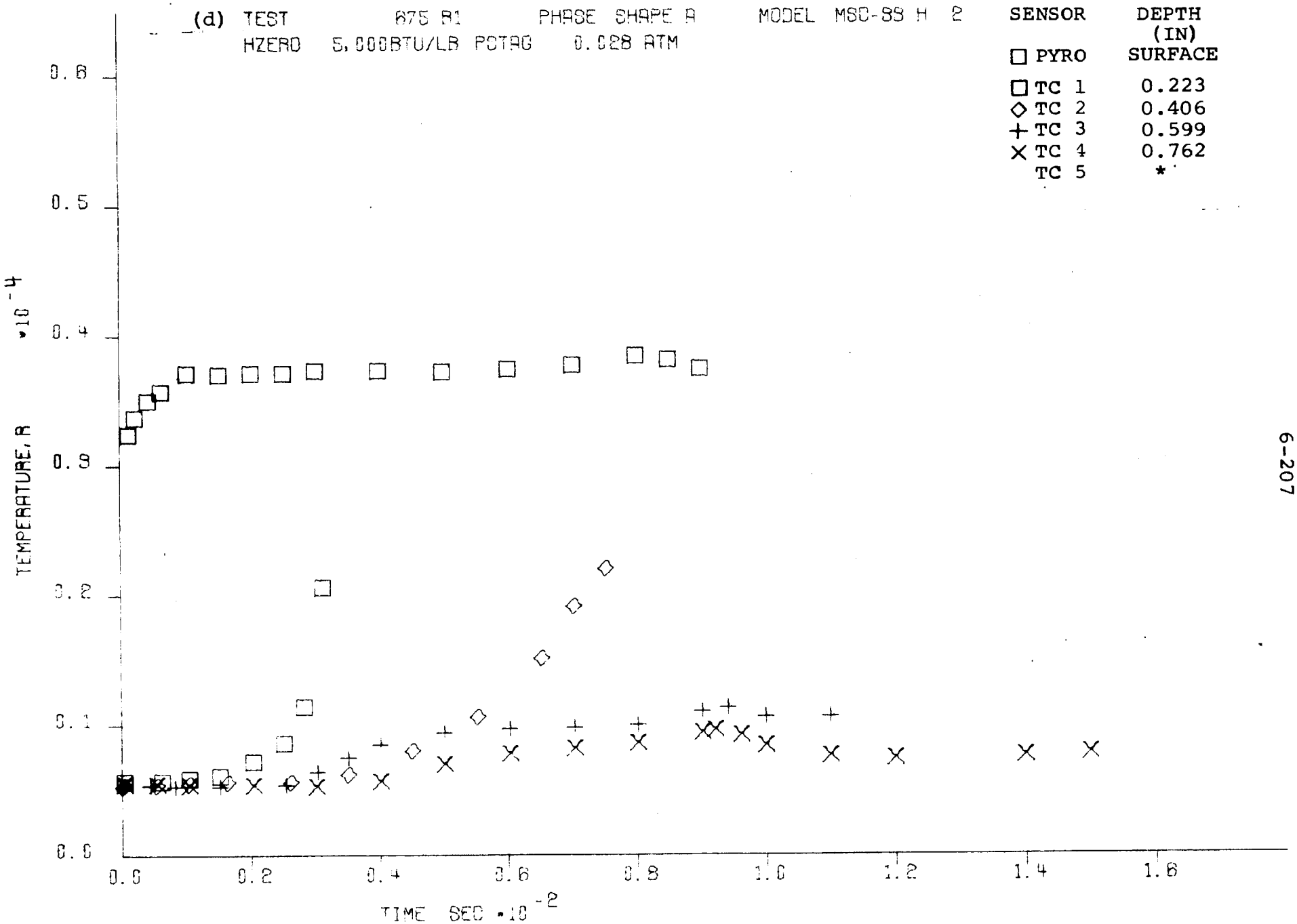

Figure 6-18. Continued.

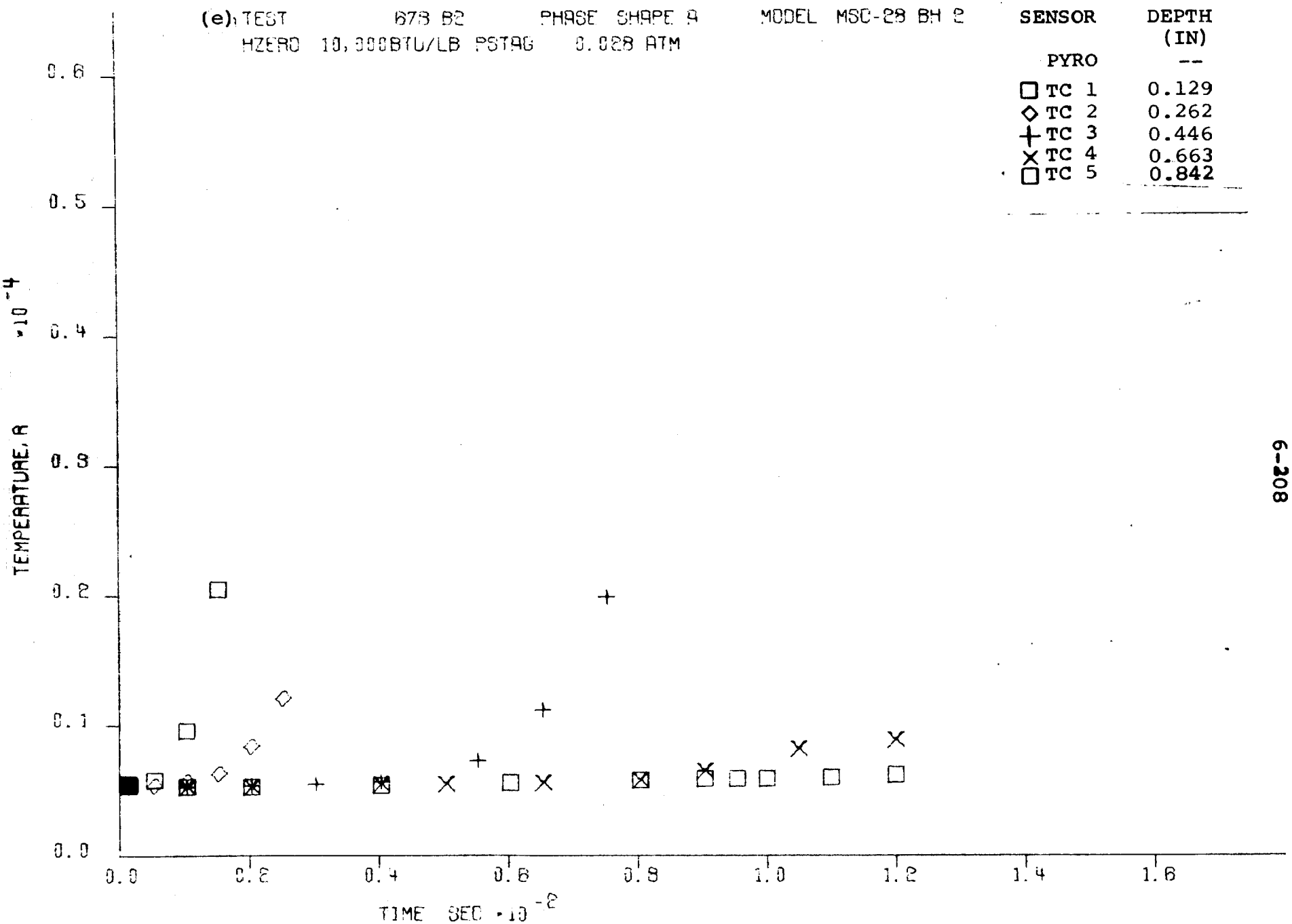

Figure 6-18. Continued.

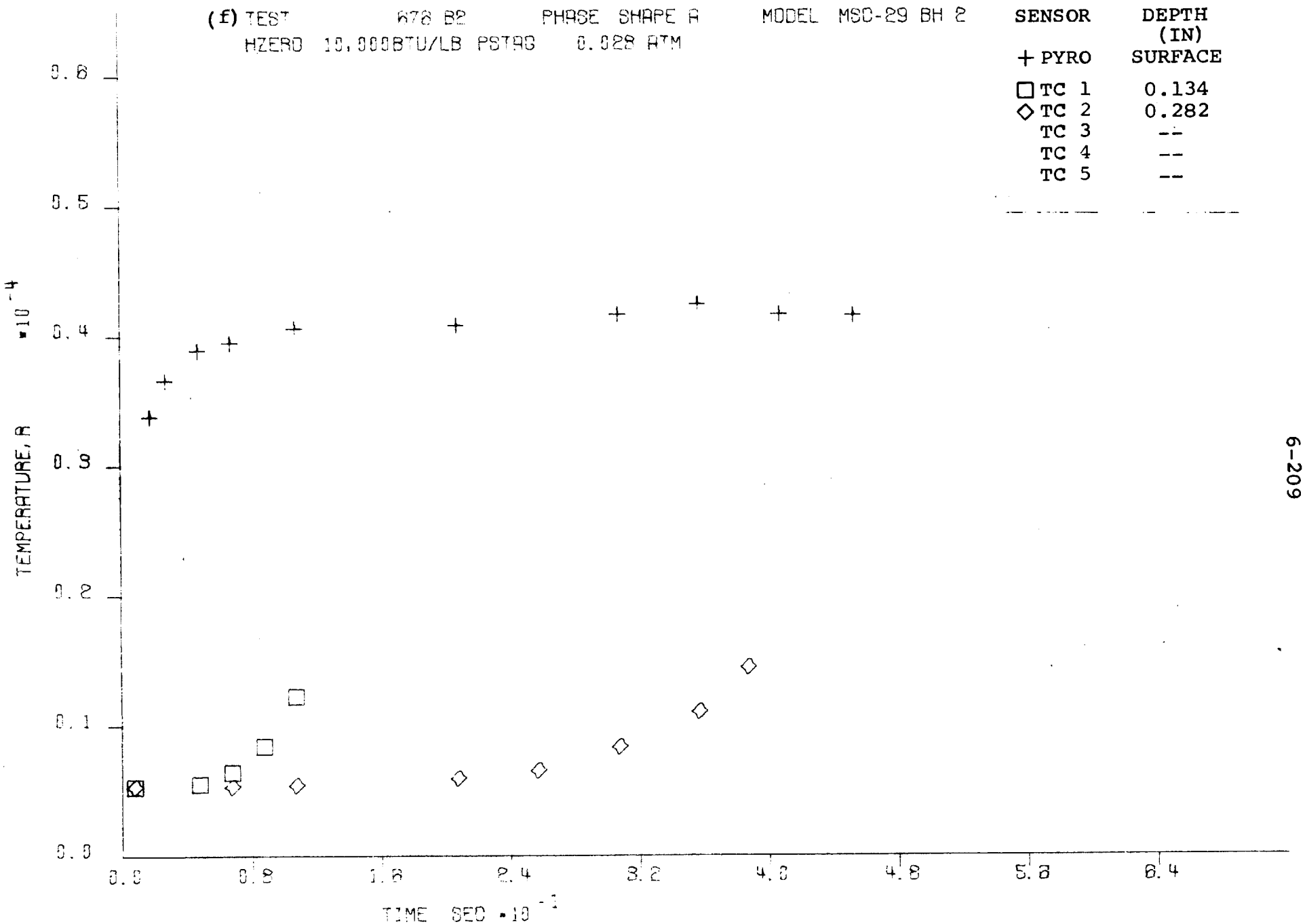

Figure 6-18. Continued.

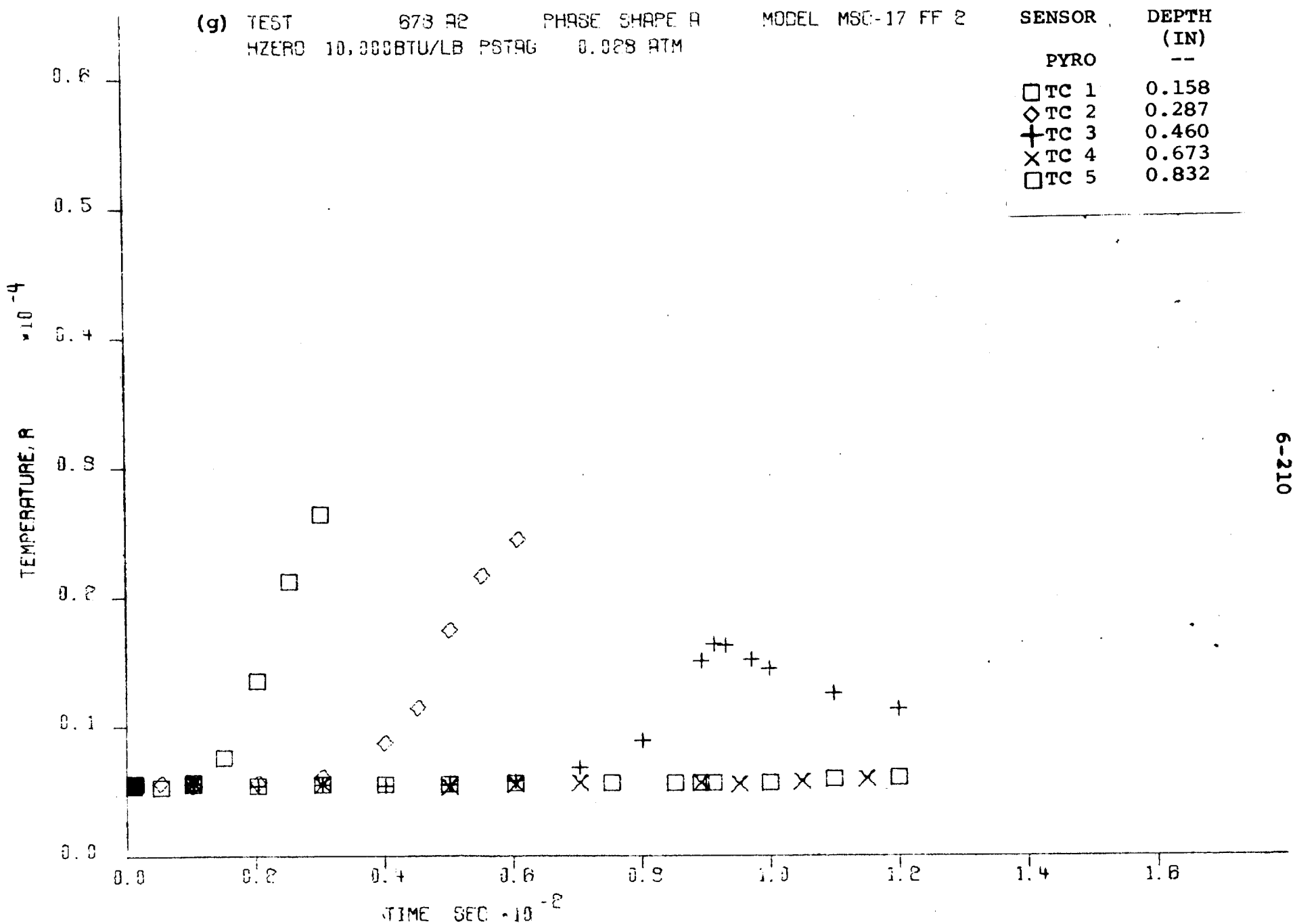

Figure 6-18. Continued.

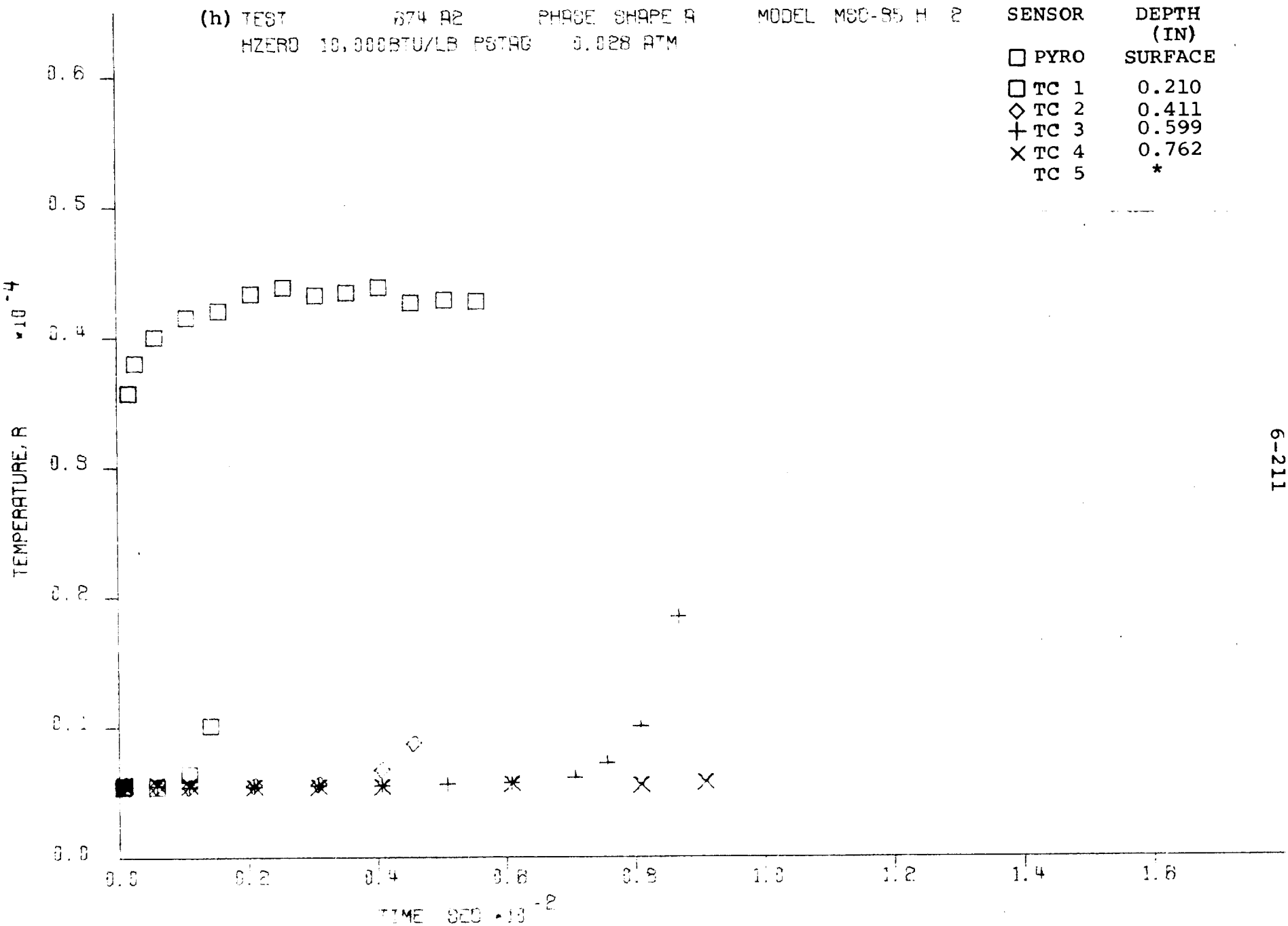

Figure 6-18. Continued.

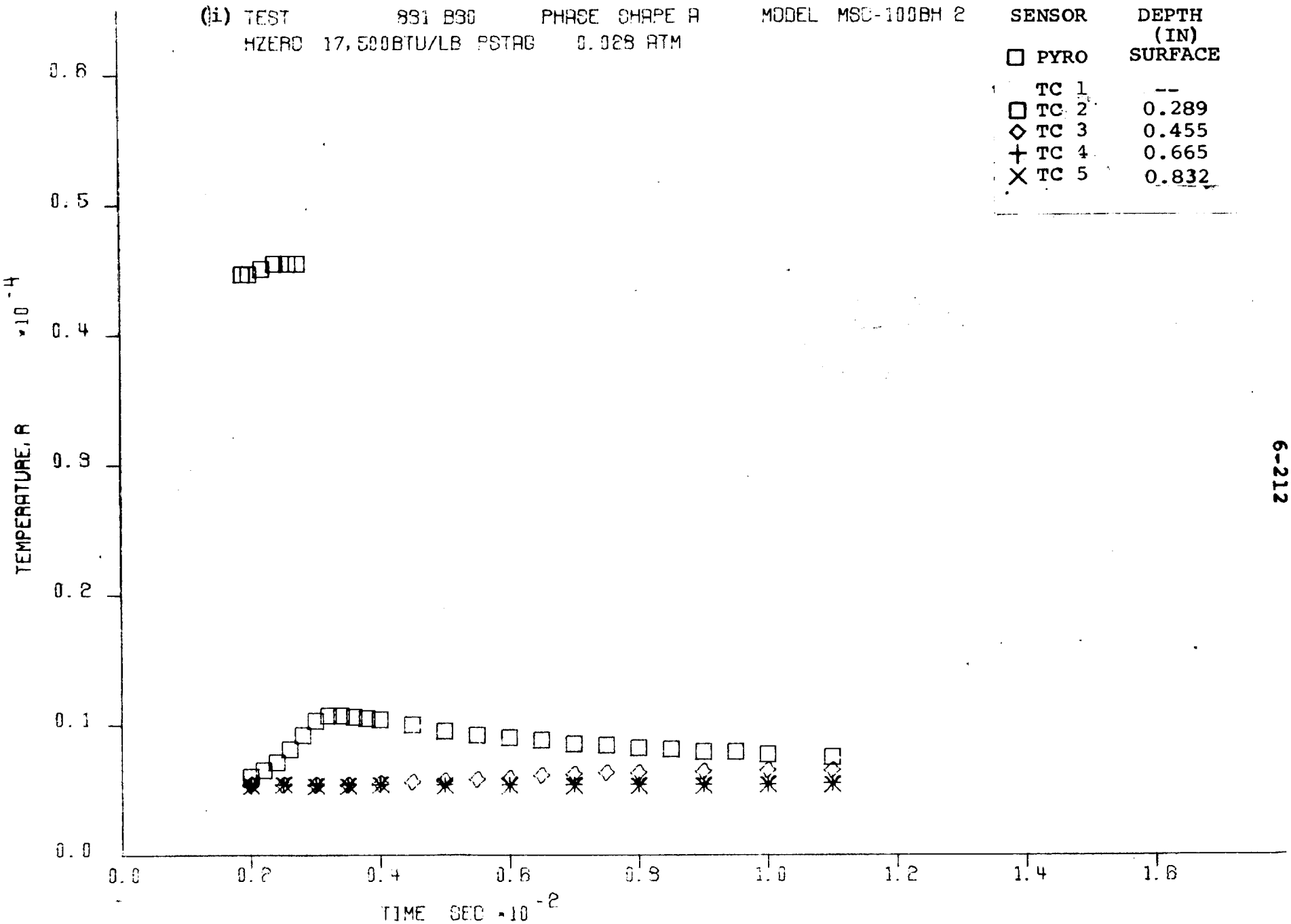

Figure 6-18. Continued.

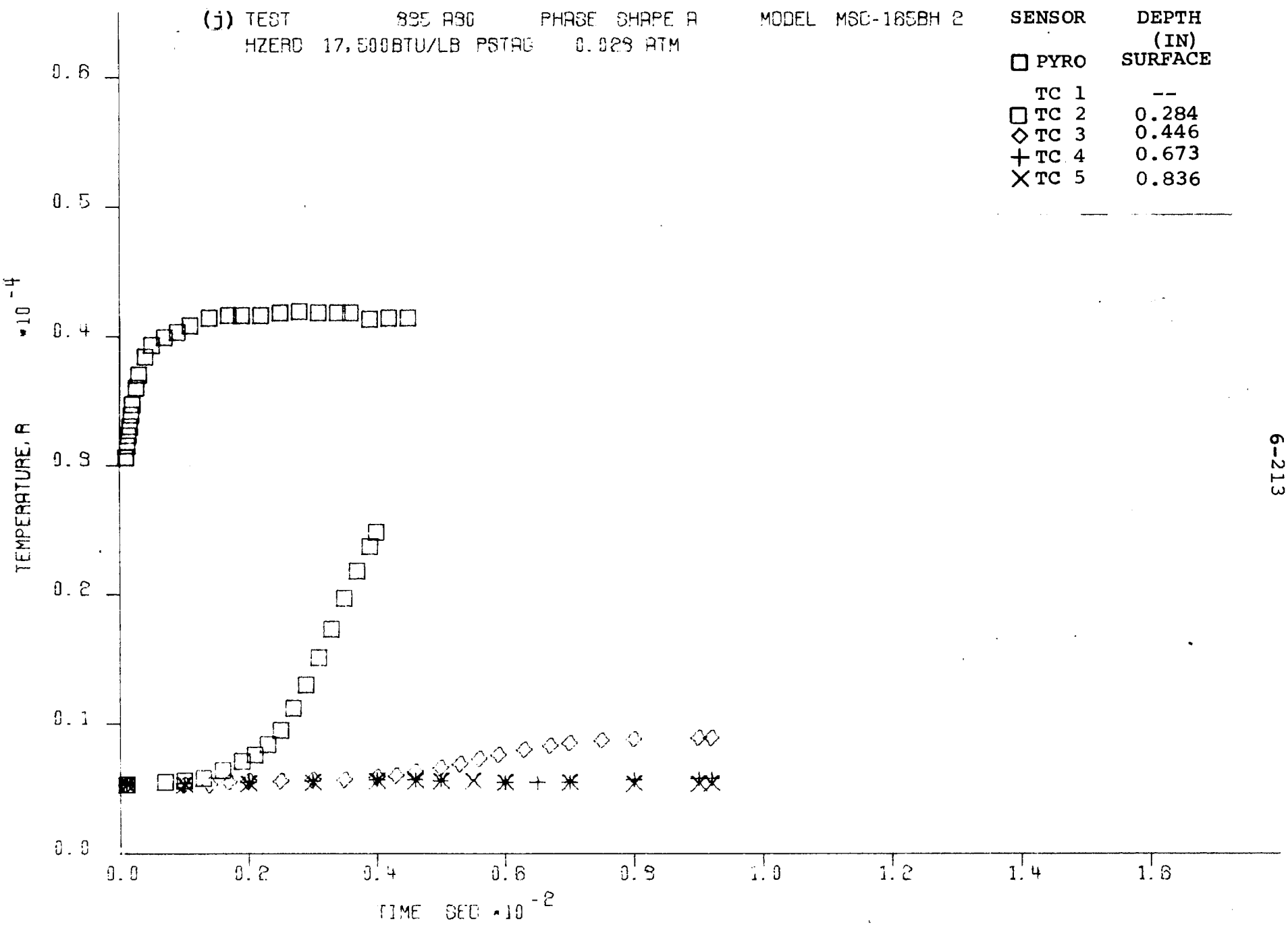

Figure 6-18. Continued.

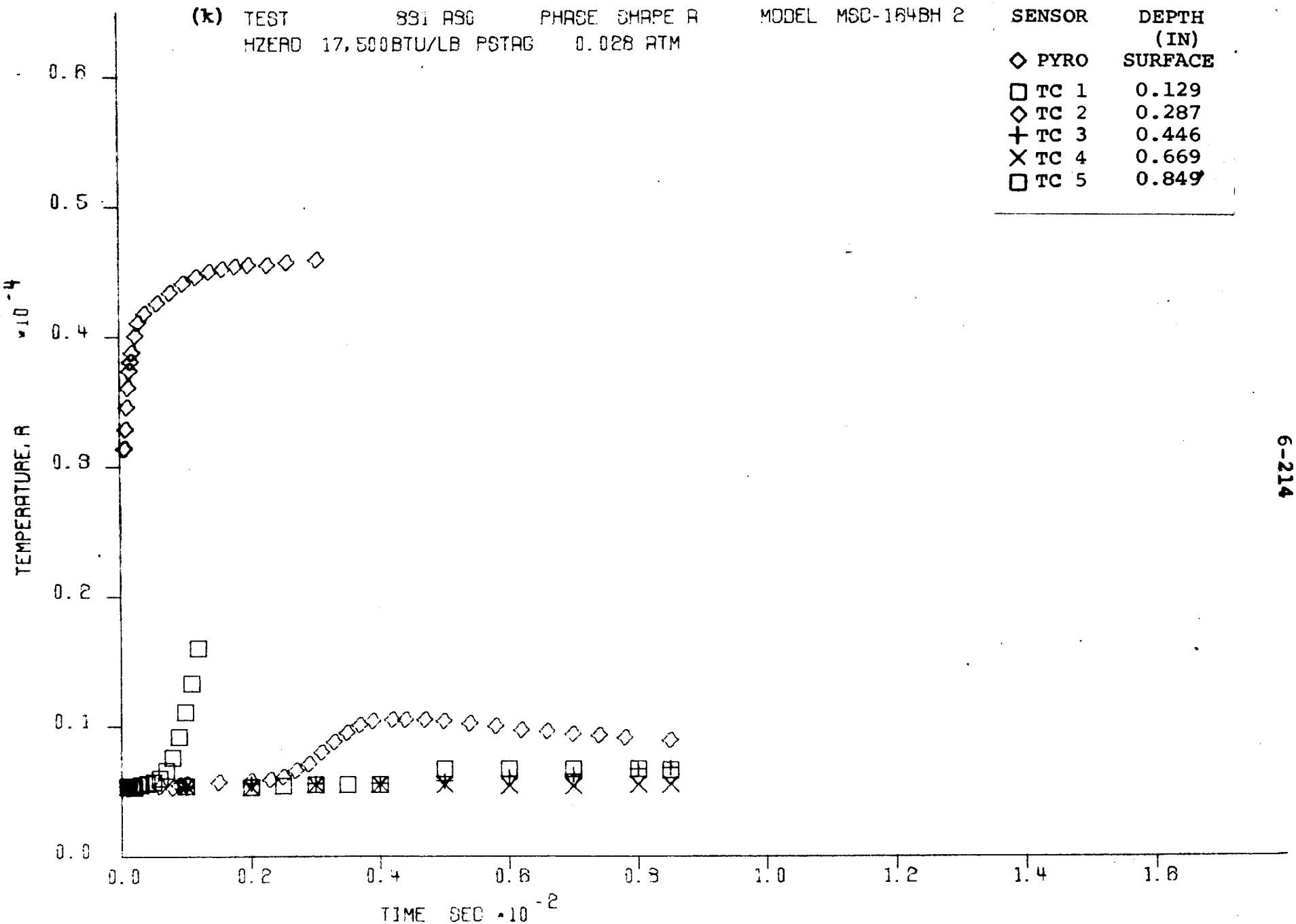

Figure 6-18. Continued.

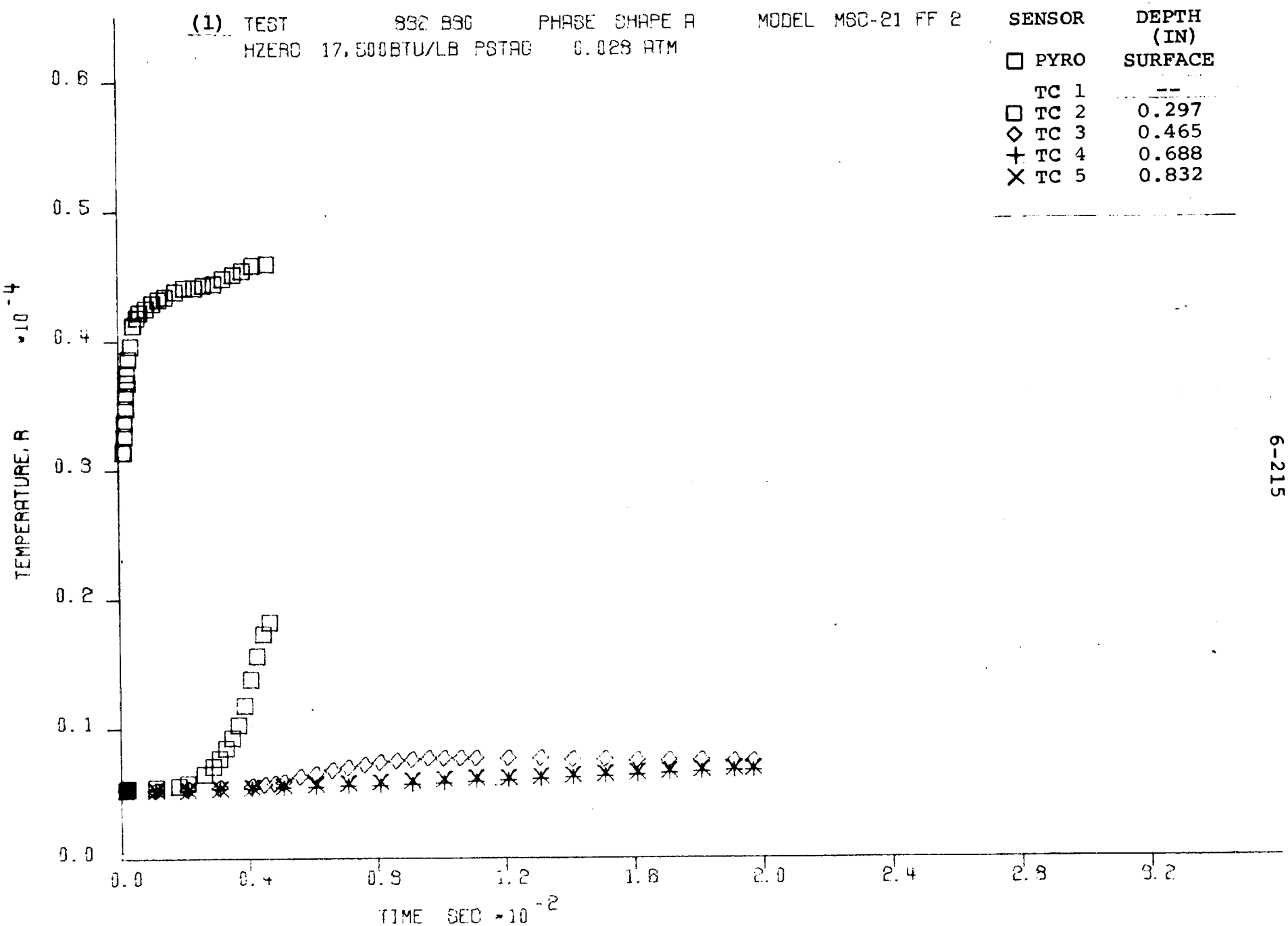

Figure 6-18. Continued.

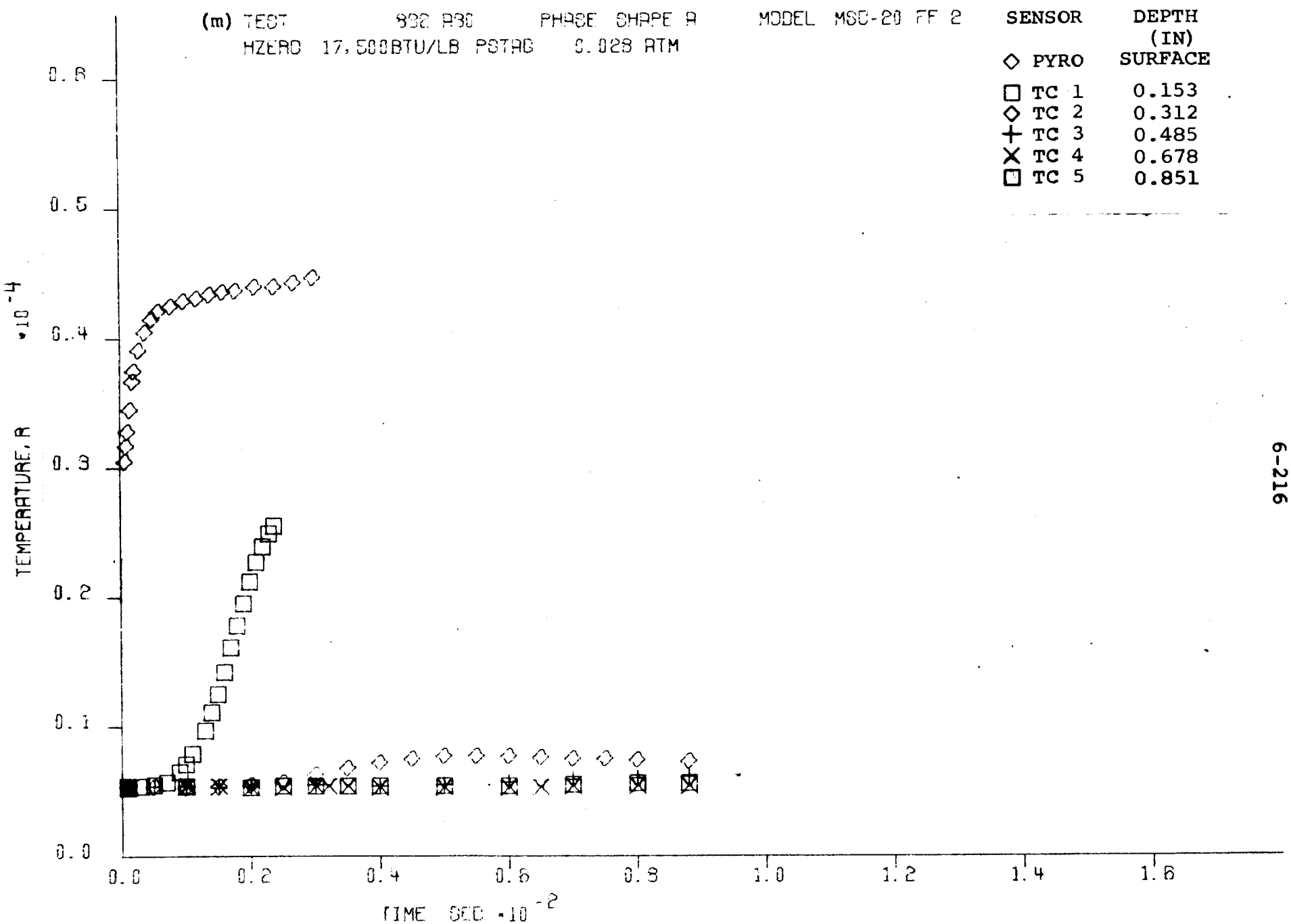

Figure 6-18. Continued.

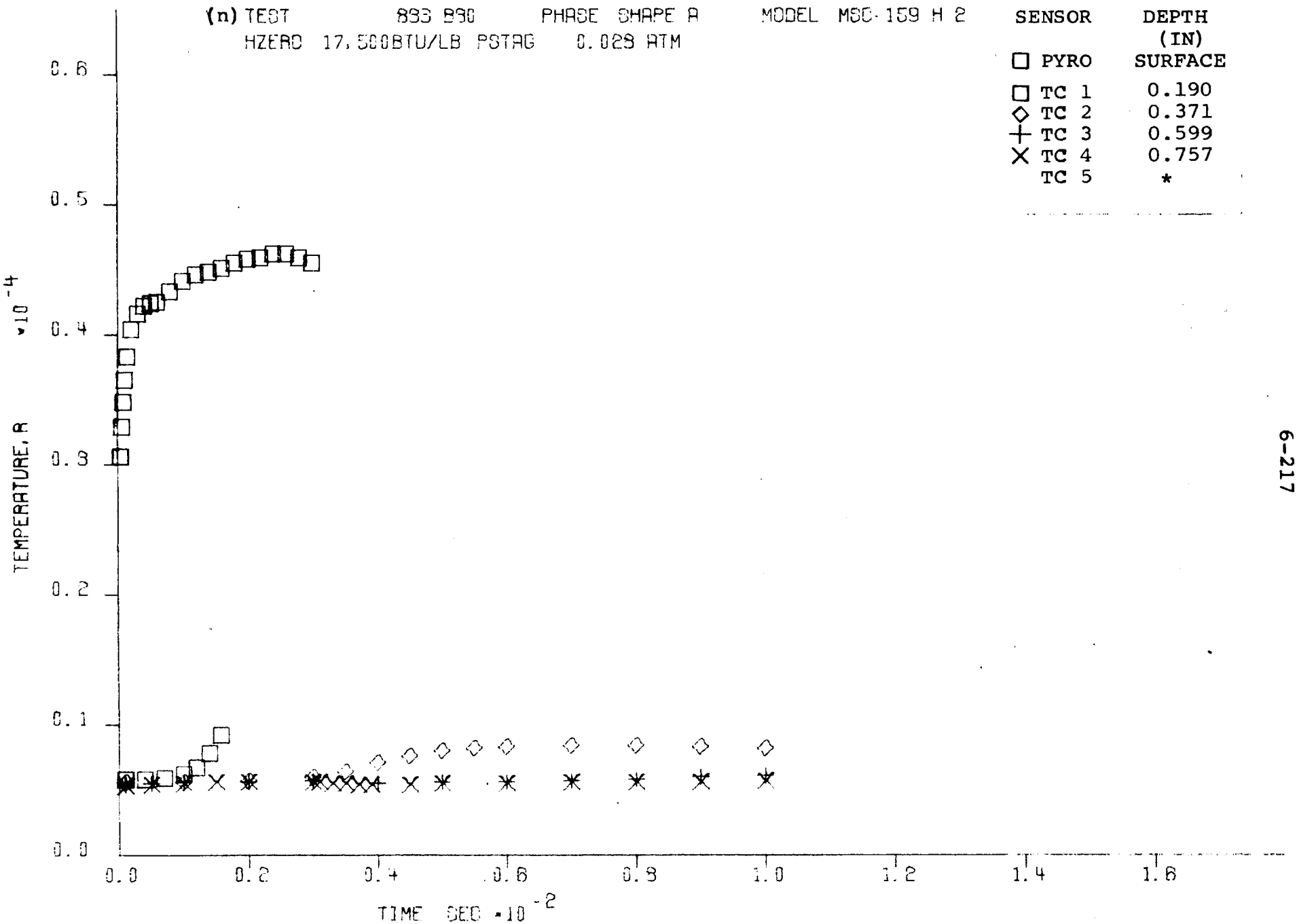

Figure 6-18. Concluded.

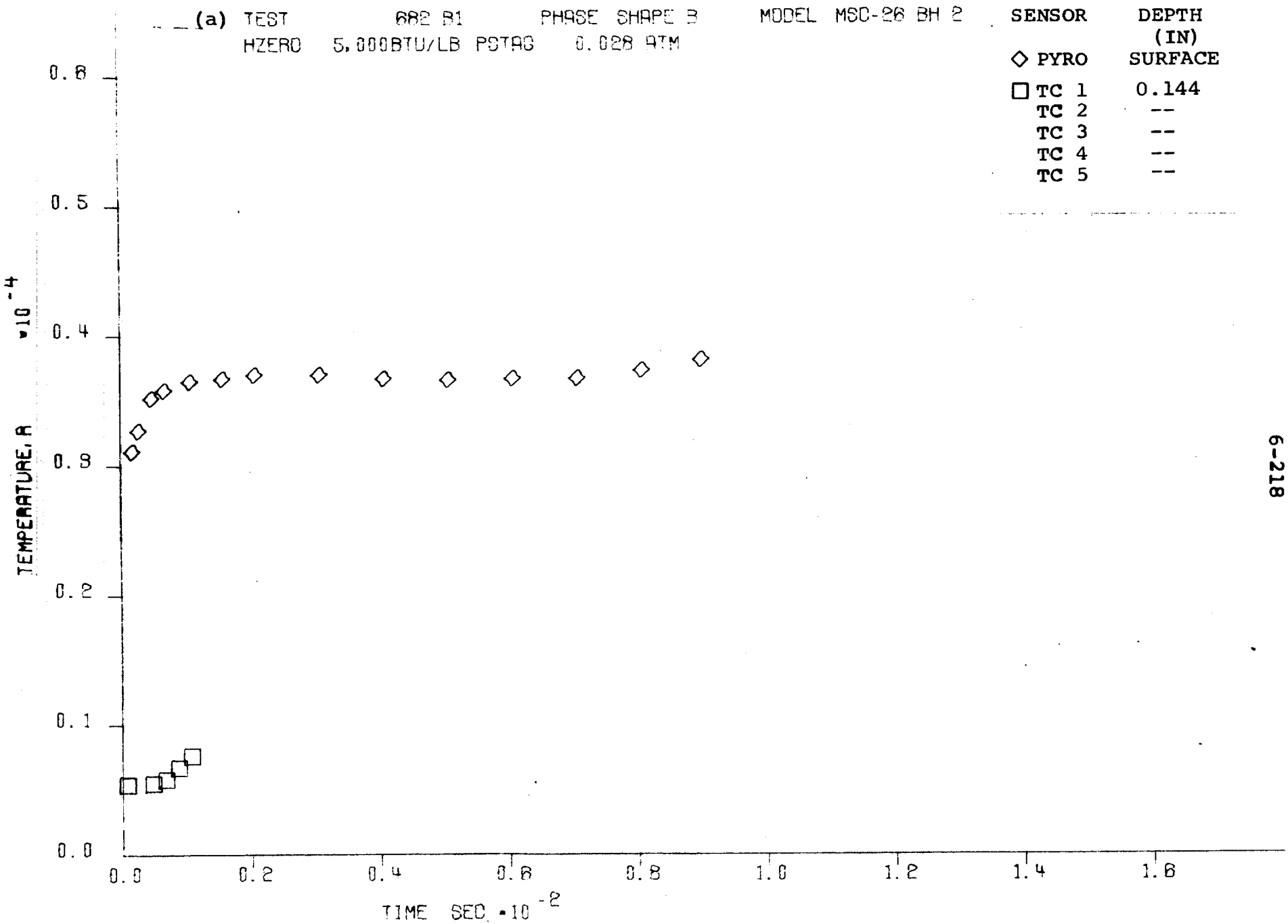

Figure 6-19. Surface and Internal Temperature Histories, Phase VI B.

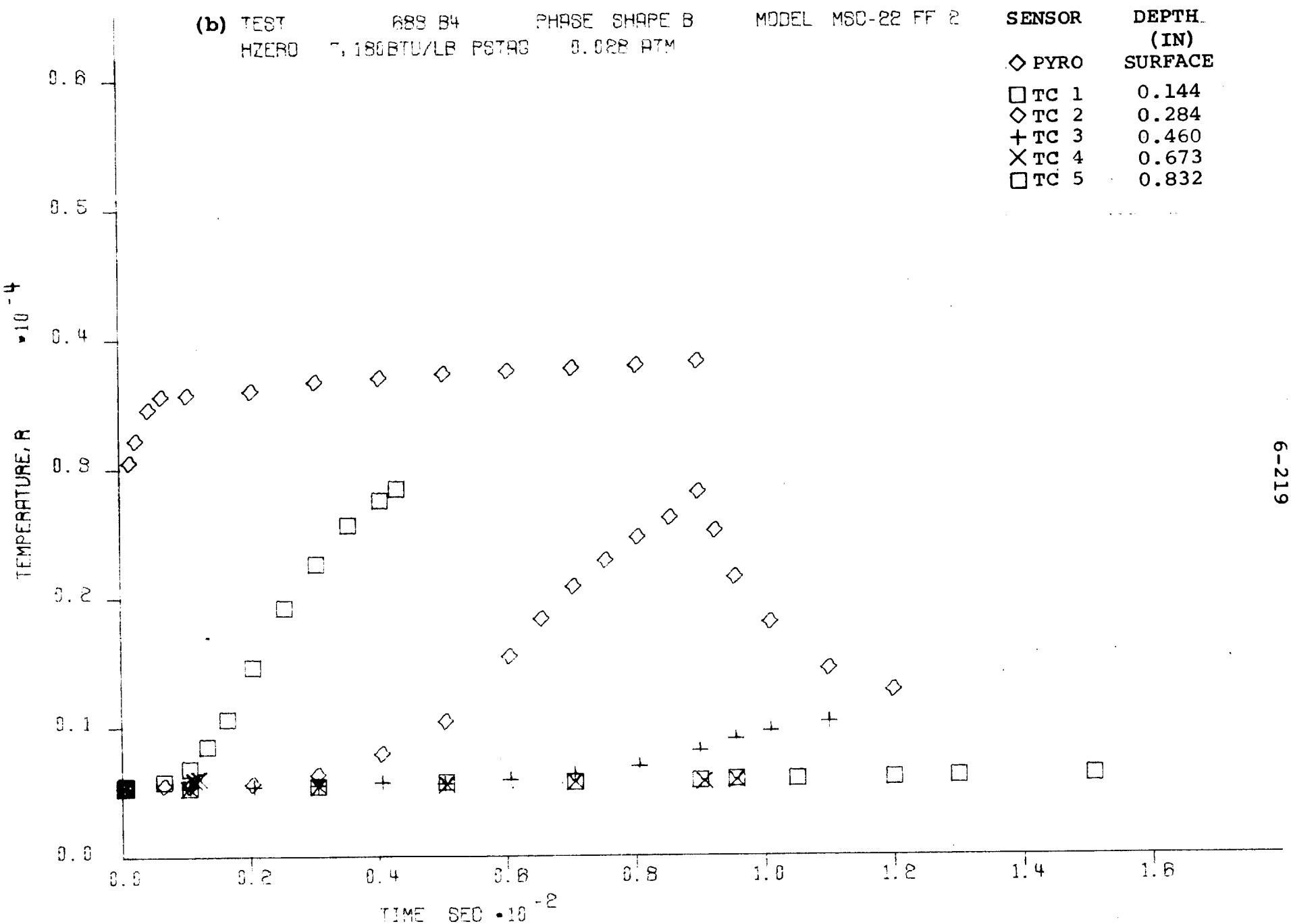

Figure 6-19. Continued.

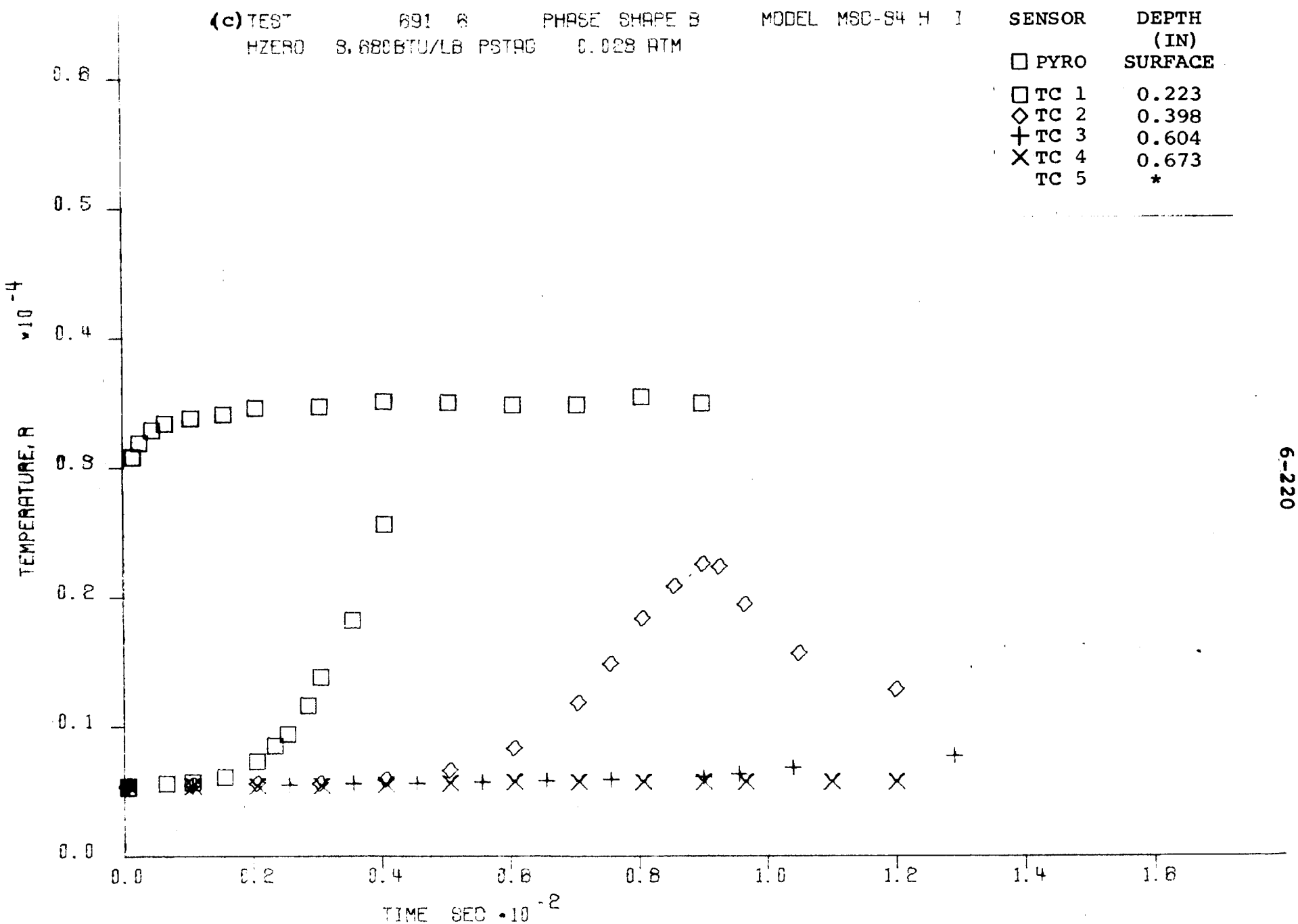

Figure 6-19. Continued.

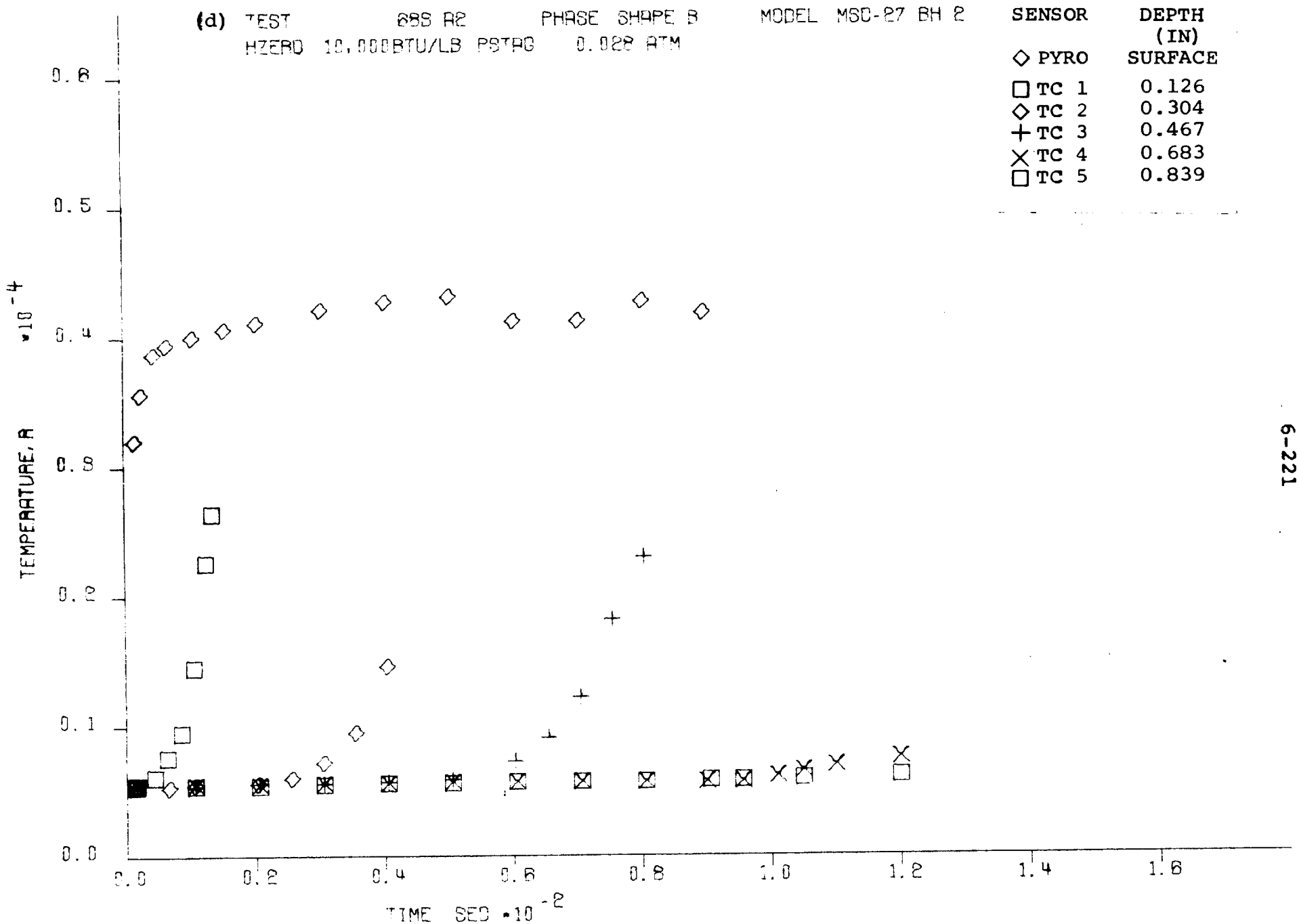

Figure 6-19. Continued.

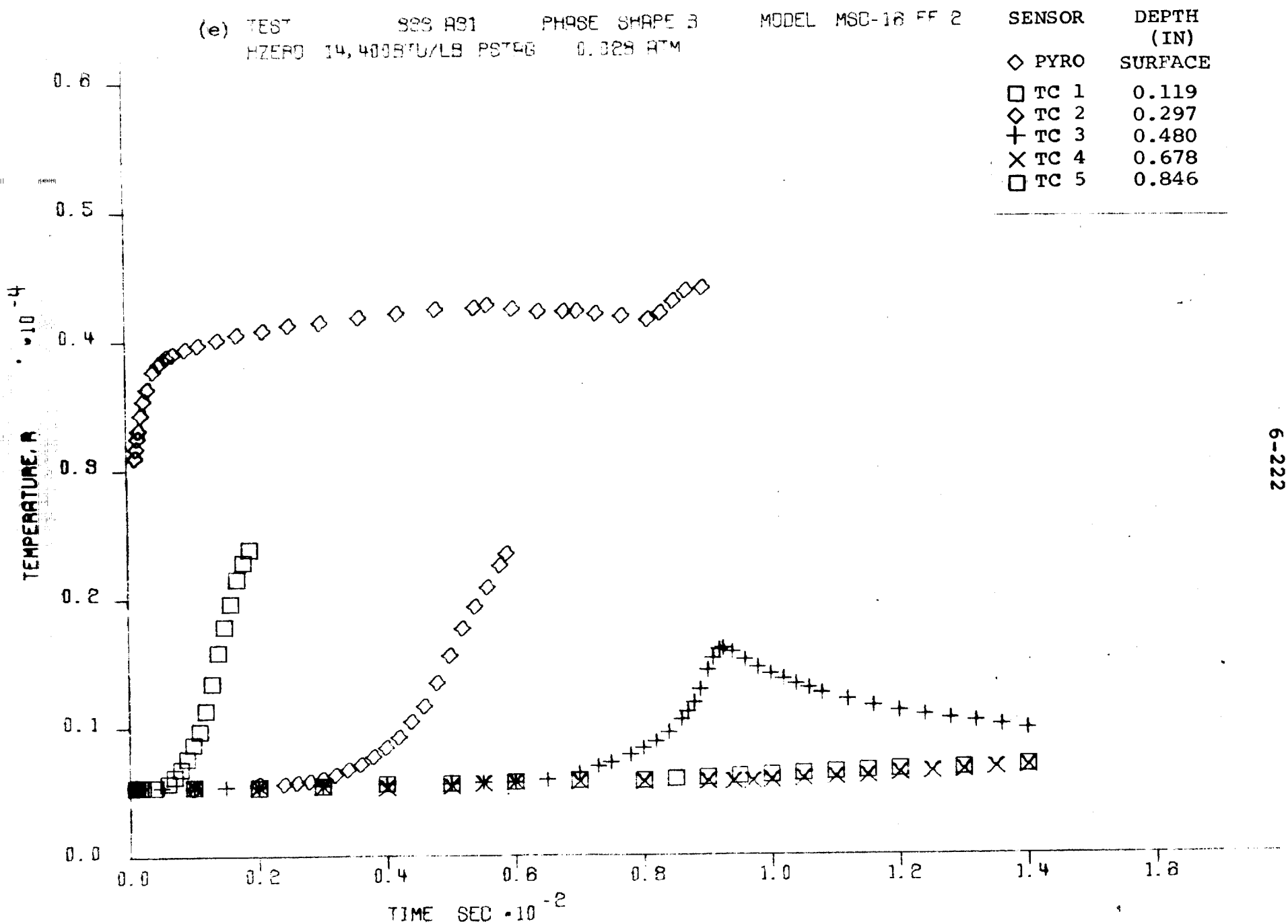

Figure 6-19. Continued.

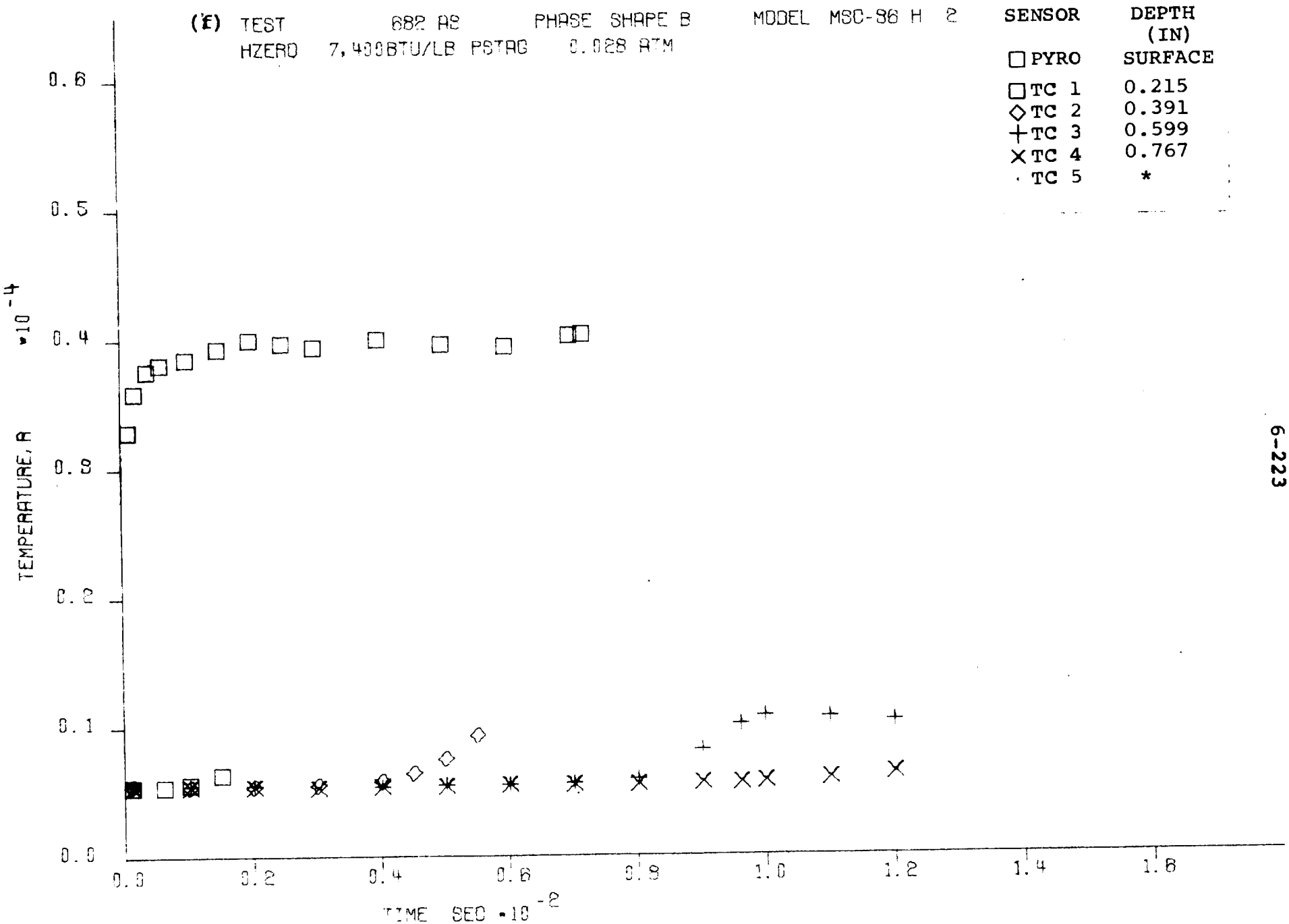

Figure 6-19. Continued.

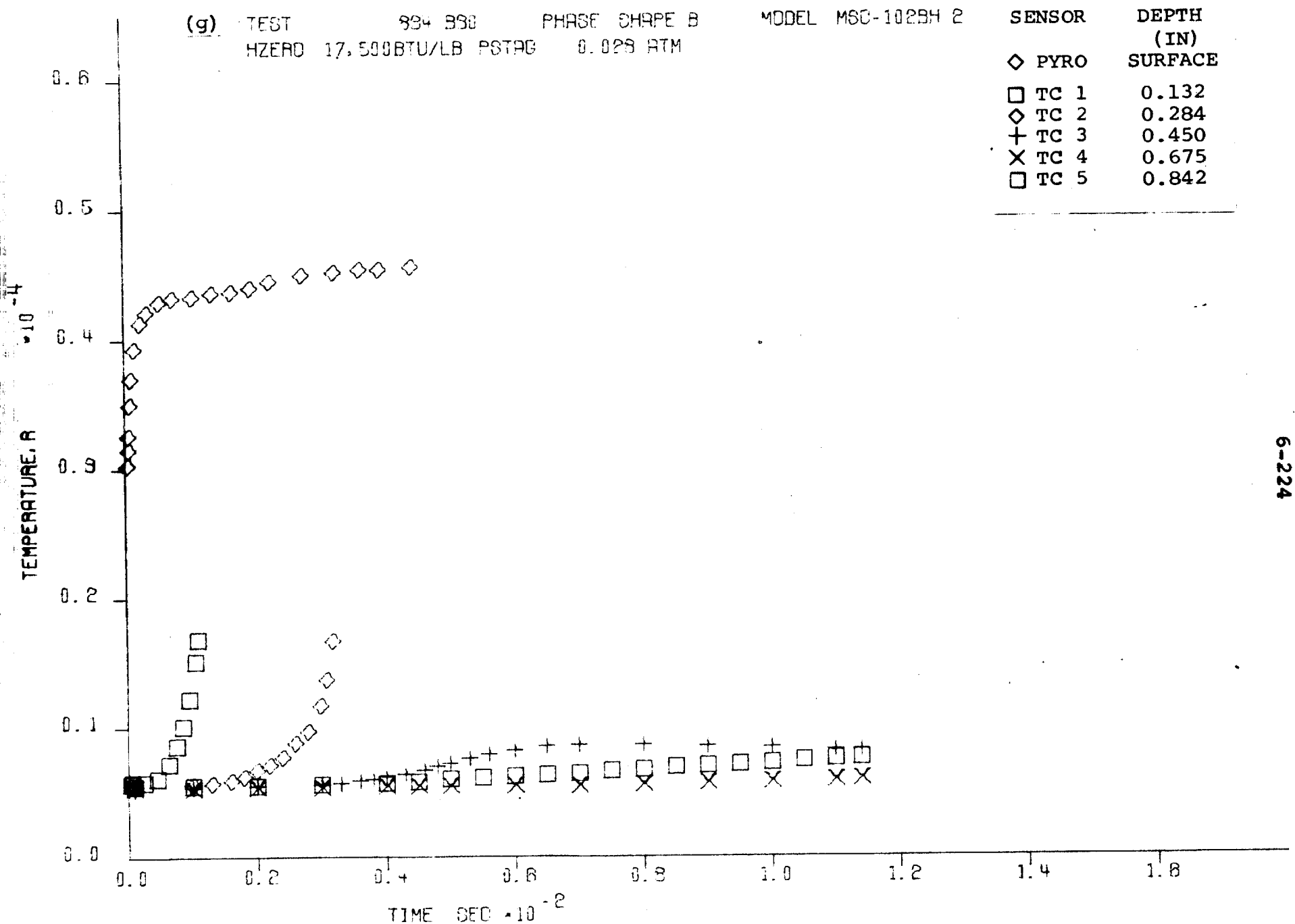

Figure 6-19. Continued.

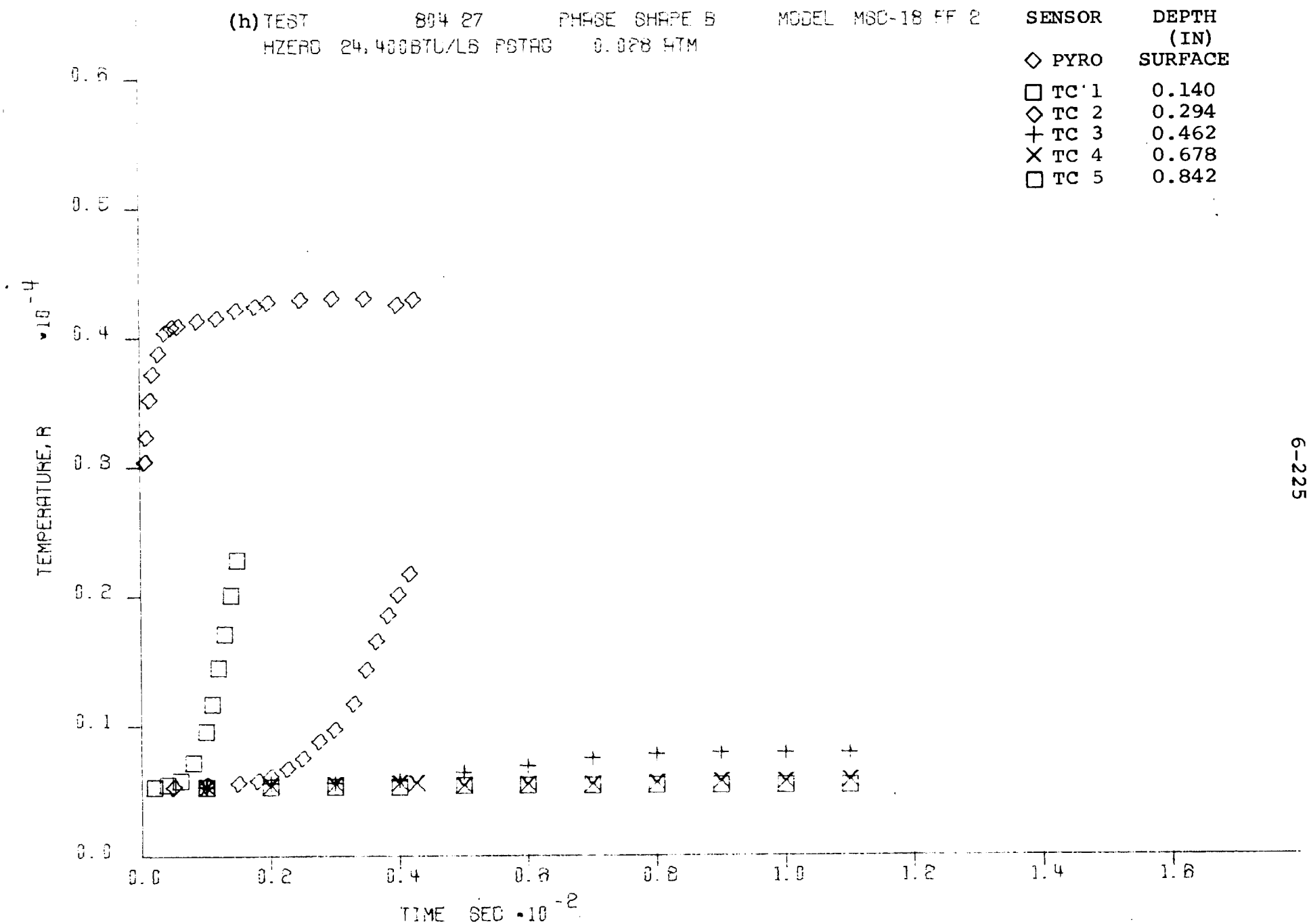

Figure 6-19. Continued.

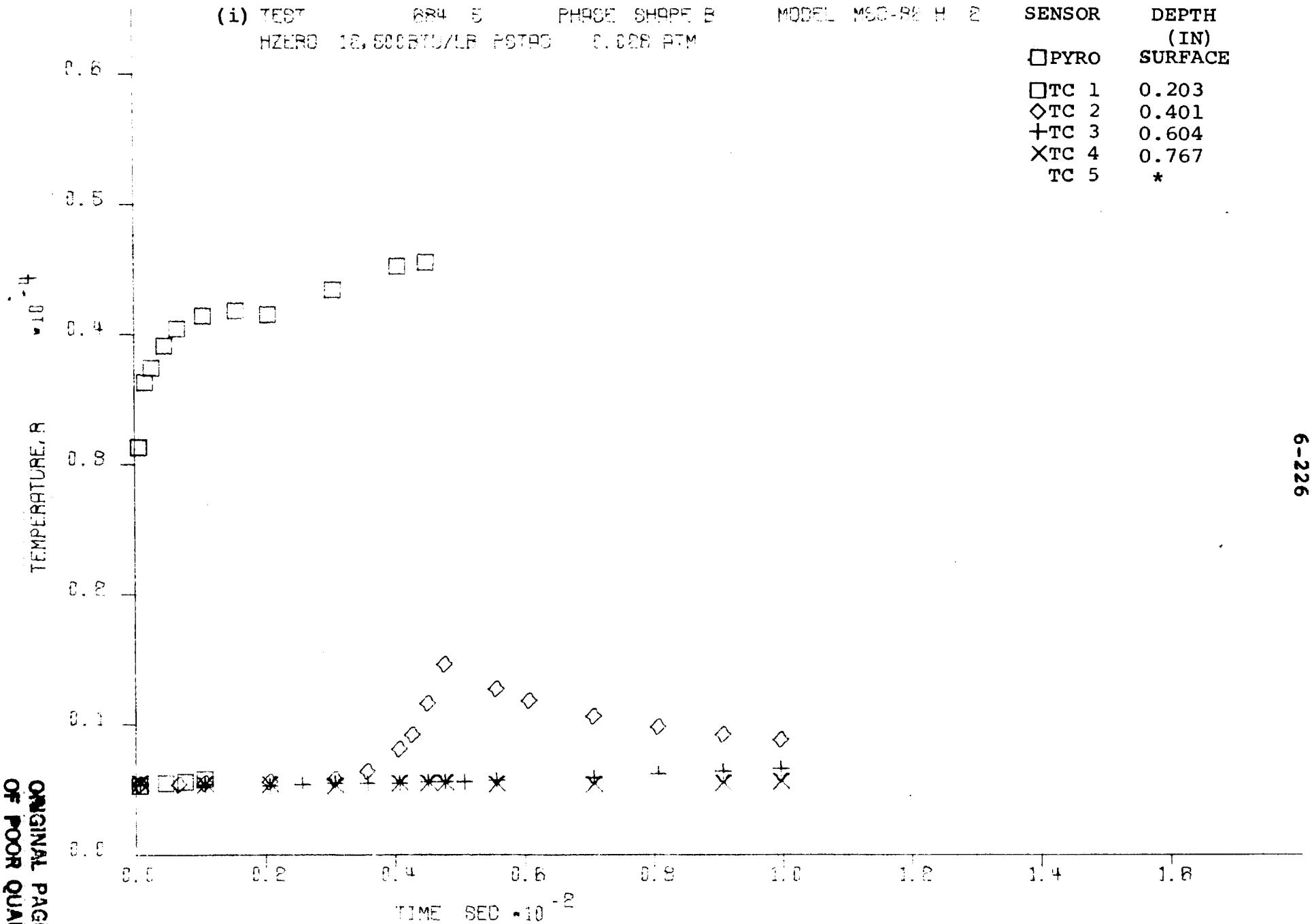

Figure 6-19. Concluded.

ORIGINAL PAGE IS OF POOR QUALITY

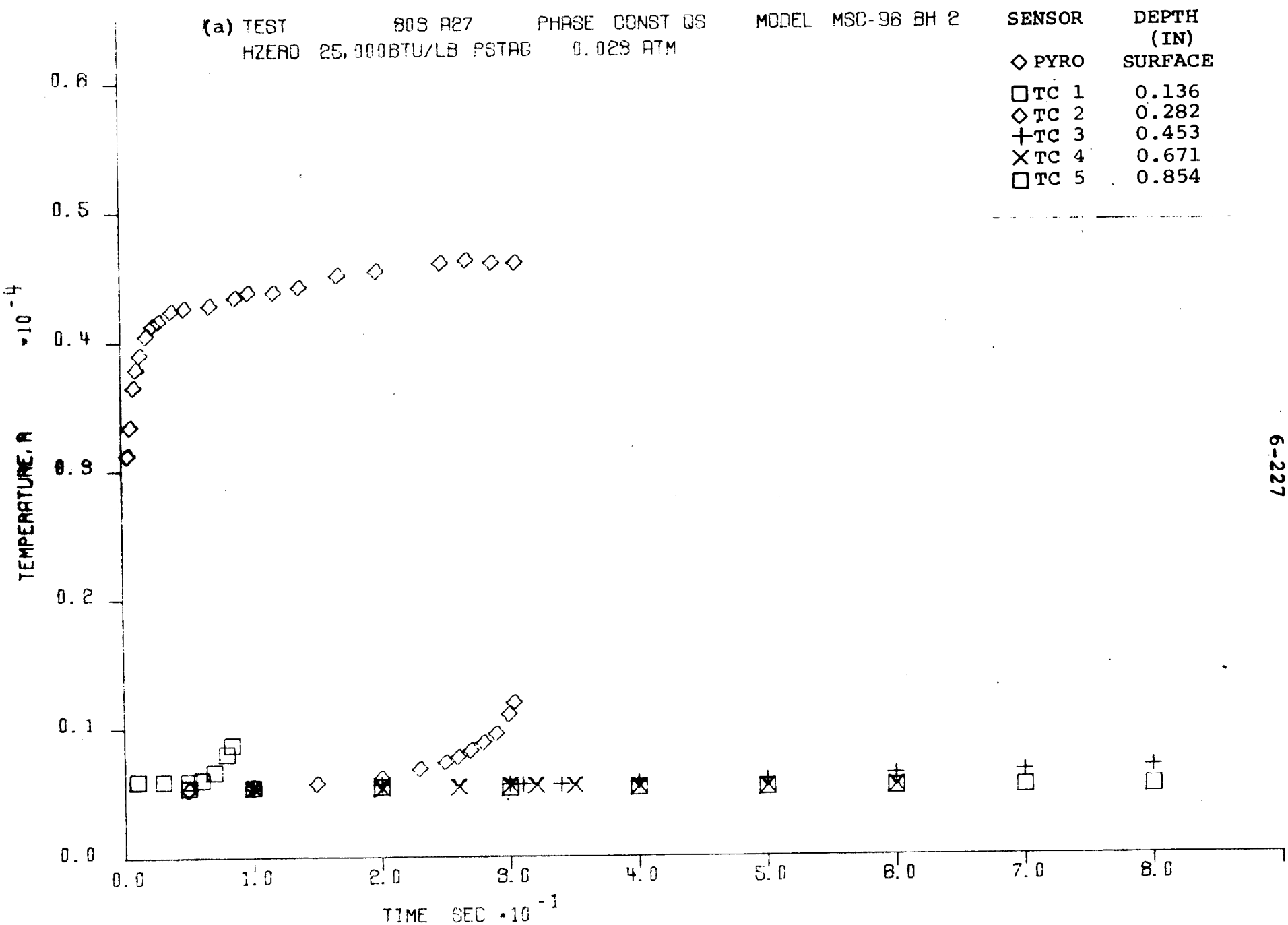

Figure 6-20. Surface and Internal Temperature Histories, Phase VII.

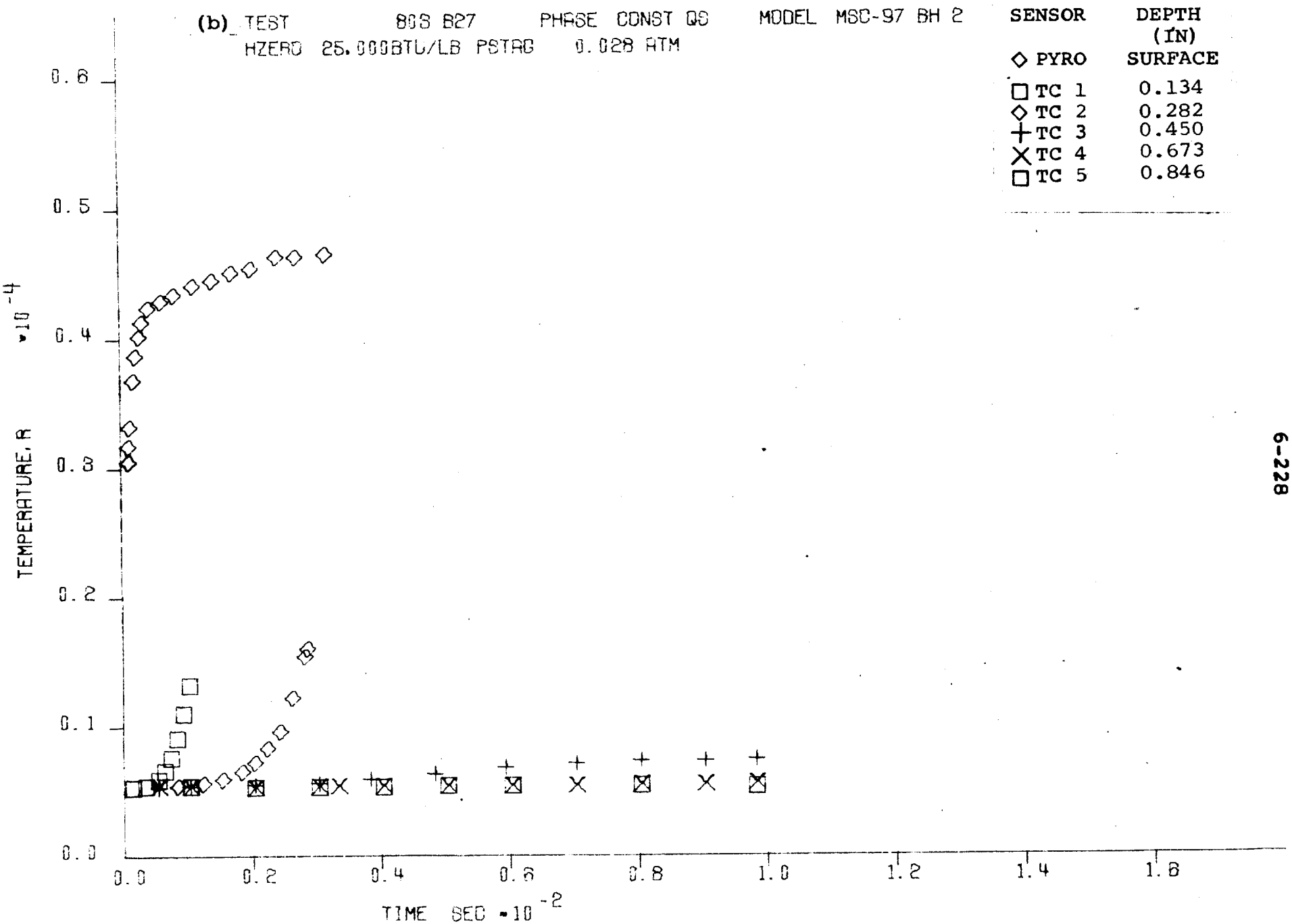

Figure 6-20. Continued.

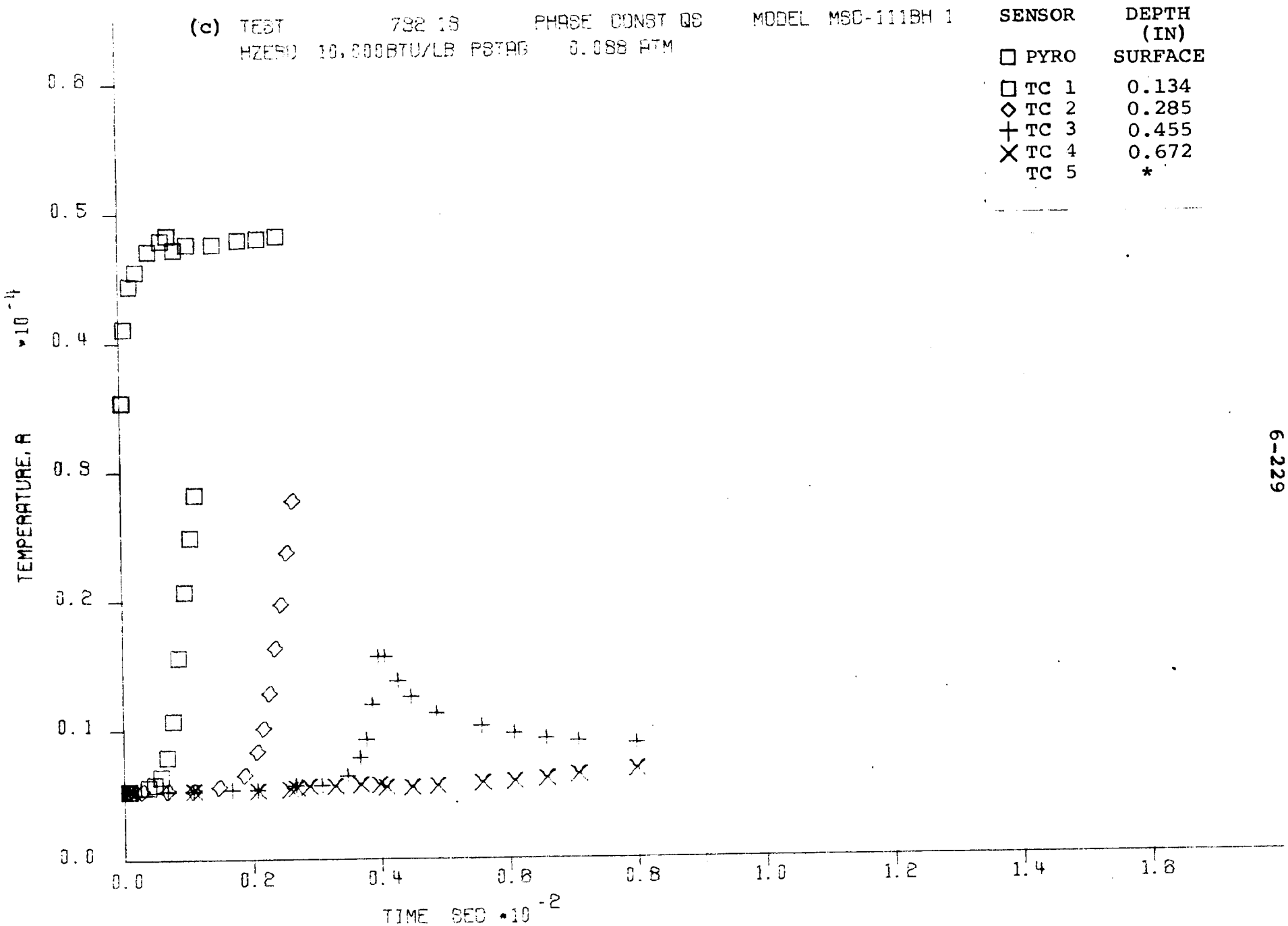

Figre 6-20. Continued.

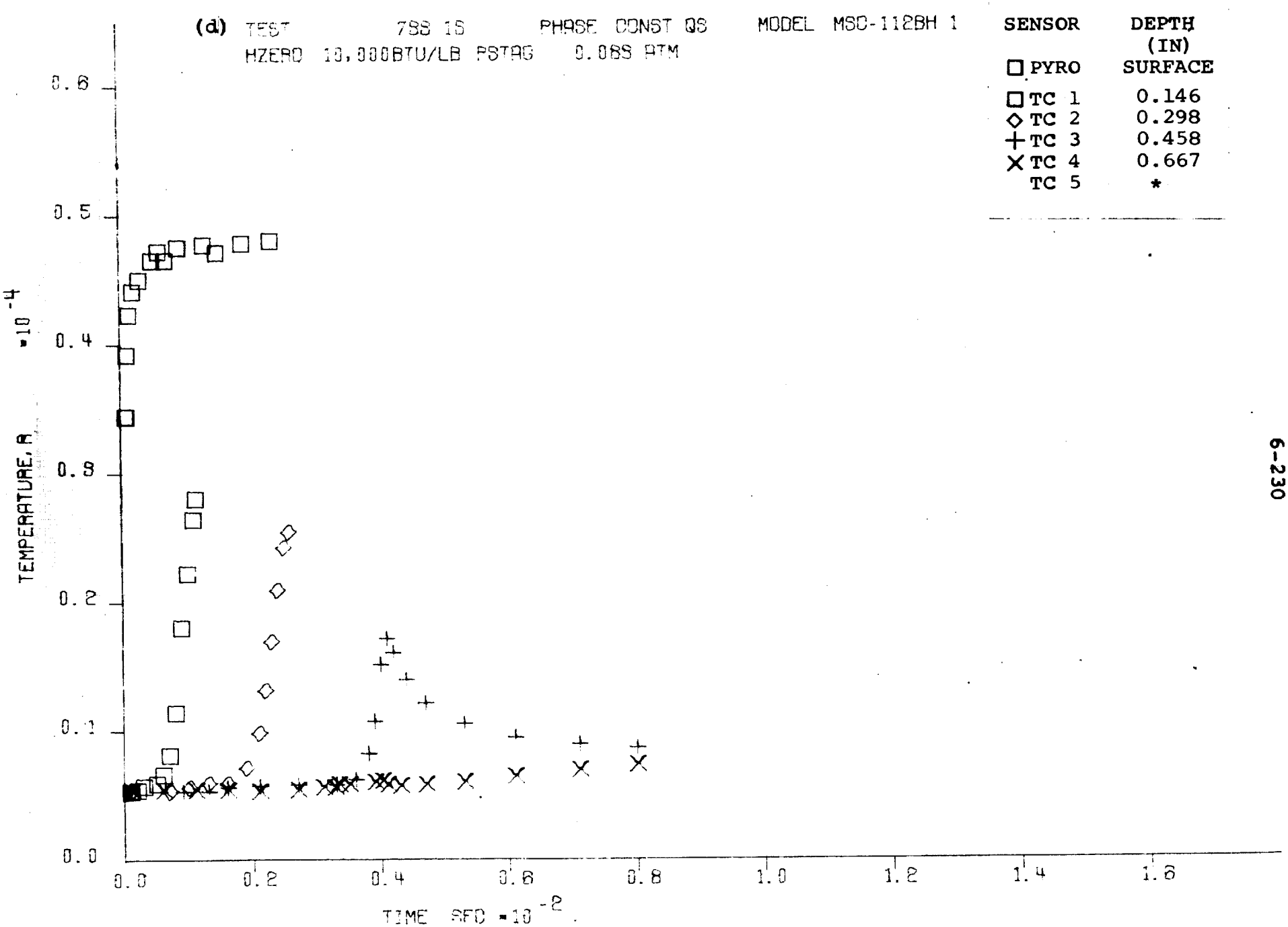

Figure 6-20. Continued.

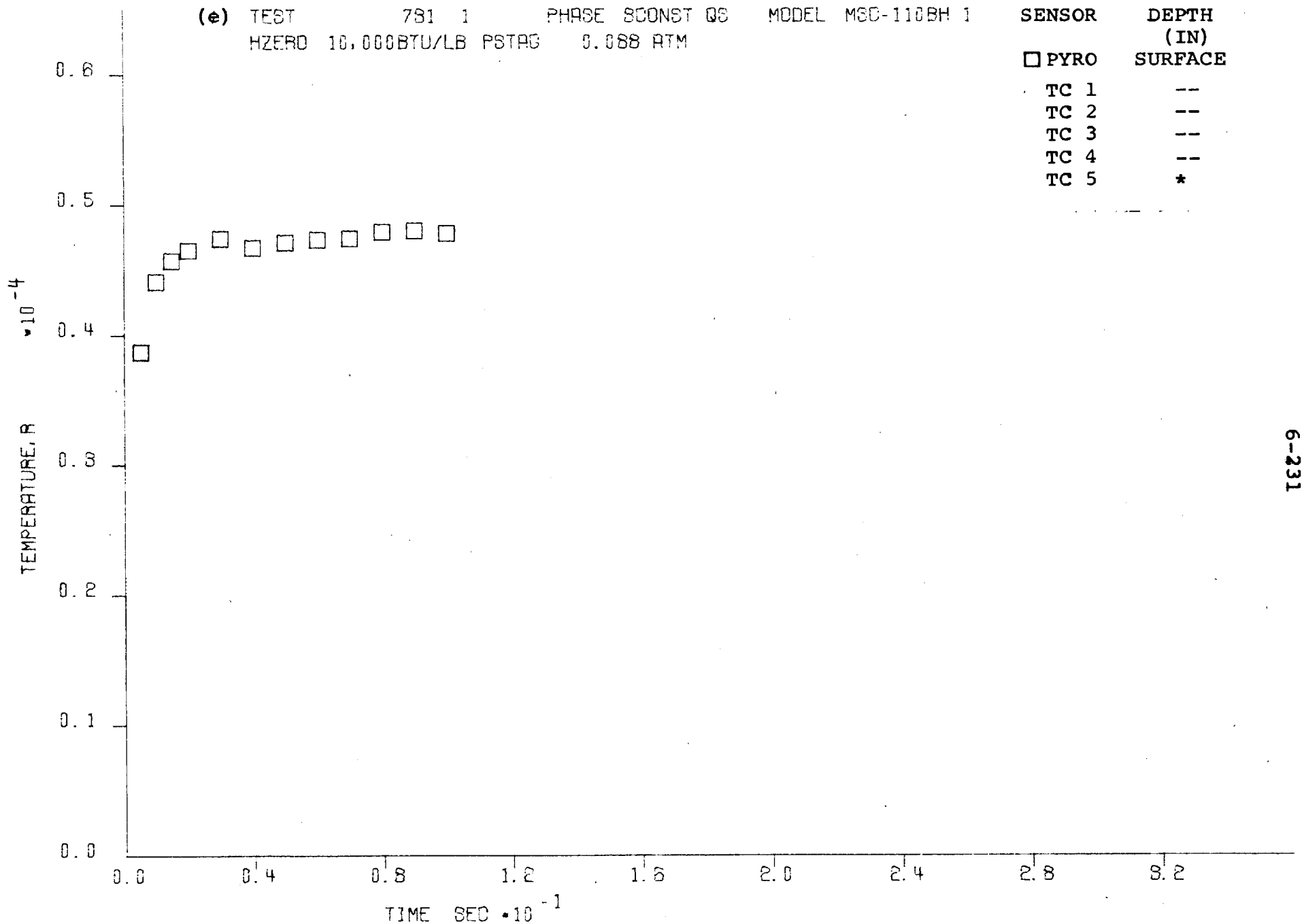

Figure 6-20. Continued.

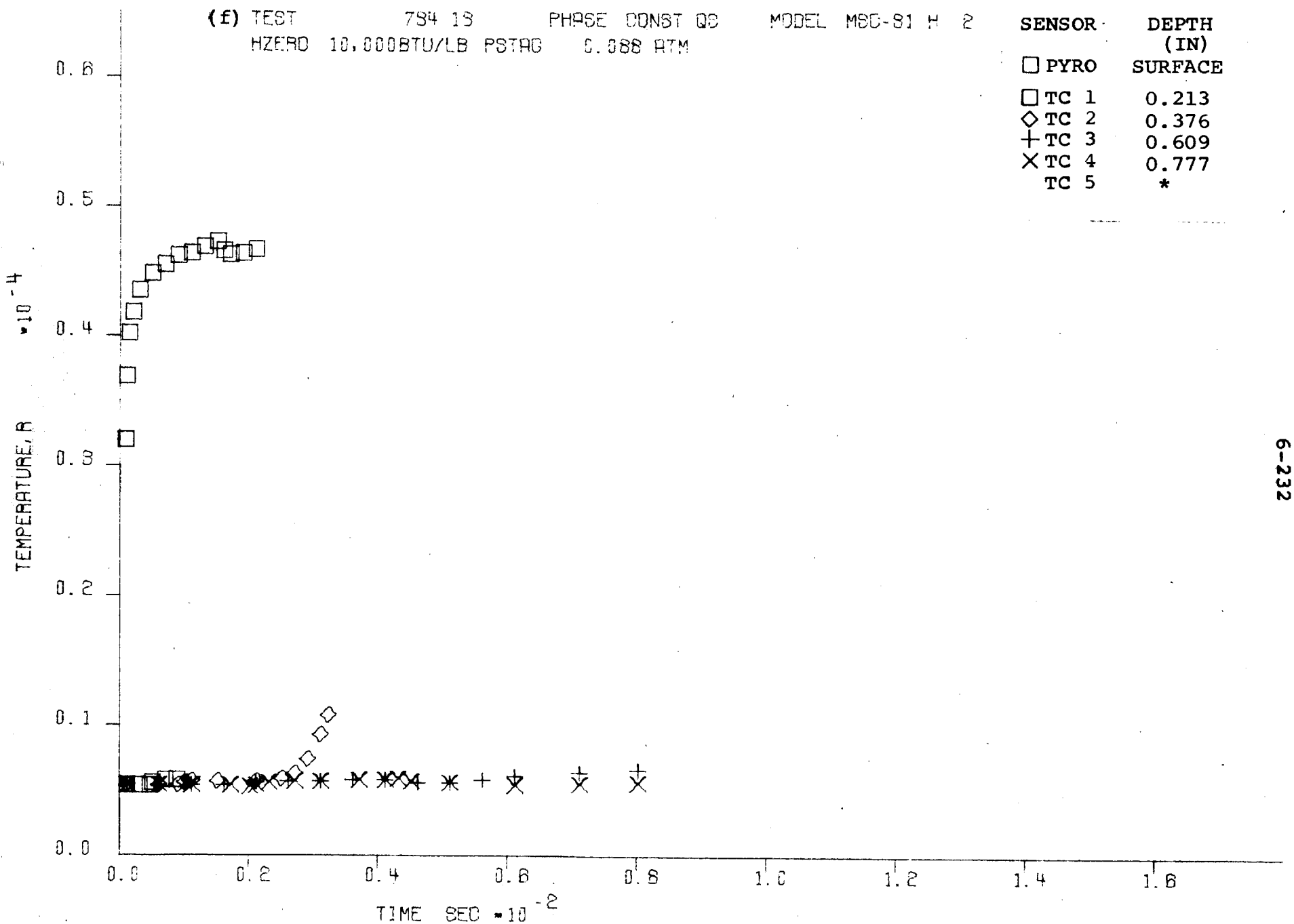

Figure 6-20. Continued.

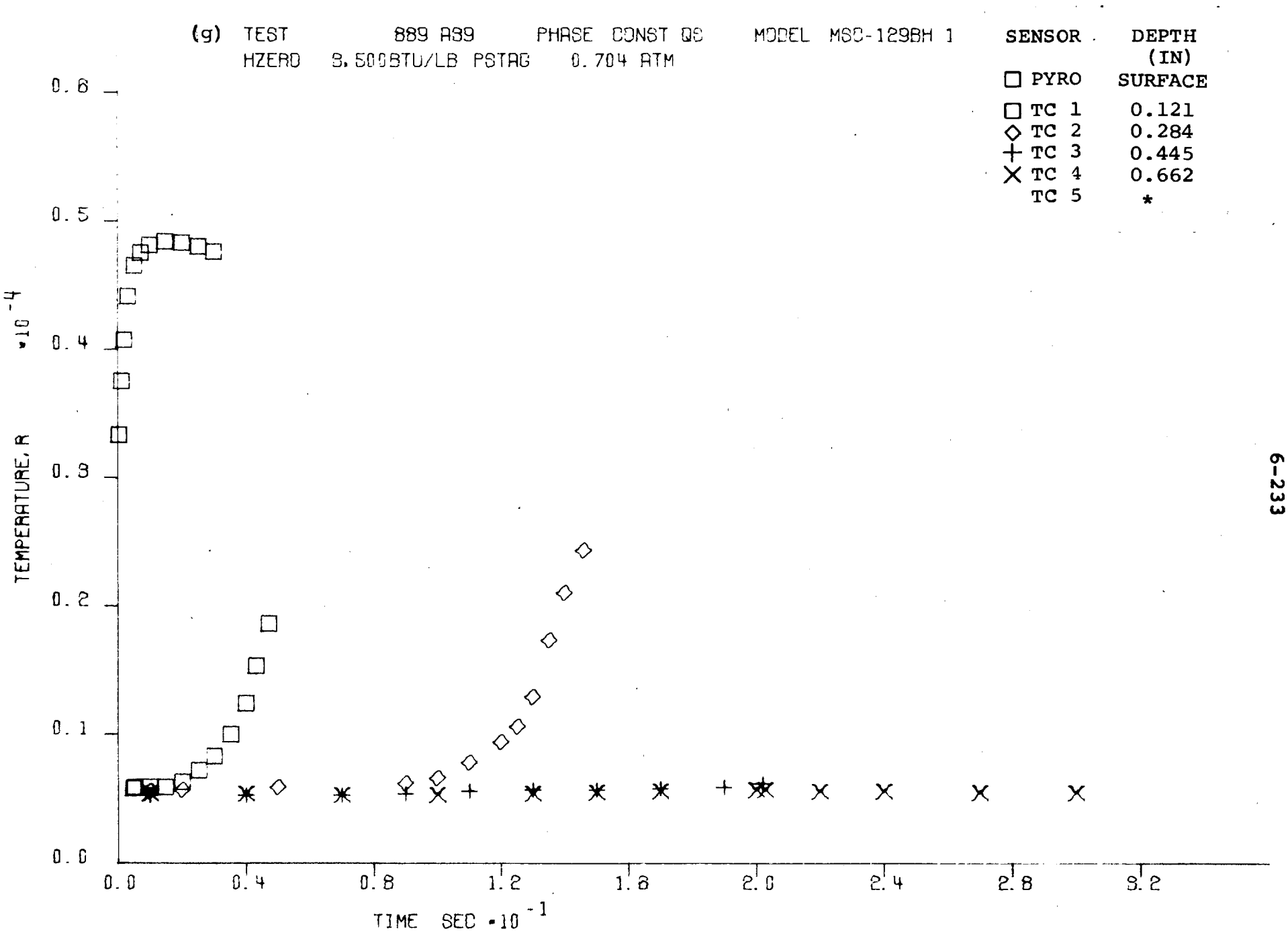

Figure 6-20. Continued.

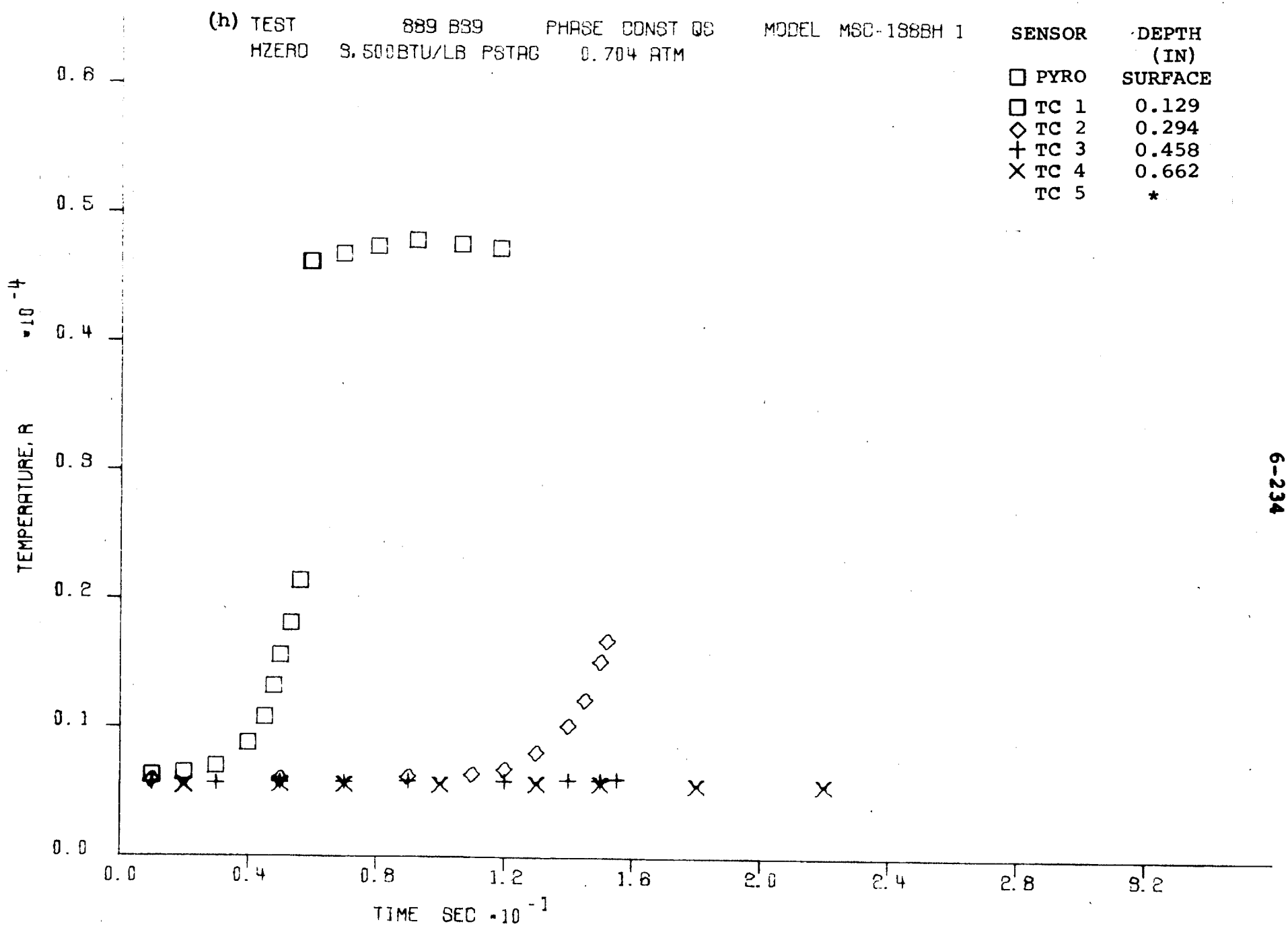

Figure 6-20. Concluded.

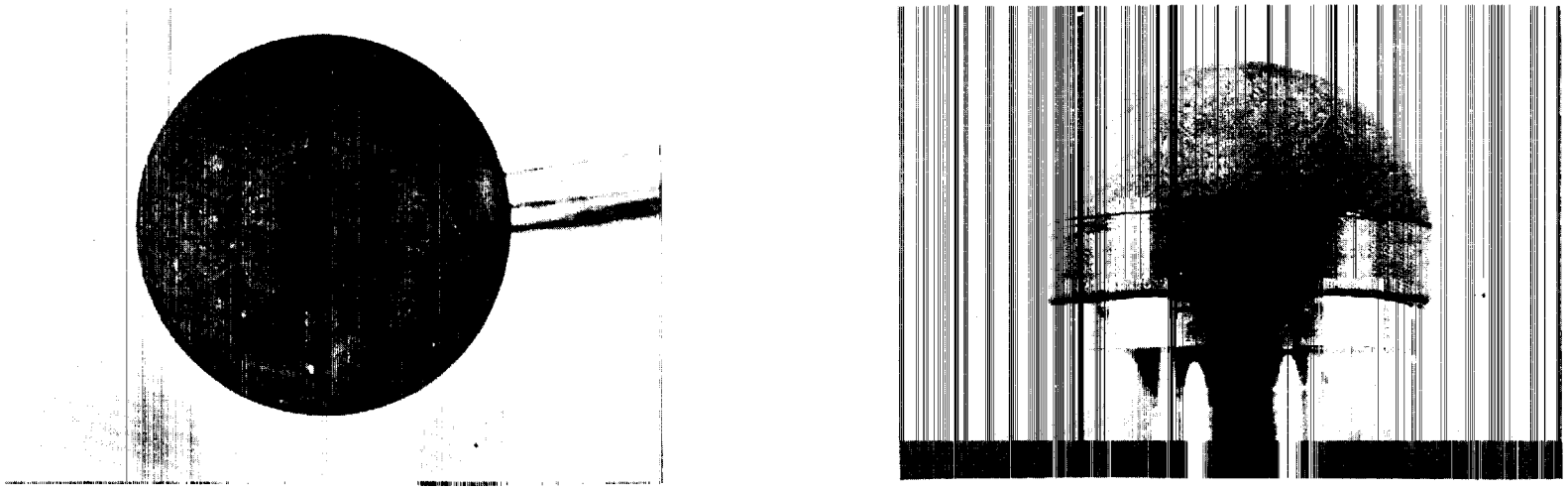

(a) 2 Inch Hemisphere

(b) 4 Inch Blunt Hemisphere

Figure 6-21 Pre Test Model Photographs.

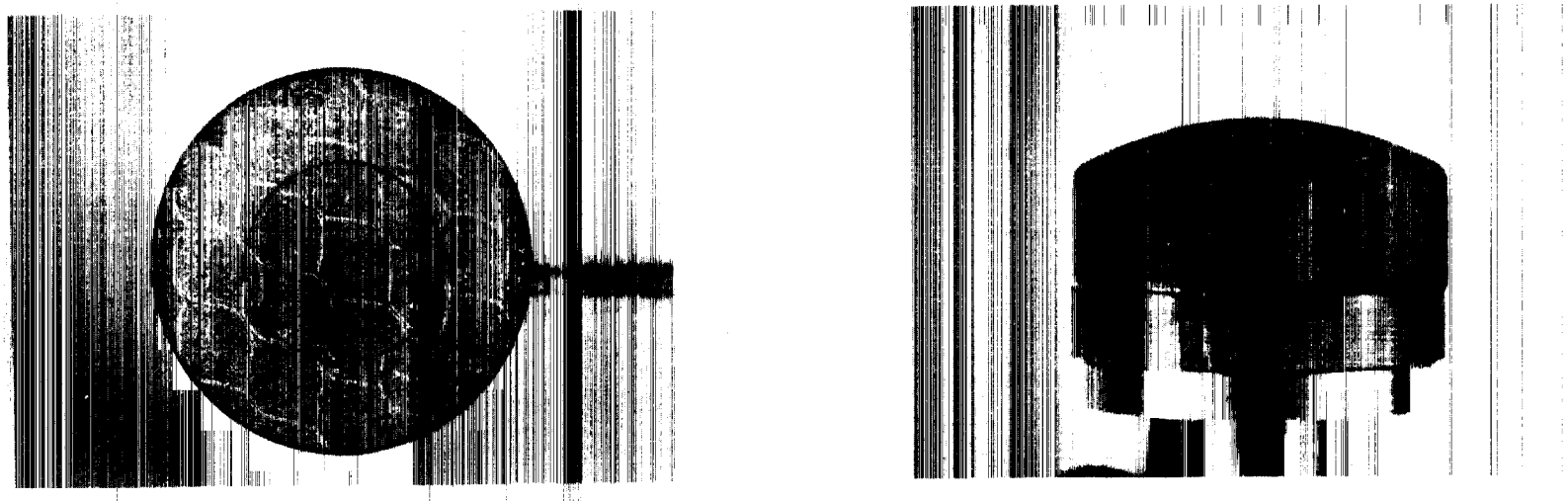

(c) 2 Inch Blunt Hemisphere

(d) 2 Inch Flat Face

Figure 6-21 Continued.

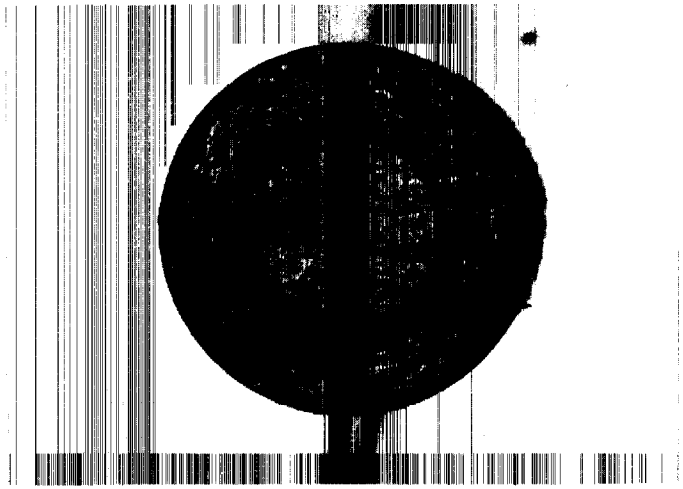

(e) 1 Inch Blunt Hemisphere

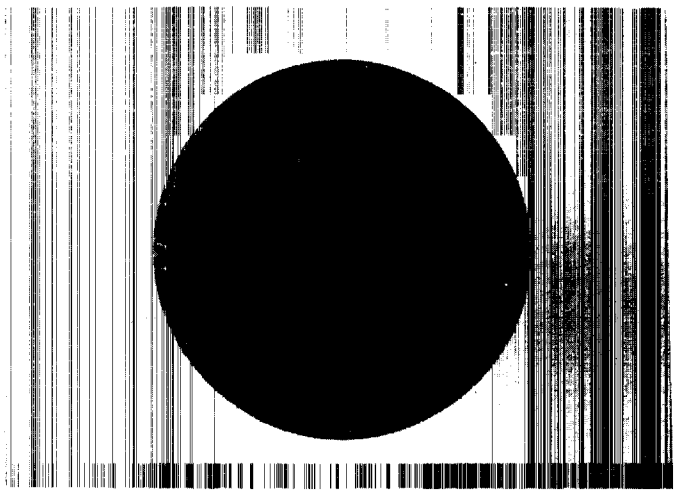

(f) 1 1/4 Inch Flat Face

Figure 6-21 Continued.

(g) 0.22 Inch Duct
Material 5026-39

(h) 0.22 Inch Duct
Material P2019

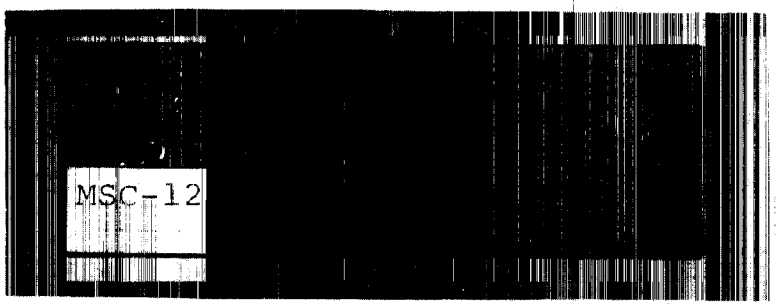

(i) 0.22 Inch Duct
Material 5026-22

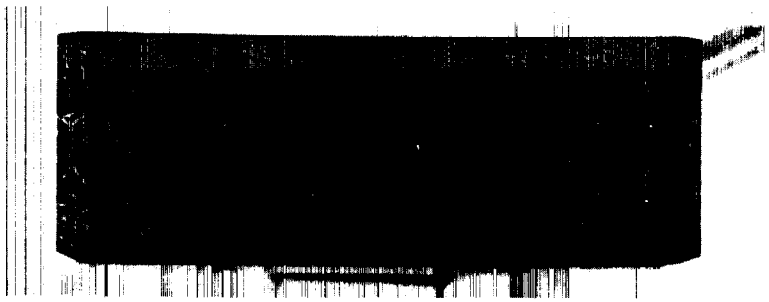

(j) 0.22 Inch Duct
Material 5026-39

Figure 6-21 Concluded.

(a) Model 6

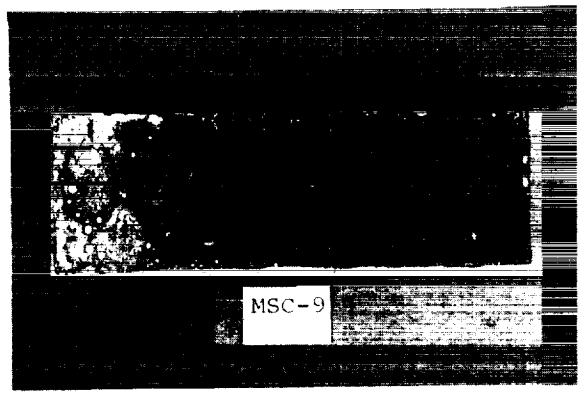

(b) Model 9

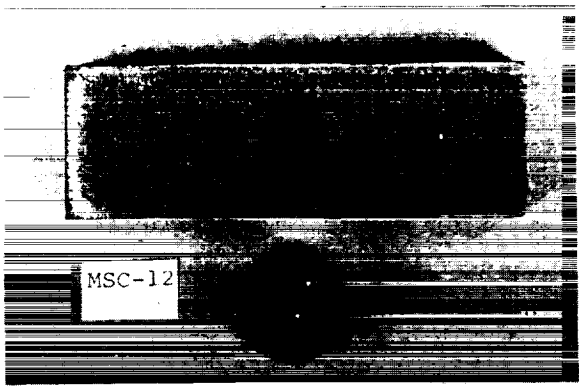

(c) Model 12

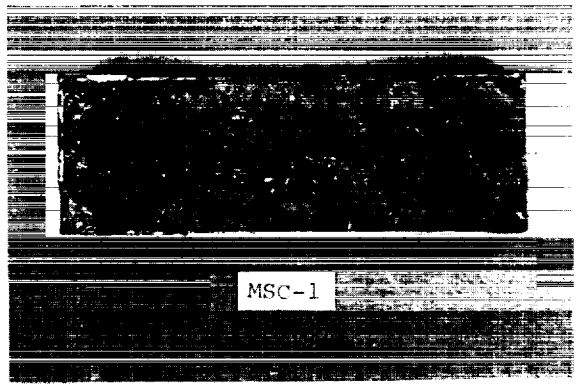

(d) Model 1

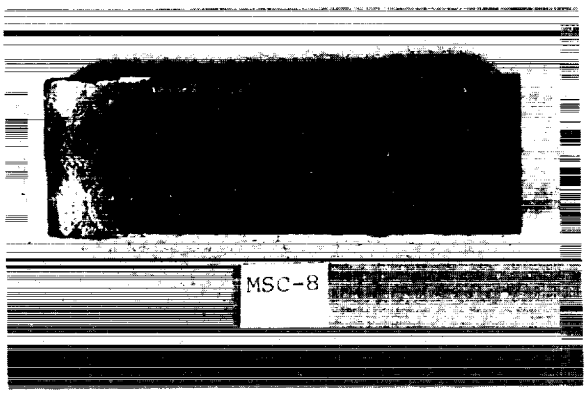

(e) Model 8

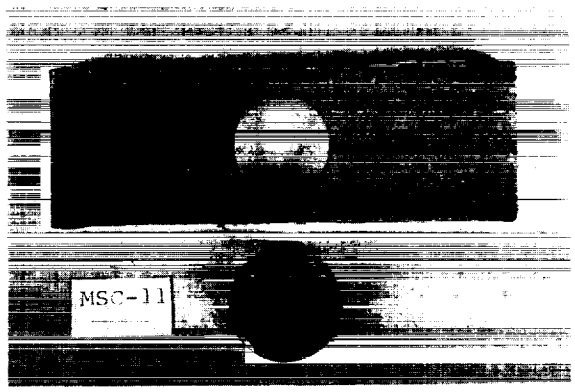

(f) Model 11

Figure 6-22 Phase I Post Test Model Photographs.

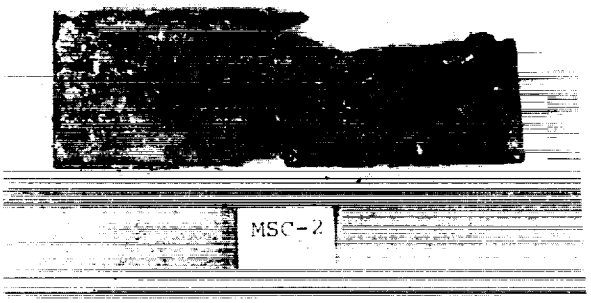

(g) Model 2

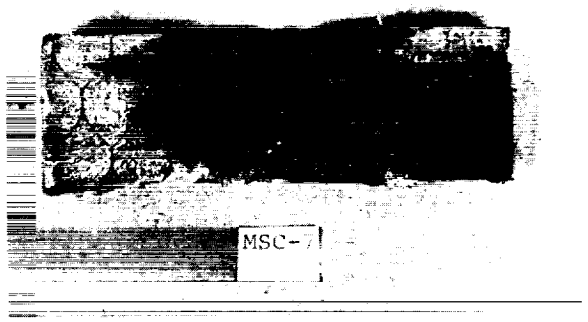

(h) Model 7

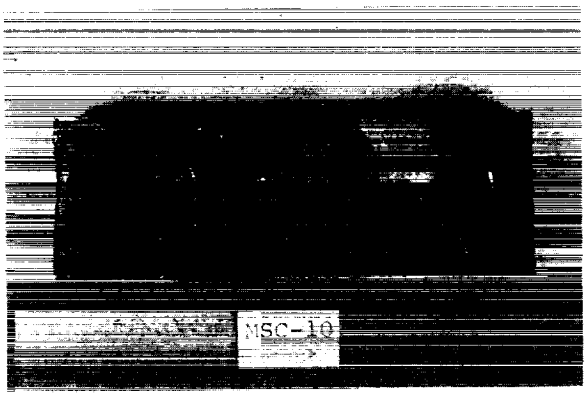

(i) Model 10

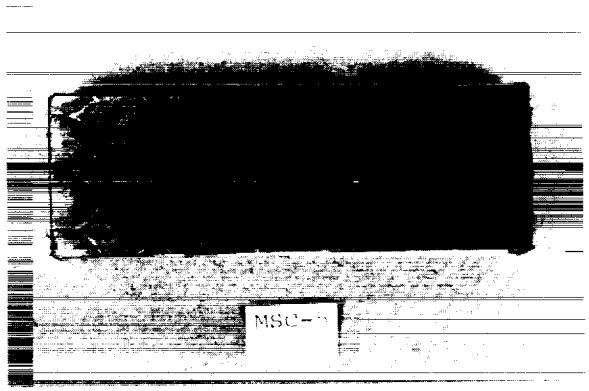

(j) Model 5

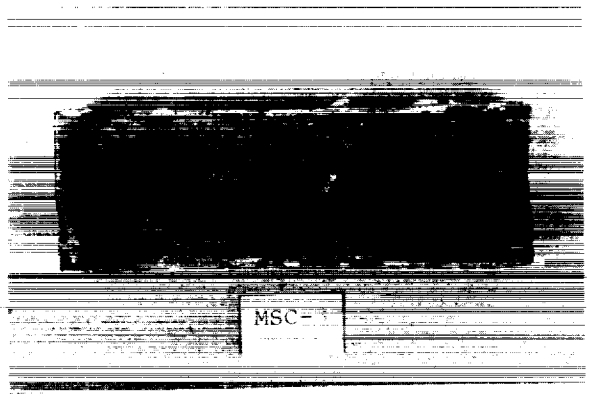

(k) Model 3

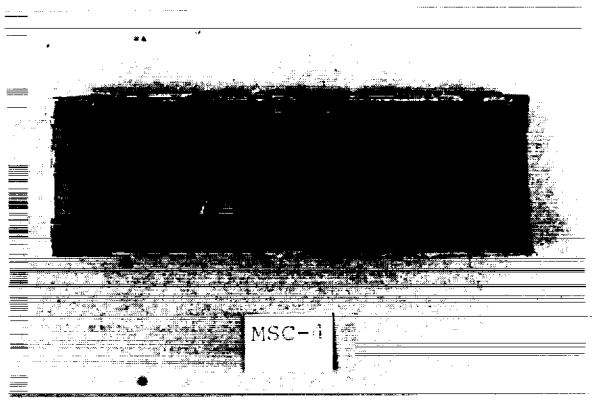

(l) Model 4

Figure 6-22 Continued.

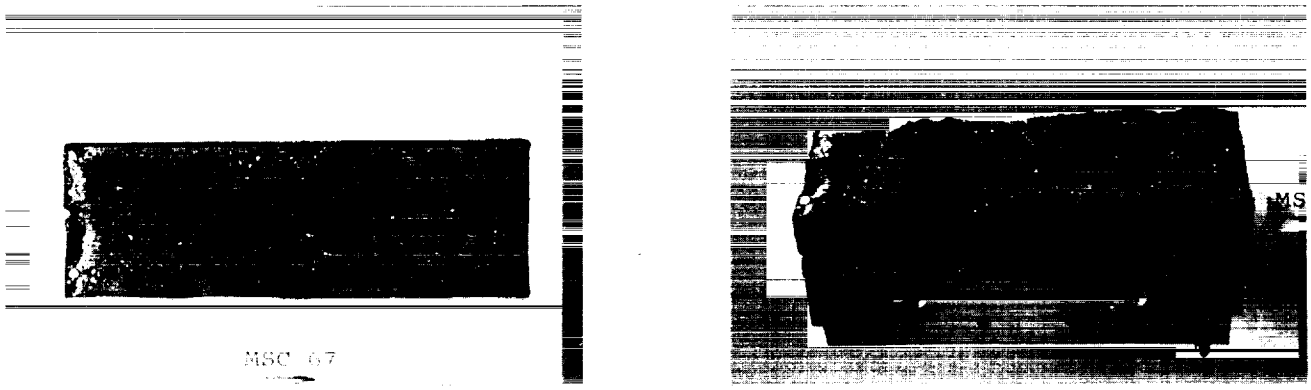

(m) Model 67

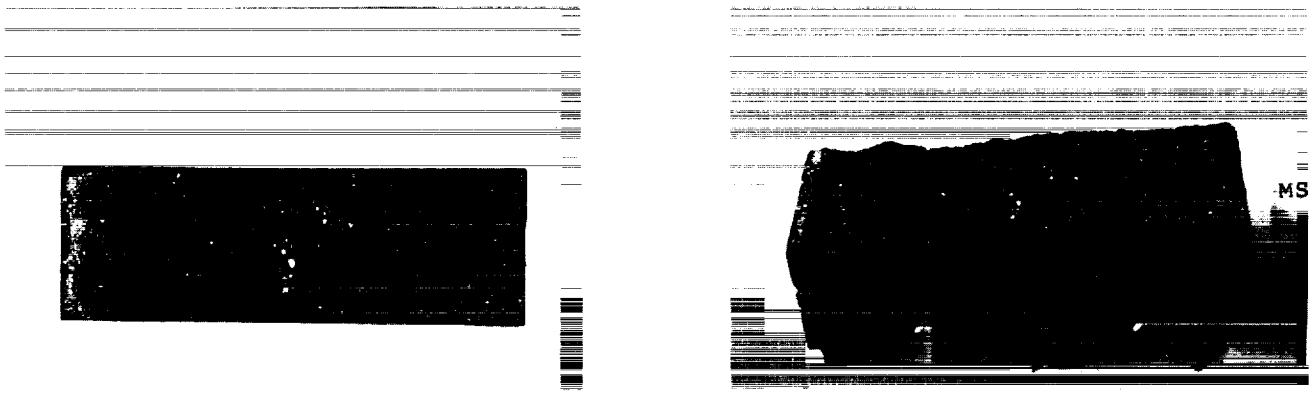

(n) Model 68

(o) Model 64

Figure 6-22 Continued.

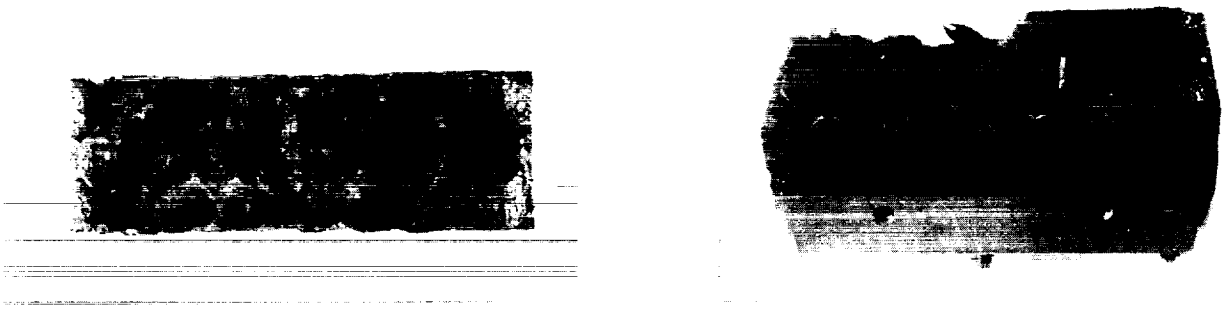

(p) Model 65

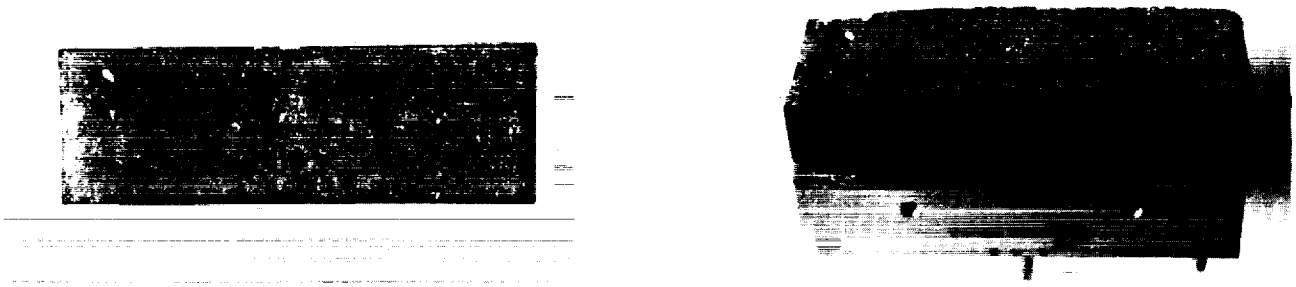

(q) Model 73

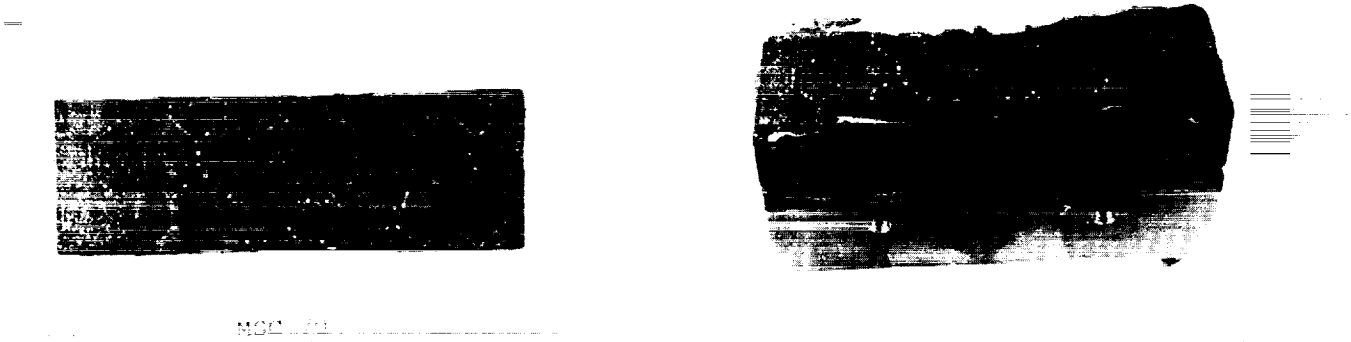

(r) Model 70

Figure 6-22 Continued.

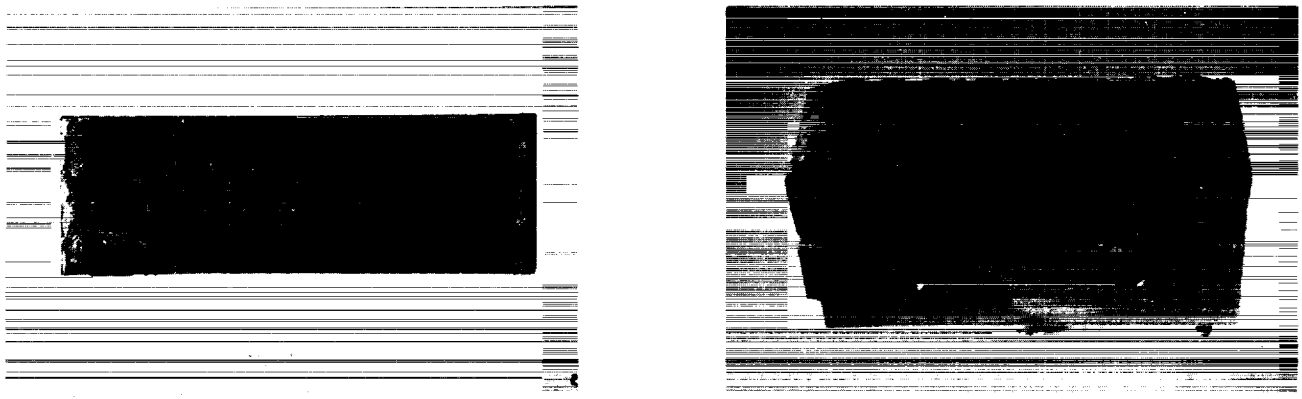

(s) Model 69

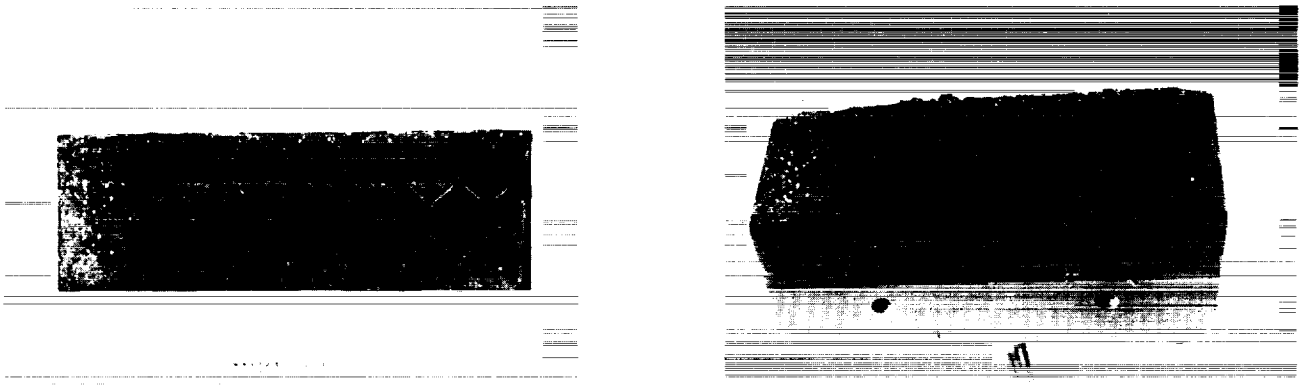

(t) Model 72

(u) Model 71

Figure 6-22 Continued.

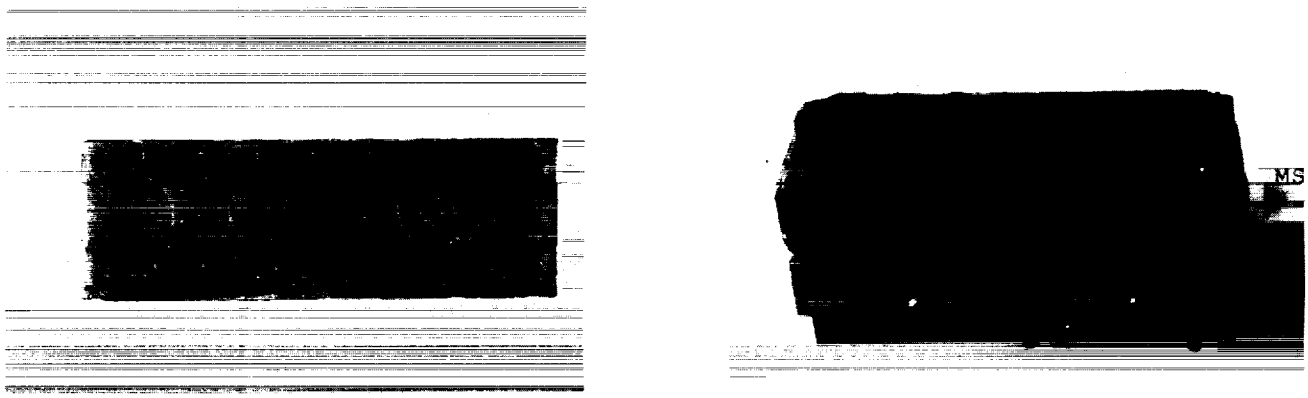

(v) Model 66

Figure 6-22 Concluded.

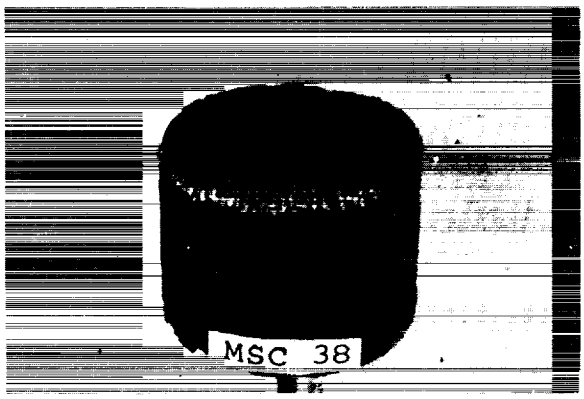

(a) Model 46

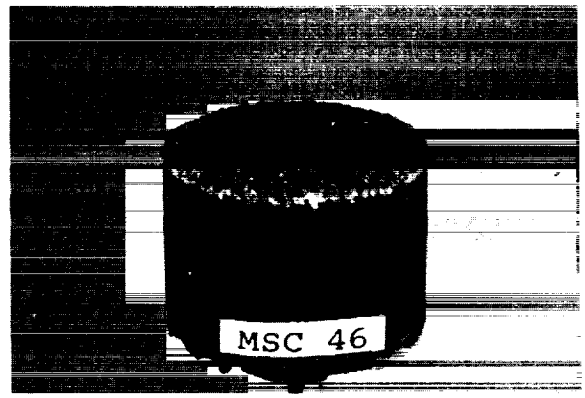

(b) Model 38

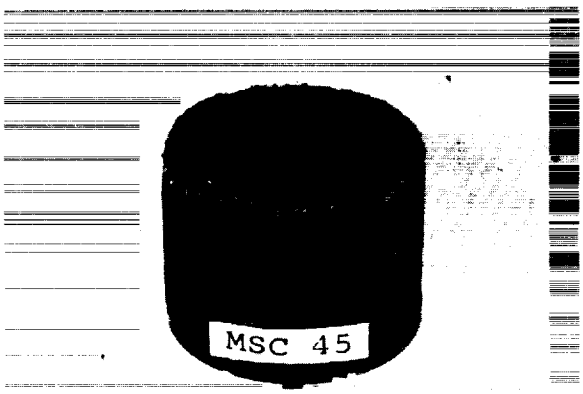

(c) Model 45

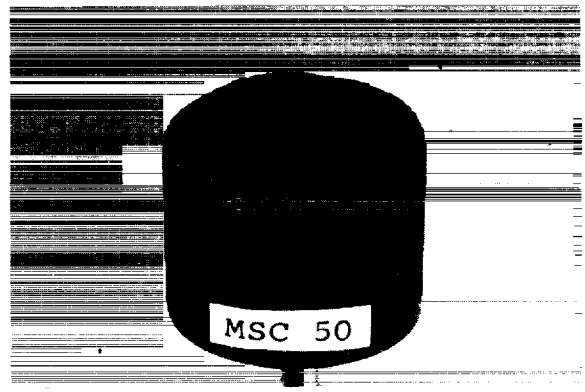

(d) Model 50

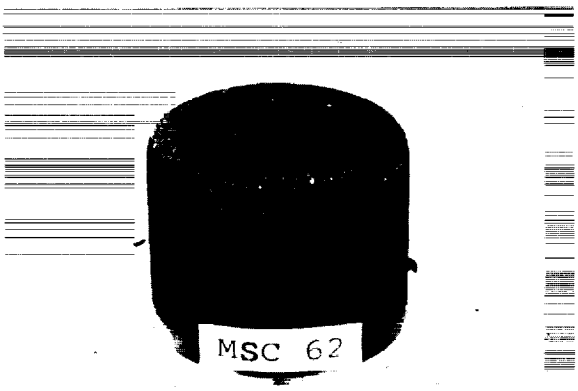

(e) Model 62

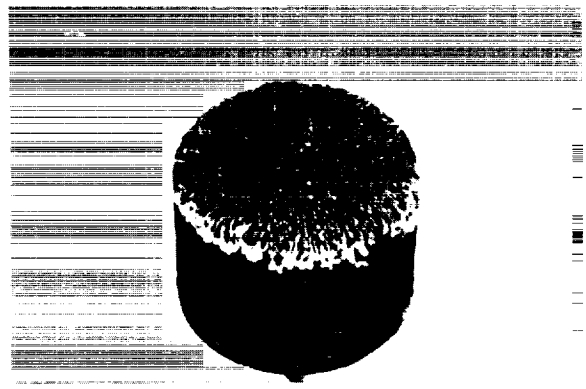

(f) Model 51

Figure 6-23 Phase II Post Test Model Photographs.

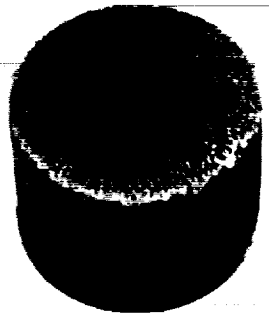

(g) Model 61

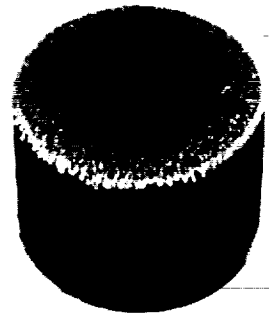

(h) Model 54

(i) Model 55

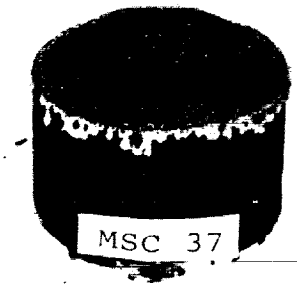

(j) Model 37

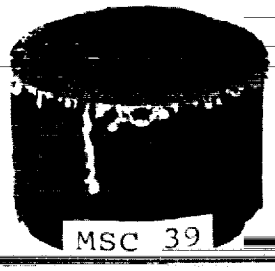

(k) Model 39

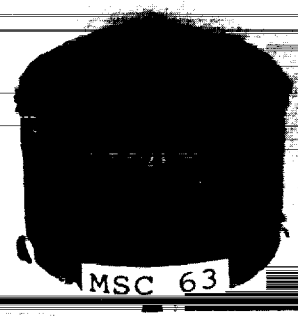

(l) Model 63

Figure 6-23 Continued.

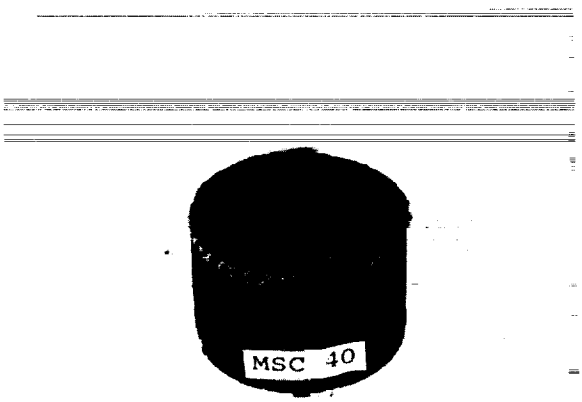

(m) Model 40

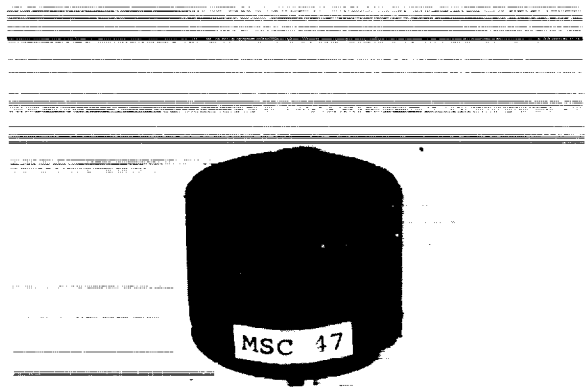

(n) Model 47

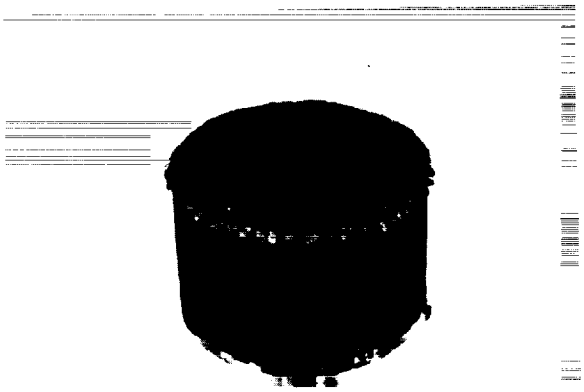

(o) Model 49

(p) Model 53

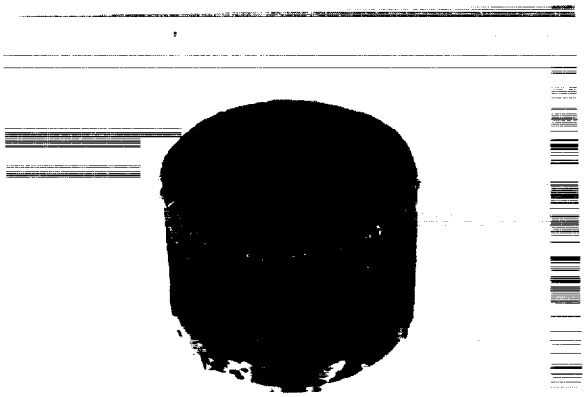

(q) Model 60

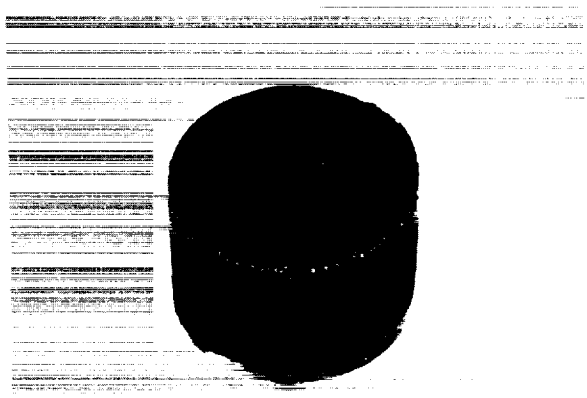

(r) Model 52

Figure6-23Continued.

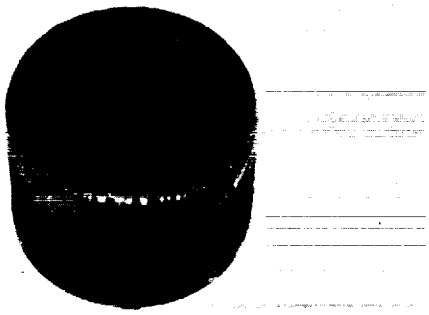

(s) Model 44

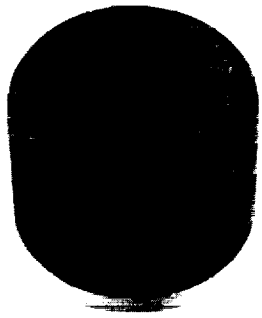

(t) Model 48

(u) Model 42

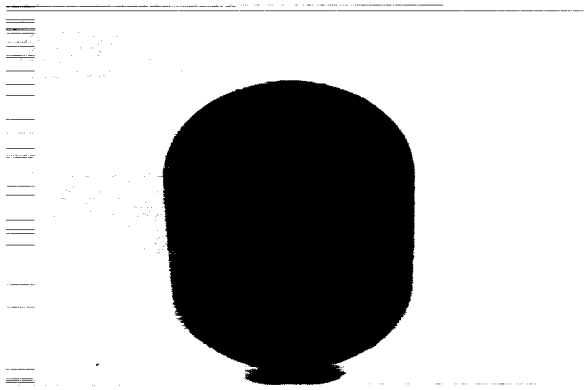

(v) Model 56

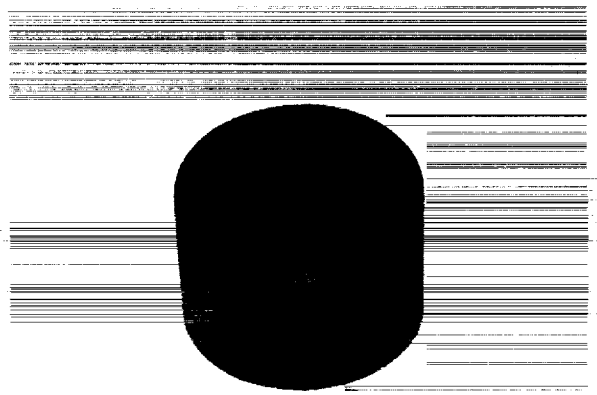

(w) Model 57

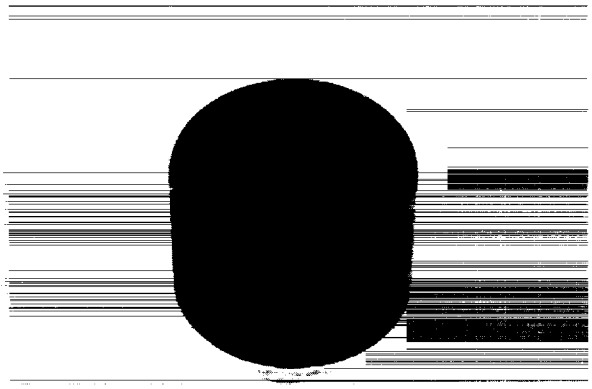

(x) Model 58

Figure 6-23 Concluded.

(a) Model 154

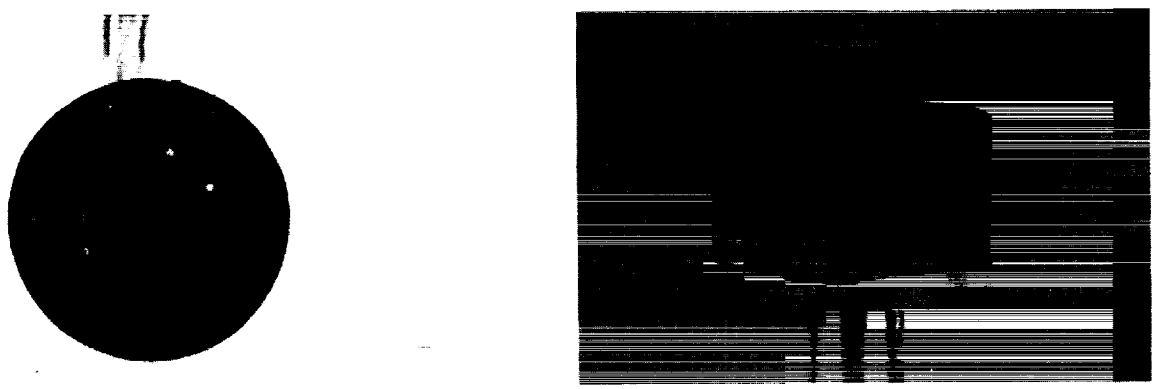

(b) Model 158

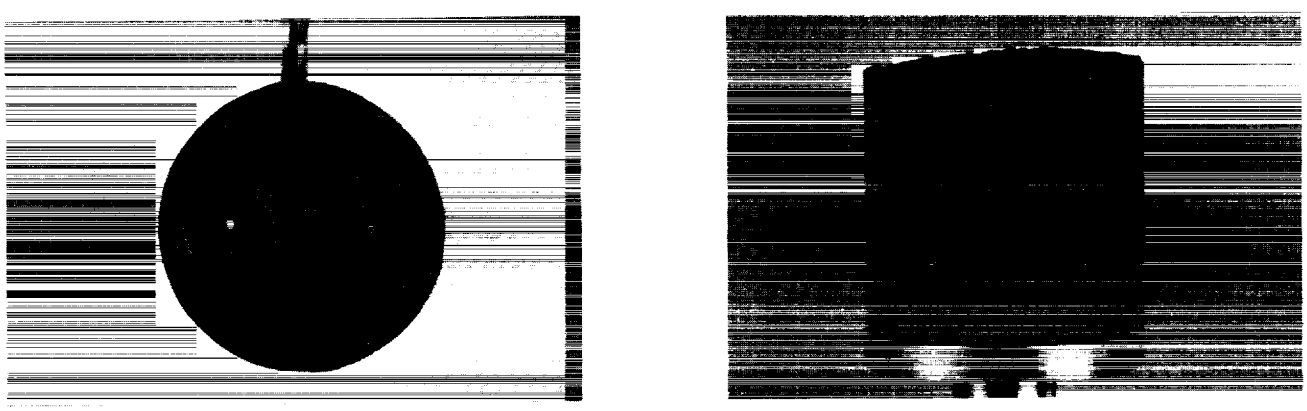

(c) Model 113

Figure 6-23 Phase III Post Test Model Photographs.

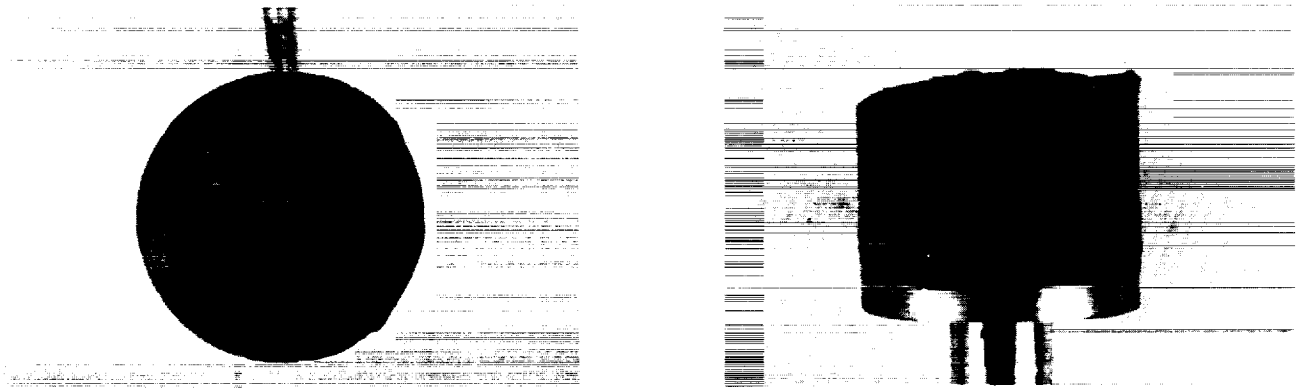

(d) Model 151

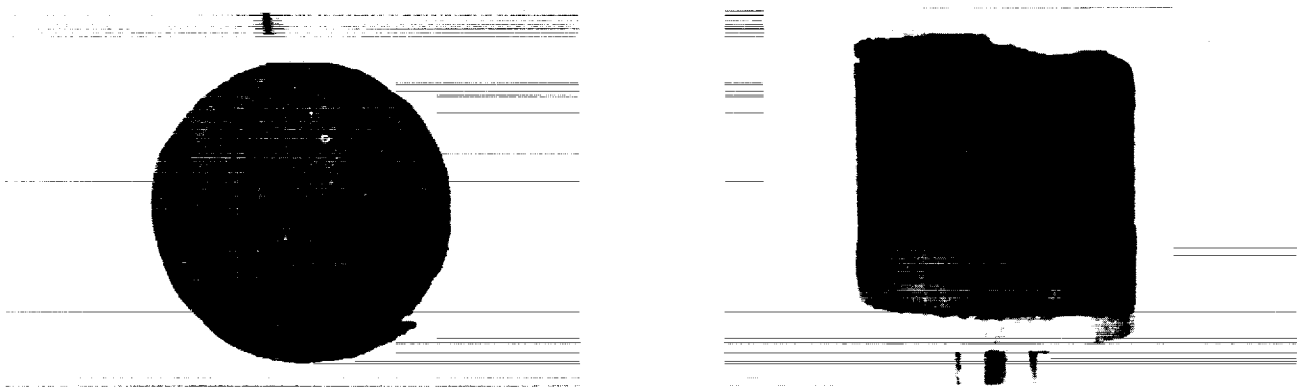

(e) Model 152

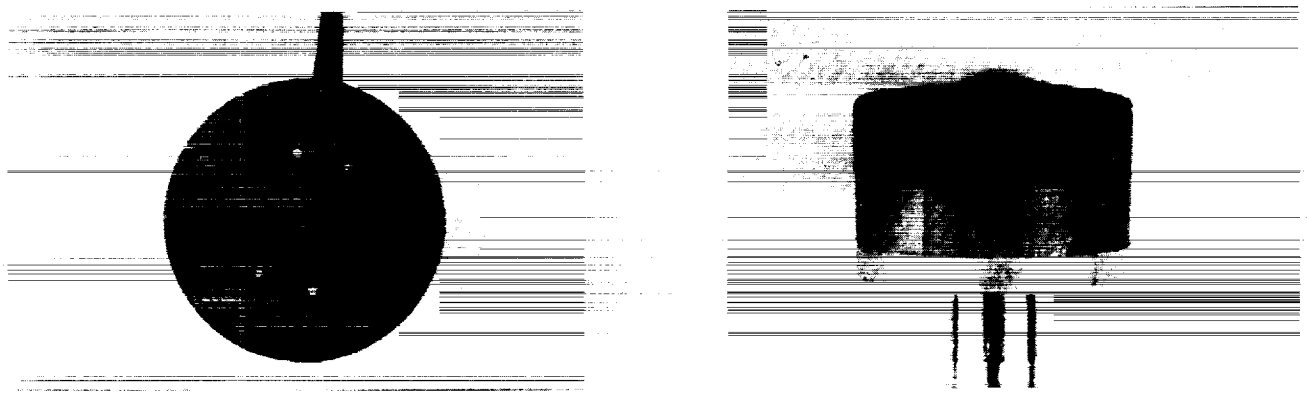

(f) Model 156

Figure 6-24 Continued.

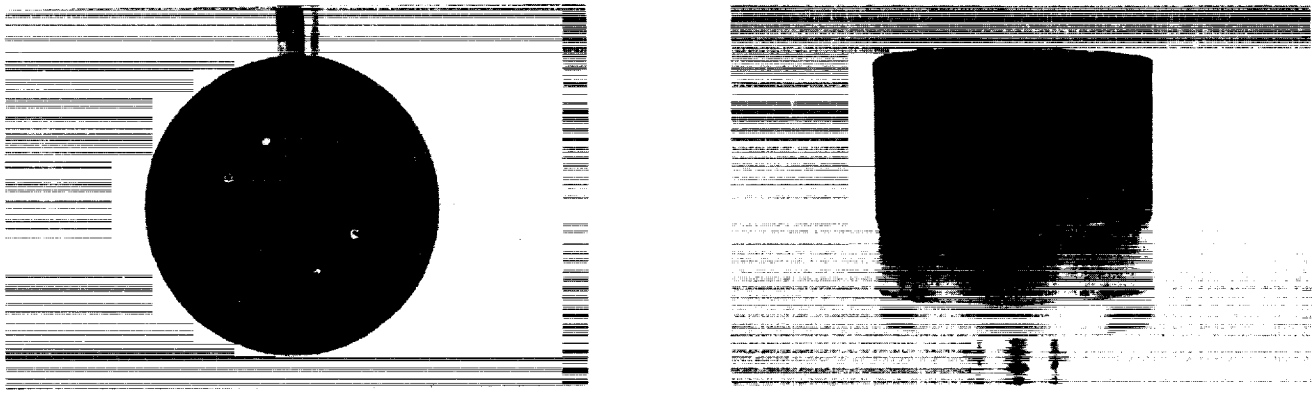

(g) Model 157

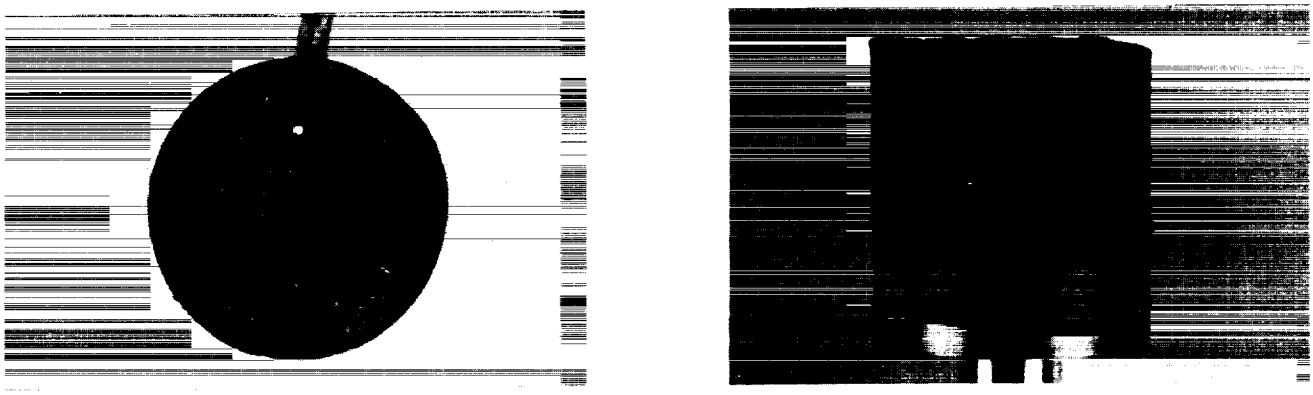

(h) Model 134

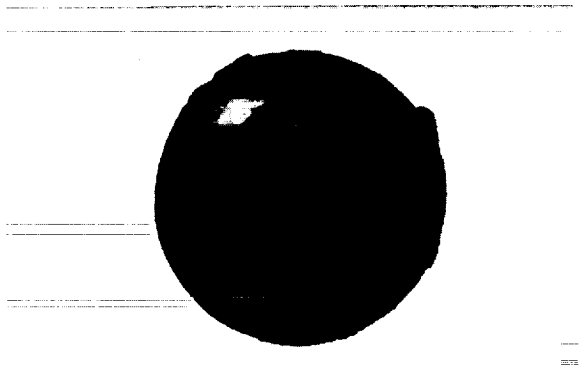

(i) Model 149

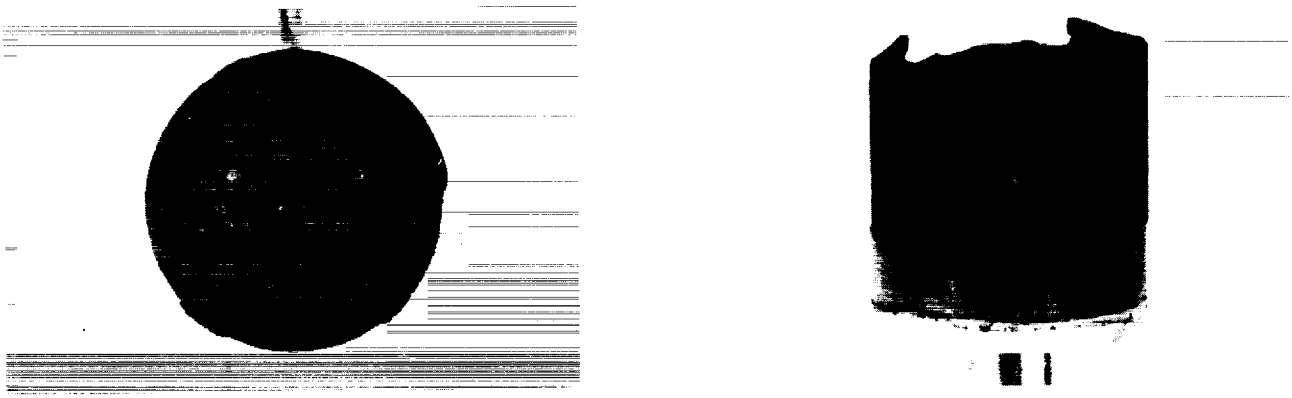

(j) Model 150

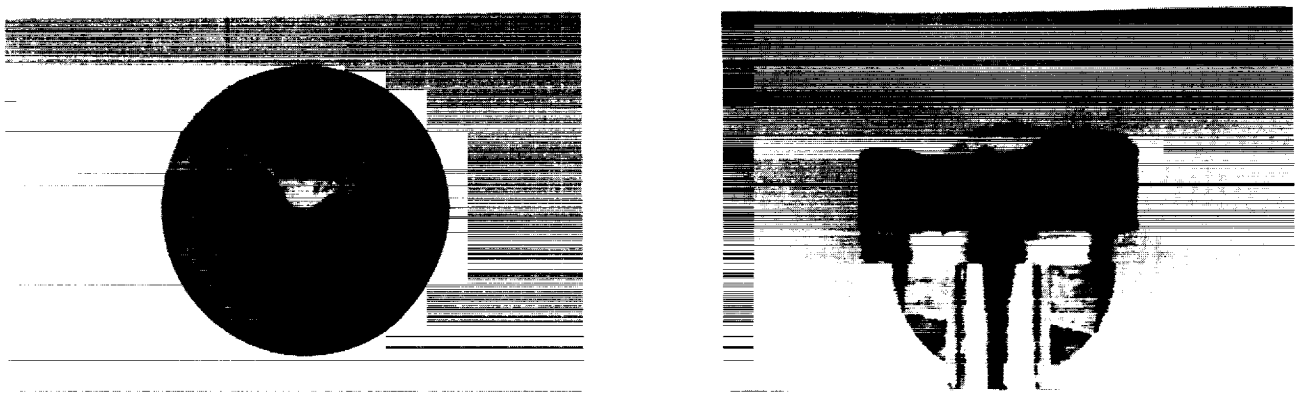

(k) Model 139

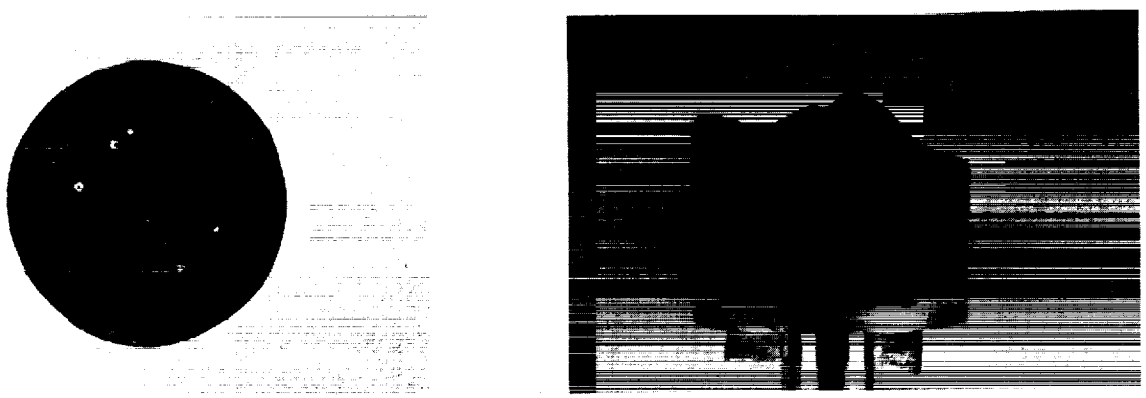

(l) Model 153

Figure 6-24 Continued.

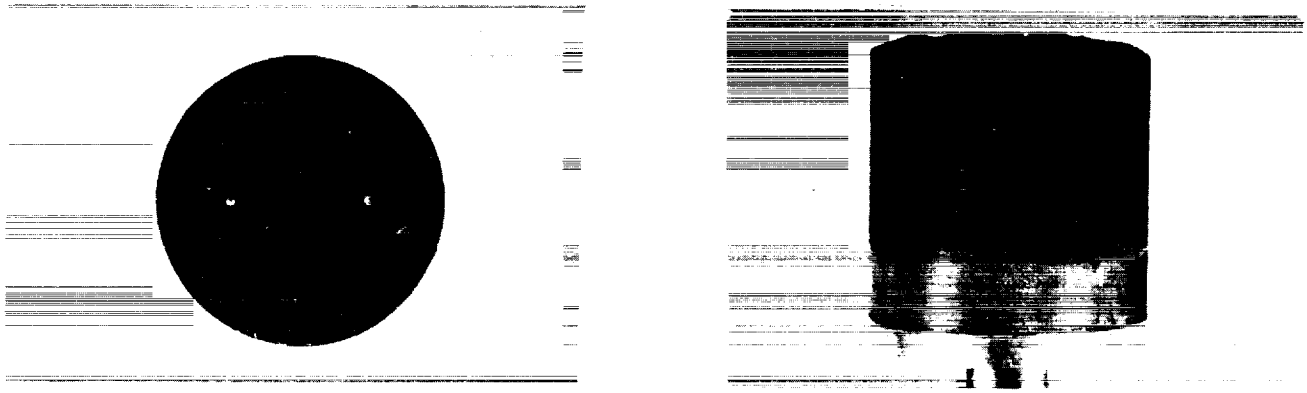

(m) Model 144

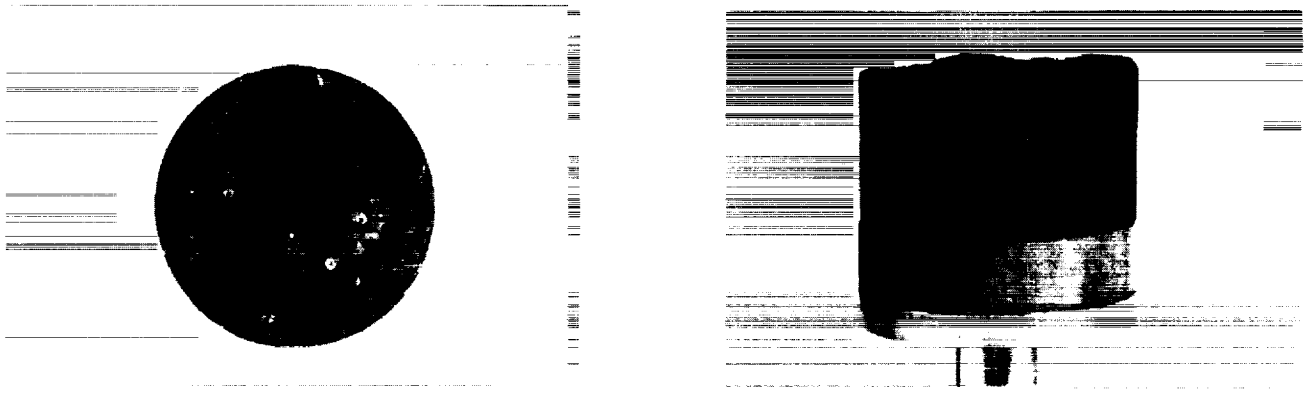

(n) Model 145

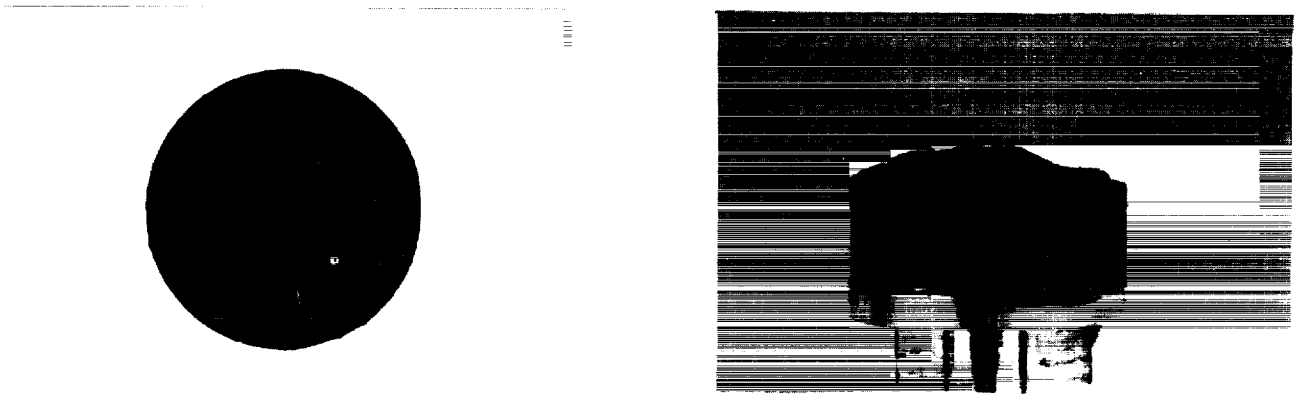

(o) Model 146

Figure 6-24 Continued.

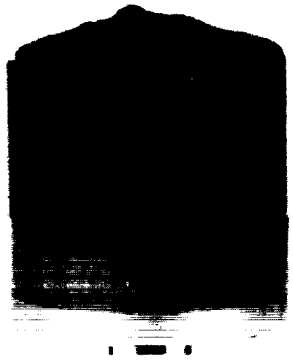

(p) Model 147

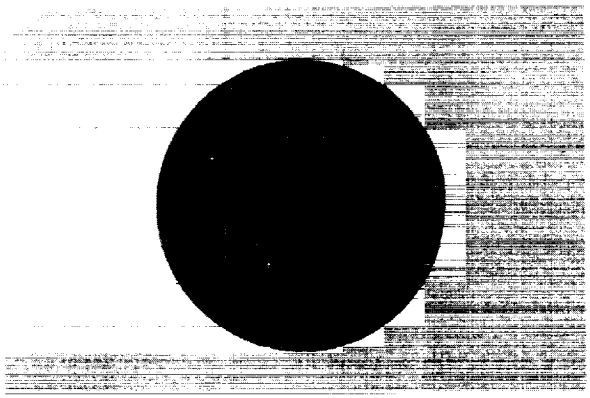

(q) Model 136

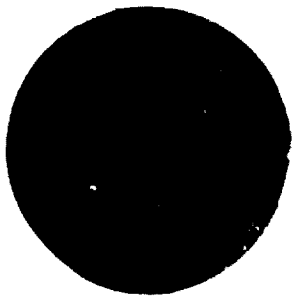

(r) Model 135

Figure 6-24 Continued.

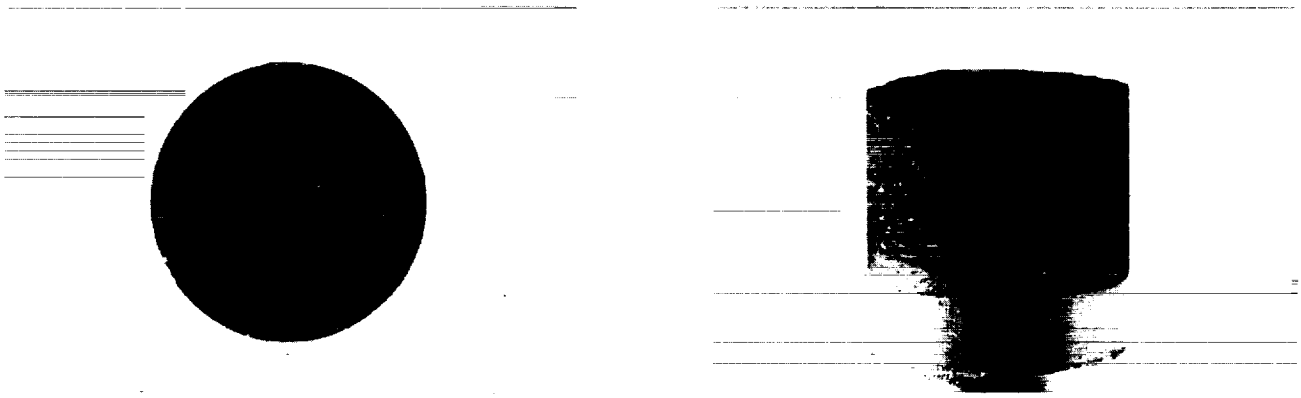

(s) Model 155

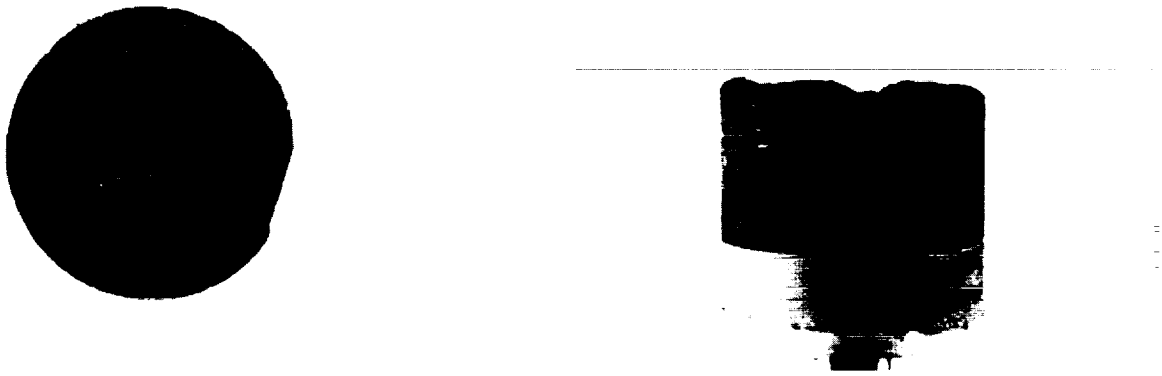

(t) Model 137

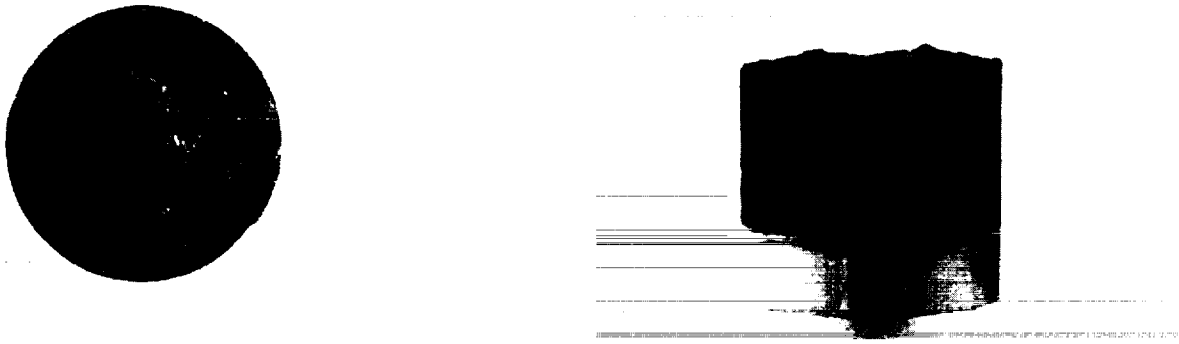

(u) Model 148

Figure 6-24 Continued.

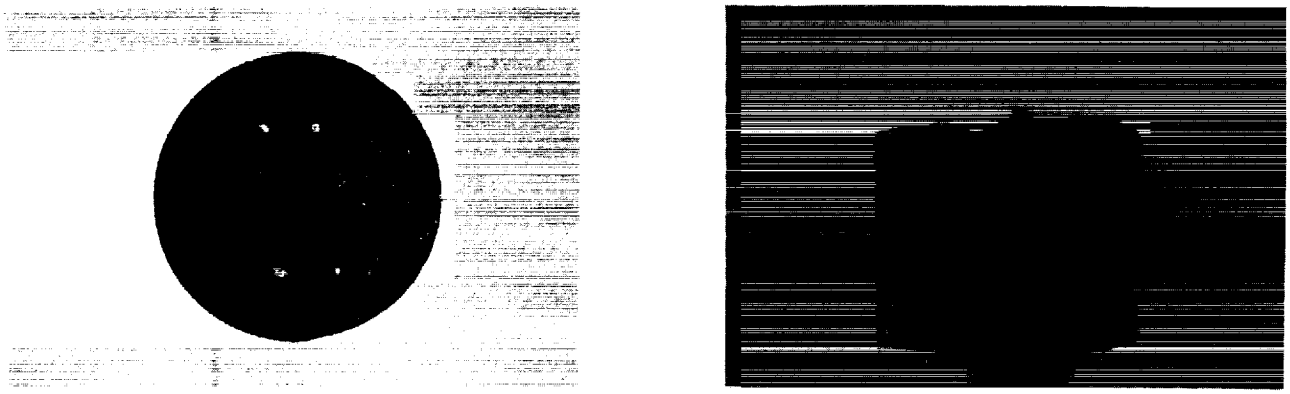

(u) Model 140

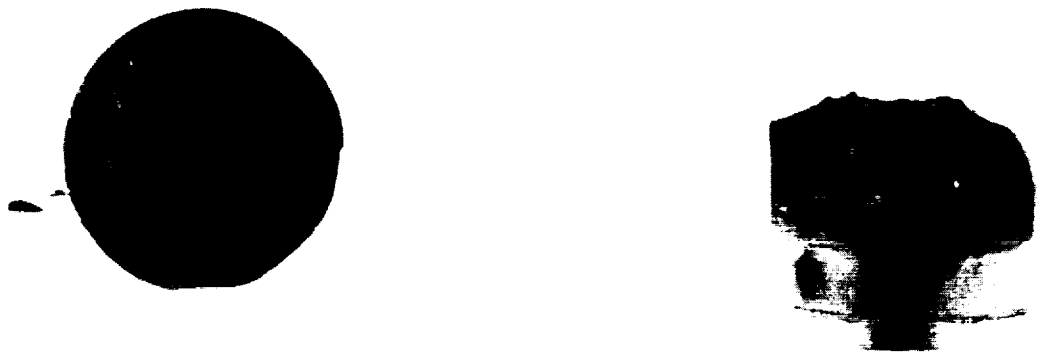

(w) Model 132

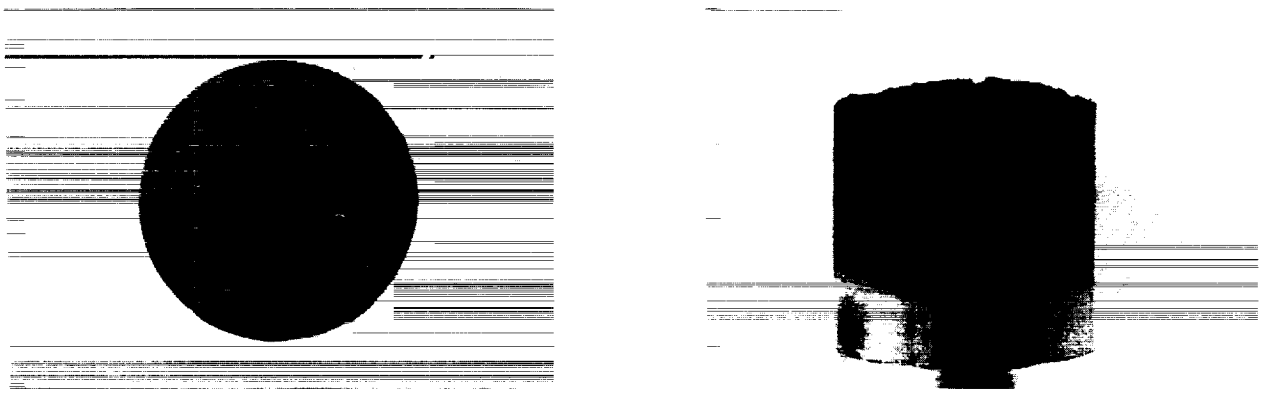

(x) Model 133

Figure 6-24 Continued.

(y) Model 142

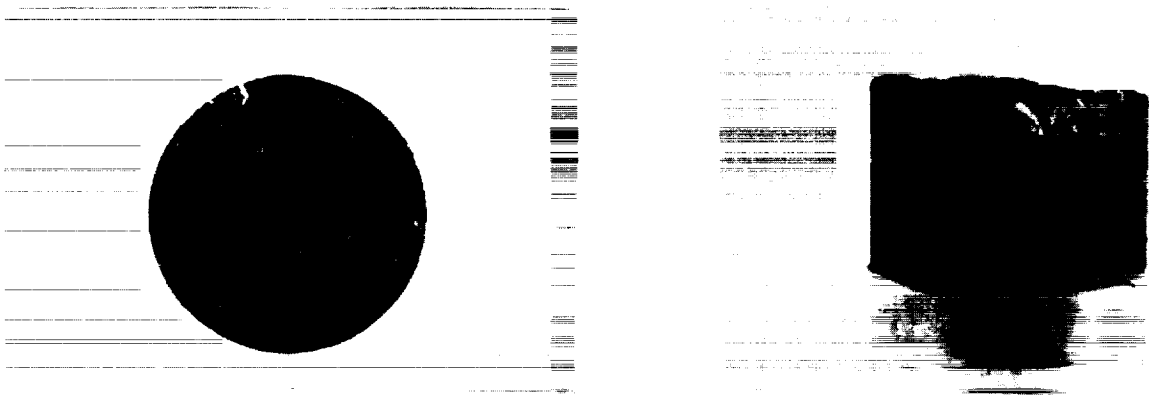

(z) Model 143

(aa) Model 141

Figure 6-24 Continued.

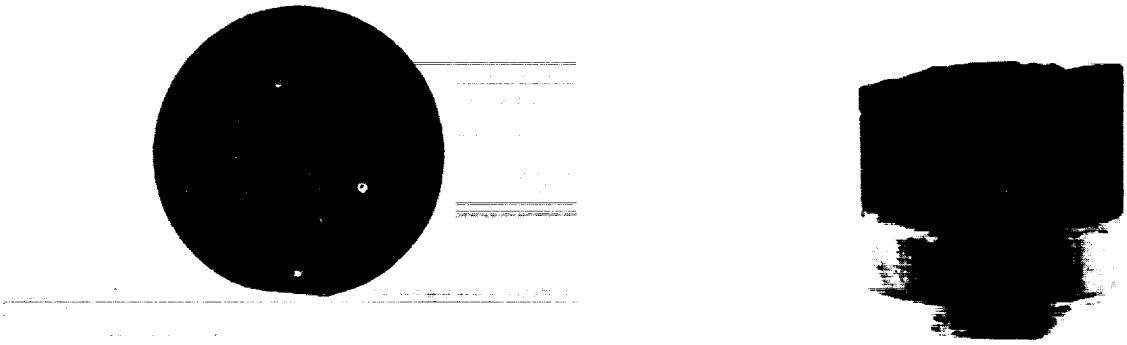

(bb) Model 130

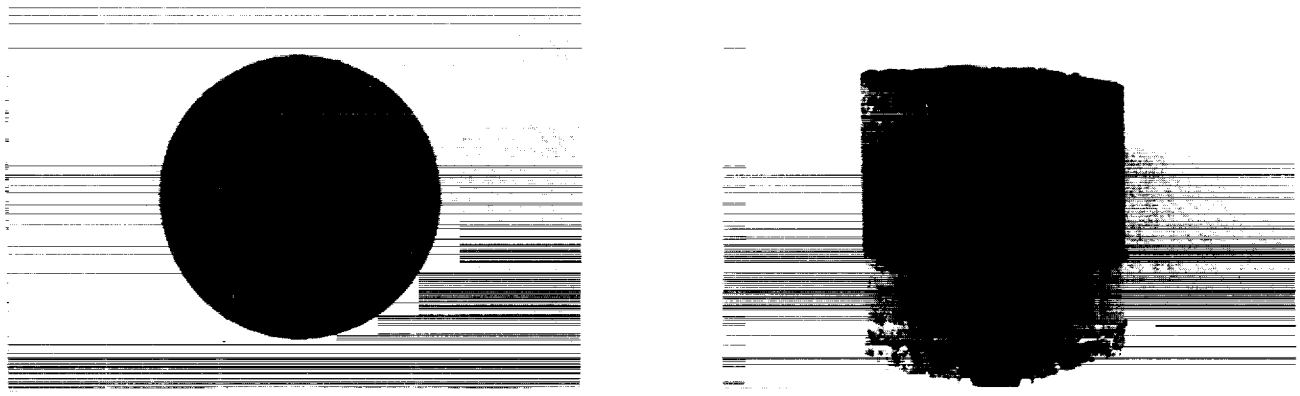

(cc) Model 131

Figure 6-24 Concluded.

(a) Model 93

(b) Model 95

(c) Model 94

Figure 6-25 Phase IV A Post Test Model Photographs.

(d) Model 89

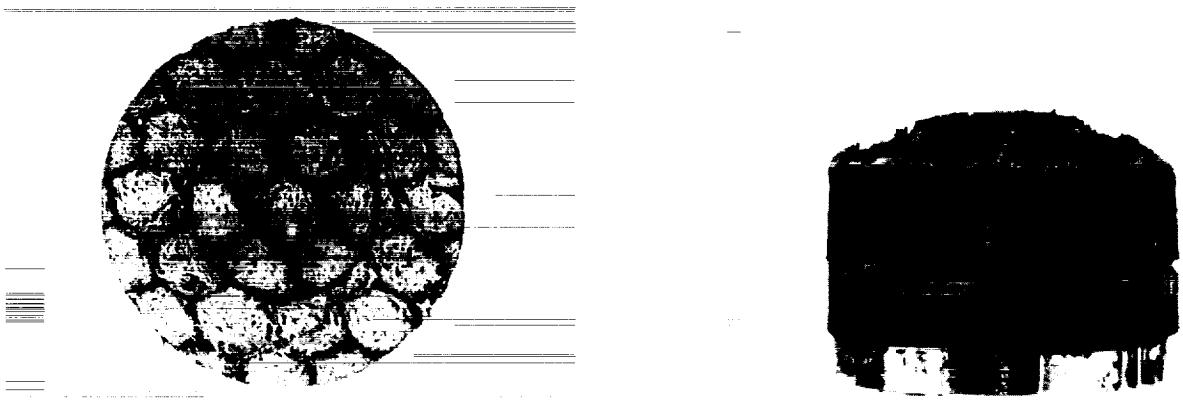

(e) Model 88

(f) Model 87

Figure 6-25 Continued.

(g) Model 92

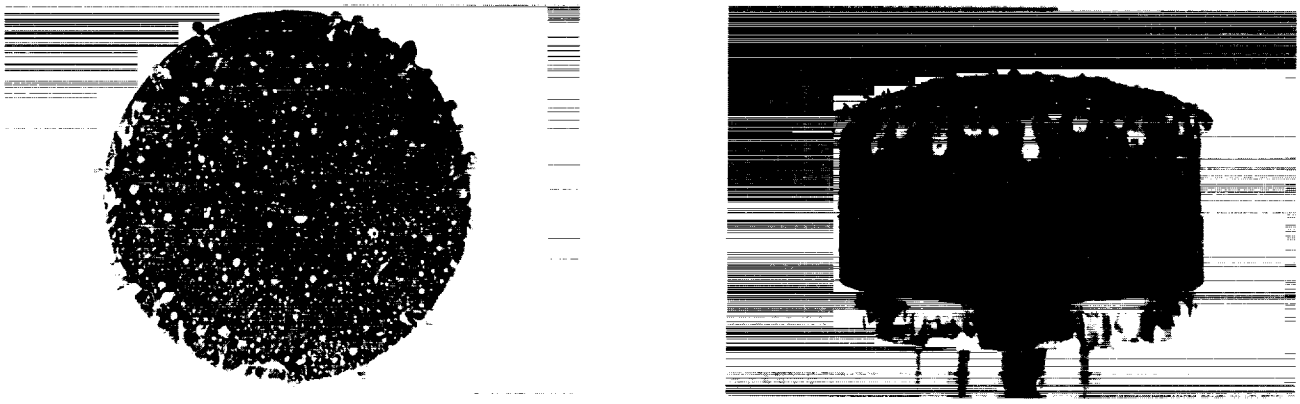

(h) Model 91

(i) Model 90

Figure 6-25 Continued.

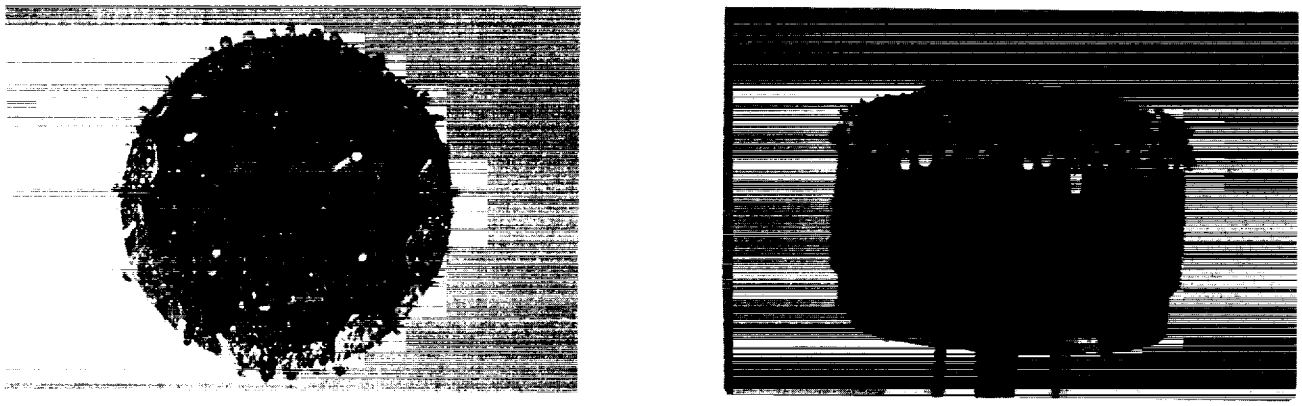

(j) Model 106

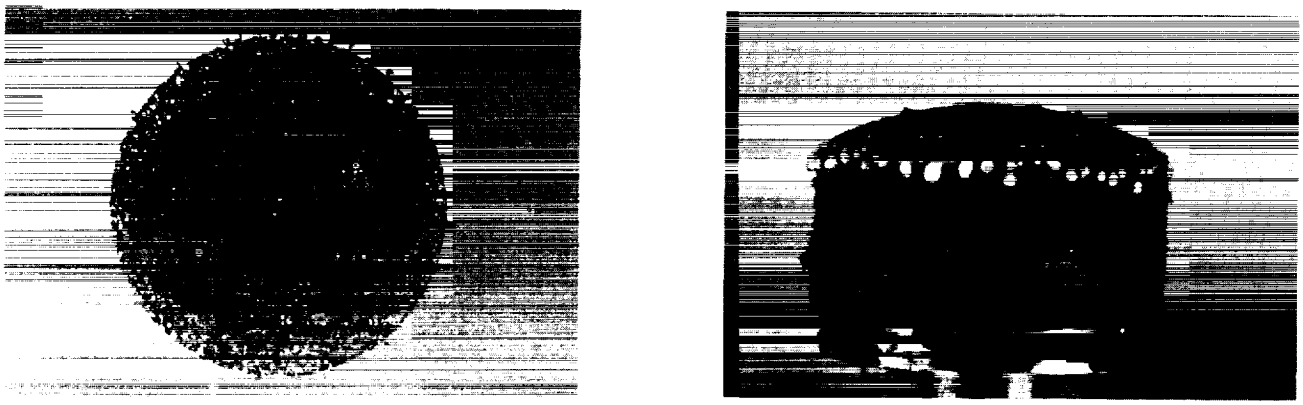

(k) Model 108

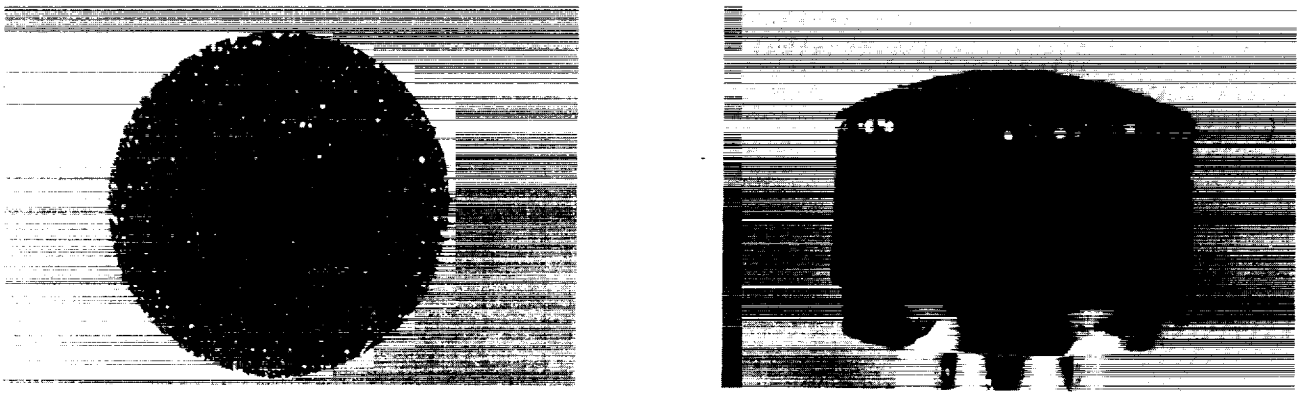

(l) Model 99

Figure 6-25 Continued.

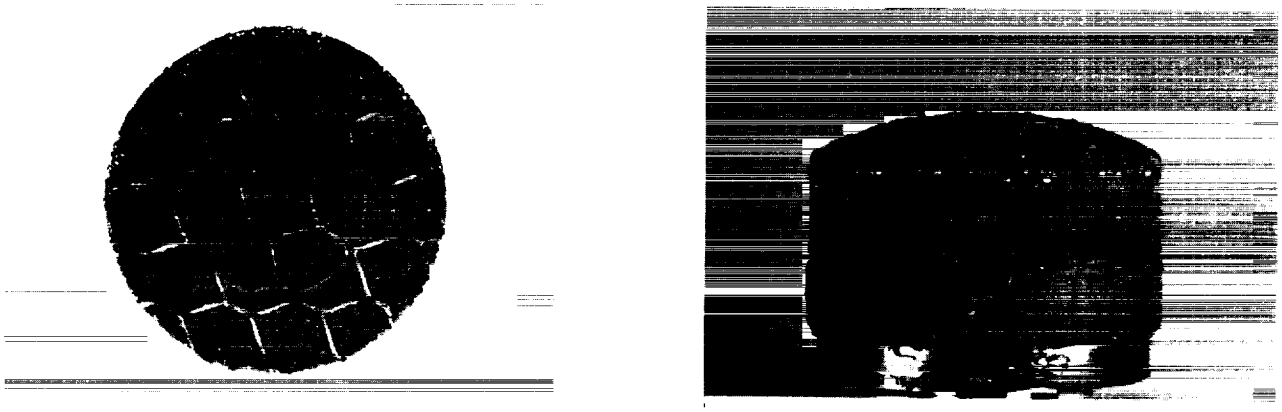

(m) Model 163

(n) Model 166

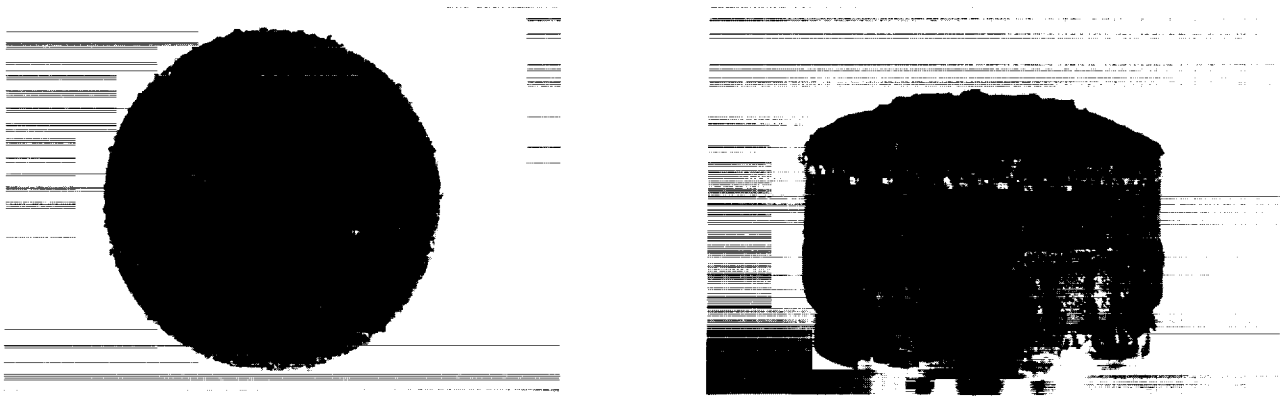

(o) Model 162

Figure 6-25 Continued.

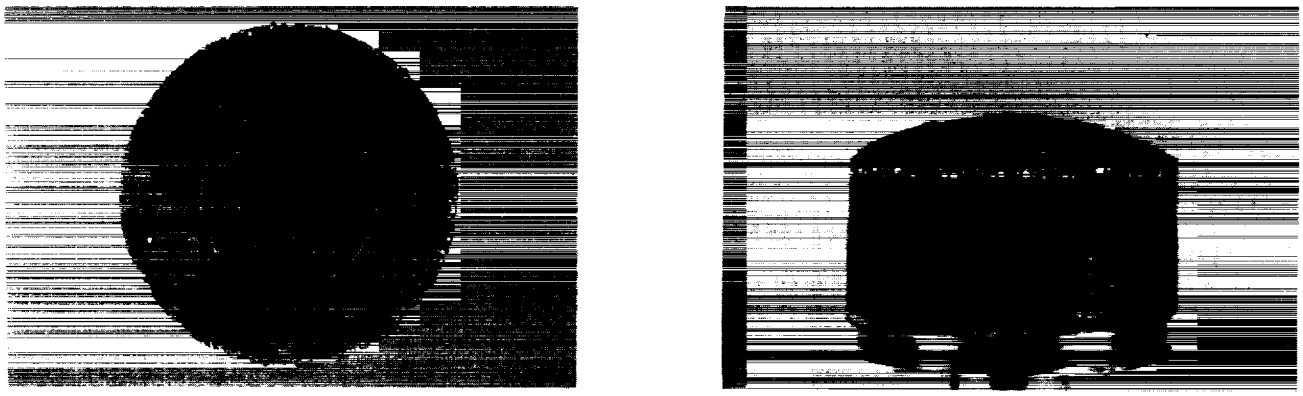

(p) Model 109

Figure 6-25 Concluded.

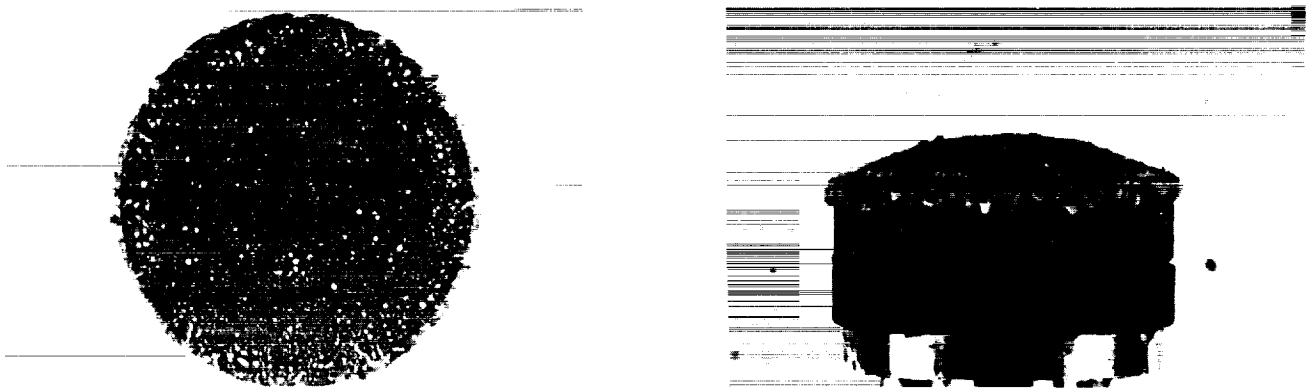

(a) Model 74

(b) Model 79

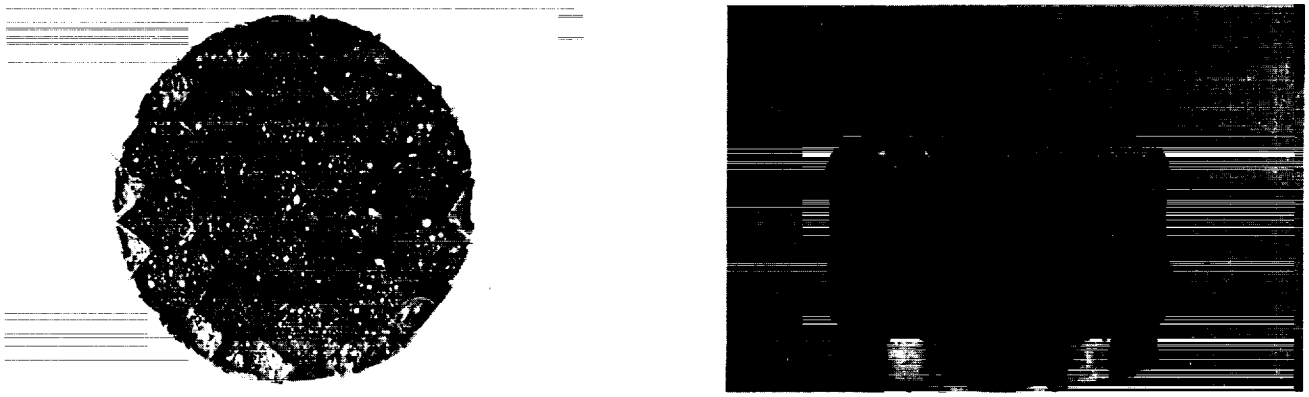

(c) Model 78

Figure 6-26 Phase IV B Post Test Model Photographs.

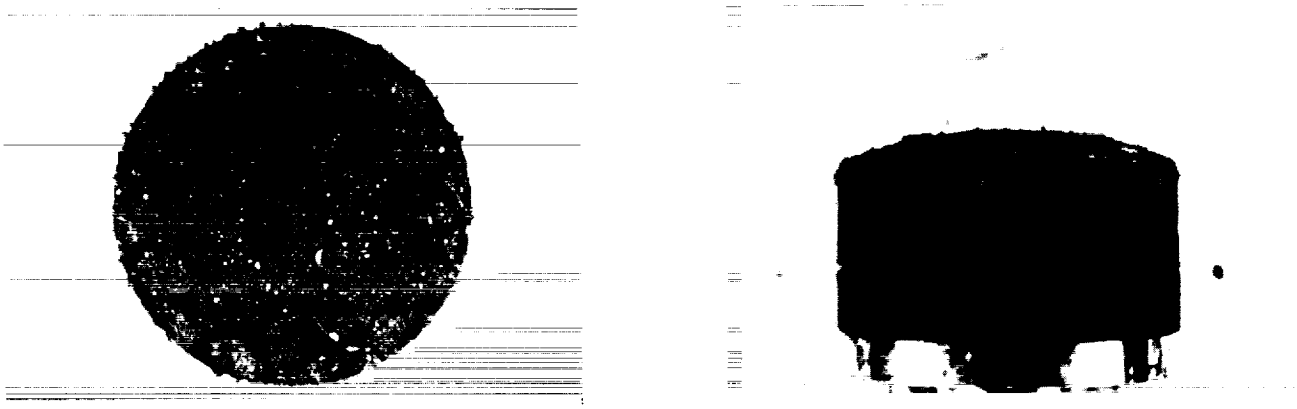

(d) Model 77

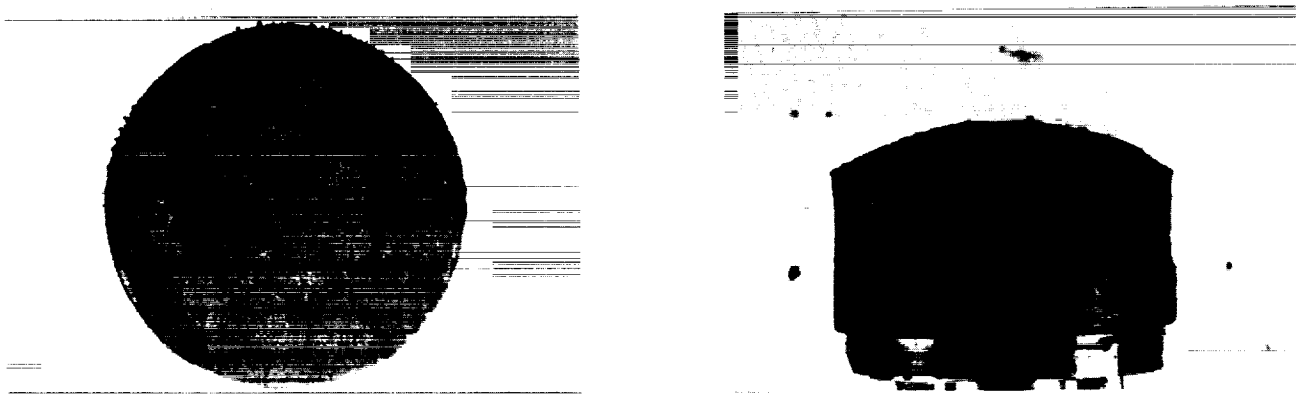

(e) Model 23

(f) Model 76

Figure 6-26 Continued.

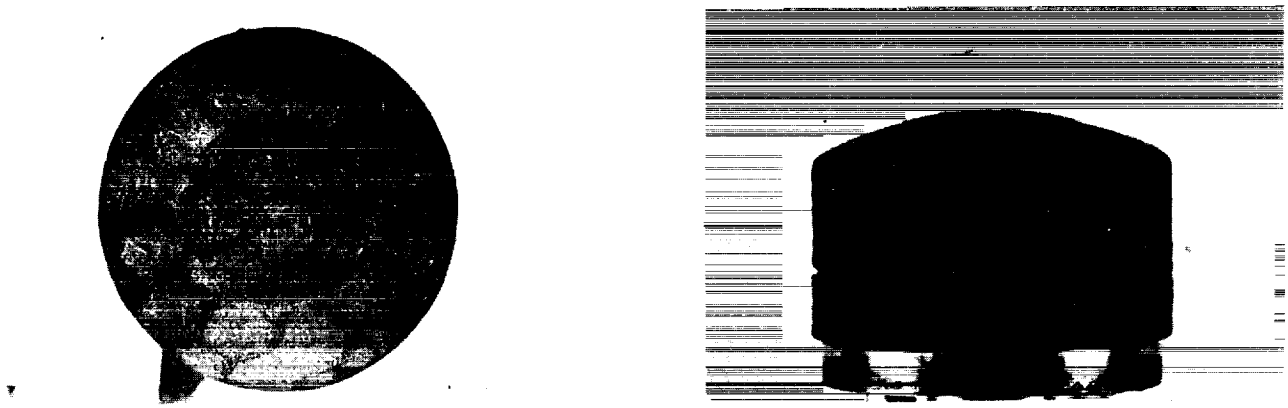

(g) Model 84

(h) Model 85

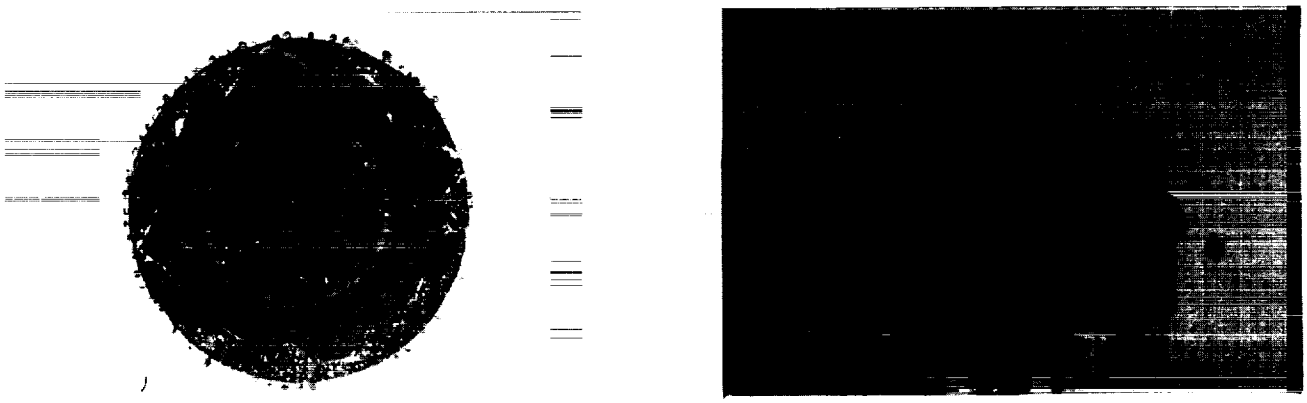

(i) Model 75

Figure 6-26 Continued.

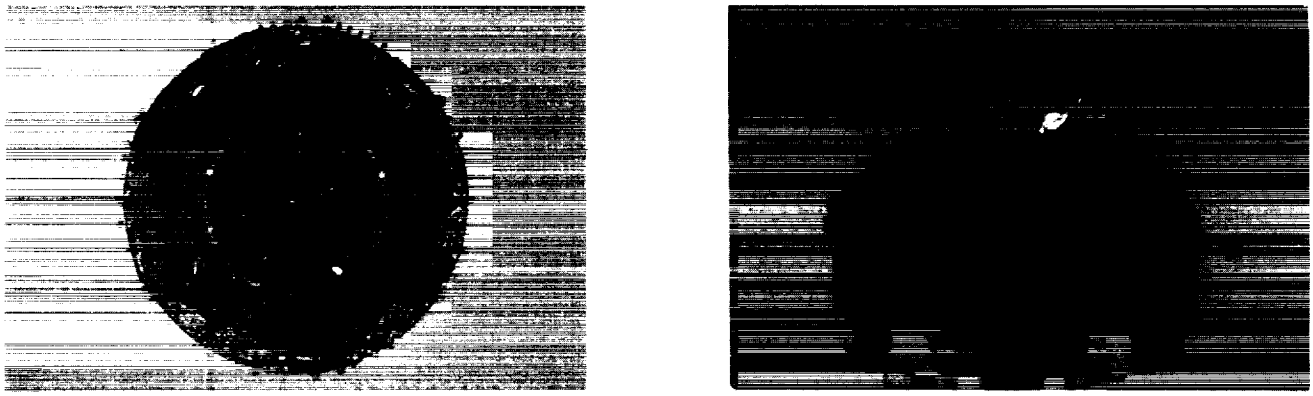

(j) Model 81

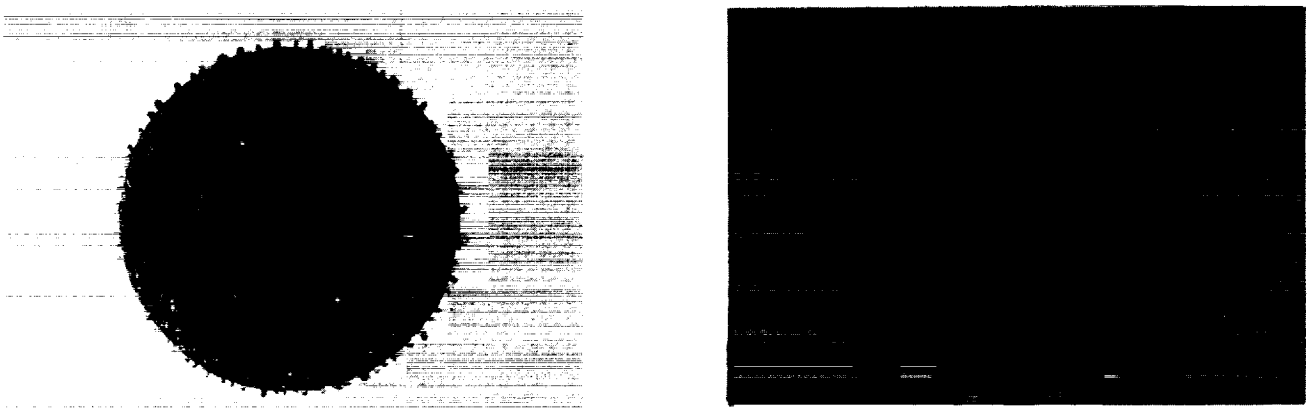

(k) Model 83

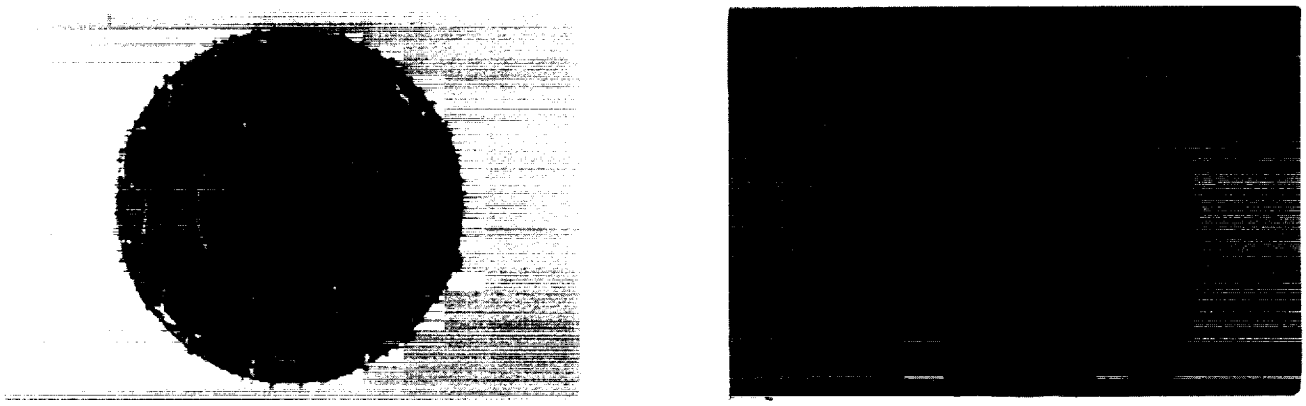

(l) Model 82

Figure 6-26 Continued.

(m) Model 80

(n) Model 24)

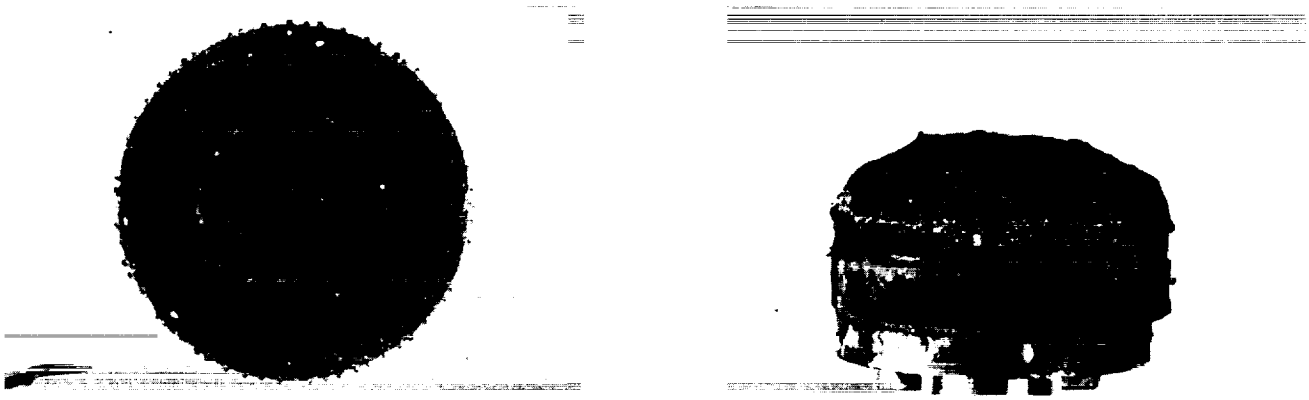

(o) Model 101

Figure6-26 Continued.

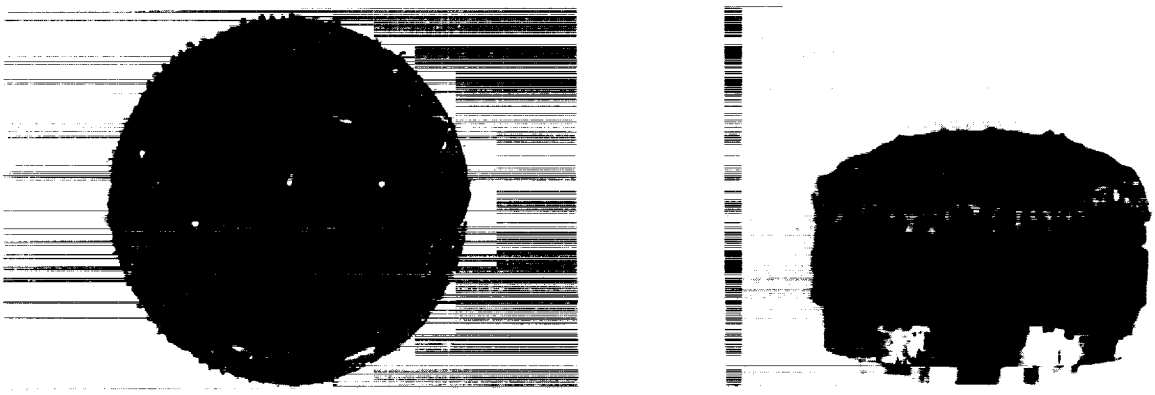

(p) Model 104

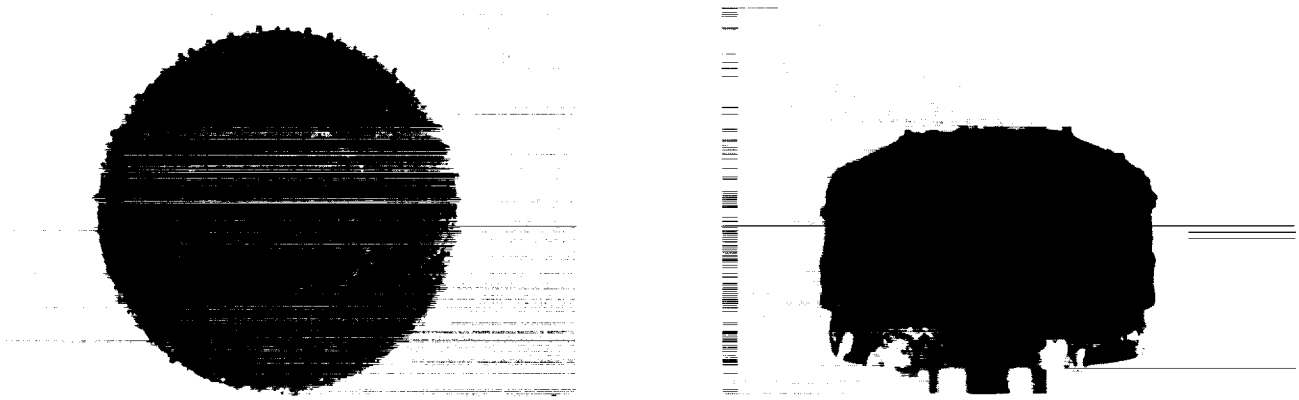

(q) Model 98

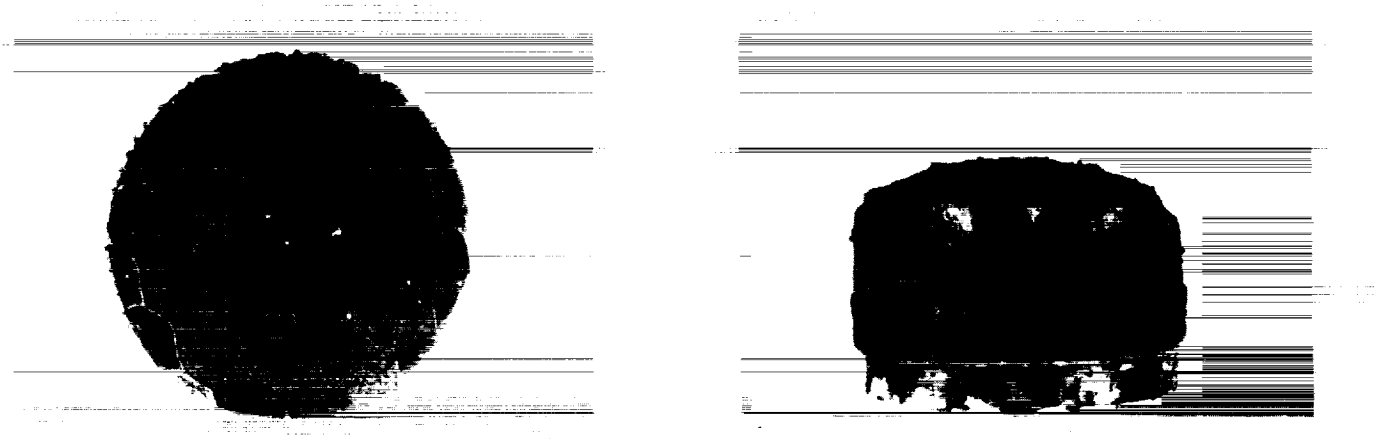

(r) Model 107

Figure 6-26 Continued.

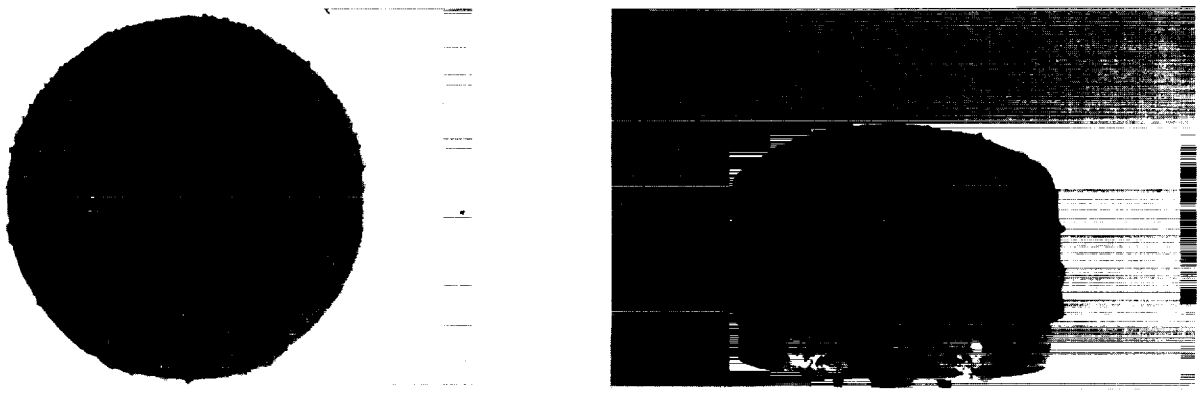

(s) Model 105

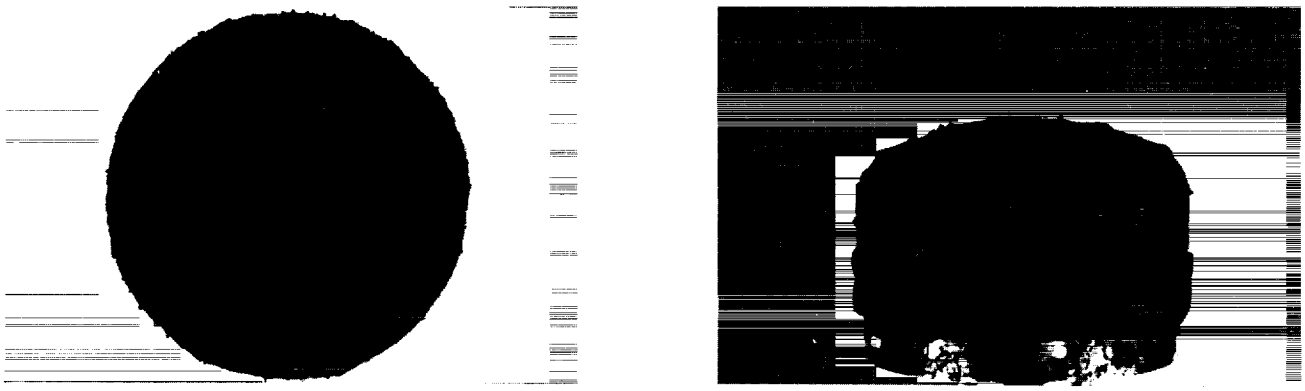

(t) Model 103

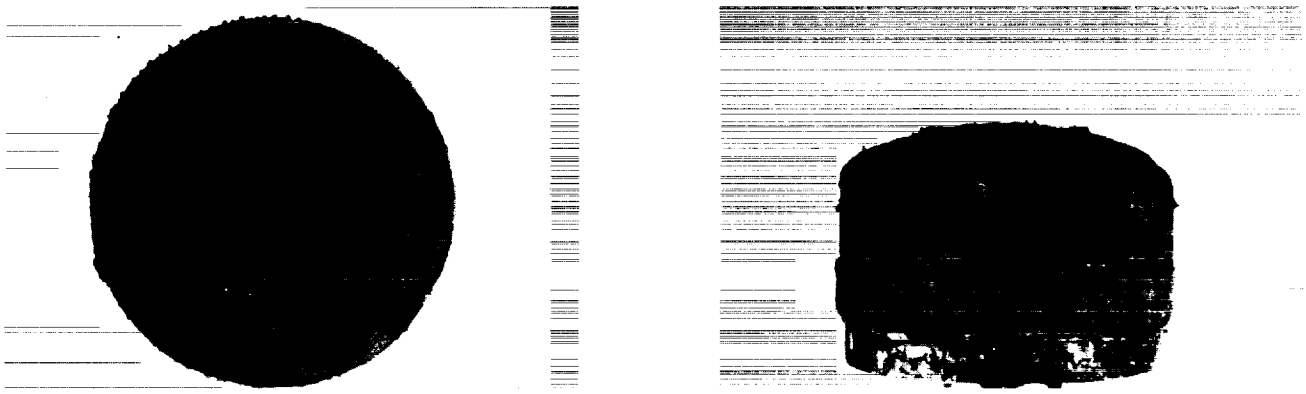

(u) Model 161

Figure 6-26 Continued.

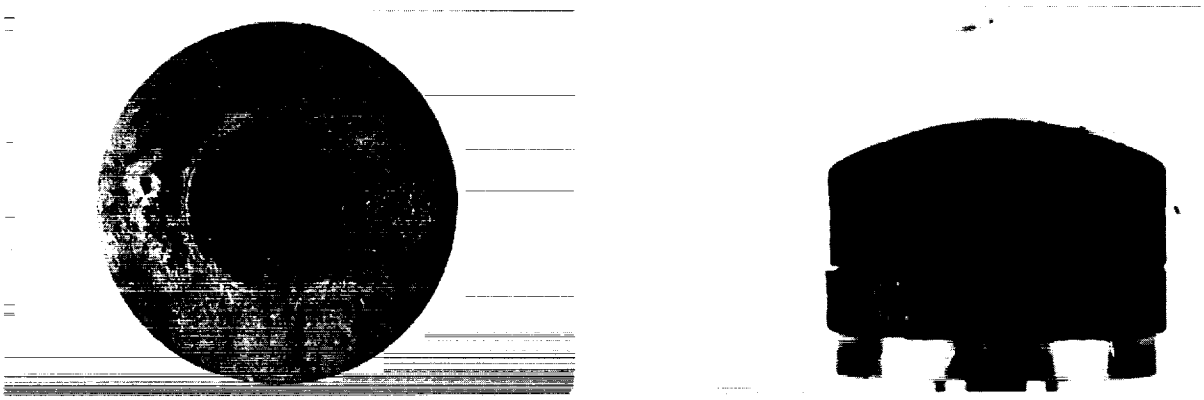

(v) Model 86

Figure 6-26 Concluded

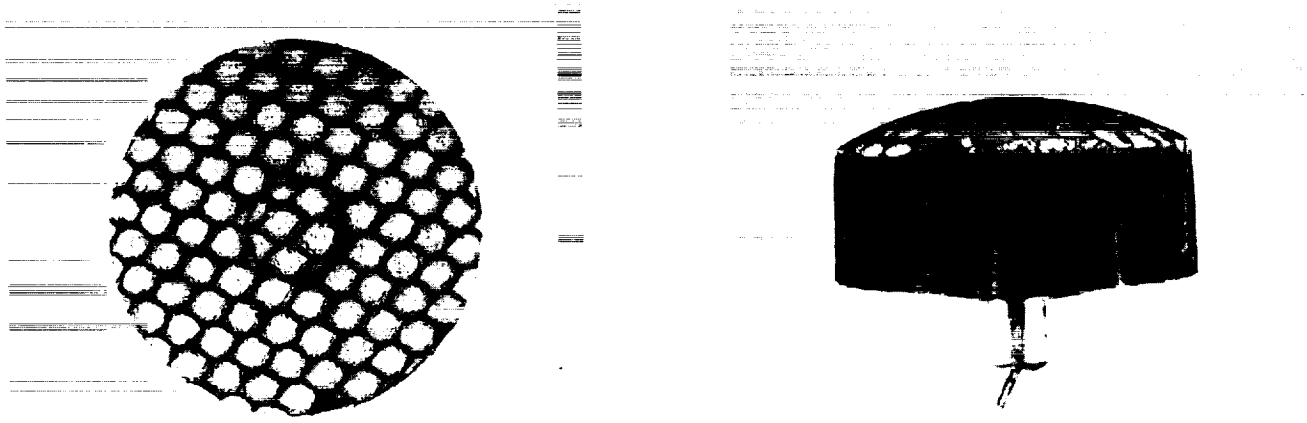

(a) Model 114

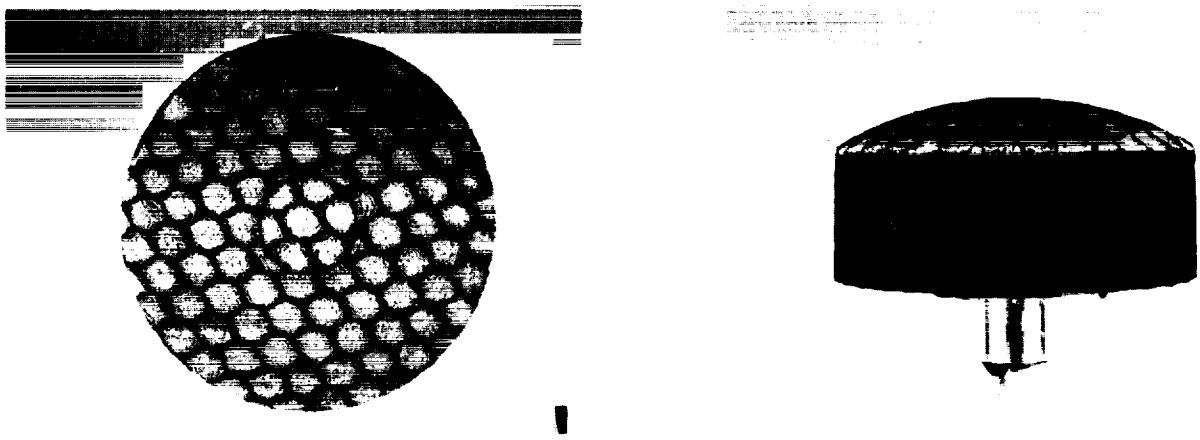

(b) Model 115

(c) Model 116

Figure 6-27 Phase V Post Test Model Photographs

(d) Model 128

(e) Model 127

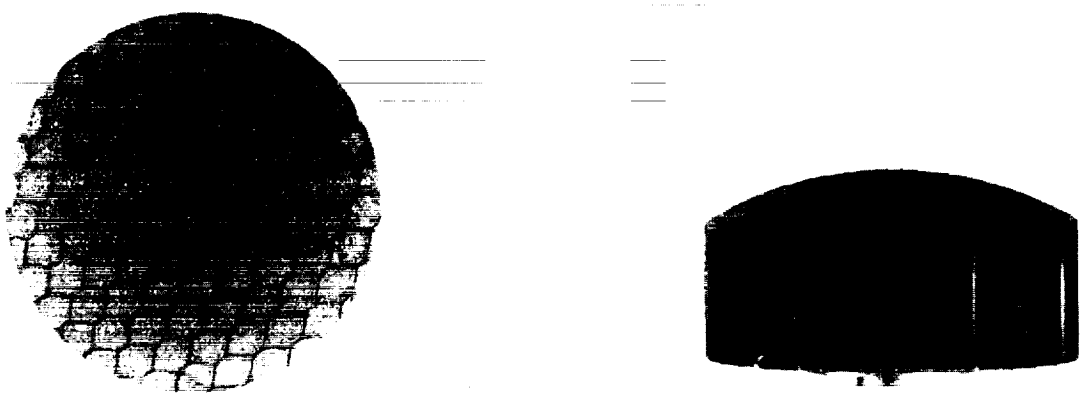

(f) Model 126

Figure 6-27 Continued.

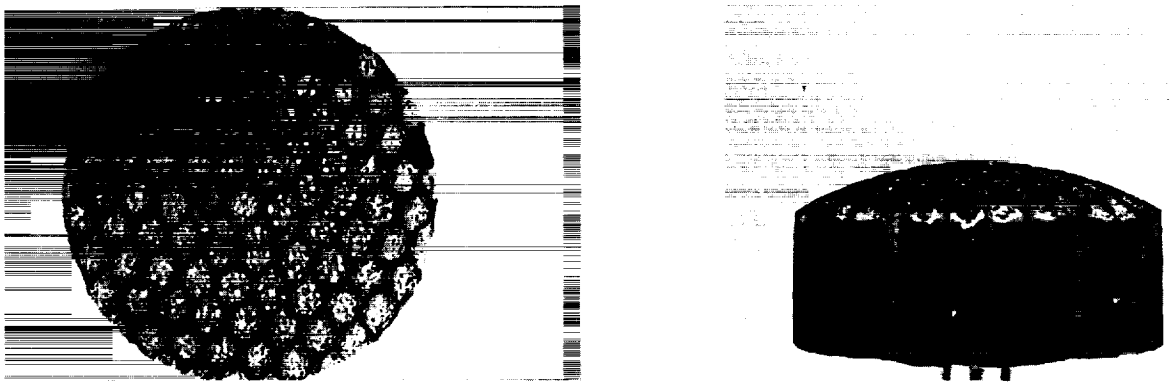

(g) Model 120

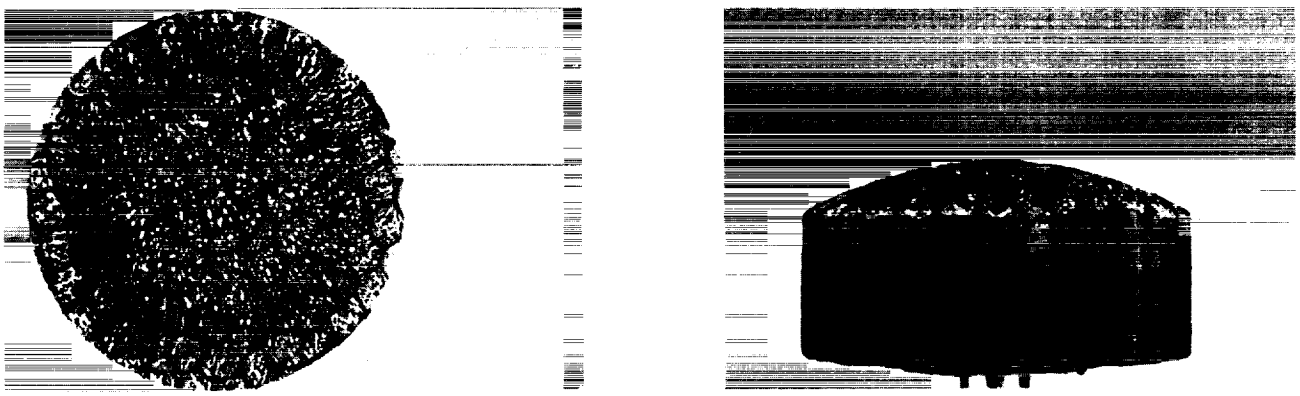

(h) Model 118

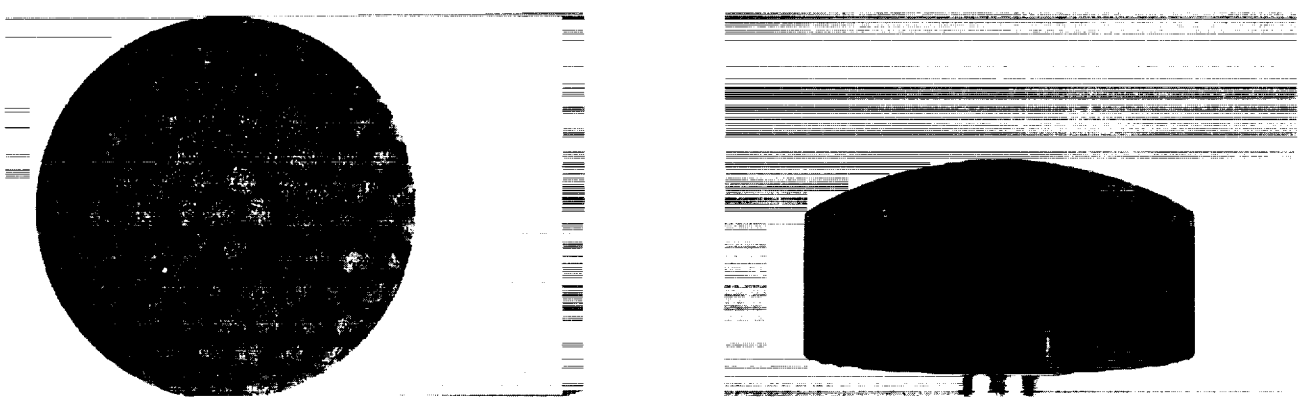

(i) Model 117

Figure 6-27 Continued.

(j) Model 122

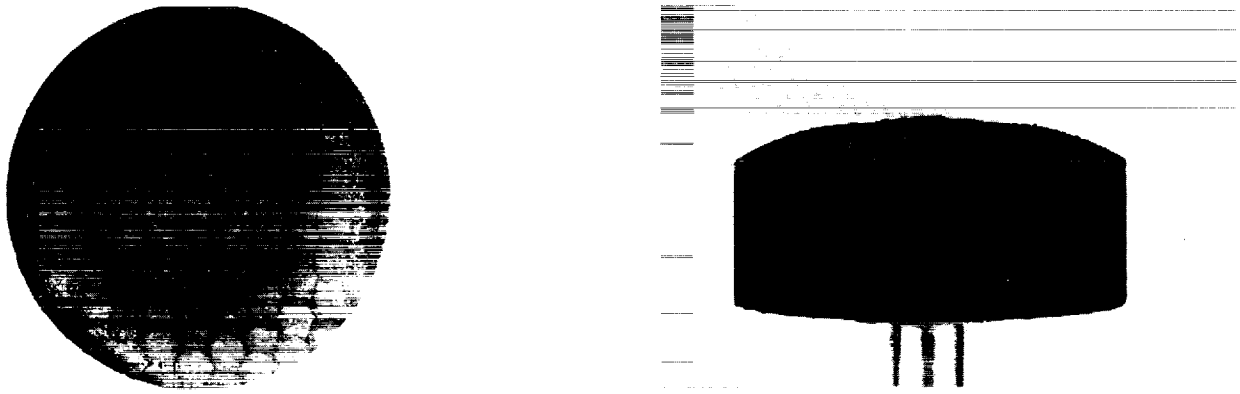

(k) Model 121

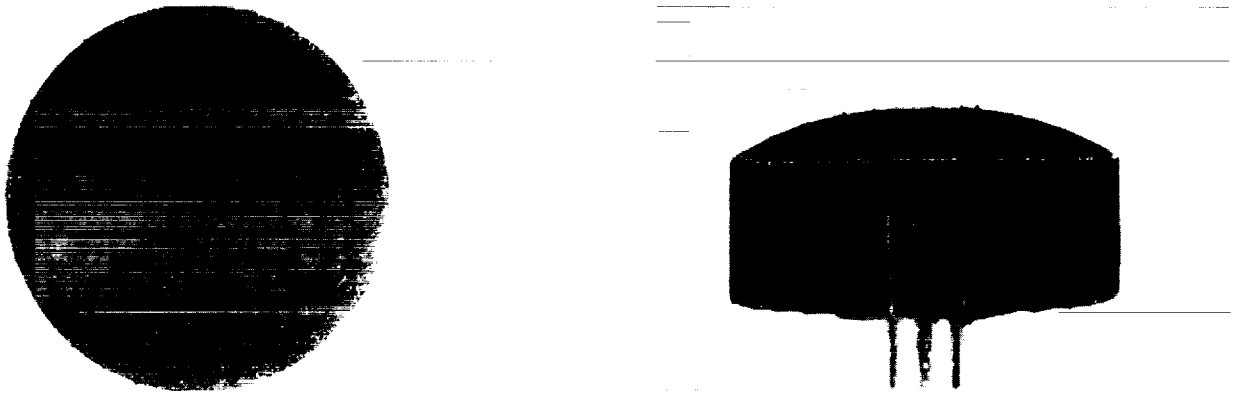

(l) Model 119

Figure 6-27 Continued.

(m) Model 123

(n) Model 125

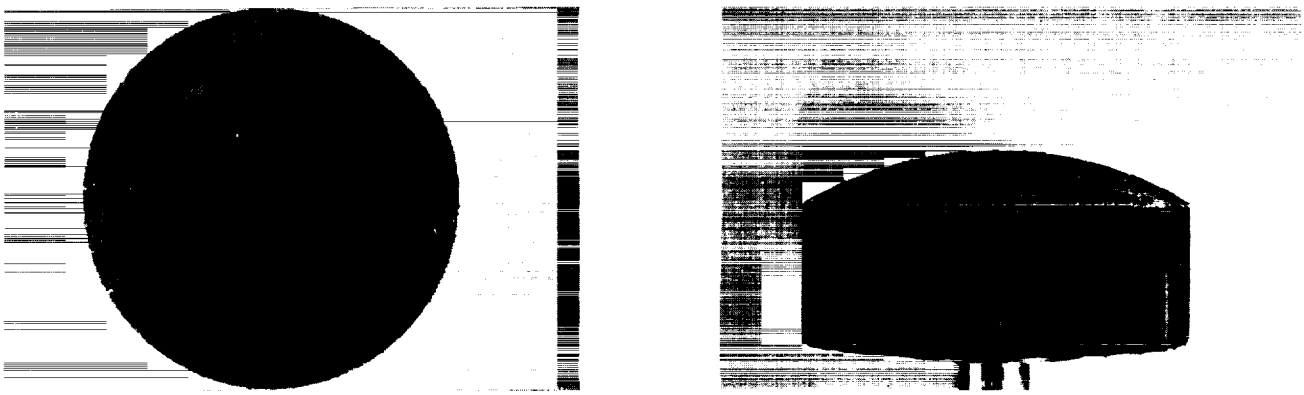

(o) Model 124

Figure 6-27 Concluded

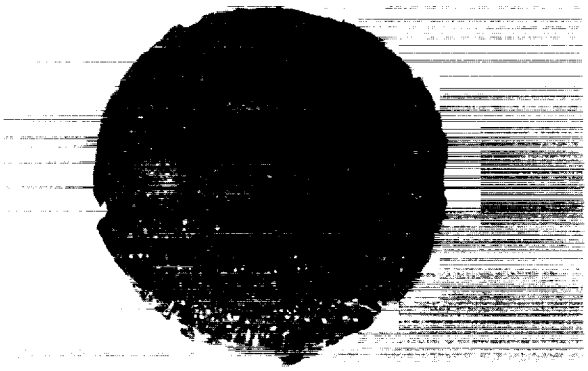

(a) Model 30

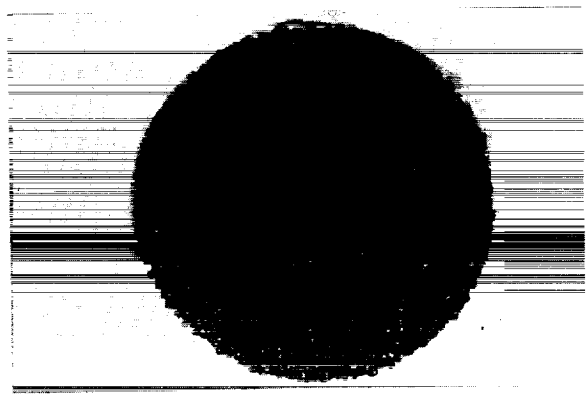

(b) Model 25

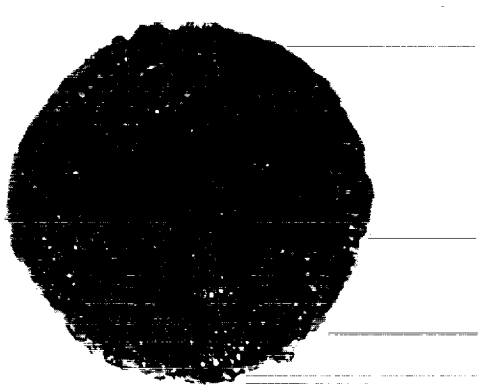

(c) Model 19

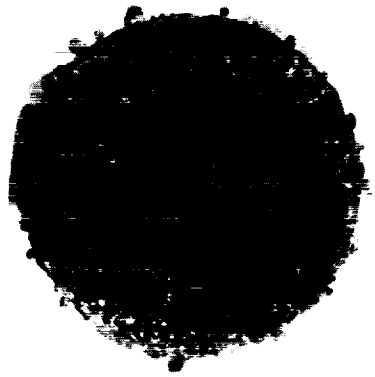

(d) Model 33

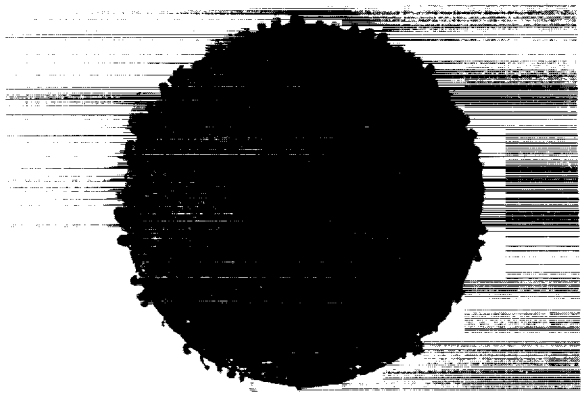

(e) Model 28

(f) Model 29

Figure 6-28 Phase VI A Post Test Model Photographs.

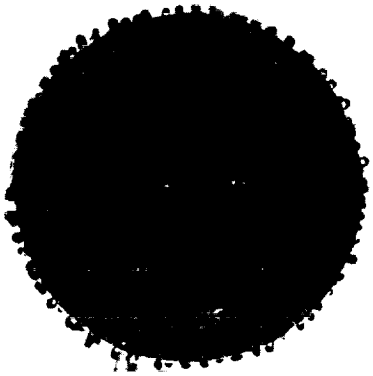

(g) Model 17

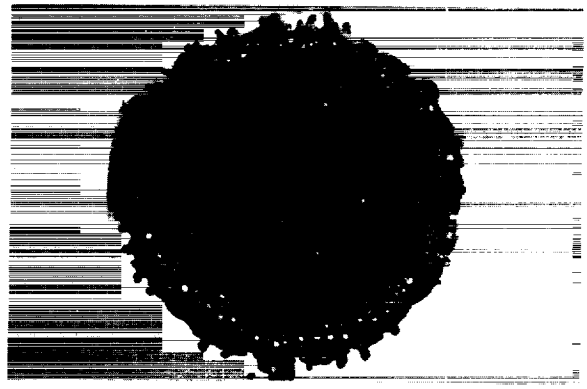

(h) Model 35

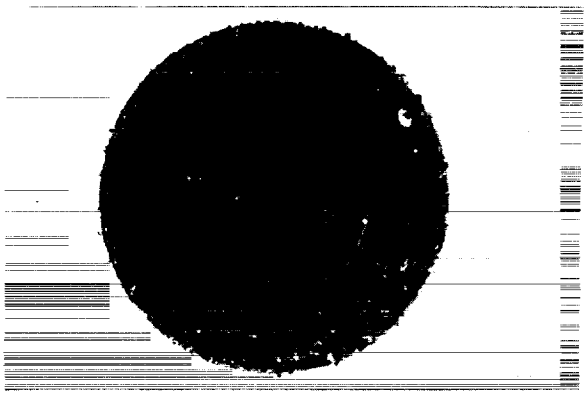

(i) Model 100

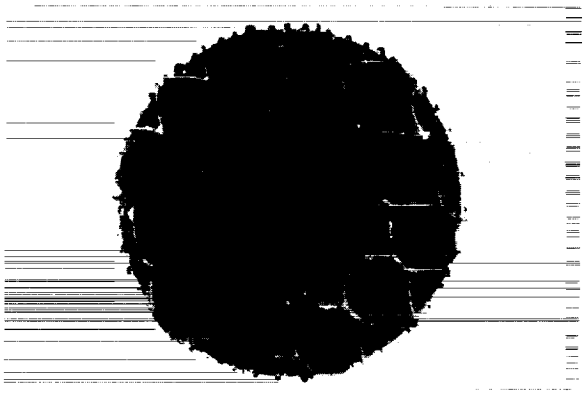

(j) Model 165

Figure 6-28 Continued.

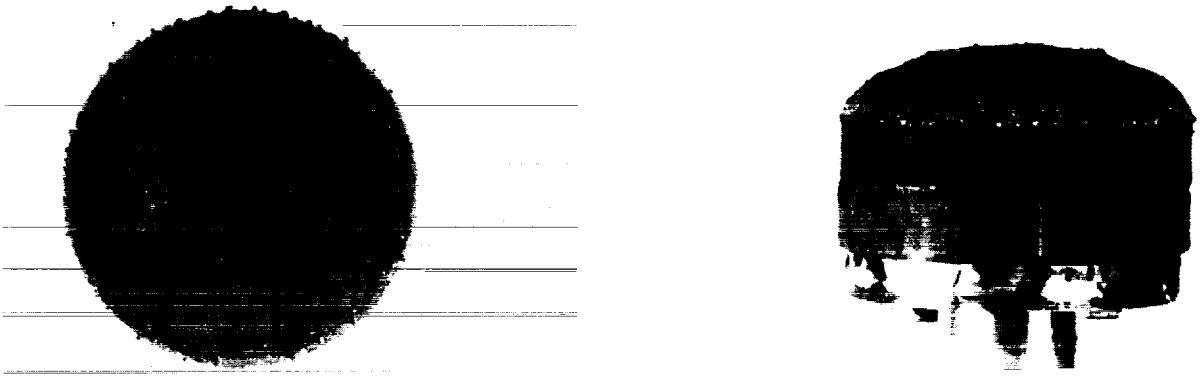

(k) Model 164

(l) Model 21

(m) Model 20

Figure 6-28 Continued.

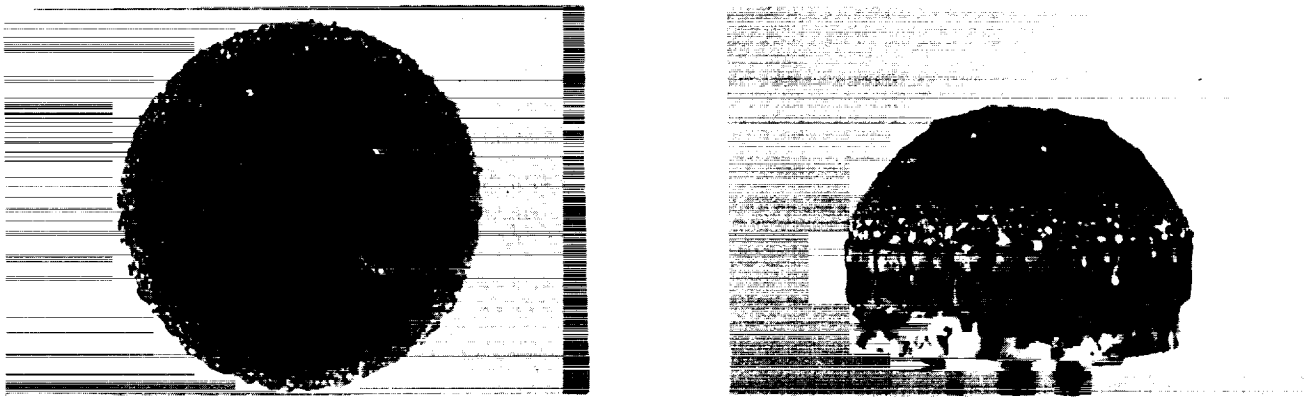

(n) Model 159

Figure 6-28 Concluded.

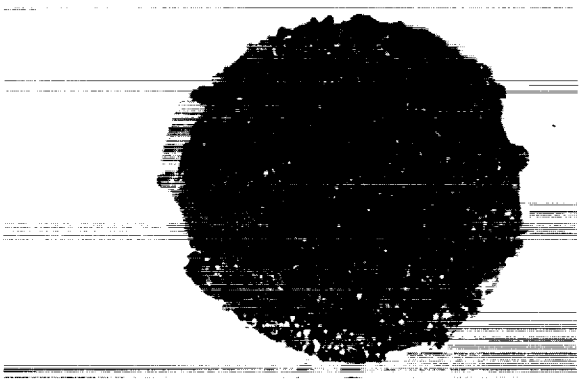

(a) Model 26

(b) Model 22

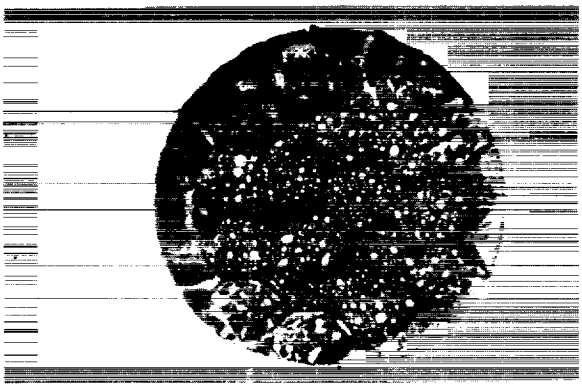

(c) Model 34

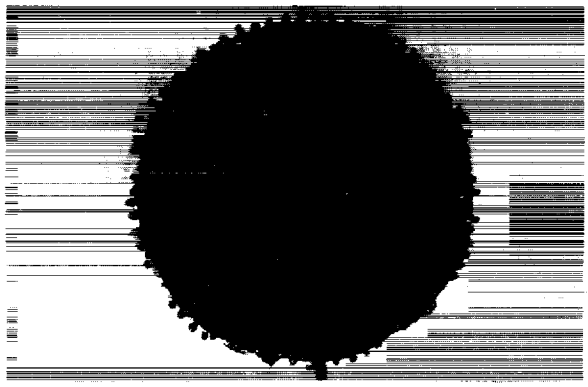

(d) Model 27

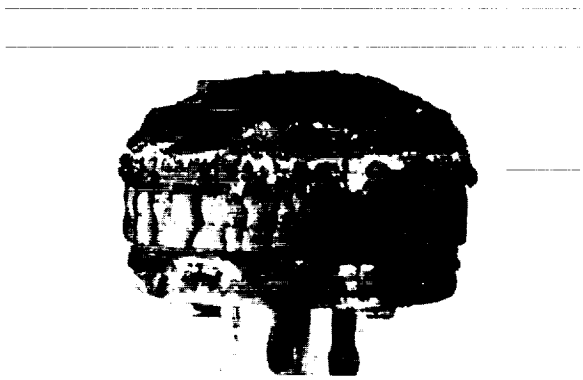

(e) Model 16

Figure 6-29 Phase IV B Post Test Model Photographs.

(f) Model 36

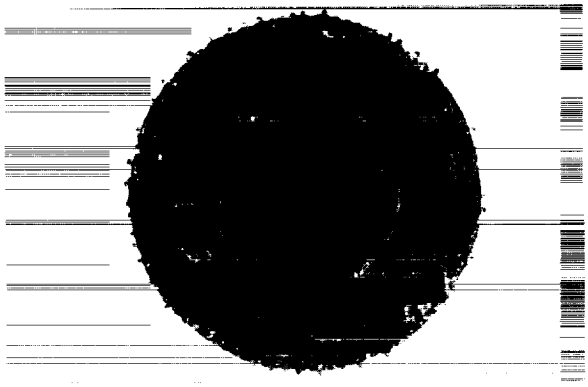

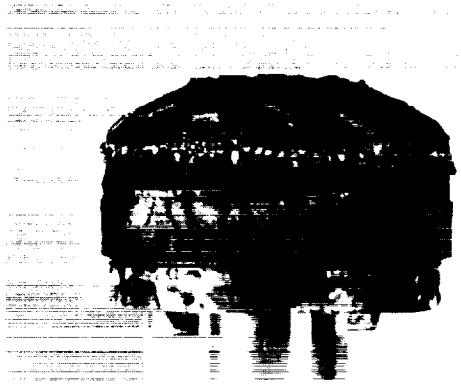

(g) Model 102

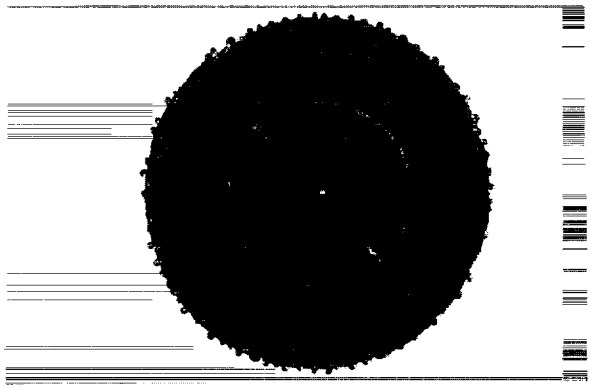

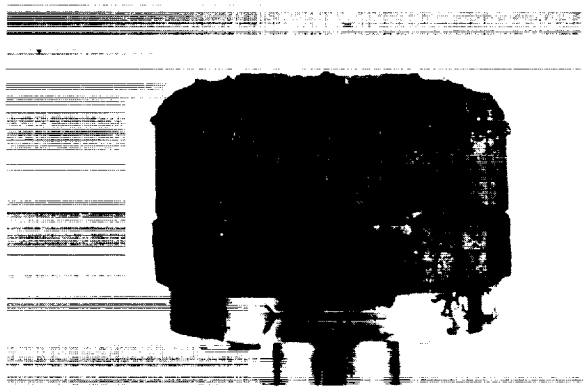

(h) Model 18

Figure 6-29 Continued

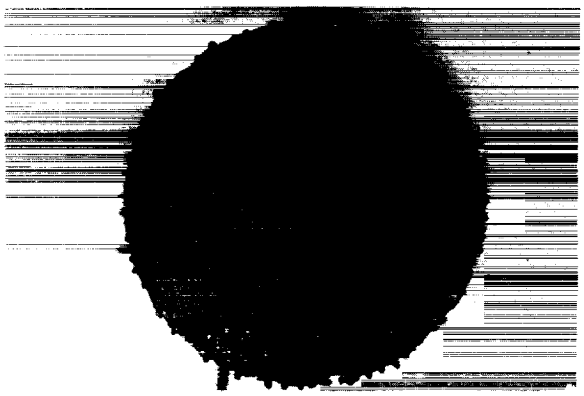

(i) Model 32

Figure 6-29 Concluded

(a) Model 96

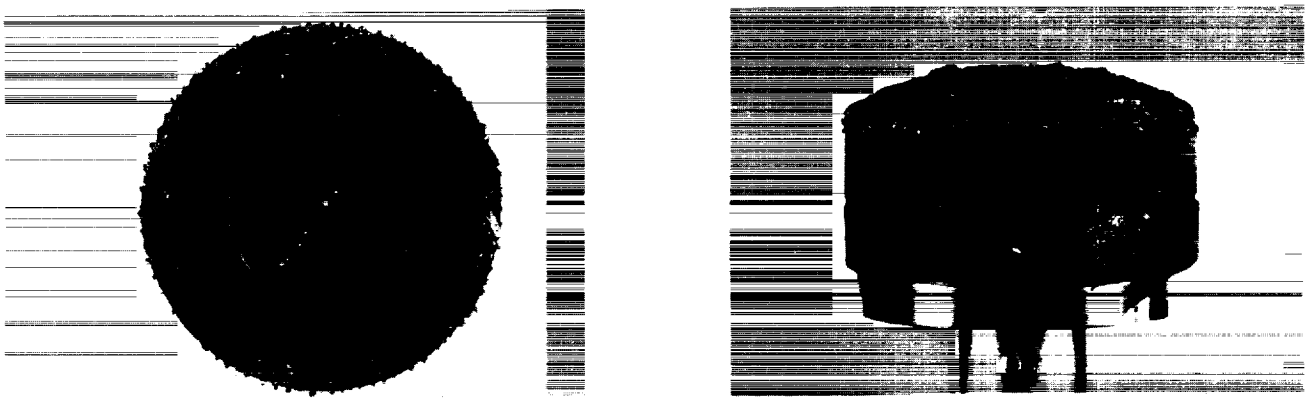

(b) Model 97

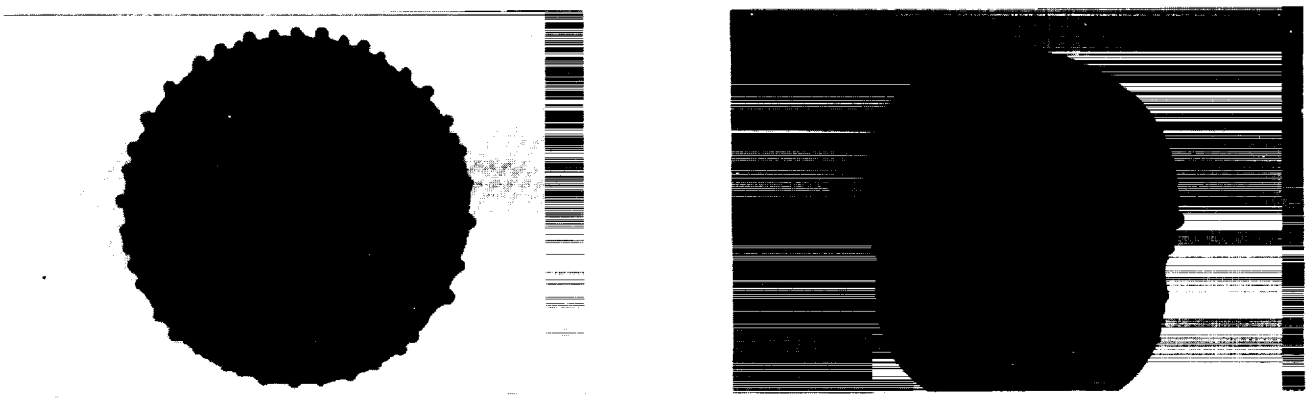

(c) Model 111

Figure 6-30 Phase VII Post Test Model Photographs.

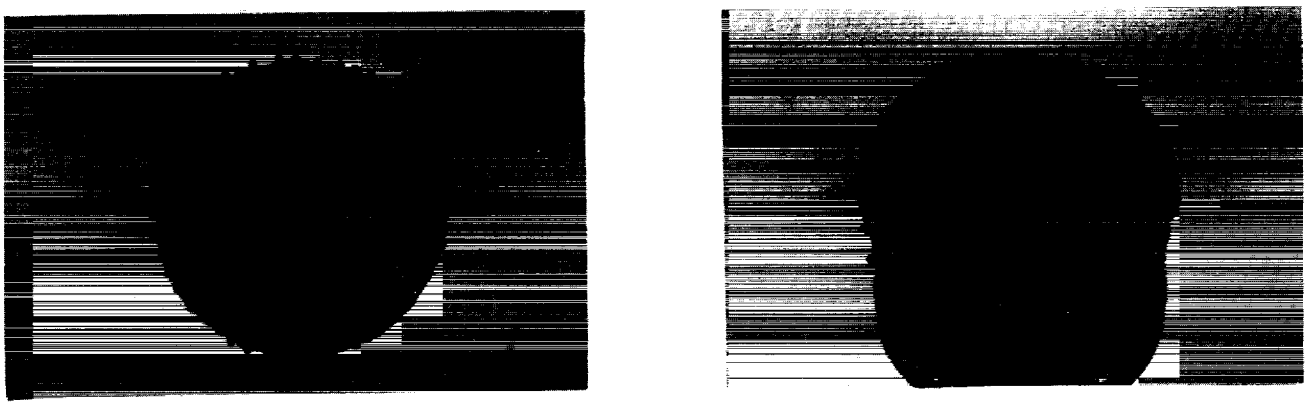

(d) Model 112

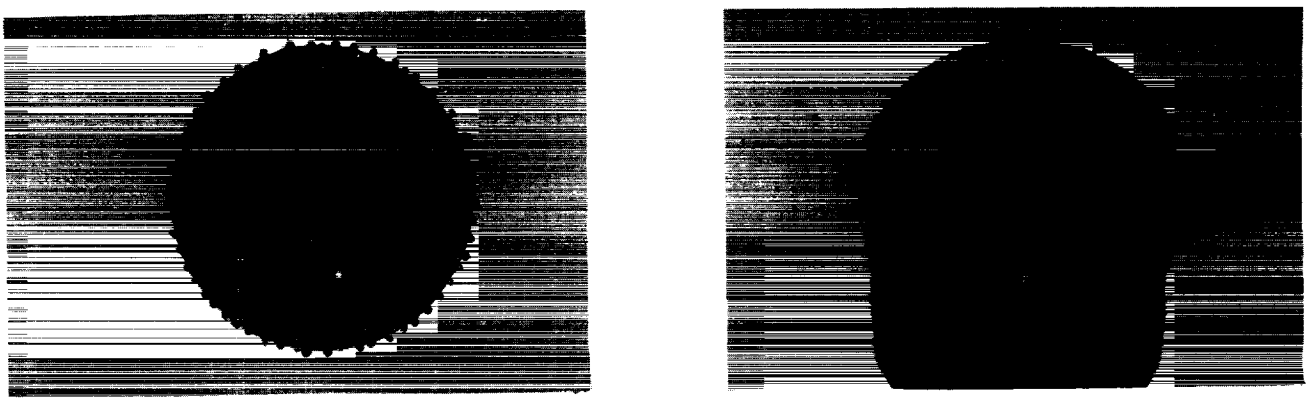

(e) Model 110

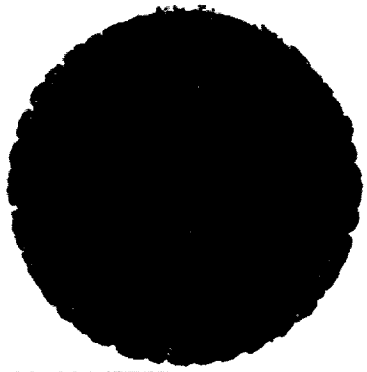

(f) Model 31

Figure 6-30 Continued.

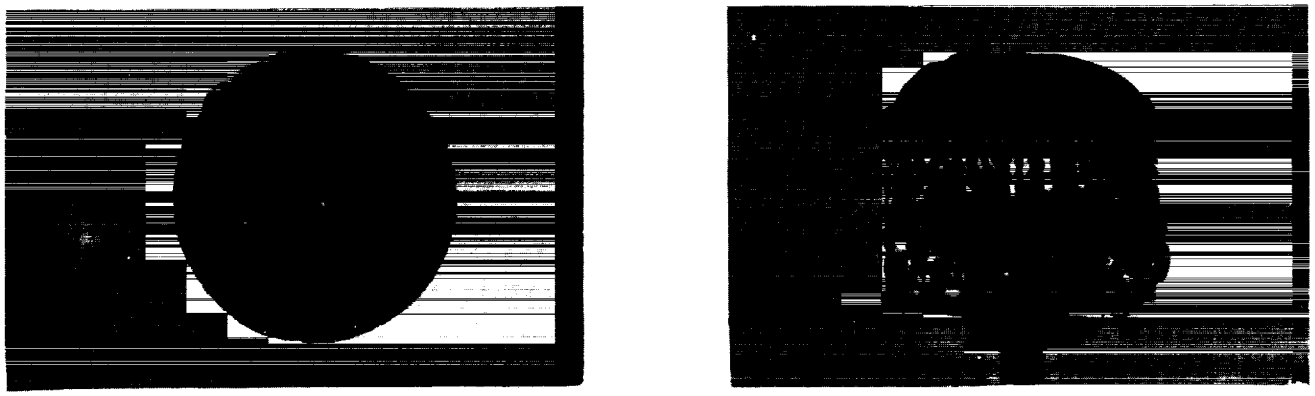

(g) Model 129

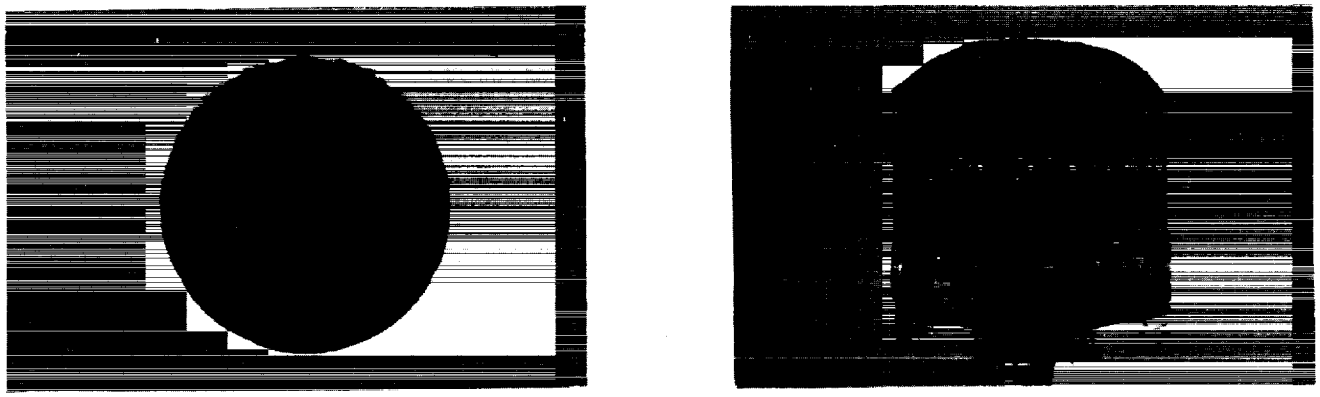

(h) Model 138

Figure 6-30 Concluded

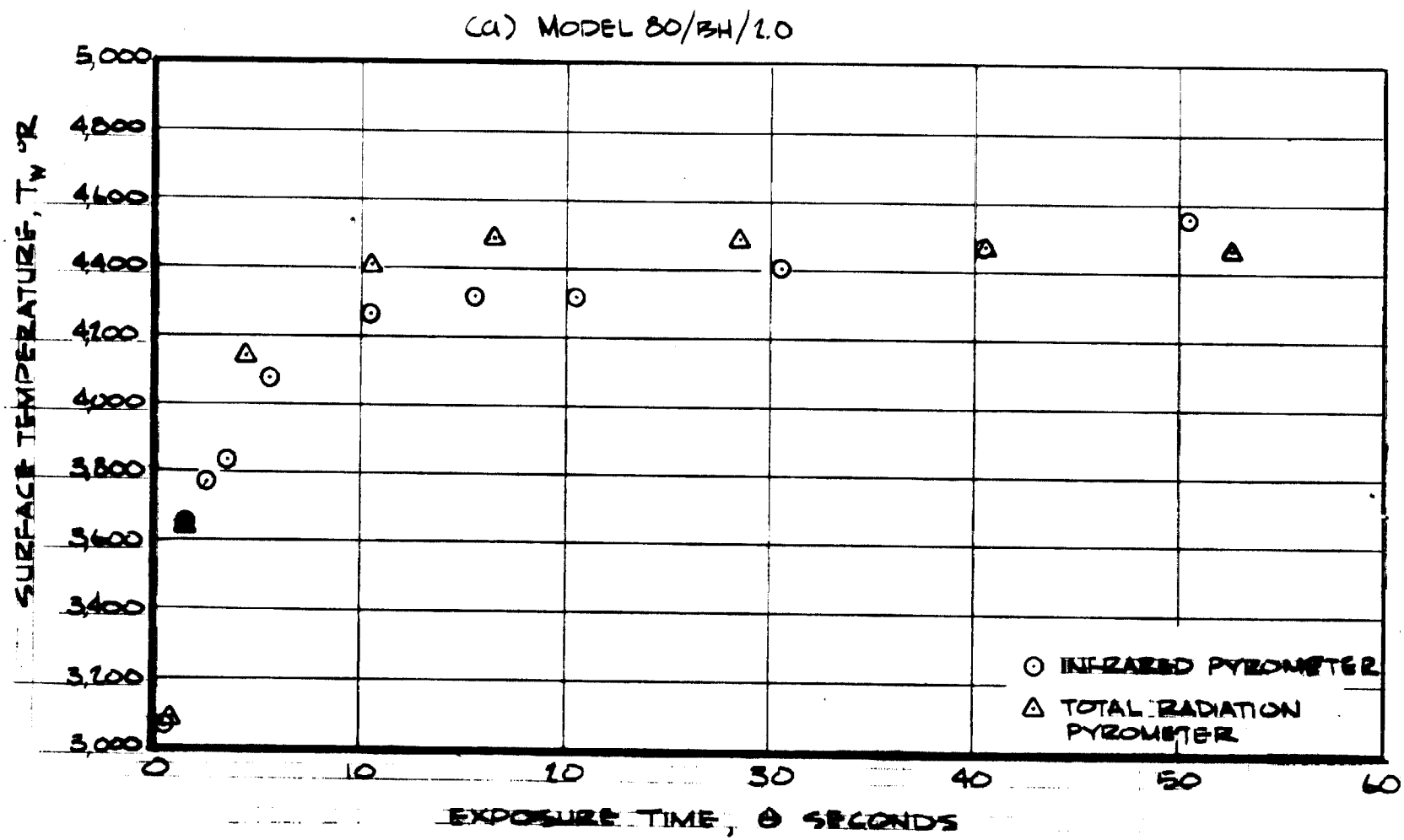

FIGURE 6-31 COMPARISON OF SURFACE TEMPERATURES INDICATED BY INFRARED AND TOTAL RADIATION PYROMETER.

(b) MODEL 29/BH/2.0

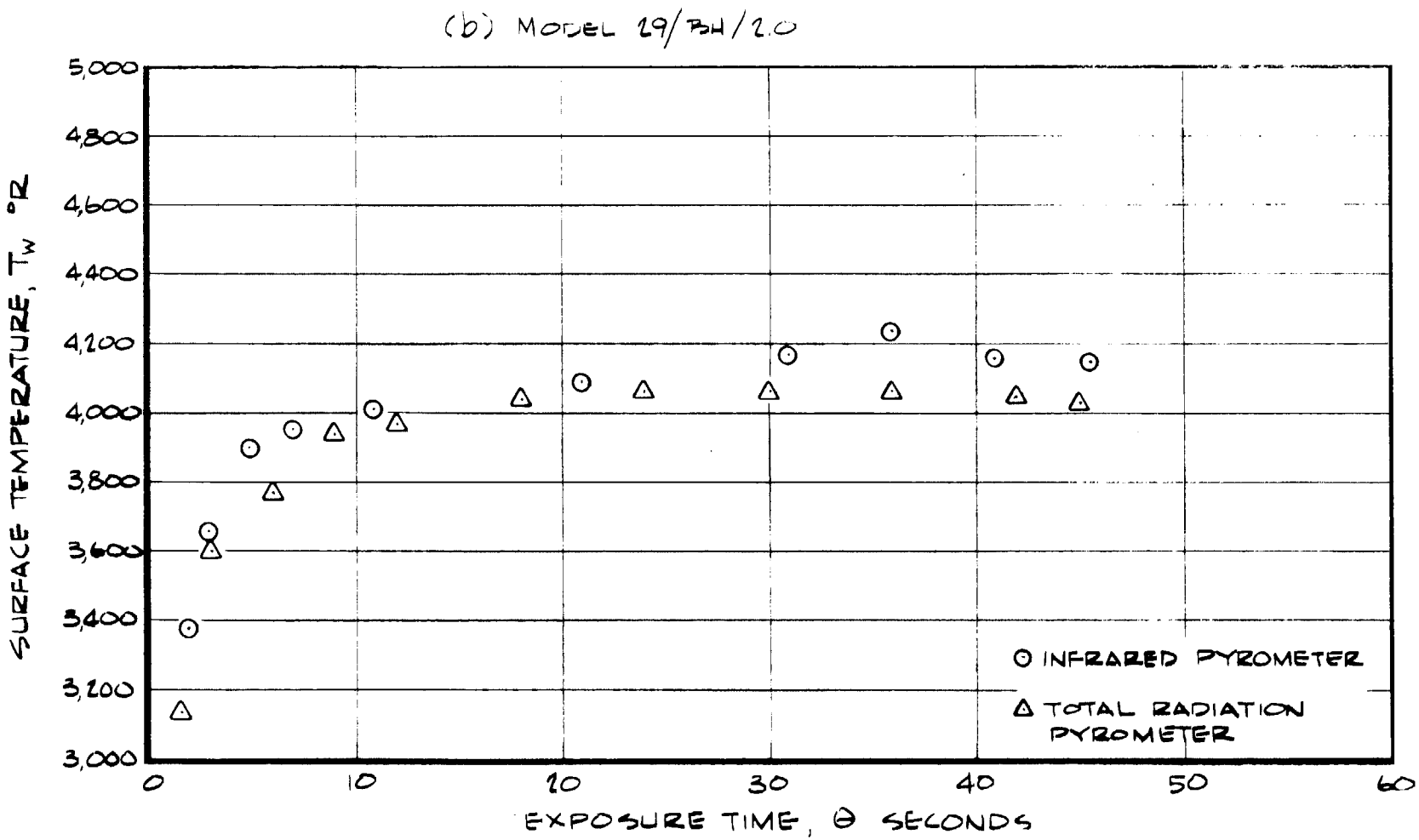

FIGURE 6-31 CONTINUED

(C) MODEL 21/FF/2.0

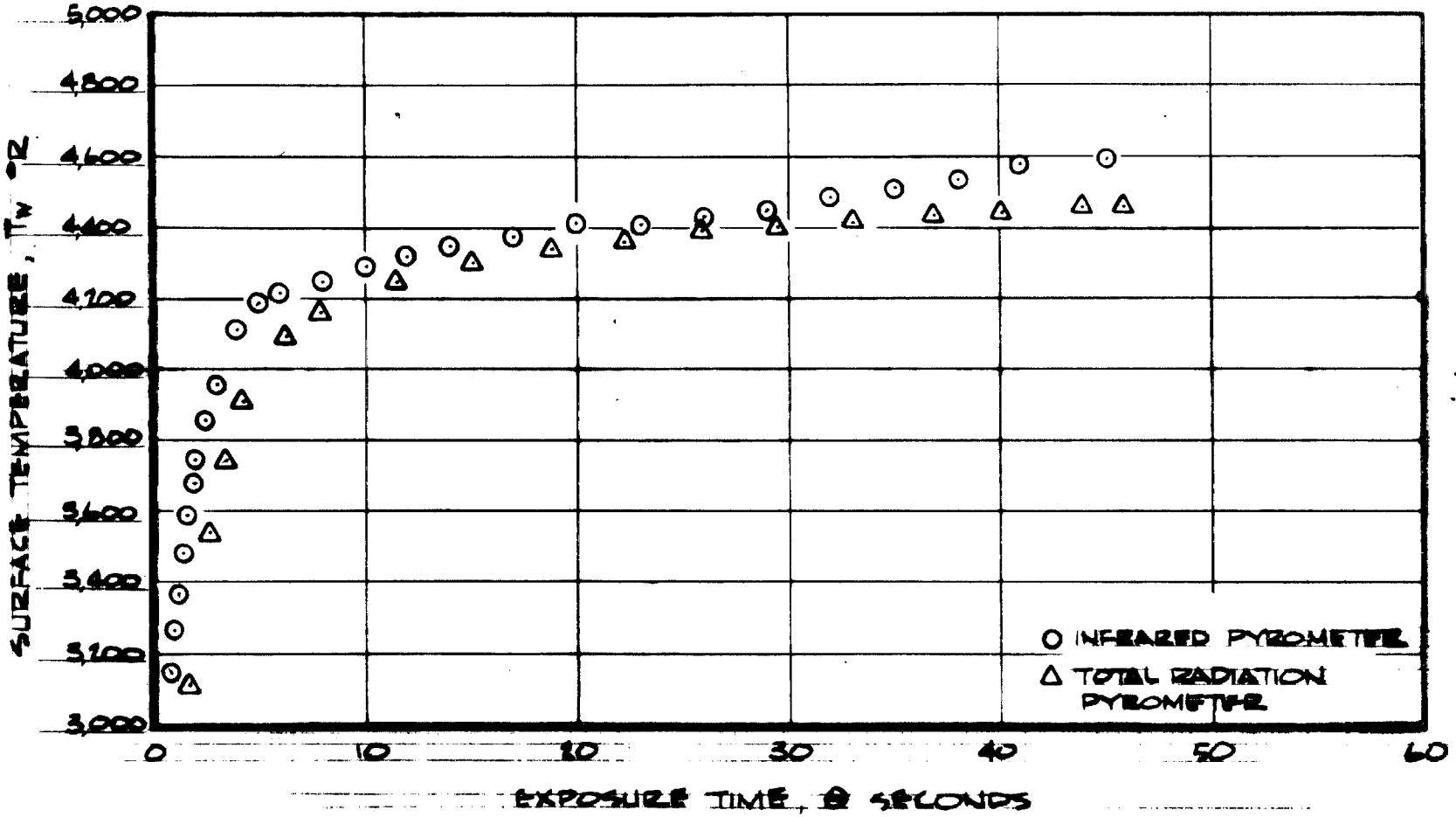

FIGURE 6-31 CONTINUED

(d) MODEL 102/BH/2.0

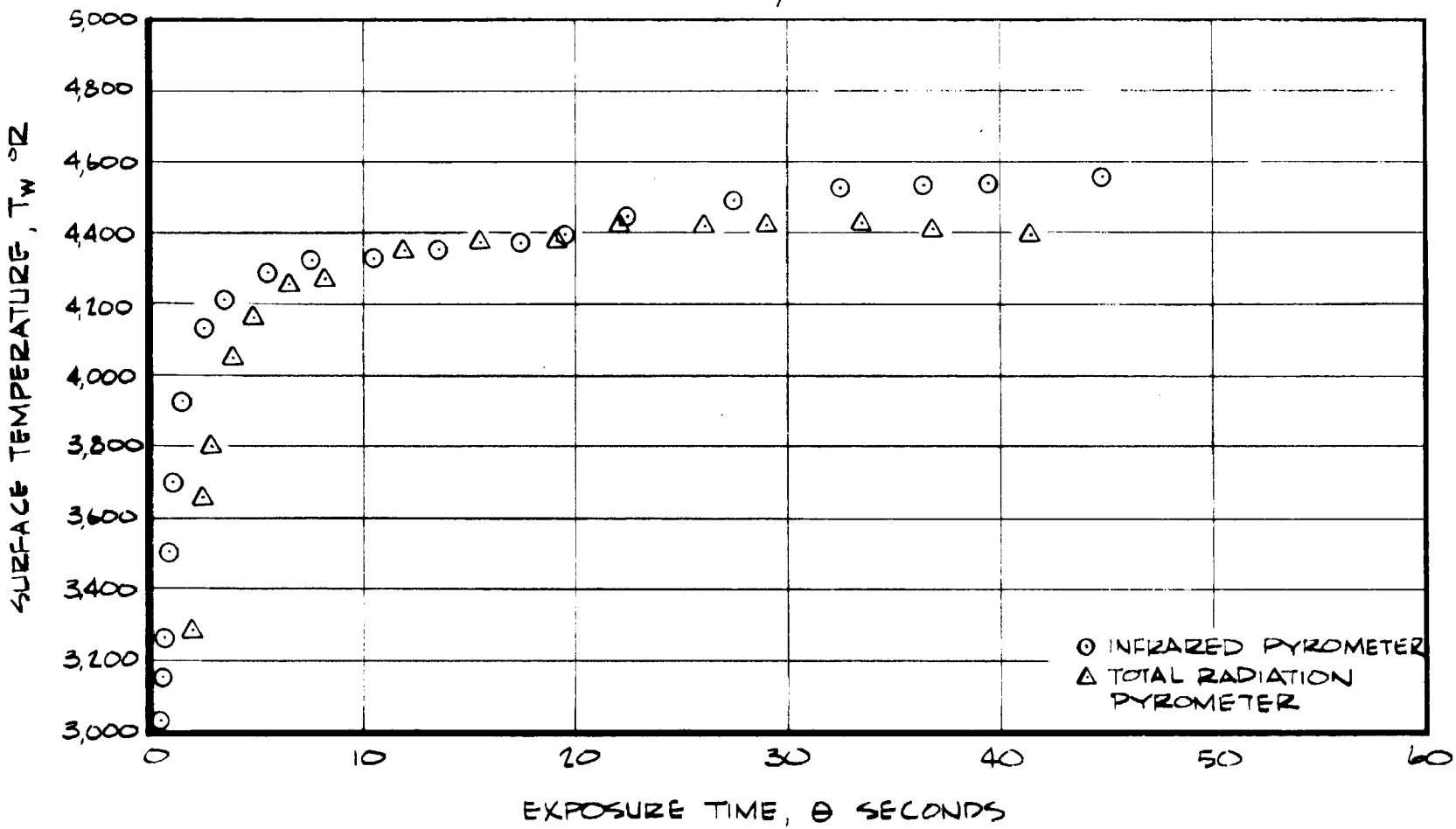

FIGURE 6-31 CONCLUDED

6.3 CHEMICAL AND PHYSICAL PROPERTIES TESTS

Chemical and physical properties tests on 12 selected models were also performed as part of the overall program. Surface and in-depth analyses of the models were performed after exposure to simulated reentry conditions through photomicrograph studies, X-ray diffraction measurements, microchemical quantitative analysis, X-ray density measurements, and infrared spectra measurements.[1] The tests were performed to provide a further characterization of the 5026-39 HCG material as an aid in understanding the response phenomena of the material and in interpreting and rationalizing the experimental results and analytical predictions. The models, test conditions, and chemical and physical properties tests performed on them are presented in Table 6-16. The tests and the test results are described in following sections.

6.3.1 Photomicrograph Study

Microscopic examinations of the surface and in-depth characteristics of the models were performed through visual inspection and photomicrograph study. Representative photomicrographs for all models and the virgin material are presented in Figure 6-32. The information obtained from this study is summarized below by model:

158/BH/1.0 - Surface

Black, porous, irregular; occasional small black globules; no discrete fibers

140/BH/1.0 - Surface

Irregular (due to erratic recession), gray fibrous material

91/BH/2.0 - Surface

Many transparent globules with large spectrum of size; large globules contained gas bubbles; black, porous, irregular; transparent fibers

108/BH/2.0 - Surface

Similar to 158

84/BH/2.0 - Surface

Gray; large amount of gray fibrous material

80/BH/2.0 - Surface

Similar to 158

114/BH/4.0 - Surface

Loose white scab of agglomerated fibers, glassy in appearance; underneath surface porous, irregular, large amount of random fibers

[1] All tests were performed by Stanford Research Institute, Menlo Park, California, under subcontract to Aerotherm Corporation.

TABLE 6-16

SUMMARY OF CHEMICAL AND PHYSICAL PROPERTIES TESTS

		Test Conditions				Analysis Techniques								
Model No.	Phase	Enthalpy h (Btu/lb)	Stagnation Pressure ps (atm)	Heating Rate q_c (Btu/ft²-sec)	Environment	Photomicrographs		X-Ray Diffraction		Micro-Chemical		X-Ray Density	Infrared Spectra	
						Surface	In-Depth	Surface	In-Depth	Surface	In-Depth		Surface	In-Depth
158/BH/1.0	III	5,031	1.06	318	Air	x		x						
140/BH/1.0		5,151	3.10	480		x		x						
91/BH/2.0	IV	10,969	0.0079	45.8		x		x		x			x	
108/BH/2.0		16,301	0.0080	60.8		x		x		x				
84/BH/2.0		10,918	0.0298	74.0	Helium	x		x		x				
80/BH/2.0		9,960	0.0276	107	Nitrogen	x		x		x				
114/BH/4.0	V	4,910	0.0112	18.5	Air	x	x	x	x	x	x	x	x	x
30/BH/2.0	VI	5,937	0.0275	45.8		x		x		x				
27/BH/2.0		10,269	0.0282	71.3		x	x	x	x	x	x	x		x
102/BH/2.0		16,517	0.0271	113		x		x		x				
97/BH/2.0	VII	18,860	0.285	133		x		x		x				
111/BH/1.0		10,588	0.0817	156		x		x		x				
Virgin Material	—	—	—	—	—		x				x	x		

(a) Surface - 158/BH/1.0 5x

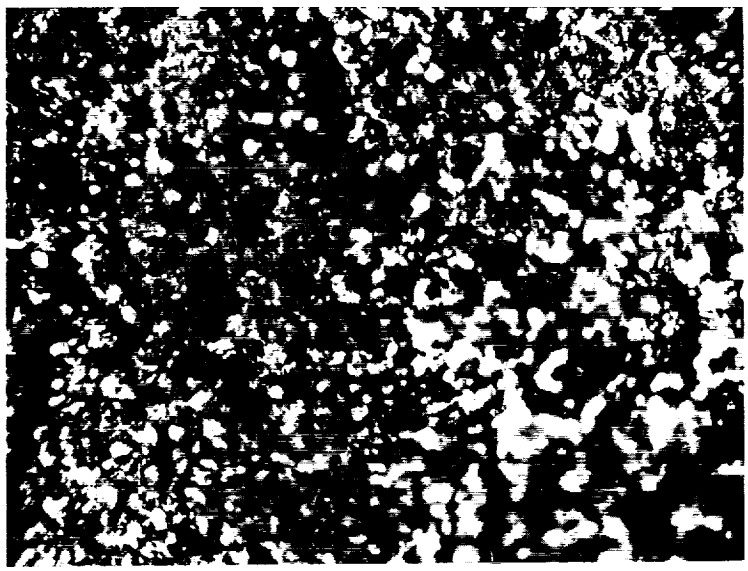

(b) Surface - 158/BH/1.0 80x

Figure 6-32. Representative Micrographs.

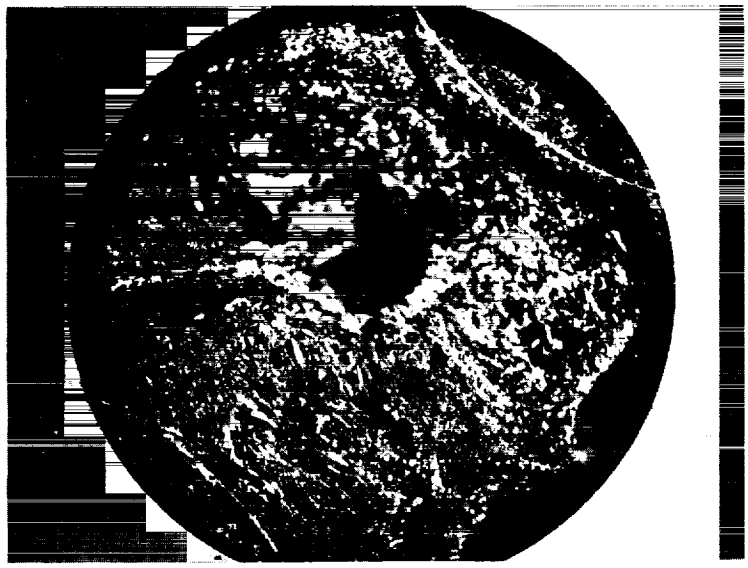

(c) Surface - 140/BH/1.0 5x

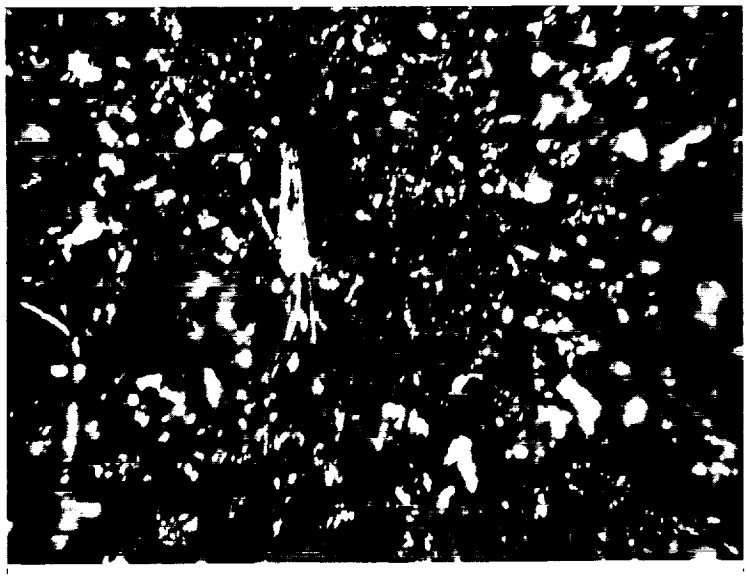

(d) Surface - 140/BH/1.0 80x

Figure 6-32. Continued.

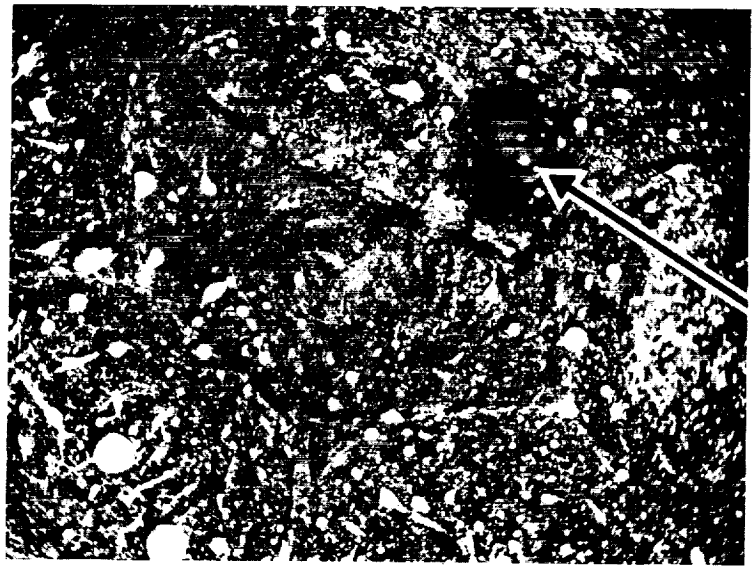

(e) Surface - 91/BH/2.0 5x

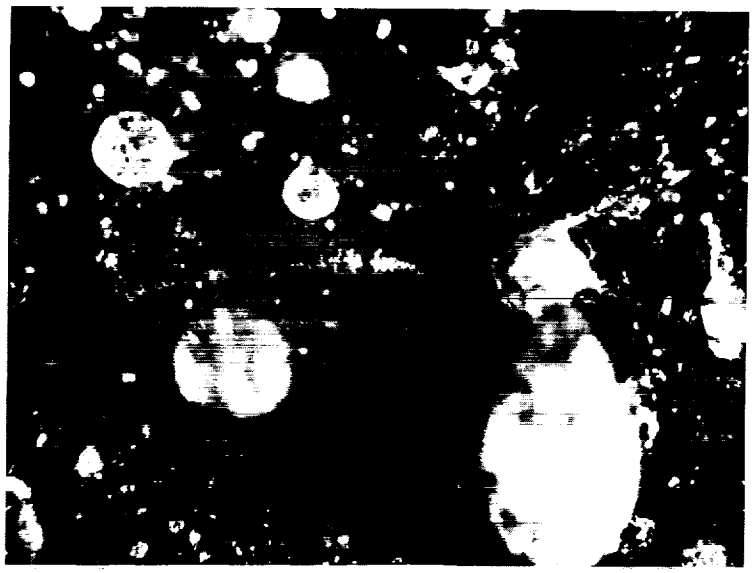

(f) Surface - 91/BH/2.0 80x

Figure 6-32. Continued.

Exposed Thermocouple Hole

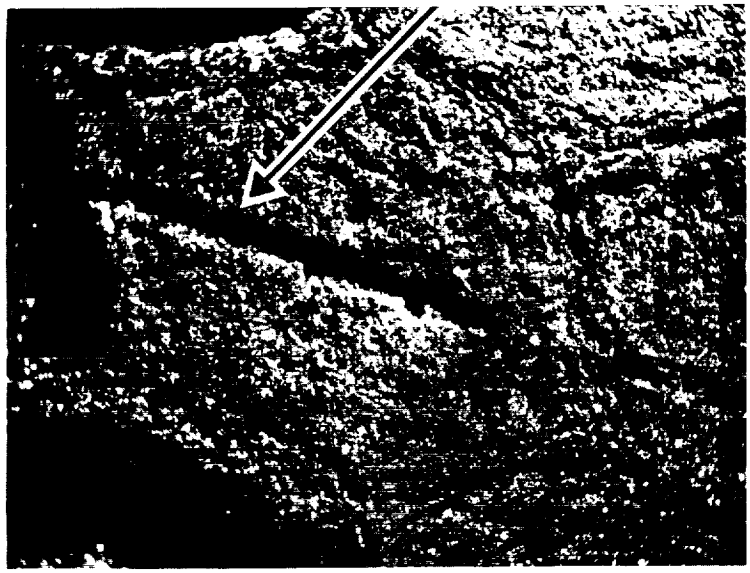

(g) Surface - 108/BH/2.0 5x

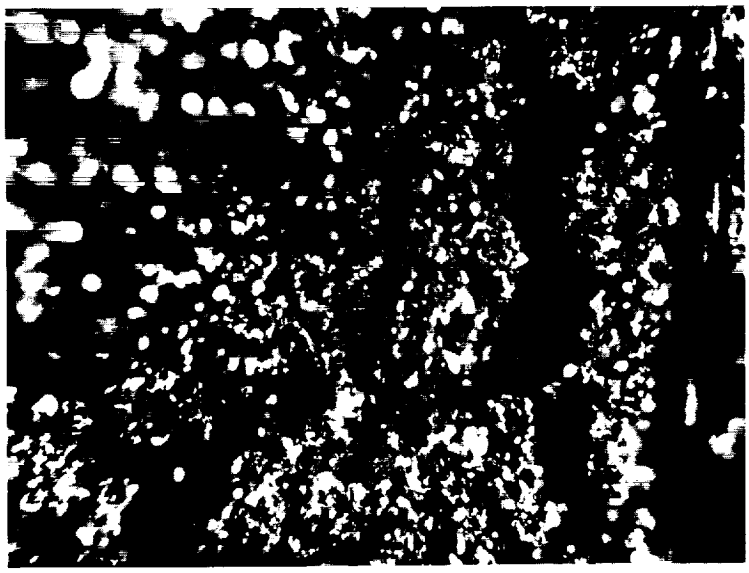

(h) Surface - 108/BH/2.0 80x

Figure 6-32. Continued.

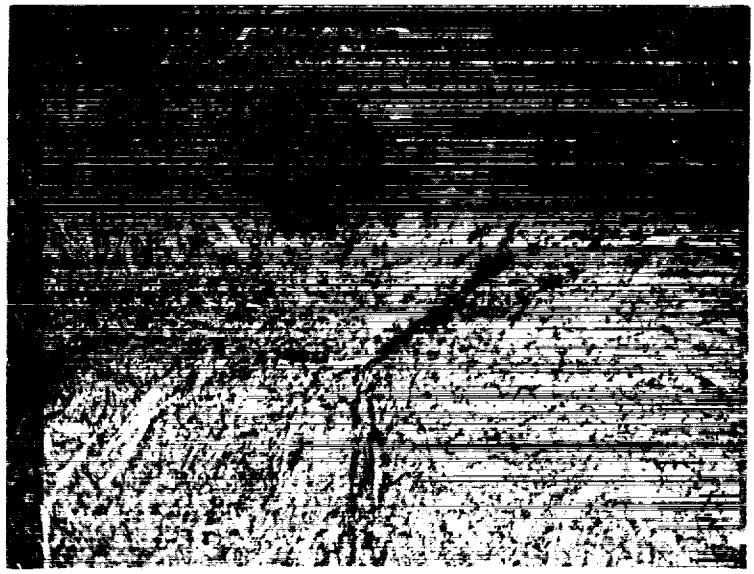

(i) Surface - 84/BH/2.0 5x

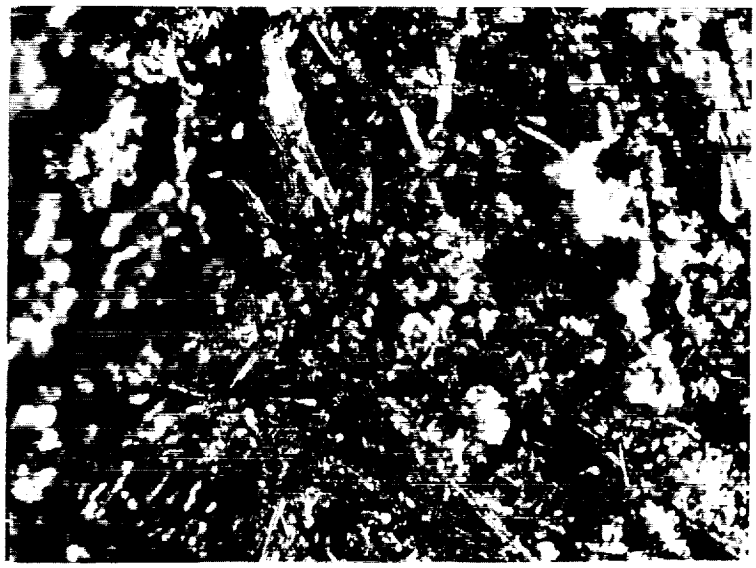

(j) Surface - 84/BH/2.0 80x

Figure 6-32. Continued.

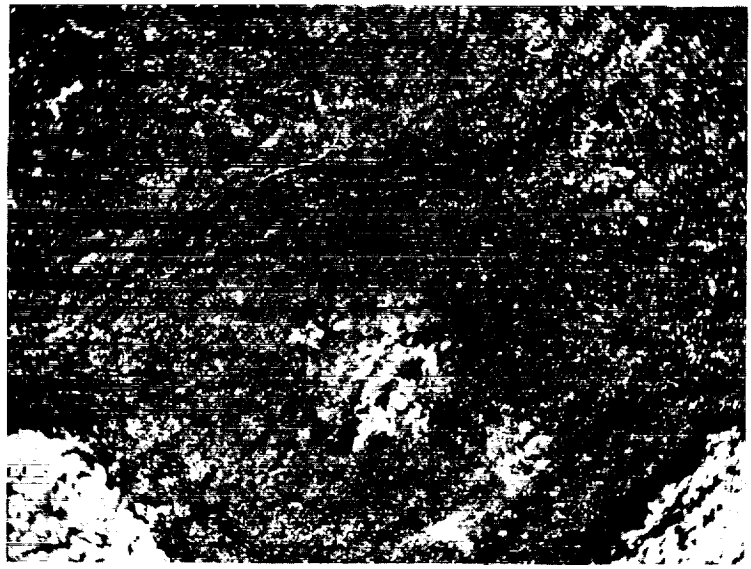

(k) Surface - 80/BH/2.0 5x

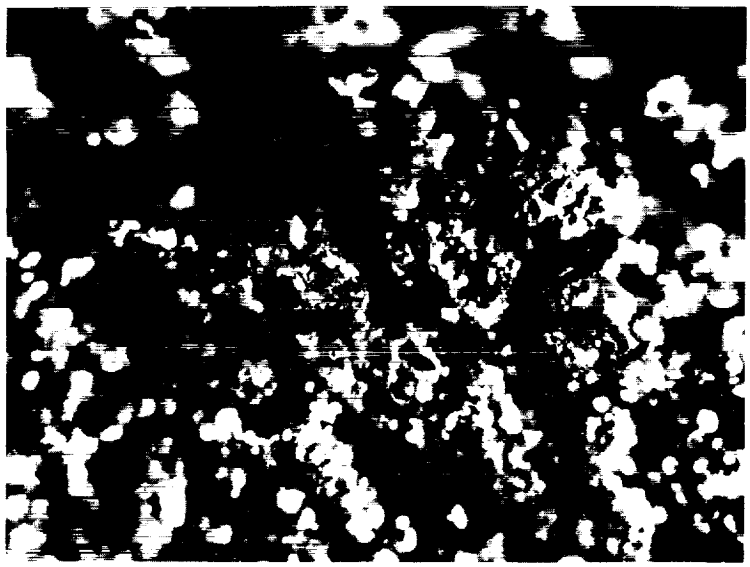

(l) Surface - 80/BH/2.0 80x

Figure 6-32. Continued.

Scab Removed

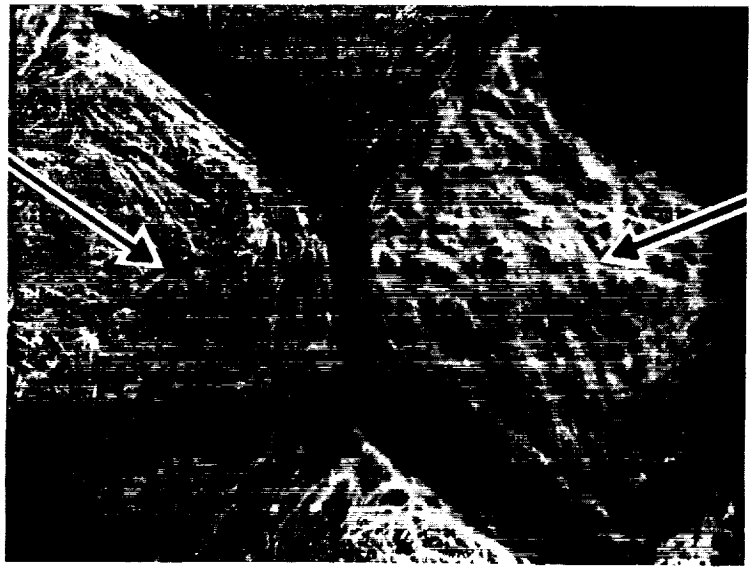

Scab

(m) Surface - 114/BH/4.0 5x

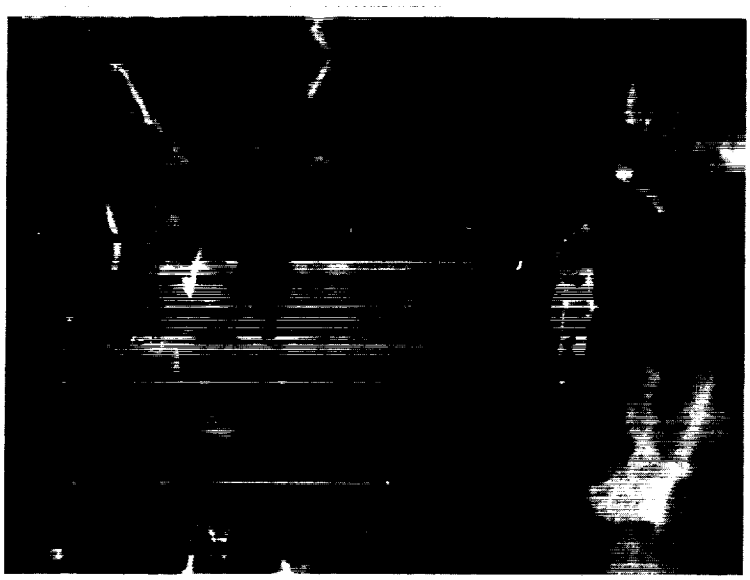

Scab

(n) Surface - 114/BH/4.0 125x

Figure 6-32. Continued.

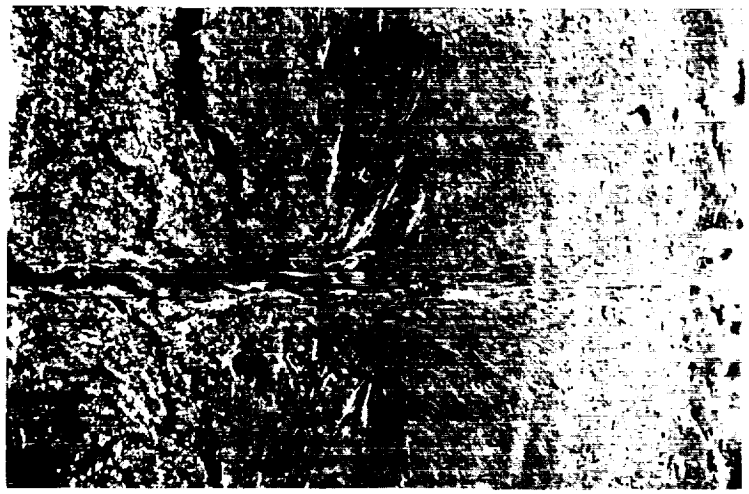

(o) In Depth - 114/BH/4.0 5x

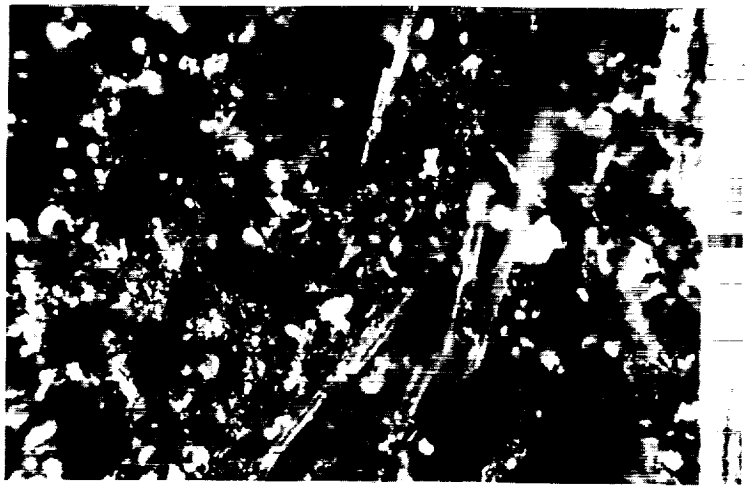

Pyrolysis Zone

(p) In Depth - 114/BH/4.0 80x

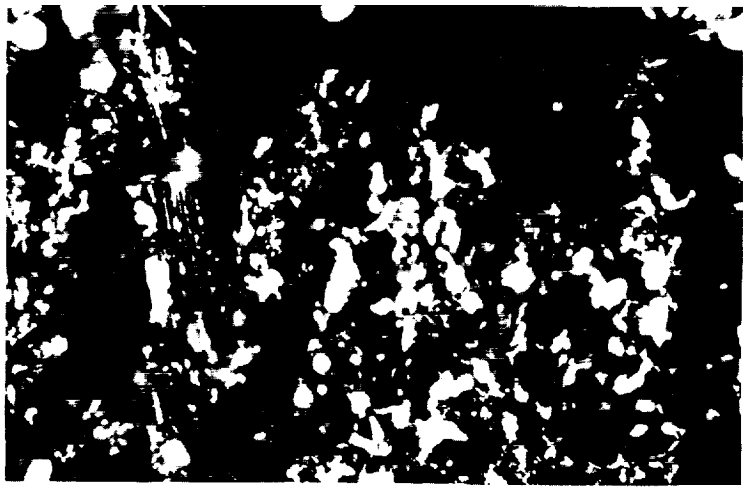

Char

(q) In Depth - 114/BH/4.0 125x

Figure 6-32. Continued.

(r) Surface - 30/BH/2.0 5x

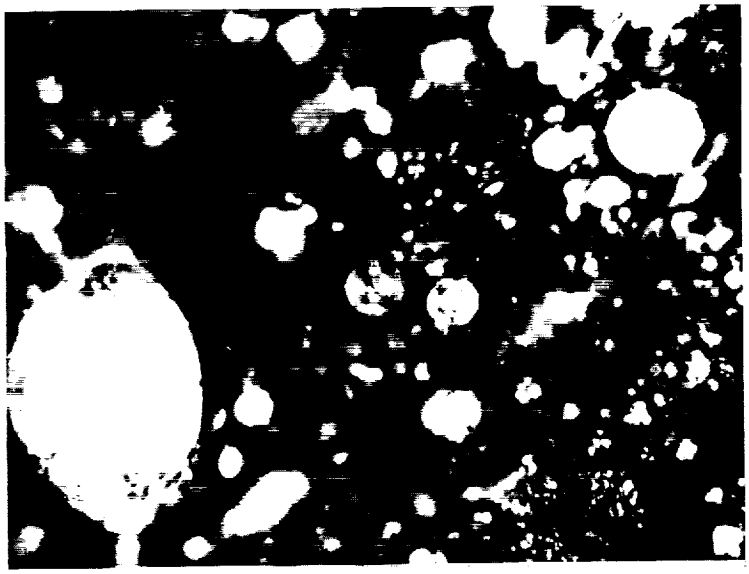

(s) Surface - 30/BH/2.0 80x

Figure 6-32. Continued.

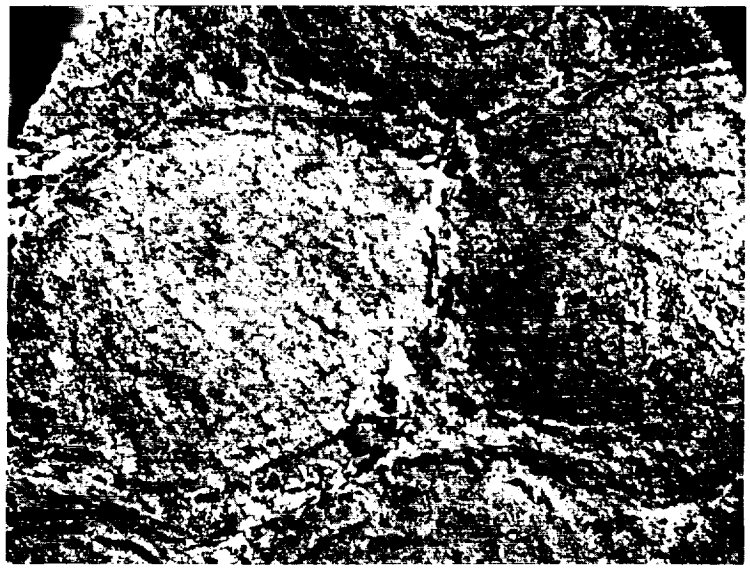

(t) Surface - 27/BH/2.0 5x

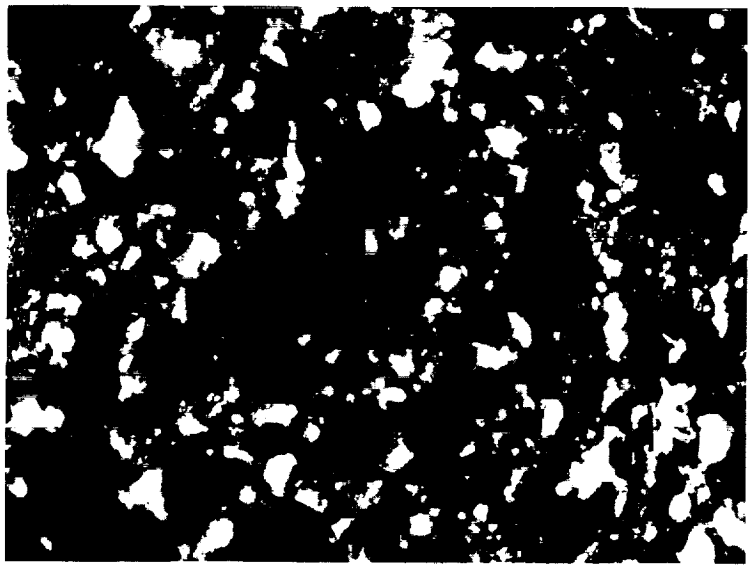

(u) Surface - 27/BH/2.0 125x

Figure 6-32. Continued.

(v) In Depth - 27/BH/2.0 5x

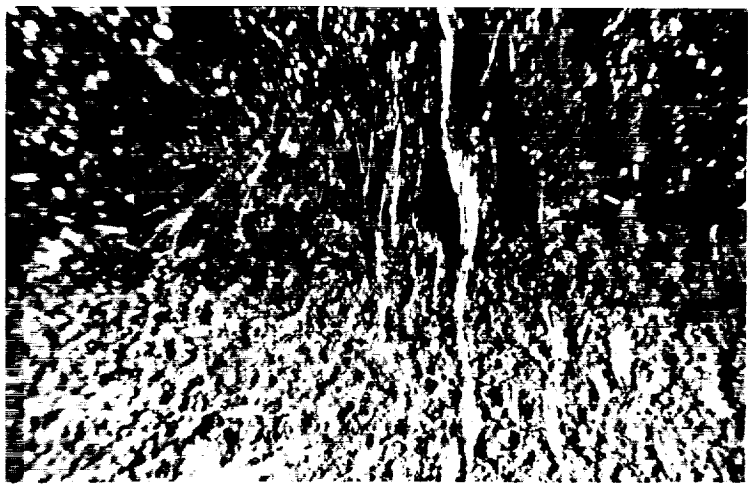

Pyrolysis Zone

(w) In Depth - 27/BH/2.0 20x

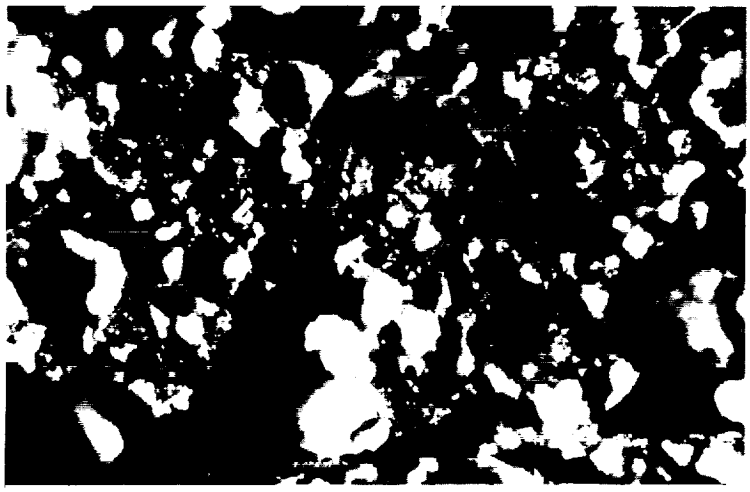

Char

(x) In Depth - 27/BH/2.0 125x

Figure 6-32. Continued.

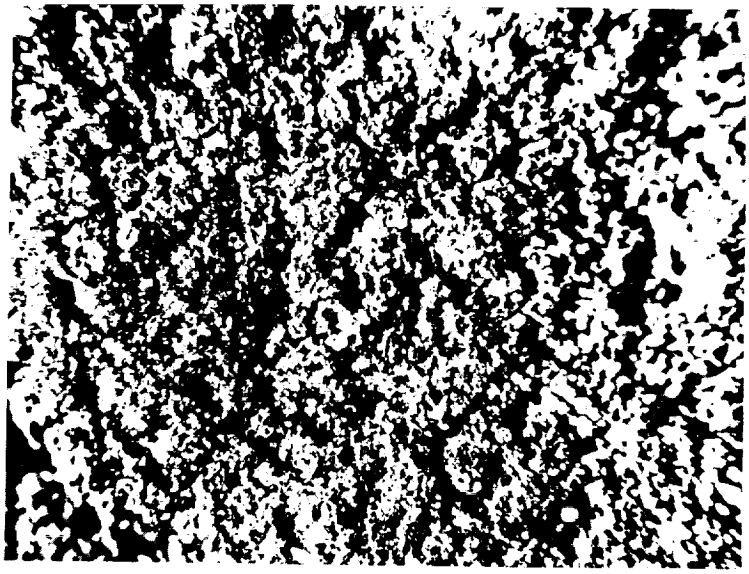

(y) Surface - 102/BH/2.0 25x

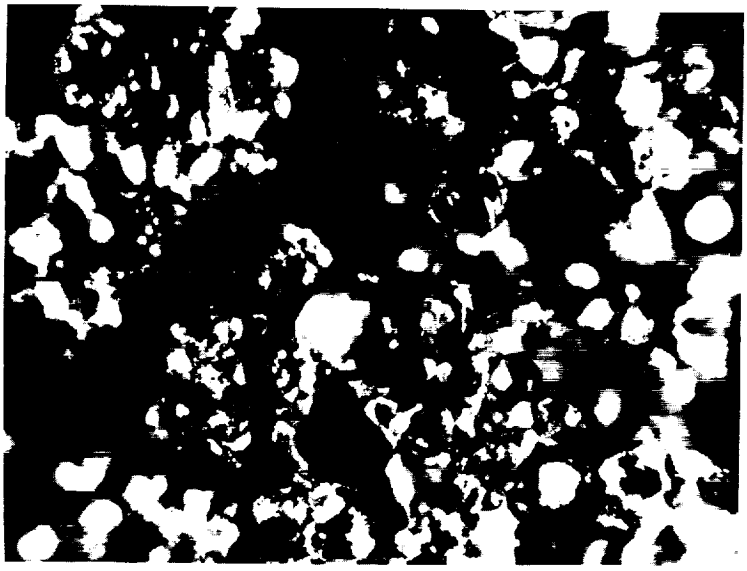

(z) Surface - 102/BH/2.0 125x

Figure 6-32. Continued.

(aa) Surface - 97/BH/2.0 5x

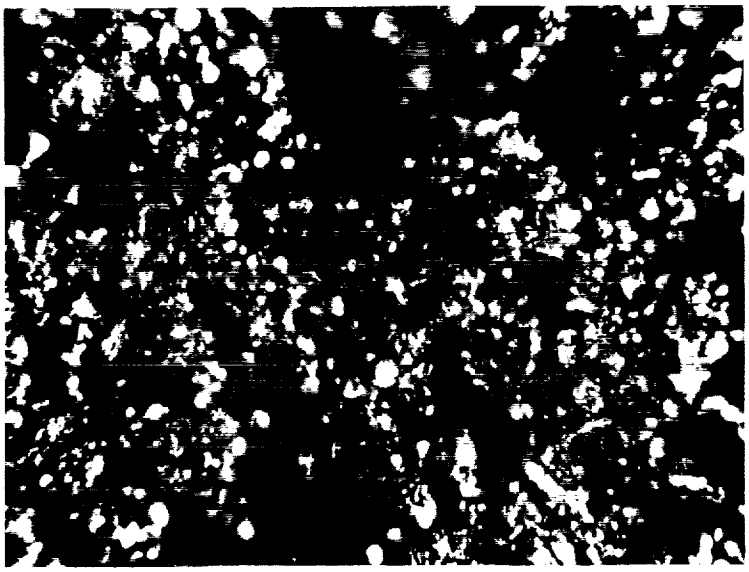

(bb) Surface - 97/BH/2.0 80x

Figure 6-32. Continued.

(cc) Surface - 111/BH/1.0 5x

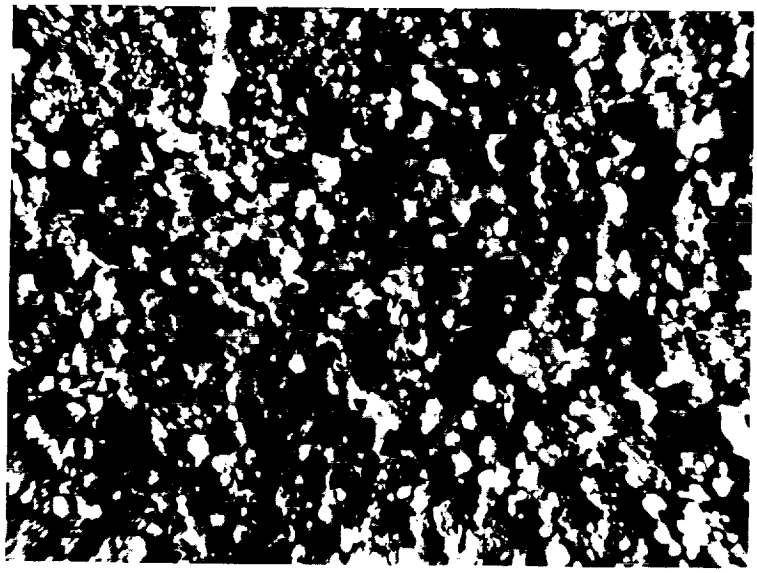

(dd) Surface - 97/BH/2.0 80x

Figure 6-32. Continued.

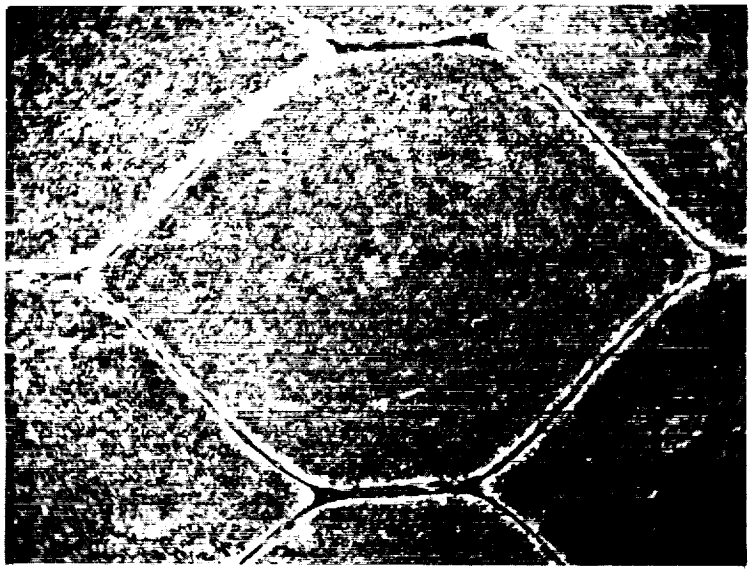

(ee) Surface - Virgin Material 5x

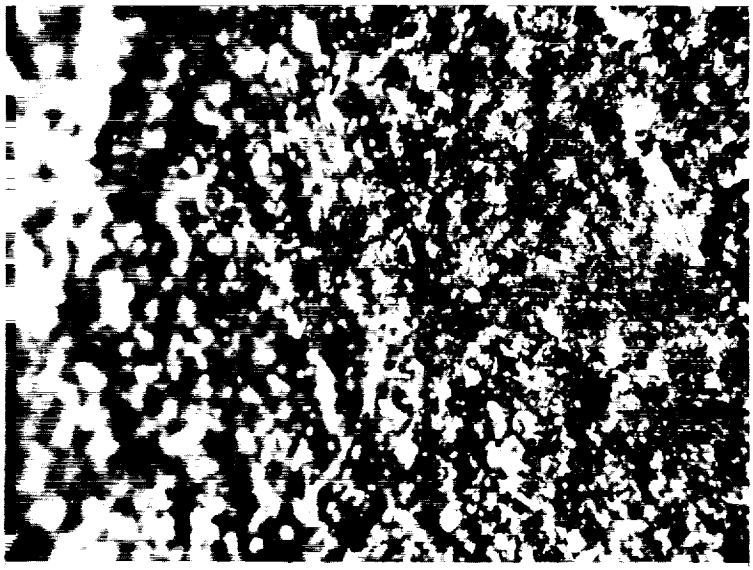

(ff) Surface - Virgin Material 80x

Figure 6-32. Concluded.

- In-Depth (Char)

Irregular, porous, fibers (generally oriented parallel to surface); few random deep fissures parallel to surface; gray central layer between black layers

30/BH/2.0 - Surface

Similar to 91

27/BH/2.0 - Surface

Similar to 158

- In-Depth (Char)

Similar to 114 but with fewer and narrower fissures

102/BH/2.0 - Surface

Similar to 158

97/BH/2.0 - Surface

Similar to 158

111/BH/1.0 - Surface

Similar to 158

Virgin Material

Rough; spherical reddish-brown particles on tan "background"; glassy fibers singly or in thick, long clumps

6.3.2 X-Ray Diffraction Analysis

X-ray diffraction patterns were obtained by placing about 5 to 10 mg of powdered sample on a thin plastic film and scanning the sample with a Norelco diffractometer. The analysis was performed for the surface materials, including the scab and globules where appropriate, and for six in-depth regions in Models 114 and 27. The compounds and the intensities of their diffraction peaks are presented in Table 6-17. The in-depth samples were taken in order of increasing depth from the surface through the entire char layer and pyrolysis zone. Sample -1 is indicative of the surface (or underneath surface in the case of the scab model), samples -2 through -5 cover the char region, and sample -6 includes the pyrolysis zone. A rough calibration of pyrolytic graphite indicated that the maximum concentration of crystalline graphite in any of the samples was less than 10 percent. Samples of α - cristobalite and β - silicon carbide were not available for a similar calibration of these compounds.

6.3.3 Microchemical Analysis

The microchemical quantitative analyses were performed using a conventional micro-carbon-hydrogen apparatus. A 5 mg sample was weighed into a platinum boat and was first heated in the apparatus at about 125°C to collect

TABLE 6-17

X-RAY DIFFRACTION ANALYSIS RESULTS

Model No. and Sample Location		Crystalline Compound, Relative Intensity in Parenthesis
158	Surface	SiC (25), C (18
140	Surface	SiC (10), C (9)
91	Globules	Amorphous
91	Surface	
108	Surface	C (7)
84	Surface	SiC (25), C (45)
80	Surface	SiC (29), C (7)
114	Scab	α-SiO_2 (45)
114-1	Surface	α-SiO_2 (28)
114-2		α-SiO_2 (60)
114-3		α-SiO_2 (65)
114-4		α-SiO_2 (13)
114-5		Amorphous
114-6		
30	Globules	
30	Surface	
27-1	Surface	SiC (9), C (13)
27-2		SiC (4), C (6)
27-3		α-SiO_2 (11)
27-4		Amorphous
27-5		
27-6		
102		SiC (13), C (15)
97		SiC (32)
111		C (4)
Virgin		Amorphous

Note: α-SiO_2 is α-cristobalite, SiC is β-SiC, C is graphite.

the water. The sample was then burned to convert carbon to carbon dioxide and hydrogen to water. The boat was reweighed to determine ash. The results for H_2O, ash, C, and H for the surface char samples totaled between 99.8 and 101.6 percent and were normalized to 100 percent. Oxygen was calculated by difference for the in-depth samples (samples 114-3 to 114-6 and 27-4 to 27-6) by subtracting the total of H_2O, ash, C and H from 101 percent (the average of the surface char samples), and then normalizing to 100 percent. Nitrogen was considered to be negligible and no analysis was performed for it. The final results for all samples tested are presented in Table 6-18. Note that no analysis was performed for Model 158 or Model 140 because the char was so thin that it was impossible to obtain a representative surface sample.

The surface sample of Model 80 exhibited an unusually high total weight percent and since silicon carbide was observed as a surface material in the X-ray diffraction measurements it was assumed that this high weight was due to its presence. Note that SiC, in combusting the sample, forms the heavier compound SiO_2. Therefore silicon carbide was calculated for the Model 80 sample to adjust the total to 101 percent and then the values were normalized to 100 percent. Other samples contained silicon carbide, but the concentrations were much lower and could not be estimated with any degree of certainty.

6.3.4 X-Ray Density Measurement

The X-ray density distribution was measured on Models 114 and 27 using the Norelco diffractometer with a scintillation counter and pulse height analyzer. The X-ray beam which passed through the sample was collimated to a height of 0.003 inch; the beam width was 1/8 inch. These dimensions define the resolution of the measurements, the 0.003-inch dimension being in the axial direction of the model. The sample was a constant thickness section of the model about 1/8-inch thick. The X-ray beam traversed the sample at a rate of 0.002 inch per minute.

With this technique, the density is deduced from the fraction of X-rays which pass through the sample; the higher this fraction, the lower the material density. Unfortunately, silica is 6 to 8 times more dense to X-rays than carbon (with the copper target of the X-ray source used) and therefore it is difficult to measure density changes due to pyrolysis for the 5026-39 HCG material with this technique. It does however provide an excellent trace of the silica content distribution.

The X-ray density results, which are indicative of silica content variations, are presented in Figure 6-33 for Models 114 and 27. No calibrations were performed to allow a quantitative presentation of the results. In both

TABLE 6-18

MICROCHEMICAL ANALYSIS RESULTS

Model No. and Sample Location		Composition, Percent by Weight							
		H_2O	Ash	C	H	O, by diff	SiC	C/H	Ash/C
91	Globules	1.1	98.2	0.7	0.00	0.0	—	> 100	—
91	Surface	0.9	45.1	54.0			—		0.84
108	Surface	0.5	34.4	65.1			—		0.53
84	Surface	0.5	18.3	81.2			—		0.23
80	Surface	1.0	25.0	72.1			1.9		0.37
114	Scab	0.3	99.6	0.1			—	—	—
114-1	Surface	2.6	70.1	27.1	0.17		—	> 100	2.61
114-2		1.4	49.5	48.7	0.25		—		1.02
114-3		1.6	53.8	41.4	0.26		—		1.30
114-4		5.1	52.3	39.6	0.46		—	86	1.32
114-5		4.4	51.4	37.6	1.27	6.3	—	30	1.37
114-6		3.3	45.6	40.4	2.28	9.4	—	18	1.13
30	Globules	1.3	98.6	0.1	0.00	0.0	—	—	—
30	Surface	0.6	58.3	41.1			—	> 100	1.42
27-1	Surface	0.0	28.6	71.4			—		0.40
27-2		0.7	44.1	55.2	0.04		—		0.80
27-3		3.3	52.3	44.2	0.21		—		1.18
27-4		2.7	57.0	36.6	0.50	3.2	—	73	1.56
27-5		3.7	45.2	40.5	2.48	8.1	—	16	1.12
27-6		3.6	29.3	48.1	4.06	14.9	—	12	0.61
102	Surface	1.1	23.2	75.6	0.05	0.0	—	> 100	0.31
97	Surface	0.5	34.4	65.1	0.00		—		0.53
111	Surface	2.0	43.8	54.0	0.12		—		0.81
Virgin	Polymer	3.2	25.7	48.3	4.23	18.5	—	11	0.53

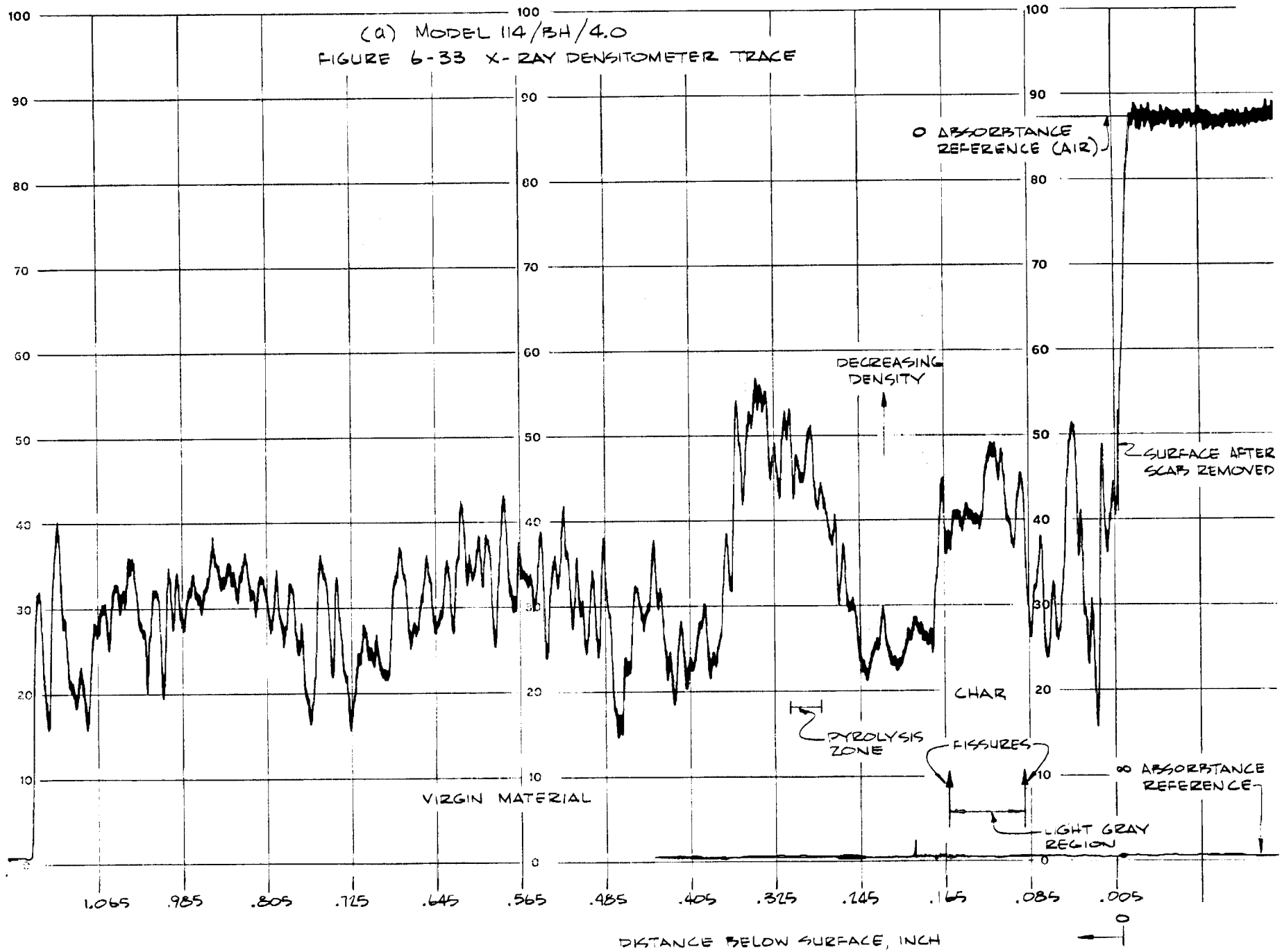
(a) MODEL 114/BH/4.0
FIGURE 6-33 X-RAY DENSITOMETER TRACE
0 ABSORBTANCE REFERENCE (AIR)
DECREASING DENSITY
SURFACE AFTER SCAB REMOVED
CHAR
PYROLYSIS ZONE
FISSURES
∞ ABSORBTANCE REFERENCE
VIRGIN MATERIAL
LIGHT GRAY REGION
100
90
80
70
60
50
40
30
20
10
0
1.065
.985
.805
.725
.645
.565
.485
.405
.325
.245
.165
.085
.005
0
DISTANCE BELOW SURFACE, INCH

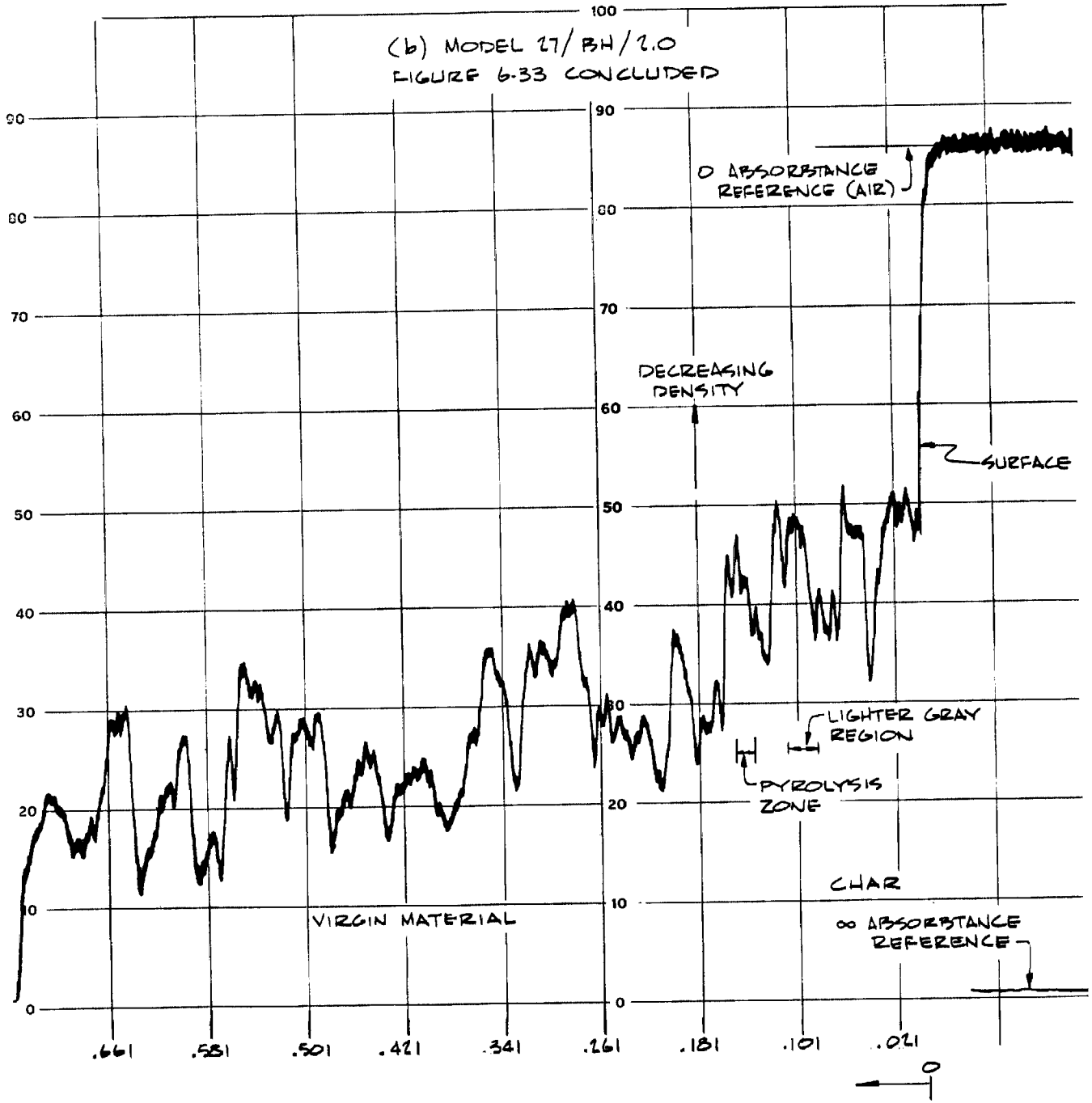
(b) MODEL 27/BH/2.0
FIGURE 6-33 CONCLUDED
100
90
80
70
60
50
40
30
20
10
0
.661
.581
.501
.421
.341
.261
.181
.101
.021
0
0 ABSORBTANCE REFERENCE (AIR)
DECREASING DENSITY
SURFACE
LIGHTER GRAY REGION
PYROLYSIS ZONE
CHAR
∞ ABSORBTANCE REFERENCE
VIRGIN MATERIAL

models, large variations in silica content in the virgin material are apparent. These variations are no less than about ±18 percent for both models. For Model 114 two large fissures were apparent in the region of the X-ray scan as noted in Figure 6-33a. These fissures approximately defined the boundaries of the gray region noted previously in Section 6.3.1. The silica density is seen to be low in this region. The pyrolysis zone is also a low density region, this region extending well beyond the bounds of the measured pyrolysis zone. The level of silica at the surface is close to that of the virgin material. Model 27 (Figure 6-33b) exhibits a generally decreasing density towards the surface even in the virgin material. The silica content at the surface is significantly lower than that in the virgin material.

Measurements of density were also attempted by slicing and weighing material samples in the process of obtaining the samples for microchemical analysis. The technique was not sufficiently accurate with the equipment at hand for its use under this program.

6.3.5 Infrared Spectra Analysis

The infrared absorption spectra of resins and other materials can be used to characterize the temperature to which the resin has been exposed and for qualitative identification of the material chemical composition (References 6-2 and 6-3). Infrared spectra analysis was therefore performed on the in-depth samples of Models 114 and 27 and on the scab and surface. The in-depth results are summarized below:

114/BH/2.0	-1 through -5	Temperature > 1,900°R
	-6	Temperature ≈ 1,550°R
27/BH/2.0	-1 through -4	Temperature > 1,900°R
	-5	Temperature ≈ 1,550°R
	-6	Temperature < 1,200°R

The temperatures indicated are not exact but rather indicate the approximate temperature level the sample achieved.

REFERENCES

6-1 Rindal, R. A., Flood, D. T., and Kendall, R. M.: Analytical and Experimental Study of Ablation Material for Rocket-Engine Application, NASA CR-54757, May 1966.

6-2 Barry, W. T. and Gaulin, C. A.: A Study of Physical and Chemical Processes Accompanying Ablation of G. E. Century Resins, Missile and Space Vehicle Department. General Electric Co., under U.S. Air Force Ballistic Systems Division, Contract 269-486.

6-3 Hunt, J. M., Wisherd, M. P. and Bonham, L. C.: Infrared Absorption Spectra of Minerals and Other Inorganic Compounds, Anal. Chem., 22 1478 (1950).

SECTION 7
ANALYTICAL PREDICTIONS

7.1 INTRODUCTION

An extensive analytical evaluation of the performance of the Avcoat 5026-39 HCG material under reentry conditions was also performed as part of the overall program. The computerized mathematical models which have been developed at Aerotherm to characterize the thermochemical response of an ablative material exposed to a high-temperature chemically-reacting environment were used in conducting the analytical investigation.

The analytical evaluation of the thermal protection system material was divided into two phases. First, theoretical predictions of material performance were made for several heating conditions which corresponded to tests in the experimental investigation under the subject contract; direct comparisons between theoretical and experimental results were then made. Second, theoretical predictions were performed for heating conditions varied in a parametric manner, with many of the conditions being outside the range of those included in the experimental investigation.

The following sections present the background and results for this part of the program. Section 7.2 describes the computer programs which embody the theoretical model to characterize ablative material thermochemical response. Section 7.3 describes the computer input information required to conduct the theoretical study, including all property data for the Avcoat 5026-39 HCG material. The results of both phases of the analytical investigation are presented in Section 7.4.

7.2 DESCRIPTION OF THE ABLATION COMPUTER PROGRAMS USED IN THE ANALYTICAL STUDY

Two computer programs were used in performing the analytical predictions under the subject contract. The Charring Material Ablation Program (CMA) was used to obtain the actual transient response predictions, (i.e., surface temperature response, internal temperature response, and erosion rate) and the Aerotherm Chemical Equilibrium Program (ACE) was used to generate the surface thermochemistry boundary conditions used by the CMA program. Sections 7.2.1 and 7.2.2 describe briefly the CMA and ACE computer programs respectively.

7.2.1 The Aerotherm Charring Material Ablation Program (CMA)

The CMA computer program is an implicit, finite-difference computational procedure for determining the one-dimensional transient transport of thermal energy in an isotropic material which can ablate from a front surface and

which can decompose in depth. The ablating-surface boundary condition for the material subjected to a heating environment can take one of two basic forms:

Option 1 - general convection-radiation heating with coupled mass transfer, including the effects of unequal heat and mass transfer coefficients (non-unity Lewis number) and unequal mass diffusion coefficients (surface thermochemistry computations presume chemical equilibrium at the surface)

Option 2 - specified surface temperature and surface recession rate.

The Option 1 form of boundary conditions is used when a completely theoretical prediction is desired. The Option 2 form of boundary conditions is convenient when an internal temperature prediction utilizing experimentally-determined surface boundary conditions is desired.

The input information required for the CMA program can be summarized as:

a. Constants for the Arrhenius decomposition equation which define the material density change as a function of time and temperature

b. A one-dimensional nodal network which defines the material configuration

c. Back wall boundary conditions

d. Material properties - specific heat, emissivity, and thermal conductivity for the fully charred and virgin materials

e. Pyrolysis gas enthalpy (chemical + sensible) as a function of temperature

f. Heats of formation for the char and virgin material

g. Heat-transfer coefficient and boundary-layer-edge pressure and recovery enthalpy as functions of time for Option 1 boundary conditions, or surface temperature and recession rate as functions of time for Option 2 boundary conditions

h. Ratio of mass-transfer to heat-transfer coefficient for Option 1 boundary conditions

i. Radiation view factor, for Option 1 boundary conditions

j. Surface equilibrium chemistry information generated by the ACE program, for Option 1 boundary conditions

Output from the CMA program includes all of the input information specified above, and the following information for each time interval desired:

a. General information - number of time steps computed, number of iterations required for the surface energy balance, wall enthalpy, edge gas enthalpy, heat transfer coefficient (corrected for blowing), ratio of corrected- to uncorrected-for-blowing heat transfer coefficient

b. Ablation rates

c. Recession and recession rates

d. Surface energy flux terms

e. In-depth energy terms

f. Nodal data - current temperature, density, and enthalpy of all nodes

g. Temperature of specified thermocouple depths

h. Locations of specified isotherms

The material property data, thermodynamic data, and geometric configuration data which are contained in the above list of input information are discussed further in Section 7.3. Further details of the CMA program are presented in References 7-1 and 7-2.

7.2.2 The Aerotherm Chemical Equilibrium Program (ACE)

The ACE computer program is a general chemical equilibrium computer program, the surface thermochemistry option of which was used to generate the CMA program Option 1 surface thermochemical boundary conditions. The program treats surface thermochemical reactions as being diffusion rate controlled (equilibrium) and considers unequal diffusion coefficients. The chemical system considered by the program consists of the boundary layer edge gases, the exposed surface material, and the pyrolysis gases of in-depth material decomposition. The surface removal mechanisms considered by the program are surface chemical reactions, including surface material decomposition, phase change, and reactions with the edge gas - pyrolysis gas species, and liquid layer removal. Liquid layer removal is treated in terms of a fail temperature, the liquid being removed mechanically if it appears as a surface specie above the specified fail temperature.

Operationally, the ACE program generates an array of surface state parameters as a function of surface recession rate, surface pressure, and material internal decomposition products injection rate. Input information includes specification of the elemental composition of the system being analyzed, a set of thermodynamic property data for each likely species in the system, and prescription of an array of mass-transfer rates for the surface material

and mass-transfer rates for the internal decomposition products. The elemental composition of the system being analyzed is defined by the relative masses of elements contained in the charred ablation material, the pyrolysis off-gas, and the boundary-layer-edge gas. The thermodynamic property data for the likely species in the system are available from such sources as the JANAF Thermochemical Tables (Reference 7-3).

The various input data to the ACE program for the 5026-39 HCG material are also discussed further in Section 7.3. Further details of the ACE program are presented in References 7-2 and 7-4.

Output information from the ACE program includes both listed and punched card data. The total output data includes system properties (viscosity, conductivity, diffusion coefficient, Prandtl number, Schmidt number, molecular weight, isentropic exponent, etc.), thermodynamic variables (temperature, enthalpy, entropy, pressure, density), the pyrolysis gas rates and char removal rates (input), and the mole fractions of each molecular specie present in the system. Each card of the punched card output is used directly as the surface thermochemistry input for the CMA program.

7.3 COMPUTER PROGRAM INPUT INFORMATION

As briefly described in Section 7.2 above, the two computer programs used in the analytical investigation require as input a wide variety of thermodynamic, material property, and geometric configuration data. The present section presents these input data for the Avcoat 5026-39 HCG material.

The various input data are conveniently divided into input requirements for the ACE program, described below in Section 7.3.1, and input requirements for the CMA program, described below in Section 7.3.2.

7.3.1 Input Information for the ACE Program

The input information to the ACE program is presented in the following sections. Section 7.3.1.1 describes the elemental chemical compositions of the boundary layer edge gas, char, and pyrolysis off-gas. Section 7.3.1.2 describes the thermodynamic property data input for each of the molecular species present in the system. Section 7.3.1.3 describes other miscellaneous input data required by the ACE program.

7.3.1.1 Elemental Composition of the Char, Pyrolysis Gas, and Boundary-Layer Edge Gas

Reference 7-5 describes the procedure used to arrive at the elemental composition of the char and pyrolysis gas for the Avcoat 5026-39 HCG material. In summary, based upon chemical analysis and TGA data supplied to Aerotherm by

NASA-MSC the following elemental compositions were determined:

Element	Elemental Mass Fractions Pyrolysis Gas	Char
H	0.0930	
B		0.0079
C	0.5470	0.4880
N	0.0190	
O	0.3410	0.2605
Al		0.0212
Si		0.1852
Ca		0.0366

Based on the data supplied by NASA-MSC, the char was assumed to consist of an ash plus carbon, with the ash being characterized by the following composition:

Specie	Ash Mass Fraction (relative to total char mass)
SiO_2	0.1869
Al_2O_3	0.0181
CaO	0.0240
B_2O_3	0.0120

Examination of the ash composition reveals that the elements Al, B, and Ca are present only in trace quantities, and to both simplify the analysis and reduce computer run time the idealization was made that the ash consists of SiO_2 only. To be consistent, the oxygen present in the deleted species Al_2O_3, CaO, and B_2O_3 was also removed; the resulting idealized composition of the char material used in the present analysis is therefore

Element	Mass Fraction in Char
C	0.488
O	0.273
Si	0.239

In specifying the boundary layer edge gas composition only the principal elements, nitrogen and oxygen, were assumed to comprise the air boundary-layer edge gas, with the mass fraction contribution due to other elements lumped into the nitrogen mass fraction. This composition is $\tilde{K}_N = 0.765$ and $\tilde{K}_O = 0.235$.

7.3.1.2 Thermodynamic Data for the Eligible Molecular Species

Thermodynamic data were input for all the molecular species which were considered in the evaluation of the surface thermochemical equilibrium. The following set of 56 species was assumed to sufficiently define the chemical system (* denotes condensed phase):

N	NO	HNO
CHN	OSi	NO_2
N_2O	O	HNO_2
HNO_3	HO	HO_2
HN	H	H_2
N_2	H_2O	O_2
CO	C	CH
CHNO	CHO	CH_2
CH_2O	CH_3	CH_4
C_2	C_2H	C_2N_2
C_2H_3	C_2H_4	C_2H_4O
C_2H_6	C_3	C_3H
C_3H_2	C_3H_3	C_3H_4
C_3H_5	C_3O_2	C_4
C_4H	HSi	H_4Si
NSi	O_2Si	Si_2
Si	C_2H_2	CN
CO_2	CSi*	O_2Si*
C*	Si*	

In addition, the following set of eight ionized species was included for calculations involving very high boundary-layer edge gas enthalpies:

e^-	N^+	N_2^+
O_2^-	NO^+	O_2^+
O^+	O^-	

Thermodynamic information for each molecular species includes

a. Heat of formation at 298°K

b. Sensible enthalpy increase from 298°K to 3,000°K

c. Three constants for an equation which gives specific heat as a function of temperature

d. Entropy at 1 atmosphere and 3,000°K

e. For the condensed-phase species, a fail temperature

The fail temperature of item e. used for the liquid-layer removal model was taken as the temperature at which the surface specie passes from the solid to the liquid state.

References 7-3, 7-6, and 7-7 are the sources of the thermodynamic data used in the present analysis. For all condensed phase species the fail temperatures were taken to be identical to melt temperatures as specified by the above references.

7.3.1.3 Miscellaneous Input Information

In addition to the elemental composition and thermodynamic property data described in the preceding two sections, ACE requires: 1) information regarding the boundary-layer edge gas thermodynamic state, and 2) a range of char and pyrolysis gas mass injection rates.

The boundary-layer edge gas state was uniquely defined by specification of elemental composition, pressure, and enthalpy. Section 7.4 contains a summary of the various edge gas states considered in the theoretical investigation. (The diffusion exponent for use in the unequal binary diffusion coefficient of the ACE program was taken to be 0.333 - see Reference 7-2.)

The following table summarizes the matrix of non-dimensional char removal and pyrolysis gas mass injection rates input to the ACE program:

Pyrolysis Gas Mass Injection Rates $\dot{m}_g/\rho_e u_e C_M$	Char Mass Removal Rates $\dot{m}_c/\rho_e u_e C_M$
20.	0.6
8.	0.45
3.	0.3
1.	0.2
0.6	0.1
0.4	0.05
0.2	0.02
0.1	0.01
0.01	0
0	

A surface mass balance, consistent with equilibrium chemistry relations, was computed by the ACE program for each combination of mass rates tabulated above.

7.3.2 Input Information for the CMA Program

Section 7.2.1 above briefly outlined the input information requirements for the CMA program. The following sections present the numerical information and a brief discussion for each category of input information.

7.3.2.1 Arrhenius Material Decomposition Equation

Material internal decomposition is characterized by a decomposition equation of the form

$$\frac{\partial \rho}{\partial \theta} = B \exp\left(\frac{-E_a}{RT}\right) \rho_p \left(\frac{\rho - \rho_c}{\rho_p}\right)^{\psi} \tag{7-1}$$

where

ρ = Instantaneous density

ρ_c = Residual or fully-charred material density

ρ_p = Virgin material density

θ = Time

T = Temperature

$B, E_a/R, \psi$ = Input constants characterizing the specific material

As described in Reference 7-5, helium atmosphere TGA data provided to Aerotherm by NASA-MSC were fit with the equation above. This determination of the densities ρ_c and ρ_p and the decomposition kinetic constants $B, E_a/R$, and ψ leads to the single rate equation which was used by the CMA program to treat the internal decomposition behavior of the 5026-39 HCG material:

$$\frac{\partial \rho}{\partial \theta} = 1.06 \times 10^6 \exp\left(-\frac{24{,}530}{T}\right) (34.0) \left(\frac{\rho - 16.0}{34.0}\right)^{2.5} \tag{7-2}$$

where the virgin material density was taken as 34.0 lb/ft^3 and the fully charred material density as 16.0 lb/ft^3.

7.3.2.2 Nodal Network

For all calculations performed under the analytical investigation the surface of the ablating material was assumed to be planar and the nodal

network one-dimensional. For analytical predictions of the experimental results obtained under the subject contract, total nodal network thicknesses corresponded to the actual model core depth (Figure 4-2). For the parametric study phase of the analytical investigation a total nodal network thickness of 2.00 inches was used.

Depending upon which total thickness was considered, the total number of nodes ranged from 36 to 49. The surface node thickness varied from 0.001 to 0.004 inch depending on the conditions considered in the calculation. In proceeding from the surface node into the material, the nodal thicknesses were progressively increased; the typically violent decomposition events occurring near the surface required that the surface nodes be relatively thin in order that the finite difference procedure could be stable, while the considerably slower transient thermal events occurring deeper in the material caused less strain on the numerical procedure and thus required only relatively thick nodes. To illustrate, the nodal arrangement for the 2.00-inch total network thickness is tabulated below:

	Thickness (inches)
Surface Node	0.001
4 Nodes	0.002
8 Nodes	0.004
8 Nodes	0.008
4 Nodes	0.016
4 Nodes	0.032
4 Nodes	0.064
2 Nodes	0.128
1 Node	0.191

7.3.2.3 Back Wall Boundary Conditions

To completely specify the boundary conditions for the solution of the material in-depth thermal conduction problem, conditions at the rear of the nodal network had to be specified. Heat transfer at the back wall is characterized by a convective heat transfer coefficient, a surface emissivity, and the temperature of the environment to which heat transfer takes place from the back wall. The heat transfer coefficient and emissivity were taken as zero, and the reservior temperature was taken as 530°R, yielding an insulated back wall boundary condition.

7.3.2.4 Material Properties

Material property data, in the form of specific heat, emissivity, and thermal conductivity for the fully-charred and virgin materials, are of course,

required input to the CMA program. All primary material property data were provided to Aerotherm by NASA-MSC. The primary data for conductivity was manipulated into a special conductivity model which accounts for both temperature and density effects on conductivity. Otherwise the data were used as provided.

Specific heat data are input for both the virgin material and the fully-charred material. The program then performs the integration

$$h = \int_{T_{ref}}^{T} C_p(T)\,dT \tag{7-3}$$

to obtain a table of sensible enthalpy as a function of temperature, for both the virgin material and fully-charred material. The sensible enthalpy of the material in a partially-degraded state at a particular temperature is then determined from a mass-weighted average of the virgin and fully-charred material enthalpies at that temperature. Reference 7-8 should be consulted for further computational details. The specific heat data used in all of the theoretical predictions are summarized in the following table:

T (^oR)	Virgin Material C_p (Btu/lb-^oR)	Fully-Charred Material C_p (Btu/lb-^oR)
210	0.100	--
460	0.260	0.190
710	0.369	--
960	0.420	0.280
1,210	0.430	0.315
1,460		0.350
1,960		0.425
2,460		0.430
5,000		

The thermal conductivity is treated in the program as a function of both temperature and density. As described in detail in Aerotherm Technical Memorandum 6007-TM-2R generated under this contract (Reference 7-9), the model used to characterize the thermal conductivity is represented by the equation

$$K(x,T) = f_1(x)K_p(T) + f_2(x)K_c(T) \tag{7-4}$$

where $K(x,T)$ is the partially-degraded material thermal conductivity, $K_p(T)$ and $K_c(T)$ are the virgin and fully-charred material temperature-dependent thermal conductivities, and $f_1(x)$ and $f_2(x)$ are empirically-determined weighting functions of the virgin material mass fraction. The functions $f_1(x)$ and $f_2(x)$ were determined by matching steady-state thermal conductivity data and partially-degraded material density data, provided to Aerotherm by NASA-MSC, to the conductivity equation above. Figure 7-1 and the following tables summarize the numerical information used in the thermal conductivity model for the 5026-39 HCG material:

T ($^\circ$R)	K_p (Btu/ft-sec-$^\circ$R)	K_c (Btu/ft-sec-$^\circ$R)
210	0.8×10^{-5}	--
460	1.33×10^{-5}	1.22×10^{-4}
710	1.64×10^{-5}	--
960	1.75×10^{-5}	1.25×10^{-4}
1,210	|	1.27×10^{-4}
1,460	|	1.29×10^{-4}
1,960	|	1.36×10^{-4}
2,460	|	1.46×10^{-4}
2,960	|	1.63×10^{-4}
3,460	|	1.90×10^{-4}
3,960	|	2.25×10^{-4}
4,460	|	|
5,000	|	|

x	$f_1(x)$	$f_2(x)$
1.000	1.000	0.0
0.975	|	|
0.932	0.794	|
0.880	0.604	|
0.640	0.0	0.520
0.375	|	0.846
0.195	|	1.000
0.0	|	|

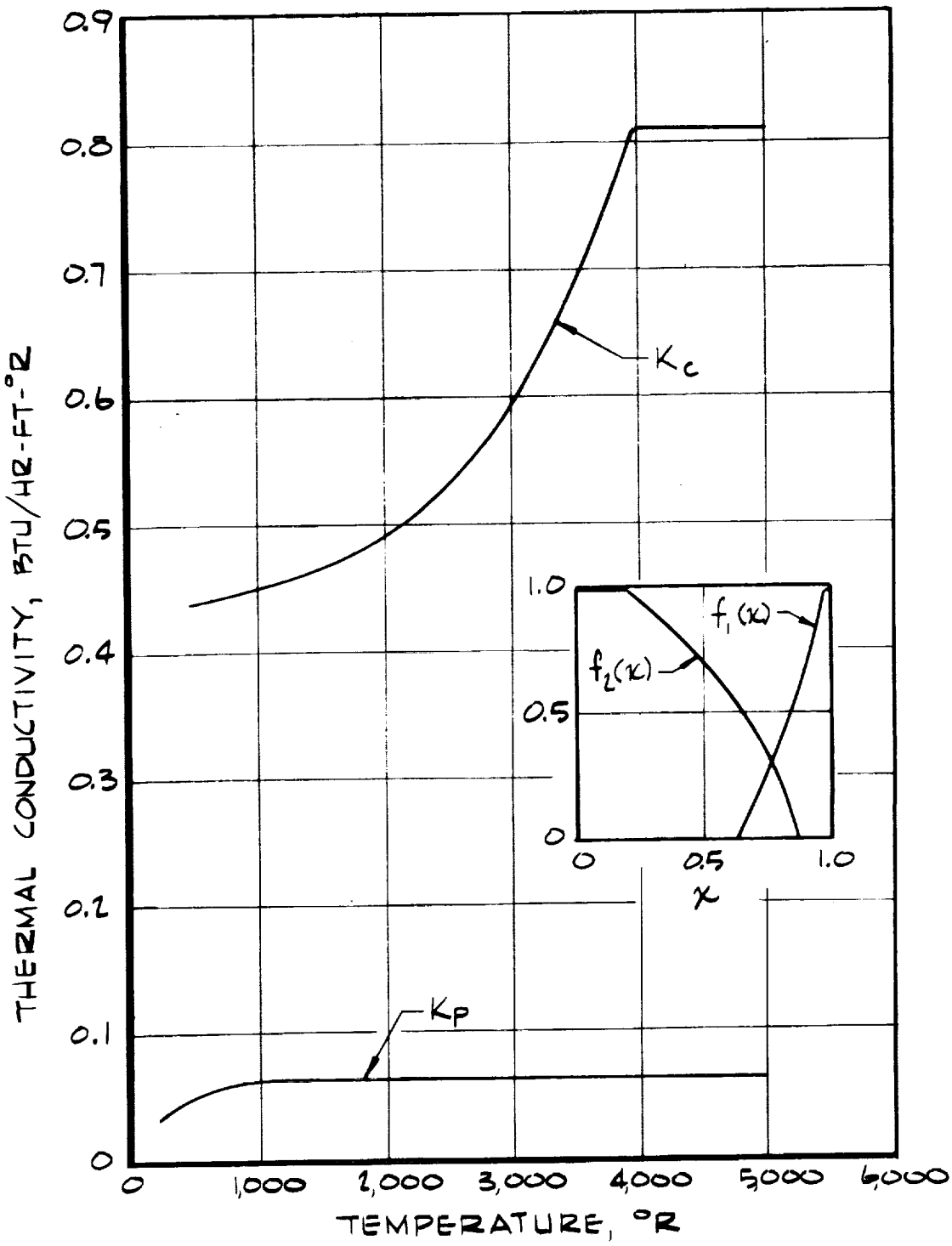

FIGURE 7-1 CHAR AND VIRGIN MATERIAL THERMAL CONDUCTIVITY AND f-FUNCTIONS.

From Reference 7-10, the material surface emittances used were 0.65 for the virgin material and 0.75 for the fully-charred material. This property was assumed to be independent of temperature for the range of temperatures of interest.

7.3.2.5 Pyrolysis Gas Enthalpy

The total enthalpy of the pyrolysis gases as a function of temperature, required as input to the CMA program, was calculated for gas-phase equilibrium conditions using the ACE program. Input information required to perform this calculation was the elemental composition of the pyrolysis gas (Section 7.3.1.1), a pressure and range of temperatures, and thermodynamic information for the eligible gas phase species comprising the system. The table of eligible molecular species in Section 7.3.1.2 contains all gas phase species appropriate to the pyrolysis gas.

For a pressure of 0.033 atm, the following table of total enthalpy as a function of temperature was calculated:

T (^{o}R)	h (Btu/lb)
900	-1,600
1,500	-900
2,000	10
2,500	806
3,000	1,687
3,600	2,222
4,500	3,720
5,400	7,600
6,300	13,290

Figure 7-2 contains a plot of the pyrolysis gas total enthalpy versus temperature for several different pressures covering a range of four orders of magnitude. Also included on the plot is the total enthalpy curve for the pressure of 0.033 atm. For convenience this single curve was input to the CMA program for all the ablation calculations.

7.3.2.6 Heats of Formation

As described in Reference 7-5, the heats of formation for the char and virgin material were determined from the known elemental compositions and molecular species heats of formation obtained from Reference 7-3. From the ash molecular breakdown (Section 7.3.1.1) an ash heat of formation of -6,460

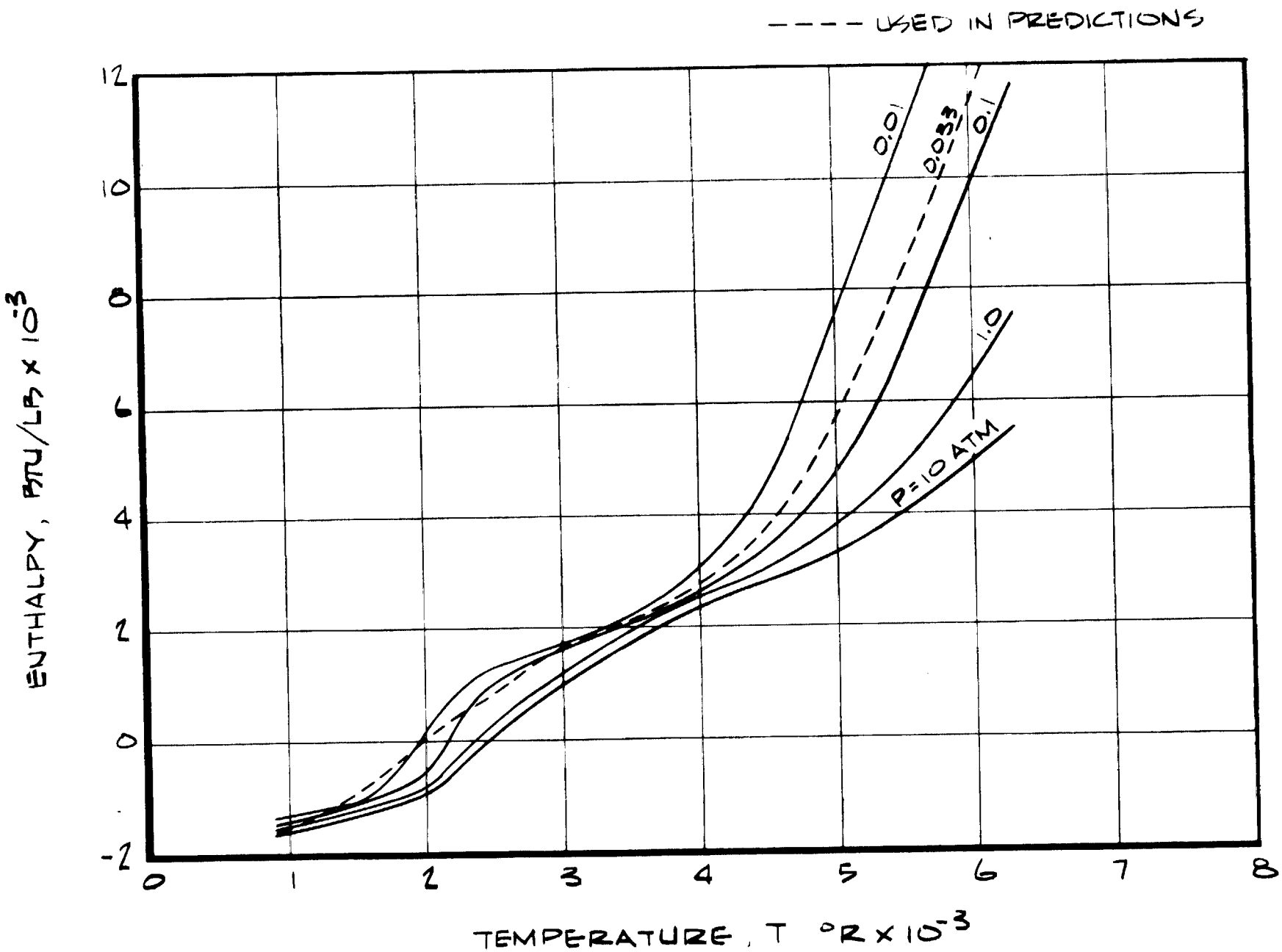

FIGURE 7.2 PYROLYSIS GAS TOTAL ENTHALPY VS TEMPERATURE

Btu/lb ash was calculated. The mass fraction of ash in the virgin material was determined to be 0.241 lb ash/lb virgin material. Assuming the remainder of the virgin material to be phenolic and epoxy novalac resin (mass fraction 0.759), with an assumed heat of formation of -1,110 Btu/lb resin (the value for phenolic resin), the virgin material heat of formation was calculated from a mass-average of the resin and ash heats of formation to be -2,390 Btu/lb virgin material.

Based upon TGA data the char residual mass fraction was determined to be 0.471 lb char/lb virgin material. Assuming the char to be composed of the ash plus carbon (the latter with a zero heat of formation), the heat of formation of the char was computed to be -3,310 Btu/lb char.

7.3.2.7 Functions of Time Boundary Conditions

The functions-of-time input depends upon the program boundary condition option being used; the heat transfer coefficient, and boundary-layer-edge pressure and recovery enthalpy being input for Option 1 and the surface temperature and recession rate being input for Option 2. For the Option 1 cases, the boundary conditions for the calculations were specified by the enthalpy, the cold wall heat flux, the stagnation pressure, and, where appropriate, the radiation heat flux. The heat transfer coefficient, required as input, was determined by the following procedure. The cold wall heat transfer coefficient, for stagnation point flow is given by

$$(\rho_e u_e C_H)_{cw} = \frac{q_c}{h - h_w} \tag{7-5}$$

where h_w was taken as the enthalpy corresponding to a wall temperature of 300°F. For constant boundary layer edge conditions, the relation between the non-ablating wall, stagnation point heat transfer coefficient and the properties affected by wall temperature is given by (References 5-3 and 7-11)

$$\rho_e u_e C_H \propto \frac{(\rho_w \mu_w)^{0.1}}{Pr_w} \tag{7-6}$$

The density and viscosity are related to temperature by

$$\rho_w \propto \frac{1}{ZT_w} \tag{7-7}$$

$$\mu_w \propto \frac{T_w^{3/2}}{T_w + 198.6} \approx T_w^{1/2} \tag{7-8}$$

where the density relation applies at constant pressure and the viscosity relation is Sutherland's formula, the approximation being valid at high temperatures. For the range of surface temperatures of interest, the Prandtl number (Equation (7-7)) does not vary significantly and the value of Z (Equation (7-7)) is always close to 1.0. With these simplifications, Equation (7-6) then reduces to

$$\rho_e u_e C_H \propto \frac{1}{T_w^{0.05}} \tag{7-9}$$

or

$$\frac{(\rho_e u_e C_H)_{hw}}{(\rho_e u_e C_H)_{cw}} = \left(\frac{T_{cw}}{T_{hw}}\right)^{0.05} \tag{7-10}$$

Typical values of material surface temperature together with the assumed 300°F cold wall temperature yielded a heat transfer coefficient ratio, Equation (7-10), of 0.925 as being representative of the range of surface temperatures calculated. The hot wall convective heat transfer coefficient input to the CMA program was therefore calculated by the equation

$$(\rho_e u_e C_H)_{hw} = 0.925 \frac{q_c}{h - h_w} \tag{7-11}$$

where h_w is the enthalpy corresponding to a wall temperature of 300°F. In the CMA program the non-ablating heat transfer coefficient as determined above is corrected for blowing according to

$$\frac{\rho_e u_e C_H}{(\rho_e u_e C_H)_o} = \frac{\Phi}{e^{\Phi} - 1} \tag{7-12}$$

where

$$\Phi = \frac{2\lambda \dot{m}_a}{(\rho_e u_e C_H)_o}$$

and λ is the blowing reduction parameter. Thus $\rho_e u_e C_H$ is entered as a constant in the functions-of-time table as calculated from Equation (7-11).

The radiation heat flux in this portion of the input data is that heat flux impinging upon the ablation material surface from the high temperature boundary-layer gas (or in the experimental situation, a separate radiation source). This flux was input as a constant value in the appropriate cases.

Boundary-layer edge pressure and recovery enthalpy were entered as constants in the functions-of-time table, recovery enthalpy being total enthalpy.

The surface temperature and recession rate as functions-of-time for the Option 2 boundary condition calculations were based upon the experimental surface recession and surface temperature data obtained from the model tests.

7.3.2.8 Ratio of Mass Transfer to Heat Transfer Coefficient

The mass transfer to heat transfer coefficient ratio (Option 1) was determined from the Chilton-Colburn analogy (see Reference 7-12)

$$\frac{\rho_e u_e C_M}{\rho_e u_e C_H} = Le^{2/3} \tag{7-13}$$

where Le is the Lewis number. The Lewis number was available from the ACE program calculations.

7.3.2.9 Radiation View Factor

For the stagnation point heat transfer considered herein, the surface radiation view factor (Option 1) was unity, and so entered as part of the input.

7.3.2.10 Surface Thermochemistry

As discussed in Section 7.3.1, the Option 1 surface thermochemistry input to the CMA program was generated by the ACE program. The results of the ACE calculations are too extensive to present in their entirety here. Some typical results are presented in Figure 7-3, however. The dimensionless char removal rate $\dot{m}_c/\rho_e u_e C_M$ is plotted against surface temperature with the dimensionless pyrolysis off-gas rate $\dot{m}_g/\rho_e u_e C_M$ as a parameter. For illustrative purposes, results are presented for only three off-gas rates, covering the spectrum from high to low. Figure 7-3a presents results which show the effect of pressure on surface thermochemistry; Figure 7-3b presents results which show the effect of enthalpy. Note that the enthalpy effect is due only to its effect on the boundary layer edge molecular composition, this composition in turn affecting the diffusion rates of chemical species through the boundary layer and therefore the surface chemical response.

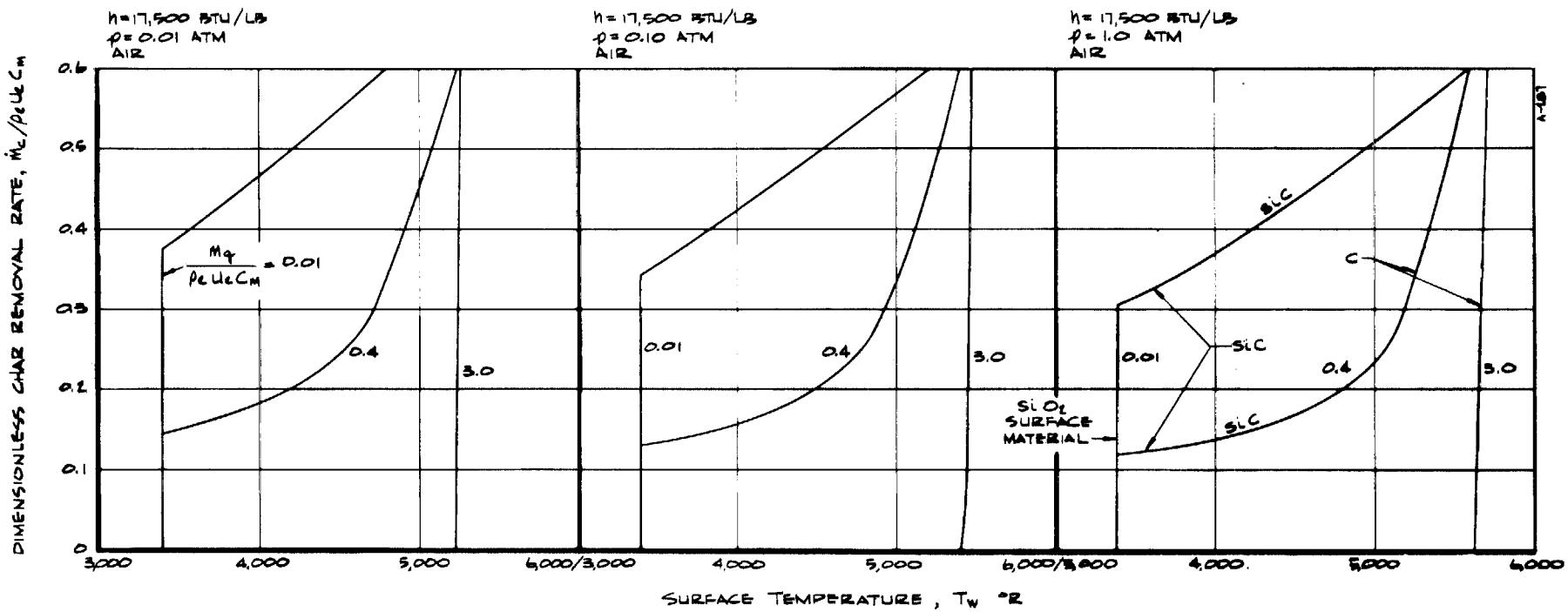

(a) EFFECT OF PRESSURE

FIGURE 7-3 TYPICAL SURFACE THERMOCHEMICAL RESPONSE RESULTS.

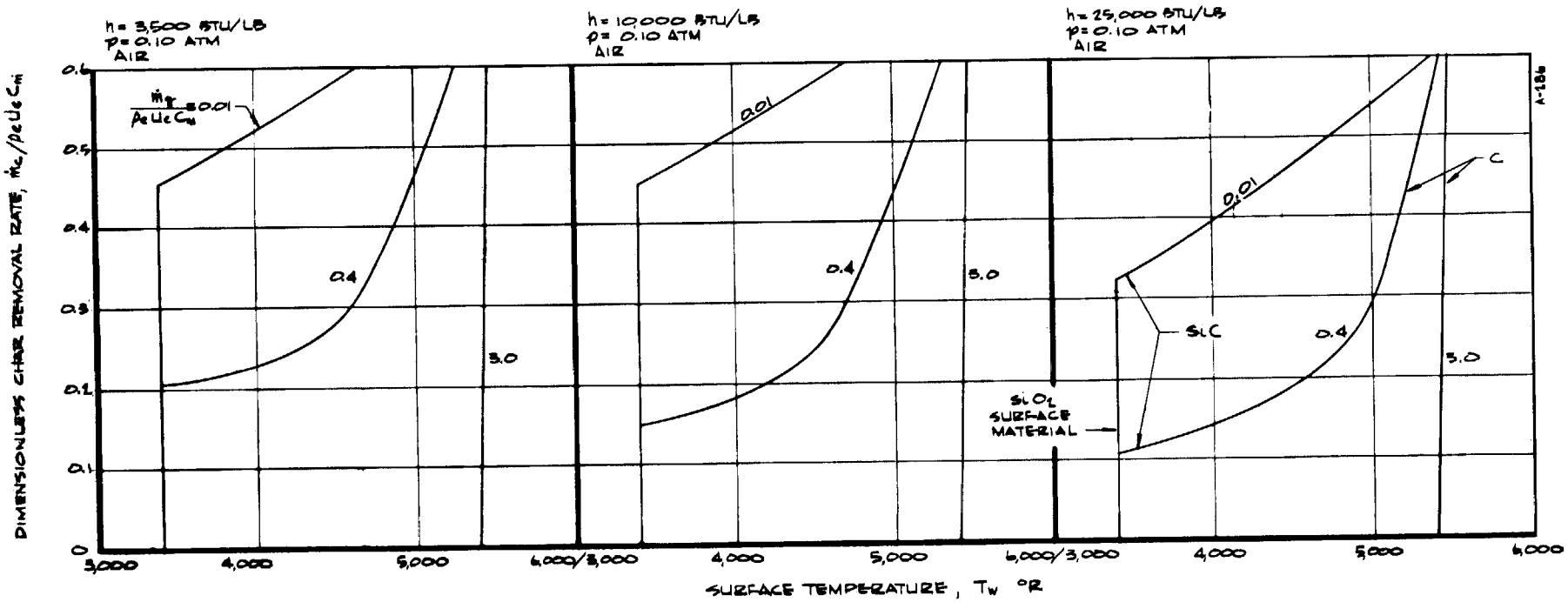

(b) EFFECT OF ENTHALPY

FIGURE 7-5 CONCLUDED

The following table lists all boundary-layer edge conditions for which surface equilibrium chemistry tables were generated for both the experimental and parametric predictions:

Edge Pressure (atm)	Edge Enthalpy (Btu/lb)	Edge Composition K
0.001	25,000	$0.77N_2/0.23O_2$
0.01		
0.1		
1.0		
10.0		
0.01	17,500	
0.1		
1.0		
0.01	10,000	
0.028		
0.1		
1.0		
0.028	5,500	
0.1	5,000	
1.0		
3.0		
0.01	4,910	
0.1	3,500	
0.0082	3,440	
0.02	3,000	
1.0	17,500	$0.85N_2/0.15O_2$
	5,000	
	17,500	$0.93N_2/0.07O_2$
	5,000	
	17,500	Nitrogen
0.028	10,000	
1.0		
	5,000	
0.029	11,000	Helium

7.4 RESULTS OF THE ANALYTICAL PREDICTIONS

The preceding sections described the ablation computer programs used and the input data required to perform the analytical investigation phase of the subject contract. This section presents the results of the theoretical predictions of the surface and in-depth response of the 5026-39 HCG material.

The material response is basically defined by the surface temperature and recession histories, and internal temperature distribution history for a given set of heating conditions. This information is presented in tabular and graphical form in Section 7.4.1 for the experimental predictions, and in Section 7.4.2 for the parametric predictions.

7.4.1 Experimental Predictions

Theoretical thermal response predictions were made for fourteen different sets of boundary conditions, corresponding to fourteen different heating conditions of the experimental phase of the program. A fully-theoretical prediction, using the Option 1 type of input boundary conditions, was made for each of the fourteen cases. Also, from the measurements of the model surface response, (surface recession rate and surface temperature), a prediction was made of the in-depth response for each of the fourteen cases, using the Option 2 type of input boundary conditions.

Table 7-1 presents the heating conditions and Options 1 and 2 predicted material performance for each of the fourteen cases. The heating condition is defined by the stagnation enthalpy, stagnation pressure, heating rate, exposure time, and chemical environment. The material response quantities included are the values of the total surface recession, char depth, pyrolysis zone depth, and surface temperature at the end of the test, and the average surface recession rate. The plots contained in Figures 7-4 and 7-5 present surface recession, char depth, pyrolysis zone depth, surface temperature, and in-depth thermocouple temperatures as a function of time for the Option 1 and Option 2 experimental predictions, respectively.

7.4.2 Parametric Predictions

Theoretical thermal response predictions were made for a total of 47 different heating conditions; as mentioned earlier, only Option 1 predictions were made for the parametric investigation. Table 7-2 presents the heating conditions and predicted thermochemical response for each of the 47 cases; this table is arranged in a manner similar to that of Table 7-1. For this part of the theoretical investigation the stagnation enthalpy was varied from 3,000 to 25,000 Btu/lb, the stagnation pressure was varied from 0.001 to 10 atm, the convective heating rate was varied from 20 to 500 Btu/ft^{2}sec, the radiative heating rate varied from 0 to 500 Btu/ft^{2}sec, and the chemical environment varied from air to pure nitrogen. Exposure time was varied from 30 to 300 sec, with cooldown periods being either 0 or 120 seconds. Plots similar to those of Figure 7-4 are available for all conditions of the parametric study and will be supplied upon request.

TABLE 7-1

PREDICTIONS OF MODEL PERFORMANCE

Phase	Model No.	Enthalpy h (Btu/lb)	Stagnation Pressure p_s (atm)	Heating Rate q_c (Btu/ft^2-sec)	Chemical Environment	Exposure Time θ (sec)	OPTION 1 Surface Recession s (inch)	OPTION 1 Char Depth (1) (inch)	OPTION 1 Pyrolysis Zone Depth (1) (inch)	OPTION 1 Average Recession Rate $\dot{s}$ (mils/sec)	OPTION 2 Surface Recession s (inch)	OPTION 2 Depth (1) (inch)	OPTION 2 Pyrolysis Zone Depth (1) (inch)	OPTION 2 Average Recession Rate (2) $\dot{s}$ (mils/sec)
III	158/BH/1.0	5,031	1.06	1,175	Air	10.2	0.391	0.400	0.413	38.3	0.537	0.537	0.542	52.6
|	140/BH/1.0	5,151	3.10	1,775	|	2.9	0.211	0.212	0.217	72.8	0.417	0.417	0.418	144
IVA	93/BH/2.0	3,440	0.0082	33.0	|	210.2	0.0023	0.351	0.468	0.0109	0.0996	0.365	0.490	0.474
|	91/BH/2.0	10,969	0.0079	116	|	60.5	0.0048	0.215	0.271	0.079	0.152	0.270	0.322	2.51
|	108/BH/2.0	16,301	0.0080	154	|	60.4	0.0006	0.225	0.282	0.0099	0.148	0.280	0.332	2.45
IVB	84/BH/2.0	11,000	0.029	173	Helium	60.3	0	0.215	0.267	0	0.0226	0.238	0.291	0.375
|	80/BH/2.0	9,960	0.0276	271	Nitrogen	60.6	|	0.276	0.321	|	0.172	0.354	0.397	2.84
V	114/BH/4.0	4,910	0.010	33.2	Air	211.4	0.0009	0.342	0.455	0.0043	0.085	0.382	0.501	0.402
|	122/BH/4.0	10,433	0.0275	134	|	60.6	0.0159	0.231	0.287	0.262	0.170	0.311	0.362	2.80
VIA	30/BH/2.0	5,500	0.028	101	|	90.0	0.0958	0.301	0.377	1.07	0.218	0.386	0.442	2.42
VIB	27/BH/2.0	10,270	0.0282	189	|	|	0.134	0.363	0.422	1.49	0.394	0.534	0.579	4.38
|	102/BH/2.0	16,517	0.0271	278	|	44.7	0.029	0.229	0.277	0.649	0.220	0.334	0.374	4.92
VII	96/BH/2.0	24,300	0.028	444	|	30.8	0.073	0.231	0.260	2.37	0.148	0.253	0.291	4.81
|	111/BH/1.0	10,000	0.088	|	|	39.6	0.253	0.345	0.374	6.38	0.388	0.450	0.475	9.80

(1) Depths include effect of cooldown after test.

(a) Input to computer program together with surface temperature history (see Figure 7-5).

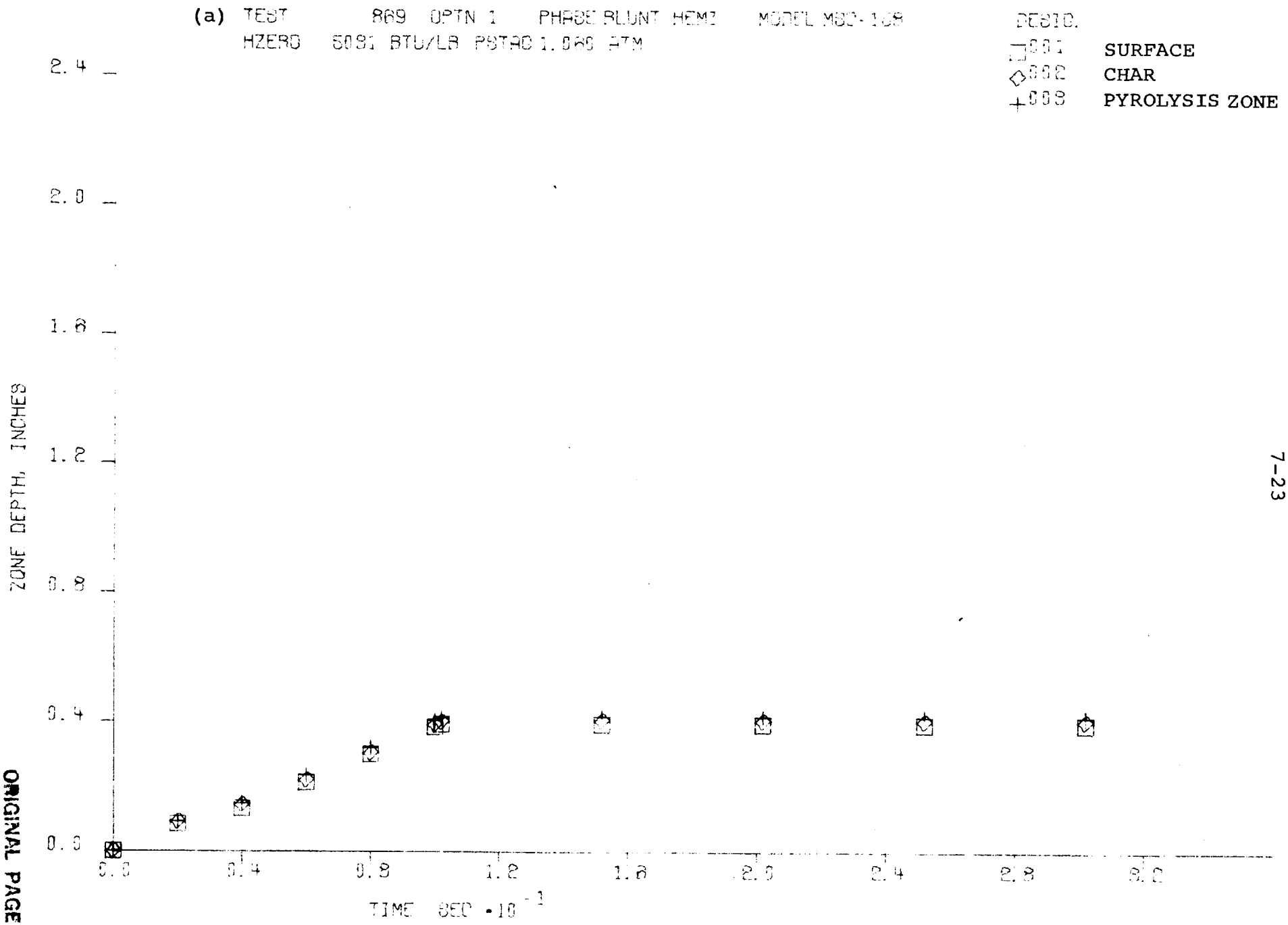

Figure 7-4. Analytical Predictions of Material Performance for Models Exposed to Simulated Reentry Conditions (Option 1)

ORIGINAL PAGE IS
OF POOR QUALITY

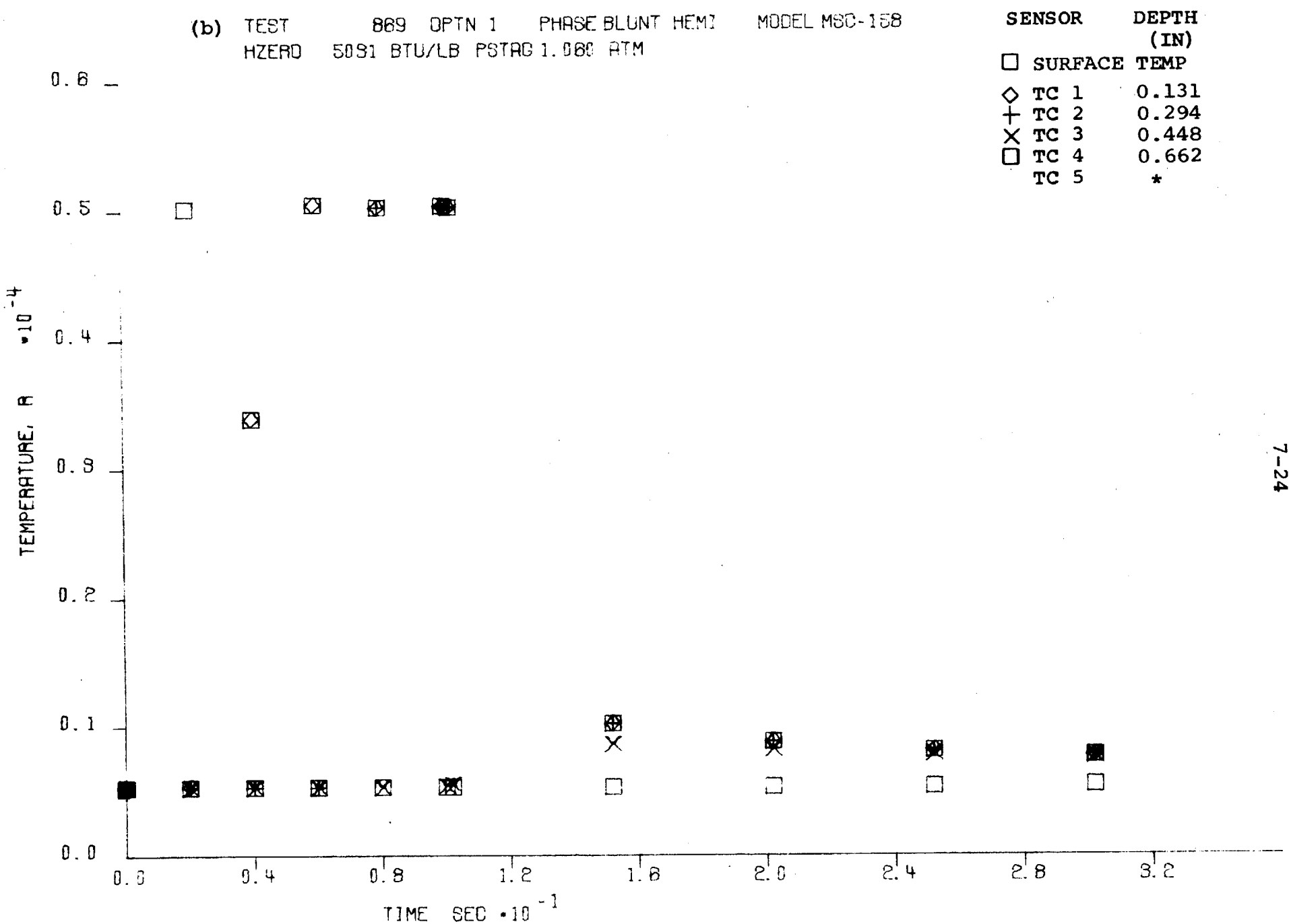

Figure 7-4. Continued.

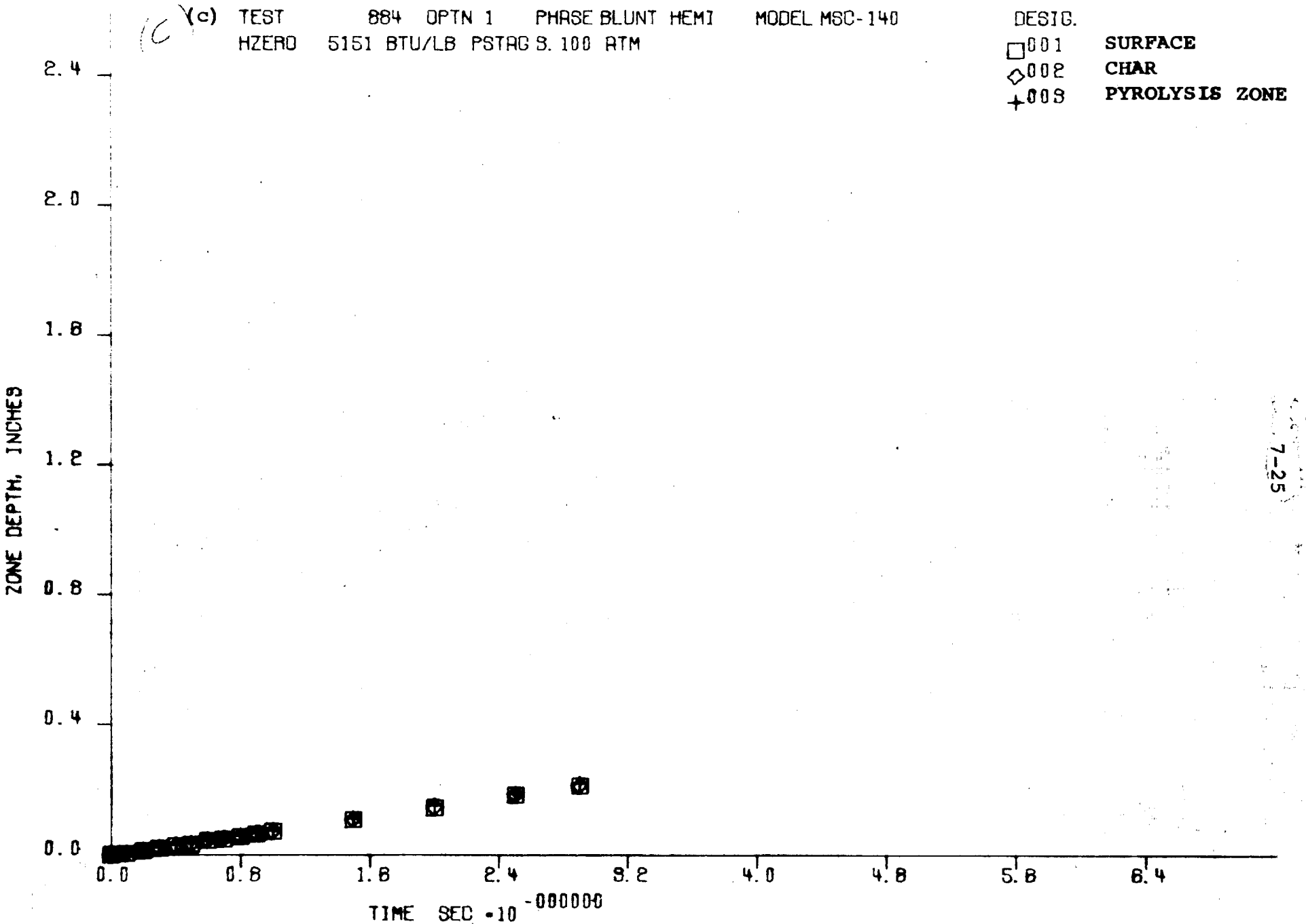

Figure 7-4. Continued.

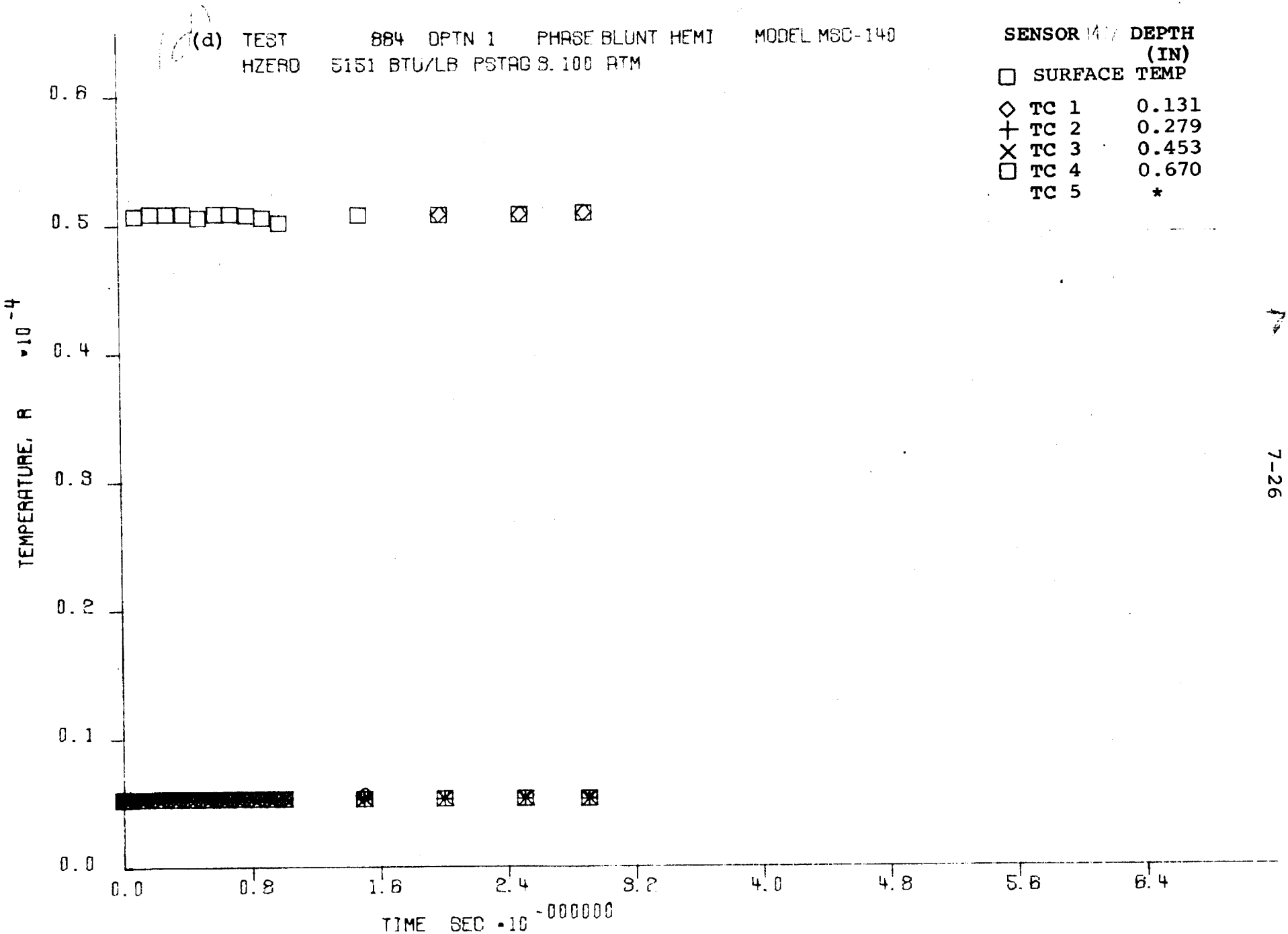

Figure 7-4. Continued.

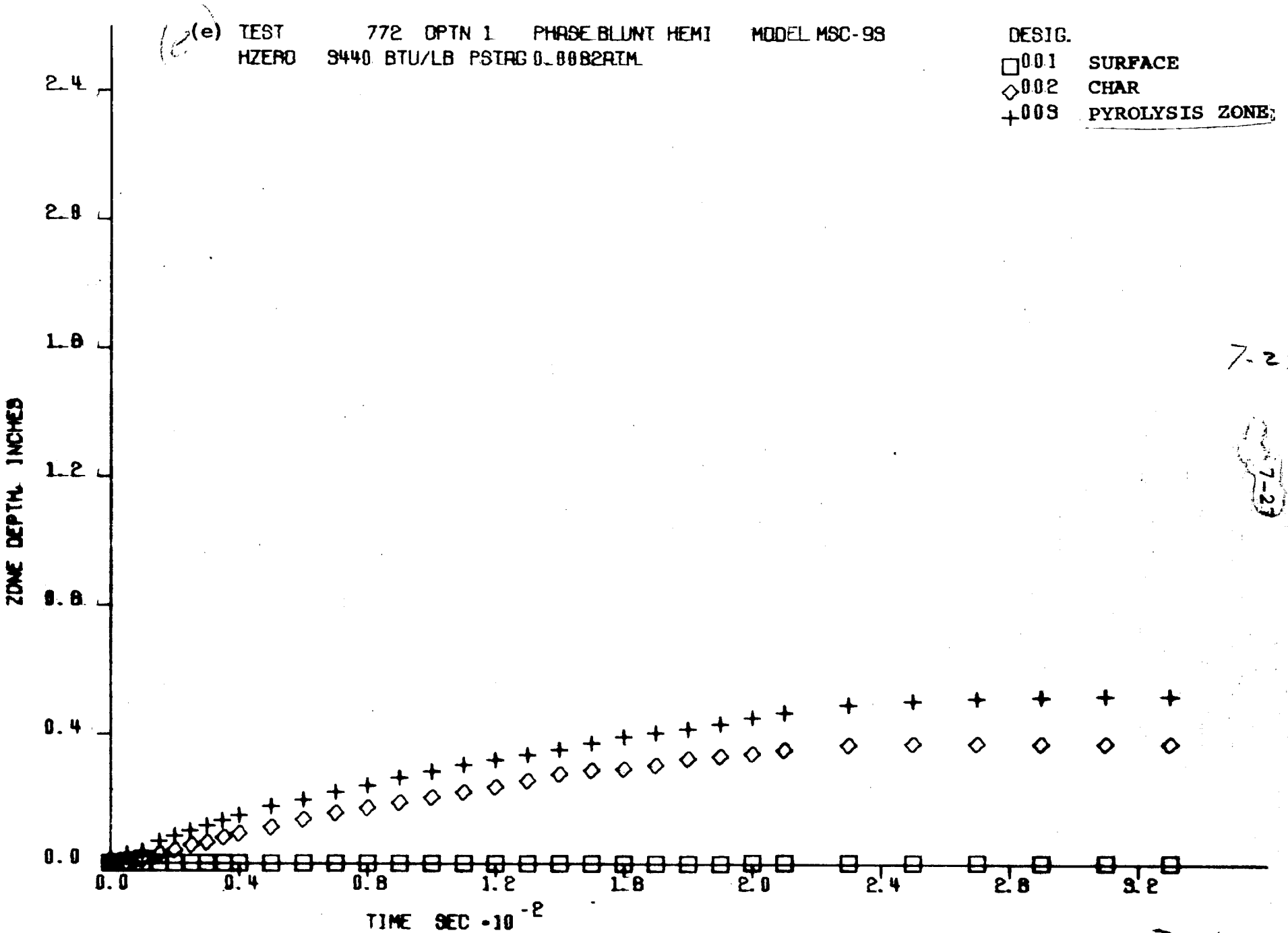

Figure 7-4. Continued.

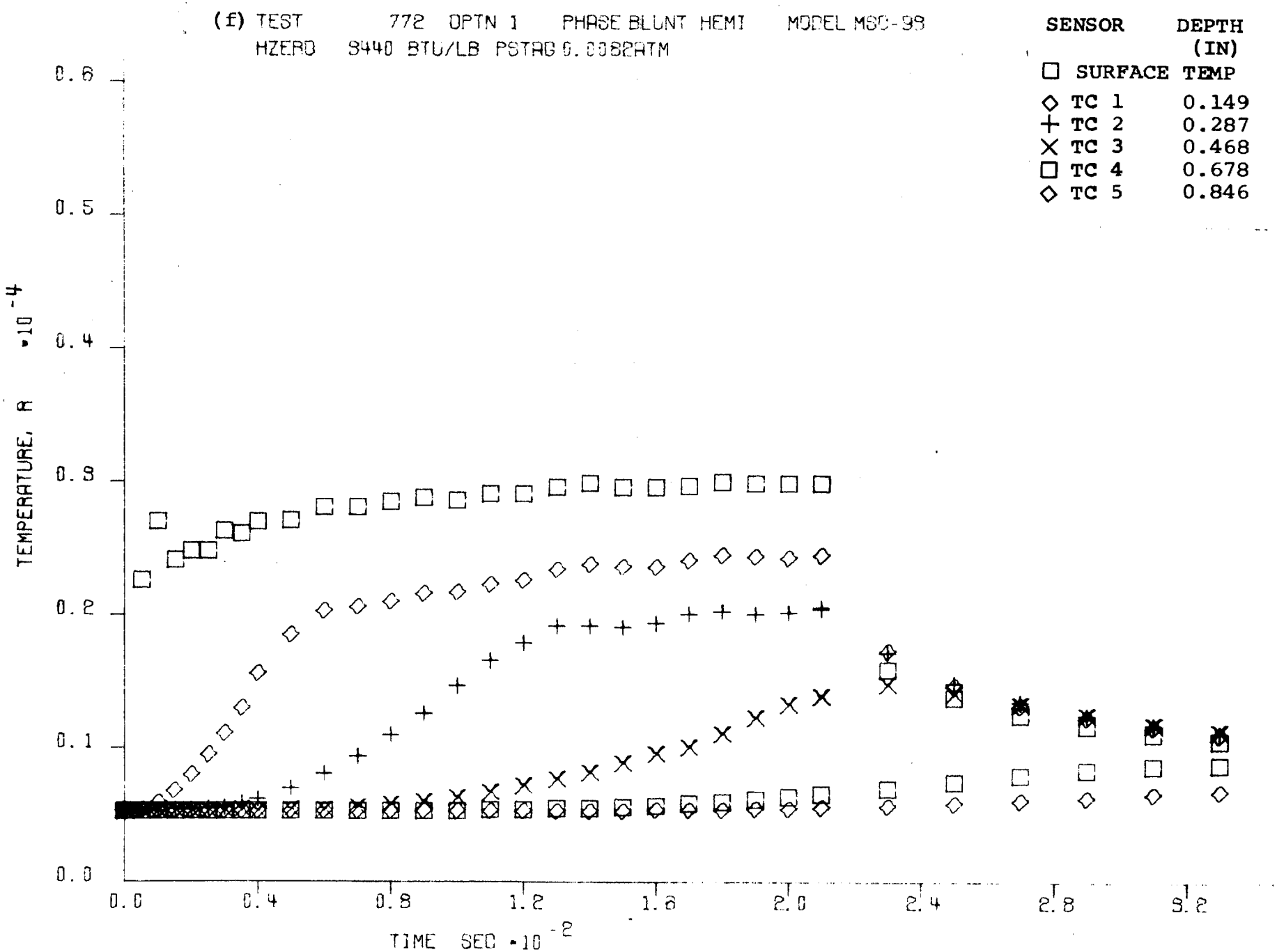

Figure 7-4. Continued.

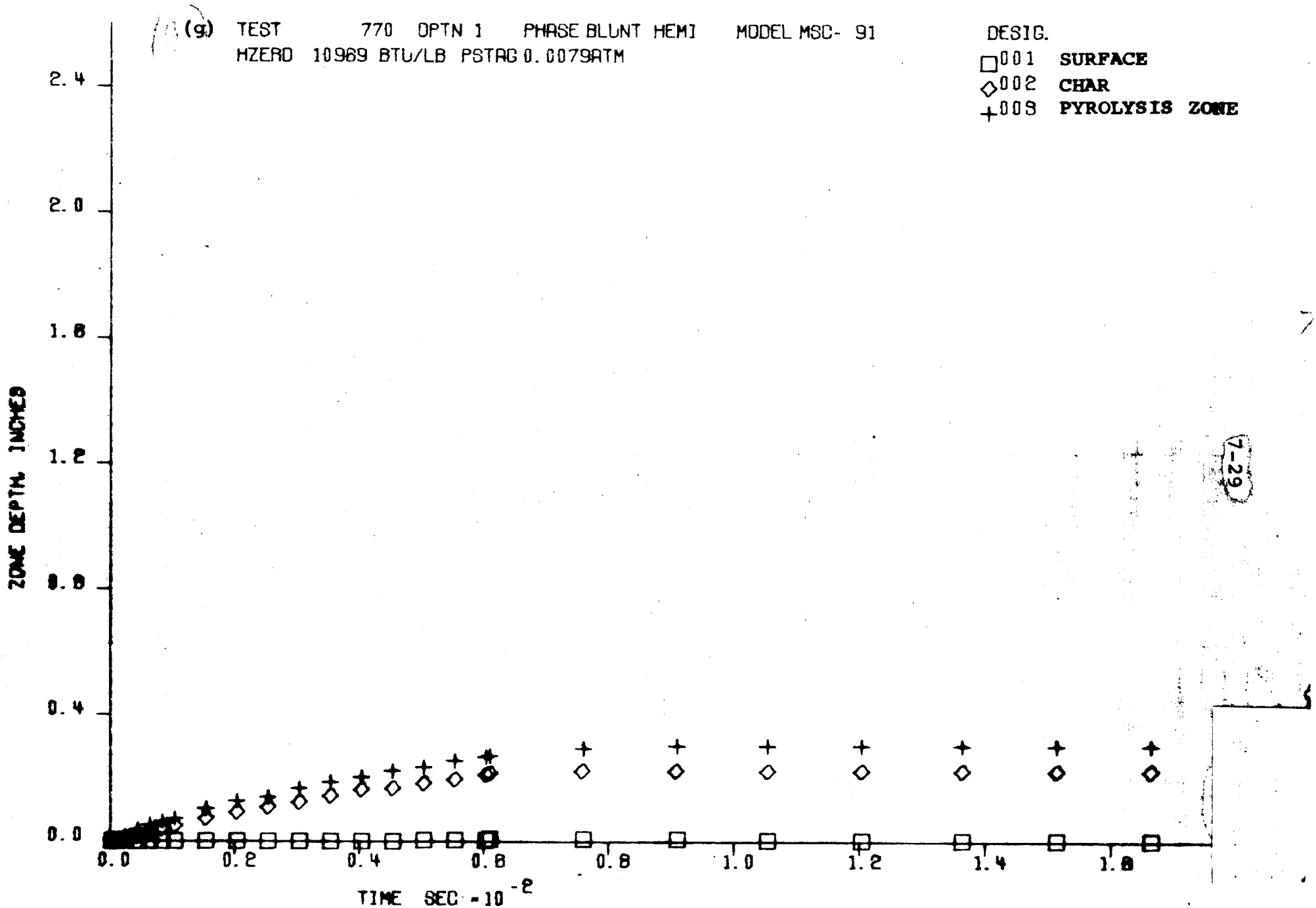

Figure 7-4. Continued.

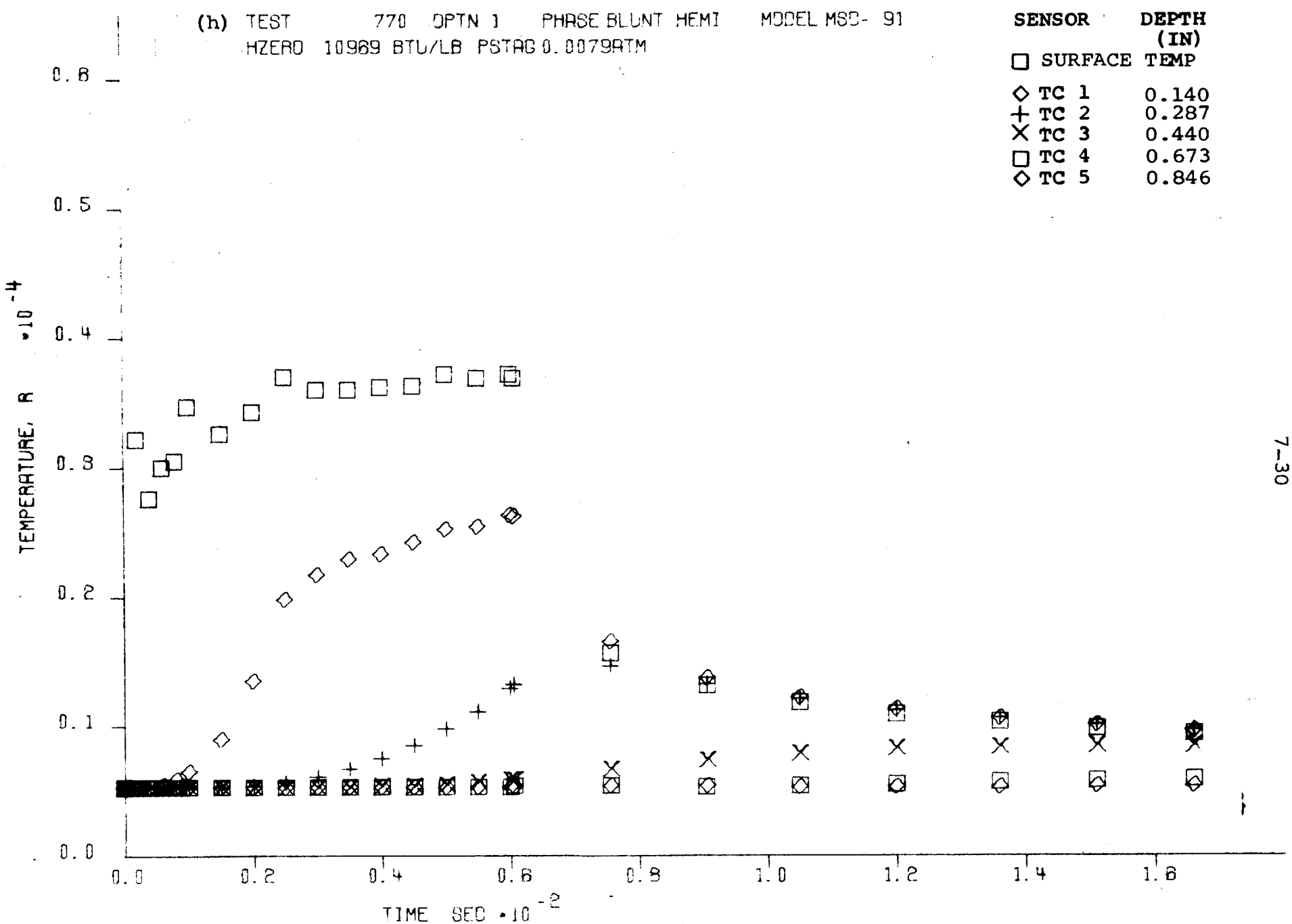

Figure 7-4. Continued.

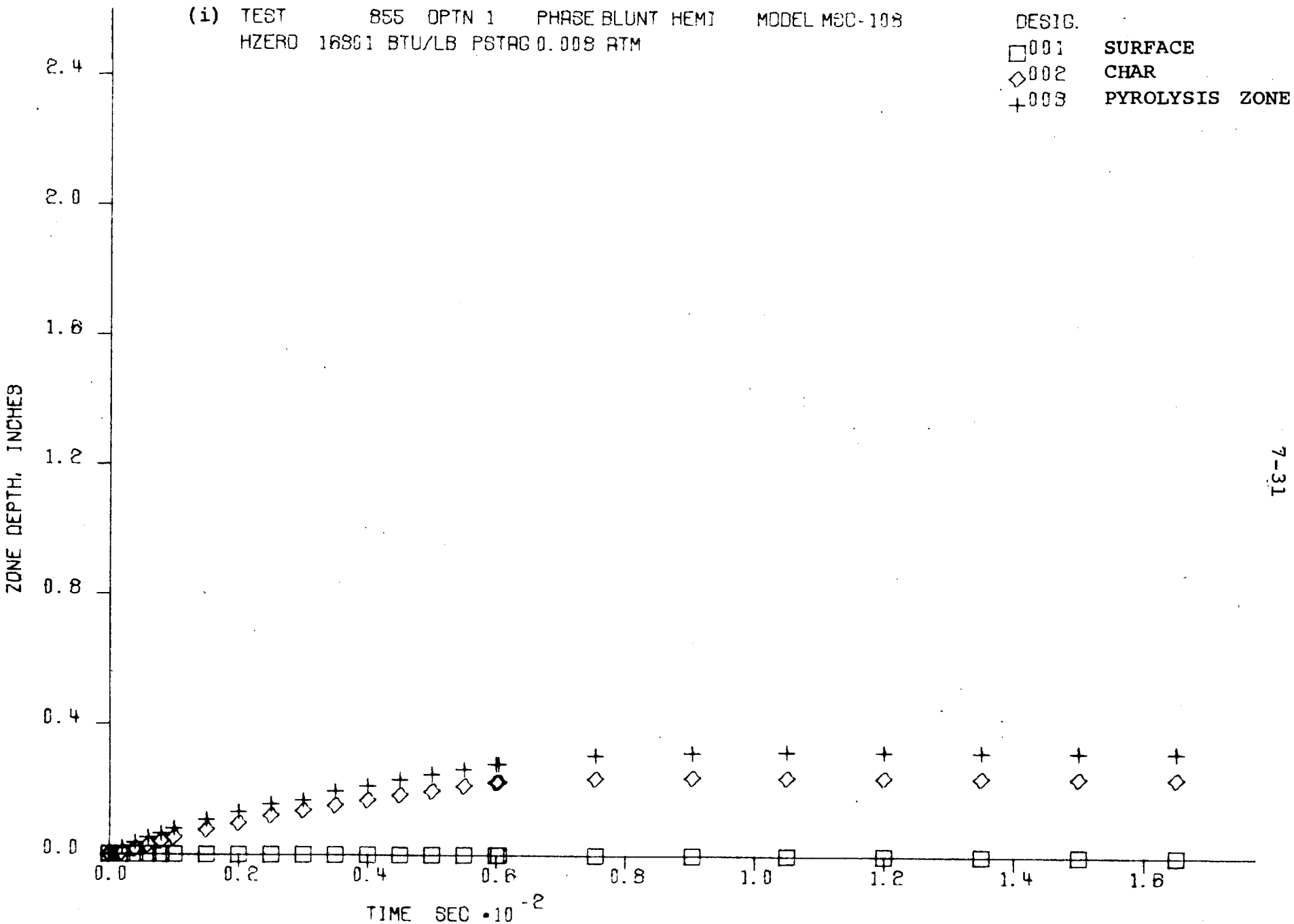

Figure 7-4. Continued.

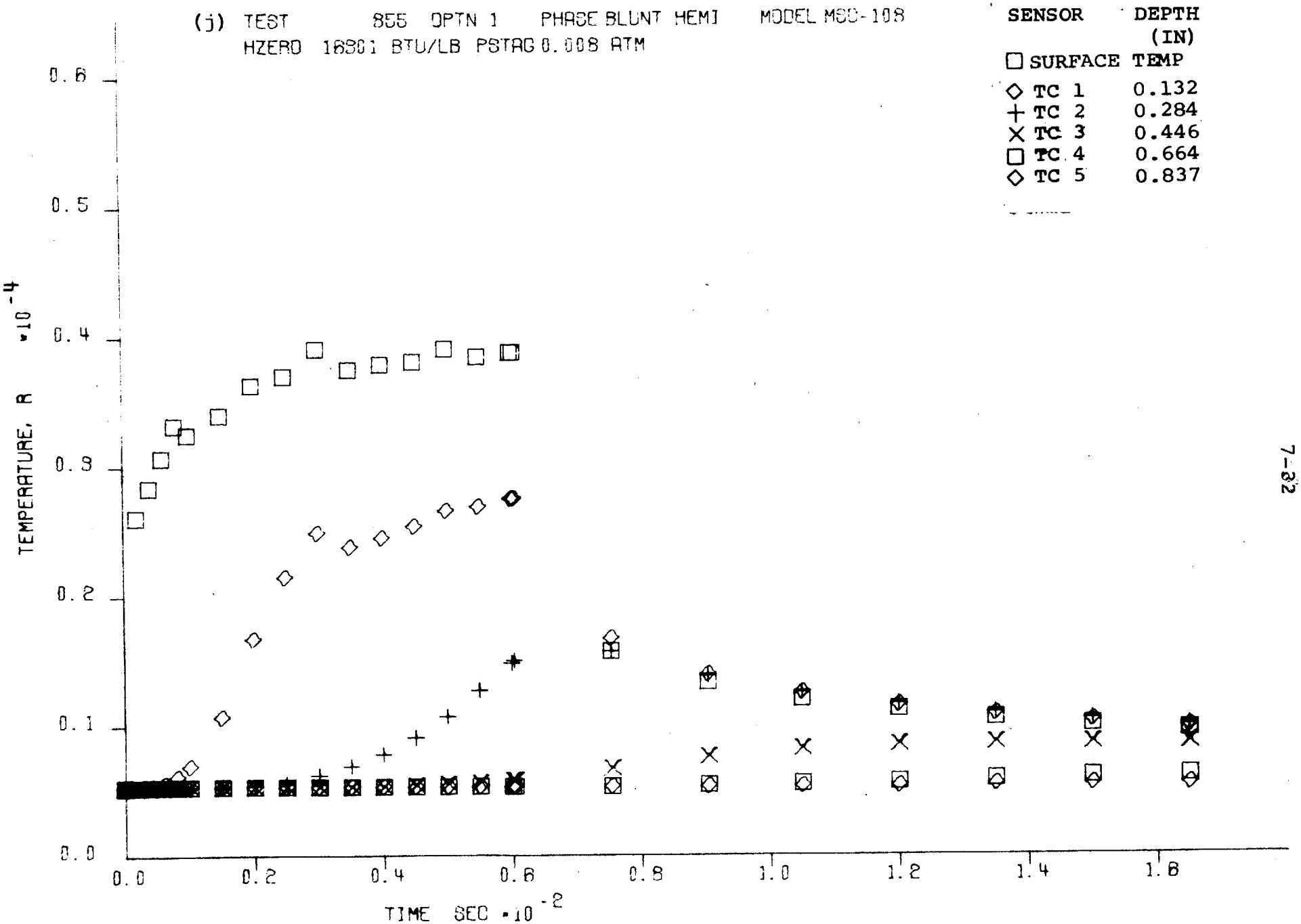

Figure 7-4. Continued.

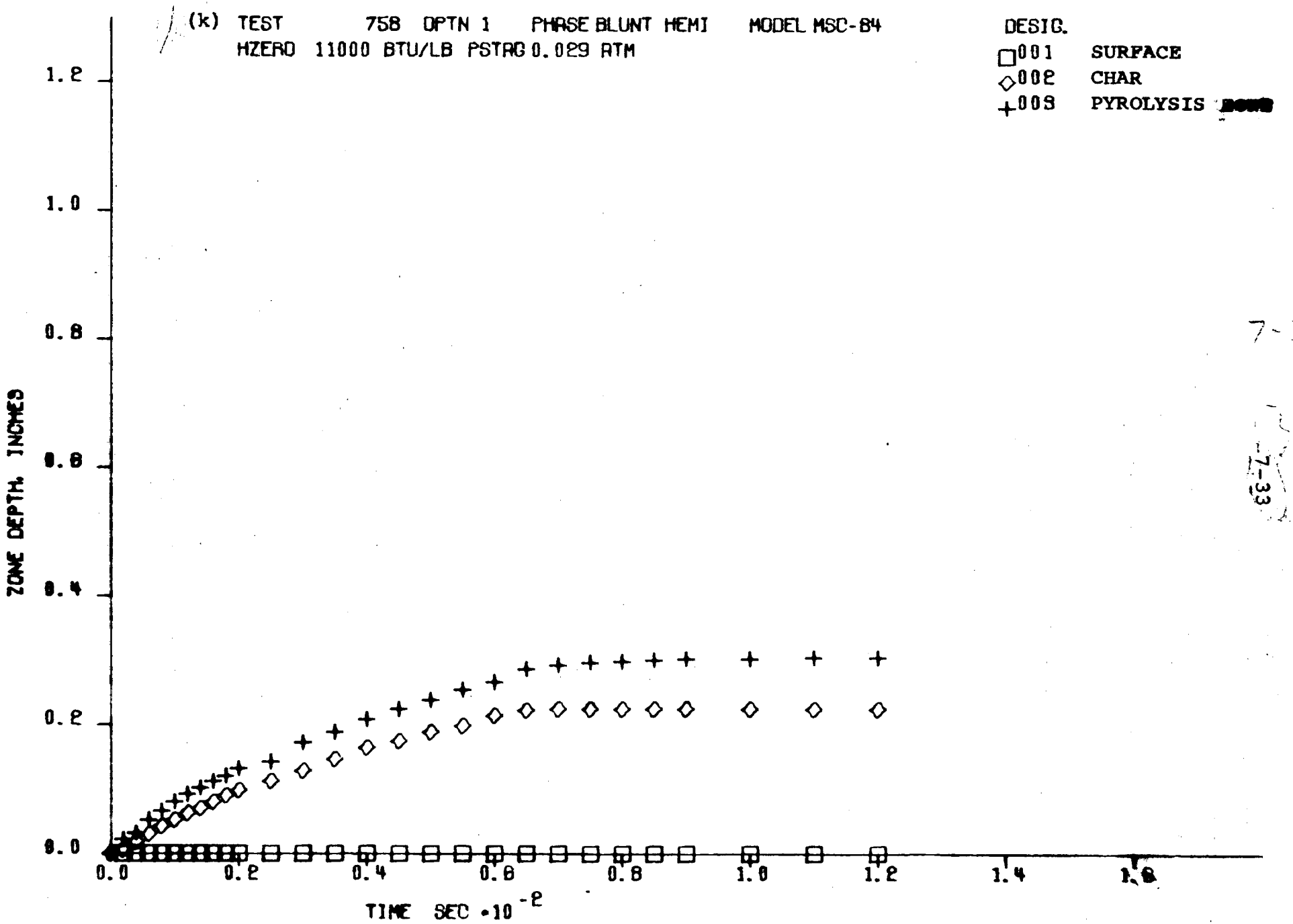

Figure Continued.

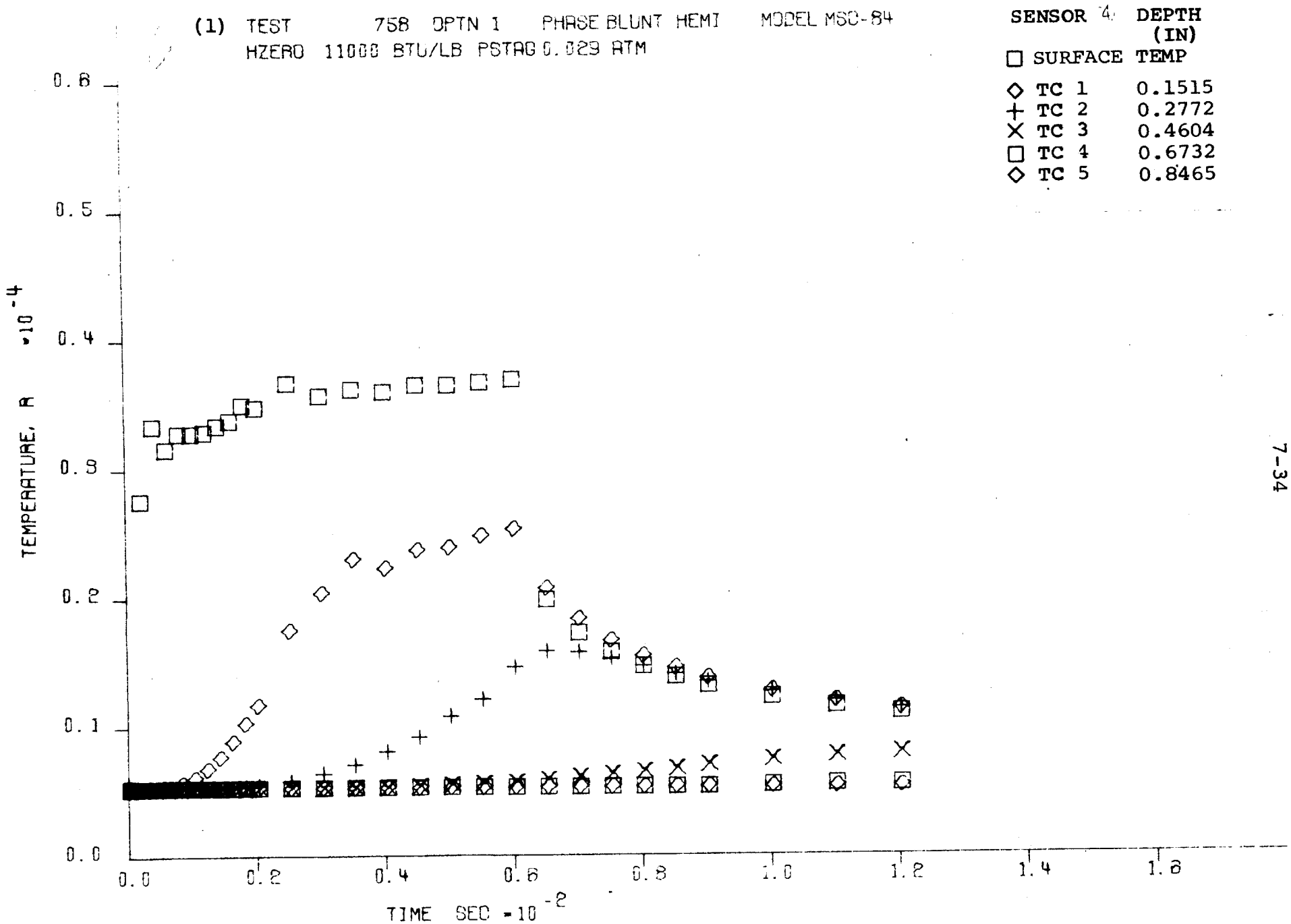

Figure 7-4. Continued.

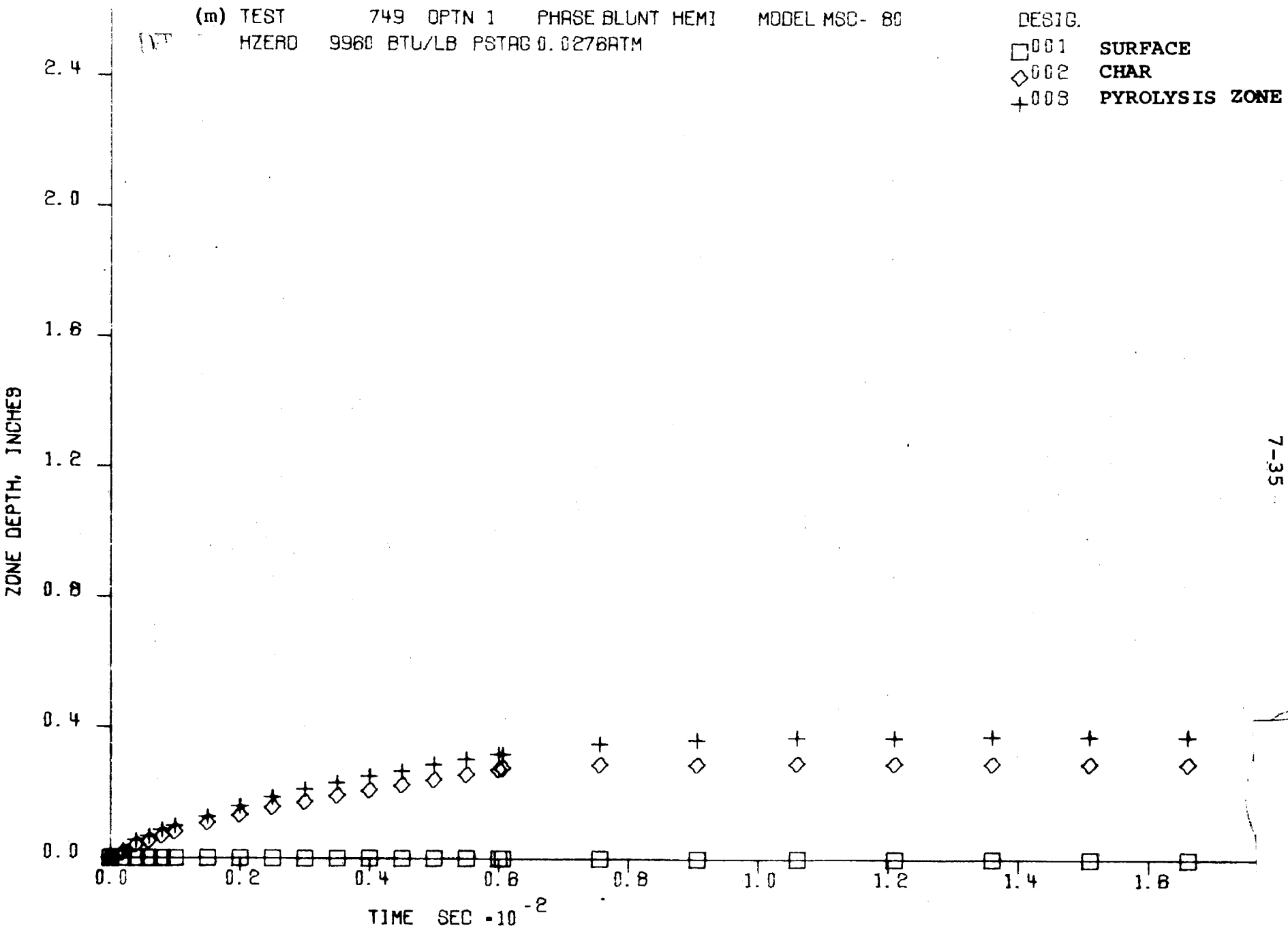

Figure 7-4. Continued.

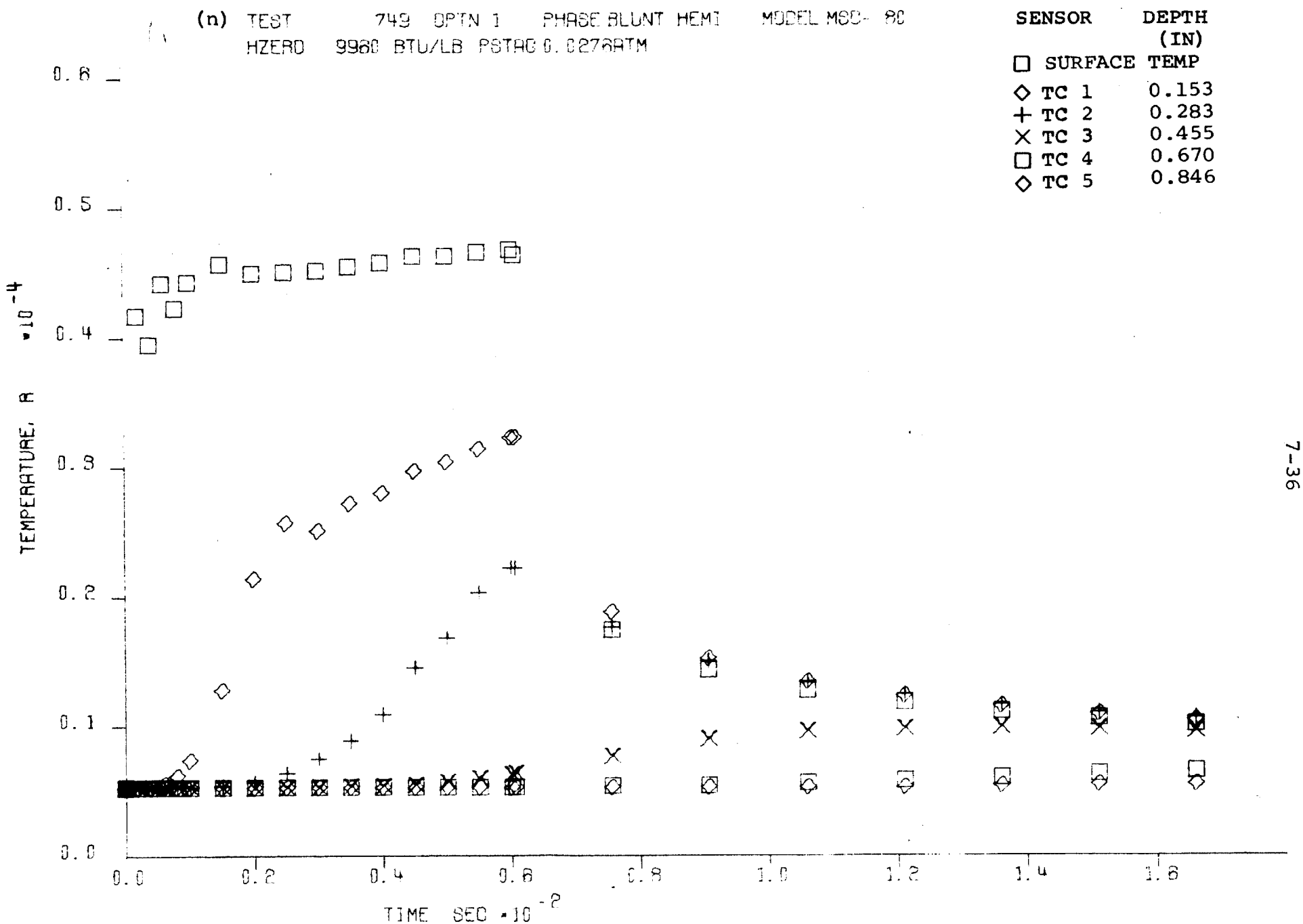

Figure 7-4. Continued.

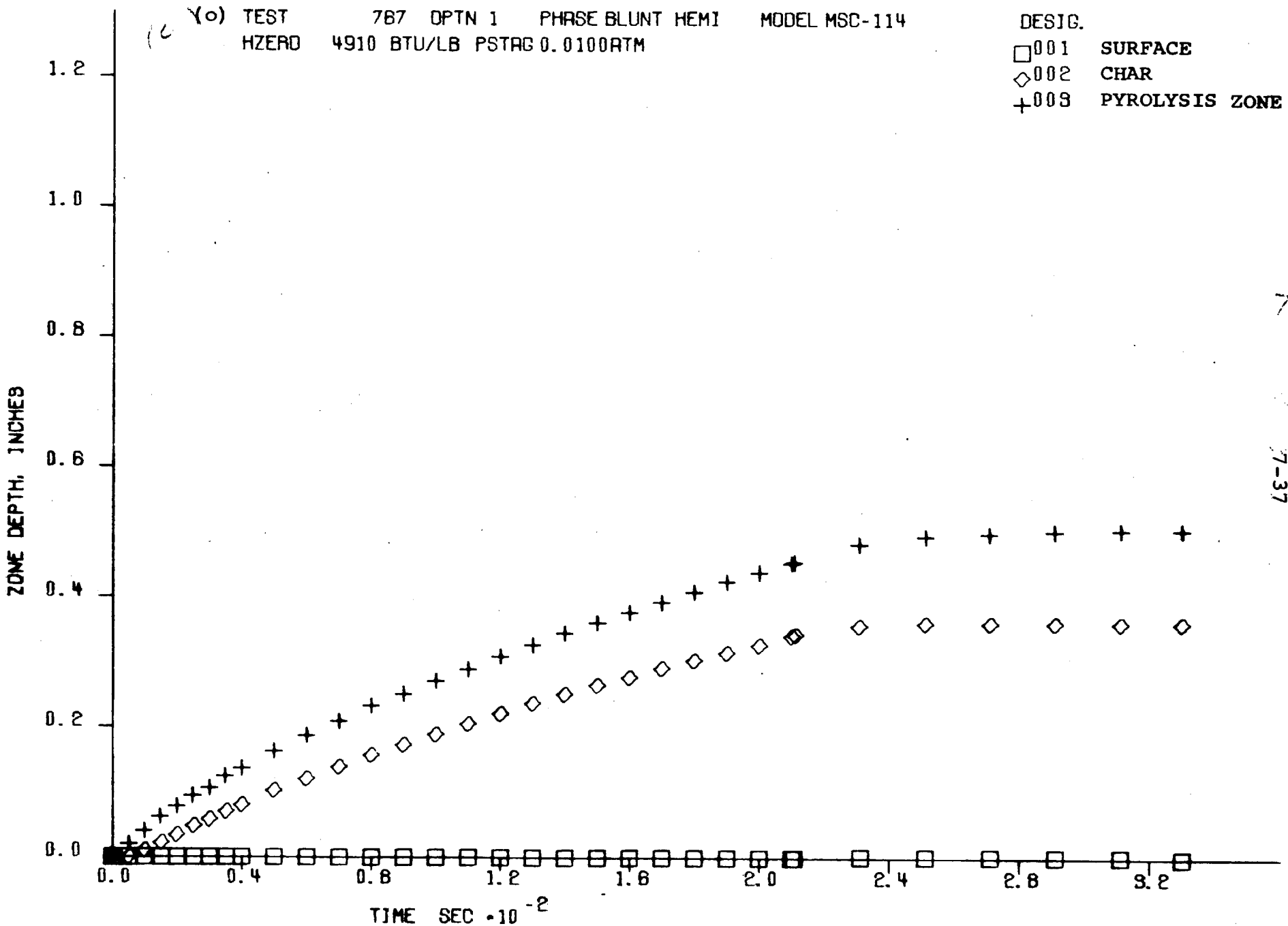

Figure 7-4. Continued.

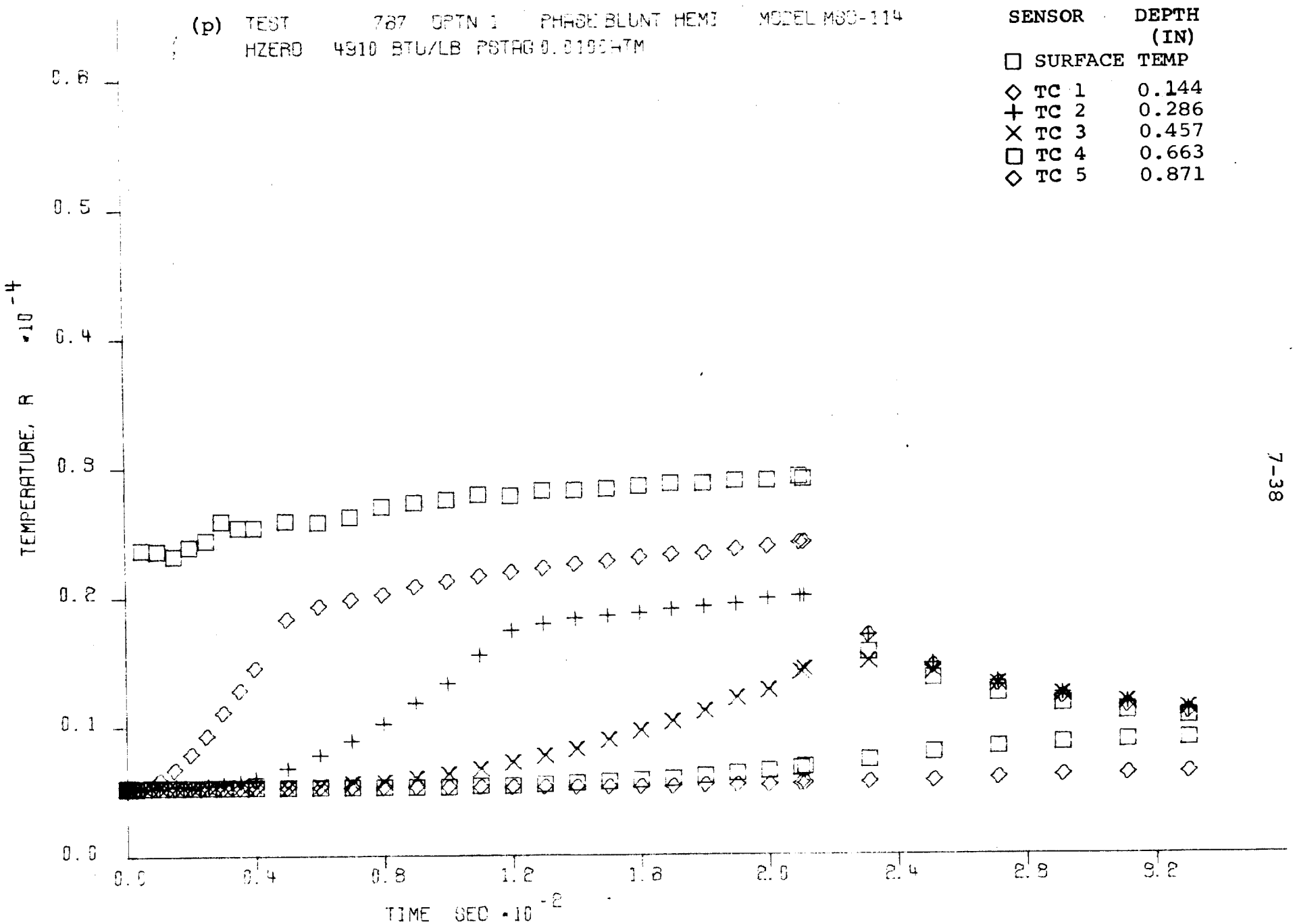

Figure 7-4. Continued.

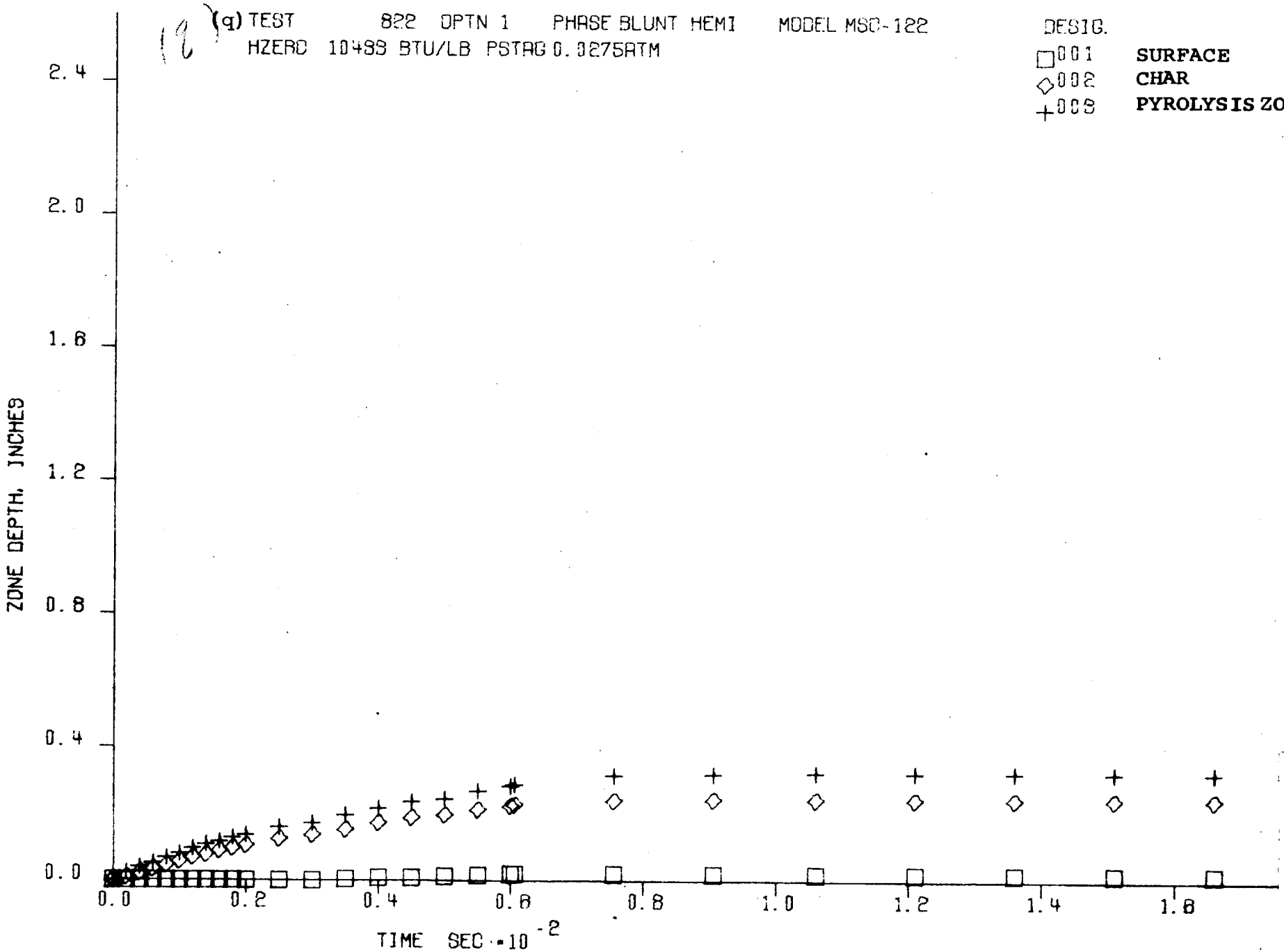

Figure 7-4. Continued.

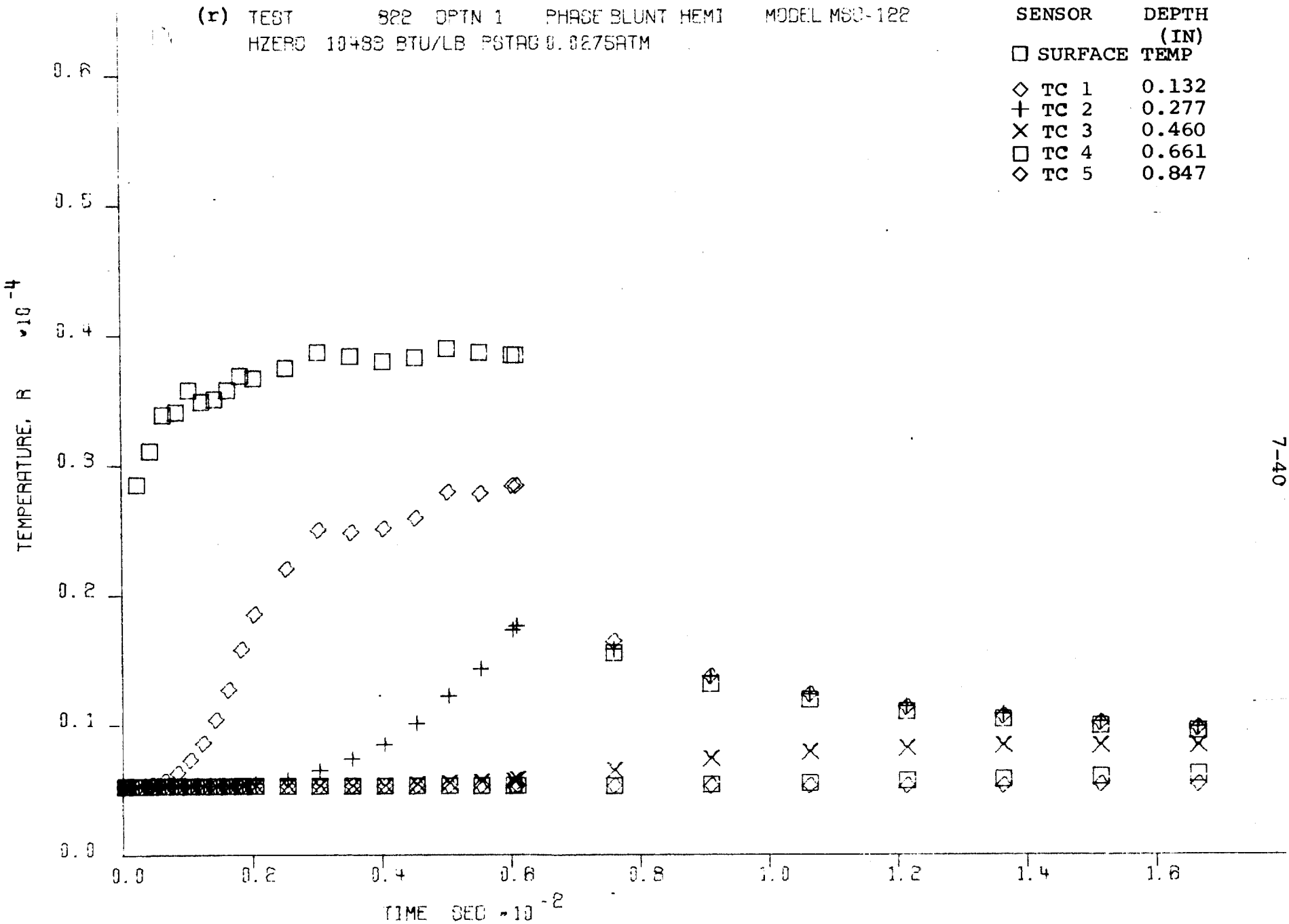

Figure 7-4. Continued.

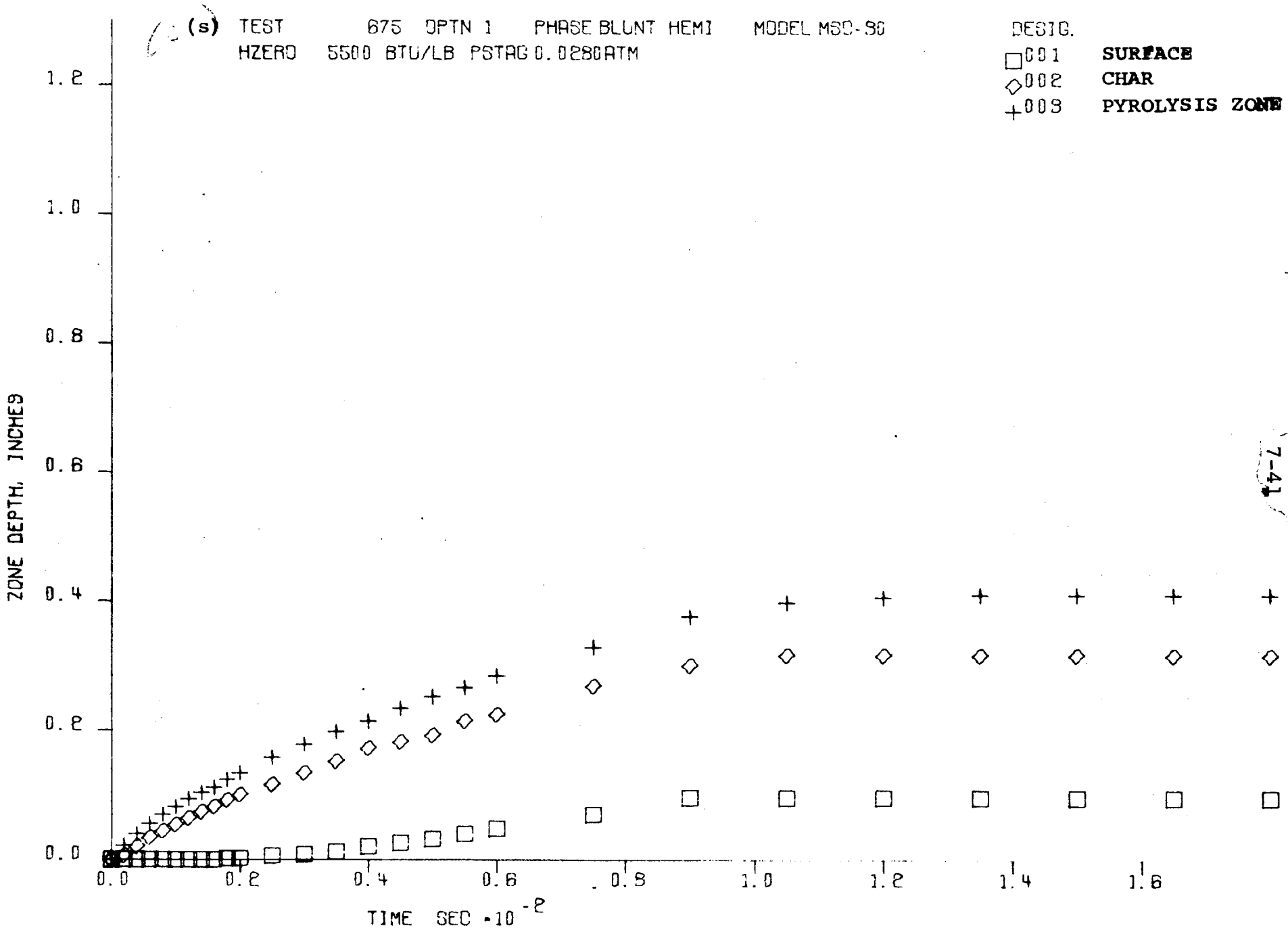

Figure 7-4. Continued.

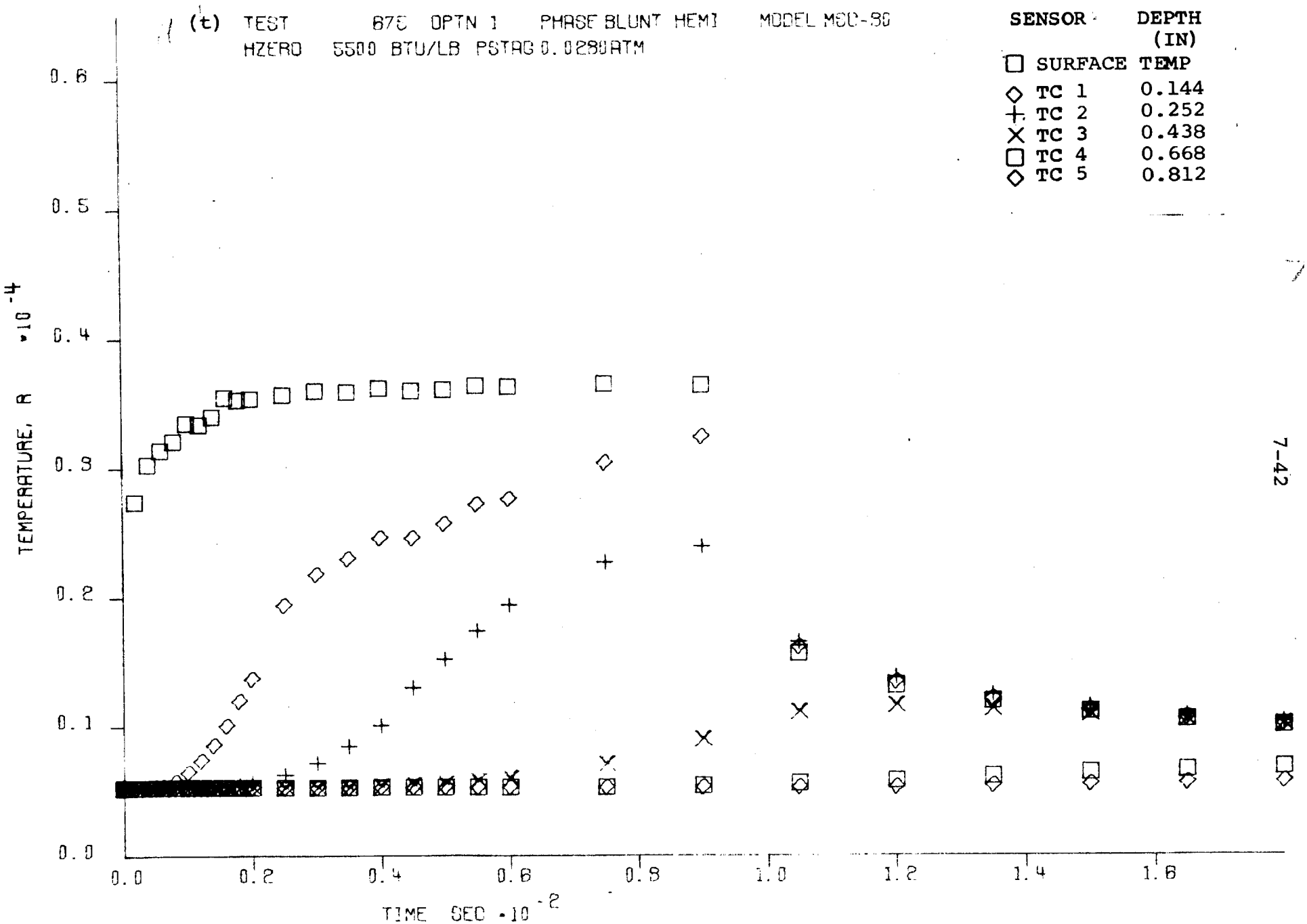

Figure 7-4. Continued.

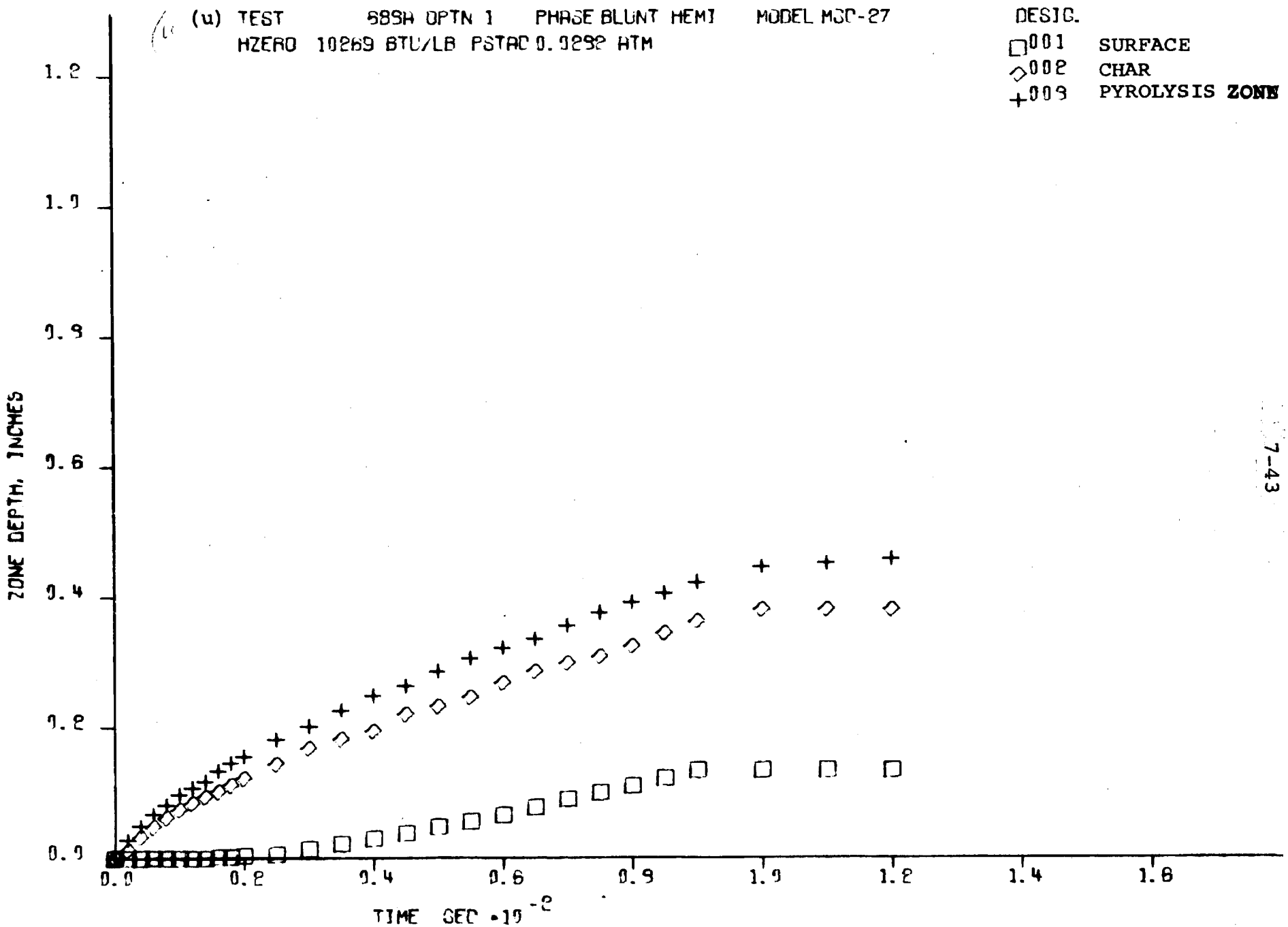

Figure 7-4. Continued.

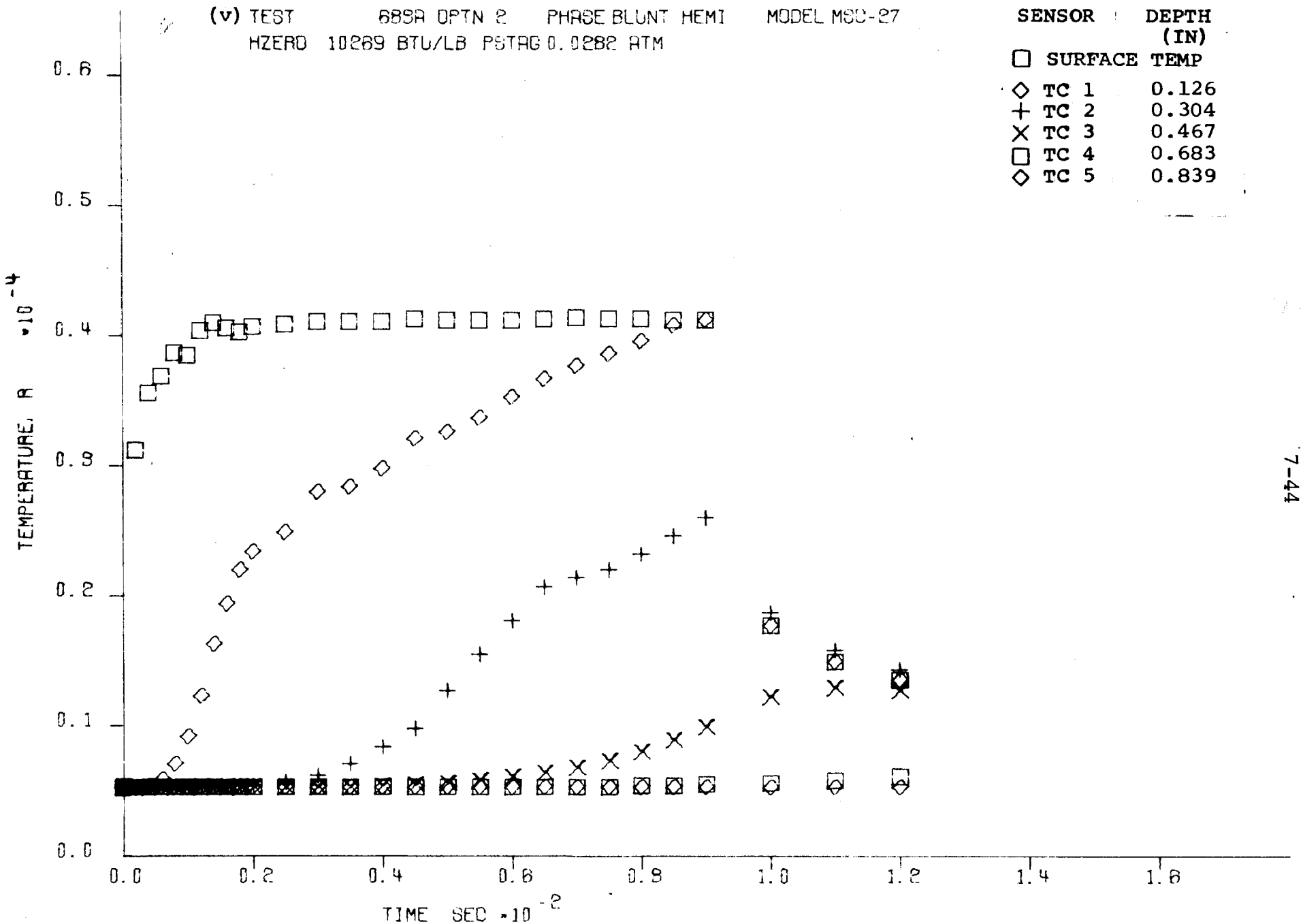

Figure 7-4. Continued.

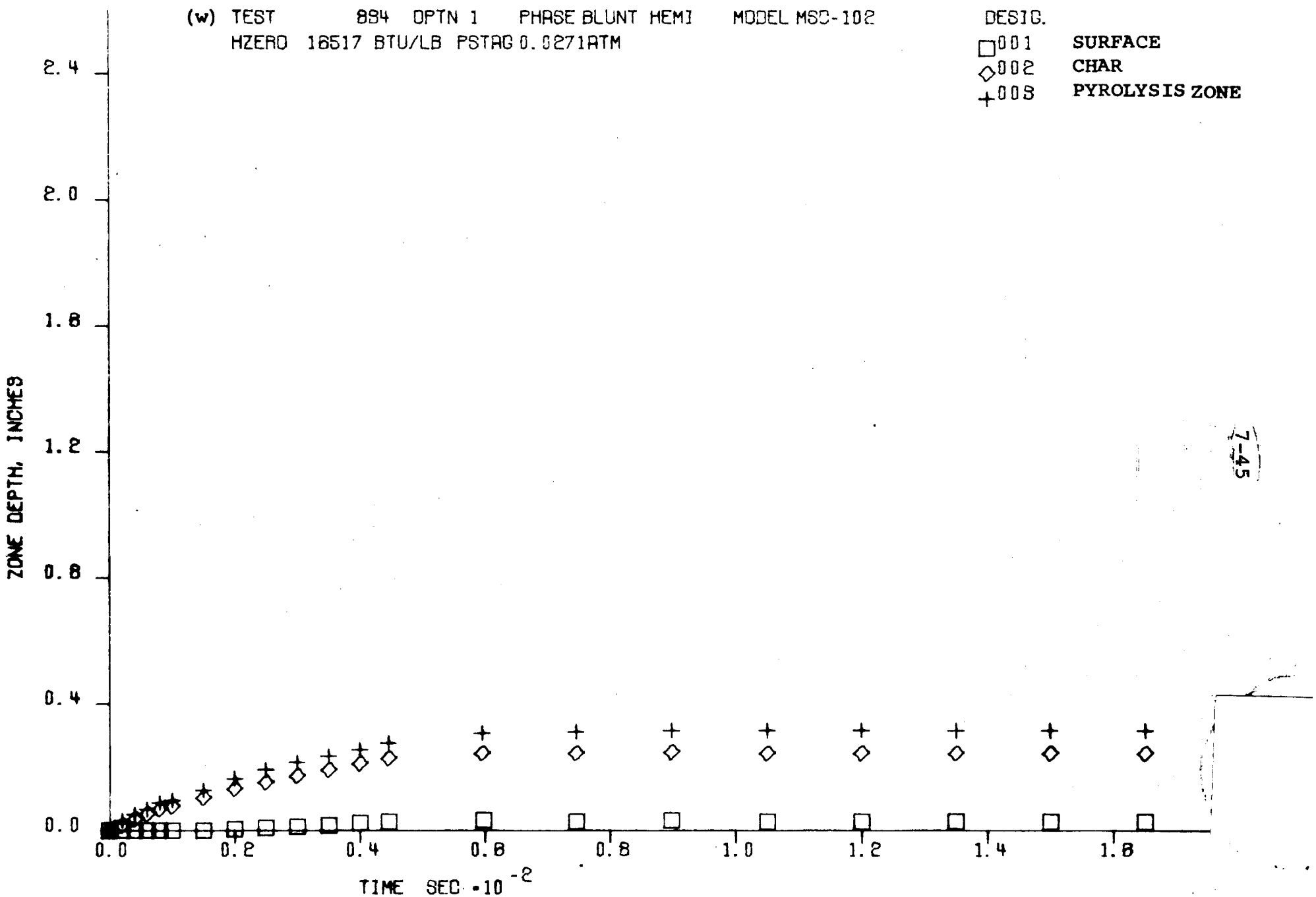

Figure 7-4. Continued.

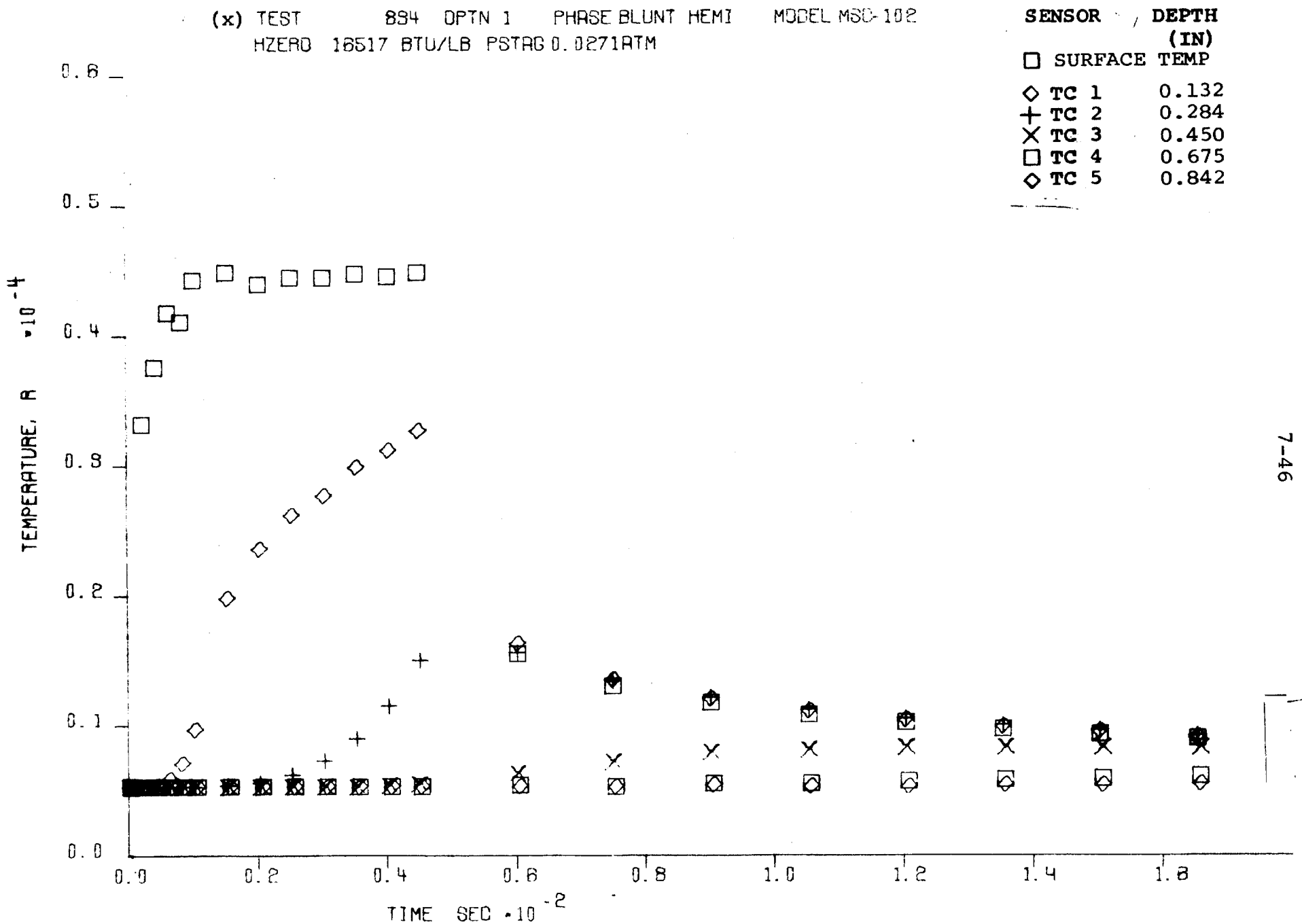

Figure 7-4. Continued.

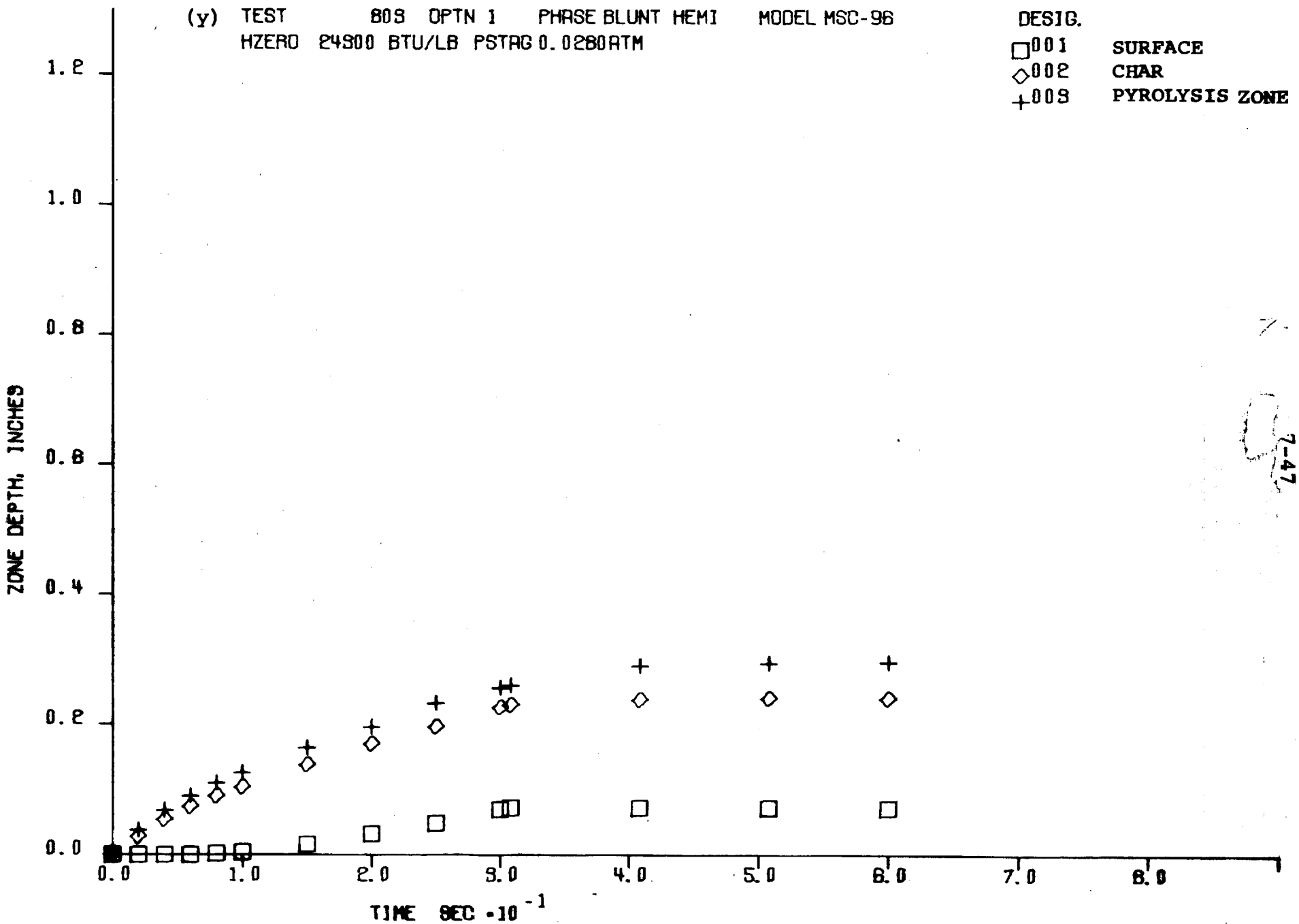

Figure 7-4. Continued.

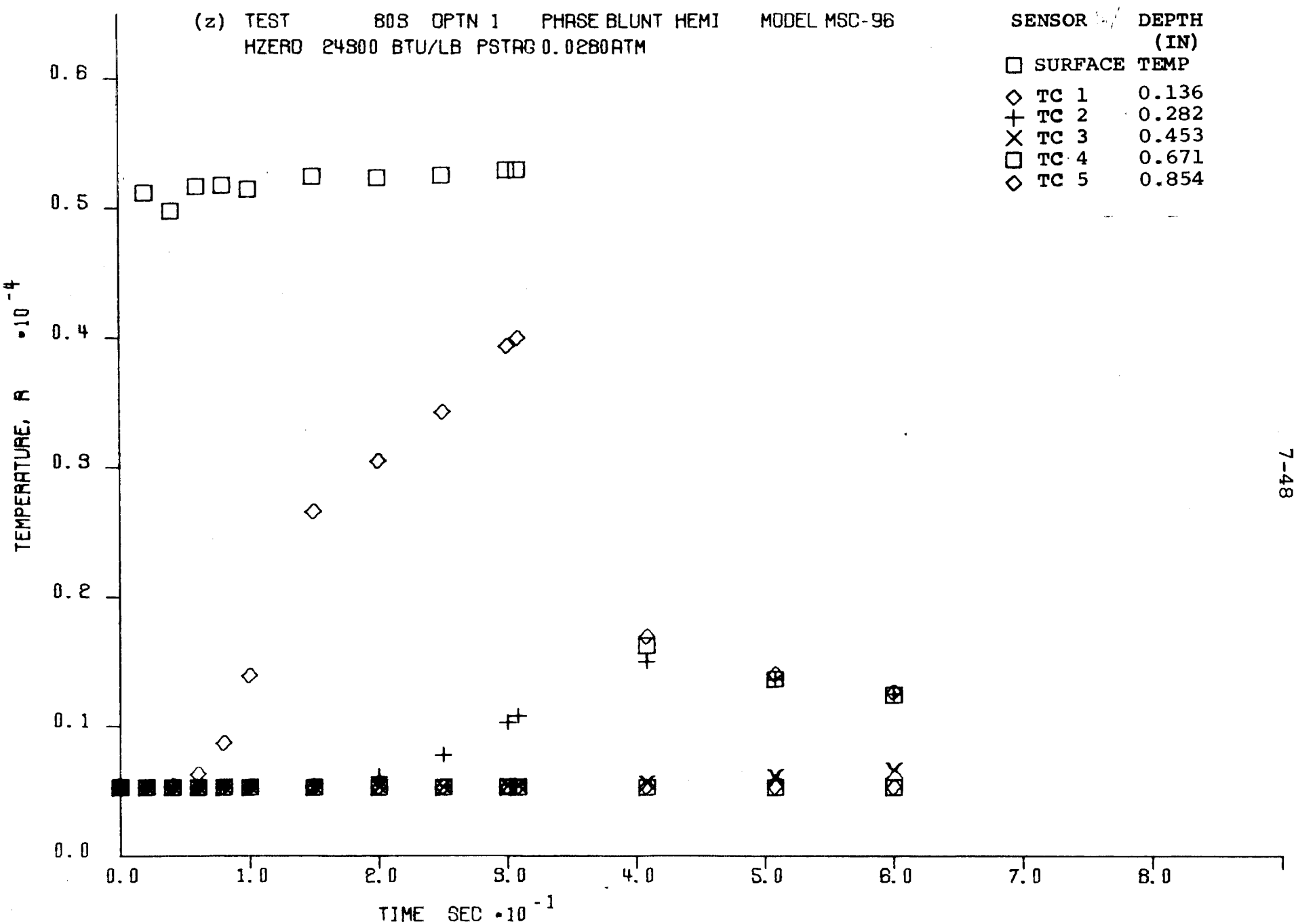

Figure 7-4. Continued.

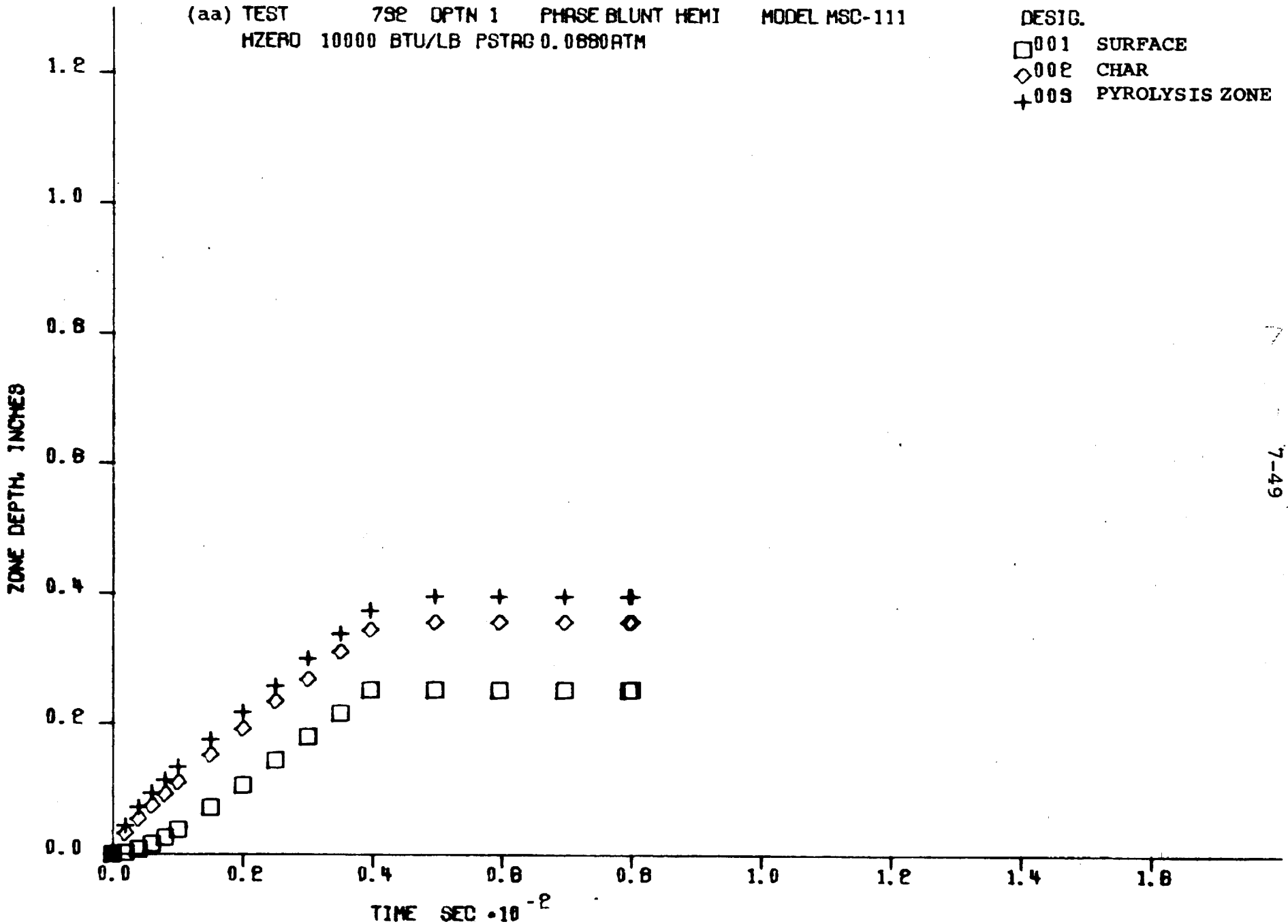

Figure 7-4. Continued.

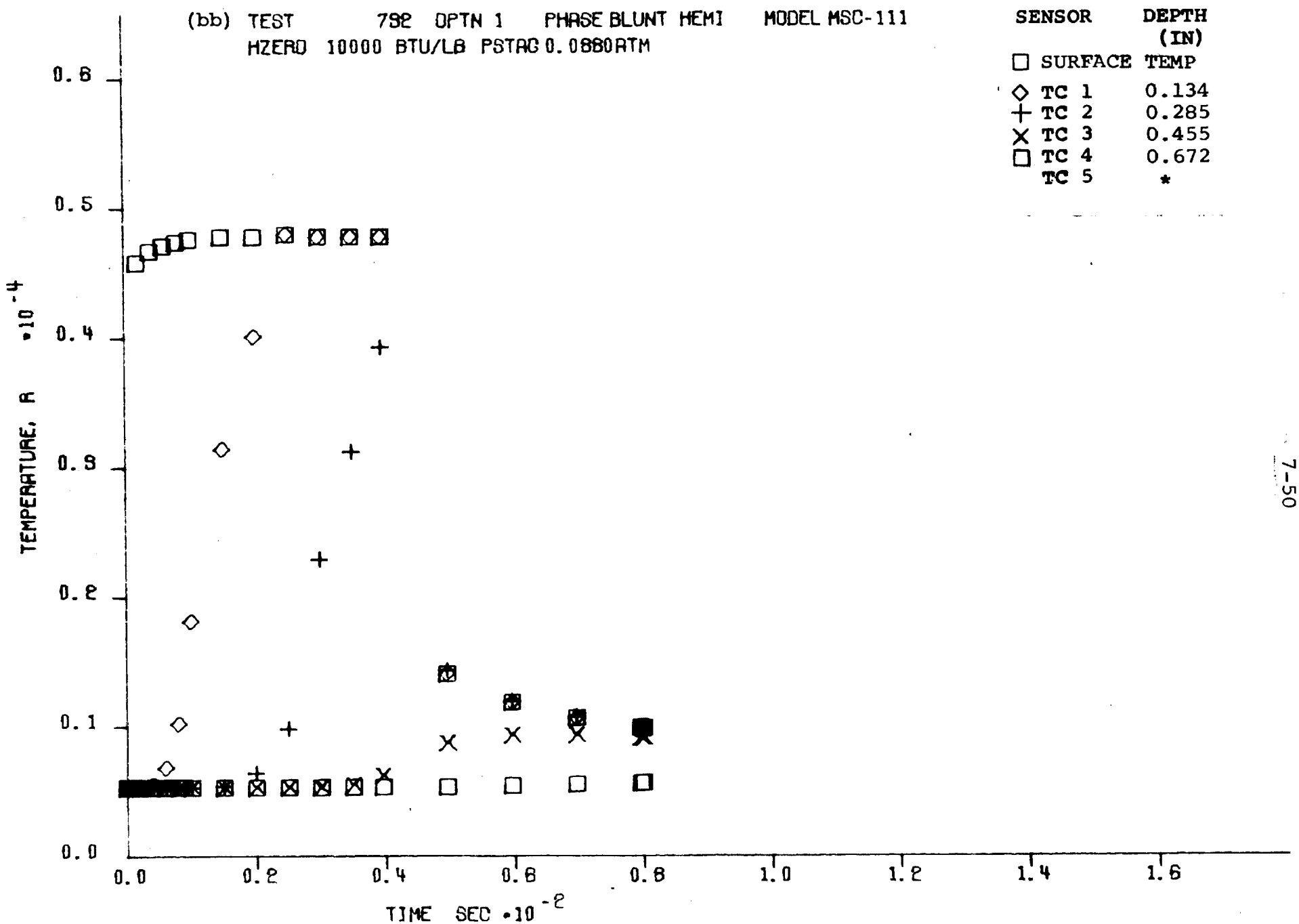

Figure 7-4. Concluded.

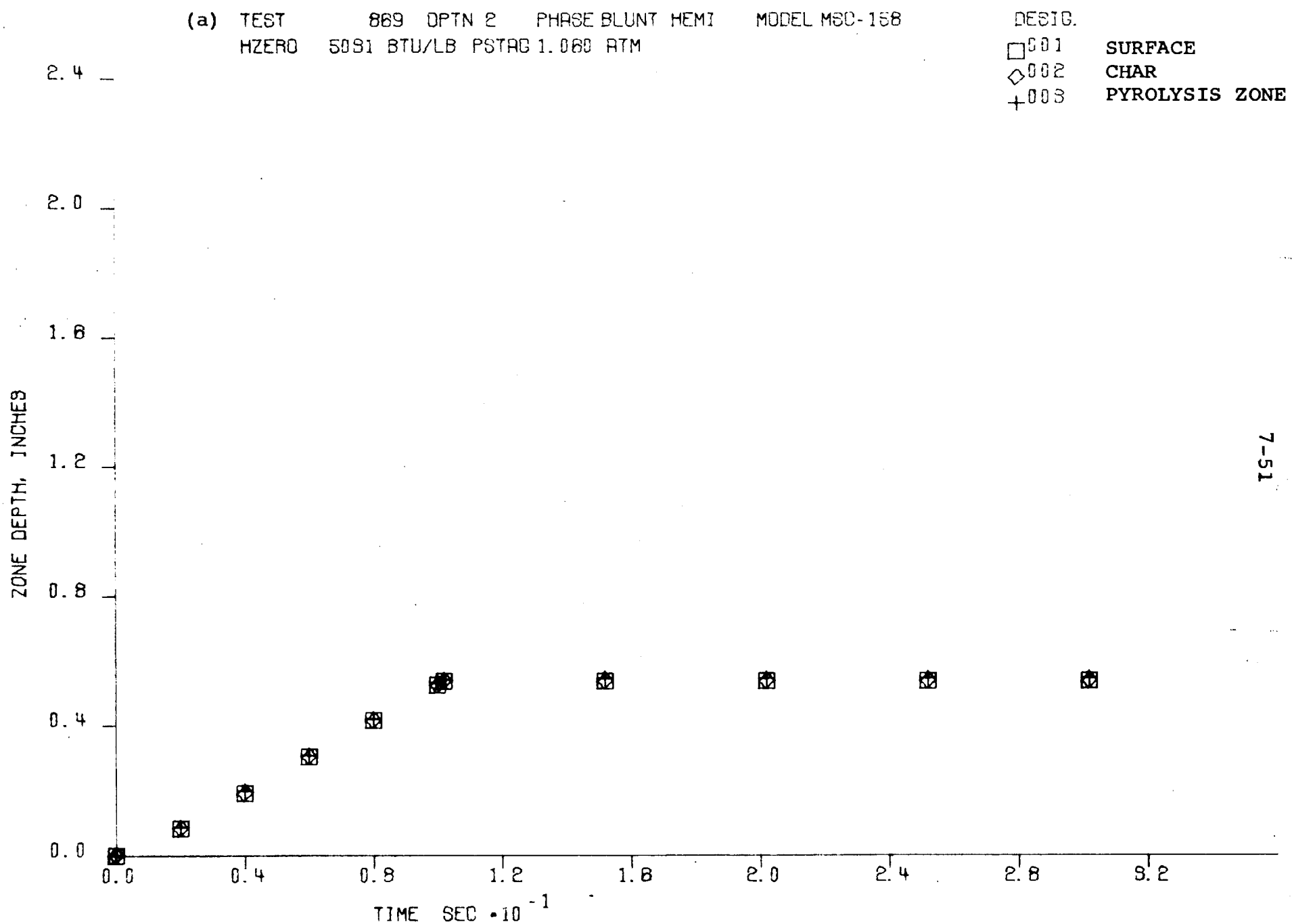

Figure 7-5. Analytical Predictions of Material Performance for Models Exposed to Simulated Reentry Conditions (Option 2).

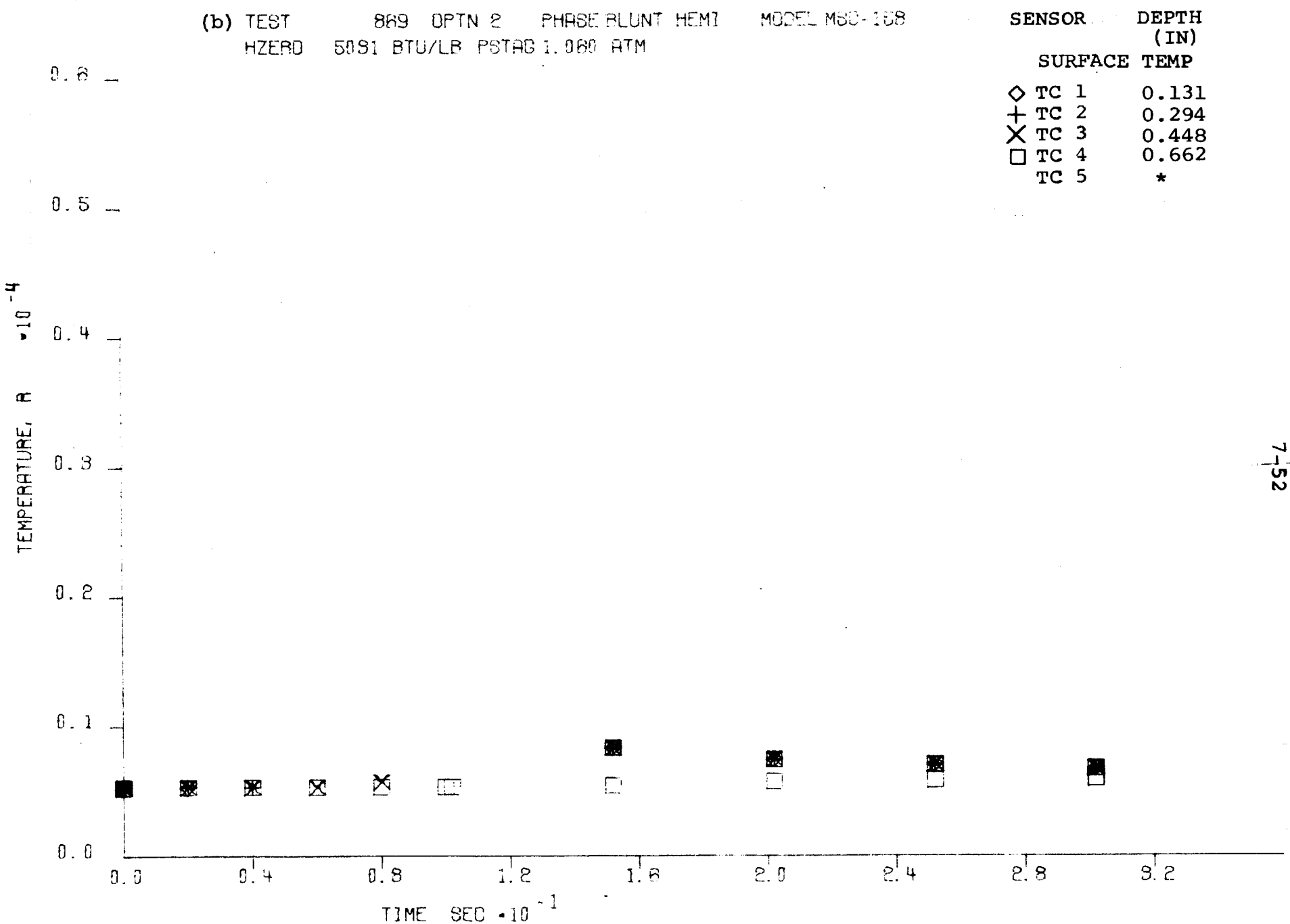

Figure 7-5. Continued.

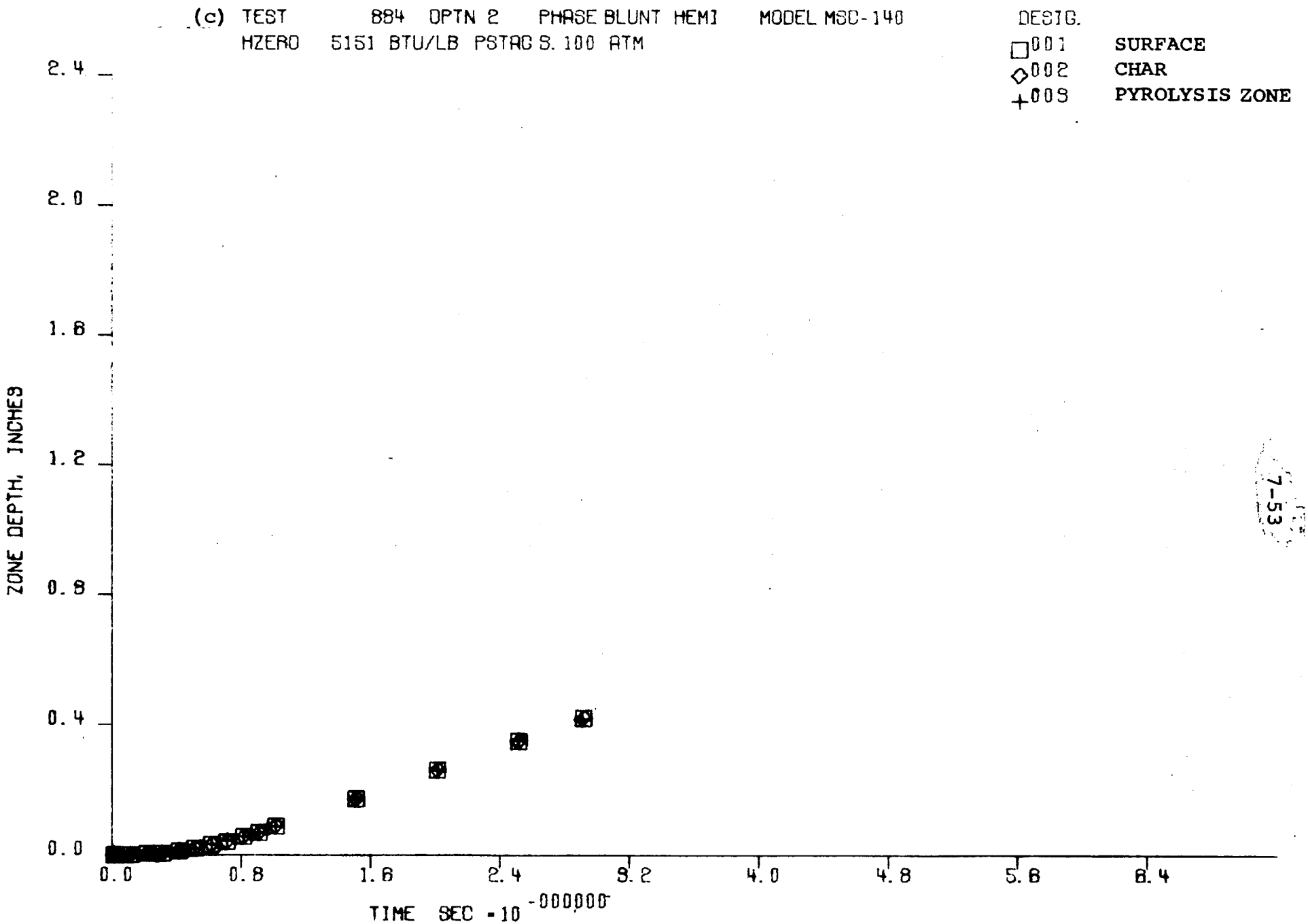

Figure 7-5. Continued.

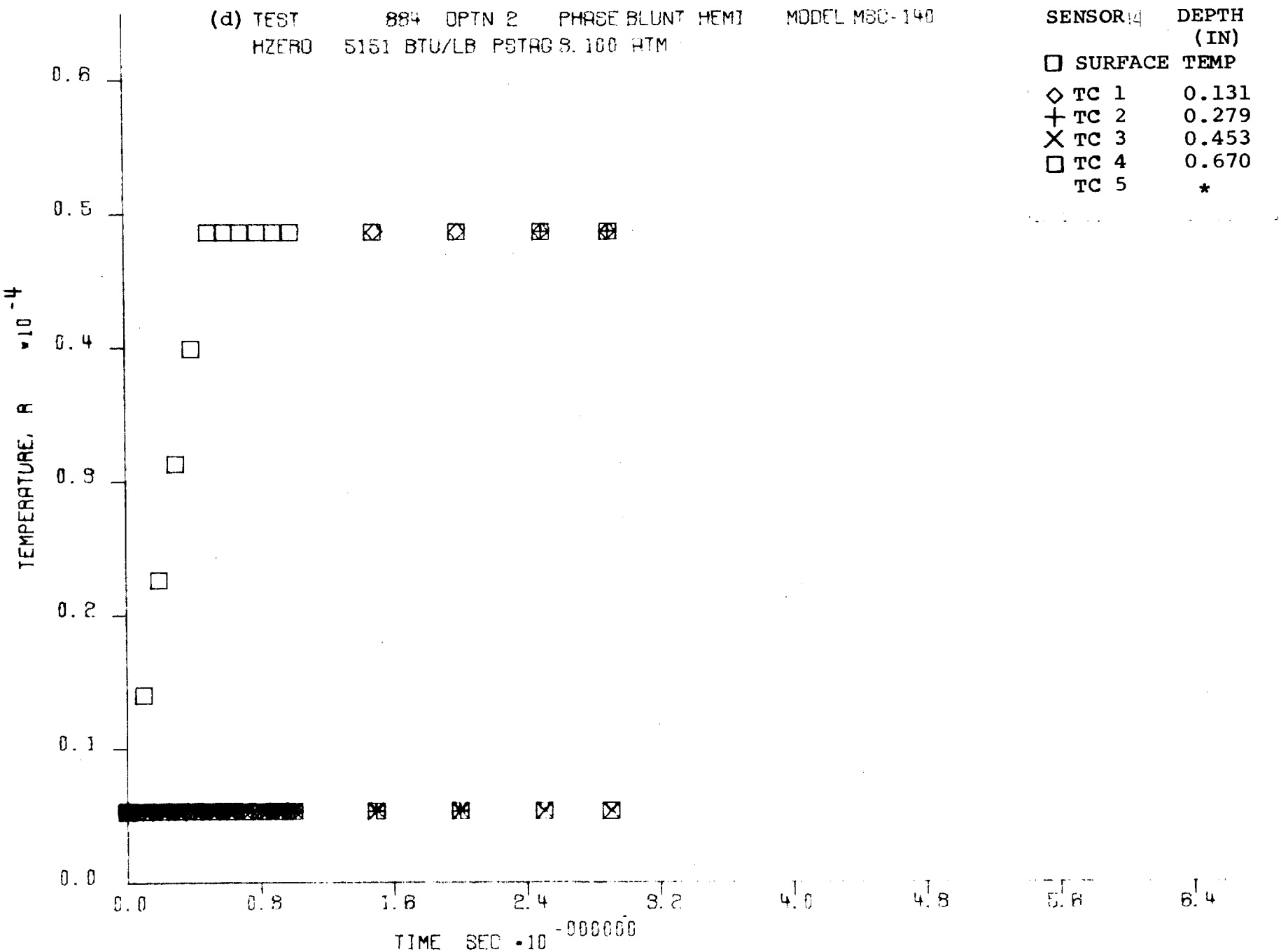

Figure 7-5. Continued.

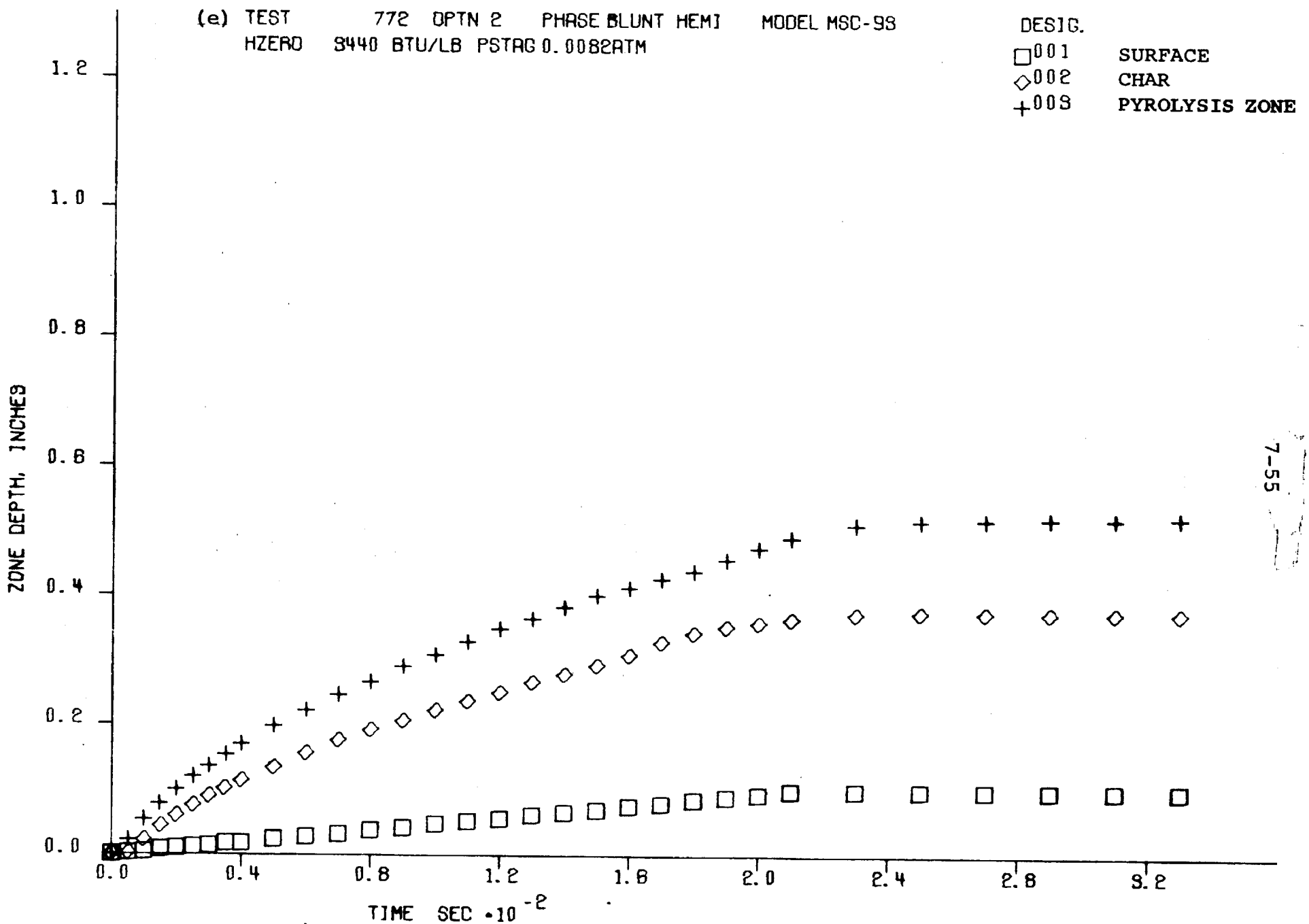

Figure 7-5. Continued.

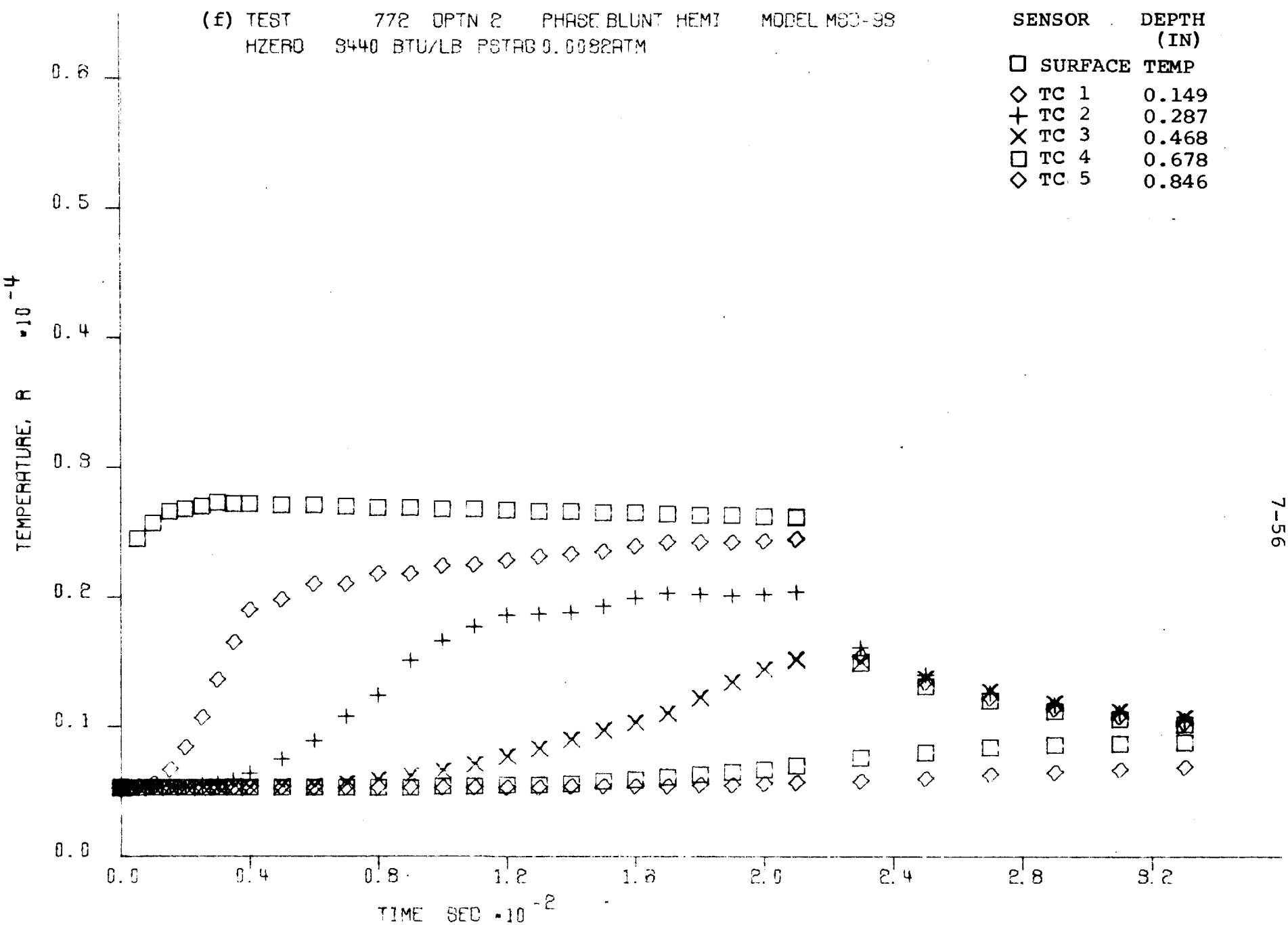

Figure 7-5. Continued.

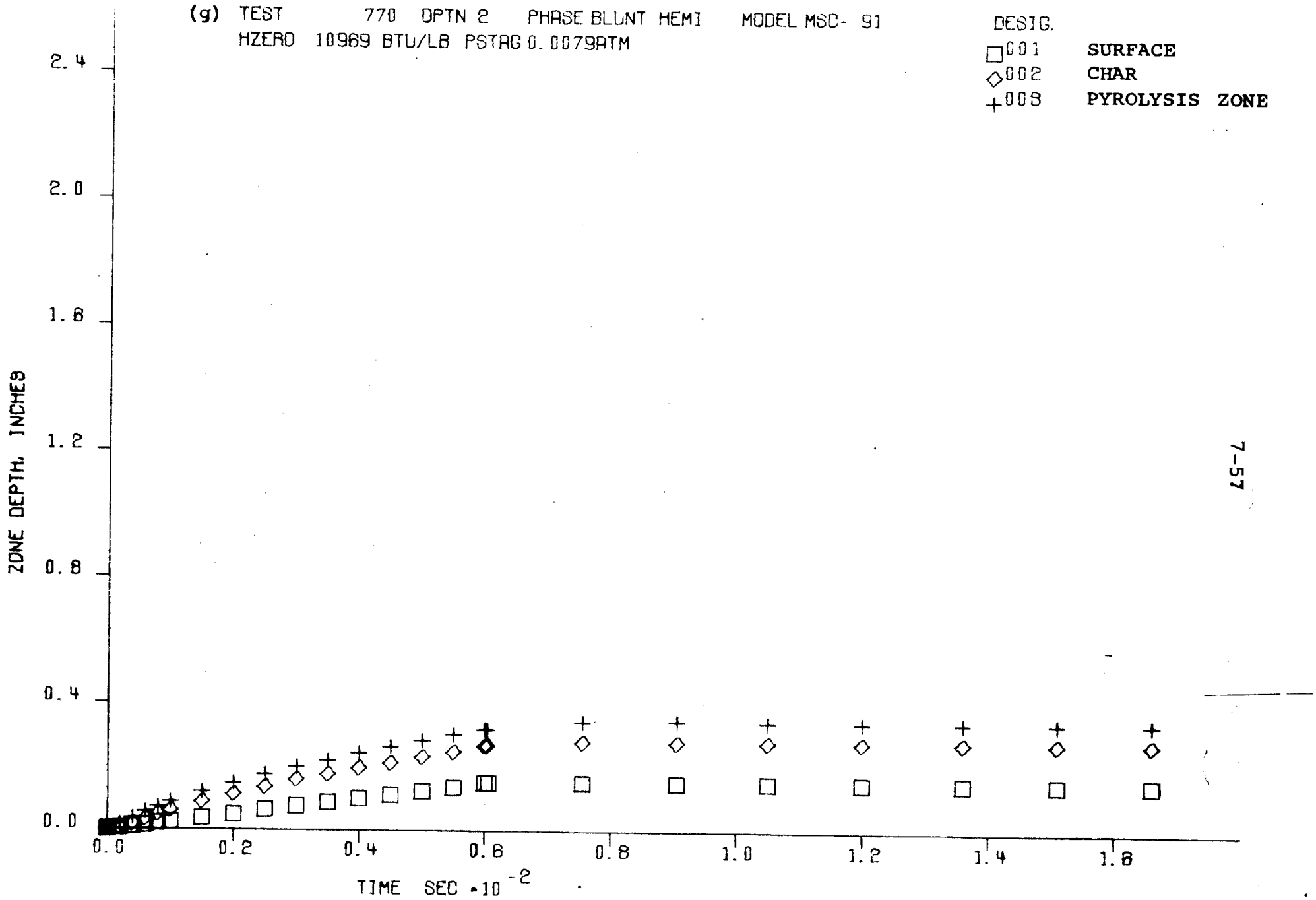

Figure 7-5. Continued.

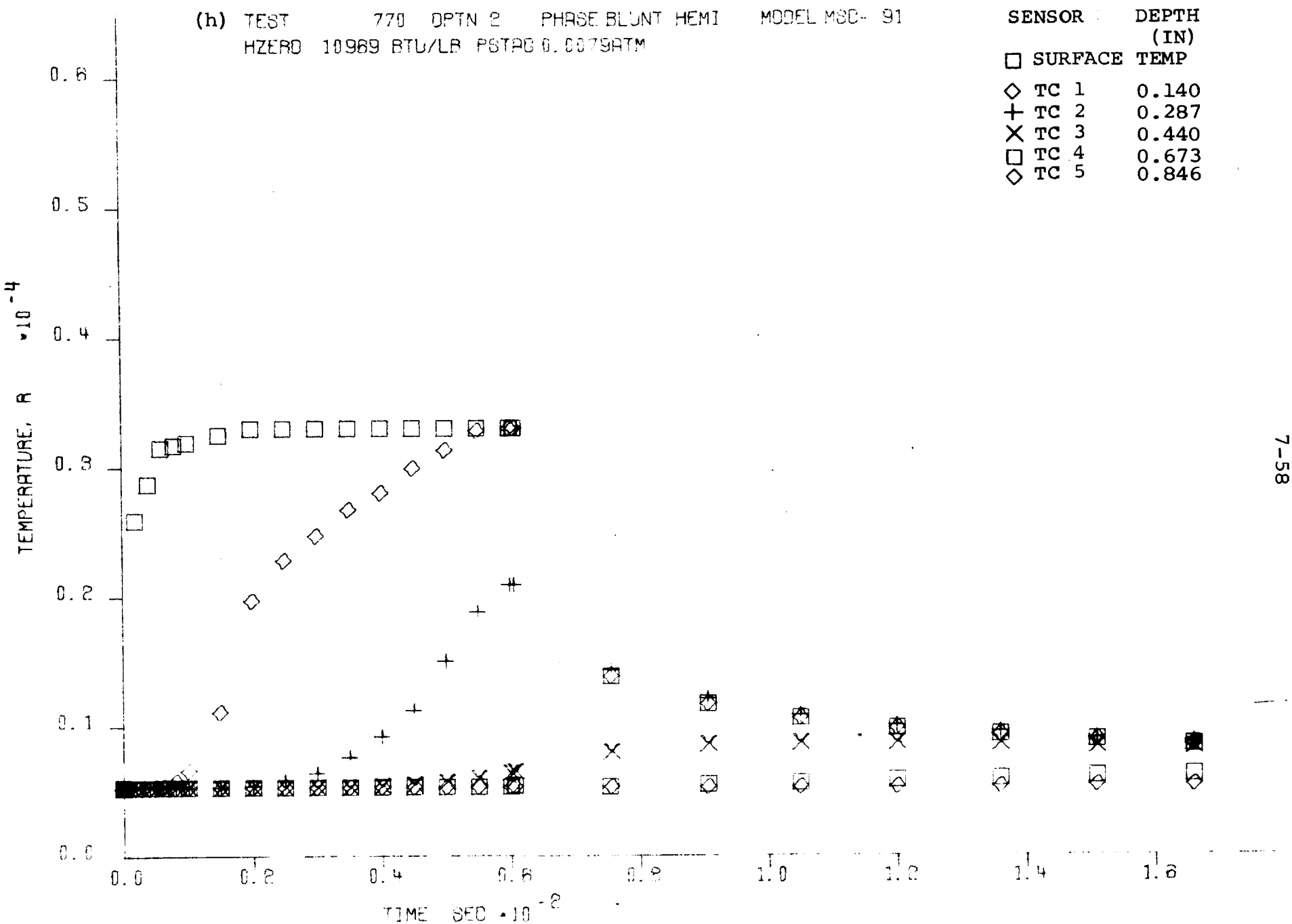

Figure 7-5. Continued.

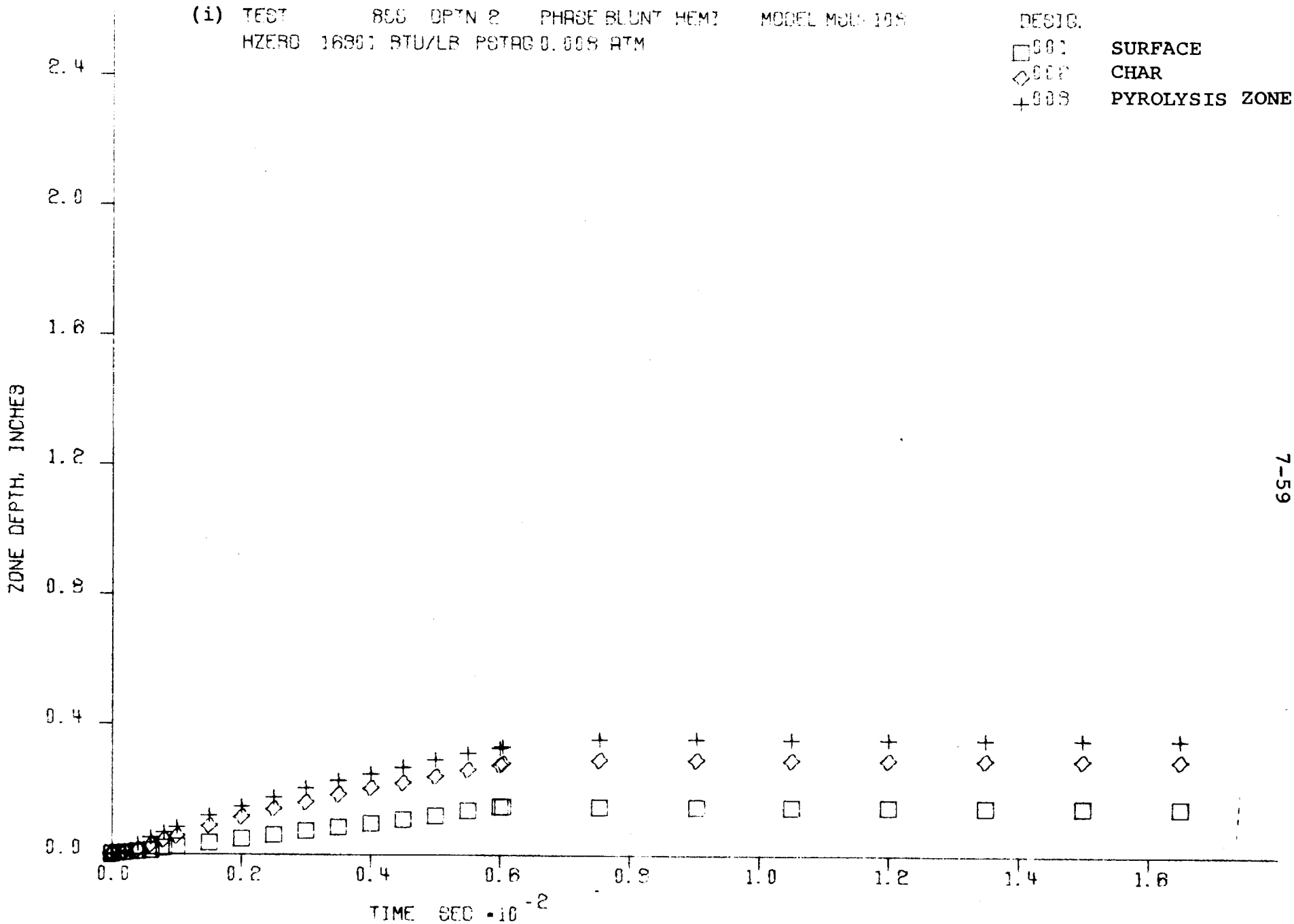

Figure 7-5. Continued.

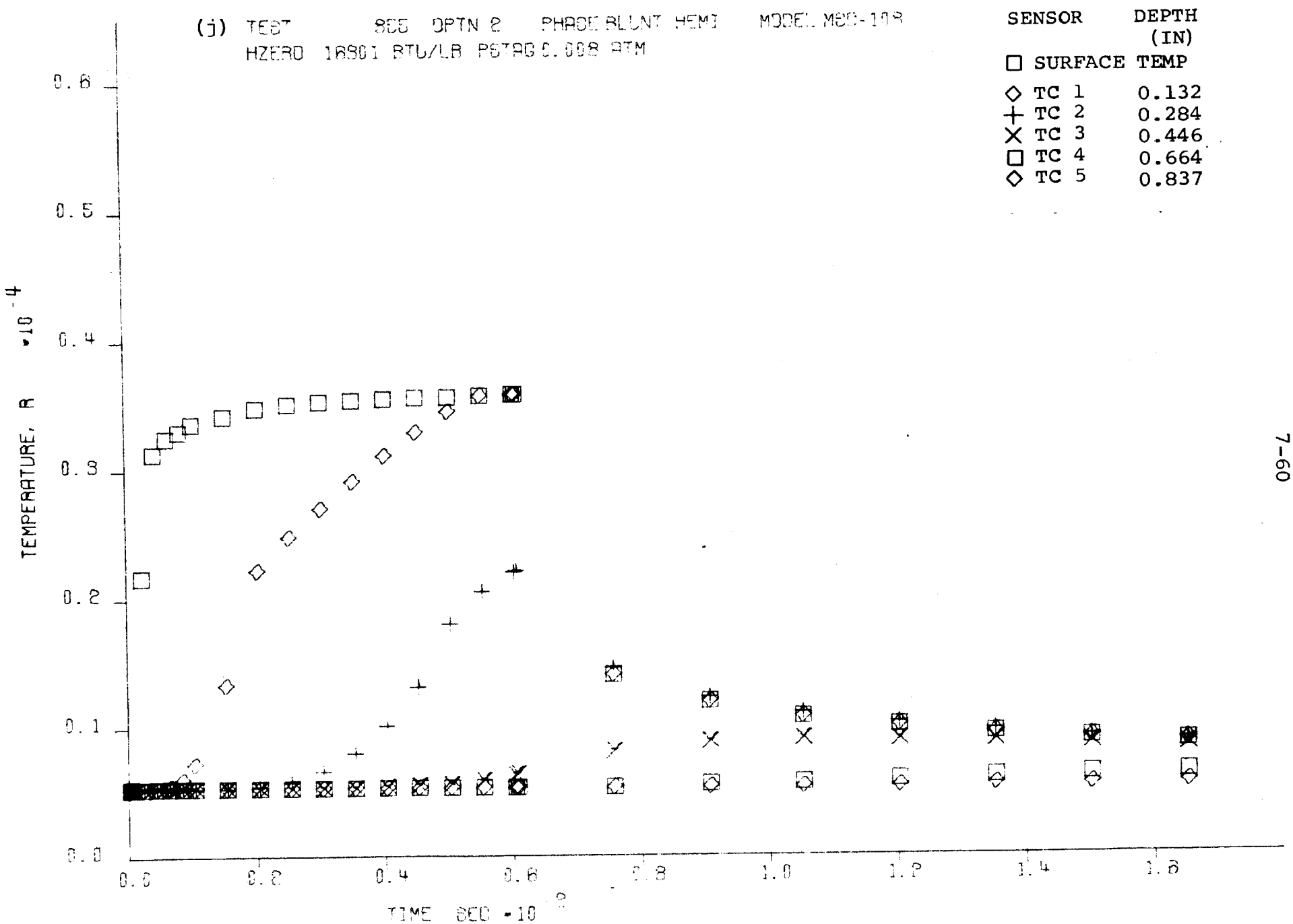

Figure 7-5. Continued.

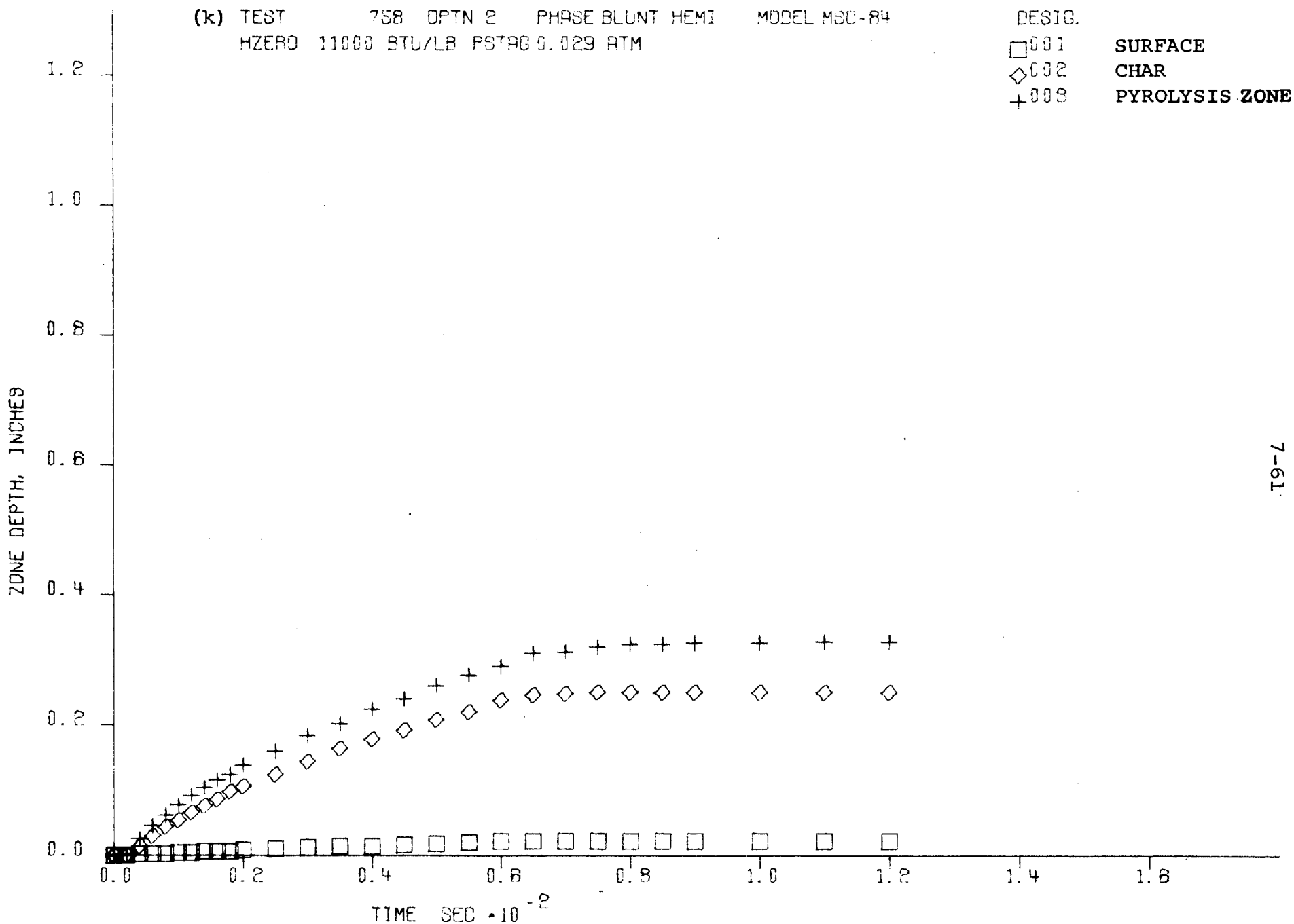

Figure 7-5. Continued.

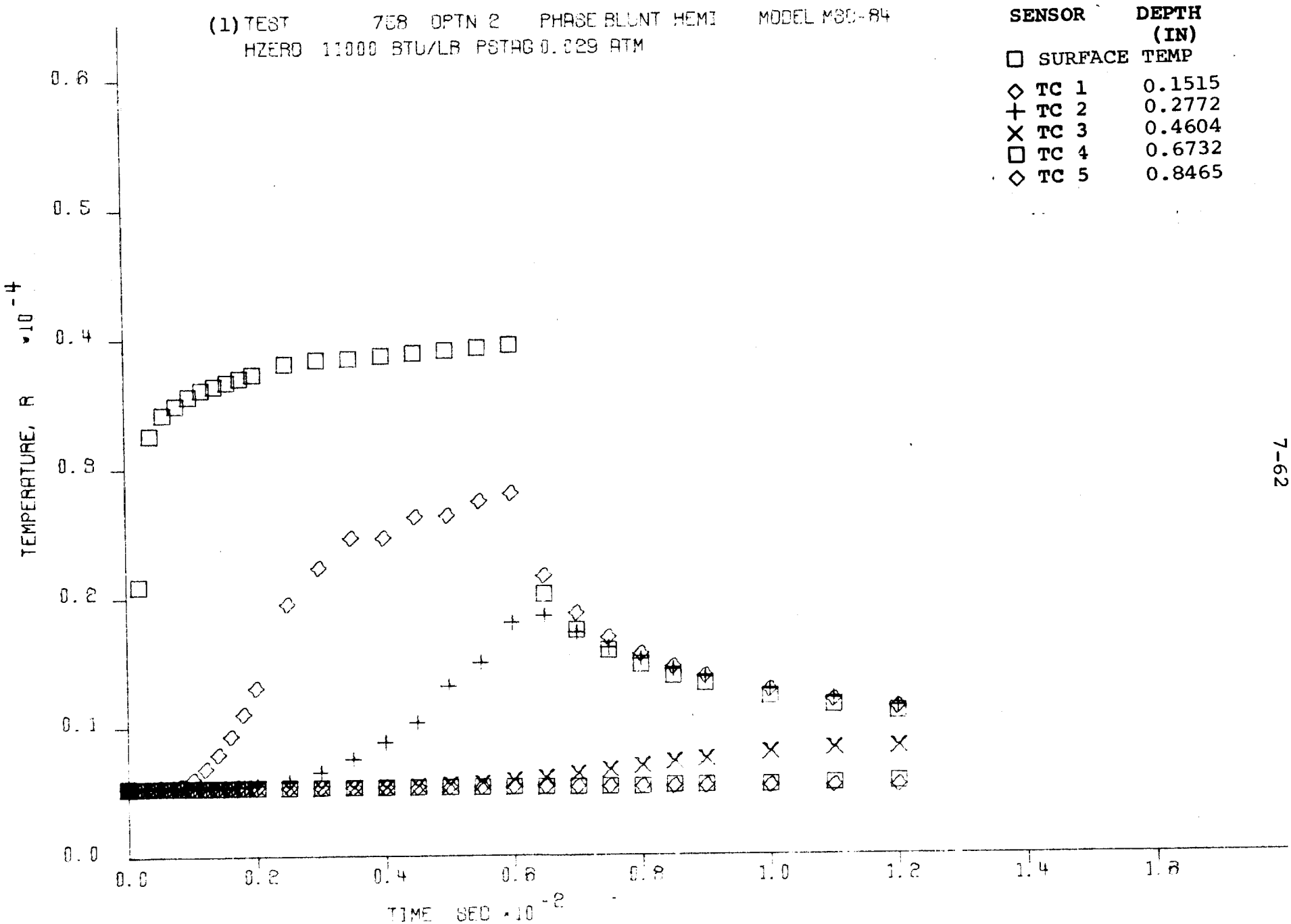

Figure 7-5. Continued.

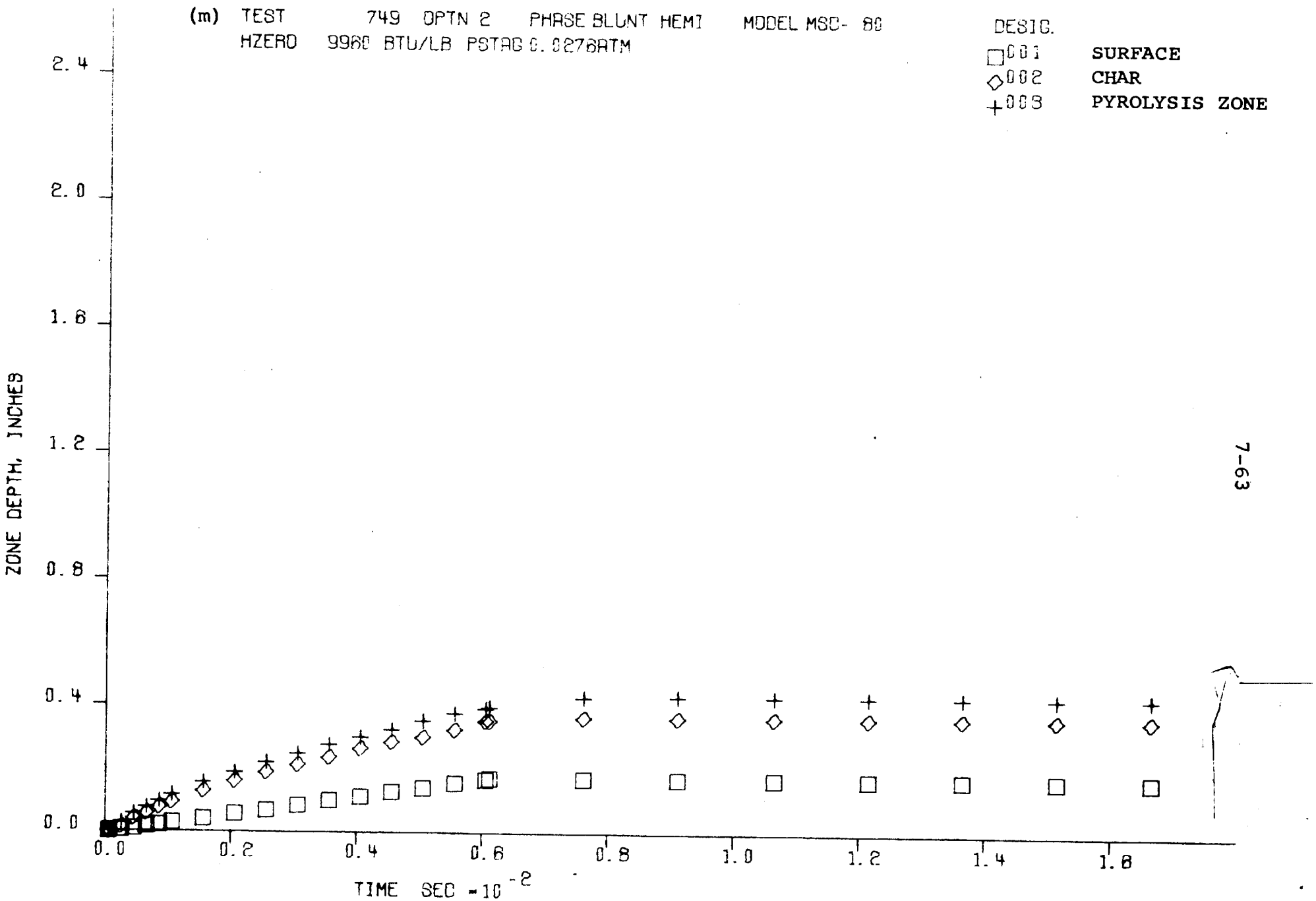

Figure 7-5. Continued.

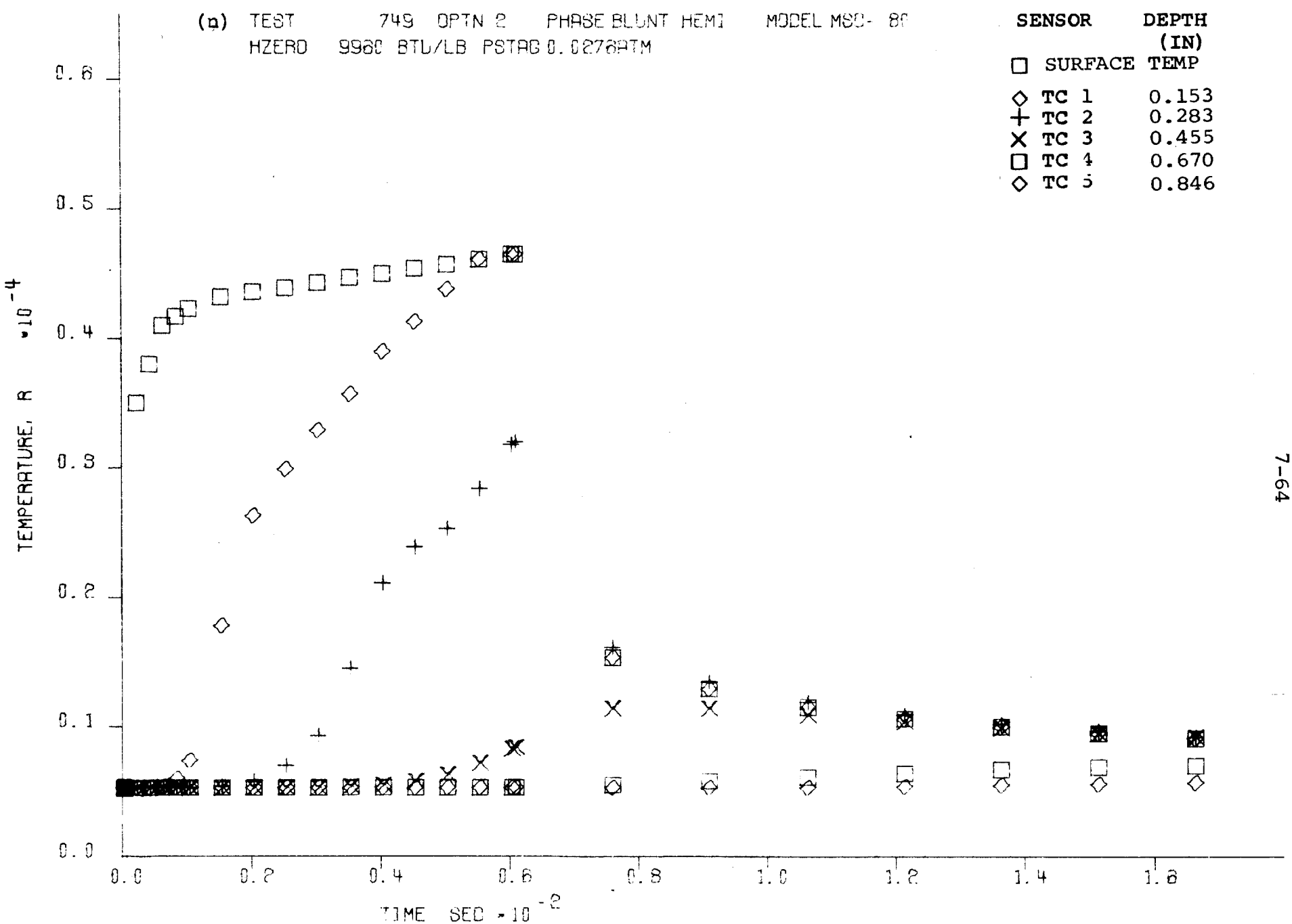

Figure 7-5. Continued.

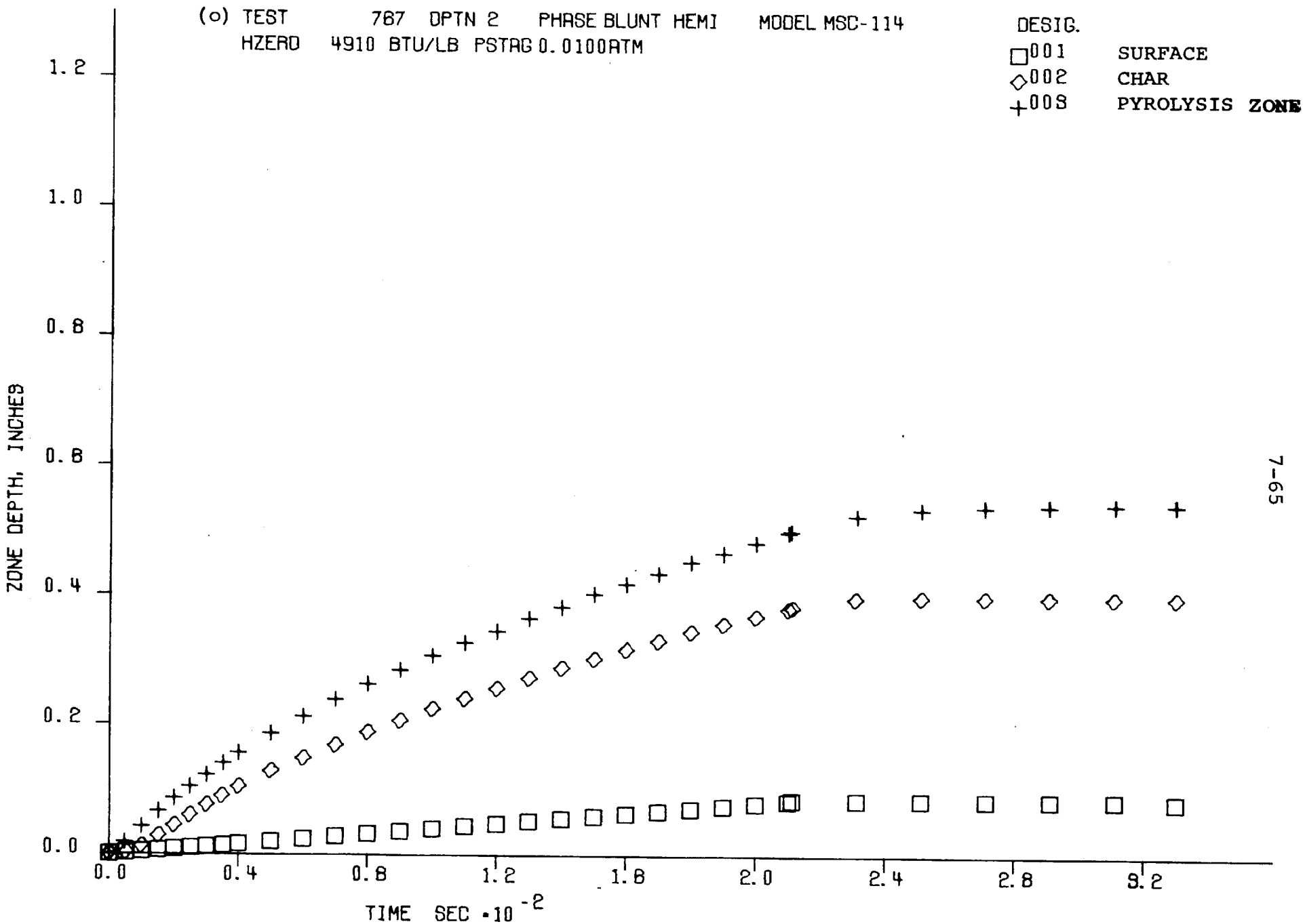

Figure 7-5. Continued.

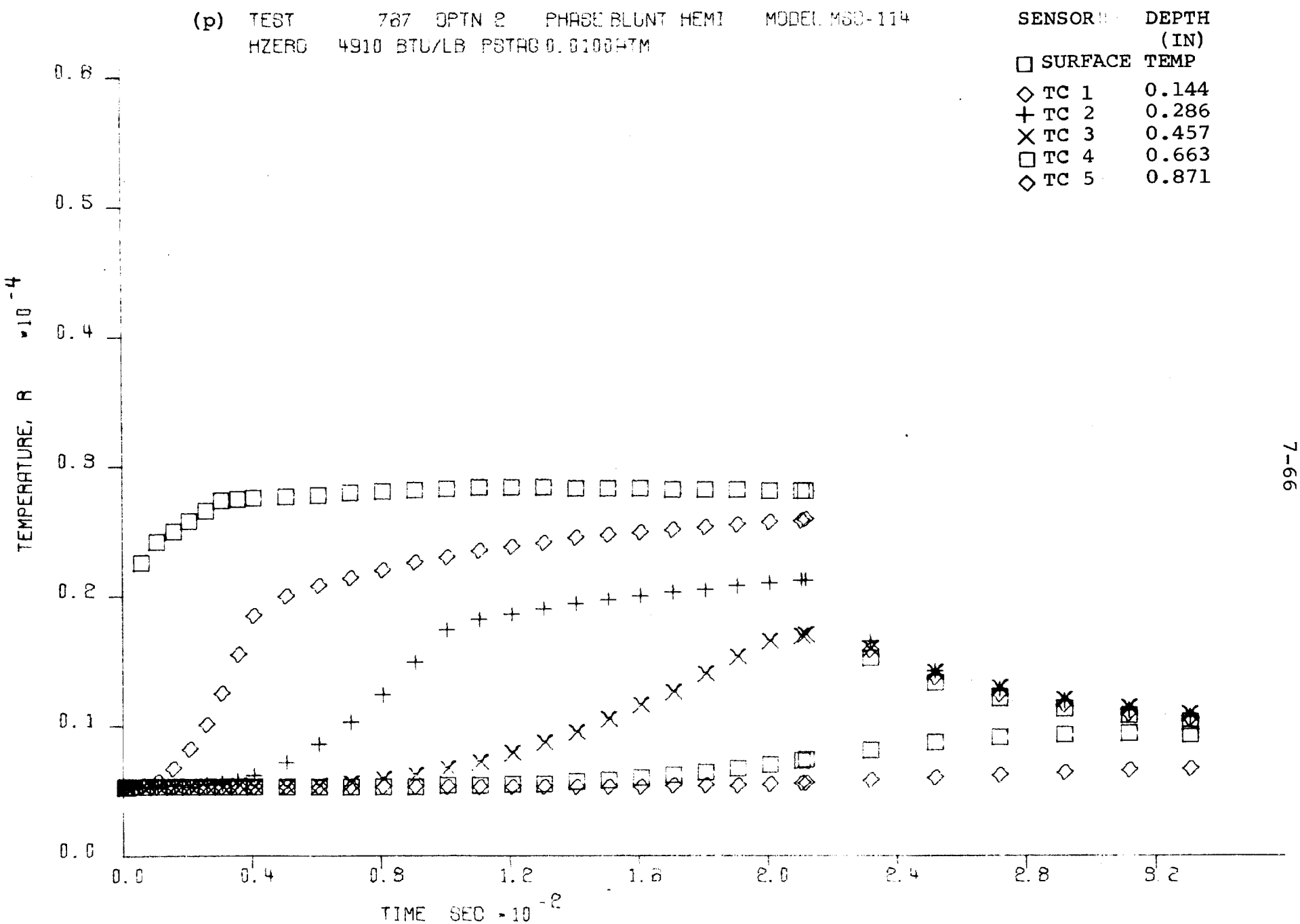

Figure 7-5. Continued.

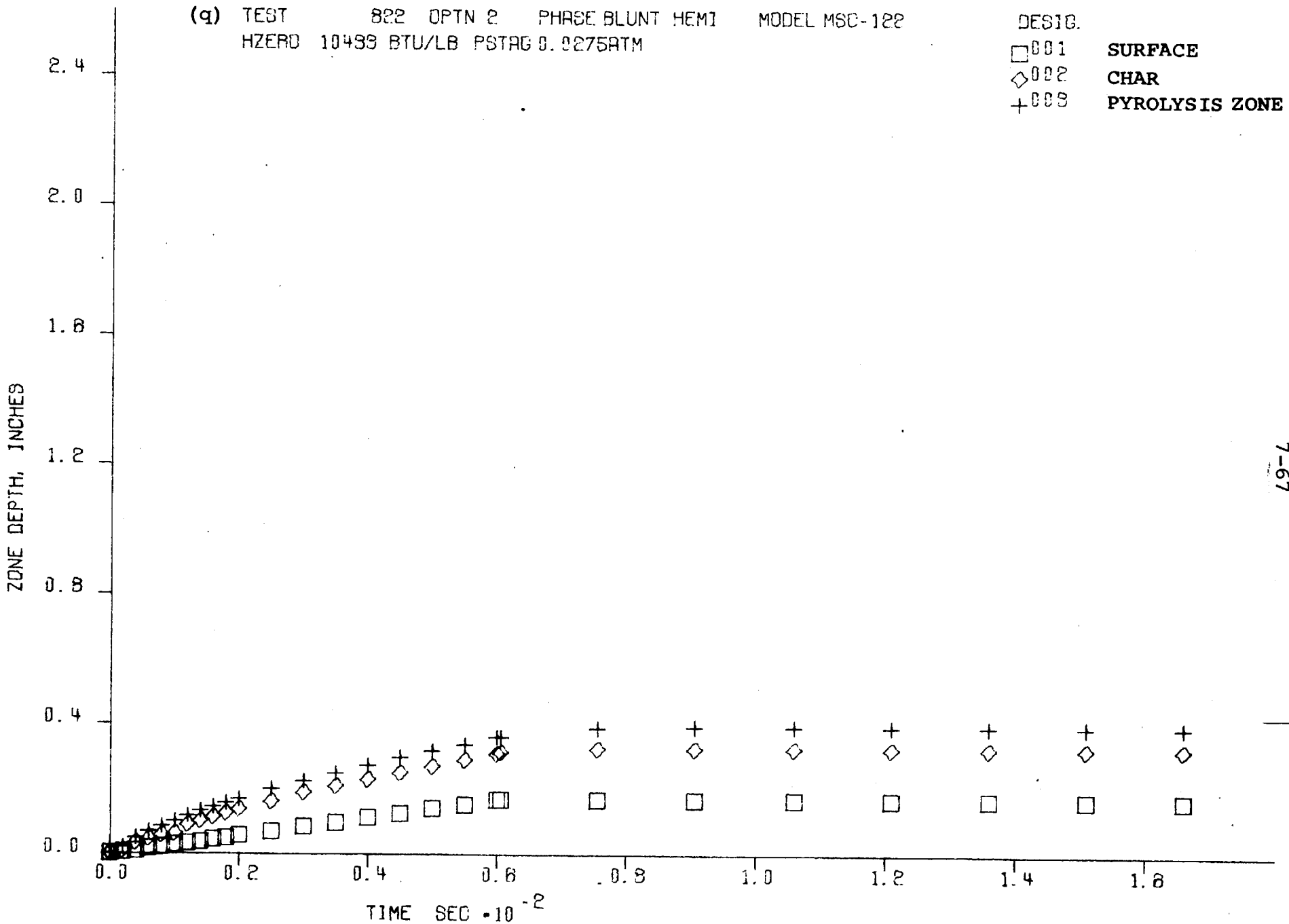

Figure 7-5. Continued.

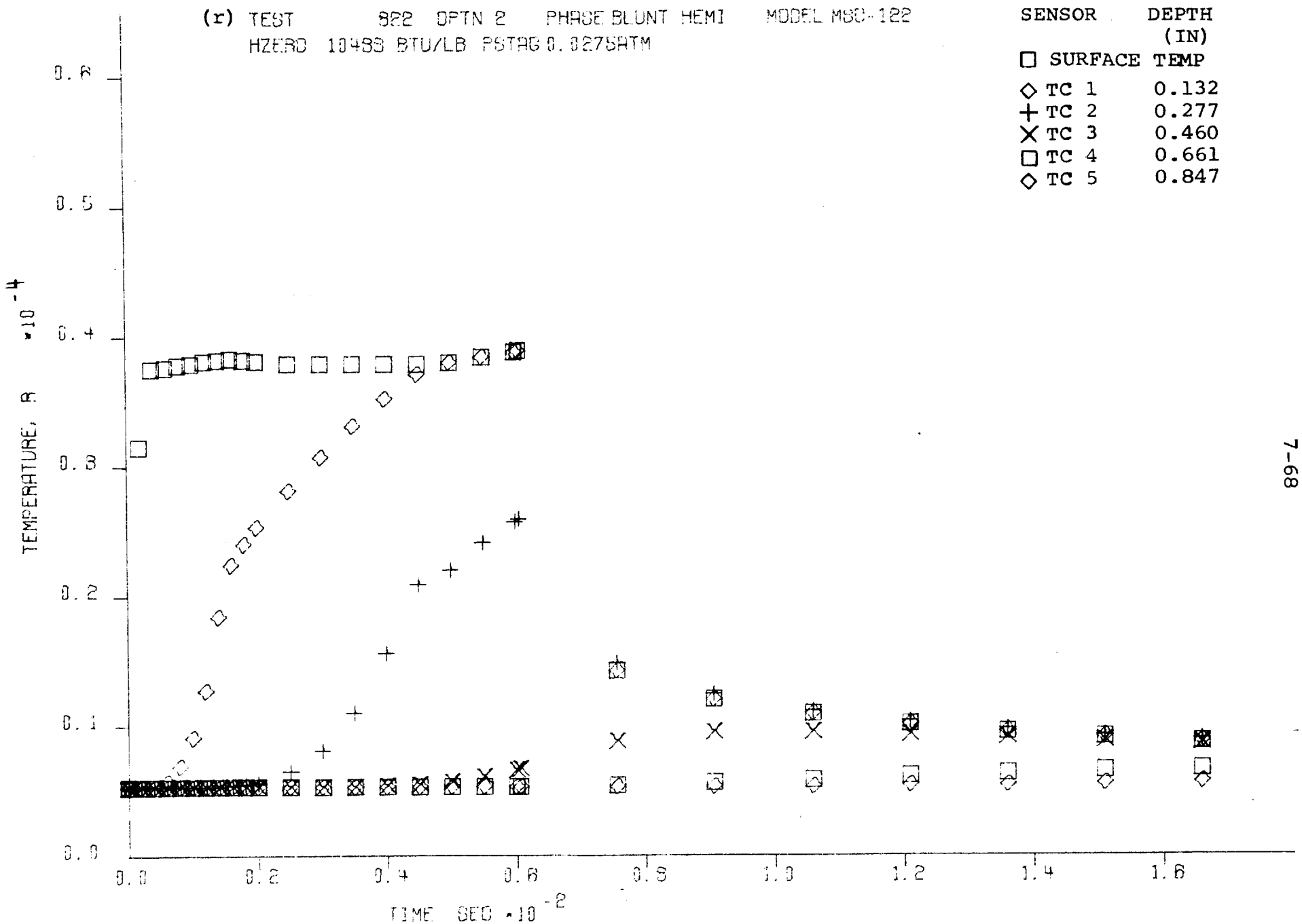

Figure 7-5. Continued.

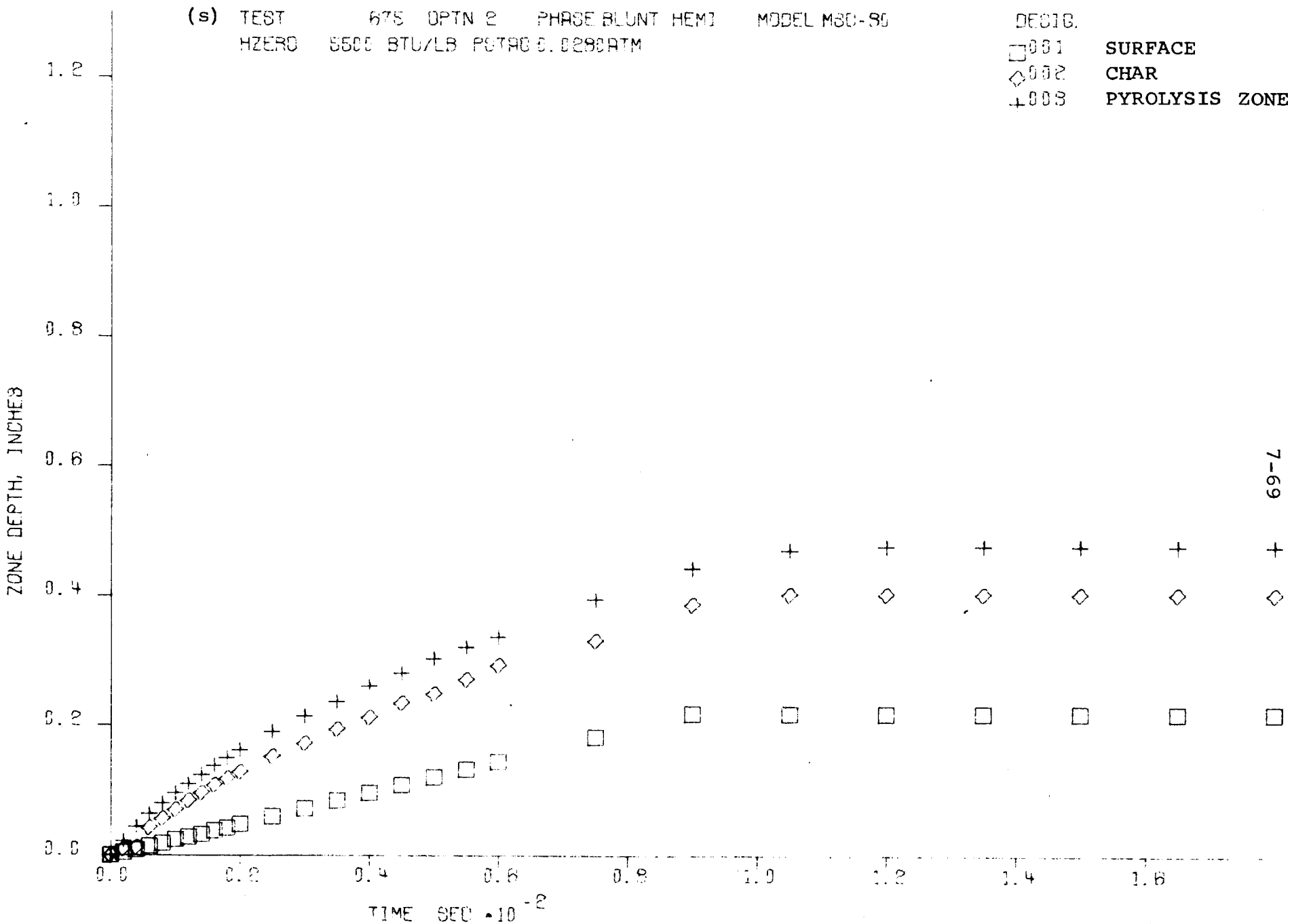

Figure 7-5. Continued.

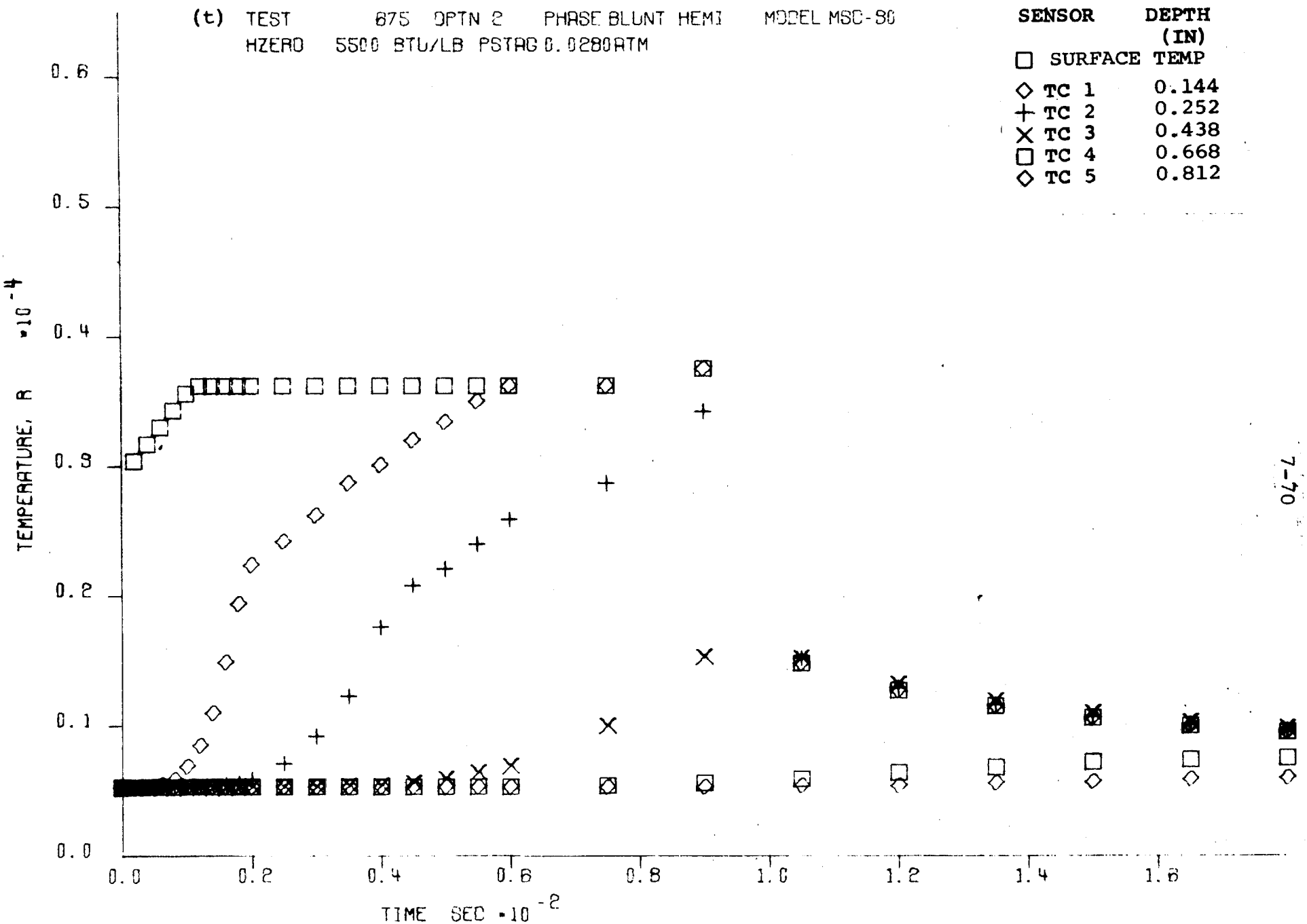

Figure 7-5. Continued.

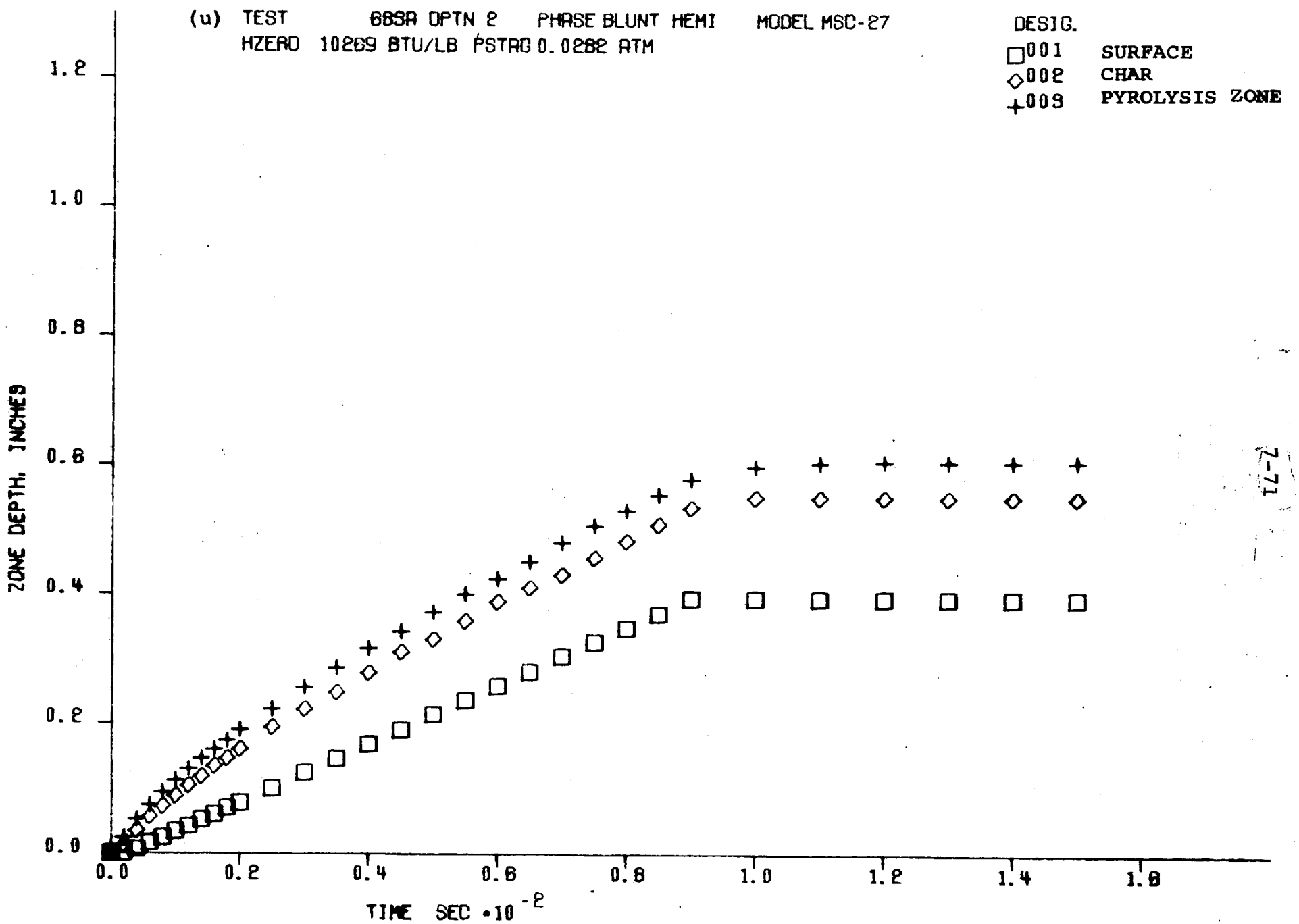
(u) TEST 68SA OPTN 2 PHASE BLUNT HEMI MODEL MSC-27
HZERO 10269 BTU/LB PSTAG 0.0282 ATM
DESIG.
001 SURFACE
002 CHAR
003 PYROLYSIS ZONE
ZONE DEPTH, INCHES
TIME SEC *10^-2
0.0
0.2
0.4
0.6
0.8
1.0
1.2
1.4
1.6

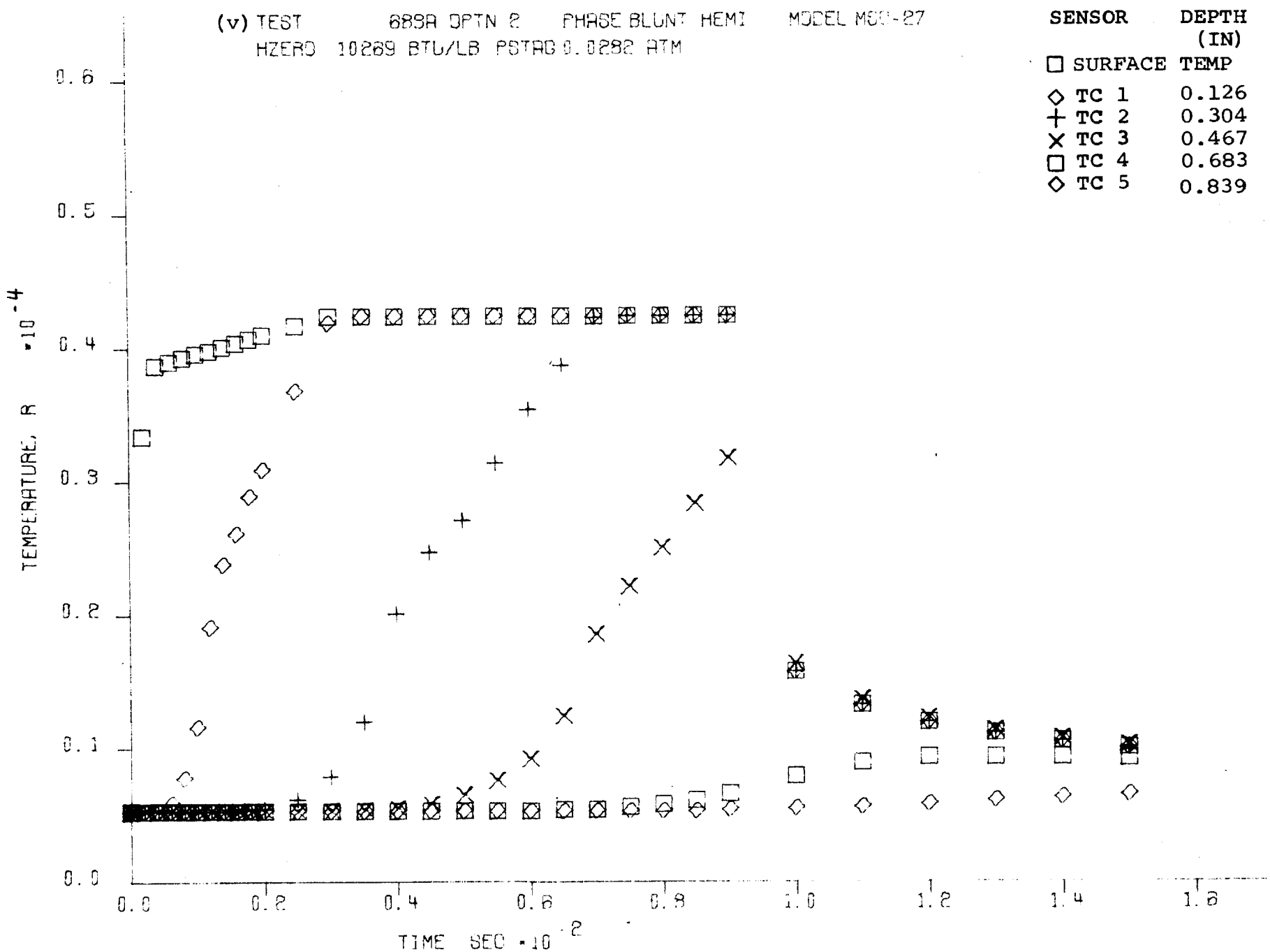

Figure 7-5. Continued.

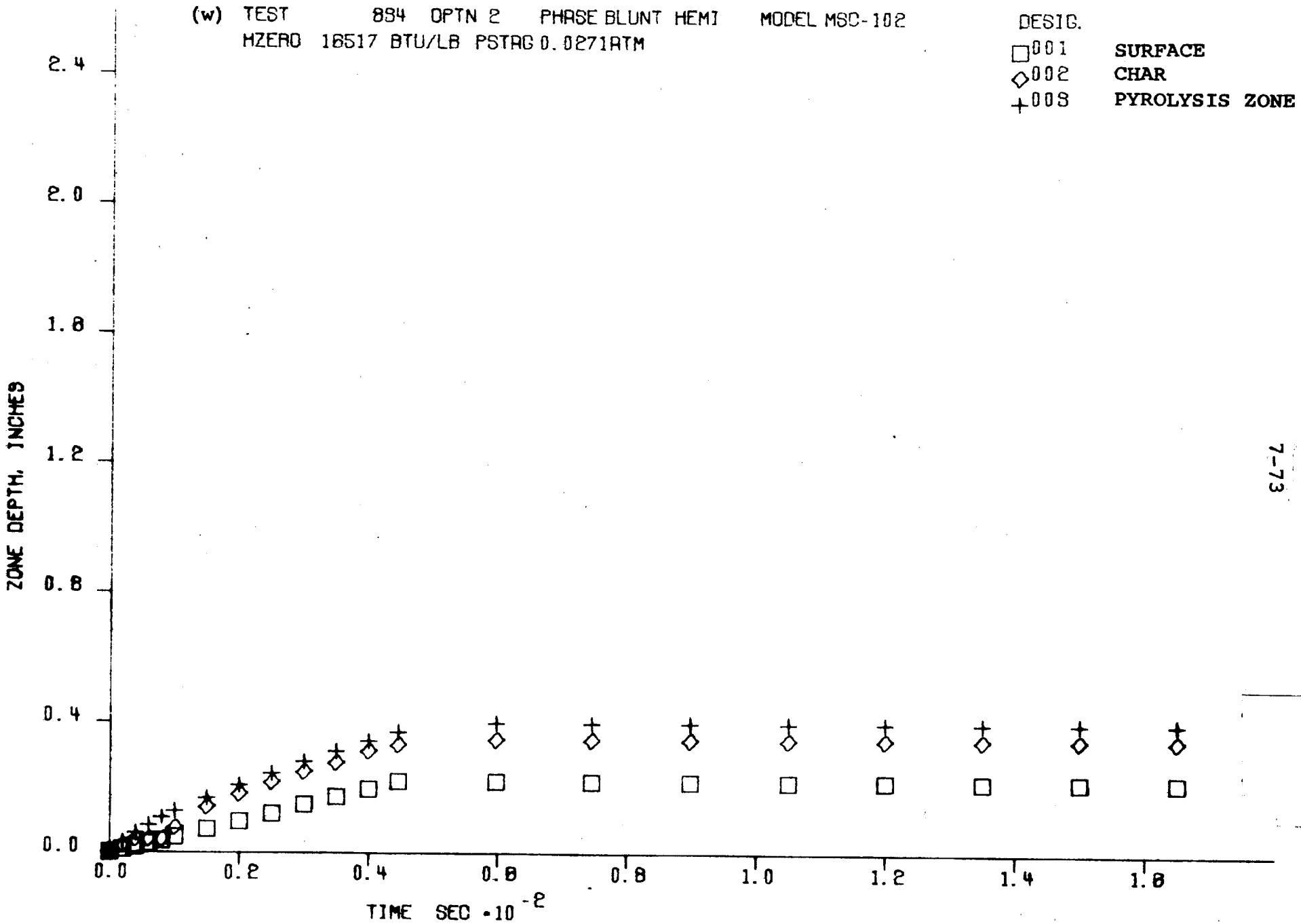
(w) TEST 884 OPTN 2 PHASE BLUNT HEMI MODEL MSC-102
MZERO 16517 BTU/LB PSTAG 0.0271ATM
DESIG.
001 SURFACE
002 CHAR
003 PYROLYSIS ZONE
ZONE DEPTH, INCHES
2.4
2.0
1.8
1.2
0.8
0.4
0.0
0.0
0.2
0.4
0.6
0.8
1.0
1.2
1.4
1.6
TIME SEC *10 -2

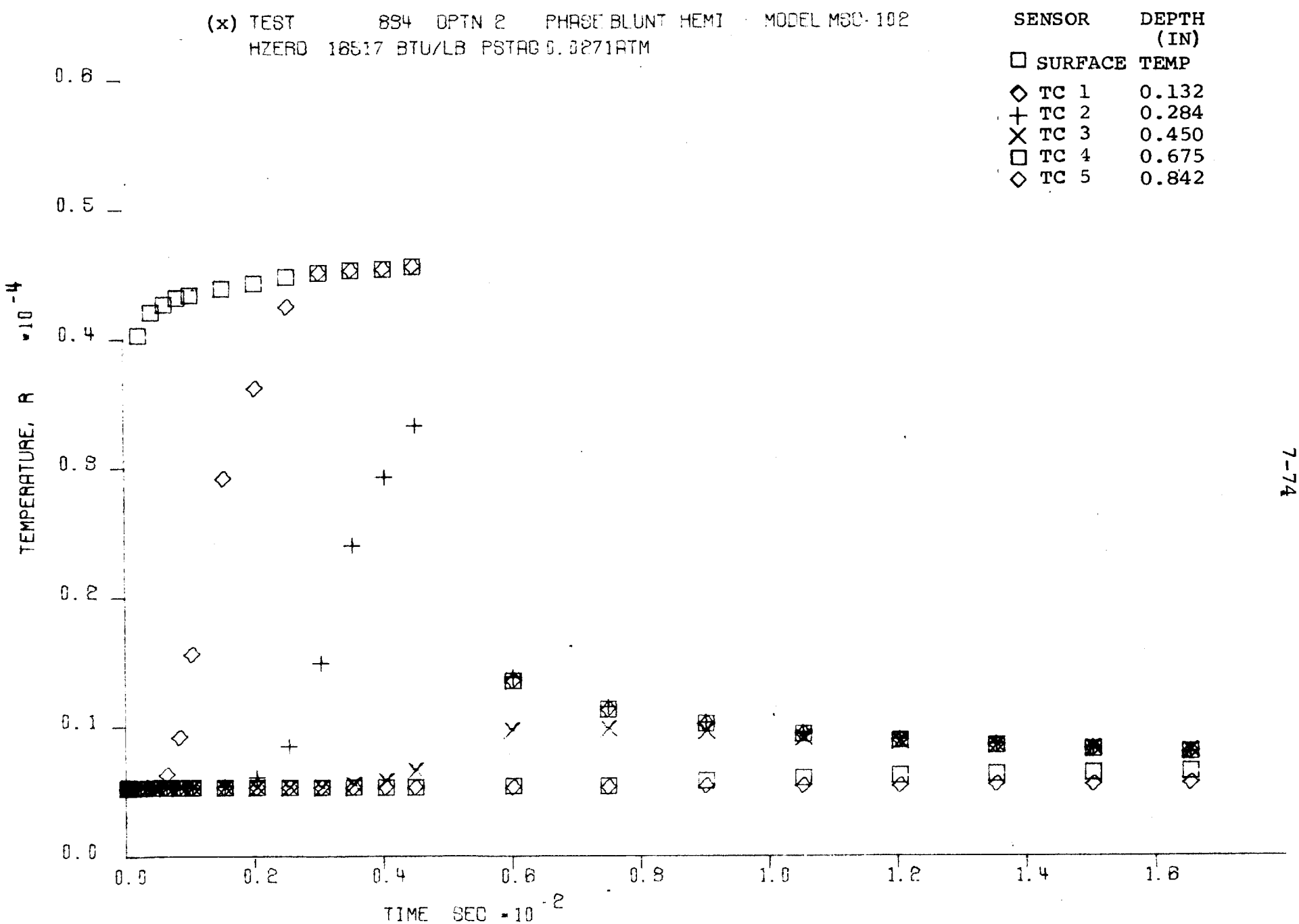

Figure 7-5. Continued.

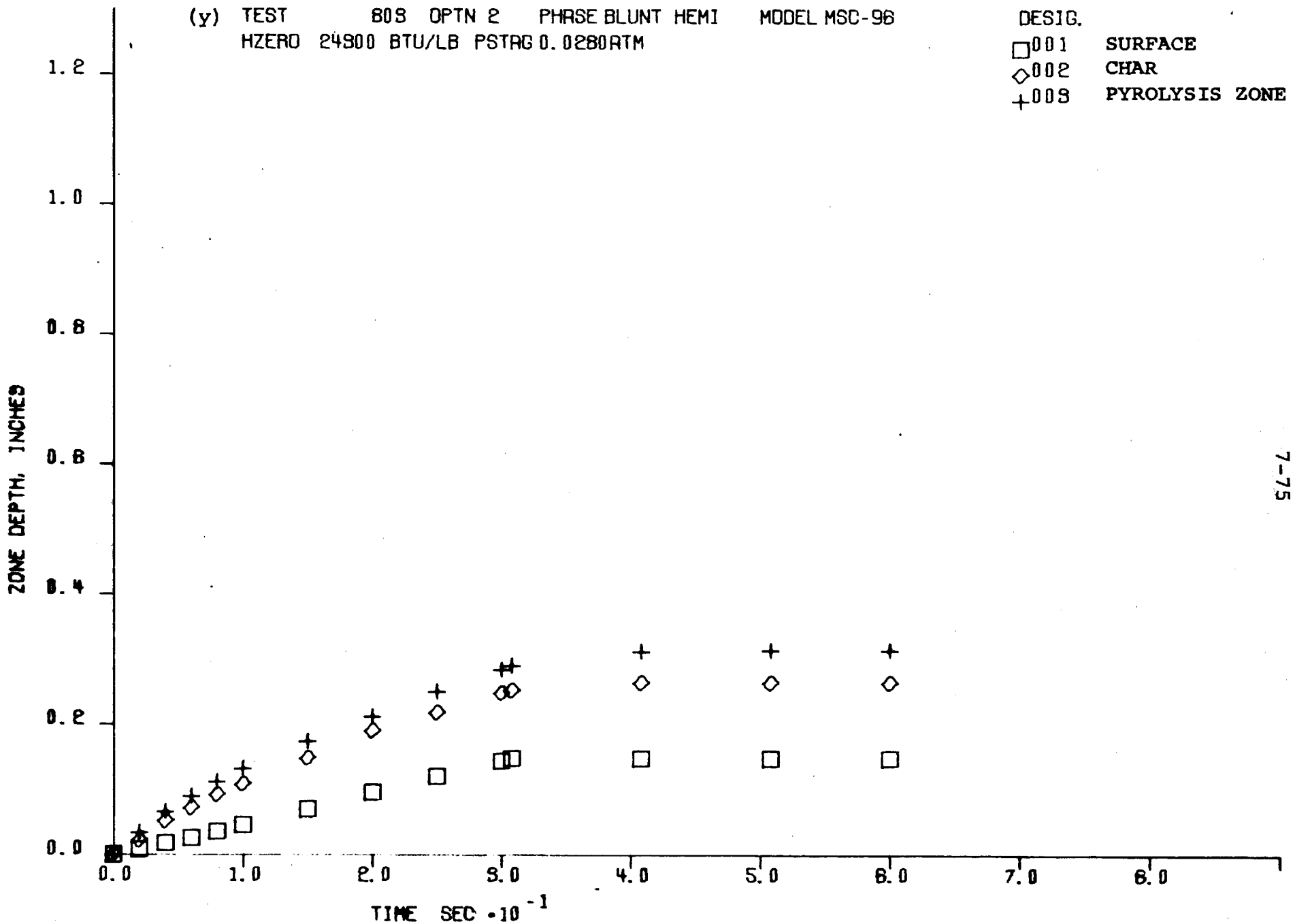

Figure 7-5. Continued.

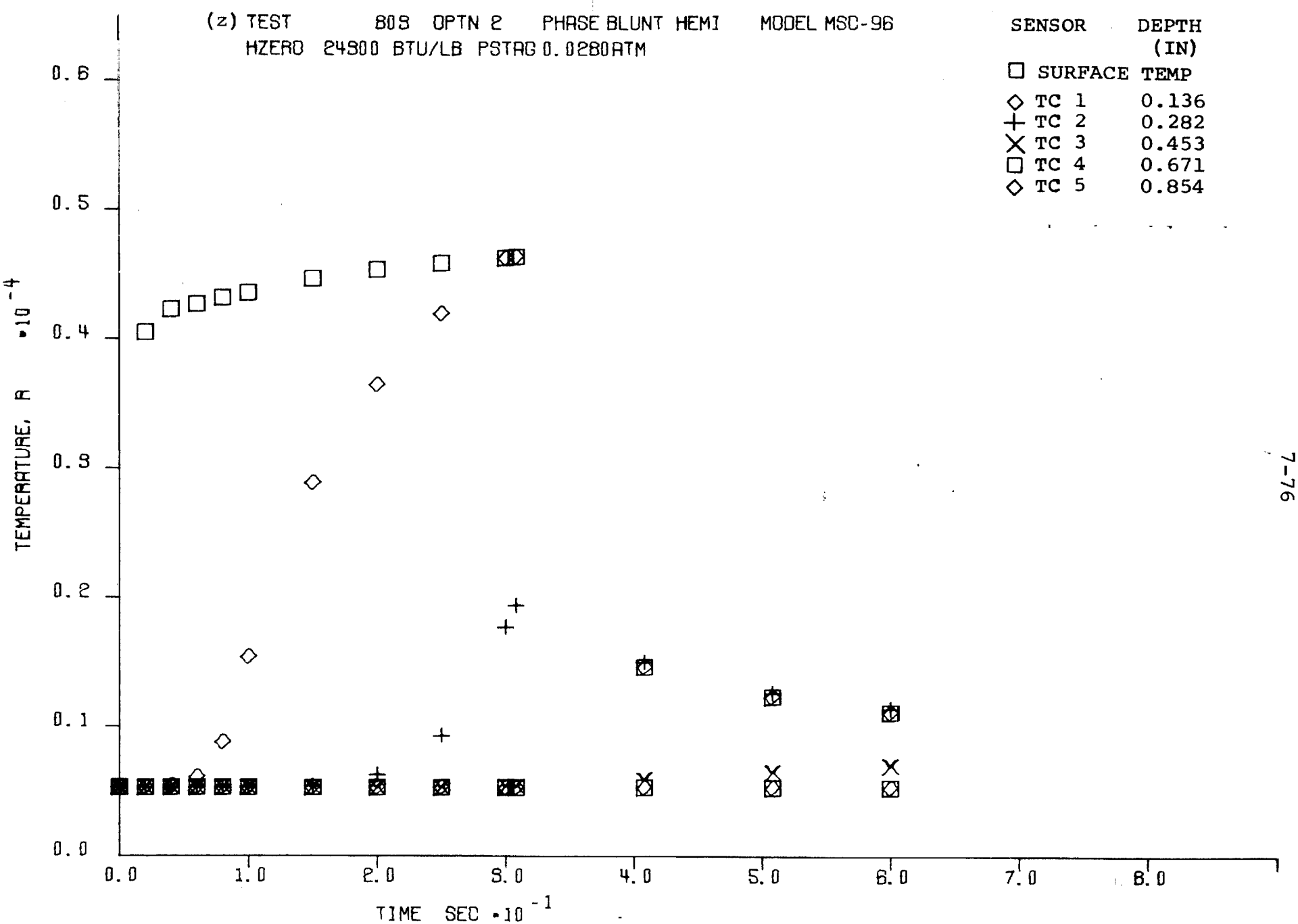

Figure 7-5. Continued.

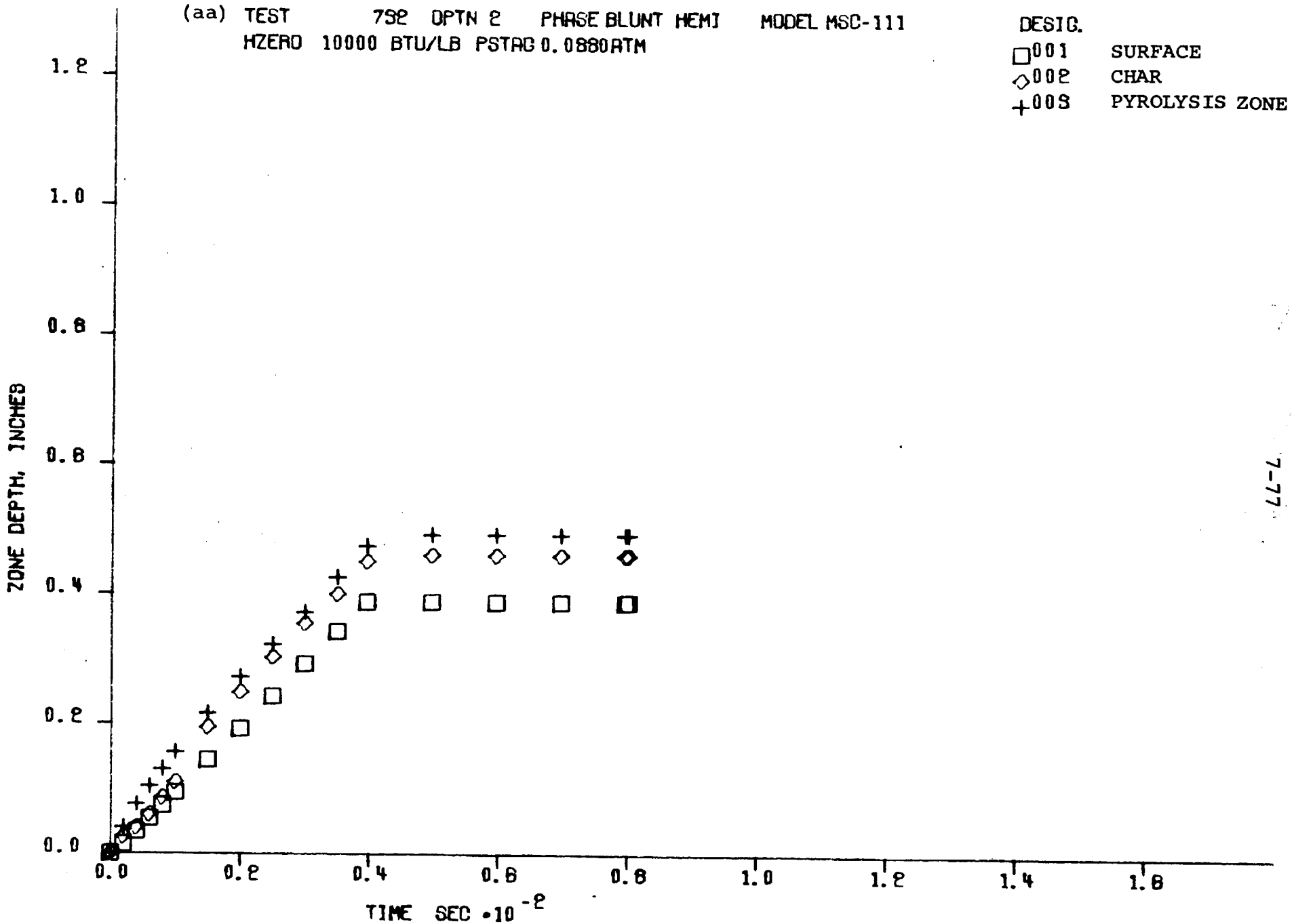

Figure 7-5. Continued.

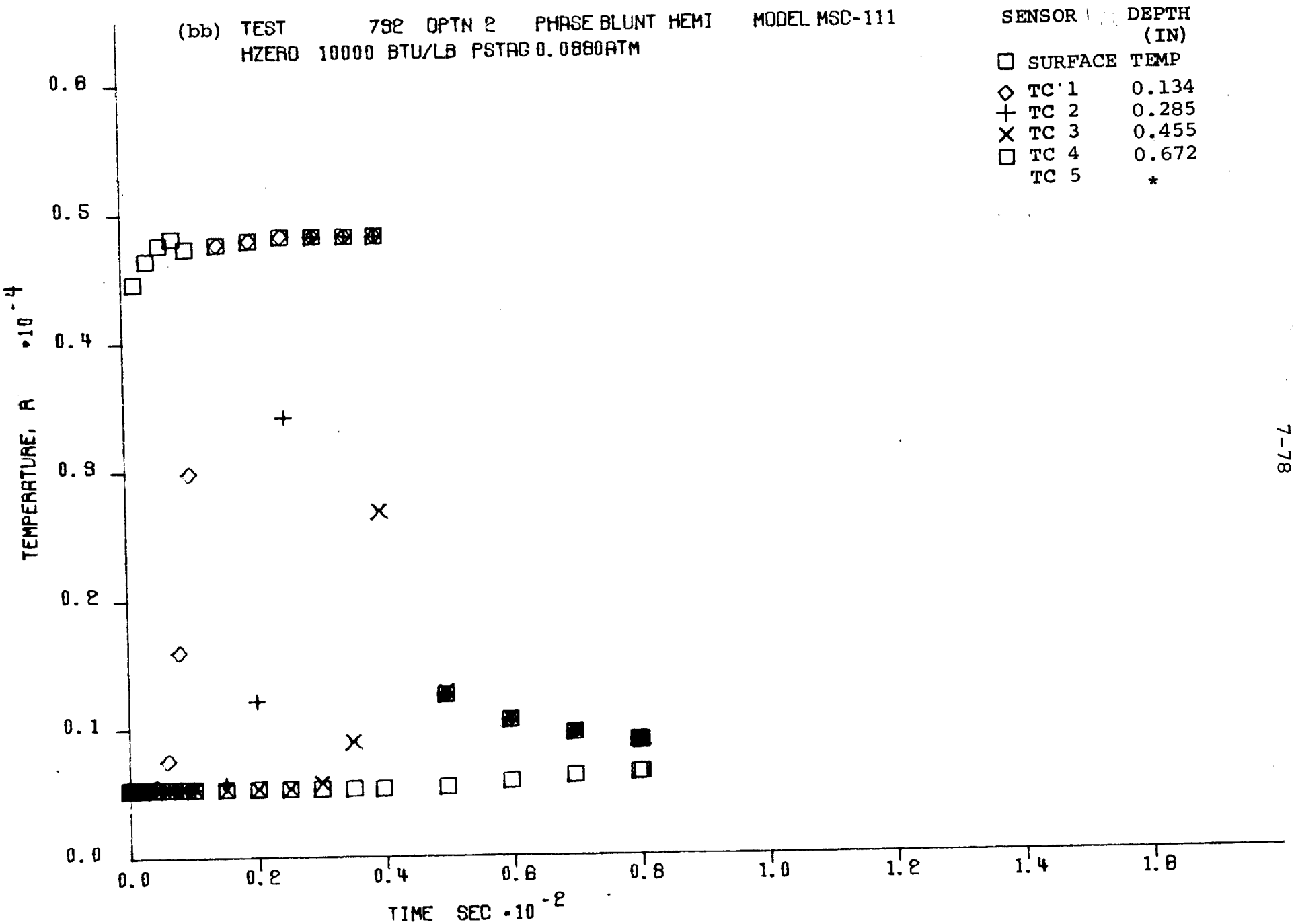

Figure 7-5. Concluded.

TABLE 7-2

RESULTS OF PARAMETRIC STUDY

Prediction No.	Enthalpy h (Btu/lb)	Stagnation Pressure P_s (atm)	Convective q_c (Btu/ft² sec)	Radiative q_r (Btu/ft² sec)	Chemical Environment	Exposure Time ϑ (sec)	Cooldown Time (sec)	Surface Recession (inch)	Char Depth (1) (inch)	Pyrolysis Zone Depth (1) (inch)	Average Recession Rate (mils/sec)	Isotherm Depths (1) 1,000°F	Isotherm Depths (1) 600°F
1	25,000	0.001	100	0	Air	240	0	0	0.515	0.614	0	0.612	0.680
2		0.01				180			0.425	0.516		0.512	0.563
3		0.1				90			0.257	0.325		0.328	0.369
4		1.0				45			0.144	0.197		0.204	0.235
5		10.0				30			0.103	0.148		0.155	0.182
6	17,500	0.1				90			0.247	0.313		0.322	0.362
7	10,000							0.008	0.261	0.328	0.089	0.330	0.369
8	5,000					180		0.385	0.588	0.653	2.14	0.657	0.697
9	3,500							0.612	0.741	0.794	5.54	0.798	0.829
10	17,500		20			90		0	0.298	0.140	0	0.137	0.199
11			50						0.158	0.239		0.243	0.289
12			200					0.021	0.325	0.391	0.233	0.3970	0.432
13	17,500		500					0.387	0.547	0.591	4.30	0.596	0.619
14	25,000	1.0				45		0.133	0.313	0.351	2.96	0.355	0.377
15			250	250				0.024	0.269	0.314	0.533	0.319	0.344
16	17,500		100	0	Nitrogen	60		0	0.178	0.237	0	0.243	0.278
17					$0.93N_2/0.07O_2$				0.177	0.238		0.244	0.278
18					$0.85N_2/0.15O_2$				0.179	0.238		0.245	0.279
19					Air				0.181	0.239		0.2458	0.280
20			500		Nitrogen				0.313	0.361		0.367	0.399
21					Air			0.205	0.385	0.422	3.42	0.427	0.451
22	10,000		100		Nitrogen	90			0.263	0.327	0	0.336	0.377
23					Air			0.008	0.272	0.343	0.088	0.348	0.388
24			500		Nitrogen			0.029	0.407	0.461	0.322	0.462	0.499
25					Air			0.725	0.814	0.838	8.06	0.844	0.859
26	5,000		100		Nitrogen	120		0	0.325	0.403	0	0.405	0.452
27					$0.93N_2/0.07O_2$			0.009	0.335	0.415	0.075	0.419	0.464
28					$0.85N_2/0.15O_2$			0.088	0.361	0.438	0.733	0.443	0.484
29					Air			0.233	0.420	0.488	1.94	0.491	0.527
30	17,500	0.1	20			30	120	0	0/0	0.053/0.589	0	0.553/—	0.097/—
31						60			0.004/0.005	0.098/0.108		0.081/—	0.151/—
32						300			0.207/0.215	0.375/0.406		0.361/1.83	0.451/0.207
33			100			30			0.101/0.107	0.148/0.166		0.152/—	0.180/—
34						60			0.181/0.192	0.239/0.271		0.244/—	0.280/1.08
35						300		0.008	0.560/0.586	0.676/0.756	0.027	0.660/0.557	0.736/0.812
36			500			30		0.087	0.227/0.238	0.262/0.291	2.93	0.269/—	0.287/—
37						60		0.234	0.390/0.407	0.643/0.462	3.90	0.431/1.96	0.454/—
38		0.01	20			30		0	0/0	0.052/0.058	0	0.054/—	0.096/—
39						60			0.001/0.002	0.096/0.106		0.063/—	0.149/—
40						300			0.200/0.208	0.370/0.400		0.355/1.85	0.446/0.218
41			100			30			0.100/0.106	0.146/0.165		0.152/—	0.178/—
42						60			0.178/0.190	0.239/0.271		0.244/—	0.280/1.08
43						300		0.009	0.588/0.586	0.675/0.756	0.030	0.658/0.567	0.735/0.811
44	3,000	0.2	200	20		45	0	0.419	0.458	0.477	9.34	0.482	0.495
45				100				0.446	0.492	0.511	9.91	0.516	0.529
46				500				0.611	0.654	0.668	13.6	0.672	0.682
47	25,000	0.1		100				0.0008	0.240	0.283	0.018	0.292	0.318

(1) At the end of exposure time / At the end of cooldown time.

REFERENCES

7-1 User's Manual; Aerotherm Charring Material Ablation Program, Version 2, Aerotherm Corp., January 1966.

7-2 Kendall, R. M.: A General Approach to the Thermochemical Solution of Mixed Equilibrium-Nonequilibrium, Homogeneous or Heterogeneous Systems, Part V of Final Report, Contract NAS9-4599, Aerotherm Project No. 6002, March 14, 1967.

7-3 JANAF Thermochemical Tables. The Dow Company, Midland, Michigan, August 1965.

7-4 User's Manual; Aerotherm Equilibrium Surface Thermochemistry Program, Version 2; Aerotherm Chemical Equilibrium Program (rough draft), Aerotherm Corporation, June 1966, December 1966, respectively.

7-5 Theoretical Simulation of the Apollo Heat Shield Material Using Existing Vidya Computer Programs, Aerotherm Draft Memorandum 6002-4, Contract NAS9-4599.

7-6 Duff, R. E. and Baur, S. H.: Equilibrium Composition of the C/H System at Elevated Temperatures, J. Chem. Phys., Vol. 36, p. 1754, April 1962.

7-7 Hochstim, Adolf R.: Equilibrium Compositions, Thermodynamic and Normal Shock Properties of Air with Additives, Vol. 1, DA-04-495-ORD-3112 and -3383, General Dynamics-Convair, Dec. 1, 1961.

7-8 Rindal, R. A., Kendall, R. M., and Moyer, C. B.: Finite Difference Equations for the Response of a One-Dimensional Charring Material of Arbitrary Geometrical Configurations, Aerotherm Corporation, Palo Alto, California, Contract No. NAS9-4599, Report 6002-TM-1, March 18, 1966.

7-9 Clark, K. J.: Thermal Conductivity Model for Avcoat 5026-39, Aerotherm Technical Memoranda 6007-TM-2 and 6007-TM-2R, October 19, 1966 and February 1, 1967.

7-10 Personal Communication, D. J. Tillian, NASA-MSC, December 1966.

7-11 Rindal, R. A. and Kratsch, K. M.: Prediction of the Ablative Material Performance on a Scout Entry Vehicle, Final Report No. 66-4, Aerotherm Project No. 6016, Aerotherm Corporation, July 15, 1966.

7-12 McCuen, P. A., Schaefer, J. W., Lundberg, R. E., and Kendall, R. M.: A Study of Solid-Propellant Rocket-Motor Exposed Materials Behavior, Report No. AFRPL-TR-65-33, Final Report, Contract No. AF 04(611)-9073, Vidya Project No. 9061, February 26, 1965.

APPENDIX A

LIST OF INSTRUMENTATION

Instrument	Make	Model
Recording Oscillograph	Consolidated Electro-dynamics Corporation	5-119
Voltage to Frequency Converter	Vidar	260
Master Scanner	Vidar	12029
Differential Temperature Transducer	Delta-T Corporation	1 inch diameter
Pressure Transducer	Consolidated Electro-dynamics Corporation	± 25 psid, 0-150 psia, 0-1 psia
	Statham	0-15 psia, 0-5 psia, ± 2 psid
Indicating Potentiometer	Minneapolis-Honeywell	
Infrared Pyrometer	Infrared Industries	Thermodot TD9CH
Total Radiation Pyrometer	Minneapolis-Honeywell Brown Instruments Div.	Radiamatic RI 2
Vacuum gage	Hastings	Model DV-6 (micron Hg) Model DV-4D (mm Hg)
Absolute pressure gage	Wallace Tiernan	0-20 mm Hg, 0-100 mm Hg, 0-200 mm Hg, 0-31 inches Hg
Differential pressure gage	Barton Instrument Corporation	0-15 psid
Motor driven movie camera	Traid	Photosonics 1B 16mm
Micrometer	Mitutoyo	0-1", No. 103-260, 0-2", No. 103-262
Analytic balance	Braun Corporation	